Methods and tools for the study of G-quadruplex DNA and RNA in human cells

Jérémie Mitteaux

DOCTORAL THESIS OF THE UNIVERSITY OF BOURGOGNE FRANCHE-COMTÉ

prepared at the Institute of Molecular Chemistry of the University of Bourgogne (ICMUB)

Graduate School n°553

« Carnot Pasteur »

Thesis for the degree of Doctor of Philosophy (PhD)

in Chemical biology

by

Mr MITTEAUX Jérémie

Methods and tools for the study of G-quadruplex DNA and RNA in human cells

---

Thesis presented and defended in Dijon, on 13th December 2023

Jury composition:

Pr DENAT Franck	Professor and Director, ICMUB (Dijon)	President
Dr MILLEVOI Stefania	Senior INSERM researcher, CRCT (Toulouse)	Reviewer
Dr BRITTON Sébastien	CNRS researcher, IPBS (Toulouse)	Reviewer
Dr AMRANE Samir	INSERM researcher, ARNA/IECB (Bordeaux)	Examiner
Dr MONCHAUD David	Senior CRNS researcher, ICMUB (Dijon)	Supervisor
Dr GOBBO Jessica	Clinical research scientist, LNC Research Centre (Dijon)	Guest

Titre : Méthodes et outils pour l'étude des G-quadruplex d'ADN et ARN en cellules humaines

Mots clés : Acides nucléiques, G-quadruplex, déstabilisateur de G4, imagerie optique, purification par affinité

Résumé : Les G-quadruplexes (ou G4s) sont des structures alternatives d'acides nucléiques (ADN et ARN) identifiées depuis 1988. Grâce à des méthodes expérimentales variées (relevant des techniques de biophysique et biochimie) d'une part, et à des outils (bio)moléculaires ciblant les G4s (*e.g.*, ligands de G4s, anticorps spécifiques des G4s) d'autre part, les rôles biologiques de ces superstructures riches en guanines (Gs) commencent à être bien compris : les G4s interviennent notamment dans la régulation de l'expression de gènes, de la réplication et de la transcription, dans le maintien de la structure des télomères, dans la réparation de l'ADN, etc. Les G4s jouent donc des rôles importants dans de nombreux processus clés de la cellule. Ces rôles, ainsi que leur forte densité génomique et transcriptomique, et les dysfonctions associées aux protéines en charge de leur résolution *in cella* (les hélicases), ont conduit à considérer les G4s comme des acteurs (et donc des cibles) important(e)s dans les maladies génétiques.

Dans ce contexte, identifier des composés chimiques capables de moduler la formation de ces structures en cellules humaines apparaît être une stratégie utile non seulement pour mieux comprendre les rôles qu'elles jouent mais aussi pour le développement de traitements potentiels de ces maladies.
Durant mon projet de doctorat, *(I)* j'ai tout d'abord identifié une molécule permettant de déstabiliser de façon fiable les G4s, le PhpC, et ce, par le développement de nouveaux tests *in vitro* ; *(II)* j'ai ensuite étudié la relation entre les G4s et les dommages à l'ADN en cellules humaines par imagerie optique *via* l'utilisation d'outils moléculaires polyvalents: les TASQs ; et finalement, *(III)* en combinant les applications des TASQs avec l'optimisation d'une méthode de purification par affinité des G4s d'ARN (G4RP), j'ai validé la capacité du PhpC à déstabiliser les G4s *in cella*, contribuant ainsi à la valorisation de ce composé dont les applications en recherche et en thérapie sont extrêmement prometteuses.

Title: Methods and tools for the study of G-quadruplex DNA and RNA in human cells

Keywords: Nucleic acids, G-quadruplex, G4-destabilizer, optical imaging, affinity purification

Abstract: G-quadruplexes (G4s) are nucleic acids (DNA and RNA) alternative structures identified since 1988. Thanks to a panel of experimental methods belonging to the biophysical and biochemical techniques on the one hand, and to the use of (bio)molecular G4 tools (*e.g.*, chemical G4 ligands, G4-specific antibodies) on the other hand, precise insights into the biological roles that these guanine (G)-rich high-order structures play have been gained: notably, G4s are involved in the regulation of gene expression, of replication and transcription in telomere maintenance and DNA repair, etc. G4s are thus key players in critical cellular processes. These roles, combined with both a high genomic and transcriptomic density and a series of dysfunctions related to the proteins in charge of their unwinding in cells (G4 helicases) led us to consider G4s as key effectors of (and thus, key targets for) genetic diseases.

In this context, the identification of compounds able to modulate these G4 structures in human cells appears to be a useful strategy not only for better delineating their cellular roles but also for the development of potential treatments for G4-associated diseases.
During my PhD project, *(I)* I identified a reliable G4-destabilizer small molecule named PhpC *via* the development of new *in vitro* assays; *(II)* I studied the relationship between G4s and DNA damage by optical imaging using home-made G4-specific multivalent molecular tools, the TASQs; and finally *(III)* combining the application of the TASQs with the optimization of a cellular G4 RNA purification method (G4RP), I validated the G4 RNA-destabilizing properties of PhpC *in cella*, thus contributing to the development of a molecule with possibly tremendous applications for G4-associated diseases.

ACKNOWLEDGMENT

Ce travail n'aurait jamais vu le jour sans la contribution de différents acteurs (économique, institutionnel, scientifique) que je tiens ainsi à remercier :

Les organismes financeurs – 1/ Le Centre National de la Recherche Scientifique (CNRS), 2/ l'ITMO Cancer d'Aviesan/INSERM (projet ANASTOMOSIS, Plan Cancer 19CP117-00, 2014-2019), 3/ l'Union Européenne (projet SEQUENTIA, PO FEDER-FSE Bourgogne n° BG0021532, 2014-2020), 4/ l'Agence Nationale de la Recherche (projet DEMENTIA, ANR-17-CE17-0010-01, 2017-2020).

Les organismes d'accueil – 1/ L'Institut de Chimie Moléculaire de l'Université de Bourgogne (ICMUB ; UMR CNRS 6302), 2/ l'Université de Bourgogne, 3/ l'École doctorale Carnot Pasteur (n° 553).

Les collaborateurs scientifiques – 1/ L'ICMUB à Dijon en France (David Monchaud, Ibai E. Valverde, Claude P. Gros, Nicolas Desbois, Pauline Lejault, Francesco Rota Sperti, Joanna Zell, Angélique Pipier, Marc Pirrotta, Baptiste Dupouy, Sandy Raevens), 2/ la Plateforme DimaCell de l'INRAE à Dijon en France (Chrystel Deulvot, Elodie Noirot), 3/ le Laboratoire Interdisciplinaire Carnot de Bourgogne à Dijon en France (Julien Boudon), 4/ l'équipe Chimie et Reconnaissance d'Acides Nucléiques de l'Institut Curie à Paris en France (Anton Granzhan), 5/ l'équipe Structure et Instabilité des Génomes du MNHN/CNRS/INSERM à Paris en France (Jean-Baptiste Boulé, Alexandra Joubert), 6/ le Département de Neurologie de l'École de médecine McGovern à Houston aux E.U.A. (Andrey S. Tsvetkov, Louise D. McCullough, Jose F. Moruno-Manchon, Fudong Liu, Natalie Tabor), 7/ le Département de Chimie de l'Université Western Ontario à Ontario au Canada (Robert H. E. Hudson, Zi Wang, Filip Wojciechowski), 8/ l'Université de la Colombie-Britannique à Vancouver au Canada (Judy M. Y. Wong, Sunny Y. Yang).

Le comité de suivi individuel de thèse – 1/ Jessica Gobbo (Centre Georges-François Leclerc à Dijon en France), 2/ Richard Decréau (ICMUB à Dijon en France), 3/ David Monchaud (ICMUB à Dijon en France).

Le jury de soutenance de thèse – 1/ Franck Denat (ICMUB à Dijon en France), 2/ Stefania Millevoi (Centre de Recherches en Cancérologie de Toulouse à Toulouse en France), 3/ Sébastien Britton (Institut de Pharmacologie et Biologie Structurale à Toulouse en France), 4/ Samir Amrane (Intitut Européen de Chimie et Biologie à Bordeaux en France), 5/ David Monchaud (ICMUB à Dijon en France), 6/ Jessica Gobbo (Centre Georges-François Leclerc à Dijon en France).

Mes remerciements vont plus particulièrement à David Monchaud qui a encadré mon projet de doctorat au sein de son équipe GATTACA, à l'ICMUB. Plus que cela, je te suis extrêmement reconnaissant de m'avoir donné ma chance et d'avoir créé dans ton équipe cet environnement positif, professionnel comme personnel, qui m'a rapidement permis d'être en confiance et a véritablement joué le rôle de soupape de sécurité. Merci de m'avoir laissé une pleine liberté sur mes choix scientifiques comme artistiques, ces derniers te laissant avec des articles (et des posters) comprenant de jolis nuanciers de couleurs, ce dont je suis plutôt fier ! Merci aussi d'avoir supporté mes doutes, mon caractère discutable et mes légers retards (que je préfère appeler « moments de perfectionnement ») malgré lesquels tu as toujours trouvé du temps

pour me relire (j'en suis sûr : parfois sur un « home trainer » autour de 22h). De façon inattendue, je n'aurais jamais cru prendre goût à la course sur piste et participer à un 10 km (presque facile), donc merci pour cet exploit, ces entraînements (négociations) passé(e)s ensemble et pour m'avoir fait connaître cette pratique salvatrice.

Je tiens aussi à remercier les corps enseignant, scientifique et technique de l'ICMUB avec qui j'ai eu plaisir à discuter au détour d'un couloir, d'une pause déjeuner ou d'un apéro : Anne, Claire B, Claire L, Christine G, Christine S, Didier, Franck, Ibai, Laurie, Marc, Marie-Jo, Mathieu M, Myriam, Nicolas, Quentin, Richard, Stéphane, Stéphanie, Thierry, Anthony (Tony), Victor.

Au cours de ces quatre années de doctorat j'ai eu la chance de faire plusieurs rencontres à l'ICMUB, sur des temps plus ou moins long. Merci à toutes ces personnes qui sont passées dans ma vie et y ont laissées une trace :

2019-2020 – Adrien, Amélie, Anne, Daïan, Delphine, Diana, Emma, Francesco, Garance, Jo, Laurie, Léa, Malorie, Mathieu B, Michael, Pauline, Pierre, Robin L, Sergeï, Thibaud B, Thibaut C, Valentin, Wassima.

2020-2021 – Baptiste D, Benjamin, Fatima, Loris, Marta, Michel, Océane, Romane, Sébastien S, Tony.

2021-2022 – Angie, Baptiste C, Camille, Dimitri, Elisa, Jelena, Matthieu, Maxime, Robin R, Sofia, Suzanna, Yoann.

2022-2023+ – Cécile, Gaëlle, Ken, Hinda, Lucas (…), Maël, Manon, Margerie, Marie (Garuche), Sandy, Sheïma, Shubham, Sophie (d'en bas), Sophie P (d'en haut), Vincent, Zoé.

Mentions spéciales :

Garance, à croire que ça devait se faire ? Une rencontre autour de la balance de précision du R10, le confinement du au SARS-CoV-2, des premiers mois difficiles pour moi et ta soutenance de thèse fin 2020. Et pourtant, voilà 4 années que notre amitié dure : on s'entraide à relativiser les choses qui nous arrivent, à définir nos objectifs, nos craintes, et ce avec une sincérité parfois tranchante. C'est réconfortant, c'est sain, c'est réel. Merci à toi.

Elisa, *Rattus elisus*, alliée et neurodivergente victime d'aliénation parentale. Nous sommes à la fois si différents et si proches… (rourouh) Ses moments de déconnexion totale avec toi ont été plus que nécessaires pour supporter le poids de la servitude volontaire. Telle la Fée Morgane (que l'on croit être Merlin…), une magie spéciale (sombre) émane de toi et me touche tout particulièrement. Ce sont cette facilité d'accès, ton humour à toute épreuve et ta lucidité qui m'ont fait marcher vers ta lumière en fin de course. Ton parcours s'achève toi aussi très bientôt, va, brise tes chaînes et vit.

Marta, sol de la noche. Tu me rappelles un New York roll : généreuse et espiègle (oulah). De gels (Angèle/Anne) aux FRET, de la musculation à la zumba, des jeux de société (« J'ai 2 fils et la bombe ») aux restaus (« C'est pour qui ces yakitoris ???! »), tu as été une présence indispensable à mon séjour sur Dijon, sans qui cette expérience n'aurait pas eu la même saveur. Madrid, Niort, Dijon, Toulouse, quel que soit le

lieu nous nous retrouverons très vite pour créer de nouveaux souvenirs ensemble et continuer de faire vivre notre langage.

Paupau, Jo, Angie, une post-doc par année pour partager mon bureau et mon quotidien. Paupau, dragonne au cœur tendre, tu as grandement contribué à rendre douce et vivante mon arrivée dans l'équipe et dans cette ville, merci mille fois pour cela. Jo, la britannique (pas anglaise !) dont la franchise implacable m'a amusé autant qu'ému. Merci pour toutes ces réflexions et ces débats (souvent un verre à la main). Angie, un temps gourou yogiste, un temps coloriste hippie, le mistral est bien arrivé sur Dijon accompagné de sa playlist « witch pop » et de sa plus belle voix pour nos karaokés-labo sur Clara et Juliette.

Wassima, on dit qu'il ne faut jamais rencontrer ses idoles. Pour ma part, je ne sais pas comment j'aurais pu faire sans : ton énergie et ta positivité communicative faisait de toi la cathode de l'ICMUB auprès de laquelle toute pensée négative disparaissait. Drôle, juste, sensible, je me suis délecté de chaque moment passé avec toi à nourrir ton « ego trip » et refaire le monde à notre image. Je n'ai pas peur du futur car nos chemins se recroiseront pour sûr, au détour d'une « Fashion Week », d'une séance de dédicace ou des thermes de Caracalla à Baden-Baden.

Zoé, ma kryptonite, « ghost shark », la bombe H, « the alien superstar », Buffy bis, Lisan al Gaib (DOL 4, « as it was written... »). Un diamant taillé sur-mesure que peu de personnes sont capables de voir, tel le « glass onion » au milieu de l'île qui est pourtant à la portée de tous d'apercevoir. Tu as radicalement crampté mon quotidien en l'agrémentant de références cinématographiques, de rire et de sarcasme. On avait au début misé sur une relation toxique, j'ai l'impression à présent qu'une jolie synergie s'est installée et, totalement accro, je ne me résoudrais jamais à m'en séparer.

Merci aussi à ma famille pour leur soutien et leur patience au fil des années : Anthony, Dominique, Émilie, Jonathan, Julien, Laura, Léa, Loïc, Maman, Mamie, Marion, Nathalie, Papa, Patrick. Et bienvenue à Cataleya et Soren.

Lydia, Pauline, le noyau dur sans qui tout aurait été différent. Vraiment différent. Vous m'accompagnez depuis ma première année post-bac (10 ans…), nos relations ont mûri, pris de l'ampleur, jusqu'à atteindre cette confiance mutuelle et intemporelle. Merci de me faire vivre cela.

À ces longues journées, soirées et même nuits de traitements de données, de montage de figures et de rédactions en tout genre accompagnées de 1/ podcasts (2 Heures de Perdues, À Bientôt de te Revoir, C Dans l'Air, FloodCast, La Réu' d'Écran Large, La Saga, Transfert, Une Bonne Fois Pour Toutes !, YESSS), 2/ albums (&, Aller-Retour, Ancient Dreams in a Modern Land, Ben, Brol, Brûler le Feu, Caméo, Chromatica, Cœur, Crash, Deja, Desire I Want to Turn Into You, Dirt Femme, El Mal Querer, Entre a mi Mundo, Future Nostalgia, How I'm Feeling Now, Joie de Vivre, L'Ère du Verseau, LSD, Mata, Matriochka, Motomami, Music is the Weapon, Nonante-Cinq, Piano Republik, Plastic Hearts, Poster Girl, Rare, Redcar les Adorables Étoiles, Renaissance, Revelación, Rumours, Sainte-Victoire, Sanctuary, Smile, Solar Power, Sorøre, Sunshine Kitty,

Tako Tsubo, The English Riviera, The Gift, Volume II) et 3/ musiques de films (Alice in Wonderland, Alien, Aliens, Arrival, Dune, Gremlins, Halloween III, Harry Potter and the Prisoner of Azkaban, It Follows, Jurassic Park, La La Land, Poor Things, Stranger Things, The Mummy, The Thing) qui m'ont sauvés de la solitude.

“But we have soothed ourselves into imagining sudden change as something that happens outside the normal order of things. An accident, like a car crash. Or beyond our control, like a fatal illness. We do not conceive of sudden, radical, irrational change as built into the very fabric of existence. Yet it is. And chaos theory teaches us that straight linearity, which we have come to take for granted in everything from physics to fiction, simply does not exist. Linearity is an artificial way of viewing the world. Real life isn’t a series of interconnected events occurring one after another like beads strung on a necklace. Life is actually a series of encounters in which one event may change those that follow in a wholly unpredictable, even devastating way.”

Michael Crichton, Jurassic Park (1990)

LIST OF CONTENTS

– APPENDICES –

ABBREVIATIONS

1,5-BisNPO: macrocyclic 1,5-bis-naphthalene
2,6-BisNPO: macrocyclic 2,6-bis-naphthalene
2,7-BisNPN: macrocyclic 2,7-bis-naphthalene
3D: three-dimensional
53BP1: (or TP53BP1) p53-Binding Protein 1
±: plus or minus
>: superior
<: inferior
%: percentage
°C: degree Celsius
Å: Angstrom
Δ: a difference between two values (resulting from subtraction)
ΔΔCt: the relative fold between two cycle threshold (Ct) values
$\Delta T_{1/2}$: Melting temperature $_{\text{condition with ligand}}$ - melting temperature $_{\text{condition without ligand}}$
γH2AX: phosphorylated variant histone H2AX, (occurring after DNA double-strand breaks)
µ: micro
a. u.: arbitrary unit
AF: Alexa Fluor
Alk: Alkyne
ALS: Amyotrophic Lateral Sclerosis
AMP: Adenosine Monophosphate
ARNA: Acides nucléiques : Régulations Naturelles et Artificielles (UMR CNRS 5320, UMR INSERM U1212)
ASO: Antisense Oligonucleotide
ATP: Adenosine triphosphate
Az: Azide
B-DNA: DNA duplex
BACH1: (or FANCJ) BRCA1-Associated C-terminal Helicase 1
BCT: BioCyTASQ
BG4: a G4-specific antibody (obtained by Biffi Giulia)
BLAST: Basic Local Alignment Search Tool
BLM: Bloom syndrome-related gene (the syndrome was firstly described by David Bloom in 1954)
BRACO-19: N,N'-(9-(4-(dimethylamino)phenylamino)acridine-3,6-diyl)bis(3-(pyrrolidin-1-yl)propenamide)
BrdU: Bromodeoxyuridine
BRIP1: BRCA1-Interacting Protein 1
BTT: BioTriazoTASQ
C-DNA: four-way junctions
c-hTelo: the oligonucleotide possessing the complementary sequence to the s-hTelo
***c-KIT1/2*:** cellular homologs (1 and 2) of the *v-kit* viral gene isolated from a feline fibrosarcoma (hence the name "kit"); a proto-oncogene
***C9orf72*:** chromosome 9 open reading from 72
***ca.*:** *circa*, meaning "approximatively"
CD: Circular Dichroism
CGIs: CpG Islands
ChIP-seq: Chromatin ImmunoPrecipitation – sequencing
CMP: Cytidine Monophosphate
CMPP: Co-binding-Mediated Protein Profiling
CNRS: Centre National de la Recherche Scientifique
CNS: Central Nervous System
CpG: Cytosine-phosphate-Guanine
CRCT: Centre de Recherches en Cancérologie de Toulouse (UMR CNRS 5071, UMR INSERM 1037)
CRISPR/Cas9: Clustered Regularly Interspaced Short Palindromic Repeats-associated Cas9 nuclease
Ct: Cycle threshold, meaning the qPCR cycle number where the fluorescence intensity is distinguishable from the background noise and representing a quantitative value of nucleic acid
CuAAC: Copper(I)-catalysed Alkyne-Azide Cycloaddition
CUT&Tag: Cleavage under targets and tagmentation
Cy3: Cyanine3
Cy5: Cyanine5
CyT: a cyanine dye
DAOTA-M2: a triangulenium derivative (or 8,12-bis(2-morpholinoethyl)-8H-benzo[ij]xantheno[1,9,8-cdef][2,7]naphthyridin-12-ium hexafluorophosphate)
DAPI: 4',6-diamidino-2-phenylindole
DBCO: Diarylcyclooctyne
DDR: DNA Damage Responses
DEPC: Diethylpyrocarbonate
DFS: Dynamic Force Spectroscopy
DLS: Dynamic Light Scattering
DMEM: Dulbecco's Modified Eagle Medium
DMSO: Dimethyl sulfoxide
DNase: Deoxyribonuclease
DNA: DesoxyriboNucleic Acid
DNMT1: DNA(cytosine-5)-MethylTransferase 1
DOTA: 1,4,7,10-tetraazacyclododecane-1,4,7,10-tetraacetic acid
DOTASQ: DOTA-templated synthetic G-quartet
Dr: Doctor
DRAQ5: 1,5-bis{[2-(di-methylamino)ethyl]amino}-4,8-dihydroxy-9,10-anthraquinone
DRP: Dipeptide Repeat Protein
DSB: Double-Strand DNA Breaks
DSC: Differential scanning calorimetry
dsDNA: double-stranded DNA

***E. coli*:** *Escherichia coli*
***e.g.*:** *exempli gratia*, meaning "for example"
EDTA: Ethylenediaminetetraacetic acid
EGTA: Ethyleneglycol-*bis*(β-aminoethyl)-N,N,N',N'-tetraacetic acid
ELISA: Enzyme-Linked Immunosorbent Assay
EMSA: Electrophoretic Mobility Shift Assay
ESI-MS: Electrospray Ionization Mass Spectrometry
***f*:** function
FA: Formaldehyde
FAM: 6-carboxyfluorescein
FAn: Fluorescence Anisotropy
FANCJ (also called BACH1 and BRIP1): Fanconi Anemia Complementation group J
FC: Fold Change
FI: Fluorescence Intensity
Figure S: supplementary figure
FITC: Fluorescein Isothiocyanate
***focus/foci*:** fireplace, meaning "light point (or object)"
FOLDeR: Footprinting Of Long 7-Deazaguanine substituted RNAs
FP: Fluorescence Polarization
FQA: Fluorescence Quenching Assay
FRET: Förster (or Fluorescence) Resonance Energy Transfer
FRET-MC: FRET coupled to melting competition
FTD: Frontotemporal Dementia
FUS: (or TLS) Fused in Sarcoma/Translocated in LipoSarcoma RNA-binding protein
FWJ: Four-Way Junction
G3BP(1): GTPase-activating protein-binding protein (1)
G4 strand: oligonucleotide with the *S. pombe* G4-1 motif (antisense strand)
G4-DNA/RNA: G-quadruplex-folding DNA/RNA sequence
G4-FID: G-quadruplex Fluorescent Intercalator Displacement
G4-GIS: G-quadruplex ligand-Guided Immunofluorescence Staining
G4-LIMCAP: G-quadruplex Ligand-Mediated Cross-linking And Pull-down
G4(s): G-quadruplex(es)
G4D: G-quadruplex(es)-destabilizing
G4DP: G-Quadruplex-DNA-specific Precipitation
G4RP: G-Quadruplex-RNA-specific Precipitation
G4S: G-quadruplex(es)-stabilizing
G4sP: G-quadruplex-specific-Precipitation (ratio)
GBA: Glycosidic Bond Angles
GEF: Guanine nucleotide Exchange Factor
GFP: Green Fluorescent Protein
GMP: Guanosine Monophosphate
Gs: Guanines
guaPhpC: 2-(6-(3-(2-(bis(tert-butyloxycarbonyl)methyleneamino)ethoxy)phenyl)pyrrolocytosin-1-yl)acetic acid
h: hour
***H. sapiens*:** *Homo sapiens*
H-DNA: DNA triplex
HaCaT cells: primary immortalized human keratinocytes
HBV: Hepatitis V Virus
HCl: hydrogen chloride
hf2: antibody n° 2 selected toward the parallel-type G4 *c-KIT2* by Himesh Fernando
HIV-1: Human Immunodeficiency Virus 1
HPV: Human Papillomavirus
hTelo: human telomeric repeat sequence
hPIF1: human helicase (enzyme) (for "Petite Integration Frequency" given that experiments with allelic mutants leading to recombination between p^- and p^+ mtDNA)
***i.e.*:** *id est*, meaning "that is"
$IC_{20/50/80}$: 20/50 (half)/80% maximal Inhibitory concentration
ICC: Immunocytochemistry
ICMUB: Institut de Chimie Moléculaire de l'Université de Bourgogne (UMR CNRS 6302)
IECB: Institut Européen de Chimie et Biologie
IgG: Immunoglobulin G
IMP: Inosine Monophosphate
IMT: Isopropyl 4-Methylbenzenesulfonate-based Thioflavin T derivatives
***in cella*:** in a compartment/room, meaning in a cellular environment
***in silico*:** with a silicon-containing computer, meaning in a digital way (with a computer)
***in vitro*:** in glass, meaning in an artificial environment
***in vivo*:** within the living, meaning in a biological environment (*e.g.*, in animal experiment)
INSERM: Institut National de la Santé Et de la Recherche Médicale
IntDen: Integrated Density
IPBS: Institut de Pharmacologie et Biologie Structurale (UMR CNRS 5089)
ITC: Isothermal Titration Calorimetry
isoFRET: Isothermal FRET
K^+: potassium ion
KCl: potassium chloride
HCT116 cells: immortalized human colon carcinoma cells
K_D: Dissociation constant
HEK293T cells: immortalized Human Embryonic Kidney 293 cells (with a temperature sensitive mutant of the SV40 large T antigen)
HeLa cells: immortalized human adenocarcinoma cells from Henrietta Lacks
KIF5A: (human) Kinesin Family member 5A

KIT: receptor tyrosine Kinase proto-oncogene
KRAS: Kirsten Rat Sarcoma viral oncogene
LC-MS/MS: Liquid Chromatography followed by tandem Mass Spectrometry
LNC: Lipides Nutrition Cancer (UMR INSERM 1231)
M: Million or Molar (*e.g.* nM: nanomolar), depending on the context
Mat&Meth: Materials and Methods
Max: Maximum
MCF7 cells: immortalized human adenocarcinoma cells (established in the Michigan Cancer Foundation, now The Barbara Ann Karmanos Cancer Institute)
MCI lymphocytes: Mild Cognitive Impairment disease-associated lymphocytes
MDC1: Mediator of DNA damage Checkpoint protein 1
$MgCl_2$: magnesium chloride
Min: Minimum or minute, depending on the context
MNase: Micrococcal Nuclease
MNHN: Muséum National d'Histoire Naturelle
mol. equiv.: molar (mol/L) equivalent
MOPS: 3-(*N*-morpholino)propanesulfonic acid (buffer)
MRC5-SV40 cells: normal SV40-transformed human fibroblast (established in the Medical Research Council; strain n° 5)
MYC: Myelocytomatosis viral oncogene
N-TASQ: Naphtho-TASQ
NaCl: sodium chloride
NCBI: National Center for Biotechnology Information
NEAT1: Nuclear paraspeckle Assembly Transcript 1
nm: nanometer (length unit)
NMM: *N*-methylmesoporphyrin IX
NMR: Nuclear Magnetic Resonance
NRAS: Neuroblastoma Rat Sarcoma viral oncogene
nt: nucleotide (length unit)
NT: Non-Treated
Ntts: N-TASQ threshold
***Nucleus/nuclei*:** core/kernel, meaning large membrane-enclosed organelle found in eukaryotic cells which contains genetic material
nX: the final working concentration of the solution (*e.g.*, n= 1X, 10X)
***o*-BMVC:** 3,6-bis(1-methyl-2-vinylpyridinium) carbazole diiodide
ODN(s): OligoDesoxyriboNucleotide(s)
ON(s): OligoNucleotide(s)
***p* value:** the probability of obtaining test results at least as extreme as the result actually observed, under the assumption that the null hypothesis is correct
PAGE: PolyAcrylamide Gel Electrophoresis
PANC-1 cells: immortalized human epithelioid carcinoma cells
PARP1: Poly(ADP-Ribose) Polymerase 1
PBS: Phosphate Buffered Saline
PCR: Polymerase Chain Reaction
PDB: Protein Data Bank
PDC: Pyrido Dicarboxamide (a PDS derivative)
PDP: PDS Derivative Probe
PDS: Pyridostatin (or 4-(2-aminoethoxy)-N2,N6-bis(4-(2-aminoethoxy)quinolin-2-yl)pyridine-2,6-dicarboxamide hydrochloride)
PEG: Polyethylene Glycol
pH: Potential of hydrogen (scale for the acidity/basicity of an aqueous solution)
Phen-DC_3: 3,3'-[1,10-Phenanthroline-2,9-diylbis(carbonylimino)]bis[1-methylquinolinium] 1,1,1-trifluoromethanesulfonate (1:2)
PhpC: ethyl 2-(6-(3-(2-(tert-butyloxycarbonylamino)ethoxy)phenyl)pyrrolocytosin-1-yl)acetate
PhpC derivatives n° 1-3: 1. (6-phenylpyrrolopyrimidin-3-yl)acetic acid; 2. ethyl 6-(2,6-(di(oxyethylaminum)phenyl)pyrrolocytosin-3-yl)acetate bis(trifluoroacetate) salt; 3. ethyl 6-(3-(oxyethylaminum)imidazolocytosin-3-yl)acetate trifluoroacetate salt
PLA: Proximity Ligation Assay
PNA: Peptid Nucleic Acids
Poly(G/rG): oligonucleotide with a repetitive sequence of 2'-deoxyguanosine-5'-triphosphate (dGTP, for DNA) or guanosine-5'-triphosphate (GTP or rGTP, for RNA)
PorphySQ: Porphyrin-templated synthetic G-quartet
POT1: Protection of Telomeres 1
PQFS: Putative G-Quadruplex Forming Sequence
Pr: Professor
(q)PCR: (quantitative) Polymerase Chain Reaction
qSa: qPCR Stop assay (related to)
QUMA-1: 7-diethylaminocoumarin-3-aldehyde (or (E)-2-(2-(7-(diethylamino)-2-oxo-2H-chromen-3-yl)vinyl)-6-fluoro-1-methyl-7-(4-methylpiperazin-1-yl)quinolin-1-ium iodide)
R: Ratio
R^2: Pearson correlation coefficient (PCC)
Rab5: Ras-associated binding protein 5
RBS: Ribosome Binding Site
RCL: Reverse Crosslinking
rG: guanosine-5'-triphosphate
(r)G4-seq: (RNA-)G-Quadruplex-sequencing
RHPS4: 3,11-difluoro-6,8,13-trimethyl-8H-quino[4,3,2-kl]acridinium methosulfate

RNA: RiboNucleic Acid
RNAi: RNA interference
RNase: Ribonuclease
ROI: Region of Interest
ROS: Reactive oxygen species
rpm: Rotation per minute
RTS: Reverse Transcriptase Stalling
***S. pombe*:** *Schizosaccharomyces pombes*
S-DNA: three-way junctions
s-hTelo: the oligonucleotidic system possessing the hTelo G4 sequence (for G4-UNFOLD)
SA: Streptavidin
SARS-CoV: Severe Acute Respiratory Syndrome Coronavirus
SD: Standard deviation
SDS: Sodium dodecyl sulfate
SDS-PAGE: denaturing SDS-composed polyacrylamide gel electrophoresis
Seq: Sequencing
SHALiPE: Selective 2'-Hydroxyl Acylation by Lithium ion (Li^+)-based Primer Extension
SILAC: Stablie Isotope Labelling by Amino acid in Cell culture
SHAPE: Selectiv
SiR-PyPDS: Silicon Rhodamine-coupled Pyrrolidine-based PDS (a PDS derivative)
SMM: Small Molecule Microarrays
SOD1: Superoxide Dismutase 1
SPAAC: Strain-Promoted Alkyne Azide Cycloaddition
SPR: Surface Plasmon Resonance
SRB: Sulforhodamine B
ssDNA: Single-stranded DNA
SYBR: cyanine-based fluorescent nucleic acid (ssDNA, dsDNA, RNA) probe
SV40: Simian Virus 40
$T_{1/2}$: Melting temperature
***t*-test:** a type of statistical analysis for comparing the mean of two dataset
Table S: Supplementary Table
TAE: Tris-Acetate-EDTA buffer
TALEN: Transcription Activator-Like Effector Nuclease
TAMRA: 6-carboxytetramethylrhodamine
TAP1: Triarylpyridine derivative n° 1
***Taq*:** *Thermus aquaticus* enzyme
TArPS: 5,10,15,20-tetrakis[3-sulfonato-4-O-[2-[2-(2-methoxy)ethoxy]ethoxy]ethylphenyl]-21H,23H-porphyrin
TASQ: Template-Assembled Synthetic G-Quartets
tau: tubulin-associated unit
TBE: Tris-borate-EDTA (buffer)
TDP-43: TAR DNA-binding protein 43 (43 kDa)
TDS: Thermal Difference Signature
TEGP: tetra-[ethylene glycol]-porphyrin, also 5,10,15,20-tetrakis-[4-(2-(2-(2-methoxy)-ethoxy)-ethoxy)-ethyl]-21H,23H-porphyrin
TEGPy: tetra-[(ethylene glycol)-pyridyl]-porphyrin, also 5,10,15,20-tetrakis-[N-(2-(2-(2-methoxy)-ethoxy)-ethoxy)-ethyl-4-pyridyl]-21H,23H-porphyrin
TERRA: Telomeric repeat-containing RNA
ThT: Thioflavin T
Tm: Melting temperature
TMP: Thymidine Monophosphate
TMPyP4: 5,10,15,20-tetrakis-[N-methyl-4-pyridyl]-21H,23H-porphyrin
TOP2Acc: human Topoisomerase IIα cleavage complex (transient TOP2α-DNA complex)
TPPS: 5,10,15,20-tetrakis[4-sulfonatophenyl]-21H,23H-porphyrin
TRAP: Telomerase Repeat Amplification Protocol
TRF2: Telomeric Repeat Factor 2
TWJ: Three-Way Junction
U2OS cells: immortalized human osteosarcoma cells
UTR: Untranslated Region
UV: Ultra-Violet light
***via*:** road/manner, meaning by way of or using
***vide infra*:** see below
***vide supra*:** see above
V_0: initial velocity (in second)
WRN: Werner gene
X-ray: (or X-radiation) high-energy electromagnetic radiation with wavelength between 10 pm (picometers) to 10 nm (nanometers)
Z-DNA: DNA zigzag
z-dimension: height dimension of an object

INTRODUCTION – State of the art relative to this thesis

I. The desoxyribonucleic acid (DNA)

The discovery and the isolation of DNA ("nuclein") by Friedrich Miescher between 1869 and 1971[1,2] was soon followed by the elucidation of its actual chemical content by Albrecht Kossel in 1881 (*i.e.*, the four bases A, T, G and C) and then,[3,4] Phoebus Levene between 1905 and 1908 (*i.e.*, the sugar, phosphate and base units).[5–7] The elucidation of its tridimensional structure in 1953 by James Watson, Francis Crick,[8] Rosalind Franklin, R. G. Gosling[9] and Maurice Wilkins[10] has launched what could be referred to as the nucleic acids realm. Despite an early discovery of the existence of alternative nucleic acid structures, that is structures that deviate from the canonical duplex-DNA (or B-DNA), their study was overlooked for quite a long time because most of the efforts at that time were invested to understand the biological implications of the B-DNA structure, thus abiding by the rules of the 'central dogma of biology' heralded by Francis Crick in 1957 which places the duplex at the very heart of all biological processes.

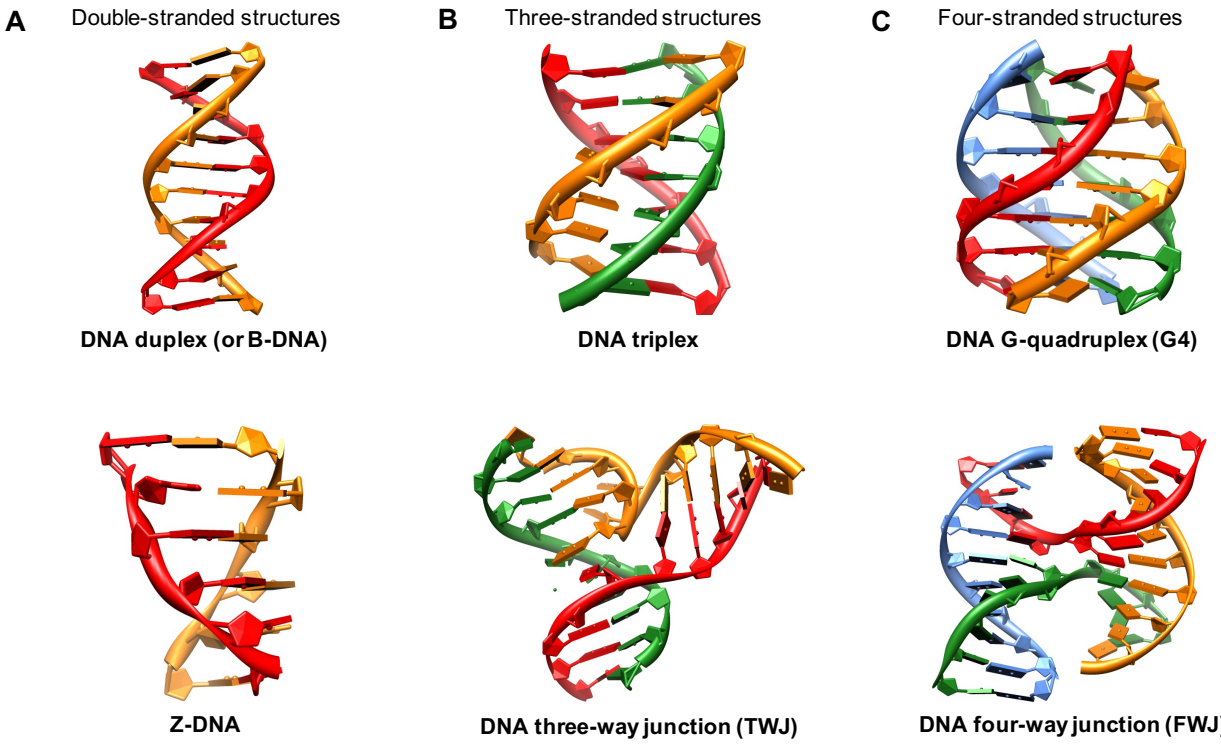

Figure 1. Structural representation of nucleic acid alternative structures. The DNA molecule can adopt different conformations, depending on the oligonucleotide sequences involved, including (**A**) DNA two-stranded structures (*e.g.*, B-DNA and Z-DNA), (**B**) DNA three-stranded structures (*e.g.*, DNA triplex and three-way junction) and (**C**) DNA four-stranded structures (*e.g.*, DNA G-quadruplex and four-way junction). Illustration from Stefan *et al.*[11]

There are numerous classes of nucleic acid alternative structures (**Figure** 1): *i.* DNA triplex (or H-DNA or hinged DNA; firstly identified in RNA in 1957),[12–14] *ii.* G-quadruplexes (or G4s, made of guanines; 1962 and 1988 for the G-quartet and G4 discoveries, respectively),[15–17] *iii.* four-way junctions (or Holliday junction or

cruciform DNA (C-DNA); modelized in 1964 but demonstrated *in vitro* in 1981),[18–20] *iv.* Z-DNA (duplex of inverted helicity, Z for zigzag; 1967),[21–23] *v.* R-loops (DNA:RNA hybrid; in 1976),[24,25] *vi.* three-way junctions (or slipped DNA or S-DNA; 1986),[26–28] *vii.* i-motifs (or C-quadruplexes, made from cytosines; 1993),[29,30] *viii.* t-loops (located on the telomeres; 1999),[31] and *ix.* G-loops (combining both G4 and R-loop structures at telomeres; 2004).[32] So far, G4s are the most studied alternative nucleic acids structures, whose cellular functions are consequently the best understood.

II. The nucleic acid G-quadruplex structure

1. The G-quadruplex discovery

Research on guanines (G) specific properties started more than 100 years ago.[33] In 1910, Ivar Bang showed a gelation effect of guanosine monophosphate (GMP) on urine and blood.[33] These analyses were associated with anticoagulant effect and toxic impacts on respiration and arterial blood pressure. These first observations paved the way for the idea that Gs can self-assemble to form high-order structures. Only 3 years after the discovery of the DNA double-helix structure in 1953,[8–10] Jerry Donohue surmised about the existence of others nucleic acids structure, even possibly a single chain oligonucleotide folded by intramolecular hydrogen bonds, highlighting the possibility for two guanines to interact with each other.[34] In 1958, Rich worked with X-ray on the inosine monophosphate (IMP), the precursor of adenosine monophosphate (AMP) and GMP, and proposed a triple-stranded right-handed helix for that nucleobase, which was disproved in 1974 and shown to be a four-stranded helix,[35] thereby nurturing interest about higher-order nucleic acid structures.[36] Then, Ralph *et al.* conduced UV-melting experiments at 260 nm, the specific nucleic acids absorption wavelength, which showed that a trinucleotide d(GGG) but also a tetranucleotide d(GGGG) can fold into a stable, thermal-dependent structure in presence of ions.[37] Finally, the firm demonstration of the self-assembling properties of rGs was provided in 1962 thanks to X-ray diffraction experiments, which allowed Gellert *et al*. for providing the fine structure of the basic unit of a fiber of Gs,[15] in which 4 Gs interact with each other *via* 8 hydrogen bonds to form a stable and planar tetramers with an ion-containing hole in the middle, referred to as G-quartets. When the Gs are embedded in a single sequence, in a continuous fashion, G-quartets can self-stack on top of each other to form the core of the G4s (**Figure 2**).

RNA molecule was first extracted from fish eggs in 1906,[6] and the first evidence of RNA four-stranded structure dates back to the work of forementioned Gellert *et al.* in 1962, then validated in 1975 by the Zimmerman *et al.* study about the fiber structure of poly(rG) in K^+ saturated solution.[38] While the G4-DNA research was intense after these discoveries, the interest about RNA remains modest for a while, which explains why the ability of the biological G-rich RNA sequence r[$^{5'}GC_2GAUG_2UA(GU)_2G_4U^{3'}$] (from the *E. coli* 5S RNA) to fold into G4 structure was studied in 1991 only.[39]

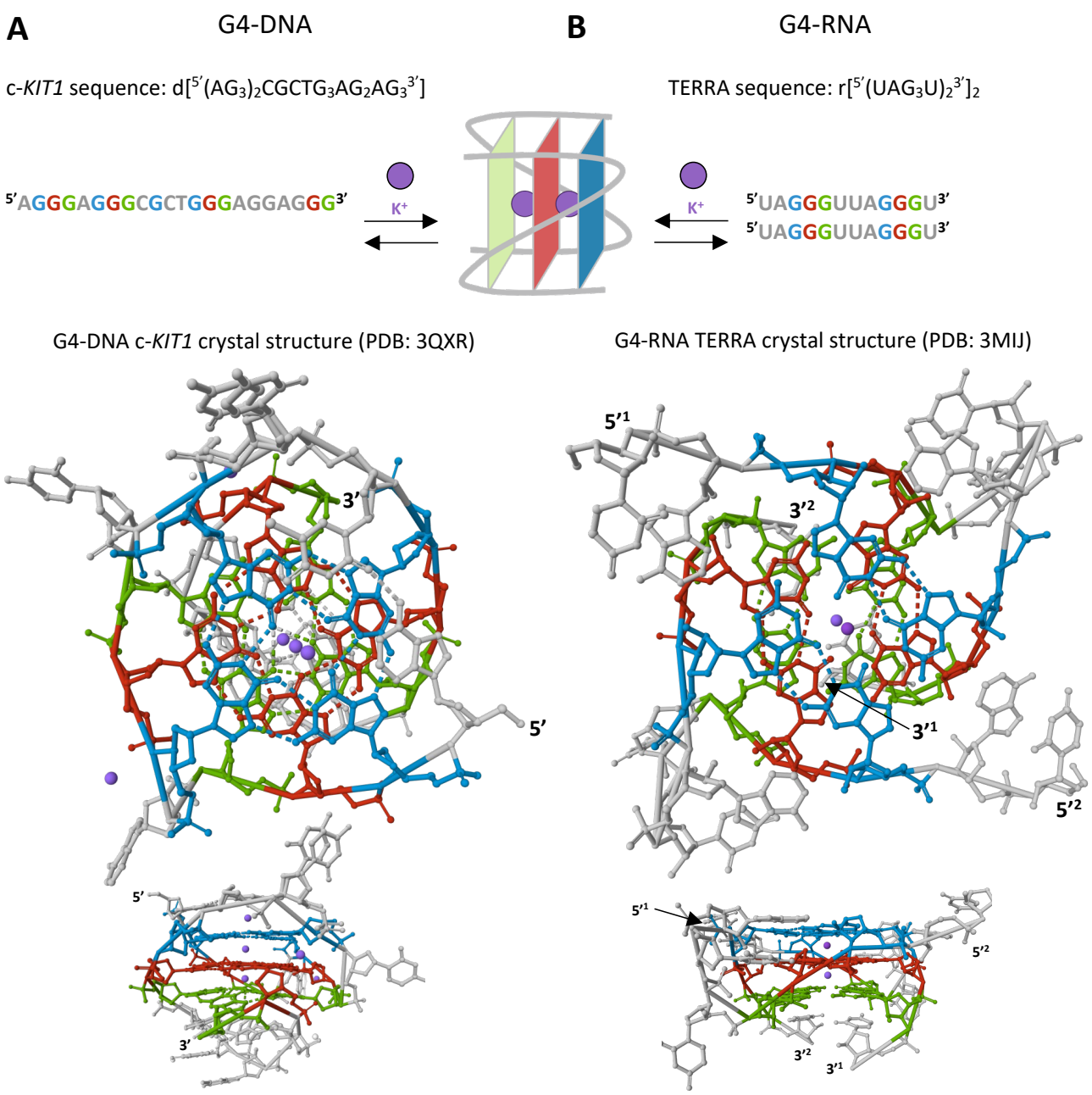

Figure 2. Schematic representation of G-quadruplex DNA and RNA structures. The proximity of G-rich sequences in a cation (K^+ > Na^+)-containing solution will induce their interaction into several G-quartet planar structures and then G-quadruplex structure. Here are shown the crystal structure of (**A**) the three-layered intramolecular parallel-type promoter region G-quadruplex c-*KIT1* obtained in 2012 (PDB: 3QXR)[40] and (**B**) of the three-layered bimolecular anti-parallel-type telomeric G-quadruplex TERRA obtained in 2011 (PDB: 3MIJ).[41]

2. Topologies of G-quadruplexes

After such a discovery, a more accurate description of G4s was obtained, notably by X-ray diffractions and NMR experiments, on both its helical nature and that of hydrogen bonds involved (Hoogsteen's hydrogen bonds).[42,43] Several studies then documented the variety of G4 topologies and provided insights into the experimental conditions needed for a G-rich sequence to fold into a G4 structure, notably through non-denaturing polyacrylamide gel electrophoresis (PAGE) and the two techniques cited above.[44,45]

Depending on the sequence involved (G-runs), the number of strands involved and their length, as well as the nature of ions found in the central channel, G4s can adopt a large number of topologies which have been globally classified as parallel, antiparallel and hybrid topologies. In more detail, this classification focused on the glycosidic bond angles (GBA) between the ribose and the nucleobase (*syn* or *anti*), the groove width[46] and the strands direction (**Figure 3**).[47,45] On the basis of a 5' -> 3' strand directionality, G4 can be parallel-type or I-type (*i.e.*, the four strands have the same 5' -> 3' direction, **Figure 3-A**), an anti-parallel-type or III-type (*i.e.* two groups of two strands respecting an opposite 5' -> 3' direction, **Figure 3-C**) and hybrid-type or mixed parallel and anti-parallel-type or II-type (*i.e.* one group of one strand and a second group of three have opposite 5' -> 3' direction, **Figure 3-B**). Finally, the molecularity of G4, *i.e.* whether the G4 is intramolecular (or unimolecular), bimolecular or tetramolecular,[44] provided a large panel of possible G4 structures, as intramolecular G4s can be parallel-type[48] but also anti-parallel-type,[49] bimolecular G4s can be anti-parallel-type[50,51] or hybrid G4s,[52] and tetramolecular parallel-type G4s.[16,53]

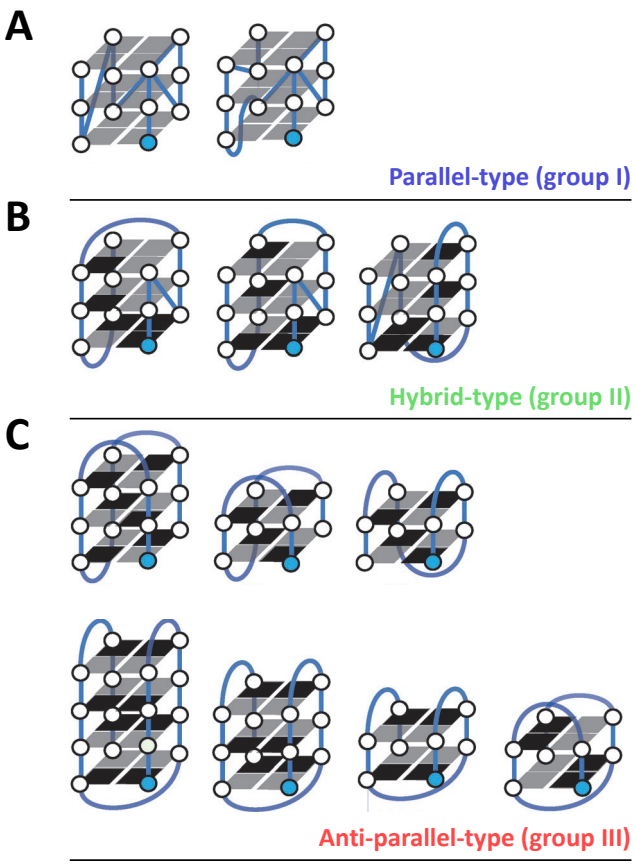

Figure 3. G-quadruplex topologies classification. Examples of the three G4 topologies based on 5' -> 3' strands direction: (**A**) parallel-, (**B**) anti-parallel- and (**C**) hybrid-type. Illustration from Karsisiotis *et al.*[47]

3. The characterization of G-quadruplexes

With all these possible topologies, fast and reliable characterization techniques were needed. To rapidly discriminate between different G4s the first technique implemented was the circular dichroism (CD): in 1974, Gray and Bollum found a different CD signature between a "single-stranded" (non-folded) and a "self-

complexed" (folded full-parallel G-quadruplex) d(G_5) oligonucleotide.[54] Through several studies on G4 structures, distinctive CD peaks were assigned for each G4 topology (**Figure 4**): *i.* a strong positive band at 260 nm and a negative band at 240 nm for parallel-type G4s, *ii.* positive bands at 240 and 290 nm and one negative at 260 nm for anti-parallel-type G4s, *iii.* positive bands at 260 and 290 nm and one negative at 240 nm for hybrid-type G4s.[45,47] Other techniques were developed such as the UV thermal difference spectrum (TDS), which allows for differentiating nucleic acids structures (*e.g.* DNA or RNA duplex, triplex, G-quadruplex, i-Motif) reliably and efficiently.[55] These methods have facilitated the study of parameters that drive conformation induction: for example, the human telomeric G-rich repeat sequence hTelo (or "HT" or "22AG") [$AG_3(T_2AG_3)_3$] folds into an anti-parallel-type G4 in Na^+ condition but a parallel and hybrid-type in K^+ condition;[56,48] its conformation depends on the nucleic acids type (DNA or RNA) as the G4-DNA [$(G_3T_2A)_3G_3$], folds into an anti-parallel-type (Na^+) or a hybrid-type G4 (K^+)[57] while its RNA counterpart [$(G_3U_2A)_3G_3$] always displays a parallel-type G4 signature, along with a more intense CD signal at its maximum (around 40.10^4 *versus* 17.10^4 deg cm^2/dmol for G4-RNA and -DNA, respectively),[57] which is associated with a higher stability.[57] This difference in stability was also shown by CD melting experiments, with a melting temperature (Tm) of 65 and 73°C for G4-DNA and G4-RNA respectively, in K^+ conditions, and 47 and 42°C in Na^+ conditions. In general, G4-DNAs can easily adopt different conformations depending on the sequence they fold from and the ionic conditions they are studied in, while G4-RNAs usually adopt a parallel topology, but not exclusively.[58]

A

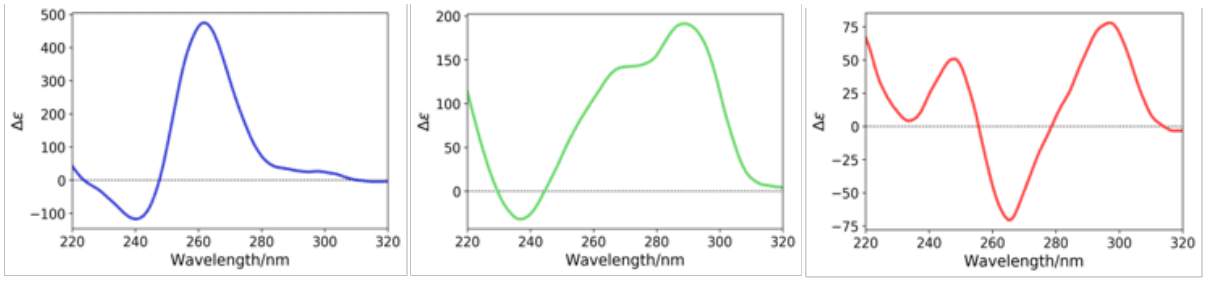

B

Wavelength (nm)	CD signature
240	-
260	+
290	∅

Wavelength (nm)	CD signature
240	-
260	+
290	+

Wavelength (nm)	CD signature
240	+
260	-
290	+

Figure 4. Circular dichroism spectra of the three G-quadruplex topologies. The three G4 topologies listed above possess (**A**) distinctive CD peaks signature at (**B**) different wavelength: negative peak at 240 (groups I-II) or 260 nm (group III) and positive peak at 240 (group III), 260 (groups I-II) or 290 nm (groups II-III). + = positive band. - = negative band. ∅ = no band. Adapted from an illustration in the article "Structure Evaluation of G-quadruplex aptamers Using High-Throughput CD Measurement System and Principal Component Analysis" on Jasco website.

4. The study of G-quadruplexes

a. *in vitro* and *in cella* methods

In silico methods for studying G4s were developed, allowing for the computational identification of Putative G-Quadruplex Forming Sequence (PQFS) by Quadparser (Huppert and Balasubramanian), the Neidle team's algorithm and more recently by G4Hunter (Bedrat, Lacroix and Mergny).[59–61] These investigations led to the presence of a substantive number of PQFS in our genome and transcriptome; however, these results must be confirmed by experimental methods and particularly *in vitro* techniques.[62]

Since the first evidence of the existence of G-rich high order structures *via* UV absorption and/or X-ray diffraction on DNA and RNA in 1962 (**Table 1**),[37,15] and the similar study on poly(dR) in 1975,[38] structural studies were conducted on G4s. Poly dG ONs signatures were firstly studied by Gray and Bollum in 1974 by CD analysis as previously discussed,[54] but the real impetus was provided in the 1990's by: 1/ PAGE experiments in 1988 for G4-DNA (with the d[$^{5'}G_5AGCTG_4{}^{3'}$] motif)[16] and 1991 for G4-RNA (with the *E. coli* r[$^{5'}GC_2GAUG_2UAGUGUG_4U^{3'}$]),[39] notably with G footprinting experiments;[49] 2/ NMR and calorimetry were used with the G-rich d[$^{5'}G_2T_2AT_2G_2{}^{3'}$] sequence to reveal its « tetraplex structure » in 1990,[63] and models of the G4 that folds from the d[$^{5'}TG_4T^{3'}$] sequence were proposed one year later with additional NMR spectroscopy;[64,56,65] the G4-RNA structure of the d[$^{5'}UG_4U^{3'}$] was also solved, providing the the first evidence of RNA quartet existence;[53] 3/ the X-ray crystallography allowed for the elucidation of the crystal structure of the *Oxytricha* telomeric sequence d[$^{5'}G_4T_4G_4{}^{3'}$] [66] and a few years later (1994) of d[$^{5'}TG_4T^{3'}$][67] and then of the first G4/drug complex in 2003;[68] 4/ another interesting analytical technique, the electrospray ionization mass spectrometry (ESI-MS), was adapted for the study of the d[$^{5'}(CGCG_4GCG)_4{}^{3'}$] G4.[69]

Progressively, most of these biophysical techniques were adapted for the study of the interaction between G4 and chemical compounds, in parallel of efforts invested to develop more accurate biophysical and biochemical methods to discover, characterize, predict or confirm new G4 structures (**Table 1**). Among them were the isothermal titration calorimetry (ITC; in 1999),[70] dynamic light scattering (DLS; 1999),[71] thermal difference spectra (TDS; 2005),[55] magnetic tweezer coupled to dynamic force spectroscopy (DFS; 2012),[55,72] surface plasmon resonance (SPR; 2007),[73,74] affinity chromatography and UV absorbance pull-down in 2010,[75,76] for instance.

Enzyme-based assays were also used given that G4s are able to interfere with the normal processivity of enzymes on ssDNA (**Table 1**). This was first used with the telomerase enzyme (1991) for the study of its interaction with the *Oxytricha* telomeric G4,[77] followed by the first use of polymerases with the DNA Polymerase Arrest assay in 1996.[78] Both enzymes were then rapidly repositioned for the identification of G4-interacting compounds with the telomerase stalling assay (1997) and the PCR-based (TRAP) assay with *Taq* polymerase (1998).[79,80] Ten year later, enzyme-based assays were extended to RNA study with the RTase stop assay (2010),[81] and more recently the use of the hPIF1 can be cited for an interesting G4 helicase assay (2015).[82] Also, qPCR can be used for detection and quantification after a G4-specific pull-down step (qPCR pull-down, 2010).[76]

A lot of assays are based on fluorescence measurements (**Table 1**) such as the previously cited G4 helicase assay along with qPCR Stop assays[83] and also now routinely used techniques such as FRET-melting assay (2001),[84] fluorescence polarization (2006),[85] gene reporter assay (2007),[86] G4 fluorescent intercalator displacement (G4-FID; 2008),[87] magnetic tweezer couplet to FRET (2013),[88] small molecule microarrays (SMMs; 2015),[89] fluorescence quenching assay (FQA; 2015),[90] fluorescence pull-down (2019),[91] BG-flow (2021),[92] G4-UNFOLD assay (2021),[93] FRET-MC (2021, also used as HTS *in vitro* assays)[94,95] and Iso-FRET (2022).[96]

Biochemical techniques were optimized for studying RNA G4s in 2002: Northern blot, RT-PCR, but also high throughput screening assay as cDNA microarray.[97] A renewed interest in RNA G4s study came a bit later (in the 2010's; **Table 1**) with the development of G4-RNA-specific quantitative approaches including the Selective 2'-Hydroxil Acylation analyzed by lithium ion (Li^+)-based Primer Extension SHALiPE (2016), inspired by the Selective 2'-Hydroxil Acylation analyzed by Primer Extension (SHALE; 2006),[98] a chemical footprinting method relying on the 2'-OH acylation of unconstrained nucleotides. The FOLDeR method (2017) was also developed and compares the behavior difference between a G4-RNA and a 7-deazaguanine-substitued RNA, *i.e.* the same RNA sequence with chemical modifications only preventing the G4 but no other secondaries structures folding. These two assays combined old and new methods to study G4s such as the reverse transcriptase stalling (RTS), primer extension (PCR) and denaturing PAGE for the SHALiPE,[99] and the enzyme digestion (ribonuclease H) and PAGE again for the FOLDeR.[100]

In order to genetically modify (in a transitory or stable manner) cells, molecular biology and genetics techniques were applied: transfection of a G4-folding sequence (2004) which acts as an aptamer in sequestering a nuclear protein factor,[101] RNA interference (2008) to study the FANCJ G4 helicase involvement in Fanconi anemia,[102] antisense oligonucleotide (ASO) strategy (2008) for silencing c-*MYC* expression,[103] CRISPR/Cas9 (2017) for SLIRP protein tagging and mapping of its binding genomic sites,[104] CRISPR/Cas9 (2017) for genomic G4 mutation into Bcl-2 gene,[105] and transcription activator-like effector nuclease (TALEN; 2021) in using a fusion protein RHAU helicase–Fok1 nuclease.[106]

Year	Technique name	Experimen-tation target	Experimen-tation type	Application	Reference
1962	UV absorption	DNA	*in vitro*	Structural G-quartet study	Khorana *et al.*, *J. Am. Chem. Soc.* **1962**, *84* (11), 2265-2266[37]
1962	UV absorption	RNA	*in vitro*	Structural G-quartet study	Gellert *et al.*, *Proc. Natl. Acad. Sci.* **1962**, *48* (12), 2013-2018[15]
1962	X-ray diffraction	RNA	*in vitro*	Structural G-quartet study	Gellert *et al.*, *Proc. Natl. Acad. Sci.* **1962**, *48* (12), 2013-2018[15]
1974	Circular dichroism	DNA	*in vitro*	Structural G4 – G4/compound interactions studies	Gray and Bollum, *Biopolymers* **1974**, *13* (10), 2087-2102[54]

1988	PAGE	DNA	*in vitro*	Structural G4 – G4/compound interactions studies	Sen and Gilbert, *Nature* **1988**, *334*, 364-366[16]
1990	Differential scanning calorimetry (DSC)	DNA	*in vitro*	Structural G4 study	Jin *et al.*, *Science* **1990**, *250* (4980), 543-548[63]
1990	NMR spectroscopy	DNA	*in vitro*	Structural G4 study	Jin *et al.*, *Science* **1990**, *250* (4980), 543-548[63]
1991	Telomerase assay	DNA	*in vitro*	Structural G4 – Functional G4 studies	Zahler *et al.*, *Nature* **1991**, *350* (6320), 718-720[77]
1991	PAGE	RNA	*in vitro*	Structural G4 – G4/compound interactions studies	Kim *et al.*, *Nature* **1991**, *351* (6324), 331-332[39]
1992	X-ray crystallography	DNA	*in vitro*	Structural G4 study	Kang *et al.*, *Nature* **1992**, *356*, 126-131[66]
1992	NMR spectroscopy	RNA	*in vitro*	Structural G4 study	Cheong and More, *Biochemistry* **1992**, *31* (36), 8406-8414[53]
1993	ESI-MS	DNA	*in vitro*	Structural G4 study	Goodlett *et al.*, *Biol. Mass Spectrom.* **1993**, *22* (3), 181-184[69]
1996	DNA Polymerase Arrest assay	DNA	*in vitro*	Structural G4 – Functional G4 studies	Weitzmann *et al.*, *J. Biol. Chem.* **1996**, *271* (34), 20958-20964[78]
1997	TRAP assay (with telomerase)	DNA	*in vitro*	G4/compound interactions study	Sun *et al.*, *J. Med. Chem.* **1997**, *40* (14), 2113-2116[79]
1998	PCR-based TRAP assay (with *Taq* polymerase)	DNA	*in vitro*	G4/compound interactions study	Perry *et al.*, *J. Med. Chem.* **1998**, *41* (17), 3253-3260[80]
1999	Southwestern blot	DNA, G4-binding proteins	*in vitro*	Qualitative G4/protein interactions study	Sarig *et al.*, *J. Biol. Chem.* **1999**, *272* (7), 4474-4482[107]
1999	ITC	DNA	*in vitro*	G4/compound interactions study	Haq *et al.*, *J. Am. Chem. Soc.* **1999**, *121* (9), 1768-1779[70]
1999	DLS	DNA	*in vitro*	Structural G4 study	Bolten *et al.*, *Biochemistry* **1999**, *38* (38), 12416-12423[71]
2001	Phage display	DNA	*in vitro*	Production of G4-binding antibody/protein	Isalan *et al.*, *Biochemistry* **2001**, *40* (3), 830-836[108]
2001	(Phage) ELISA	G4-binding proteins	*in vitro*	Selection of (phage) G4-binding antibody/protein	Isalan *et al.*, *Biochemistry* **2001**, *40* (3), 830-836[108]
2001	FRET-melting	DNA, RNA	*in vitro*	Structural G4 – G4/compound interactions studies	Mergny and Maurizot, *ChemBioChem* **2001**, *2 (*2), 124-132[84]

2001	Immunofluorescence	DNA, RNA	*in vivo* (*Stylonychia lemnae*)	Qualitative or quantitative G4 – Colocalization – G4/compound interactions studies	Schaffitzel *et al*., *Proc. Natl. Acad. Sci. U.S.A.* **2001**, *98* (15), 8572-8577[109]
2002	cDNA microarray	RNA (cDNA)	*in cella*	Qualitative G4 – Functional G4 – G4/compound interactions studies	Grand *et al.*, *Mol. Cancer Ther.* **2002**, *1* (8), 565-573[97]
2002	Northern blot	RNA	*in cella*	Qualitative G4 – Functional G4 – G4/compound interactions studies	Grand *et al.*, *Mol. Cancer Ther.* **2002**, *1* (8), 565-573[97]
2002	RT-PCR	RNA	*in cella*	Qualitative G4 – Functional G4 – G4/compound interactions studies	Grand *et al.*, *Mol. Cancer Ther.* **2002**, *1* (8), 565-573[97]
2002	Western blot	Protein (from a G4-containing gene)	*in cella*	Qualitative protein – Functional G4 – G4/compound interactions studies	Grand *et al.*, *Mol. Cancer Ther.* **2002**, *1* (8), 565-573[97]
2004	Transfection (of a G4-folding sequence)	DNA	*in cella*	G4/DNA/protein interactions studies	Cogoi *et al.*, *Biochemistry* **2004**, *43* (9), 2512-2523[101]
2005	TDS	DNA, RNA	*in vitro*	Structural G4 study	Mergny *et al*., *Nucleic Acids Res.* **2005**, *33* (16), e138[55]
2006	Fluorescence polarization (FP) (or anisotropy; FAn)	DNA, RNA, G4-binding proteins	*in vitro*	Structural G4 – G4/compound/ protein interactions studies	Juskowiak *et al.*, *Spectrochim. Acta. A Mol. Biomol. Spectrosc.* **2006**, *64* (4), 835-843[85]
2006	SHALE	RNA	*in vitro*	Quantitative G4 study	Wilkinson *et al*., *Nat. Protoc.* **2006**, *1* (3), 1610-1616[98]
2007	SPR	DNA	*in vitro*	G4/compound interactions study	White *et al*., *Biophy. Chem.* **2007**, *126* (1-3), 140-153[73]
2007	Gene reporter	DNA	*in cella*	Functional G4 – G4/compound interactions studies	Kumari *et al*., *Nat. Chem. Biol.* **2007**, *3* (4), 218-221[86]
2008	RNA interference	RNA	*in cella*	Functional G4-DNA helicase study	Wu *et al*., *Mol. Cell. Biol.* **2008**, *28* (12), 4116-4128[102]
2008	G4-FID	DNA	*in vitro*	G4/compound interactions study	Monchaud *et al*., *Biochimie* **2008**, *90* (18), 1207-1230[87]
2008	Antisense oligonucleotide (ASO) strategy	DNA	*in vivo* (zebrafish embryos)	Functional G4 study	Kumar *et al.*, *Biochem.* **2008**, *47* (50), 13179-13188[103]

2010	RTase stop assay	RNA	*in vitro*	Functional G4 – G4/compound interactions studies	Hagihara *et al., Bioorg. Med. Chem. Lett.* **2010**, *20* (7), 2350-2253[81]
2010	Affinity chromatography	DNA	*in vitro*	G4 extraction – G4/compound interactions studies	Smith and Johnson, *Methods Mol. Biol.* **2010**, *608*, 207-228[75]
2010	Chromatin immuno-precipitation (ChIP)	G4-binding proteins	*in cella*	Quantitative G4 extraction	Law *et al., Cell* **2010**, *143* (3), 367-378[110]
2010	UV absorbance pull-down	DNA, RNA	*in vitro*	Qualitative G4 extraction – G4-binding compound evaluations	Müller *et al.*, *Nat. Chem.* **2010**, *2* (12), 1095-1098[76]
2010	qPCR pull-down	DNA	*in cella*	Quantitative G4 extraction – G4-binding compound evaluations	Müller *et al.*, *Nat. Chem.* **2010**, *2* (12), 1095-1098[76]
2012	Chemofluorescence	DNA, RNA	*in cella*	Qualitative or quantitative G4 – Colocalization – G4/compound interactions studies	Rodriguez *et al*., *Nat. Chem. Biol.* **2012**, *8* (3), 301-310[111]
2012	Magnetic tweezer (coupled to DFS)	DNA	*in vitro*	Structural G4 – G4/compound interactions studies	De Messieres *et al., Phys. Rev. Lett.* **2012**, *109* (5), 058101[72]
2013	Magnetic tweezer (coupled to FRET)	DNA	*in vitro*	Structural G4 – G4/compound interactions studies	Long *et al., Nucleic Acids. Res.* **2013**, *41 (*4), 2746-2755[88]
2015	Fluorescence quenching assay (FQA)	DNA, RNA	*in vitro*	Quantitative G4/compound interactions study	Le *et al*., *J. Chem. Commun.* **2015**, *51* (38), 8048-8050[90]
2015	hPIF1 helicase assay	DNA	*in vitro*	G4/compound interactions study	Mendoza *et al., Nucleic Acids Res.* **2015**, *43* (11), e71[82]
2015	Small molecule microarrays (SMMs)	DNA	*in vitro*	G4/compound interactions study	Felsenstein *et al., ACS Chem. Biol.* **2015**, *11* (1), 139-148[89]
2016	SHALiPE and DMSLiPE	RNA	*in vitro*	Quantitative G4 study	Kwok et al., *Angew. Chem. Int. Ed.* **2016**, *55* (31), 8958-8961[99]
2017	FOLDeR	RNA	*in vitro*	Quantitative G4 study	Weldon et al., *Nat. Chem. Biol.* **2017**, *13* (1), 18-20[100]
2017	Proximity ligation assay (PLA)	RNA, G4-binding proteins	*in cella*	Semi-quantitative G4/protein interactions study	Lista *et al.*, *Nat. Commun.* **2017**, 8, 16043[112]
2017	CRISPR/Cas9 (for protein tagging)	G4-binding proteins	*in cella*	Quantitative G4/protein study	Williams *et al.*, *J. Am. Chem. Soc.* **2017**, *139* (36), 12426-12429[104]

2017	CRISPR/Cas9 (for G4 mutation)	DNA	*in cella*	Functional G4 study	Serikawa *et al*., *FEBS Lett.* **2017**, *591* (21), 3649-3659[105]
2019	Fluorescence pull-down	DNA, RNA	*in vitro*	Qualitative G4 extraction – G4-binding compound evaluations	Renard *et al*., *Nucleic Acids Res.* **2019**, *47* (11), 5502-5510[91]
2021	BG-flow	DNA, RNA	*in cella*	Quantitative G4 study	De Magis *et al., BMC Biol.* **2021**, *19* (1), 45[92]
2021	FRET-MC	DNA	*in vitro*	Structural G4 – G4/compound interactions studies	Luo *et al., Biopolymers* **2021**, *112* (4), e23415[94]
2021	Transcription activator-like effector nuclease (TALEN)	DNA	*in vitro*	Functional G4 study	Dang *et al.*, *Chem. Commun.* **2021**, *57* (37), 4568-4571[106]
2021	G4-UNFOLD assay	DNA	*in vitro*	G4/compound interactions study	Mitteaux *et al., J. Am. Chem. Soc.* **2021**, *143* (32), 12567-12577[93]
2021	G4-GIS	DNA, RNA	*in cella*	Semi-quantitative G4 study	Masson *et al., Nucleic Acids Res.* **2021**, *49* (22), 12644-12660[113]
2022	Iso-FRET	DNA, RNA	*in vitro*	Structural G4 – G4/compound interactions study	Luo *et al., Nucleic Acids Res.* **2022**, *50* (16), e93[96]

Table 1. Non exhaustive summary list of *in vitro* and *in cella* methods developed for G4s study. Several techniques were specifically developed for the study of G4-DNAs (telomerase assay, DNA polymerase assay, TRAP and PCR-based TRAP assays, gene reporter assay, G4-FID, hPIF1 helicase assay, SMMs, FRET-MC, G4-UNFOLD assay), G4-RNAs (cDNA microarray, Northern blot, RT-PCR, RTase stop assay SHALiPE, DMSLiPE, FOLDeR) but also both structures (UV absorption, X-ray diffraction, CD, PAGE, DSC, NMR, crystallography, ESI-MS, ITC, DLS, FRET-melting, immunofluorescence, transfection, fluorescence polarization, RNA interference, ASO strategy, TDS, SPR, affinity chromatography, ChIP, UV absorbance pull-down, qPCR pull-down, chemofluorescence, magnetic tweezer, FQA, CRISPR/Cas9, fluorescence pull-down, BG-flow, TALEN, G4-GIS, Iso-FRET) and G4-binding proteins (Southwestern blot, phage display, ELISA, Western blot, ChIP, PLA, CRISPR/Cas9).

Another, qualitative approach for the characterization of G4 is their visualization *in cella*, by either cytochemistry or immunocytochemistry protocols (**Table 1**). These methods rely on the use of antibodies or G4 probes: the first observation of G4s was reported in 2001 by the immunodetection of G4s in eukaryotic cells (*Stylonychia lemnae*) using the anti-G4 antibody Sty49;[109] more than 10 years later was reported the first visualization of G4s in human cells by chemofluorescence thanks to the fluorophore-labelled PDS G4 ligand (2012).[111] These results were then confirmed by the immunodetection using the G4-specific antibody BG4 on G4-DNA in 2013 and G4-RNA in 2014,[114,115] and more recently by a technique that combines the two approaches referred to as G4 ligand-guided immunofluorescence staining, or G4-GIS (2021).[113] Interaction between genomic G4 and proteins can also be studied *via* indirect (colocalization with GFP-hPif1)[111] or direct (proximity ligation assay (PLA) with NCL; 2017)[112] imaging techniques.

The G4/proteins interactions were also studied by some molecular biology and biochemical routine techniques as Southwestern blot (1999),[107] Western blot (2002)[97] and chromatin immunoprecipitation (ChIP; 2010).[110]

G4-interacting proteins, usually obtained by phage display and ELISA test,[108] as well as chemical G4 probes were thus abundantly used for the direct or indirect visualization of G4 in cells, and their description will be developed further.

c. Genome-, transcriptome- and G4/protein interactome-wide methods

The G4 research field was recently reinvigorated by a series of genome wide, sequencing-based techniques (**Table 2**).[116,117] The G4-seq (2015) used extracted and purified DNA and relied on a DNA sequencing step performed in conditions favoring G4 folding (K^+ or with the G4-stabilizer PDS) or not (Li^+) to compare the polymerase stalling sites in both conditions, which are then ascribed to G4 sites *bona fide*.[118] This method was then adapted for the study of G4-RNA with the development of rG4-Seq (2015).[119] An alternative, so called '*in vivo*' technique was developed for the study of G4-DNA, G4-ChIP-Seq (2018),[116] which relies on the use of the BG4 antibody to fish G4s out from cell lysates, followed by an Chromatin ImmunoPrecipitation (ChIP), a PCR amplification and then a final high-throughput sequencing to identify isolated sequences folded into G4s in physiological condition. We developed another '*in vivo*' approach for the study of G4-RNA, G4RP-Seq,[120,121] which relies on the purification of G4s using a small molecule (the Template-Assembled Synthetic G-Quartet, or TASQ) prior to their identification of G4s by sequencing (or by RT-qPCR for the G4RP-RTqPCR version). This technique, which was developed in collaboration with the group of Judy Wong (UBC Vancouver, CA), will be detailed in Chapter III.

Recently, the G4RP-Seq was adapted to DNA (2023) with the development of the G4DP-Seq technique,[122] but also to viral G4-RNA.[123] Other techniques were also developed: the G4 CUT&Tag methods (2021-2022) and G4access (2023).[124–126,95] The Cleavage Under Targets and Tagmentation (CUT&Tag; 2019) method allows the tethering of ON tag (adapter) sequences at specific chromatin sites by a combination of G4-specific antibodies and a Tn5 transposase (*i.e.*, an enzyme which is able to cut DNA and insert transposon into it), followed by PCR amplification of the Tn5-tagged sequences and DNA sequencing.[127] The G4 CUT&Tag and SG4 CUT&Tag were developed using either the BG4 antibody or SG4 nanobody;[126,125] another version of this approach was published as a single-cell method, the snG4 CUT&Tag, using genomics microfluidic platform for the cells partitioning and barcoding.[124] The G4access (2023) does not use antibody but the micrococcal nuclease (MNase) acting on ssDNA (open chromatin, where G4s fold), followed by the DNA library preparation and sequencing.

Year	Technique name	Experimentation target	Experimentation type	Application	Reference
2015	G4-Seq	DNA	*in cella*	Qualitative G4 genome study	Chambers *et al., Nat. Biotechnol.* **2015**, *33* (8), 877-881[118]
2015	rG4-Seq	RNA	*in cella*	Qualitative G4 transcriptome study	Kwow & Balasubramanian, *Angew. Chem. Int. Ed.* **2015**, *54* (23), 6751-6754[119]
2016	SHALiPE and DMSLiPE + Seq	RNA	*in cella*	Quantitative G4 transcriptome study	Guo & Bartel, *Science*, **2016**, *353* (6306), 5371-5371[128]
2016	G4-ChIP-Seq	DNA	*in cella*	Quantitative G4 genome study	Hänsel-Hertsch *et al., Nat. Genet.* **2016**, *48* (10), 1267-1272[116]
2017	SILAC	G4-binding proteins	*in vitro/in cella*	Quantitative G4/protein interactome study	Williams *et al.*, *J. Am. Chem. Soc.* **2017**, *139* (36), 12426-12429[104]
2018	G4RP-Seq	RNA	*in cella*	Quantitative G4 transcriptome study	Yang *et al*., *Nat. Commun.* **2018**, *9* (1), 4730-4740[120]
2021	G4-LIMCAP	G4-binding proteins	*in cella*	Qualitative G4/protein interactome study	Su *et al., J. Am. Chem. Soc.* **2021,** *143* (4), 1917-1923[129]
2021	CMPP	G4-binding proteins	*in cella*	Qualitative G4/protein interactome study	Zhang et al., *Nat. Chem.* **2021**, *13* (7), 626-633[130]
2021	snG4-CUT&Tag	DNA	*in cella*	Quantitative G4 genome study	Hui et al., *Sci. Rep.* **2021**, *11* (1), 23641[124]
2022	G4 CUT&Tag	DNA	*in cella*	Quantitative G4 genome study	Lyu et al., *Nucleic Acids Res.* **2022**, *50* (3), e13[125]
2022	SG4 CUT&Tag	DNA	*in cella*	Quantitative G4 genome study	Galli et al., *J. Am. Chem. Soc.* **2022**, *144* (50), 23096-23103[126]
2023	G4DP-Seq	DNA	*in cella*	Quantitative G4 genome study	Feng et al., *iScience* **2023**, *26* (6), 106846[131]
2023	G4access	DNA	*in cella*	Quantitative G4 genome study	Esnault et al., *Nat. Genet.* **2023**, *55*, 1359-1369[95]

Table 2. Non exhaustive summary list of genome-, transcriptome- and G4/protein interactome-wide methods developed for G4s study. Several techniques were specifically developed for the study of the G4 genome (G4-Seq, G4-ChIP-Seq, snG4-CUT&Tag, G4 CUT&Tag, SG4 CUT&Tag, G4DP, G4access), the G4 transcriptome (rG4-seq, SHALiPE and DMSLiPE (± sequencing), G4RP-Seq) and the G4-binding proteins interactome (SILAC, G4-LIMCAP, CMPP). Seq = sequencing.

All these techniques, used for the identification of either G4-DNA and G4-RNA were implemented to study their biological functions, better understand the G4-associated diseases and assess the relevance of therapeutic strategies targeting G4s. Recently, the G4-interacting proteome was highlighted with the development of two methods: the G4 ligand-mediated cross-linking and pull-down (G4-LIMCAP) and the co-binding-mediated protein profiling (CMPP).[129,130] These methods combine 1/ the crosslinking of G4-binding

proteins with photoactivable G4 ligand (PDS derivatives), 2/ the G4/protein complex pull-down after the addition of a biotin moiety to the G4 ligand by click reaction, 3/ the separation of proteins by SDS-PAGE and 4/ the analysis and identification of proteins by LC-MS/MS. Of note, there was a first attempt to study G4/protein complexes in 2017 but in using biotinylated synthetic G4-forming sequences for the interaction with and the precipitation of G4-binding proteins, followed by LC-MS/MS analyses.[104]

5. The G-quadruplexes functions and dysfunctions

The aforementioned techniques allowed for the identification of >700 000 PQFS and >10 000 G4-forming sequences by G4-Seq and G4-ChIP-Seq,[116,118] respectively. It is now predicted that >1.5 M sequences can fold into G4 in our genome (by G4Hunter),[60] and >1.1 M sequences in our transcriptome (by G4RNA screener).[132] This wide distribution of G4s gave new insights into the biological processes involving G4s (**Figure 5**): with a prevalence of G4s in intergenic regions,[59,133] in particularly in gene promoters, 5-UTRs and telomeres, G4s have been rapidly associated with gene regulation at both the transcriptional and translational levels. They have also been associated with genome stability maintenance *via* their implication in telomeres protection and telomerase regulation.[17,134,135] Translation and alternative splicing of RNAs are governed by the presence of G4s near the ribosome binding sites or in introns,[136,137] but in some case even in exon.[138] However, G4s regulation mechanism is often related to the capacity of these tridimensional structures to block enzymes processivity (*e.g.* DNA and RNA polymerases, telomerase) and/or to allow for the recruitment of molecular effectors (*e.g.* RNA-binding proteins) promoting activation or inhibition of biological pathways.[137,139] To tackle the stability of G4s and their consequences on the cellular mechanisms, cells have developed regulatory enzymes able to bind to and then unwind these structures: the G4-helicases.[140,141] G4-helicases are involved in the maintenance of a healthy physiological state by unwinding secondary structures that might arise during DNA transactions, at replication forks and transcription bubbles.

G4s have also been related to others functions (**Figure 5**) like gene regulation in mitochondrial DNA,[142] immunoglobulin class-switch recombination[143] and regulation of key viral steps in many viruses (*e.g.* HBV and HPV for DNA viruses and SARS-CoV-2 and HIV-1 for RNA viruses).[144] Epigenetic regulation might also be influenced by G4s because of the higher affinity of DNA methyltransferases to G4-DNA than dsDNA resulting in DNMT1 sequestration on G4s at CpG islands (CGIs).[135] CGIs hypermethylation can also impact various biological processes such as ageing or cancers.[145] Regarding G4-RNAs, results have demonstrated their roles in alternative splicing, mRNA translation and telomere maintenance (as cited above) but also in mRNA localization in neurons and miRNA maturation too.[146,147]

As G4s are involved in many key biological processes, the dysregulation of G4 landscapes can lead to severe genetic diseases (**Figure 5**). G4s participate to the regulation of the cancer-associated telomerase recruitment,[135] the under-expression of oncogenes with G4-containing promoter (*MYC*, *KRAS*, *KIT*), but also to the metastatic process inhibiting the epithelial-mesenchymal transition,[137] making them closely linked to cancer mechanisms.[148,149] Also the overrepresentation of G4s in chromosome 9, due to the $^{5'}$d[GGGGCC]$^{3'}$

hexanucleotide repeat expansion in the *C9orf72 locus* leads to the development of neurodegenerative diseases: the *C9orf72*-mediated Amyotrophic Lateral Sclerosis (ALS) and Fronto-Temporal Dementia (FTD).[150–152] The $^{5'}$d[GGGGCC]$^{3'}$ repeat expansion promotes *i.* toxic gain-of-function of G-rich mRNAs-mediated aggregation of mRNAs and RNA-binding proteins, resulting in RNA foci in nuclei, *ii.* toxic gain-of-function of the dipeptide repeat proteins (DPR) resulting from these abnormal and extreme G-rich mRNAs and which cause inclusions in the frontal cortex, and *iii.* the loss-of-function of the C9orf72 protein which is a GEF protein implicated in Rab-dependent vesicular trafficking and autophagy.[153] More generally, these two diseases are closely associated to 1/ pathological protein aggregation (*e.g.*, TDP43, tau, SOD1, UFS and DPRs), 2/ synaptic and neuronal network defects (*e.g.*, neuronal hyperexcitability, synaptic disconnection between motor neurons and muscle), 3/ cytoskeletal abnormalities (*e.g.*, kinesin KIF5A-dependent axonal transport and cytoskeletal dynamics defects), 4/ altered energy homeostasis (*e.g.*, low ATP availability, mitochondrial dysfunction), 5/ DNA and RNA defects (*e.g.*, ROS-associated mutagenesis, chromosome rearrangements, RNA transcription arrest, DNA replication fork collapse), 6/ inflammation (*e.g.*, microgliosis) and 7/ neuronal cell death (*e.g.*, accumulation of age-associated DNA/lipids/proteins damage, cell replication dysfunction, high energy requirements), leading to amyotrophy, muscular strength decrease and spasticity.[153,154,152] Popular neurodegenerative disorders are also starting to be associated, even partially, with G4 dysfunctions, including Parkinson's and Alzheimer's disease along with Fragile X Syndrome.[154]

Others genetic diseases are linked to G4s but in a different manner, *i.e.*, the G4 helicases-mediated diseases (**Figure 5**).[135,140,141] Indeed, when mutations occur in G4-helicases coding genes, this loss-of-function mutations result in an overrepresentation of genomic G4s, which leads to replication and transcription dysregulations, excessive DNA damage and genome instability. A disease exists for almost each of the G4-helicase affected: the Bloom syndrome (for the G4-helicase BLM),[155,156] Werner syndrome (WRN)[157,158], Fanconi anemia (FANCJ, BACH1 or BRIP1),[102,159–162] etc. The treatment of these G4-associated diseases requires molecular and/or biological tools to address causal factors or pathological consequences. To this end, G4-interacting small molecules can be used to study G4 structures in pathological context and to treat related molecular dysfunctions (further detailed hereafter).

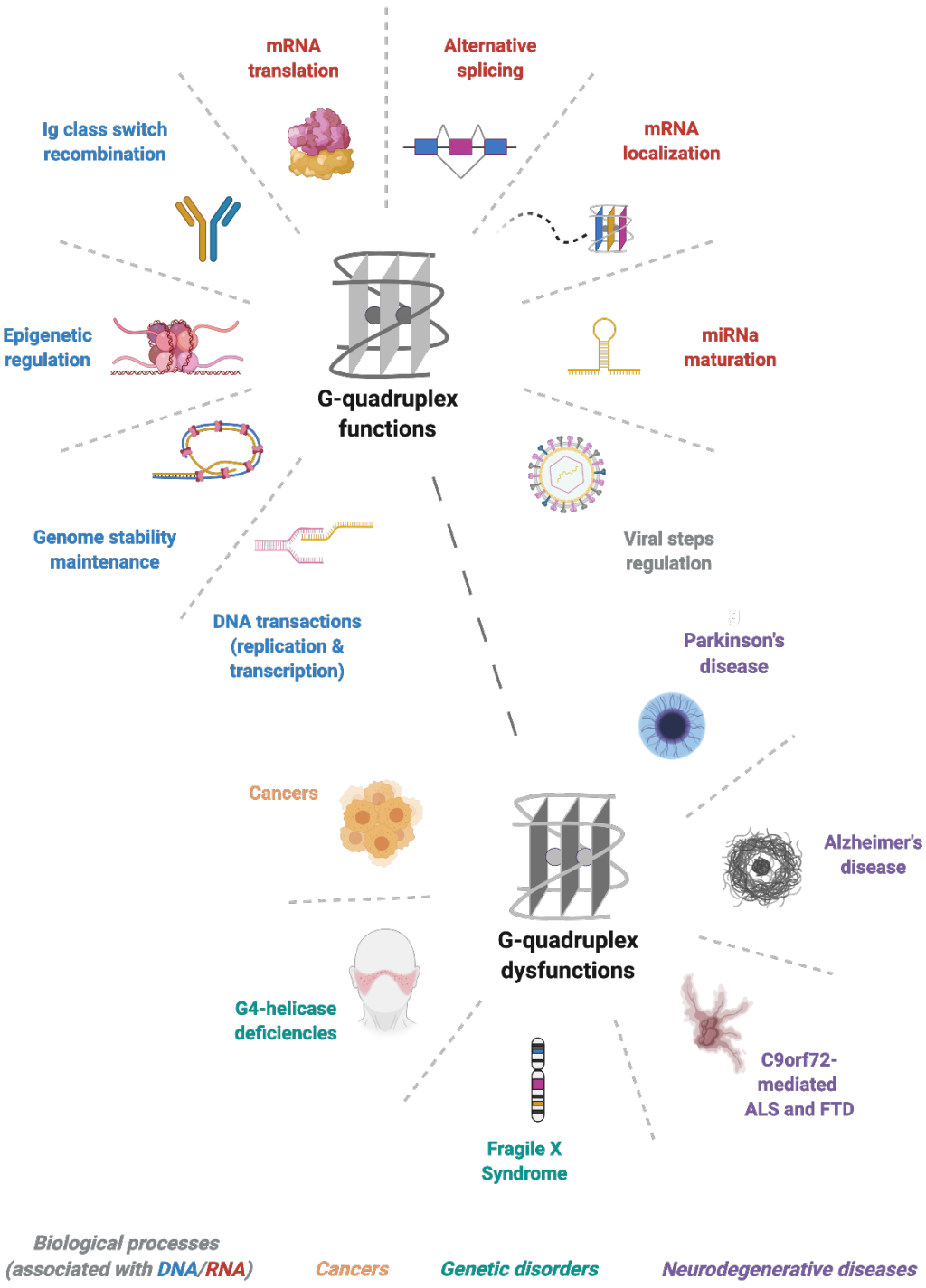

Figure 5. Schematic overview of the G4-associated biological functions and dysfunctions. The G4 structures were associated to several biological processes involving DNA G4s (DNA transactions, genome stability maintenance, epigenetic regulation, Ig class switch recombination) as well as RNA G4s (mRNA translation, alternative splicing, mRNA localization, miRNA maturation). These structures also have functions into viral steps regulation. Dysfunctions of G4s were linked to cancers, genetic disorders (G4-helicase deficiencies, fragile X syndrome) and neurodegenerative diseases (C9orf72-mediated ALS and FTD, Alzheimer's and Parkinson's diseases).

III. The G-quadruplex ligands

1. The G-quadruplex stabilizers

Considered as the textbook example of cancer biomarkers, the telomerase enzyme began to be considered as a key player of a new and promising anticancer strategy more than 30 years ago.[163] Attempts to modulate

the telomerase activity were based on small molecule or ONs with direct (*e.g.*, the d[$^{5'}$(TAG$_3$T$_2$AGACA$_2$$^{3'}$] GRN163 ON renamed imetelstat)[164,165] or indirect (*e.g.*, G4 ligands as TMPyP4)[166] anti-telomerase action. This enzyme acting on telomeric DNA, which are highly G4-prone sequences, several *in vitro* assays have been developed using a G4-folded ON to assess the capacity of small molecules to bind to telomeric G4s and block telomerase processivity. The first telomeric G4-interacting small molecule, a 2,6-diamidoanthraquinone (**Figure 6**), was discovered by Sun *et al*. in 1997 and its ability to inhibit human telomerase activity confirmed.[79] Next, the modified TRAP assay was used to assess the G4-stabilizing property of various small molecules.[80] This assay, adapted from an older one,[163] comprises a first step of telomerase-catalyzed extension of a primer, the primer being a non-telomeric ON, which will be extended by telomerase with a number of telomeric sequences depending on the action of small molecules (*i.e.* if molecules rapidly stick on the newly formed G4, the telomerase processivity is stopped, the extended DNA is thus shorter than without molecules). The second step is a PCR amplification of the extended primer followed by an electrophoretic separation. In order to have a real measure of the G4 stabilization and not an inhibition of the polymerase activity by small molecule during PCR, a *Taq* polymerase stop assay has to be performed. This technique allowed for the discovery of various G4-interacting compounds including TMPyP4 (IC_{50} = 0.3 µM; 1998),[166] telomestatin (IC_{50} = 5 nM; 2001),[167] BRACO-19 ($IC_{50\ v}$ = 95 nM; 2002),[168] 360A (IC_{50} = 0.3 µM; 2005)[169] and Phen-DC_3 (IC_{50} = 16 nM; 2007) (**Figure 6**).[170] All these molecules were also reevaluated by an improved assay, so called the Direct assay,[171] which allowed for a more accurate determination of the ability of the candidates to inhibit telomerase activity *per se* (and not the other steps of the TRAP protocol). The most used G4 ligand nowadays, the pyridostatin, or PDS (2008), was not assessed by TRAP but by a series of alternative *in vitro* assays and by a series of optical imaging investigations: this molecule was shown to uncap the GFP-POT1 fusion protein from telomeres, and to colocalize at DNA double-strand break sites (with γH_2AX labelling).[172]

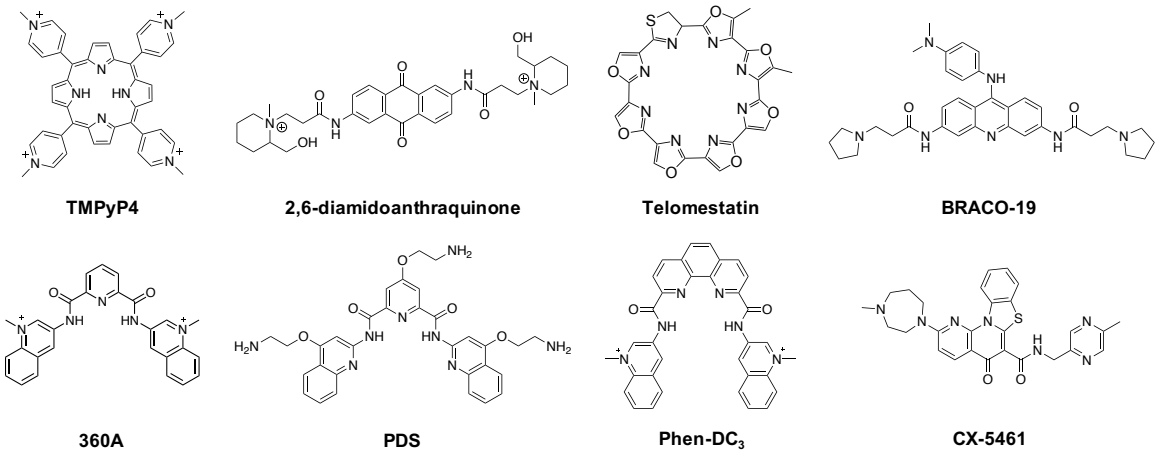

Figure 6. Chemical structures of eight well-known G4-stabilizers (TMPyP4, 2,6-diamidoanthraquinone, telomestatin, BRACO-19, 360A, PDS, Phen-DC_3 and CX-5461).

The properties of these ligands were assessed by a series of *in vitro* studies to evaluate their cellular effects and/or their therapeutic potential, including their ability to modulate G4 topology,[139] regulate G4-

containing oncogenes,[135] virus viability (DNA or RNA)[144] and G4-mediated cellular processes, exhibit tumor inhibitory activity, etc.[139] Among them, only two molecules went to clinical trials for solid tumors: CX-3543,[173] which was stopped in phase III trials because of its off-target effects, and CX-5461 in 2022 (**Figure 6**),[174–176] which recently showed drawback effects in promoting genetic instabilities (*i.e.*, mutagenesis, mainly *via* single base substitutions).[177]

In this context, we developed a series of Template-Assembled Synthetic G-Quadruplex (TASQ) ligands: this approach, born in 2008,[178,179] has been furthered by our group till the very first prototype of biomimetic G4 ligand in 2011, named DOTASQ (**Figure 7**).[180] Different derivatives were synthesized over the past years in order to optimize their G4-interacting properties: the PorphySQ in 2012 (with a porphyrin template instead of DOTA),[181] the ^{PNA}DOTASQ in 2013 (with cationic appendages around the synthetic G-quartet to increase selectivity and affinity to G4s),[182,183] and the ^{PNA}PorphySQ in 2014.[184]

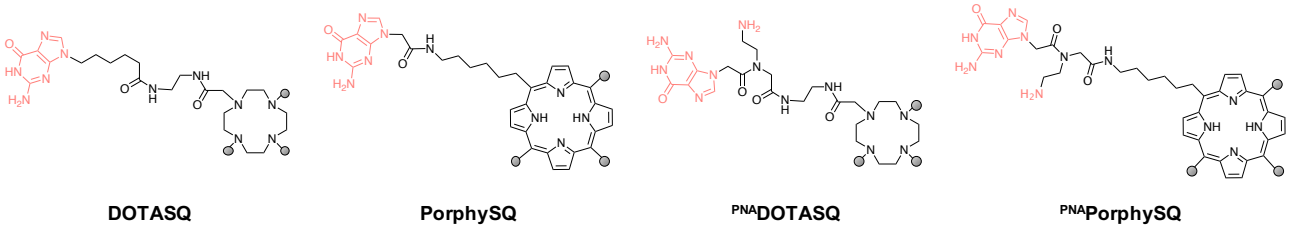

Figure 7. Chemical structures of our first TASQ generation (DOTASQ, PorphySQ, ^{PNA}DOTASQ and ^{PNA}PorphySQ).

2. The G-quadruplex destabilizers

Very recently, a search for a new type of G4-interacting molecules has emerged: the G4-destabilizing molecules, which can be small molecules, peptides and even proteins.[141] The quest for G4-destabilizers can be explained by the involvement of G4s in aforementioned key biological processes, notably those implicated in *C9orf72*-mediated neurodegenerative diseases and G4 helicase-associated genetic diseases. G4-stabilizers can be used to investigate the mechanisms underlying these diseases but also for therapeutic purposes as these genetic disorders are associated with an over-representation of G4s (because of a G4-prone repeat expansion or a lack of G4-helicase). A new therapeutic approach would thus rely on G4-destabilizers, used to iron G4s out and rescue G4-helicases deficiency. The identification of G4-destabilizers is thus becoming a new challenge in the G4 field and particularly in the neuropathology field that currently suffers from severe therapeutics attrition.

Surprisingly, the first small molecule which was described as a possible G4-destabilizer was also one of the first G4-stabilizers to be discovered, the TMPyP4 (**Figure 8**).[185–190] Evidence of its G4-destabilizing and/or aggregating capacity have been reported in 1980 with agarose gel experiment.[185] Weisman-Shomer *et al*. demonstrated in 2003 that TMPyP4 is able to open a G4-structure, leading to a less condensed structure visible by non-denaturing electrophoresis gel in K^+ condition.[186] They also demonstrated this by gene reporter assay, in a manner that was previously used to assess G4-stabilizing properties of several candidates. Another

G4-destabilizer was reported in 2009 by the Balasubramanian's group, TAP1,[191] whose properties were assessed through different *in vitro* experiments (*i.e.* CD experiment, RT-qPCR quantification and NMR study), which was followed by a third one in 2011, identified by Kaluzhny *et al.* through a series of spectroscopic experiments: an anthrathiophenedione.[192] Finally, in 2019, a stiff-stilbene[193] was demonstrated to govern G4 folding and unfolding by CD investigations, FRET-melting experiments and NMR studies.

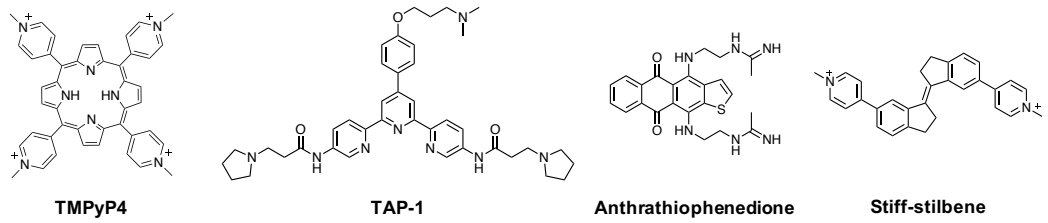

Figure 8. Chemical structures of four presumed G4-destabilizers (TMPyP4, TAP1, anthrathiophenedione and stiff-stilbene).

The description of the properties of these putative G4-destabilizing small molecules were hand-waving as most of them were collected *via* 1 or 2 assays only. Combining data collected through a series of assays seems to be the key to identify G4-destabilizers in a reliable manner. So far, no therapeutic strategies based on G4-destabilizers have emerged, which can be explained by the novelty of these molecules and the difficulty to assess their G4-destabilizing properties in an accurate and reliable manner (further discussed below).

3. The G-quadruplex probes

Research in the G4 field also relies on the visualization of G4s in their native biological involvement.[194] Only a handful of antibodies were described as G4-specific antibodies (**Table 3**). Historically, the first antibody was the me^V-IIB4 (formerly called me^V-αQ_1) in 1998 which was only used *in vitro*.[195] As described above, the first G4 antibody really used for immunodetection of these structures in cells was the Sty49 antibody (coupled to FITC-labelled secondary antibody) on *Stylonychia lemnae* in 2001.[109] Balasubramanian *et al*. obtained firstly the Hf2 antibody used for the isolation of G4 structures from genomic DNA extracted from MCF7 cells[196] and then BG4 antibody (2013) which is now commonly used for immunodetection of G4s,[114,115] G4 counting (BG-flow)[92] and quantitative G4 genome-wide studies (G4-ChIP-Seq, G4 CUT&Tag).[116,125] Recently, the same team produced the SG4 nanobody, which was used for both optical imaging and CUT&Tag investigations (2022).[126] Of note, two others antibodies were also reported but far less used, 1H6 (2013)[197] and D1 antibodies (2016).[198]

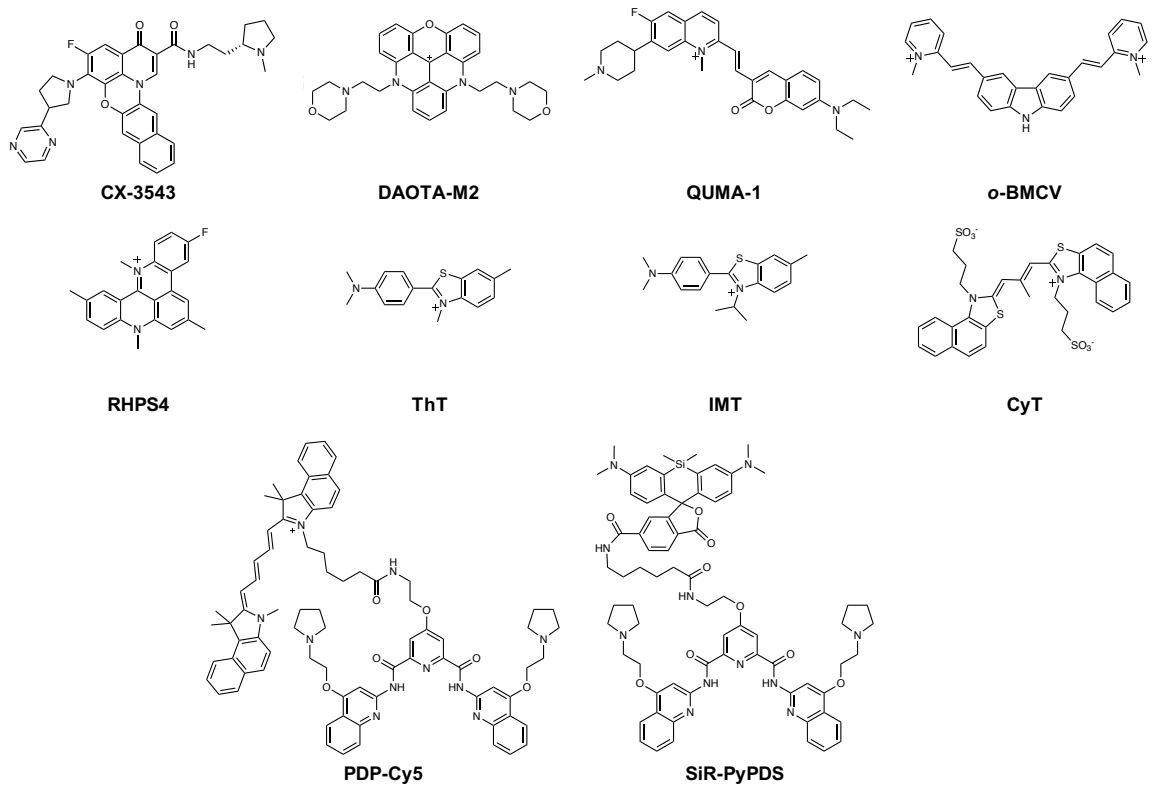

Figure 9. Chemical structures of ten G4 probes (CX-3543, DAOTA-M2, QUMA-1, *o*-BMCV, RHPS4, ThT, IMT, CyT, PDP-Cy5, SiR-PyPDS).

Since 1996, fluorescent small molecules were synthesized for the visualization of G4s (**Figure 9**, **Table 3**). While some were only used *in vitro* (*e.g.*, DODC, NMM, thiazole orange, crystal violet),[199–202] others were used in cells and showed: *i.* global cellular signals for CX-3543 (2009)[203] and DAOTA-M2 (live cell incubation for 24 h; 2015),[204] *ii.* global but precise cellular signals for N-TASQ (fixed cells; 2016),[205] QUMA-1 (fixed cells; 2018)[206] and *o*-BMCV (fixed cells; 2018),[207] *iii.* mostly nuclear/nucleolar signal for RHPS4 (live cell incubation for 30 min; 2002),[208] ThT (fixed cells; 2018)[209] and IMT (fixed cells; 2018),[210] and *iv.* cytoplasmic RNA signals for CyT (fixed cells; 2015)[211] and N-TASQ again (live cell incubation for 24-48 h; 2015-2016).[205,212] It has to be noted that due to the general polyaromatic nature of these dyes, they usually suffer from "turn-off" limitations, which explained why most of G4 ligands cannot be used as fluorescent G4 probes.[213] Also, well-known G4 ligands were modified to be used directly labelled with a fluorophore as for the PDS derivatives: PDP-Cy5 (live cell incubation for 2 h; 2016)[214] and SiR-PyPDS (live cell incubation for 30 min; 2020).[215]

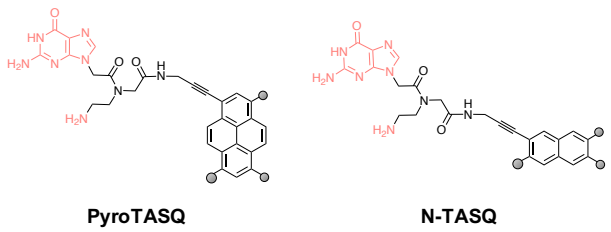

Figure 10. Chemical structures of our fluorescent G4 probes TASQs (PyroTASQ and N-TASQ).

Our TASQs were also improved with an additional fluorescent functionality, forming the new category of smart fluorescent TASQs (**Figure 10**): the PyroTASQ in 2014 and the NaphthoTASQ (or N-TASQ) in 2015.[184,216] These TASQs are turn-on fluorescence probes, *i.e.*, they are fluorescent only upon interaction with their G4 targets. The first cell-based studies began with the cell-permeable N-TASQ, which was used to detect G4-DNA as well as G4-RNA in cancer and neural cells.[205,212,217,218]

Year	Molecule name	Category	Conjugated with	Application	Reference
1996	DODC	G4 probe	/	G4 visualization in gel	Chen *et al.*, *Proc. Natl. Acad. Sci. U.S.A.* **1996**, *93* (7), 2635-2644[199]
1998	me^{V}-αQ_1	Antibody	/	/	Brown *et al.*, *Biochemistry* **1998**, *37* (46), 16325-16337[195]
2001	Sty49	Antibody	Incubated with FITC-labelled antibody	G4 visualization in cell (global)	Schaffitzel *et al.*, *Proc. Natl. Acad. Sci. U.S.A.* **2001**, *98* (15), 8572-8577[109]
2002	RHPS4	G4 probe	/	G4 visualization in cell (nuclear, nucleolar)	Heald *et al.*, *J. Med. Chem.* **2001**, *45* (3), 590-597[208]
2006	Thiazole orange	G4 probe	/	G4 labelling *in vitro* by fluorescence recording	Allain *et al.*, *J. Am. Chem. Soc.* **2006**, *128* (36), 11890-11893[201]
2007	Phen-DC_3	G4 stabilizer	/	G4 study – Model for multivalent G4 molecular tool	Cian *et al.*, *J. Am. Chem. Soc.* **2007**, *129* (7), 1856-1857[170]
2008	Hf2	Antibody	/	/	Fernando *et al.*, *Biochemistry* **2008**, *47* (36), 9365-9371[196]
2008	Pyridostatin (PDS)	G4 stabilizer	/	G4 study – Model for multivalent G4 molecular tool	Rodriguez *et al.*, *J. Am. Chem. Soc.* **2008**, *130* (47), 15758-15759[172]
2009	Crystal violet	G4 probe	/	G4 labelling *in vitro* by fluorescence recording	Kong *et al.*, *Chemistry* **2009**, *15* (4), 901-910[202]
2009	CX-3543	G4 probe	/	G4 visualization in cell (global)	Drygin *et aL*, *Cancer Res.* **2009**, *69* (19), 7653-7661[203]
2012	PDS-α	Multivalent G4 molecular tool	Clicked with Alexa Fluor 594-azide	G4 visualization in cell (nuclear, nucleolar)	Rodriguez *et al.*, *Nat. Chem. Biol.* **2012**, *8* (3), 301-310[111]
2013	1H6	Antibody	/	G4 visualization in cell (global)	Henderson *et al.*, *Nucleic Acids Res.* **2013**, *42* (2), 860-869[197]
2013	BG4	Antibody	Incubated with anti-FLAG beads or anti-FLAG plus anti-specie antibodies, plus	G4 visualization in cell (global but precise) – Purification of G4 – G4-DNA mapping in cell	Biffi *et al.*, *Nature Chem.* **2013**, *5* (3), 182-186[114] – Hänsel-Hertsch *et al.*, *Nat. Protoc.* **2018**, *13* (3), 551-564[116] – Lyu *et al.*, *Nucleic Acids Res.* **2022**, *50* (3), e13[125]

			recombinant pA-Tn5 transposase)		
2014	PyroTASQ	G4 probe	/	G4 visualization in gel	Laguerre *et al.*, *J. Am. Chem. Soc.* **2014**, *136* (35), 12406-12414[216]
2015	N-TASQ	G4 probe	/	G4 visualization in cell (global but precise in fixed cell; cytoplasmic in live cell)	Laguerre *et al.*, *J. Am. Chem. Soc.* **2015**, *137* (26), 8521-8525[212] – Laguerre *et al.*, *Sci. Rep.* **2016**, *6* (1), 32141[205]
2015	CyT	G4 probe	/	G4 visualization in cell (cytoplasmic, RNA)	Xu *et al.*, *Nucleic Acids Res.* **2015**, *43* (20), 9575-9586[211]
2015	DAOTA-M2	G4 probe	/	G4 visualization in cell (global)	Shivalingam *et al.*, *Nat. Commun.* **2015**, *6* (1), 8178[204]
2016	D1	Antibody	Fused with EGFP	G4 visualization in cell (global but precise)	Liu *et al.*, *Cell Chem. Biol.* **2016**, *23* (10), 1261-1270[198]
2016	PDP-Cy5	G4 probe	/	G4 visualization in cell (global but precise; cells transfected with G4-forming ONs)	Wu *et al.*, *Sens. Actuators B Chem.* **2016**, *236*, 268-275[214]
2017	Phen-DC_3-alk	Multivalent G4 molecular tool	Clicked with Cy5-azide	G4 visualization in cell (global but precise)	Lefebvre *et al.*, *Angew. Chem. Int. Ed.* **2017**, *56* (38), 11365-11369[219]
2017	Phen-DC_3-az	Multivalent G4 molecular tool	Clicked with Cy5-DBCO	G4 visualization in cell (global but precise)	Lefebvre *et al.*, *Angew. Chem. Int. Ed.* **2017**, *56* (38), 11365-11369[219]
2018	QUMA-1	G4 probe	/	G4 visualization in cell (global but precise)	Chen *et al.*, *Angew. Chem. Int. Ed.* **2018**, *57* (17), 4702-4706[206]
2018	*o*-BMCV	G4 probe	/	G4 visualization in cell (global but precise)	Tseng *et al.*, *Molecules* **2018**, *24* (1), 35[207]
2018	ThT	G4 probe	/	G4 visualization in cell (nuclear, nucleolar)	Zhang *et al.*, *Biochim. Biphys. Acta* **2018**, *1862* (5), 1101-1106[209]
2018	IMT	G4 probe	/	G4 visualization in cell (nuclear, nucleolar)	Zhang *et al.*, *Nucleic Acids Res.* **2018**, *46* (1), 7522-7532[210]
2018	BioTASQ	Multivalent G4 molecular tool	Incubated with Cy3-labelled or beads coated with streptavidin	G4 visualization in cell (global but precise) – Purification of G4-DNA/RNA from cell	Yang *et al.*, *Nat. Commun* **2018**, *9* (1), 4730-4740[120] – Rota Sperti *et al.*, *ACS Chem. Biol.* **2021**, *16* (5), 905-914[220] – Feng *et al.*, *iScience* **2023**, *26* (6), 106846[131]
2020	SiR-PyPDS	G4 probe	/	G4 visualization in cell (cytoplasmic)	Di Antonio *et al.*, *Nat. Chem.* **2020**, *12* (9), 832-837[215]

2020	L2H2-6OTD-Az	Multivalent G4 molecular tool	Clicked with CO-1-alkyle	G4 visualization in cell (global)	Yasuda *et al.*, *Chem. Commun.* **2020**, *56* (85), 12905-12908[221]
2021	PDB-DA-A	Multivalent G4 molecular tool	Photoactivated at 365 nm	Purification of G4-interacting proteins from cell – G4 visualization in cell (global but precise)	Su *et al.*, *J. Am. Chem. Soc.* **2021**, *143* (4), 1917-1923[129]
2021	BioCyTASQ	Multivalent G4 molecular tool	Incubated with Cy3-labelled or beads coated with streptavidin	G4 visualization in cell (global but precise) – Purification of G4-DNA/RNA from cell	Rota Sperti *et al.*, *ACS Chem. Biol.* **2021**, *16* (5), 905-914[220] – Feng *et al.*, *iScience* **2023**, *26* (6), 106846[131] – Rota Sperti *et al.*, *RSC Chem. Biol.* **2023**, *4* (7), 456-465[222]
2021	photoPDS-1	Multivalent G4 molecular tool	Photoactivated at 365 nm	Purification of G4-interacting proteins from cell	Zhang *et al.*, *Nat. Chem.* **2021**, *13* (7), 626-633[130]
2021	PDC-4,3-Alk	Multivalent G4 molecular tool	Clicked with BrdU-azide, plus anti-BrdU Alexa Fluor 488-labelled antibody	G4 visualization in cell (global but precise)	Masson *et al.*, *Nucleic Acid Res.* **2021**, *49* (22), 12644-12660[113]
2022	SG4	Nanobody	Fused with GFP and FLAG (plus anti-FLAG and anti-specie antibodies, plus recombinant pA-Tn5 transposase)	G4 visualization in cell (global) – G4 mapping in cell	Galli *et al.*, *J. Am. Chem. Soc.* **2022**, *144* (50), 23096-23103[126]
2022	BioTriazoTASQ	Multivalent G4 molecular tool	Incubated with Cy3-labelled streptavidin	G4 visualization in cell (global but precise)	Rota Sperti *et al.*, *JACS Au* **2022**, *2* (7), 1588-1595[223]
2023	MultiTASQ	Multivalent G4 molecular tool	Incubated with Cy3-labelled streptavidin	G4 visualization in cell (global but precise)	Rota Sperti *et al.*, *RSC Chem. Biol.* **2023**, *4* (7), 456-465[222]
2023	^{az}MultiTASQ	Multivalent G4 molecular tool	Incubated with beads coated ith streptavidin	Purification of G4-RNA from cell	Rota Sperti *et al.*, *RSC Chem. Biol.* **2023**, *4* (7), 456-465[222]
2024	TOR-G4	G4 probe	/	G4 visualization in cell (cytoplasmic)	Robinson *et al.*, *J. Am. Chem. Soc.* **2024**, *146* (1), 1009-1018[224]

Table 3. Non exhaustive summary list of protein and molecular tools developed for G4s study. Several antibodies, nanobody, G4 probes and multivalent G4 molecular tools were developed for the study of DNA and/or RNA G4s (*e.g.*, visualization in cell, purification from cell, mapping). Some molecular tools are derived from G4 stabilizers PDS (*e.g.*, PDS-α, PDP-Cy5, SiR-PyPDS, PDB-DA-A, photoPDS-1, PDC-4,3-Alk,) and Phen-DC_3 (*e.g.*, Phen-DC_3-alk, Phen-DC_3-az).

4. The multivalent G4 molecular tools

Others G4 ligands were developed to both visualize G4 in cells and fish them out from cell extracts in order to study their genomic and transcriptomic distribution. To this end, these ligands must be either biotinylated or clickable (**Table 3**). Indeed, well-known G4 ligands were functionalized and either pre-clicked or clicked once in interaction with G4s by click chemistry with a fluorophore (**Figure 11**): *i.* the PDS derivative PDS-α (post-fixed incubation and clicked with Alexa Fluor 594-azide; 2012),[111] *ii.* Phen-DC_3-alk (live cell incubation for 24 h, then clicked with Cy5-azide by CuAAC; 2017), *iii.* Phen-DC_3-az (same conditions; clicked with Cy5-DBCO by SPAAC; 2017),[219] and *iv.* L2H2-6OTD-Az (post-fixed incubation and clicked with CO-1-alkyle fluorescent dye; 2020).[221]

While the previous G4 ligands were clicked with fluorophores for the G4 detection in cells, another approach was chosen with the G4 ligand PDC-4,3-Alk (**Figure 11**) which was firstly clicked with a BrdU-azide before immunodetection with α-BrdU antibody (2021).[113] Of note, a better G4 *foci* resolution seemed to be obtained with the PDC-4,3-Alk (live cell incubation for 16 h, then clicked with BrdU-azide in fixed cell and immunodetection) compared to the already clicked PDC-4,3-BrdU (live cell incubation for 16 h, then immunodetection).[113]

Recently, G4 ligands with photoactivable group (*e.g.*, diazirine) were implemented for investigating G4-interacting proteins *in situ*. Su *et al*. reported the G4 ligand-mediated cross-linking and pull-down (G4-LIMCAP) method and Zhang *et al*. developed the co-binding-mediated protein profiling (CMPP) (coupled to LC-MS/MS proteomics analysis) in using the two clickable PDS derivatives PDB-DA-A (2021)[129] and photoPDS-1 (2021),[130] respectively.

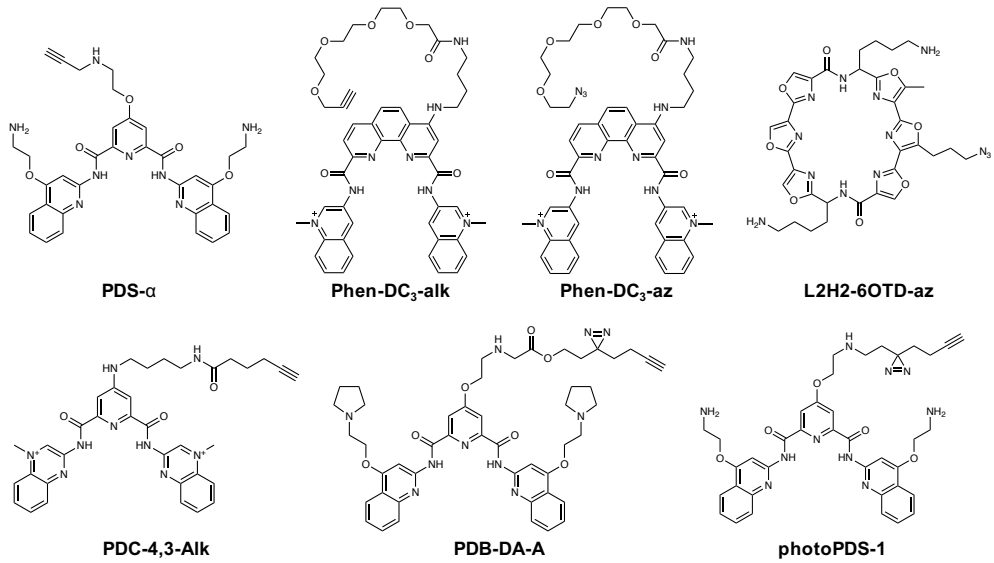

Figure 11. Chemical structures of seven multivalent G4 molecular tools (PDS-α, Phen-DC_3-alk, Phen-DC_3-az, L2H2-6OTD-az, PDC-4,3-Alk, PDB-DA-A and photo-PDS-1).

Our team also developed new TASQ generations for diversifying their applications: the biotinylated TASQs (**Figure 12**) BioTASQ, BioCyTASQ and BioTriazoTASQ were used for both *in vitro* and *in cella* studies

thanks to their strong affinity and exquisite selectivity for G4s. Their biotin appendage was exploited for *i.* the study of endogenous G4-DNA and G4-RNA landscape by affinity precipitation (pull-down) from cell lysate with streptavidin-coated beads (G4RP-seq and G4DP-seq methods)[91,120,121,131] and *ii.* the fluorescence visualization of G4s in cells (pre-targeted G4 imaging) using labelled streptavidin with BioCyTASQ and BioTriazoTASQ since 2021,[220,223] both applications that will be further detailed in the following chapters.

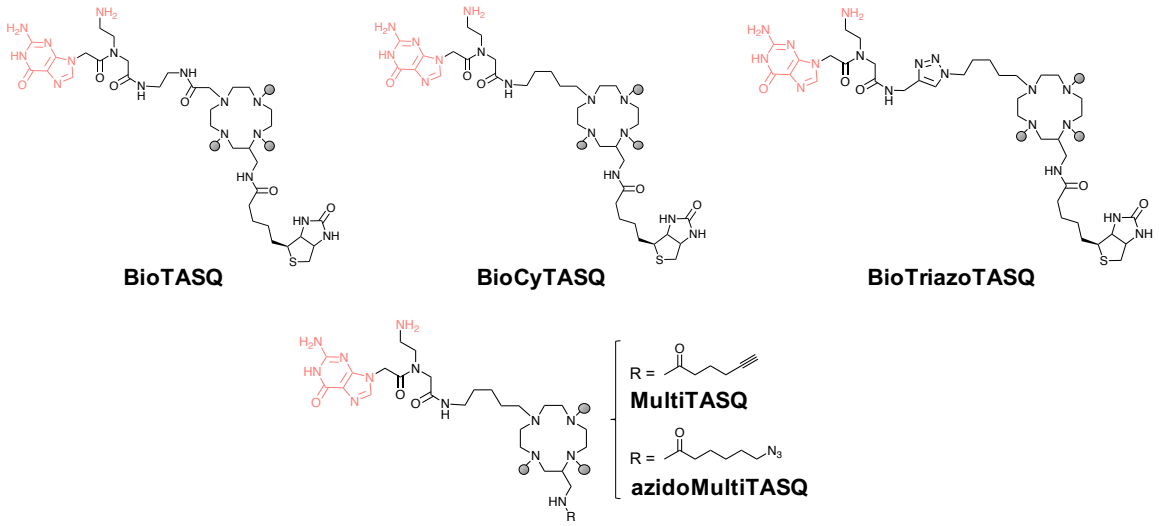

Figure 12. Chemical structures of our G4 molecular tools: the biotinylated TASQs (BioTASQ, BioCyTASQ and BioTriazoTASQ) and the clickable TASQs (MultiTASQ and ^{az}MultiTASQ).

More recently, the clickable TASQs (**Figure 12**) MultiTASQ and azidoMultiTASQ (or ^{az}MultiTASQ) benefit from the versatility of click chemistry to expand the scope of TASQ applications. Indeed, a biotin (for affinity purification) or a fluorophore moiety (for *in situ* click imaging) can be clicked, depending on the intended applications.[222,225] This patented technology[226,227] was recently licensed by Merck KGaA, and one of these compounds, along with a biotinylated TASQ, was made commercially available (Sigma-Aldrich cat. n° SCT246 and 247 for BioCyTASQ and MultiTASQ, respectively). These clickable TASQ also benefit from the very positive context around click chemistry with the Nobel Prize in Chemistry 2022 recently awarded to K. Barry Sharpless, Morten Meldal and Carolyn R. Bertozzi for the discovery of the copper-catalyzed azide-alkyne cycloaddition (CuAAC, in 2001)[228–230] and the copper-free version for biological study, the strain-promoted azide-alkyne cycloaddition (SPAAC, in 2004).[231] The use of G4 probes, as well as G4-stabilizers, has provided invaluable information on G4s including their cellular localization, the G4-prone sequences involved, the identification of biological partners, which together lead to a better understanding of their involvement in key cellular processes.[139,17,213]

The next chapters will be devoted to the development of methodologies for the study of G4-DNA and -RNA as well as the applications of TASQs: Chapter I is focused on the development of a workflow based on *in vitro* assays for the evaluation of small molecules effect on G4s, and on the identification of compounds

with G4-destabilizing capacity; Chapter II is focused on the applications of fluorescent as well as biotinylated TASQs in cells and the way numerical data can be extracted from the optical images; Chapter III is focused on both the optimization of a quantitative method of cellular G4-RNAs (G4RP) and the application of several multivalent G4 tools, both biotinylated and clickable TASQs to this end.

Chapter I – Development of a screening method for the identification of G-quadruplex-destabilizing small molecules

A. Introduction to the chapter I

For years, one of the main research axes of our team was the specific targeting of nucleic acids secondary structures,[11] particularly G4[120,180–182,184,212,216,220] and three-way junctions (TWJ).[232–235] To do so, we developed structure-specific G4-/TWJ-probes in the aim of using them as chemical biology tools. We recently became interested in G4-destabilizing small molecules. Several studies seeking to demonstrate the G4-destabilizing properties of candidates were yet reported,[187,191–193] but they globally failed to provide an undebatable G4-destabilizer prototype relying on a single or a handful of non-standardized methods.

To tackle this issue, and reach this goal, my first objective was to develop a reliable screening assay implementable to assess the G4-destabilizing properties of series of molecules. This project ultimately aims at discovering new small molecules that may find tremendous applications in a therapeutic area that currently suffers from drug attrition, that is, managing age-related and helicase deficiency-associated diseases.[135,140,141,150,151,153]

B. Project organization and implementation

I. The identification of G-quadruplexes-destabilizing small molecules: from initial considerations to adaptation

1. Ligands selection

This project started with our will to combine two *in vitro* techniques to analyze arrays of molecules in a two-dimensional manner. These techniques relied on the FRET phenomenon that takes place between two fluorophores, FAM and TAMRA (**Figure S1**), located on both ends (5' and 3', respectively) of a G4-forming sequence. Small molecule candidates that may impact the stability of a G4 structure will thus influence the distance between the two ends of the oligonucleotide (ON), resulting thus in a variation of the FAM fluorescence readily recorded with a plate-reader. The two techniques were the FRET-melting assay (performed in a temperature gradient from 25 to 90 °C) and the isothermal FRET (or isoFRET) assay (performed at 25 °C). The idea was thus to compare the effect of small molecules on the thermal and isothermal stability of G4 in order to discriminate G4-stabilizers (maintaining the two fluorophores close to each other) from potential G4-destabilizers (pushing the two fluorophores away from each other).

We first assembled a library of about 30 small molecules coming from our lab or from collaborations. After performing the first FRET-melting and isoFRET experiments with this first series of compounds, a two-dimension chart was created combining $T_{1/2}$ and T_{iso} values (not shown here), but this did not lead to the identification of reliable G4-destabilizing small molecules. We thus sought to develop a novel technique

allowing for measuring more easily a G4-destabilization. To this end, we also selected a smaller portfolio of compounds, comprising 14 candidates (**Figure 13**) including *i.* TMPyP4: a G4-stabilizer for which some G4-destabilization has also been reported,[185–187,236,189,190] *ii.* 4 TMPyP4 derivatives to study the contribution of charges and arms, *i.e.*, TEGPy, TPPS, TArPS and TEGP,[237–239] *iii.* 3 well-known G4-stabilizers to calibrate our assay, *i.e.*, Phen-DC_3, PDS and BRACO-19, and *iv.* 6 potential G4-destabilizers including a TAP1 derivative (*i.e.*, Terpy),[191] 2 G-clamp molecules (*i.e.*, PhpC and guaPhpC),[240] which are analogues of cytosine capable to form an additional hydrogen bond with guanines, and 3 azacyclophanes (*i.e.*, 1,5-BisNPO, 2,6-BisNPO and 2,7-BisNPN),[241] enabling the stabilization of isolated aromatic compounds, likely here isolated guanines. G-clamps and azacyclophanes were thus chosen to bind to guanines that possibly go out from the top G-quartet of a G4 as our hypothesis was that the opening of this upper G-quartet should be enough to trigger the collapse of the whole G4 structure. For the following assays we used different G4-forming oligonucleotide sequences (**Table Mat&Meth 1**) whose structure was characterized by both circular dichroism (CD) measurement and thermal difference signature (TDS) calculation (**Figures Mat&Meth 1-4**, **Tables Mat&Meth 2-3**).

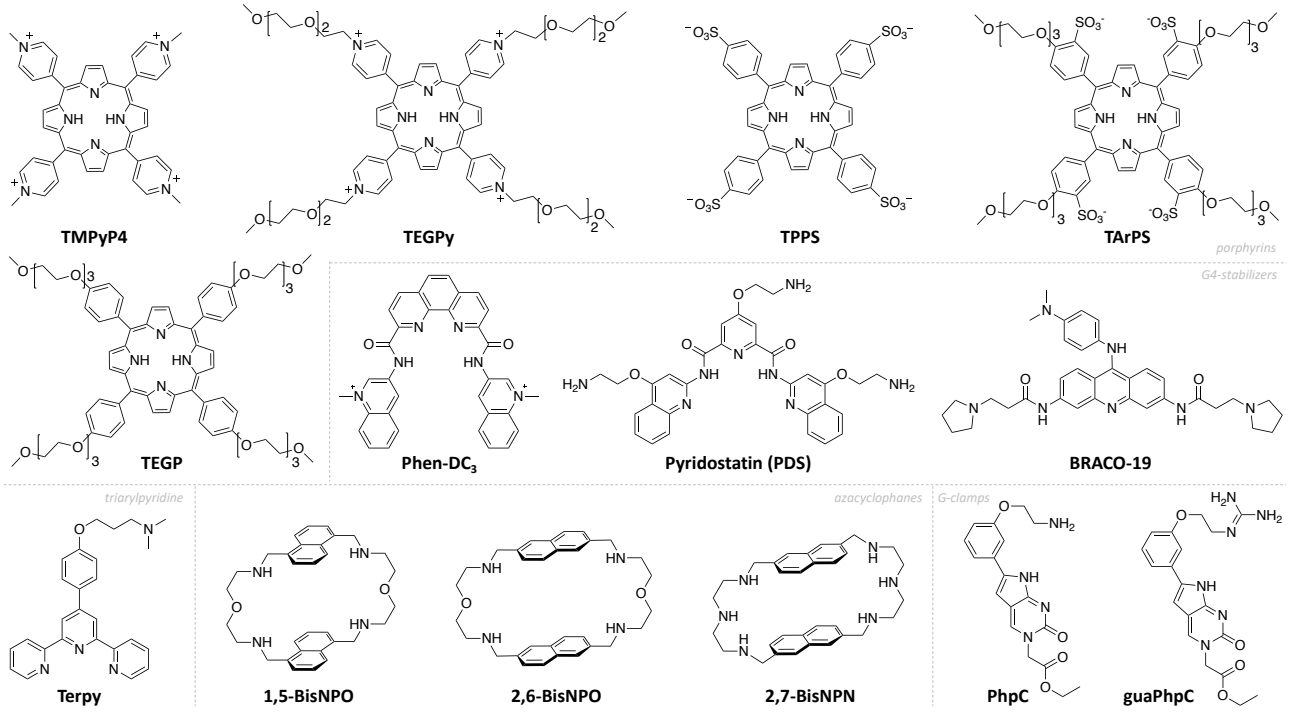

Figure 13. Chemical structures of the 14 small molecules studied as G4-stabilizing/-destabilizing ligands. This small library comprises 5 porphyrins (TMPyP4, TEGPy, TPPS, TArPS, TEGP), 3 well-known G4-stabilizers (Phen-DC_3, PDS, BRACO-19), 1 triarylpyridine (Terpy), 3 azacyclophanes (1,5-BisNPO, 2,6-BisNPO, 2,7-BisNPN) and 2 G-clamps (PhpC, guaPhpC).

2. the G4-UNFOLD assay

Given that potential G4-destabilizers should be used to alleviate G4-helicase deficiency, we first focused on *in vitro* assays initially developed to study the way G4-helicases do actually unfold G4s, notably those

dedicated to hPIF1 helicase:[82] this assay relies on the use of s-hTelo (**Figure Mat&Meth 1**, **Tables Mat&Meth 1-3**) obtained by the hybridization of a dabcyl-labelled 49-nt ON and a complementary FAM-labelled 15-nt ON. The resulting construct thus possesses ssDNA, G4 and dsDNA units (**Figure 14**). s-hTelo is used as a template for the hPIF1 helicase, whose processivity is monitored through the modification of the FAM fluorescence intensity (FI): when fully hybridized, the FAM FI is low because the hybridization brings FAM close to dabcyl (**Figure S1-A**); when hPIF1 is activated upon ATP addition, the two strands of s-hTelo are separated, restoring the FAM emission. To avoid the re-hybridization step, two complementary ON are used: *i.* the Trap ON, which is complementary to FAM-labelled 15-nt ON, and *ii.* the c-hTelo ON, which is complementary to dabcyl-labelled 49-nt ON, in order to obtain the maximum FAM FI at the end of the reaction.

The main limitation of this assay stands in the hPIF1 enzyme itself, whose activity varies from an experiment to another. That is why our first investigations were intended to create an alternative assay, independent on the use of hPIF1. We indeed observed that the addition of the G4-stabilizing ligand TMPyP4 influences the hybridization kinetics of the dabcyl-labelled 49-nt ON with c-hTelo. We thus quantified this through the calculation of V_0 (expressed in s^{-1}), which represents the slope of the FI curve right after the c-hTelo addition (**Figure 15**). To systematically obtain exploitable curves, and thus, V_0 values, the c-hTelo concentration was decreased from 5 mol. equiv. compared to s-hTelo (*i.e.*, 166.7 nM, used in the initial conditions) to 2.2 mol. equiv. (84.3 nM). Others technical simplifications were also made, removing the ATP (necessary for the hPIF1 helicase activity) and the Trap ON (because its presence did not influence the FAM FI). We also adjusted the buffer, using 20 mM Tris-HCl, 5 mM $MgCl_2$, 1 mM KCl, 99 mM NaCl, pH 7.2 for the solution of the small molecules (so called Tris-HCl buffer 1), and 20 mM Tris-HCl, 10 mM $MgCl_2$, 1 mM KCl, 99 mM NaCl, pH 7.2 (Tris-HCl buffer 2) that we use now for all conditions (*i.e.*, control and treated conditions). The G4-UNFOLD assay (**Table Mat&Meth 4**) thus simply relies on the study of the effect of small molecules on the kinetics of the c-hTelo hybridization (**Figure 15**).

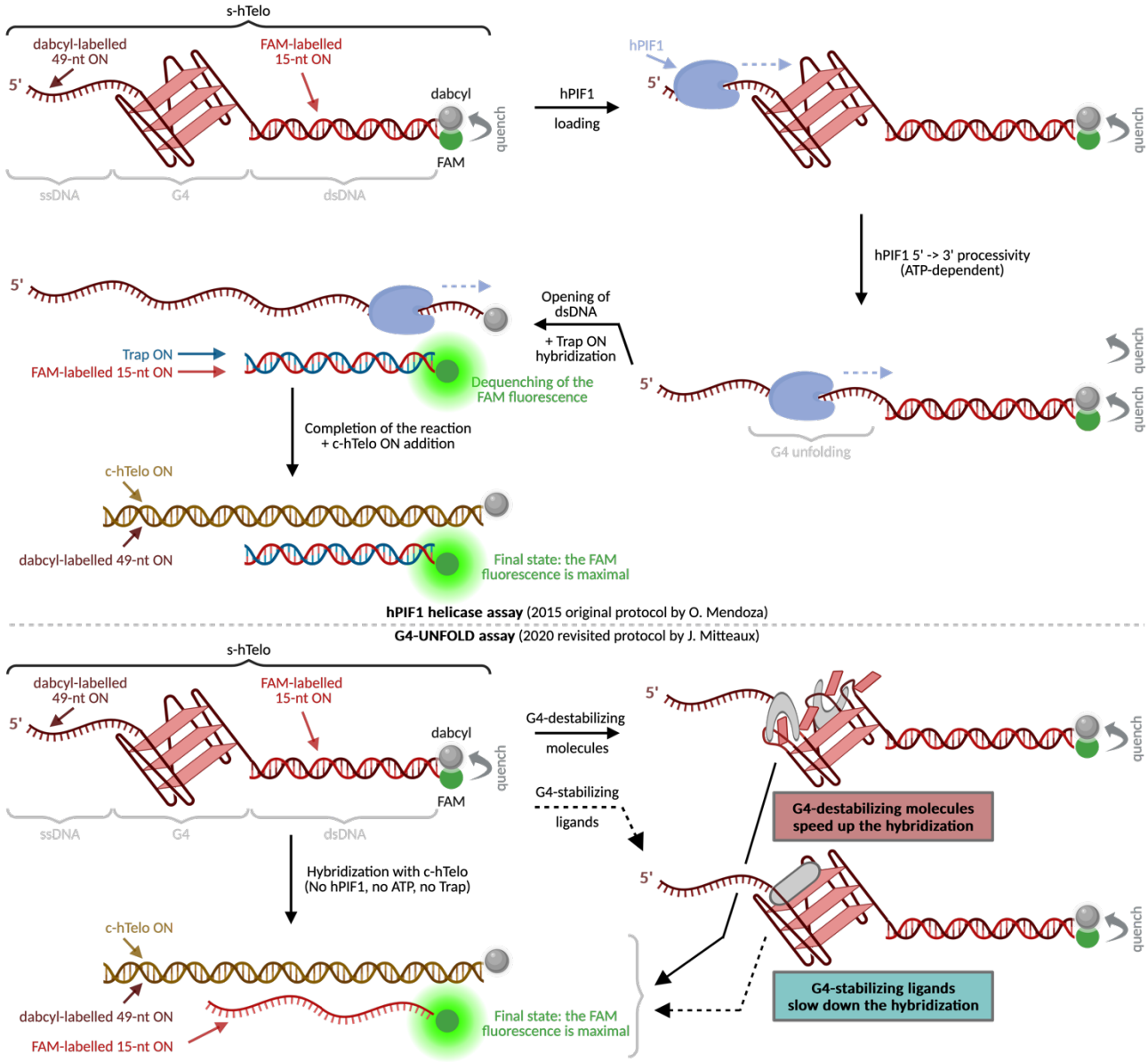

Figure 14. Schematic representation and comparison of the hPIF1 helicase and G4-UNFOLD assays. (Top) The hPIF1 helicase assay, described by Mendoza *et al.*,[82] relies on the s-hTelo ON that possess a G4 structure, the hPIF1 helicase that catalyzes the dehybridization of s-hTelo ON with a 15-nt complementary sequence labelled with a FAM, used to monitor the efficiency of the process. (Bottom) The G4-UNFOLD assay, developed by our team,[93] shares the same oligonucleotides but does not relies on hPIF1 helicase, providing information about G4-stabilization/-destabilization monitoring the c-hTelo hybridization kinetics. Created with BioRender.com

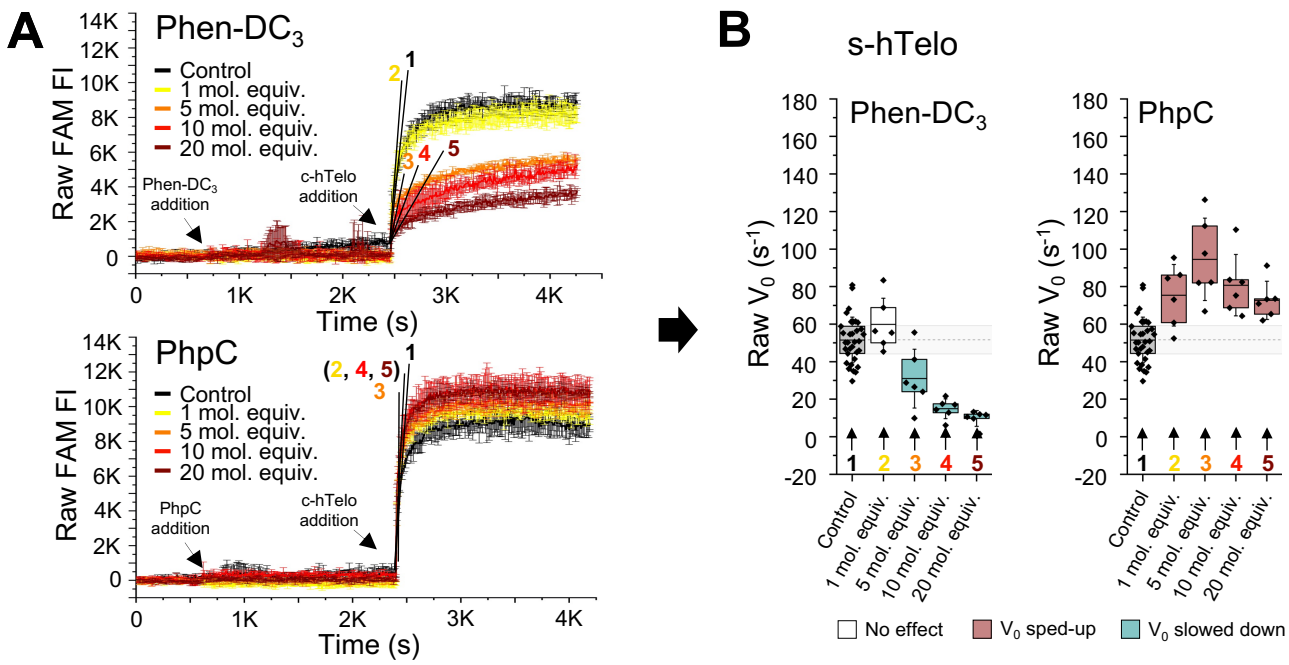

Figure 15. Schematic representation of the data treatment of the G4-UNFOLD assay. For the final representation of G4-UNFOLD assay results, (**A**) the individual FAM fluorescence intensity = *f*(time) curves were used to calculate (**B**) the initial velocity V_0 (s^{-1}). To this end, a linear fit function was applied on the first 5 points and then the calculated slope used as a V_0 value. Here Phen-DC_3 and PhpC have been used as G4-stabilizer and G4-destabilizer examples, respectively.

The 14 small molecules described above were thus investigated at 4 different concentrations: 1, 5, 10 and 20 mol. equiv. (with respect to s-hTelo). Individual FAM FI = *f*(time) curves for each candidate (see results summary cards, **Figures S2-S15**) were used to calculated V_0 values (**Figure 15**). FAM FI values were normalized (0.0-1.0) or not to calculate Normalized V_0 (**Figure S16-S17**) or Raw V_0 (**Figure 16**), respectively. ΔV_0 values were also calculated for a better comparison between small molecules represented as a heat map (**Table 4**). We found that the G4-stabilizers PDS, Phen-DC_3 and TMPyP4 slowed down the c-hTelo hybridization speed especially at medium and high concentrations (10-20 mol. equiv., **Figure 16-C-D**) with a $\Delta V_0 < -30$ s^{-1} (**Table 4**). On the contrary, PhpC, TArPS, Terpy and TPPS were found to speed up the hybridization, particularly at low (*i.e.*, 1 mol. equiv.) and/or medium concentrations (*i.e.*, 5-10 mol. equiv.) with a $\Delta V_0 > 30$ s^{-1} for TArPS and Terpy and even $\Delta V_0 > 40$ s^{-1} for PhpC and TPPS (**Table 4**). A series of molecules did not showed a particular effect on V_0: 1,5-BisNPO, 2,6-BisNPO, 2,7-BisNPN, BRACO-19, guaPhpC, TEGP and TEGPy ($-20 < \Delta V_0 < 20$, **Table 4**). Interestingly, the ranking seen in **Table 4** is not dependent on normalization, thus removing some possible biases. Also, our experimental setup allows for taking the influence of the ligands on the background FAM FI (**Figure S18**, **Table S1**).

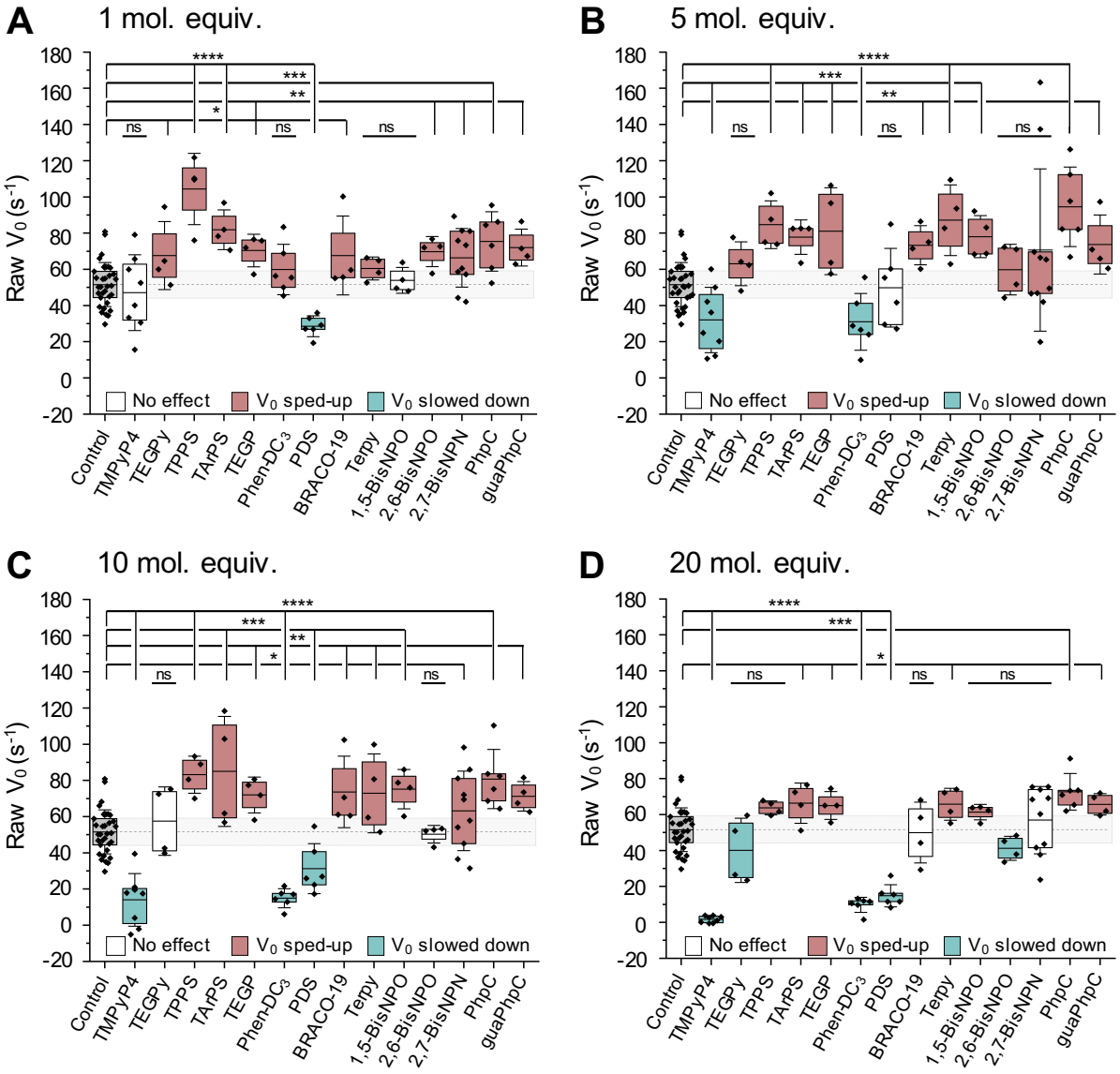

Figure 16. G4-UNFOLD raw results obtained with 4 different concentrations of 14 candidates. The G4-UNFOLD assay was performed without (*i.e.*, V_0 Control, ON only in 20 mM Tris-HCl, 10 mM $MgCl_2$, 1 mM KCl, 99 mM NaCl, pH 7.2) or with the presence of a small molecule candidate at 4 different concentrations of small molecules: (**A**) 1, (**B**) 5, (**C**) 10 and (**D**) 20 mol. equiv. Mean V_0 values calculated correspond to the slope from the linear fit applied on the first five points after the c-hTelo addition. The capacity of small molecules to speed up (red boxes) or slow down (blue boxes) the c-hTelo hybridization was attributed comparing Mean V_0 values (in s^{-1}): *i.* No effect if -SD V_0 Control < Mean V_0 small molecule < +SD V_0 Control, *ii.* G4-stabilizing effect if Mean V_0 small molecule < Mean V_0 Control or *iii.* G4-destabilizing effect if Mean V_0 small molecule > Mean V_0 Control. Error bars represent SD from the mean for at least four independent experiments. For statistical hypothesis tests, Student's *t*-test and Welch's unequal variances *t*-test were used depending on variances equality. * $p < 0.05$, ** $p < 0.01$, *** $p < 0.001$, **** $p < 0.0001$.

Collectively, this technique has validated the G4-stabilizing effect of some well-known G4-stabilizers (*e.g.*, PDS, Phen-DC_3, TMPyP4) and the G4-destabilizing properties of promising candidates: PhpC, TArPS, Terpy and TPPS. Terpy was already suspected to have G4-destabilizing property, which constitutes here another element comforting the reliability of this technique.[242] PhpC was a good surprise given that its G-clamp properties were what originally guided us to use it in the G4 field.[240] For TArPS and TPPS, these two negatively charged porphyrins highlight how negative/positive charges drive the effect of porphyrins on G4,

with a strong G4-destabilizing effect for negative porphyrins (TArPS, TPPS), a mild G4-destabilizing effect for neutral porphyrin (TEGP) and a G4-stabilizing effect for positive porphyrins (strong for TMPyP4 and mild for TEGPy). It seems the chains length has also an influence on their strength because we can clearly separate short chains with strong effect (TMPyP4 and TPPS) *vs.* long chains with mild or no effect (TEGPy, TArPS and TEGP).

Raw data (V_0 in s^{-1})

1 mol. equiv.	Control 51.5	TMPyP4 47.1	TEGPy 67.6 *	TPPS 104.0 ****	TarPS 81.9 ****
	TEGP 70.4 **	PhenDC3 59.9	PDS 28.5 ****	BRACO19 67.6 *	Terpy 60.5
	1,5-BisNP-O 53.9	2,6-BisNP-O 69.8 **	2,7-BisNP-N 66.3 **	PhpC 75.4 ***	guaPhpC 72.0 **
5 mol. equiv.	Control 51.5	TMPyP4 32.0 ***	TEGPy 63.0	TPPS 84.6 ****	TarPS 77.8 ***
	TEGP 81.0 ***	PhenDC3 31.0 ****	PDS 49.8	BRACO19 73.3 **	Terpy 87.1 ****
	1,5-BisNP-O 78.0 ***	2,6-BisNP-O 59.8	2,7-BisNP-N 70.7	PhpC 94.5 ****	guaPhpC 73.6 **
10 mol. equiv.	Control 51.5	TMPyP4 14.0 ****	TEGPy 57.5	TPPS 83.2 ****	TarPS 85.0 ***
	TEGP 71.9 **	PhenDC3 14 ,9 ****	PDS 31.2 ***	BRACO19 73.6 **	Terpy 72.9 **
	1,5-BisNP-O 75.2 ***	2,6-BisNP-O 50.3	2,7-BisNP-N 63.2 *	PhpC 80.8 ****	guaPhpC 71.2 **
20 mol. equiv.	Control 51.5	TMPyP4 1,7 ****	TEGPy 40.1	TPPS 63.7	TarPS 66.3 *
	TEGP 65.0 *	PhenDC3 9,7 ****	PDS 14.8 ****	BRACO19 49.9	Terpy 65.7 *
	1,5-BisNP-O 61.3	2,6-BisNP-O 41.2	2,7-BisNP-N 56.9	PhpC 72.7 ***	guaPhpC 65.7 *

$-\infty < \Delta V_0 < -40$ | $-40 < \Delta V_0 < -30$ | $-30 < \Delta V_0 < -20$ | $-20 < \Delta V_0 < -10$ | $-10 < \Delta V_0 < 10$ | $10 < \Delta V_0 < 20$ | $20 < \Delta V_0 < 30$ | $30 < \Delta V_0 < 40$ | $40 < \Delta V_0 < +\infty$

Normalized data ($V_0 . 10^3$ in s^{-1})

1 mol. equiv.	Control 9,7	TMPyP4 8,6	TEGPy 12,5	TPPS 16,3 ****	TarPS 13,1 **
	TEGP 13.0 *	PhenDC3 12,9	PDS 6,7 **	BRACO19 12,5	Terpy 9,1
	1,5-BisNP-O 8,3	2,6-BisNP-O 12,2 *	2,7-BisNP-N 11	PhpC 11,4	guaPhpC 11,8
5 mol. equiv.	Control 9,7	TMPyP4 8,3	TEGPy 11,2	TPPS 13,6 **	TarPS 11,6
	TEGP 13,2 *	PhenDC3 8,25	PDS 10,3	BRACO19 12,7 *	Terpy 12,5
	1,5-BisNP-O 12,2 *	2,6-BisNP-O 10,7	2,7-BisNP-N 11,1	PhpC 14,5 **	guaPhpC 11,8
10 mol. equiv.	Control 9,7	TMPyP4 5,8	TEGPy 11,4	TPPS 12,9 **	TarPS 9,6
	TEGP 11,5	PhenDC3 4,6 ****	PDS 7,1 *	BRACO19 12,2	Terpy 10,8
	1,5-BisNP-O 11,2	2,6-BisNP-O 8	2,7-BisNP-N 10,1	PhpC 11,6	guaPhpC 10
20 mol. equiv.	Control 9,7	TMPyP4 2,3 ****	TEGPy 11,5	TPPS 9,8	TarPS 10,4
	TEGP 10,5	PhenDC3 3,5 ****	PDS 4,9 ***	BRACO19 8,5	Terpy 9,5
	1,5-BisNP-O 10	2,6-BisNP-O 7,1 *	2,7-BisNP-N 9,2	PhpC 10,8	guaPhpC 10

$-\infty < \Delta V_0 < -4$ | $-4 < \Delta V_0 < -3$ | $-3 < \Delta V_0 < -2$ | $-2 < \Delta V_0 < -1$ | $-1 < \Delta V_0 < 1$ | $1 < \Delta V_0 < 2$ | $2 < \Delta V_0 < 3$ | $3 < \Delta V_0 < 4$ | $4 < \Delta V_0 < +\infty$

Table 4. Heat map representing the raw and normalized V_0 values of the 14 small molecules panoply obtained by G4-UNFOLD assay. The G4-UNFOLD assay was performed without (*i.e.*, V_0 Control, ON only in 20 mM Tris-HCl, 10 mM $MgCl_2$, 1 mM KCl, 99 mM NaCl, pH 7.2) or with the presence of a small molecule at 4 different concentrations: 1, 5, 10 and 20 mol. equiv. For normalized data (right panel), a (0;1) normalization was applied to raw data (left panel) before the V_0 calculation. Mean V_0 values (in s^{-1}) calculated correspond to the slope from the linear fit applied on the first five points after the c-hTelo addition. ΔV_0= V_0 with small molecule – V_0 Control. ΔV_0 values toward dark red are above the Control (V_0= 51.5 s^{-1}) and those toward dark blue are below the Control. Means were calculated with data from at least four independent experiments. For statistical hypothesis tests, Student's *t*-test and Welch's unequal variances *t*-test were used depending on variances equality. * $p < 0.05$, ** $p < 0.01$, *** $p < 0.001$, **** $p < 0.0001$.

To go a step further, we selected 6 of these candidates for the subsequent experiments: the 2 strongest G4-stabilizers Phen-DC_3 and TMPyP4, the 2 strongest G4-destabilizers PhpC and TPPS, and 2 intermediate candidates 1,5-BisNPO and 2,7-BisNPN, respectively (**Figure 17**).

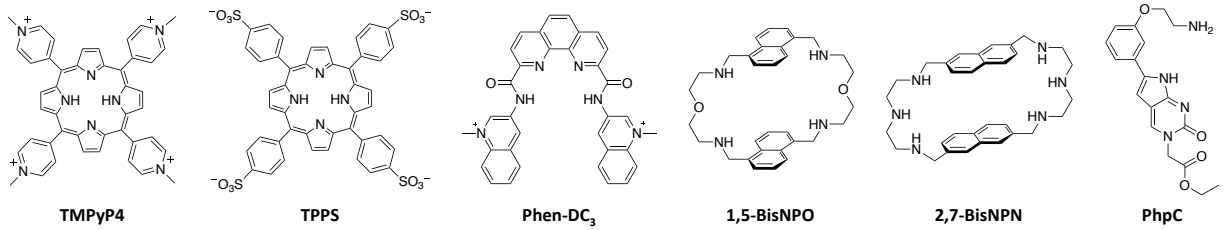

Figure 17. Chemical structures of the 6 selected small molecules further studied with classical *in vitro* assays. This panel comprises 2 porphyrins (TMPyP4, TPPS), 1 well-known G4-stabilizer (Phen-DC_3), 2 azacyclophanes (1,5-BisNPO, 2,7-BisNPN) and 1 G-clamp (PhpC).

3. Classical *in vitro* assays

In the field of the G4s, the identification and/or validation of G4 ligands usually relies on classical *in vitro* techniques such as the FRET-melting assay, CD (± UV-Vis) titration and Polyacrylamide Gel Electrophoresis (PAGE, or EMSA for Electrophoretic Mobility Shift Assay). The FRET-melting assay (**Table Mat&Meth 5**), as discussed above, uses the FAM/TAMRA fluorophores couple (**Figure S1-B**, **Figure Mat&Meth 5**) and allows for the measurement of the G4 thermal stability imparted by a ligand. The CD titration (**Table Mat&Meth 6**) is usually performed with a G4 and increasing concentrations of a small molecule in order to assess the influence of the molecule on the G4 secondary structure. The PAGE (**Table Mat&Meth 7**) is a common electrophoresis technique separating biomolecules depending on their apparent molecular size, which will be used here for determining whether a ligand act or not on this size parameter.

The FRET-melting assay, performed with the F21T ON (**Figure Mat&Meth 2**, **Tables Mat&Meth 1-3**), clearly showed that the 2 G4-stabilizers Phen-DC_3 (green box, **Figure 18**) and TMPyP4 (blue box) do indeed stabilize G4 efficiently, with $T_{1/2}$ values going up to 81.5 ± 0.4 and 70.5 ± 0.5 °C (thus $\Delta T_{1/2}$ = 30.9 and 19.9 °C, **Table S2-A,B**), respectively, at 10 mol. equiv. The two previously identified G4-destabilizers PhpC (orange box, **Figure 18**) and TPPS (yellow box) led to opposite effect (**Figure 18**) with negative $\Delta T_{1/2}$ values (down to -1.4 °C at 1 mol. equiv. for PhpC and -1.6 °C at 10 mol. equiv. for TPPS, **Table S2**). 1,5-BisNPO (burgundy box, **Figure 18**) displayed weak G4 stabilization only (with a $\Delta T_{1/2}$ value of 1.2 °C at 10 mol. equiv., **Table S2**), while 2,7-BisNPN (red box, **Figure 18**) showed a good, and dose-dependent G4-stabilization, with $\Delta T_{1/2}$ = 3.2, 5.4, 7.5 and 13.8 °C at 1, 2, 5 and 10 mol. equiv. (**Table S2-B**), respectively.

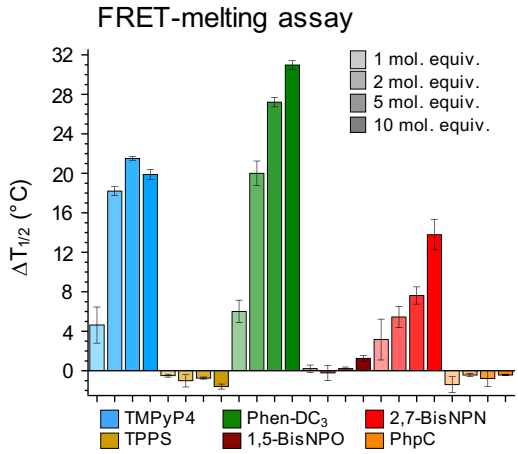

Figure 18. FRET-melting assay results obtained with the 6 selected small molecules. The FRET-melting assay was performed without (*i.e.*, $T_{1/2}$ Control, ON only with CacoK10 buffer) or with small molecules (TMPyP4 in blue, TPPS in yellow, Phen-DC_3 in green, 1,5-BisNPO in burgundy, 2,7-BisNPN in red, PhpC in orange) at 4 different concentrations: 1, 2, 5 and 10 mol. equiv. (from light to dark hue). Mean $T_{1/2}$ (or T_m, in °C) values calculated correspond to the melting temperature of the F21T G4. $\Delta T_{1/2}$= $T_{1/2}$ with small molecule – $T_{1/2}$ Control. Error bars represent SD from the mean for three independent experiments.

Using the same G4-folding sequence than for FRET-melting assay (F21T, d[$^{5'}$(G$_3$T$_2$A)$_3$G$_3$$^{3'}$]) but without label (hTelo G4, d[$^{5'}$A(G$_3$T$_2$A)$_3$G$_3$$^{3'}$], **Figure Mat&Meth 2**, **Tables Mat&Meth 1-3**)), 5 small molecules (TMPyP4, TPPS, 1,5-BisNPO, 2,7-BisNPN, PhpC) were found here to induce a proportional decrease of the 293 nm CD peak, characteristic of anti-parallel type G4 (**Figure 19-A**), which could be associated with a G4 denaturation. At the highest concentration (10 mol. equiv.), these molecules effectively make the 293 nm CD peak varied of -68.7, -20.5, -27.3, -52.1 and -17.5% (**Table S3**) for TMPyP4, TPPS, 2,5-BisNPO, 2,7-BisNPN and PhpC, respectively. Phen-DC$_3$ is the only small molecule which make this CD peak slightly increased with a CD variation between 0.2-2.5%. These results could be ascribed to a global G4 destabilization; to confirm/deny this possibility, we thus performed parallel UV-Vis titrations (**Figure 19-B**): first, we checked that none of these small molecules absorb light at 257 nm (*i.e.*, the absorbance peak of the hTelo G4, **Table S4-A**) and found that only TMPyP4 and Phen-DC$_3$ weakly absorb at the highest concentrations. Upon addition on hTelo G4, these small molecules did not strongly influence the hTelo absorbance at 257 nm: TPPS and PhpC trigger a small increase (13.1 and 7.6% at 10 mol. equiv., **Table S4-B**), 1,5-BisNPO and 2,7-BisNPN a more significant decrease (-26.4 and -11.8% at 10 mol. equiv.), and TMPyP4 and Phen-DC$_3$ a marked increase (36.7 and 22.0% at 10 mol. equiv.). However, the contribution of the molecule alone (dashed lines in Figure 7B) clearly contributes to the modification of the UV-Vis. Altogether, these results show that a great caution must be exercised when interpreting CD and UV-Vis titrations because these two techniques provide results that are the results of the combination of different parameters (*i.e.*, screening effects, induced CD, etc.), which cannot be readily related to G4-stabilisation/destabilization.

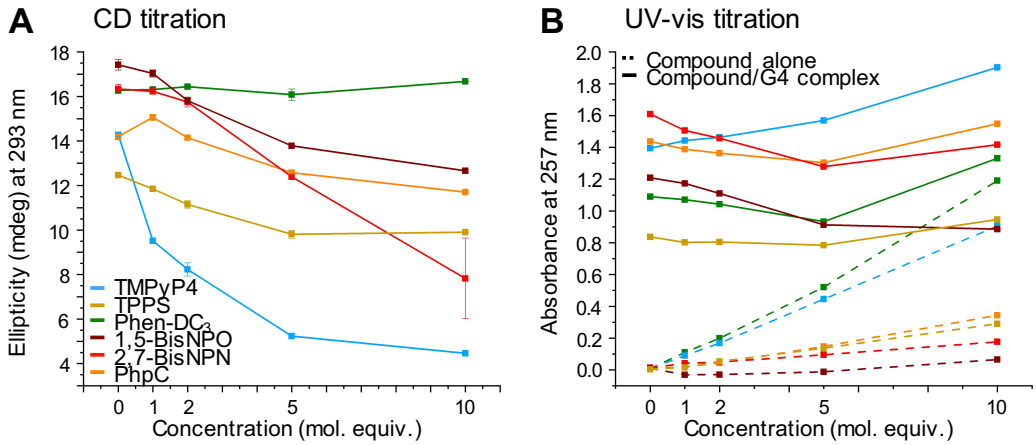

Figure 19. CD and UV-Vis results obtained with the 6 selected small molecules. The (**A**) CD (at 293 nm; in mdeg; positive peak of the hTelo G4) and (**B**) UV-Vis (at 257 nm; positive peak of the hTelo G4) titrations were performed without (*i.e.*, CD or UV-Vis Control, ± ON only with CacoK10 buffer) or with small molecules (TMPyP4 in blue, TPPS in yellow, Phen-DC$_3$ in green, 1,5-BisNPO in burgundy, 2,7-BisNPN in red, PhpC in orange) at 4 different concentrations: 1, 2, 5 and 10 mol. equiv., in a titration manner. CD titration was performed in the presence of the hTelo ON while UV-Vis titrations were performed without (Compound alone, dashed lines) or with the hTelo ON (Compound/G4 complex, solid lines). CD or UV-Vis ± SD (error bars) values calculated correspond to the CD or UV-Vis signals monitored during 10 min.

To go a step further, the 6 candidates were evaluated by the PAGE method (**Figure 20**): both TMPyP4 and Phen-DC_3 (blue and green boxes, respectively) behave alike as increasing concentrations (from 0 to 20 mol. equiv.) trigger an increase of the apparent molecular size of the G4 ON, visible by a delayed migration, which ultimately make the resulting complex disappear (with a FI down to -76.1 and -89.4%, **Figure 20-A, Figure 20-B**, **Table S5-B**) without creating a shifted band. This led us to consider that the complexes aggregate with too high ligand concentration. For the four others small molecules, a similar pattern was observed: a shifting of the hTelo G4 band with the appearance of an upper band and/or smear (**Figure 20-A**). Both 1,5-BisNPO and 2,7-BisNPN (burgundy and red boxes, respectively) trigger a stronger shift (FI down to -49.3 and -41.7% at 20 mol. equiv., **Figure 20-B**, **Table S5-B**) than TPPS and PhpC (yellow and orange boxes, respectively), for which the shift slowly starts at 20 mol. equiv. (FI down to -4.7 and -13.1, **Figure 20-B**, **Table S5-B**). These shifts and/or smears could be attributed to a partial hTelo G4 unfolding, as a partly unwound G4 displays a bigger apparent molecular size.

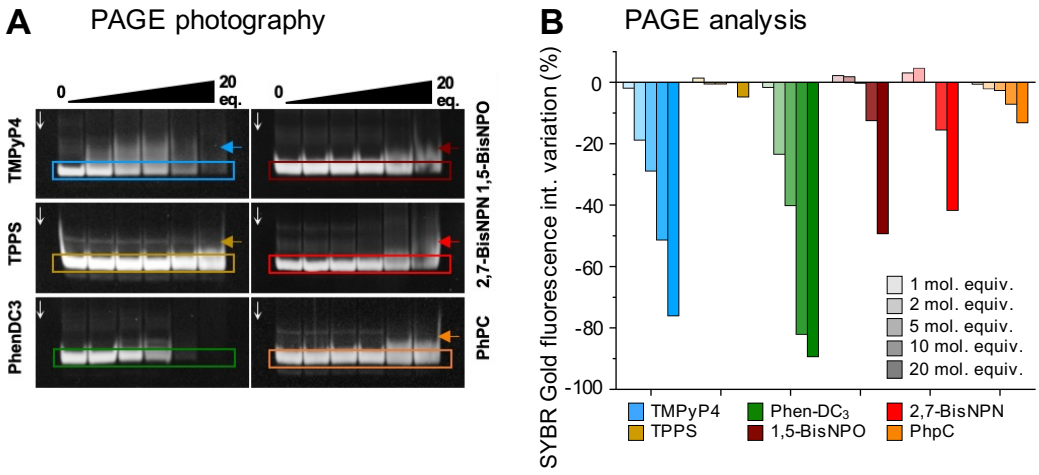

Figure 20. PAGE results obtained with the 6 selected small molecules. The (**A**) PAGE photography quantification allows for obtaining the (**B**) SYBR Gold FI and thus, the FI variation (in %) from the PAGE analysis performed without (*i.e.*, FI Control, ON only with CacoK10 buffer) or with a small molecule (TMPyP4 in blue, TPPS in yellow, Phen-DC_3 in green, 1,5-BisNPO in burgundy, 2,7-BisNPN in red, PhpC in orange) at 5 different concentrations: 1, 2, 5, 10 and 20 mol. equiv. (from light to dark hue). FI values calculated correspond to the FI of the hTelo band in gel (colored boxes). FI variation= [(FI small molecule * 100)/FI Control] – 100.

Altogether, the results collected through several *in vitro* techniques show the ability of candidates to destabilize a G4 ON depends on both the experimental conditions and the concentrations used. TPPS and PhpC seem to be the two best candidates since all the results point towards G4-destabilization; 1,5-BisNPO might be a good candidate but the results are less definitive. We thus needed another assay, considered to be orthogonal to the FRET-melting, CD, UV-Vis and PAGE experiments, to gain confidence about the actual properties of our candidates.

4. The qPCR Stop assay

To go a step further, we developed a qPCR/Polymerase stop assay. This technique relies on the ability of a polymerase to replicate a G4-containing ON possessing a G4-folding sequence. Among the recent published examples, the techniques developed by Sabouri's team[83] were interesting: the *Taq* DNA polymerase stop assay (performed with synthetic ON) and the qPCR Stop assay (performed with *S. pombe* genomic DNA). The latter was notably used to identify several new *S. pombe* G4s, playing on their stability by either modulating the K^+ concentration or adding G4-stabilizers TMPyP4, BRACO-19 and Phen-DC_3. These experiments provided interesting insights into genomic G4 sequences stabilized by the ligands, in a dose-response manner, possessing also a complementary sequence (*i.e.*, a "NonG4", C-rich, sequence) non affected by the presence of the ligand treatments. Four G4 sequences were thus of interest (G4-1, G4-4, G4-5 and G4-12); we selected G4-1 for our preliminary investigations.

With the two primers they used to amplify the genomic DNA region containing the G4-1 motif (*i.e.*, the NS390R and NS389F primers, then renamed G4-1 reverse and G4-1 forward primers, **Table Mat&Meth 1**), this genomic region was located in the chromosome 2 of *S. pombe* by sequence alignment *via* the NCBI's Nucleotide BLAST tool (https://tinyurl.com/ytcftxa3) (**Figure 21**).[243] This precise genomic location allows us to define the antisense strand possessing the G4-1 motif (the G4-strand, (**Figure Mat&Meth 3**, **Tables Mat&Meth 1-3**)) and its complementary (sense) strand (the Non G4-strand) (**Figure 21**). The principle of the qPCR Stop assay is schematically depicted in **Figure 22**: without ligand, the G4 structure of the G4-strand acts as a roadblock to the *Taq* enzyme activity, which is slowed down and creates a heterogenous population of neo-synthesized ON with varied length; at the end of the assay, the FI level will be proportional to the total ON amount and their lengths (**Figure 23-A**). The G4 stabilization by a ligand accentuates this phenomenon, thus generating less of neo-synthesized ON (the final FI is lower than the control); on the contrary, the G4 destabilization must help the enzyme unravel the G4 structure during the replication, and thus improve the amplification (the final FI value is higher than the control).

G4-1 reverse (NS390R) primer (25 nt):

5′ TTA-GAT-ACC-ATC-AAA-CAC-CAT-TAG-G 3′

Sequence alignment on NCBI > Nucleotide BLAST
Database: Standard databases > Nucleotide collection
Organism: Not specified for the alignement

G4-1 forward (NS389F) primer (20 nt):

5′ TAG-CCA-TTC-AGC-CGT-AAC-AG 3′

Description	Scientific Name	Max Score	Total Score	Query Cover	E value	Per. Ident	Acc. Len	Accession
Schizosaccharomyces pombe antisense RNA (predicted), possible alternative UTR (SPNCRNA.1367),...	Schizosaccharo...	50.1	50.1	100%	0.005	100.00%	2339	NR_150243.1
Schizosaccharomyces pombe uncharacterized protein (SPBC1685.12c), mRNA	Schizosaccharo...	50.1	50.1	100%	0.005	100.00%	2940	NM_001355872.1
Schizosaccharomyces pombe chromosome II, complete sequence	Schizosaccharo...	50.1	50.1	100%	0.005	100.00%	4539804	CU329671.1
Hibiscus tridactylites genome assembly, chromosome: 15	Hibiscus tridact...	42.1	42.1	84%	1.1	100.00%	93344650	OY288279.1
Hibiscus tridactylites genome assembly, chromosome: 14	Hibiscus tridact...	42.1	42.1	84%	1.1	100.00%	94381702	OY288278.1
Acronicta psi genome assembly, chromosome: 9	Acronicta psi	42.1	42.1	84%	1.1	100.00%	14829812	OX276477.1
Pammene fasciana genome assembly, chromosome: Z	Pammene fasci...	40.1	40.1	80%	4.4	100.00%	46694440	OU452272.1
Furcula furcula genome assembly, chromosome: 18	Furcula furcula	40.1	120	80%	4.4	100.00%	23890832	OU452260.1
Taeniopygia guttata clone TG_Ba-289B15, complete sequence	Taeniopygia gut...	40.1	40.1	80%	4.4	100.00%	55628	AC183473.3
Coregonus sp. 'balchen' genome assembly, chromosome: 18	Coregonus sp. '...	40.1	40.1	80%	4.4	100.00%	51949489	LR778270.1

Description	Scientific Name	Max Score	Total Score	Query Cover	E value	Per. Ident	Acc. Len	Accession
Schizosaccharomyces pombe uncharacterized protein (SPBC1685.12c), mRNA	Schizosaccharo...	40.1	40.1	100%	2.2	100.00%	2940	NM_001355872.1
Schizosaccharomyces pombe antisense RNA (predicted), possible alternative UTR (SPNCRNA.1367),...	Schizosaccharo...	40.1	40.1	100%	2.2	100.00%	2339	NR_150243.1
Schizosaccharomyces pombe chromosome II, complete sequence	Schizosaccharo...	40.1	40.1	100%	2.2	100.00%	4539804	CU329671.1
Plectropomus leopardus DNA, chromosome 12, nearly complete sequence	Plectropomus l...	38.2	38.2	95%	8.7	100.00%	34117940	AP022711.1
Ctenicera cuprea genome assembly, chromosome: 8	Ctenicera cuprea	38.2	38.2	95%	8.7	100.00%	48500970	OY284493.1
Mythimna impura genome assembly, chromosome: 1	Mythimna impura	38.2	38.2	95%	8.7	100.00%	36229551	LR990340.1
Borostomias antarcticus genome assembly, chromosome: 16	Borostomias an...	36.2	36.2	90%	34	100.00%	25280591	OX465219.1
Nematopogon swammerdamellus genome assembly, chromosome: 6	Nematopogon s...	36.2	36.2	90%	34	100.00%	26662671	OX336339.1
Sacculina carcini genome assembly, chromosome: 4	Sacculina carcini	36.2	72.4	90%	34	100.00%	11963827	OU696574.1
Autographa gamma genome assembly, chromosome: 11	Autographa ga...	36.2	36.2	90%	34	100.00%	12761877	LR989860.1

10 nucleotide sequence hits

First DNA hit:
Schizosaccharomyces pombe chromosome II, complete sequence (DNA)
NCBI GenBank: CU329671.1 ; Length: 4 539 804 nt

For G4-1 reverse primer:

Schizosaccharomyces pombe chromosome II, complete sequence
Sequence ID: CU329671.1 Length: 4539804 Number of Matches: 1

Range 1: 524270 to 524294 GenBank Graphics Next Match

Score	Expect	Identities	Gaps	Strand
50.1 bits(25)	0.005	25/25(100%)	0/25(0%)	Plus/Plus

```
Query  1       TTAGATACCATCAAACACCATTAGG  25
               |||||||||||||||||||||||||
Sbjct  524270  TTAGATACCATCAAACACCATTAGG  524294
```

For G4-1 forward primer:

Schizosaccharomyces pombe chromosome II, complete sequence
Sequence ID: CU329671.1 Length: 4539804 Number of Matches: 1

Range 1: 524347 to 524366 GenBank Graphics Next Match

Score	Expect	Identities	Gaps	Strand
40.1 bits(20)	2.2	20/20(100%)	0/20(0%)	Plus/Minus

```
Query  1       TAGCCATTCAGCCGTAACAG  20
               ||||||||||||||||||||
Sbjct  524366  TAGCCATTCAGCCGTAACAG  524347
```

Schizosaccharomyces pombe chromosome II, complete sequence
NCBI Reference Sequence: NC_003423.3
GenBank FASTA

Amplicon containing the G4-1 motif: 524 270-524 366 (97 nt): (CDS: 5′ 523 887-524 240 3′ ; FHN1 gene: 5′ 525 509-526 642 3′)

524 270 524 294

5′ TTA GAT ACC ATC AAA CAC CAT TAG GTT CTA CTG TAC TGC CCT GCC CTG CCC TGC CCT GTC TGT CTC TCT TCC ACT GCC TGT TAC GGC TGA ATG GCT A 3′
Sense/Coding/Plus strand (5′ > 3′) → Non G4-strand

524 308 524 325 524 347 524 366

3′ AAT CTA TGG TAG TTT GTG GTA ATC CAA GAT GAC ATG ACG GGA CGG GAC GGG ACG GGA CAG ACA GAG AGA AGG TGA CGG ACA ATG CCG ACT TAC CGA T 5′
Antisense/Non coding/Minus strand (3′ > 5′) → G4-strand G4-1 motif (Jamroskovic *et al.*, *DNA Repair* **2019**, *82*, 102678)

Figure 21. Designing of the *S. pombe* sequences G4-strand et Non G4-strand for the qPCR Stop assay. The qPCR Stop assay protocol, initially developed by Jamroskovic *et al.*,[83] uses primers to amplify a G4-containing *S. pombe* genomic region (G4-1 motif). This representation indicates the complete DNA sequence found in the yeast chromosome 2 as well as the location of the G4 motif.

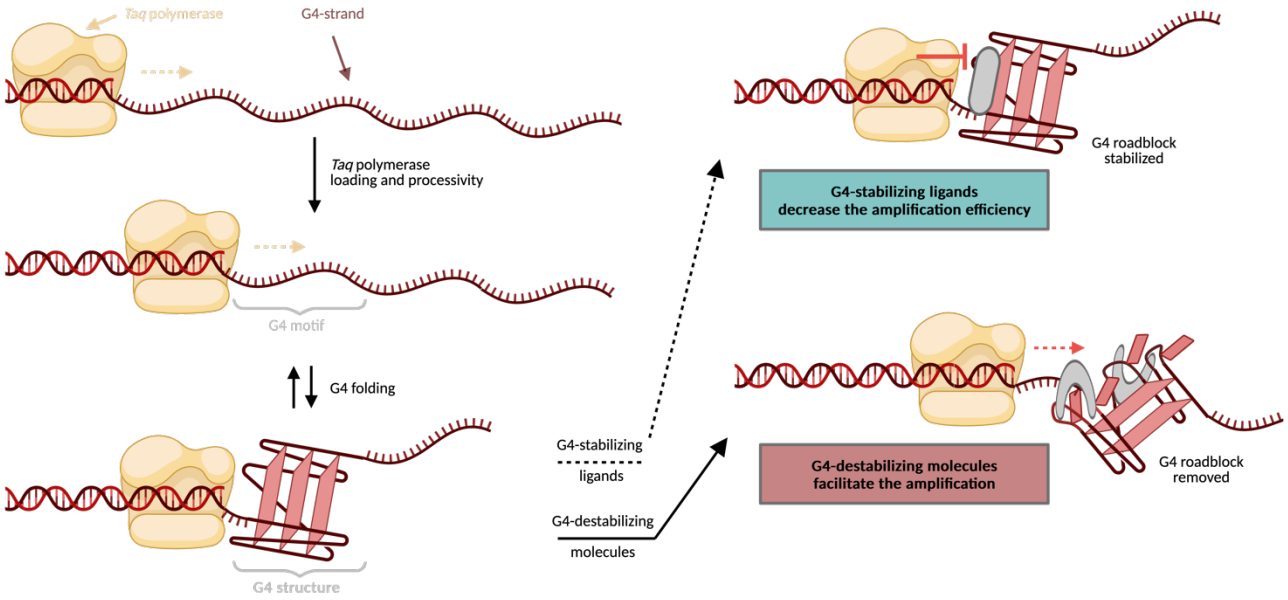

Figure 22. Schematic representation of the qPCR Stop assay. The qPCR Stop assay, intially described by Jamroskovic *et al.*,[83] relies on the G4-strand ON that possess a G4 structure and a *Taq* polymerase enzyme which catalyzes the replication of this ON during 33th qPCR cycles. The efficiency of the reaction is monitored by the use of DNA intercalating agent (SYBR Green) whose fluorescence intensity is proportional to the total ON amount and length. This technique allows for assessing the small molecules effect on G4 stability given that they affect the enzyme efficiency and then the final FI value. Created with BioRender.com

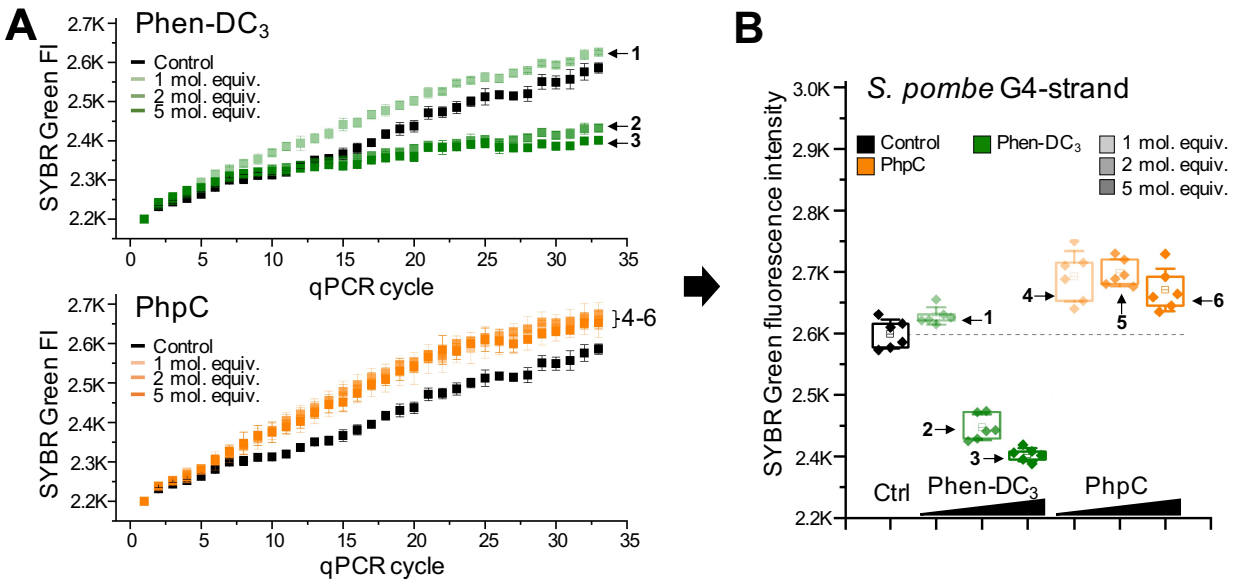

Figure 23. Data treatment of the qPCR Stop assay. For the final representation of qPCR Stop assay results, (**A**) the individual SYBR Green FI = *f*(qPCR cycle) curves were used but only (**B**) the FI values at the 33th (and last) qPCR cycle were kept, being proportional to the total ON amount and length. Here, Phen-DC$_3$ (green boxes) and PhpC (orange boxes) have been used as G4-stabilizer and G4-destabilizer examples, respectively.

For the treatment and representation of the qPCR Stop assay results, the initial SYBR Green FI value, *i.e.*, the FI at the end of the first qPCR cycle, was fixed at 2200.0 (a.u., **Figures S2-S15**) to make all results readily comparable. The FI values at the 33th (and last) qPCR cycle (**Figure Mat&Meth 6**, **Table Mat&Meth 8**) were used to compare the effect of the small molecules (**Figure 23-B)**. In order to calculate a G4 selectivity

value, the qPCR Stop assay was also done with the Non G4-strand; the effect of the small molecules on these two ONs was incorporated in a Selectivity factor S (see the **Figure S19** for the Non G4-strand FI curves).

The qPCR Stop assay was performed with the most interesting candidates (**Figure 24**), that is, the two strongest G4-stabilizers Phen-DC_3 and TMPyP4 and the two strongest G4-destabilizers TPPS and PhpC; we also included the PDS, as a reference ligand (intended to be used in subsequent cell-based studies).

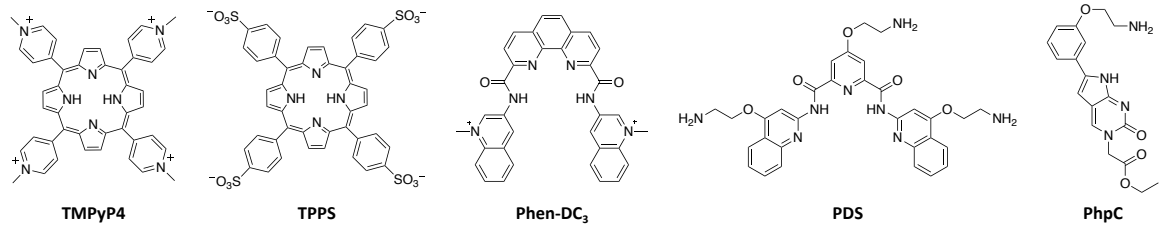

Figure 24. Chemical structures of the 5 small molecules selected for qPCR Stop assay evaluation. This panel of molecules, selected on the basis of results collected through 4 *in vitro* assays comprises 2 porphyrins (TMPyP4, TPPS), 2 well-known G4-stabilizer (Phen-DC_3, PDS) and 1 G-clamp (PhpC).

Reminiscently of what was obtained with the other *in vitro* assays, Phen-DC_3 (green boxes, **Figure 25**) was found to be a better G4-stabilizer than TMPyP4 (blue boxes; on *S. pombe* G4-strand**, Figure 25-A**), with a difference in SYBR Green FI (or ΔFI) of -195.8 *vs*. -60.2 at 5 mol. equiv. (**Table S6-A**). However, these two G4-stabilizers impacted the same way the Non G4-strand (ΔFI= -172.3 for TMPyP4 and -116.2 for Phen-DC_3 at 5 mol. equiv., **Figure 25-B**, **Table S6-B**), resulting in a Selectivity factor S (= $\Delta FI_{\text{G4-strand}} - \Delta FI_{\text{Non G4-strand}}$**, Table S6-C**) of 0.3 and 1.7 for TMPyP4 and Phen-DC_3, respectively, expressing thus their lack of G4 selectivity. By comparison, the PDS (pink boxes, **Figure 25**) demonstrated a great (ΔFI = -116.3 at 5 mol. equiv.) and selective (S= 6.3 at 5 mol. equiv.) G4-stabilization, making it the best real G4-stabilizer from this series. TPPS and PhpC (yellow and orange boxes, respectively, **Figure 25**) were found to efficiently destabilize G4, with ΔFI = 94.2 and 93.8 at 1 mol. equiv., respectively, an effect that disappears for TPPS (ΔFI= 11.3) at 5 mol. equiv., but was maintained with PhpC (ΔFI = 71.8). TPPS displayed the same dose-dependent effect on the Non G4-strand (**Figure 25-B**, resulting in a S value of -0.2 at 5 mol. equiv.), while PhpC had no effect on this control (ΔFI = 34.7, S= 2.1 at 5 mol. equiv.). Although subtle, the G4-destabilizing effect of PhpC is here confirmed.

Driven by curiosity, other small molecules were assessed through this qPCR Stop assay at a single dose (5 mol. equiv.): 1,5-BisNPO, 2,6-BisNPO, 2,7-BisNPN, BRACO-19 and TEGPy. The results obtained allow for ranking them in four categories: *i.* the mild G4-stabilizer 2,7-BisNPN (**Figure S13-G**, ΔFI= -14.7, **Table S7**), *ii.* the strong G4-stabilizer TEGPy (**Figure S3-C** ΔFI= -48.7), *iii.* the mild G4-destabilizer 2,6-BisNPO (**Figure S12-C**, ΔFI= 20.3) and *iv.* the strong G4-destabilizers 1,5-BisNPO and BRACO-19 (**Figure S11-G** and **Figure S9-C**, ΔFI= 44.3 and 48.7, respectively). All these results will be further discussed in the next section.

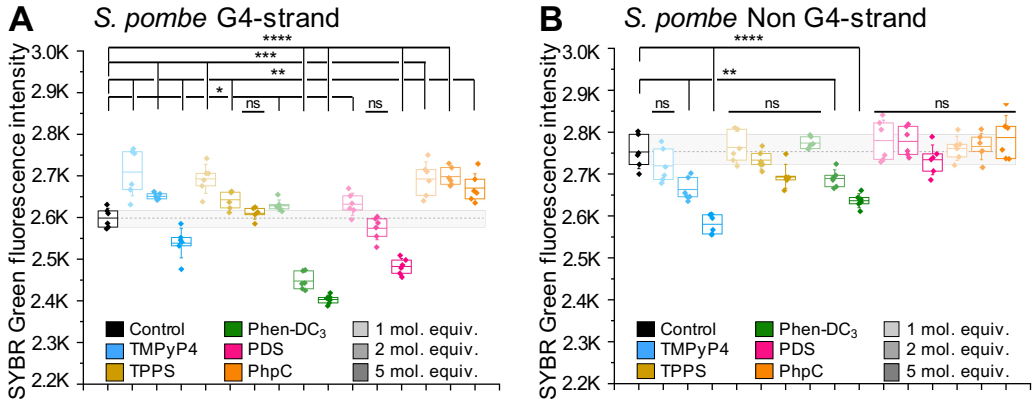

Figure 25. qPCR Stop assay results obtained with 5 small molecules. The qPCR Stop assay was performed with the *S. pombe* (**A**) G4-strand or (**B**) Non G4-strand, without (*i.e.*, SYBR Green FI Control, ON only with the KCl) or with a small molecule (TMPyP4 in blue, TPPS in yellow, Phen-DC_3 in green, PDS in pink, PhpC in orange) at 3 different concentrations: 1, 2 and 5 mol. equiv. (from light to dark hue). Mean FI values calculated correspond to the FI value at the 33th (and last) qPCR cycle. Error bars represent SD from the mean for six independent experiments. For statistical hypothesis tests, Student's *t*-test and Welch's unequal variances *t*-test were used depending on variances equality. * $p < 0.05$, ** $p < 0.01$, *** $p < 0.001$, **** $p < 0.0001$.

Collectively, these results confirm the G4-destabilizing capacity of both PhpC and TPPS, and the G4-stabilizing properties of Phen-DC_3, TMPyP4 and PDS (which closes the debate about the possible G4-destabilizing properties of TMPyP4).

5. Scoring the *in vitro* results

The screening of 14 small molecules through 5 *in vitro* assays (*i.e.*, G4-UNFOLD assay, FRET-melting assay, CD/UV-Vis titrations, PAGE analysis, qPCR Stop assay) is a long and meticulous task, and comparing the wealth of results collected an even longer task. The common concentration used in these different assays was 5 mol. equiv., which is generally enough to reliably assess a G4-stabilization/-destabilization. With a single concentration (5 mol. equiv., without taking account the replicate experiments), 54 different conditions were tested. In order to make a simple but reliable comparison of all results obtained at 5 mol. equiv., two scores were created: the G4-destabilizing score (G4D) and the G4-stabilizing score (G4S). This scoring had to be proportional and adapted to the different assays to allow the integration of results nuances.

For each technique, a maximal score of 1.0 can be attributed to each small molecules and the type of this score (*i.e.*, G4-destabilizing or G4-stabilizing) will depend on the results obtained and the scoring rules applied (*e.g.*, increment and decrement operators, **Table S8**):

- **(1)** G4-UNFOLD assay: if the strongest G4-stabilizer inhibits totally the c-hTelo hybridization and then the release of the FAM-labelled 15-nt ON too, there will be no FI increase after the addition of c-hTelo and thus the V_0 calculated will be of 0.0 s^{-1}. The mean V_0 of the Control being 51.5 s^{-1} (**Table 4**), the minimum ΔV_0 value is thus -51.5 s^{-1} ($V_{0\,min}$ = 0.0 s^{-1}) and the maximum ΔV_0 will be 51.5 s^{-1} ($V_{0\,max}$ = 103.0 s^{-1}). Small molecules which showed a $-51.5 < \Delta V_0 < 0.0$ s^{-1} will have a G4D score, those between $0.0 < \Delta V_0 < 51.5$ s^{-1} will have a G4S

score proportional to its value (see the exact scoring rules in **Table S8**). The principle is the same for the others *in vitro* techniques.

- **(2)** qPCR Stop assay: if the strongest G4-stabilizer inhibits totally the *Taq* polymerase replication of the G4-strand, there will be no SYBR Green FI increase above the initial FI value (*i.e.*, the FI at the first qPCR cycle) and thus the FI will be of 2200.0. The mean FI of the Control being 2598.8 (**Table S6**), the minimum ΔFI value is thus -398.8 (FI_{min} = 2200.0) and the maximum ΔFI will be 398.8 (FI_{max} = 2997.6). We will thus apply the same graduated scoring for G4-stabilizers as G4-destabilizers.

- **(3)** FRET-melting assay: if the strongest G4-destabilizer denatures totally the G4 at room temperature (25 °C), the FAM emission will not be quenched and will reach its maximal FI at 25 °C (the minimum temperature in the FRET-melting program). The T_{max} but also the $T_{1/2}$ will be thus 25.0 °C. The mean $T_{1/2}$ of the Control being 50.6 (**Table S2**), the minimum $\Delta T_{1/2}$ value is thus -25.6 ($T_{1/2\ min}$ = 25.0 °C) and the maximum $\Delta T_{1/2}$ will be 25.6 ($T_{1/2\ max}$ = 76.2 °C). We will thus apply the same graduated scoring for G4-stabilizers as G4-destabilizers.

- **(4)** CD titration: if the strongest G4-destabilizer denatures totally the G4, the CD peak at 293 nm will totally decrease until 0 mdeg, corresponding to a minimum CD variation of -100% (CD_{min} = 0.0 mdeg). The maximum CD variation will be thus 100% (CD_{max} = Mean CD of Control*2 mdeg). For this assay, the mean CD of Control depends on the small molecule titrated (**Table S3**).

- **(5)** PAGE experiments: for this assay, we cannot only rely on numeric values only but we also have to take the band physical aspect into consideration. The total decrease of the SYBR Gold FI of the G4 band to 0.0 will correspond to a minimum FI variation of -100% (FI_{min} = 0.0). However, when using the same amount of G4 for the Control experiments, the FI cannot increase and a FI variation of 100% is impossible. We thus used an unidirectional FI variation for G4-destabilizers and -stabilizers, and discriminate them using another parameter*:* if a small molecule stabilizes the G4, the apparent molecular size of the G4 band can either remain unchanged, decrease (appearance of a lower band) or disappear (aggregation), while a small molecule that destabilizes G4 could trigger an increase of the band size (appearance of an upper, or shifted band). On this basis, we will ascribe a G4-stabilizing score (*scenario* n° 1) or a G4-destabilizing score (*scenario* n° 2).

For each of these techniques, the variations in the results obtained (*e.g.*, ΔV_0, ΔFI, $\Delta T_{1/2}$, CD variation (%) and FI variation (%)) allow for assigning a G4S (G4-stabilizing) or a G4D (G4-destabilizing) score to each small molecule, with a possible decrement of -0.1 if the value is comprised into the SD values of the Control reference (see the exact scoring rules in **Table S8**).

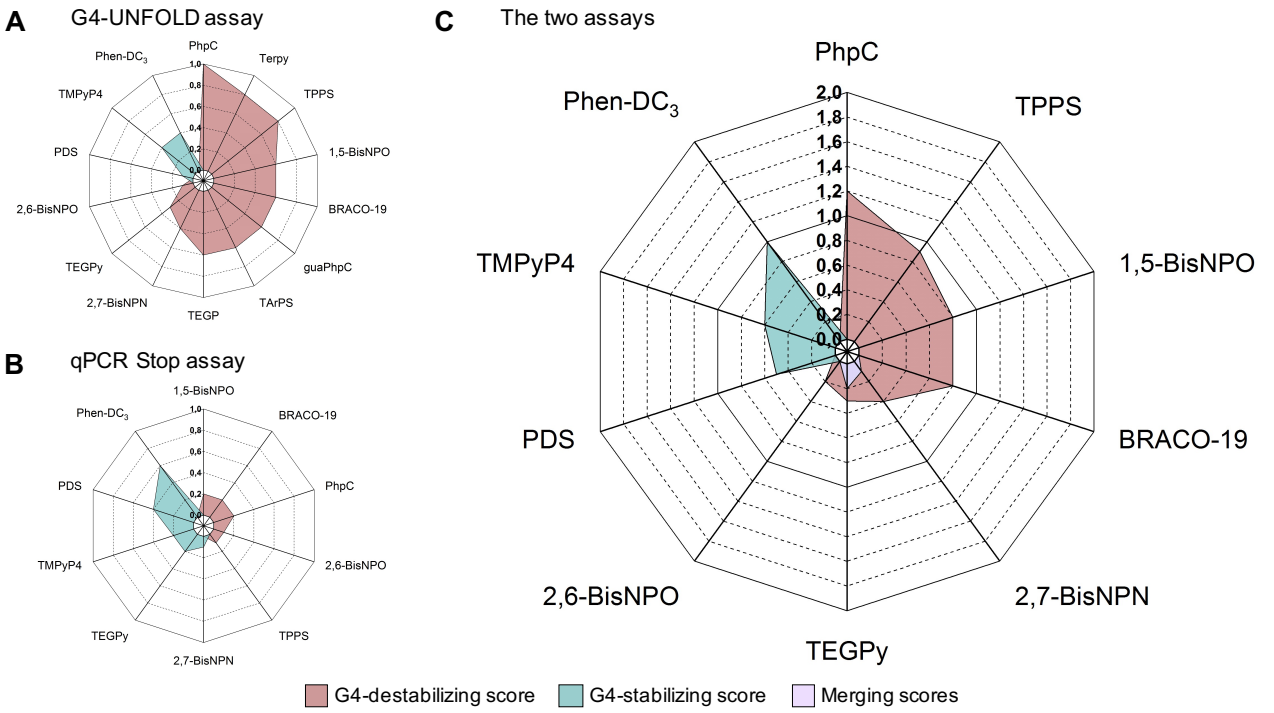

Figure 26. Radar plots of the G4 scores calculated for small molecules evaluated by G4-UNFOLD and qPCR Stop assays. Several small molecules from the panel of 14 compounds were assessed at 5 mol. equiv. by (**A**) G4-UNFOLD and (**B**) qPCR Stop assays. With the different scoring rules established (**Table S8**), G4-destabilizing (G4D, red box) and G4-stabilizing (G4S, blue box) scores were calculated and assigned to each small molecule in order to study and compare their effect on G4. Here each assay is represented separately with their scores by small molecules. (**C**) Combining the scores calculated for the two assays, a total score is obtained: the small molecules are ranked in starting at the top position and according to G4D score decrease (and then G4S score increase) in a clockwise direction. For a small molecule, the merging score (purple box) corresponds to the shared value between G4D and G4S scores.

We first focused on the G4-UNFOLD results only, collected with 14 small molecules: we observed that the 3 small molecules showing the strongest G4-destabilizing effect are the PhpC, Terpy and TPPS with a G4D score between 0.8 and 1.0 (**Figure 26-A**, **Table S9-A**); the three strongest G4-stabilizers are Phen-DC_3, TMPyP4 and PDS, with a G4S score between 0.1 and 0.4. For the qPCR Stop assay, the 3 strongest G4-destabilizers are 1,5-BisNPO, BRACO-19 and PhpC, with a G4D score of 0.2 (**Figure 26-B**, **Table S9-A**) and the 4 strongest G4-stabilizers are Phen-DC_3, PDS, TMPyP4 and TEGPy with a G4S score between 0.2 and 0.6. Compiling these 2 scores, we obtained the following G4D score ranking: PhpC > TPPS > 1,5-BisNPO = BRACO-19 > 2,7-BisNPN > TEGPy > 2,6-BisNPO > PDS > TMPyP4 > Phen-DC_3 (**Figure 26-C**), PhpC and TPPS being the best G4-destabilizers (G4D = 1.2 and 0.9, respectively) and Phen-DC_3 and TMPyP4 the best G4-stabilizers (G4S = 1.0 and 0.6, respectively). These results being fully in line with what we observed at the end of the five assays, this means that the implementation of the G4-UNFOLD and qPCR Stop assays could be sufficient to determine the G4-stabilizing/-destabilizing capacity of a candidate.

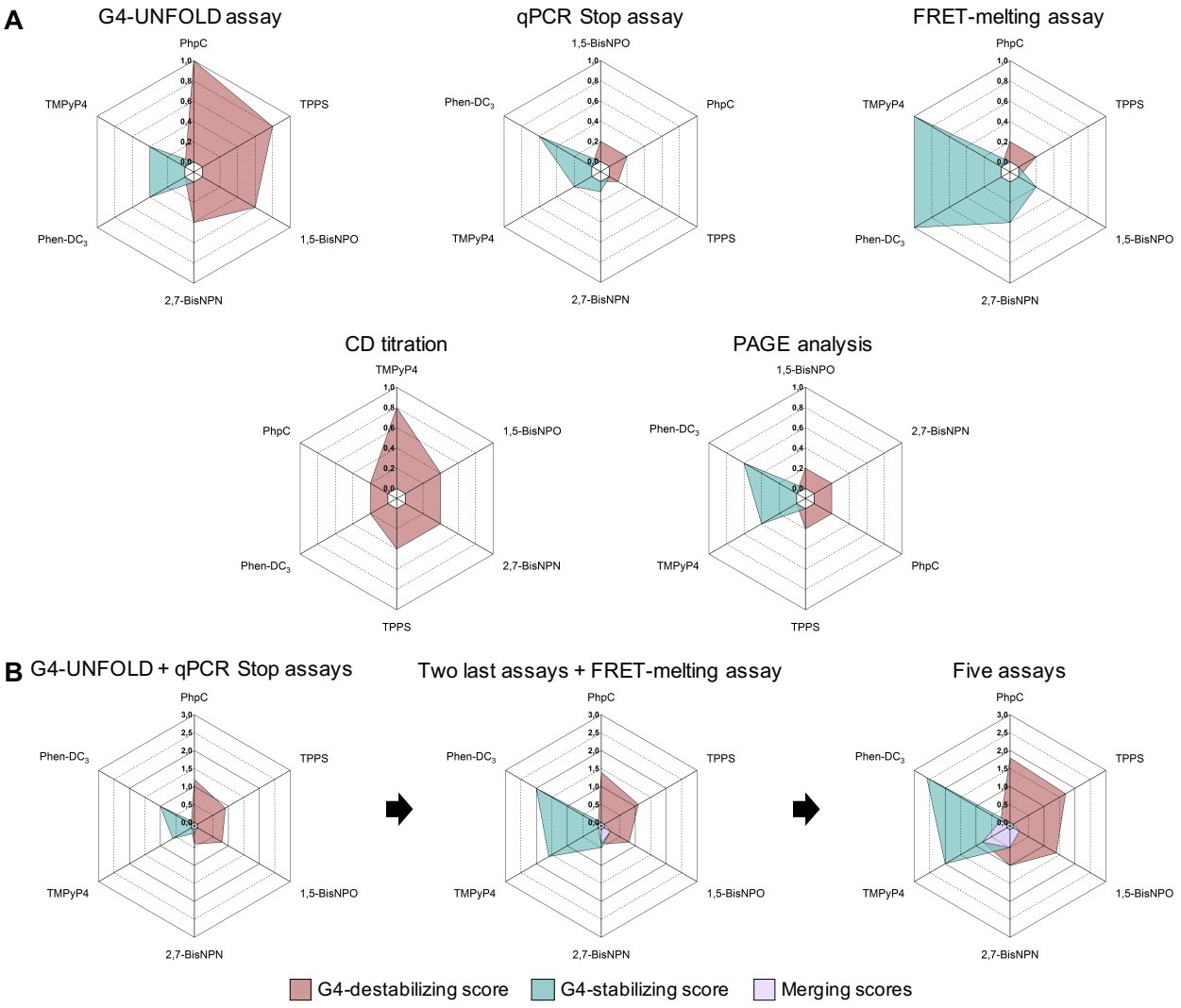

Figure 27. Radar plots of the G4 scores calculated for 6 selected small molecules evaluated by 5 different *in vitro* assays. (**A**) The 6 selected small molecules were assessed at 5 mol. equiv. by 5 *in vitro* assays. With the different scoring rules established (Table S8), G4-destabilizing (G4D, red box) and G4-stabilizing (G4S, blue box) scores were calculated and assigned to each small molecule in order to study and compare their effect on G4. Here each assay is represented separately with their scores by small molecules. (**B**) Combining the scores calculated for 2 (G4-UNFOLD plus qPCR Stop assays, left), 3 (G4-UNFOLD, qPCR Stop plus FRET-melting assays, middle) or 5 assays (right), several total scores are obtained for the 6 small molecules. The small molecules are ranked in starting at the top position and according to G4D score decrease (and then G4S score increase) in a clockwise direction. For a small molecule, the merging score (purple box) corresponds to the shared value between G4D and G4S scores.

Next, we analyzed the 6 compounds (TMPyP4, TPPS, Phen-DC_3, 1,5-BisNPO, 2,7-BisNPN and PhpC, **Figure 17**) that were assessed by the 5 *in vitro* assays. We confirmed that PhpC and TPPS are the best G4-destabilizers and Phen-DC_3 and TMPyP4 the best G4-stabilizers (**Figure 27-A**). It has to be noted that TPPS and PhpC are the only candidates that display G4D scores exclusively (**Figure S20**), while both Phen-DC_3 and TMPyP4 are the best G4-stabilizers in 4 out of 5 assays, being found inefficient during CD titrations. Given that CD titrations do not provide reliable information, and that PAGE analysis is subjective (that is, bias-prone), we discarded these 2 assays during the score calculations (**Figure 27-B**). We rightly classified 6 small molecules only on the basis of the G4-UNFOLD and qPCR Stop assays results (PhpC > TPPS > 1,5-BisNPO > 2,7-BisNPN > TMPyP4 > Phen-DC_3), but we do believe that the integration of FRET-melting results could be

interesting for a more solid scoring (**Figure 27-B**, **Figure S20**). As an example, the total scores originating from the integration of these 3 assays are: $G4D_{PhpC}$ = 1.4, $G4D_{TPPS}$ = 1.1, $G4D_{1,5\text{-}BisNPO}$ = 0.8, $G4S_{2,7\text{-}BisNPN}$ = 0.5, $G4S_{TMPyP4}$ = 1.6 and $G4S_{Phen\text{-}DC3}$ = 2.0 (**Table S9-B**).

6. Additional evaluations of the PhpC properties

We thus showed the PhpC possesses a good G4-destabilizing capacity (**Figure 26**) and triggers an increase in the apparent molecular size of the hTelo G4 ON (**Figure 20**) while TMPyP4 is mostly a good G4-stabilizer (**Figure 25**) displaying possible and concentration-dependent G4-destabilizing effects, as seen by CD titration (**Figure 19**) and qPCR Stop assay (**Figure 25**), triggering also G4-aggregation, as seen by PAGE (**Figure 20**). To go a step further, we performed Dynamic Light Scattering (DLS) experiments (**Table Mat&Meth 9**): results obtained showed that PhpC seems to decrease the size of the hTelo G4 (from 2.7 nm to 0.8 nm at 5 mol. equiv., orange line, **Figure 28-A**, **Table S10**) while TMPyP4 (blue line) decreases it at 1 mol. equiv. (from 2.7 to 0.7 nm) and increases it at 5 mol. equiv. (up to 1281.3 nm size). The size decrease triggered by PhpC could indeed originate in a G4-destabilization (for example, if PhpC destabilizes the external G-quartet of the G4) but these results are not accurate and must not be over-interpreted. In contrast, the results obtained with the TMPyP4 are much more understandable as it behaves like PhpC at low concentration (as already seen in the qPCR Stop assay) and triggers a strong aggregation at high concentration (in line with PAGE results).

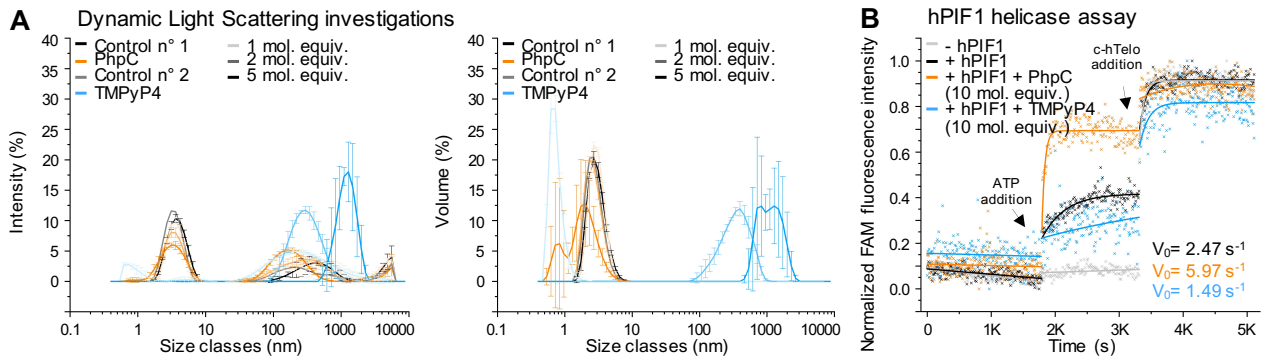

Figure 28. Results obtained with PhpC and TMPyP4 by DLS and hPIF1 helicase assays. (**A**) The DLS investigations were done without (black and grey lines) or with PhpC (orange line) or TMPyP4 (blue line) at 3 different concentrations: 1, 2 and 5 mol. equiv. (from light to dark hue). Results are shown according to the intensity (left) and volume (right) of particles. Error bars represent SD from the mean for three technical replicate experiments. (**B**) The hPIF1 helicase assay was performed without hPIF1 (grey line) and with hPIF1, without (black line) or with PhpC (orange line) or TMPyP4 (blue line) at 10 mol. equiv. concentration. hPIF1 was used at 144 nM. V_0 values calculated correspond to the slope from the linear fit applied on the five first points after the ATP addition.

We also performed the original hPIF1 helicase assay (**Figure 14**, **Table Mat&Meth 10**) with these two compounds, using the hPIF1 kindly provided by Alexandra Joubert from the laboratory of Jean-Baptiste Boulé (MNHN Paris). The preliminary results obtained (*i.e.*, with 3 experiments with PhpC; only 1 with TMPyP4) confirmed the G4-destabilization of s-hTelo G4 by PhpC at 10 mol. equiv. (with a V_0 sped up of 2.42, 2.23 and 1.54-fold, compared to control, **Figure 28-B**, **Figure S21**, **Table S11**) and the G4-stabilization (or aggregation)

by TMPyP4 at 10 mol. equiv. too (with a V_0 slowed down of 0.60-fold, compared to control). Even if preliminary, these results are important since they show that the interaction that takes place between G4 and PhpC is strong enough to destabilize the G4 but not enough to preclude the processivity of enzymes in charge of G4 unwinding, which is of critical importance for the future cell-based investigations.

Finally, the intrinsic spectroscopic properties of PhpC were exploited: PhpC indeed fluoresces when irradiated at 365 nm, which has been used to investigate its interaction with G4s. These fluorescence titrations showed that increasing concentrations of hTelo do indeed quench the PhpC emission (-14.0% and -36.3% at 1 and 5 mol. equiv., respectively, in 1 mM K^+, **Figure 29-A**, **Table S12**), which originates in a close interaction, and that this quench is mitigated by increasing concentrations of K^+ (-36.3% and -25.3% in 1 and 100 mM K^+, respectively, at 5 mol. equiv.). This correlation between PhpC FI quench and K^+-induced G4-stabilization (R^2 = 0.962 linear correlation, **Figure 29-B**), compared to the lack of quenching effect by GMP under identical experimental conditions, suggest the interaction of the PhpC with the hTelo G4 is more complex than a simple PhpC-guanine interaction, likely involving π-stacking interactions with the top G-quartet.

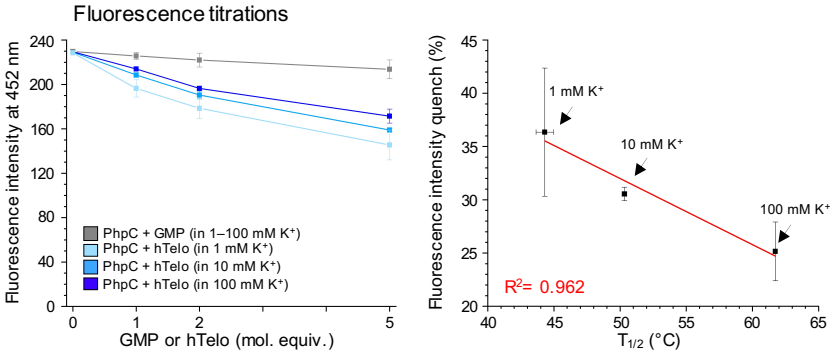

Figure 29. Fluorescence titrations of PhpC with hTelo G4. The fluorescence titrations at 452 nm (left) (and FRET-melting assay, right) were performed with PhpC, without or with the presence of the GMP (grey box) or hTelo (blue box) at 3 different concentrations of K^+: 1, 10 and 100 mM (from light to dark blue). For the FI quench, FI titration values at 5 mol. equiv. were used as well as $T_{1/2}$ values obtained with the hTelo alone in FRET-melting assay. Error bars represent SD from the mean for two technical replicate experiments.

II. New uses of the two *in vitro* screening assays

1. Improvement of the qPCR Stop assay

The qPCR Stop assay was developed with the *S. pombe* G4-1 motif by Jamroskovic *et al.*[83] The G4-strand used herein possesses a G4 sequence that is different from the others used throughout our in vitro investigations, notably from hTelo G4. The *S. pombe* G4-1 motif (orange sequence, **Figure 30**) was thus changed for hTelo (blue), *c-MYC* (pink) or *c-KIT2* (green) G4 sequences leading to the hTelo qSa (for "qPCR Stop assay"), *c-MYC* qSa and *c-KIT2* qSa ONs, respectively (**Figure 30**, **Figures Mat&Meth 3-4**, **Tables Mat&Meth 1-3**), whose the G4 stability was assessed by FRET-melting assay (**Figure S22**). A scrambled version of each of these G4 was also designed: Sc hTelo qSa, Sc *c-MYC* qSa and Sc *c-KIT2* qSa, in which some guanines of G-tracts were changed

for adenines or thymines. These ONs sharing the same 3' end sequence complementary to the G4-1 reverse primer sequence, this last primer was used for the qPCR Stop assay with the new templates.

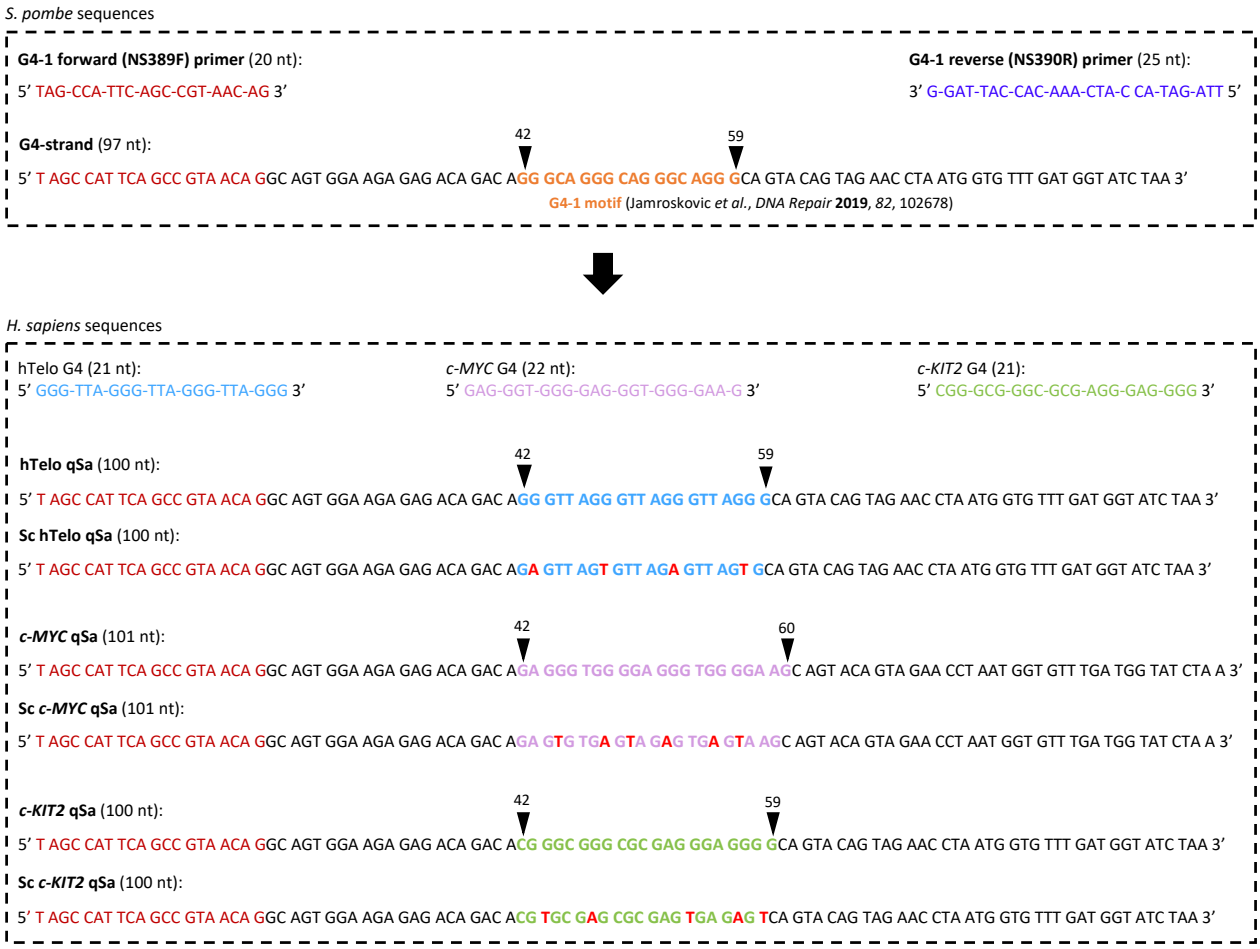

Figure 30. Adaptation of the qPCR Stop assay ONs for *H. sapiens* G4 sequences study. In the aim of developing new qPCR Stop assay templates based on *H. sapiens* G4s, the hTelo, *c-MYC* and *c-KIT2* G4 sequences were introduced in place of the *S. pombe* G4-1 motif into the long G4-strand ON to create the hTelo qSa, *c-MYC* qSa and *c-KIT2* qSa ONs. Scrambled versions were also made in replacing some guanine of the G-tracts, leading to the Sc hTelo qSa, Sc *c-MYC* qSa and Sc *c-KIT2* qSa ONs. All these ONs still possess the same 3' end sequence allowing the use of the G4-1 reverse primer for all of them.

These new qPCR Stop assay G4 templates were used with the best prototypes of G4-destabilizer, *i.e.*, PhpC (orange boxes, **Figure 31**) and G4-stabilizer PDS (pink boxes). Results obtained with the hTelo qSa and *c-KIT2* qSa were similar to that obtained with *S. pombe* G4-strand, with ΔFI_{PhpC} = 101.0 and ΔFI_{PDS} = -63.3 with hTelo qSa (at 5 mol. equiv., **Figure 31-A**, **Table S13-A**), ΔFI_{PhpC} = 107.0 and ΔFI_{PDS} = -138.3 with *c-KIT2* qSa (at 5 mol. equiv., **Figure 31-C**, **Table S13-A**) and ΔFI_{PhpC} = 71.8 and ΔFI_{PDS} = -116.3 with G4-strand (at 5 mol. equiv., **Figure 25**, **Table S6-A**). However, PDS was found to interact with Sc hTelo qSa control, which was not observed with the *S. pombe* templates. The *c-MYC* qSa was not a good template (**Figure 31-B**) likely because the control FI (black boxes) is really low compared to the controls of the others qSa ONs ($FI_{control}$ = 2961.0, 2441.8 and 2916.5 for hTelo qSa, *c-MYC* qSa and *c-KIT2* qSa, respectively, **Figure 31-A**), which could be attributed to a very stable G4 structure that strongly hampers the *Taq* polymerase processivity. This

explanation is possible but rather speculative at present and, without further investigations, the *c-MYC* qSa should not be used as template in this assay.

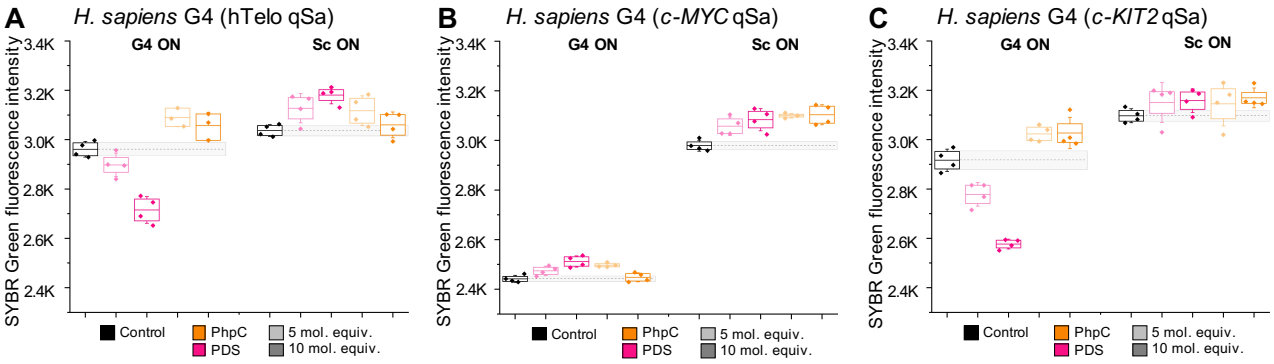

Figure 31. qPCR Stop assay results obtained with PhpC and PDS with *H. sapiens* G4 motifs. The qPCR Stop assays were performed with the *H. sapiens* (**A**) hTelo qSa, Sc hTelo qSa, (**B**) *c-MYC* qSa, Sc *c-MYC* qSa, (**C**) *c-KIT2* qSa, Sc *c-KIT2* qSa without (*i.e.*, SYBR Green FI Control, ON only with the KCl), with PhpC (orange) or PDS (pink) at 2 different concentrations: 5 and 10 mol. equiv. (from light to dark hue). Mean FI values calculated correspond to the FI value at the 33th (and last) qPCR cycle. Error bars represent SD from the mean for one experiment.

2. Application of the two adapted *in vitro* screening assays for the evaluation of PhpC derivatives

To confirm the promising results obtained with PhpC, our Canadian collaborator Robert H. E. Hudson (London, Ontario, CA) sent us 3 PhpC derivatives simply referred to as derivative n° 1, n° 2 and n° 3 (**Figure 32**). These molecules are characterized by a lack of the -O(CH$_2$)$_2$NH$_2$ amino sidechain (n°1), by 2 amino sidechains in the ortho positions (n°2), and a C->N modification within the molecule core (n°3).

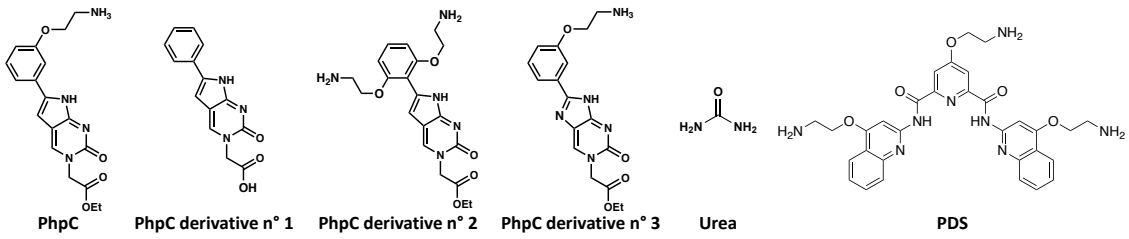

Figure 32. Chemical structures of PhpC derivatives, urea and PDS studied by G4-UNFOLD and qPCR Stop assays with *H. sapiens* hTelo G4.

The properties of these 3 PhpC derivatives plus 3 controls (PhpC, PDS and urea, a well-known denaturing agent) were assessed by both the G4-UNFOLD (using the s-hTelo G4 ON) and qPCR Stop assays (using hTelo G4, **Figure 33**, **Figures S23-S26**). As expected, PhpC (orange box, **Figure 33-A**) and PDS (pink) showed G4-destabilizing (ΔV_0 = 40.1 s^{-1}, **Table S14**) and G4-stabilizing (ΔV_0 = -32.1 s^{-1}) effects, respectively, *via* G4-UNFOLD assay. Quite pleasingly, the urea, used here to mimick G4-destabilizers, was indeed found to be an efficient destabilizer (light green, ΔV_0= 54.5 s^{-1}). The 3 new PhpC derivatives had a well measured G4-destabilizing effect as well, but a bit smaller than that of PhpC (ΔV_0 = 31.2, 37.0 and 23.5 s^{-1} for the derivative

n° 1 (burgundy), n° 2 (blue) and n° 3 (dark green), respectively). With the qPCR Stop assay (**Figure 33-B**), results were fairly similar with a high G4-destabilizing properties for both PhpC (ΔFI = 101.3, **Table S14**) and urea (ΔFI = 97.1), a good G4 stabilization for PDS (ΔFI = -15.3), even if rather weak here, and excellent to fair G4 destabilization for derivative n° 3 (ΔFI = 165.8), n° 2 (ΔFI = 91.4) and n° 1 (ΔFI = 69.3). These good results were confirmed (once) with a qPCR Stop assay performed with *S. pombe* G4-strand: the 2 references PhpC and PDS display normal effects (ΔFI= 176.0 and -204.7 at 5 mol. equiv., respectively, **Figure S27-A**, **Table S15**), derivatives n° 1 and 2 behave as G4-destabilizers (ΔFI = 95.7 and 55.3 at 5 mol. equiv., respectively), while the results obtained with derivative n° 3 were more puzzling (ΔFI = -17.2 at 5 mol. equiv.). These results must be confirmed by repeating the experiments.

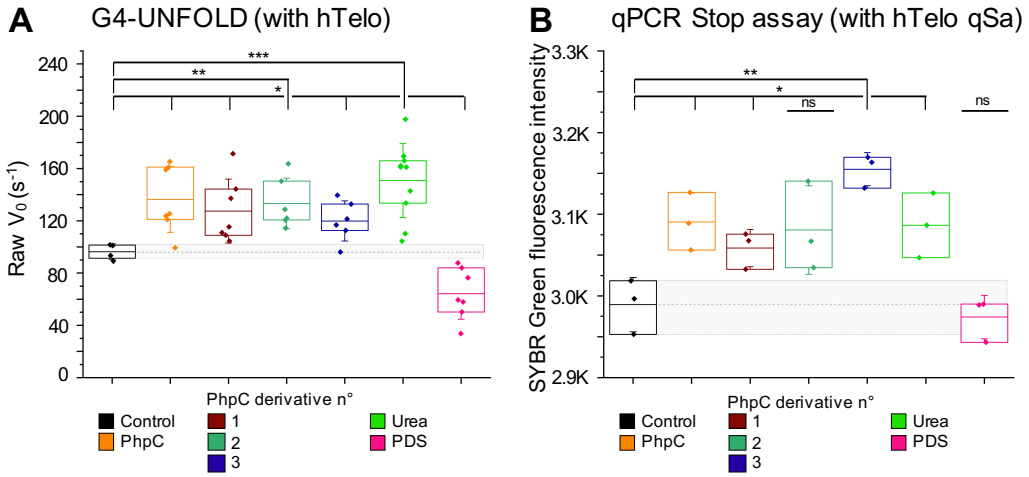

Figure 33. Results obtained with PhpC derivatives by G4-UNFOLD and qPCR Stop assay on human hTelo G4. (**A**) The G4-UNFOLD assay was performed with the s-hTelo ON, without (*i.e.*, V_0 Control, ON only in 20 mM Tris-HCl, 10 mM $MgCl_2$, 1 mM KCl, 99 mM NaCl, pH 7.2) or with small molecules at 5 mol. equiv. concentration. Mean V_0 values calculated correspond to the slope from the linear fit applied on the first five first points after the c-hTelo addition. Error bars represent SD from the mean for at least four independent experiments. (**B**) The qPCR Stop assay was performed with the *H. sapiens* hTelo qSa, without (*i.e.*, SYBR Green FI Control, ON only with the KCl) or with small molecules at 5 mol. equiv. concentration. Mean FI values calculated correspond to the FI value at the 33th (and last) qPCR cycle. Error bars represent SD from the mean for three independent experiments. (**A-B**) The small molecules used here are PhpC (orange box), PhpC derivative n° 1 (burgundy), n° 2 (dark green), n° 3 (dark blue), urea (light green) and PDS (pink). For statistical hypothesis tests, Student's *t*-test and Welch's unequal variances *t*-test were used depending on variances equality. * $p < 0.05$, ** $p < 0.01$, *** $p < 0.001$, **** $p < 0.0001$.

The scoring of these small molecules (**Table S16**) and the corresponding radar plots (**Figure 34**) confirm the G4-stabilizing ability of PDS (G4S = 0.5, **Figure 34-C**, **Table S17**) and the G4-destabilizing capacities of the 3 PhpC derivatives ($G4D_{n°1}$ = 0.6, $G4D_{n°2}$ = 0.6, $G4D_{n°3}$ = 0.8) with a slightly better capacity for derivative n° 3 which reaches the performances of PhpC (G4D = 0.8) and urea (G4D = 0.8). Quite interestingly, although urea is not a G4-destabilizer *per se* but a denaturing agent, the similarity of its effect with PhpC in these two *in vitro* assays makes it a potential G4-destabilizer reference for the development and/or the calibration of others assays aiming at identifying new G4-destabilizers.

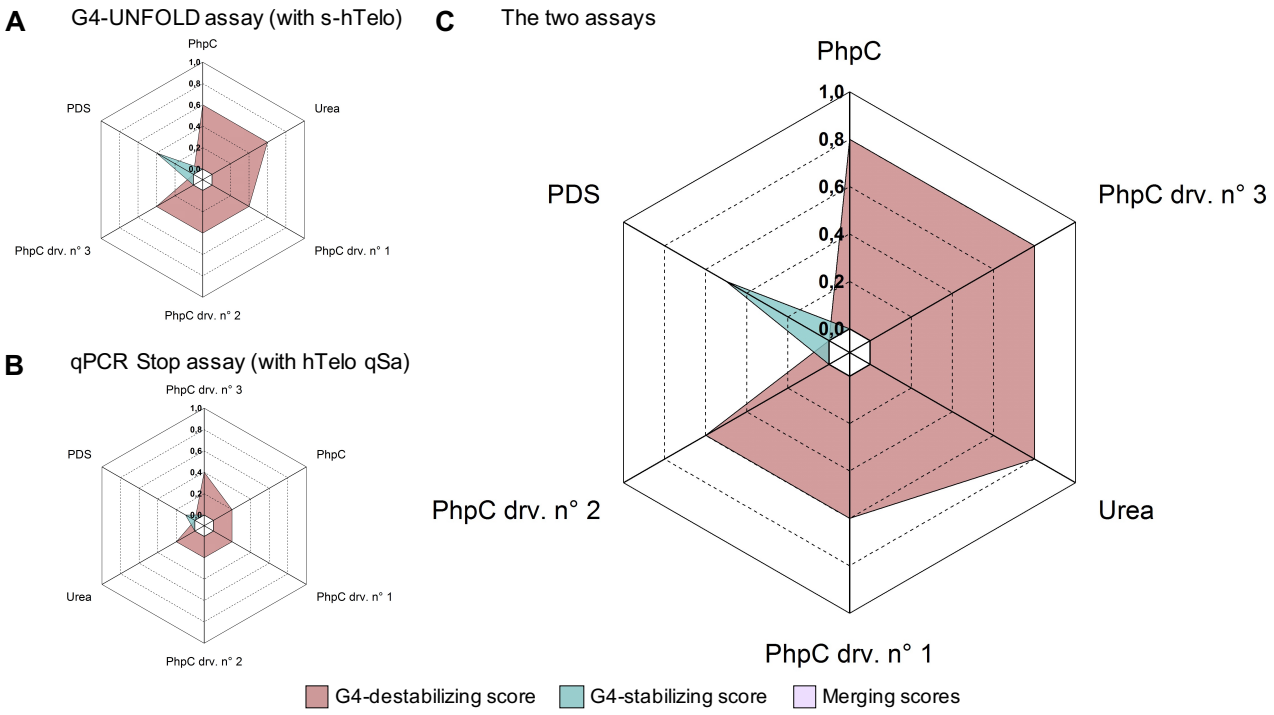

Figure 34. Radar plots of the G4 scores calculated for PhpC derivatives assessed by G4-UNFOLD assay and qPCR Stop assay with the *H. sapiens* hTelo qSa. The small molecules were assessed at 5 mol. equiv. by (**A**) G4-UNFOLD assay and (**B**) qPCR Stop assay with the *H. sapiens* hTelo qSa. With the different scoring rules established and adapted (Table S16), G4-destabilizing (G4D, red box) and G4-stabilizing (G4S, blue box) scores were calculated and assigned to each small molecule in order to study and compare their effect on G4. Here each assay is represented separately with their scores by small molecules. (C) In adding the scores calculated for the two assays, a total score is obtained for the small molecules. The small molecules are ranked in starting at the top position and according to G4D score decrease (and then G4S score increase) in a clockwise direction. For a small molecule, the merging score (purple box) corresponds to the shared value between G4D and G4S scores.

C. Discussion and perspectives about the project outcomes

Solid results were obtained *via* both fluorescence-based (G4-UNFOLD and FRET-melting assays), enzyme-based assays (*Taq* polymerase for qPCR Stop assay and hPIF1 for the G4 helicase assay), and physico-chemical assays (CD/UV-Vis titrations, PAGE analysis, DLS investigations and fluorescence titration). They showed the constant and reliable G4-destabilizing capacity of small molecules including PhpC, TPPS and 1,5-BisNPO, PhpC being the best and more selective G4-destabilizer. Despite these good properties, efforts must now be invested to decipher the way this molecule interacts with G4; in the meantime, the use of PhpC in a pathological context (*e.g.*, cancer and neuropathology) is being investigated.

This study also allowed for confirming the G4-stabilizing properties of Phen-DC_3, TMPyP4 and PDS. TMPyP4, especially, showed contradictory but interesting effects as it triggers *i.* a G4-destabilization at low concentration in qPCR Stop assay (1 and 2 mol. equiv.) and DLS investigation (at 1 mol. equiv.), *ii.* a G4-stabilization in FRET-melting and hPIF1 helicase assays and at high concentration in qPCR Stop assay (5 mol. equiv.), and *iii.* a G4 aggregation in PAGE and DLS at middle to high concentration (2-5 mol. equiv.). These observations thus confirm the contradictory effects of TMPyP4, regularly documented,[185–187,236,189,190] which makes TMPyP4 an interesting but unreliable G4 ligand. We can also notice that BRACO-19 exhibits strange

effects here notably a quite surprising G4-destabilization highlighted by both the G4-UNFOLD and qPCR Stop assays; we do not have at present satisfying explanations for this effect but we are currently gathering information from the literature that indeed points towards a rather complex, TMPyP4-like behavior. An important part of these results: the development of assays as the assessment of compounds, was reported via a publication in the Journal of the American Chemical Society in 2021.[93]

Two of the *in vitro* assays implemented here, the G4-UNFOLD and qPCR Stop assays, were found to be reliable to assess quickly the G4-stabilizing/-destabilizing properties of series of candidates. Using the scoring rules we developed, these two assays, possibly coupled with FRET-melting assay results, this workflow allows for the systematic evaluation of, and thus an easy comparison between all compounds studied. We do believe that it is now poised to be used as a standard method for the identification of G4-stabilizers/-destabilizers in a quick and reliable manner.

We also upgraded the qPCR Stop assay with incorporation of the *H. sapiens* hTelo qSa G4 sequence and extended our study to 3 new PhpC derivatives, among which the derivative n° 3 could be quite interesting. In the future, this workflow will be applied to a library of 20 new PhpC derivatives that have now been synthesized by R. Hudson (London, Ontario, CA), with the hope of finding an even more efficient G4 destabilizer.

From a technical point of view, the qPCR Stop assay (with the *S. pombe* G4-strand) was also integrated into a new *in vitro* technique allowing to assess the properties of molecules used a G4-baits. Indeed, in collaboration with Francesco Rota Sperti, another PhD student of our team, we combined an affinity precipitation (pull-down) technique using biotinylated TASQ (see Chapter II) with a qPCR Stop assay to create what we called the qPCR pull-down assay: this technique comprises a pull-down step in which the TASQs interact with the G4-strand followed by an affinity precipitation using Streptavidin MagneSphere® Paramagnetic Particles, and then quantification of the precipitation efficiency by a qPCR analysis. This technique allows for assessing the ability of TASQs to precipitate G4s embedded in long DNA sequences; we reported on the corresponding results twice, in 2022 and 2023.[222,223] This technique was recently extended by Dr Angélique Pipier, still from our team, for the isolation and identification of another nucleic acid alternative structure, the three-way junctions (TWJ).

Chapter II – Study of the cellular dynamics of G-quadruplexes by optical imaging

A. Introduction to the chapter II

The relationship between DNA damage and higher-order DNA structure stabilization is currently undergoing in our group for another type of non B-DNA structure, the three-way junctions (TWJ), and related TWJ ligands (*e.g.*, TrisNP).[244,245] Such a relationship has already been established for G4s: pioneering investigations have indeed established that G4 ligands (*e.g.*, CM03, CX-5461, EMICORON, PDS, TMPyP4) do trigger DNA damage efficiently (induction of 53BP1, γH2AX or MDC1 *foci*). The G4 ligand PDS was massively used to promote DNA damage at G4 sites: 1/ Rodriguez *et al.* (2012)[172,111] reported a 8.5-fold increase of γH2AX positive MRC5-SV40 cells (from ~10% to ~85%), 2/ Zimmer *et al.* (2016)[246] a 2.5-fold increase of HEK293T cells with > 4 γH2AX *foci* (from ~4 to 10% cells), 3/ Moruno-Manchon *et al.* (2017)[247] a ~1.6-fold increase of 53BP1 *foci* in primary cortical neurons, 4/ Pipier *et al.* (2021)[248] a 4.5-fold increase of γH2AX *foci* in HeLa cells and 5/ Bossaert *et al.* (2021)[249] a 1.5/11.1-fold increase of γH2AX *foci* in HeLa cells. These results thus confirm the existence of PDS-induced DNA damage sites and thus, the involvement of G4s at these genomic sites. The G4 ligand CX-5461 showed an even more pronounced capacity to induce DNA damage, with a 35.0- and 6.5-fold increase in HCT116 cells with > 4 γH2AX *foci* (from ~2 to 70% cells) and > 2 53BP1 *foci* (from ~10 to 65%) (Xu *et al.*, 2017),[174] respectively, and a 2.5/13.1-fold increase in γH2AX *foci* in HeLa cells (Bossaert *et al.*, 2021).[249] Other G4 ligands have been more sparingly studied: a 1.5-fold increase in γH2AX positive cells/mm^2 tumor section (from 11 to 17) in a metastatic lymph node tissue, a 3.8-fold increase in γH2AX *foci* in primary cortical neurons and a 1.9-fold increase in 53BP1 *foci* per nucleus (from 11 to 21) in PANC-1 cells were obtained after a treatment with EMICORON (Porru *et al.*, 2015),[250] TMPyP4 (Moruno-Manchon *et al.*, 2017)[247] and CM03 (Marchetti *et al.*, 2018),[251] respectively. This results again confirm that G4s are likely related to DNA damage sites.

Quite surprisingly however, the co-localization of DNA damage sites (53BP1, γH2AX, MDC1 or TOP2Acc *foci*) and G4 sites (with BG4 or 1H6 G4-specific antibodies) has only been marginally reported and precisely quantified in the literature: 1/ no significant effect of PDS on BG4/1H6-γH2AX *foci* in U2OS cells or of γ-irradiation on 1H6/γH2AX-53BP1-MDC1 *foci* in HeLa and HaCaT were noticed by Lee *et al.* (2021)[252] and Komurkova *et al.* (2021),[253] respectively; 2/ a qualitative relationship only was established between BG4 and γH2AX *foci* in MCI lymphocytes by François *et al.* (2016);[254] 3/ a great co-localization between BG4 and 53BP1 *foci* (1, 15 and 17% of co-localized *foci* per nucleus in untreated, CX-3543- and PDS-treated HCT116 cells, respectively, 3 and 6 co-localized *foci* per nucleus in untreated and CM03-treated PANC-1 cells, respectively) was reported by Xu *et al.* (2017)[174] and Marchetti *et al.* (2018);[251] and 4/ an important co-localization between BG4 and TOP2Acc *foci* (with 5.5, 14.4 and 12.5% of co-localized *foci* per nucleus in untreated, CX-3543- and

PDS-treated HeLa cells, respectively) was also reported by Bossaert *et al.* (2021).[174] Globally, the G4 and DNA damage sites were found to co-localized with a significant increase under G4 ligand treatment.

Remarkably, chemical G4 probes have not been used for the detection of G4 sites in these studies, despite the number and diversity of available probes (*e.g.*, QUMA-1, N-TASQ, PDS-α, Phen-DC_3-alk).[111,206,212,219] Two home-made molecules, the biotinylated TASQs BioTASQ and BioCyTASQ, were previously used to visualize G4s in cells using the so-called pre-targeting G4 imaging approach;[220] we thus decided to develop a strategy for studying the co-localization of TASQ *foci* (that is, G4 sites *bone fide*) and γH2AX *foci* (that is, DNA damage sites).

B. Project organization and implementation

I. G-quadruplexes localization by biotinylated TASQs and their involvement in DNA damage

1. G-quadruplexes and γH2AX marker localization and quantification in cells

We decided to use 2 recent G4 probes BioCyTASQ (BCT) and BioTriazoTASQ (BTT) for localizing G4 in cells (**Figure 13**). The antiproliferative properties of BCT was first assessed by the Sulforhodamine B (SRB) cytotoxicity assay (of note, the choice of the final SRB protocol is discussed in the next Chapter) (**Figure Mat&Meth 7**, **Table Mat&Meth 11**), which showed that this TASQ, like all other TASQs, has no cytotoxicity (with a IC_{50} = 386.3 ± 89.7 µM, blue box, **Figure S28**, **Table S18**, **Table S19**); we assumed that it is also the case for BTT.

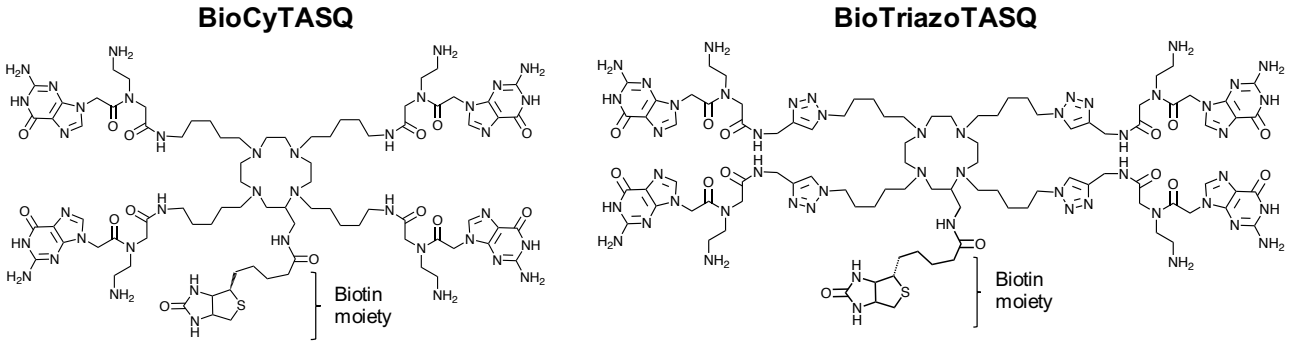

Figure 35. Chemical structures of the two biotinylated G4 probes used within cells, BioCyTASQ and BioTriazoTASQ.

Our idea was to benefit from the versatility of the biotinylated TASQs for optical imaging purposes using the biotin moiety to label the TASQ/G4 complexes *in situ via* its association with a streptavidin-Cy3 (SA-Cy3) fluorophore ($\lambda_{exc\ max}$ = 553 nm, $\lambda_{em\ max}$ = 566 nm, **Figure S29**, **Table S20**). This approach, referred to as pre-targeting G4 imaging, turned out to be quite efficient: indeed, BCT was found to accumulate mostly into the nucleoli and in the cytosol in a more discrete manner (**Figure S30**). To gain insights into a possible co-localization of DNA damage and G4 sites, MCF7 cells were fixed in methanol, incubated with a mixture of TASQ (10 µM, 16 h, at 4 °C) and anti-γH2AX primary IgG (1 µg/mL), then with a mixture of SA-Cy3 (1 µg/mL, 45 min, at 25 °C, in dark chamber) and secondary IgG–Alexa Fluor 647 (AF 647; 4 µg/mL). Then, the nuclei

were stained with DAPI (1 µg/mL, 5 min, at 25 °C, in dark chamber) in order to provide multicolor images, the TASQ *foci* in green (**Figure 36**, **Figures S31-S34**), γH2AX *foci* in red and the nuclei *in* blue.

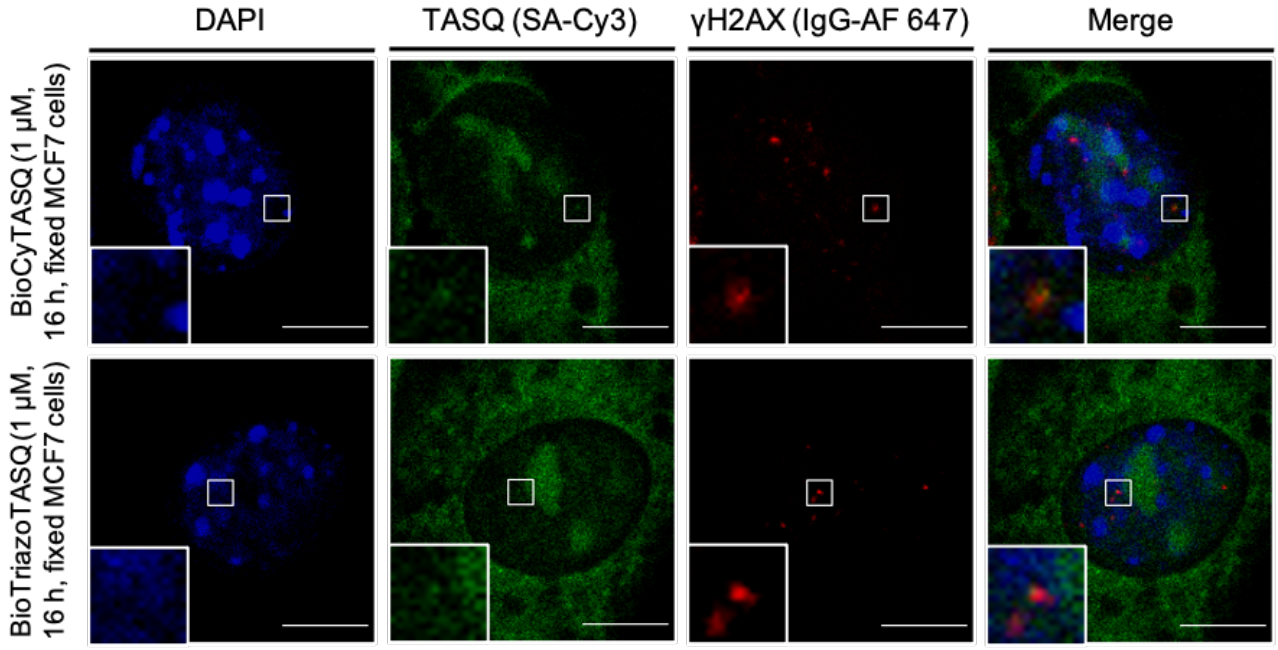

Figure 36. Optical images of MCF7 cells in which G4 sites are labelled with BioCyTASQ and BioTriazoTASQ. Optical imaging was performed with MCF7 cells treated after cell fixation with BioCyTASQ or BioTriazoTASQ (1 µM, 16 h), tagged with SA-Cy3 (green), which is followed by immunodetection of DNA damage nuclear γH2AX *foci* (with IgG-Alexa Fluor 647, red) and chromatin staining by DAPI (blue). Images are representative of the mean number of γH2AX *foci* per nucleus. Insets highlight nucleoplasmic sites where both nuclear TASQ and γH2AX *foci* co-localize. 63x oil objective, then digital magnification plus 3.9x magnification for insets (scale bar = 10 µm).

To exploit these images in a more quantitative manner, a macro program (a co-localization macro program) was developed by Dr. Angélique Pipier (**Table 5**), currently post-doc in our group. The macro-guided analysis was implemented to calculate both the number of TASQ and γH2AX *foci* per nucleus and the number of co-localized TASQ-γH2AX *foci* per nucleus. As a control, we also counted manually the number of the γH2AX *foci* as well as the co-localized TASQ-γH2AX *foci* (thus, the co-localized *foci*) per nucleus in a quite high number of cells (between 172 and 232 cells, **Figure 37-A**) and found a mean number of 4.06, 4.92 and 5.69 γH2AX *foci* per *nucleus* for the Control, BCT- and BTT-treated cells (**Table S21**) and a mean ratio of 2.7 and 2.9% of co-localized *foci*/all γH2AX *foci* per nucleus. On this basis, the macro was adjusted and then implemented it with a higher number of cells (between 719 and 793 cells, **Figure 37-B**): the number of γH2AX *foci* was very close to the manually counted number (4.09, 5.44 and 5.28 γH2AX *foci* per *nucleus* for Control, BCT- and BTT-treated cells, **Figure 37**, **Table S22**), as was the number of co-localized *foci*/all γH2AX *foci* per nucleus (4.0 and 4.9% for BCT- and BTT-treated cells, respectively).

As introduced above, several teams have studied the co-localization between DNA damage sites (53BP1, γH2AX, MDC1 or TOP2Acc *foci*) and G4 sites (with BG4 or 1H6 G4-specific antibodies). As an example, Marchetti *et al.* counted 297 BG4 *foci*, 11 53BP1 *foci* and around 3 co-localized *foci* per nucleus, and then calculated a ratio of 1.0% of co-localized *foci*/all BG4 *foci* per nucleus, and of 27.3% of co-localized *foci*/all

53BP1 *foci* per nucleus. These results are thus 5.6/6.8-fold higher than what we observed with the TASQs. This could be explained by the 10-fold difference in G4 *foci* (~30 TASQ *foci vs.* ~300 BG4 *foci*) and the only 2.2-fold difference in DNA damage sites (~5 γH2AX *foci vs.* 11 53BP1 *foci*). They also observed a 1.9-fold increase in the number of 53BP1 *foci* upon treatment with the G4 ligand CM03, in line with previous reports (see above) notably using PDS. We thus decided to perform similar experiments, live-incubating MCF7 cells with PDS with the hope of increasing number of colocalized G4/DNA damage sites.

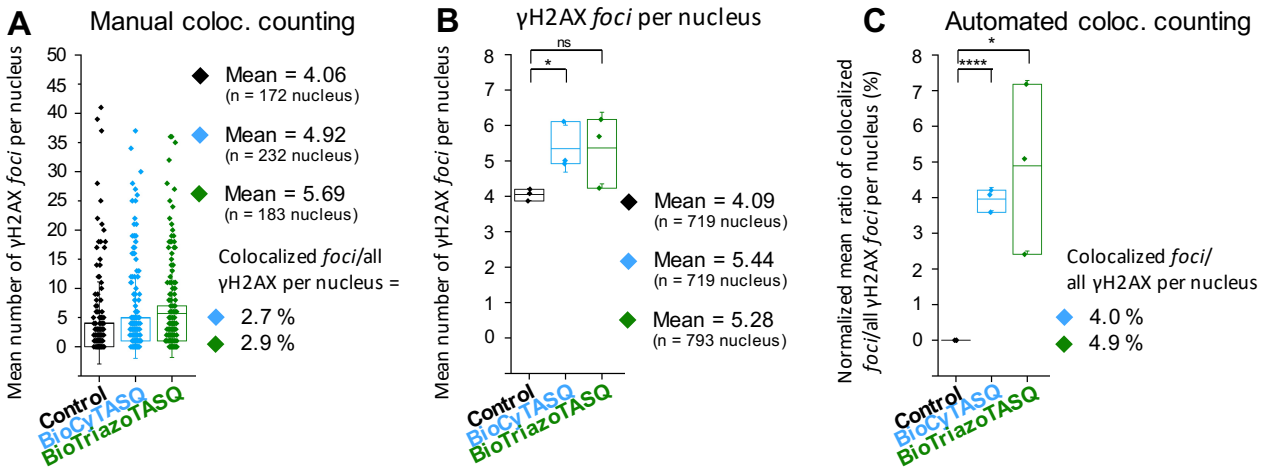

Figure 37. Quantitative results obtained from the optical images acquired with BioCyTASQ and BioTriazoTASQ. The optical imaging was performed with MCF7 cells non-treated (Control; black boxes) or treated after cell fixation with BioCyTASQ (blue) or BioTriazoTASQ (green) (1 µM, 16 h), tagged with SA-Cy3, which is followed by immunodetection of DNA damage nuclear γH2AX *foci* (with IgG-Alexa Fluor 647) and chromatin staining by DAPI. Optical images were processed with the co-localization macro program in order to count nuclei (with the DAPI channel), (**A-B**) nuclear γH2AX *foci* (with the IgG-AF 647 channel) and nuclear TASQ *foci* (with the SA-Cy3 channel). The co-localization of nuclear γH2AX *foci* and nuclear TASQ *foci* was counted (**A**) manually (on 23-32% of cells) and (**C**) automatically with the macro program in order to configure it. Error bars represent SD from the mean for three independent experiments (**B-C**). For statistical hypothesis tests, Student's *t*-test and Welch's unequal variances *t*-test were used depending on variances equality. * $p < 0.05$, ** $p < 0.01$, *** $p < 0.001$, **** $p < 0.0001$. Coloc. = co-localization.

2. Study of the PDS-induced effects on the G-quadruplexes/DNA damage relation by semi-quantitative analysis

PDS (**Figure S35**), contrarily to TASQs, has a strong cytotoxic effect (IC_{50} = 2.40 ± 0.26 µM, **Table S19**) which explained why we limited the live cell incubation time to 6 h at 5 µM concentration (**Table Mat&Meth 9**).

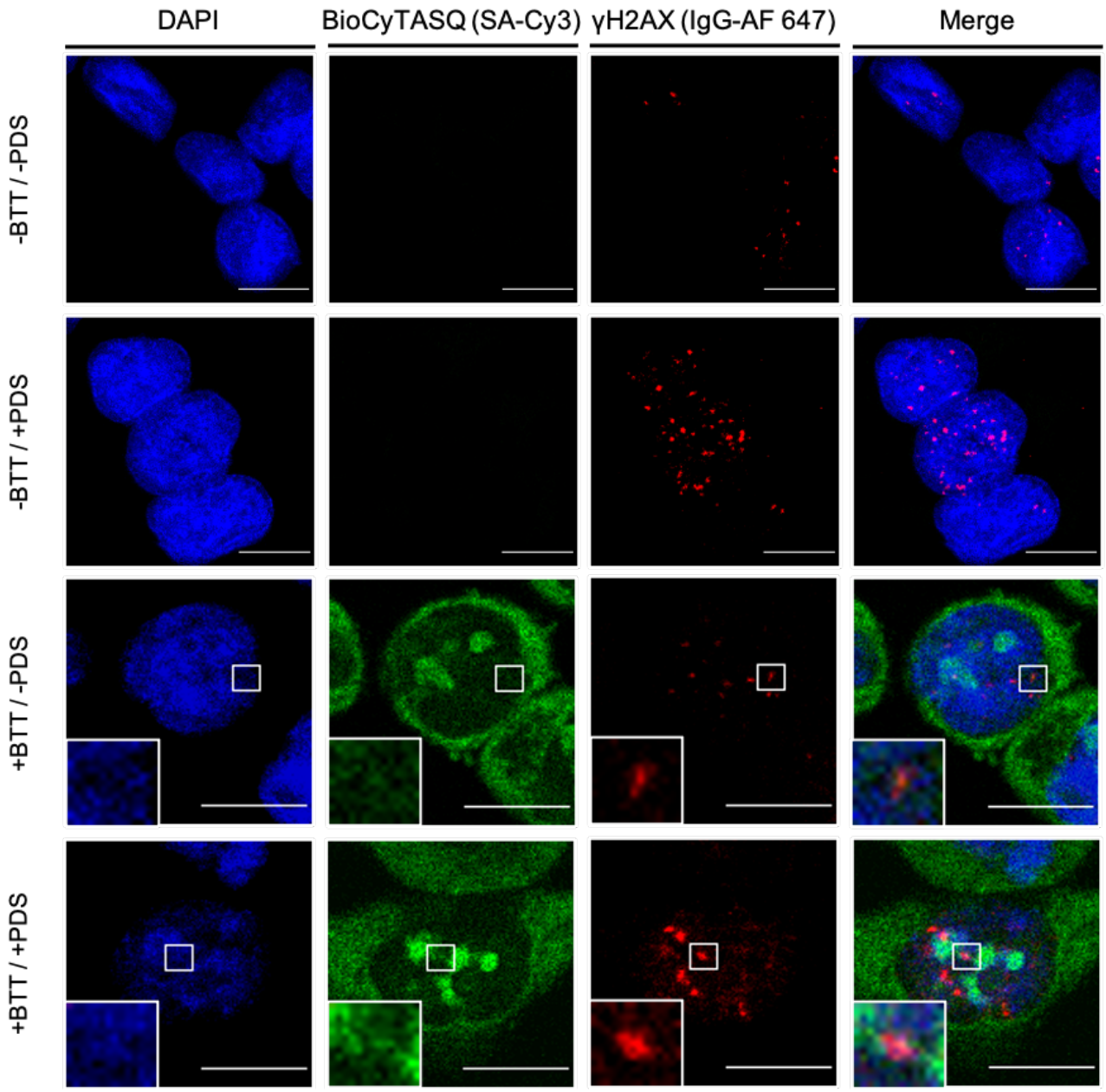

Figure 38. Optical images acquired with BioTriazoTASQ and +/- PDS treatment. Optical imaging was performed with MCF7 cells live treated or not with PDS (+/- PDS; 5 µM, 6 h) and then treated after cell fixation with BioTriazoTASQ (+/- BTT; 1 µM, 16 h), tagged with SA-Cy3 (green), which is followed by immunodetection of DNA damage nuclear γH2AX *foci* (with IgG-Alexa Fluor 647, red) and chromatin staining by DAPI (blue). Images are representative of the mean number of γH2AX *foci* per nucleus. Insets highlight nucleoplasmic sites where both TASQ and γH2AX *foci* co-localize. 63x oil objective, then digital magnification plus 3.9x magnification for insets (scale bar = 10 µm).

Control cells, without or with BTT post-fixation labelling, have a mean number of 4.8 and 4.3 γH2AX *foci* per *nucleus* (Control -PDS and BTT -PDS conditions, respectively, **Figure 38**, **Table S23**) which is consistent with the data previously obtained (above). The live incubation of the Control cells (*i.e.*, without BTT) with PDS increased more than twice this number, with an average of 10.2 γH2AX *foci* per *nucleus* (Control +PDS, **Table S23**) which is in line too with the previously mentioned studies. For cells live treated with PDS and then labelled with BTT, the increase in γH2AX *foci* is yet smaller but still significant (6.4 per *nucleus*).

When comparing cells incubated with BTT, without or with PDS treatment, the increase in γH2AX *foci* is also small but significant (1.49-fold, **Figure 39**, **Table S23**) but more importantly the increase in co-localized

TASQ/γH2AX *foci* per *nucleus* is also significant (1.89-fold). This result indicates the additional γH2AX *foci* triggered by PDS partially occurred at G4 sites, thus providing a straightforward demonstration that stabilized G4s are indeed hotspots for genetic instability. They also show that biotinylated TASQs are interesting molecular tools for this type of investigations, which can be used as reliable surrogates for the BG4 antibody.[223]

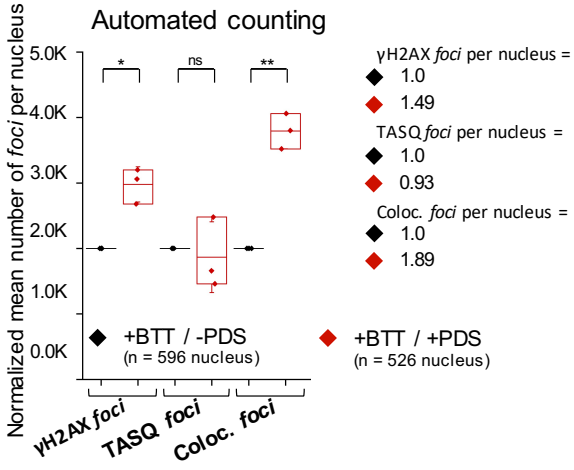

Figure 39. Quantitative results obtained from the optical images acquired with BioTriazoTASQ +/- PDS treatment. Optical imaging was performed with MCF7 cells live treated or not with PDS (+/- PDS; 5 µM, 6 h) and then treated after cell fixation with BioTriazoTASQ (+/- BTT; 1 µM, 16 h), tagged with SA-Cy3, which is followed by immunodetection of DNA damage nuclear γH2AX *foci* (with IgG-Alexa Fluor 647) and chromatin staining by DAPI. Here are shown the +BTT/-PDS control (black boxes) and +BTT/+PDS (red) conditions. Optical images were processed with the co-localization macro program in order to count nuclei (with the DAPI channel), nuclear γH2AX *foci* (with the IgG-AF 647 channel) and nuclear TASQ *foci* (with the SA-Cy3 channel). The co-localization between nuclear γH2AX *foci* and nuclear TASQ *foci* was counted automatically with the macro program. Error bars represent SD from the mean for three independent experiments. For statistical hypothesis tests, Student's *t*-test and Welch's unequal variances *t*-test were used depending on variances equality. * $p < 0.05$, ** $p < 0.01$, *** $p < 0.001$, **** $p < 0.0001$. BTT = BioTriazoTASQ. Coloc. = co-localized.

II. G-quadruplexes localization with smart G4 probe (N-TASQ) and their cellular compartmentalization

The above-described experiments provided interesting insights into several aspects of cellular imaging protocols, including slide preparation and mounting steps, and the development and use of a macro program for the analysis of cell images. As discussed in the Chapter I, the small molecule PhpC showed promising G4-destabilizing capacity *in vitro* and the question about its *in cella* effect is still pending. This demonstration in cells was of particular importance because these investigations were done in parallel with the first attempts of affinity precipitation of G4s in cells in *in vivo*-like conditions *via* the so-called G4RP technique, which will be further discussed in Chapter III. Our first approach was thus more straightforward, assessing whether and how PhpC does modulate G4 landscapes in MCF7 cells by optical imaging using another TASQ, the twice-as-smart G4 probe Naphtho-TASQ (or N-TASQ).

1. Implementation of the N-TASQ use conditions in cellular environment

The highly fluorescent background observed when using the biotinylated TASQ as imaging agents (through a 2-step protocol) is likely due to the presence of endogenous biotin in cells, which can interact with the streptavidin-Cy3 fluorophore. We thus decided to set the biotinylated TASQs aside (using them for affinity purification of cellular G4s; see Chapter III) and explore the possible modulation of G4s in cells using the turn-on fluorescent G4 probe N-TASQ.[212] Indeed, when interacting with a G4, and more particularly its top G-quartet, the four synthetic Gs (in blue, **Figure 40**) of the N-TASQ assemble into a synthetic G-quartet that stacks atop the native G-quartet of a G4 (**Figure 40**). This like-likes-like interaction stabilizes the TASQ/G4 edifice (as for all other TASQs) but in the particular case of N-TASQ, it allows the central template of N-TASQ for being emissive again (**Figure S29**). Briefly, in its open conformation, the fluorescence of the N-TASQ template is quenched by intramolecular photoelectron transfer (iPET) from the four isolated Gs, a transfer that is precluded when the synthetic G-quartet is folded, which thus relieves the fluorescence of the naphthalene core.[212]

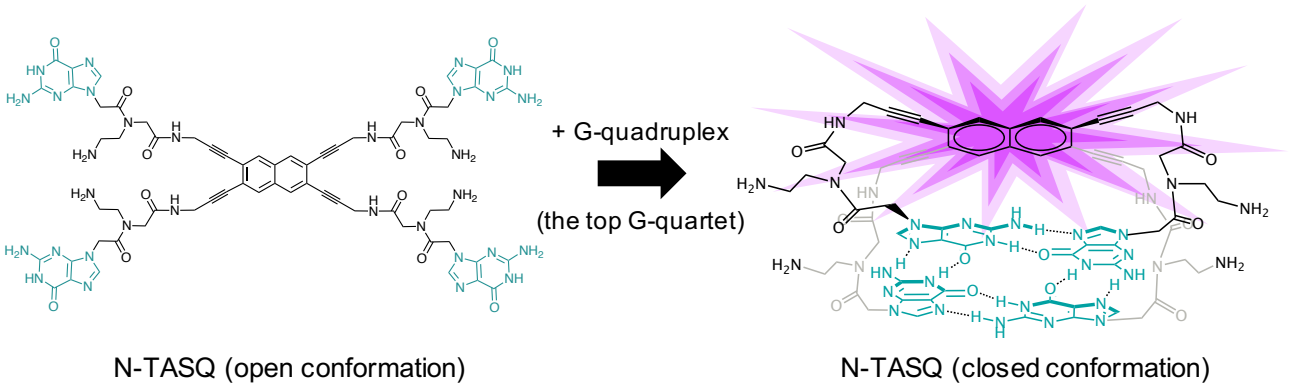

Figure 40. Chemical structure of N-TASQ and schematic representation of its interaction with G4s. N-TASQ (left) folds into its closed conformation (right) upon interaction with G4, which frees the fluorescence of its naphthalene template (**Figure S29-B**, **Table S20**).

As for the other TASQs, N-TASQ displays a poor cytotoxicity (IC_{50} = 308.5 µM, **Figure S28**, **Tables S18-S19**). Several attempts were made to determine the best conditions for the use of N-TASQ in cells:

(1) first, MCF7 cells were live incubated with 100 µM N-TASQ for 24 h before being fixed with 100% methanol. Using a confocal microscope, N-TASQ was found to be efficiently excited with both 405 and 448 nm lasers, with an emission until 600-700 nm. We thus selected the 405 nm laser for following studies, keeping in mind that this fluorescence properties make N-TASQ usable in sequential manner only with others fluorescent probe, because of the wide window of emission.

(2) The cells' autofluorescence was checked using the 405 nm laser, which was found to be quite high with 10-20% power but not with a < 5% power.

(3) N-TASQ must thus be used with the 405 nm laser at a maximum power of 5%; to this end, we optimized the width of the emission wavelengths: upon incubation with 100 µM N-TASQ for 3 h, and after cell fixation with methanol, N-TASQ is mostly visible in both the 450-500 and 500-550 nm emission windows;

we thus refined this window to 450-530 nm, in which the N-TASQ fluorescence is readily observable, even with a laser adjusted at 1% power.

(4) With these parameters (**Table Mat&Meth 9**), the fixing conditions, N-TASQ concentration and incubation time were optimized: first, N-TASQ *foci* are more defined with methanol fixation (instead of 2% (w/v) formaldehyde); second, we found that 5 µM of N-TASQ is not enough after 24 or 48 h incubation. Therefore, the N-TASQ concentration was increased concomitantly decreasing the incubation time to 10 h: with 10-20 µM of N-TASQ, *foci* are visible using a laser power of 20-30% for while a power of 1-5% only is required for 50-100 µM concentration. We finally fixed the N-TASQ concentration at 50 µM concentration and tried to further decrease the incubation time to 2, 4 or 6 h: we found that 6-h incubation was enough.

These experiments allowed for defining the optimized N-TASQ conditions, incubating MCF7 cells with 50 µM N-TASQ for 6 h before a methanol fixation and a fluorescence acquisition using the following parameters: λ_{exc}= 405 nm (2%); λ_{em}= 450-530 nm (gain = 100%).

2. Study of the PhpC-induced effects on G-quadruplexes by semi-quantitative analysis

The experimental conditions being fixed, the macro program previously used for co-localization studies has been adapted to the use of N-TASQ. The lines of code about the DAPI and the TASQ/γH2AX *foci* co-localization were removed and the whole organization and methods redesigned.

```
selectWindow("mask_stack_ntasq"+number+".TIF");
        Dialog.create("Enter the number of selection type tool");
        Dialog.addNumber("Number of selection type tool: ", 2); Choice of the type of selection tool (2 = polygon)
        Dialog.show();
        stt=Dialog.getNumber();
        setTool(stt); Use of the selection tool on image to surround cells
        waitForUser("1. Select areas (cells) with the selection tool, 2. Add it to ROI manager (right click), 3. Continue
for each areas, 4. Press OK to continue the macro"); Instructions for the use of the tool (which are posted on the
screen) for the conversion of cells to ROI

        for(c=0;c<roiManager("count");c++){
        selectWindow("mask_stack_ntasq"+number+".TIF");
        roiManager("Select",c); Selection of the ROI (cells) previously defined
        roiManager("rename", img+"/"+c+1);
        }
        roiManager("save", path_ntasq_roi_save); Saving of the ROI
```

Figure 41. Lines of code of the N-TASQ macro program 1.0 for the surrounding of cells and their saving as ROI. This part of the N-TASQ macro program 1.0 allows to surround cells with a selection tool (here a polygon) and define them as digital regions of interest (ROI) on a z-stacked image of the N-TASQ channel. Explanations about the function of some methods are in blue.

Our first optimization was made to absorb the variations of the FI in the different cell fields. To take this into account, I added a method allowing for the quantification of background FI (*i.e.*, the FI of the cell field outside the cells) used to normalize the raw FI obtained with the calculated mean background FI which

is specific of each cell field (**Figure S36**). To this end, some squared areas must be randomly positioned on different images, where there is no cell, for the quantification of background FI for different fields.

Also, to count not only the nuclear TASQ *foci* but also the global cellular *foci*, a method of manual selection of cells was added (**Figure 41**): selected cells must be manually delimited on a z-stacked images (*i.e.*, resulting of the stacking of each z-dimension images) of the N-TASQ channel to precisely define the cells contours. This method allows for the selection of cells and their conversion into digital regions of interest (ROI) identified by a number and a localization on the image (**Figure 42**, left panel).

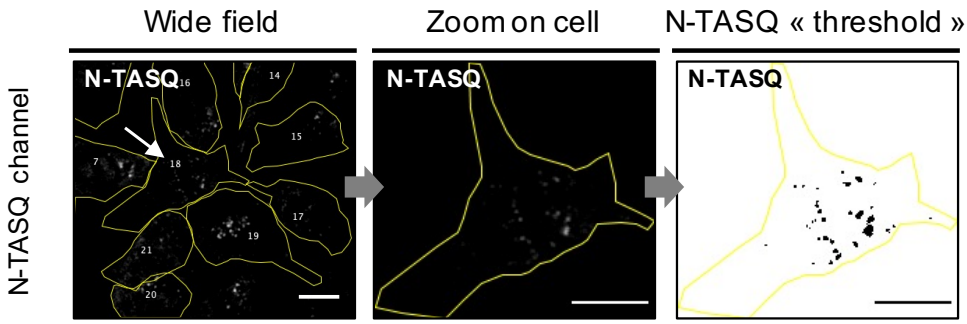

Figure 42. Processing of the optical images with the N-TASQ macro program 1.0. The optical imaging was performed with MCF7 cells live treated with N-TASQ (50 µM, 6 h). Optical image was processed with the N-TASQ macro program 1.0 in order to study the N-TASQ *foci*: after manual surrounding of cells (and the cell of interest, shown with the white arrow) to create Regions of Interest (ROI; surrounded with yellow line), these ROI are counted and numbered (left), then separated and treated ("Clear outside" and "Smooth" methods; middle) and N-TASQ *foci* inside are studied (N-TASQ "Threshold" and "3D Object Counter" methods; right). 63x oil objective, then digital magnification (scale bar = 10 µm).

This macro program, named 'N-TASQ macro program 1.0' is thus able to localize cells on images; to go step further, a loop was created for a better characterization of these images, including methods already used for the co-localization macro program (*e.g.*, the "Smooth", "Clear outside" and "3D Objects Counter") as well as for the quantification of FI (IntDen: integrated density) and volume (in μm^3) of each cell (**Figure 43**). In this program loop, cells are selected (with the previously created digital ROI), isolated (in deleting the pixels values outside the cells and then attributing to them a new value of 1 corresponding to real black pixels) and treated with a threshold of 1 (for count all pixels except those with a value of 1). This process permits to study all cells and to provide all related parameters (**Figure 42**, middle panel). Additionally, a final series of lines of code was added for recording a summary image of each cell fields studied in order to readily localize the cells of interest in each image (**Figure S37**).

The 'N-TASQ macro program 1.0' was thus designed and implemented to characterize cells *per se*, but not yet the N-TASQ *foci* in each cell, we thus needed to add another program loop (**Figure S38**). Contrarily to the cells quantification loop, the N-TASQ *foci* quantification loop includes a different threshold value for the selection of the object of interest. While a threshold of 1 was selected for the study of cells, a personalized N-TASQ threshold (or "ntts") must be defined and applied to our images. For this, each image has to be scrutinized to define a threshold allowing the selection of well separated *foci* only, and not *foci* clusters or

entire cells. To this end, a personalized ntts value for each condition is defined, thanks to which the macro program will consider these digital structures only, *in fine* leading to the characterization (*i.e.*, quantification of number, FI and volume) of each N-TASQ *focus*. These personalized ntts values allow the adaptation of the N-TASQ *foci* selection (**Figure S39**) as the mean background FI values allow the normalization of data (**Figure S40**), which are both necessary due to the background FI difference between conditions.

```
for(c=0;c<roiManager("count");c++){ Beginning of the loop allowing to go to the next cell (ROI)
	close("Results");
	selectWindow("ntasq_"+number+"_roi.TIF");
	roiManager("Select",c); Selection of a cell
	run("Duplicate...", "title=int-ntasq_roi_"+number+"/"+c+1+" duplicate range=stack"); Duplication of the cell
	run("Smooth", "stack"); Blurring of the cell
	run("Clear Outside", "stack"); Deletion of the pixels values outside of the cell
	run("Set 3D Measurements", "volume nb_of_obj._voxels integrated_density mean_gray_value
minimum_gray_value maximum_gray_value dots_size=5 font_size=10 show_numbers white_numbers");
	run("3D Objects Counter", "threshold=1 slice=1 min.=2 max.=20000000 objects statistics"); Calculation of the
FI (IntDen), the volume and the voxel number of the cell

			selectWindow("Results");
			m=nResults();
			NTroiVolume=0;
			NTroiNbvoxel=0;
			NTroiIntDen=0;
			if (m>0) {
				for(l=0; l<m; l++) { Addition of the FI, volume and voxel number values (below)
				NTroiVolume = NTroiVolume + getResult("Volume (micron^3)", l);
				NTroiNbvoxel = NTroiNbvoxel + getResult("Nb of obj. voxels", l);
				NTroiIntDen = NTroiIntDen + getResult("IntDen", l);

			}
				print("int-ntasq-roi_"+number+"/"+c+1+":", "Volume:", NTroiVolume, "nb_of_obj._voxels:",
NTroiNbvoxel, "IntDen tot:", NTroiIntDen); Saving of the FI, volume and voxel number values in a file
				}
			else {
				print("int-ntasq-roi_"+number+"/"+c+1+":", m);
				}

	close("int-ntasq_roi_"+number+"/"+c+1); Close of the duplicated cell used for quantification
	close("Objects map of int-ntasq_roi_"+number+"/"+c+1); Close of the image generated after quantification
	} Change of cell
```

Figure 43. Lines of code of the N-TASQ macro program 1.0 for the quantification of cells number, FI and volume. This part of the N-TASQ macro program 1.0 allows to quantify the number, FI and the volume (as well as the voxel number) of each cell. To do this, each cell is duplicated, blurred, isolated and then their number, FI and volume are quantified and saved in a worksheet precising the name of the experiment, the cells number and for each the quantified values. Explanations about the function of some methods are in blue.

Collectively, the N-TASQ macro program 1.0 comprises 287 lines of code (*versus* 423 lines for the co-localization macro program) allows for the characterization of both cells and N-TASQ *foci* inside cells. This macro was thus applied for the characterization of cells treated with N-TASQ (using the optimized conditions previously defined) without or with pre-incubation with the G4-destabilizer PhpC (**Figure 44**, **Figure S41**).

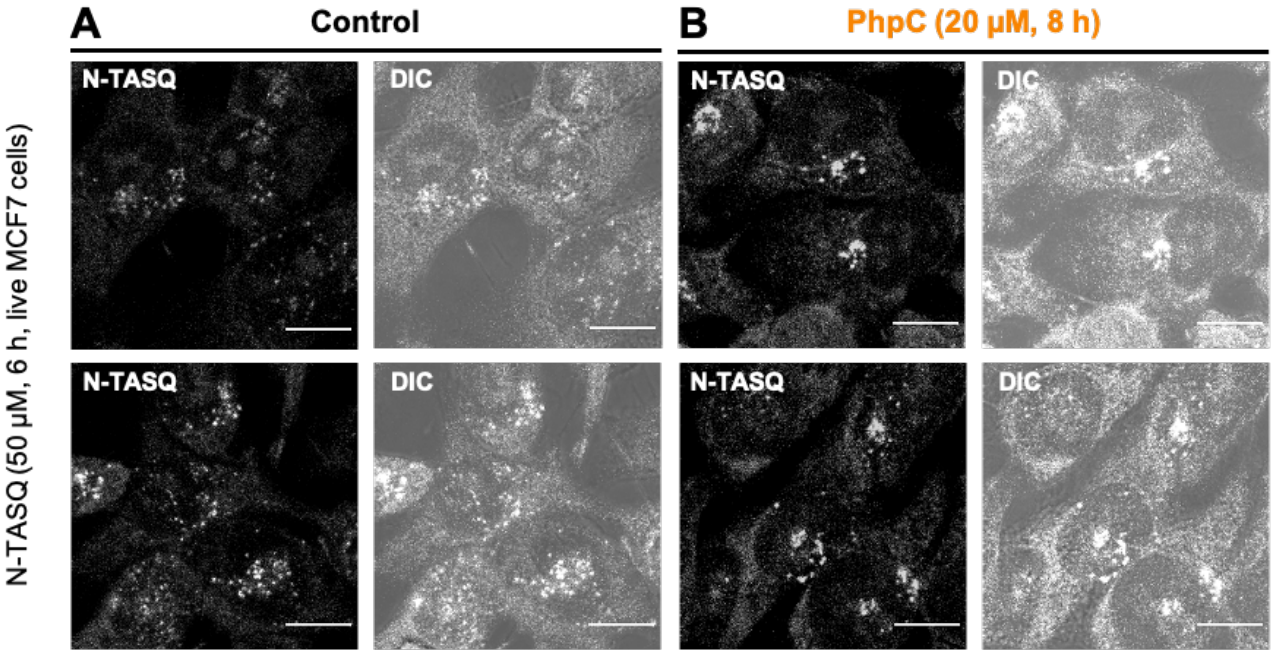

Figure 44. High-resolution optical images acquired with N-TASQ without or with PhpC pre-treatment. The optical imaging was performed with MCF7 cells (**A**) non-treated (Control) or (**B**) live treated with PhpC (20 µM, 8 h) and (**A-B**) N-TASQ (50 µM, 6 h; white) simultaneously. Images are representative of the mean number of N-TASQ *foci* per cell. 63x oil objective, then digital magnification (scale bar = 10 µm).

For these investigations, we analyzed 84 MCF7 cells as Control cells (*i.e.*, without PhpC pre-incubation): a mean number of 86.6 N-TASQ *foci* per cell was obtained, with a normalized mean FI of 19.7 (black, **Figure 44-A**, **Figure S41-A**, **Figure 45**, **Table S24**) and an average volume of 0.63 μm^3 (**Figure S42**, **Table S24**).The crystal structure of the telomeric G4 showed that the dimension of a G4 structure is 41 Å (length and width) and 6.1 Å (height),[48] resulting in a volume of 10.25 nm^3, thus indicating that N-TASQ *foci* do actually correspond to clusters of G4s (*ca*. 60 G4s) rather than isolated G4s. Even bigger N-TASQ *foci* were detected (corresponding to a volume twice bigger than the mean volume), but marginally (3.2 *foci*/cells). A further analysis of the FI results indicates that the N-TASQ *foci*-related FI represents 0.13% only of the total cell FI (**Table S24**). We then analyzed 118 cells pre-treated with PhpC (20 µM for 8 h, orange, **Figure 44-B**, **Figure S41-B**, **Figure 45**, **Table S24**): while the cellular N-TASQ *foci* kept the same volume (0.59 μm^3), their normalized FI was 38.6% lower (12.1 per *foci*) and, more importantly, these *foci* were 3.2-fold less abundant (with a mean of 27.0 N-TASQ *foci*/cell). These results thus show that the preincubation of cells with the G4-destabilizer PhpC treatment triggers a decrease in both the number and density of the cellular N-TASQ *foci*, which could represent the very first evidence that PhpC does indeed modulate G4 landscapes in cells. Of note, the bigger N-TASQ *foci* were also impacted by the presence of PhpC since their number dropped to 1.8 *foci*/cell.

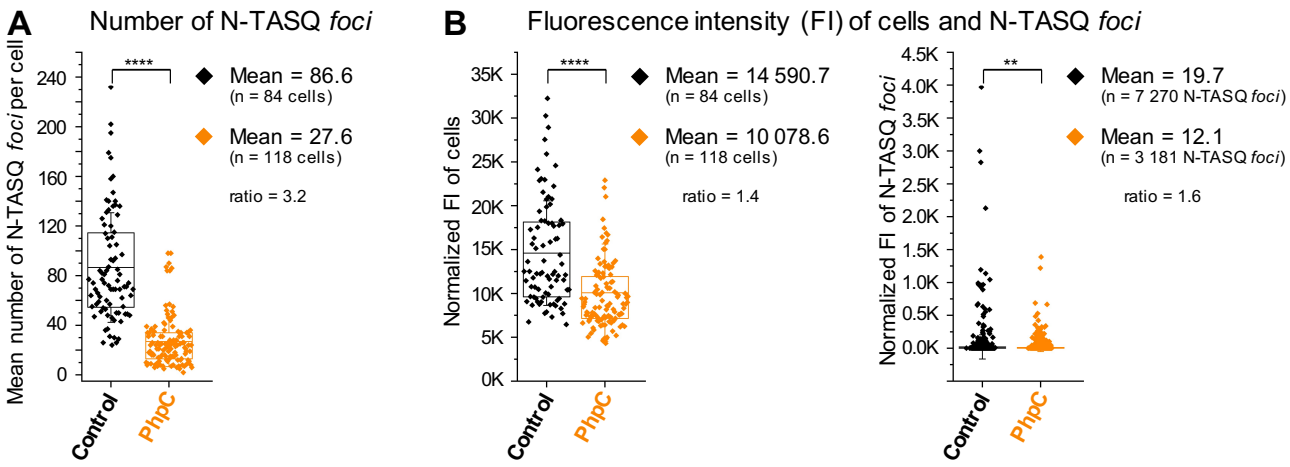

Figure 45. Quantitative optical imaging results obtained upon treatment with N-TASQ and/or PhpC. The optical imaging was performed with MCF7 cells non-treated (Control; black boxes) or live treated with PhpC (20 µM, 8 h; orange) and N-TASQ (50 µM, 6 h) simultaneously. Optical images were processed with the N-TASQ macro program 1.0 in order to count cells and (**A**) N-TASQ *foci* per cell as well as their (**B**) FI and volume (with the N-TASQ channel). A normalization was applied with the mean background FI of each image. Error bars represent SD from the mean for one technical experiment. For statistical hypothesis tests, Student's *t*-test and Welch's unequal variances *t*-test were used depending on variances equality. * $p < 0.05$, ** $p < 0.01$, *** $p < 0.001$, **** $p < 0.0001$.

These results thus show that PhpC can modulate G4s not only *in vitro* but also in cells. These optical imaging data remains however qualitative (or semi-quantitative at best) by nature, meaning that they must be further substantiated by a truly quantitative analysis, which is precisely the topic developed in the next chapter. Also, we quantified the apparent affinity of both molecules (N-TASQ and PhpC) by fluorescence quenching assay (FQA)[90] using the labelled G4-RNA $^{5'}$Cy5-*NRAS* sequence (Cy5-r[$^{5'}$G$_3$AG$_4$CG$_3$UCUG$_3{}^{3'}$]): the >2-log difference between the apparent dissociation constant of N-TASQ ($^{app}K_D$ = 0.51 µM; **Figure S43-A**, **Table S25**) and PhpC ($^{app}K_D$ > 100.0 µM) rule out a direct competition between them for G4 binding. This lack of competition was confirmed by a competitive FRET-melting assay[91] performed with the doubly labelled F-*NRAS*-T ON (FAM-r[$^{5'}$G$_3$AG$_4$CG$_3$UCUG$_3{}^{3'}$]-TAMRA): the stabilization induced by N-TASQ ($\Delta T_{1/2}$ = 11.9 °C; **Figure S43-B**, **Table S26**) was not affected by an excess of PhpC (up to 20 mol. equiv., $\Delta T_{1/2}$ = 11.7 °C).

However, before moving to this quantitative method, we decided to further exploit the wealth of optical imaging data acquired to investigate whether our workflow could be used to study the subcellular distribution of N-TASQ.

3. Development of a computing tool for the G-quadruplexes subcellular compartmentalization

To go a step further in our analyses, we thus decided to improve this macro program to discriminate between cytoplasmic and nuclear N-TASQ *foci*. This additional information could be invaluable for the study of the modulation of either G4-DNA or G4-RNA, under specific conditions including cellular stress, helicase-depletion or G4 ligands treatment.

To this end, a nuclear staining agent was used for delimiting the nucleus; the spectroscopic properties of this dye must be compatible with the N-TASQ's ones, that is why we selected DRAQ5, a red-emitting dye

($\lambda_{exc\ max}$ = 597 nm and $\lambda_{em\ max}$ = 695 nm, **Figure S29**, **Table S20**). The script of this updated macro, consequently named 'N-TASQ macro program 2.0', begins with the same steps with: *i.* the manual delimitation of cells on a z-stacked image (N-TASQ channel) to create a digital ROI, *ii.* the conversion of colors to shades of gray, *iii.* the blurring of cells for a better visualization of isolated *foci* ("Smooth" method), and *iv.* the isolation of ROI deleting the value of pixels outside of these ROI ("Clear outside" method) in both N-TASQ and DRAQ5 channels (**Figure 46**, **Figure 47**, **Figure S44**).

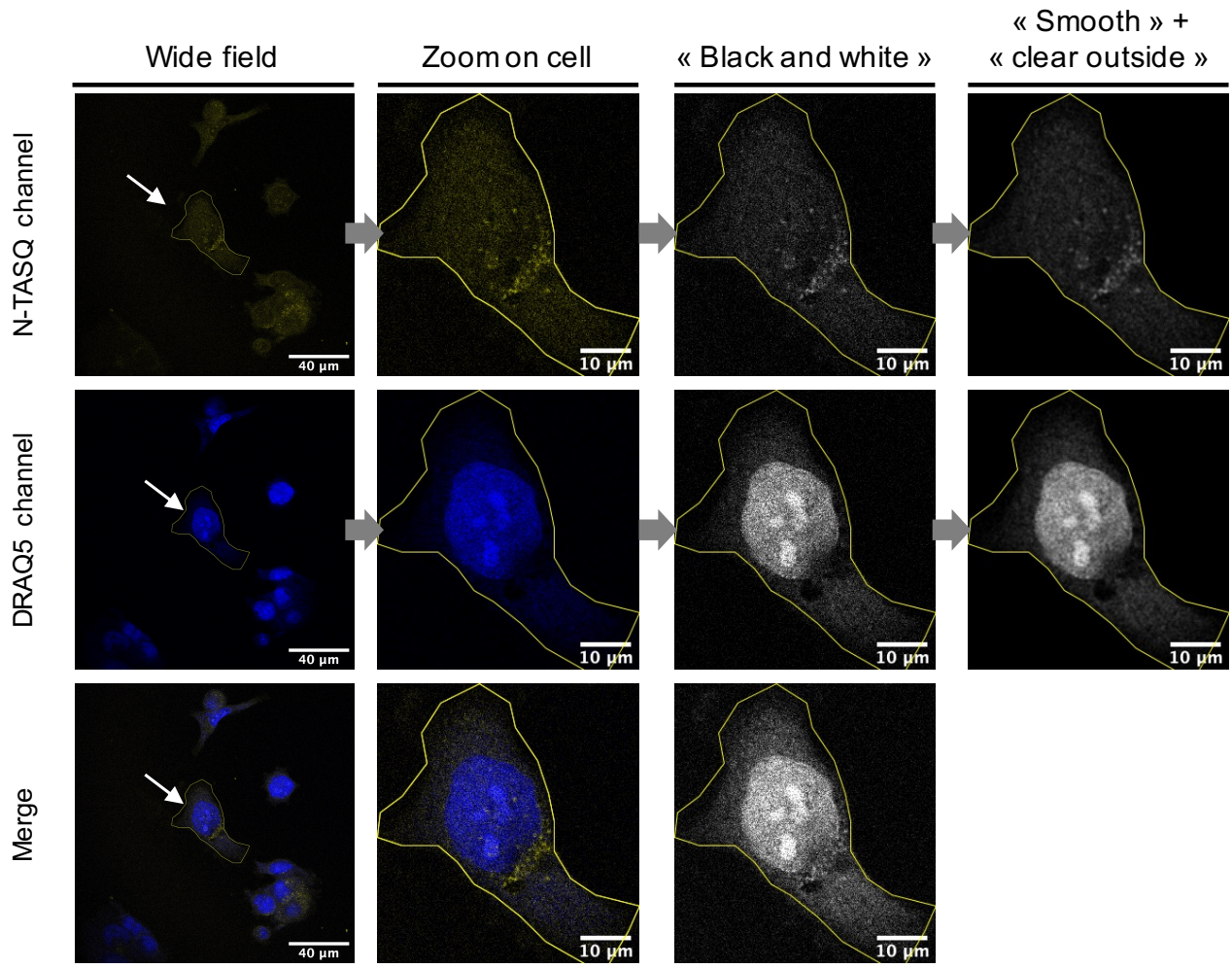

Figure 46. Processing of the optical images with the N-TASQ macro program 2.0 (Part 1/2). The optical imaging was performed with MCF7 cells live treated with N-TASQ (50 µM, 6 h), which is followed by a post-fixation nuclear staining by DRAQ5 (blue). Optical image was processed to study the N-TASQ *foci* subcellular compartmentalization: after manual surrounding of cells (and the cell of interest, shown with the white arrow) to create Regions of Interest (ROI; surrounded with yellow line), these ROI are counted, numbered, separated and treated ("Black and white", "Smooth" and "Clear outside" methods) for the N-TASQ (yellow) as well as the DRAQ5 (blue) channel. 63x oil objective, then digital magnification (scale bar = 10-40 µm).

Once the cells localized, recorded, isolated and treated, a new part of the script is launched, according to the following step *i.* in the DRAQ5 channel, a mask is created to delineate the nucleus only ("Threshold", "Fill holes" and "Subtract background" methods, **Figure 47**, **Figure 48**), *ii.* this nucleus mask is then subtracted from the cell in the N-TASQ channel to delete this nuclear and provide the cytoplasmic N-TASQ fluorescent data ("Image calculator (SUBTRACT)" method, **Figure 47**, **Figure 48**), and *iii.* the cytoplasmic N-TASQ *foci* are

then studied as above, with some minor changes in the lines of code for the extraction of data as their number, FI and volume (**Figure 47**, **Figure 48**).

```
For(c=0;c<roiManager("count");c++){ Beginning of the loop allowing to go to the next cell (ROI)
close("Results");

selectWindow("ntasq_"+number+"_nuccoloc.TIF");
roiManager("Select",c); Selection of a cell (N-TASQ channel)
run("Duplicate...", "title=ntasq_cytocoloc_"+number+"/"+c+1+" duplicate range=stack"); Duplication n° 1 of the cell
selectWindow("ntasq_cytocoloc_"+number+"/"+c+1);
run("Smooth", "stack"); Blurring of the cell copy n° 1
run("Clear Outside", "stack"); Deletion of the pixels values outside of the cell copy n° 1

selectWindow("nuc_"+number+"_nuccoloc.TIF");
roiManager("Select",c); Selection of the same cell (DRAQ5 channel)
run("Duplicate...", "title=nuc_cytocoloc_"+number+"/"+c+1+" duplicate range=stack"); Duplication n° 2 of the cell
selectWindow("nuc_cytocoloc_"+number+"/"+c+1);
run("Smooth", "stack"); Blurring of the cell copy n° 2
run("Clear Outside", "stack"); Deletion of the pixels values outside of the cell copy n° 2
setThreshold(nucts, 255); Isolation of the nucleus with DRAQ5 FI
run("Convert to Mask", "method=MaxEntropy background=Dark"); Creation of the nucleus mask
run("Fill Holes", "stack");
run("Subtract Background...", "rolling=3 light create stack");

imageCalculator("Subtract create stack", "ntasq_cytocoloc_"+number+"/"+c+1,"nuc_cytocoloc_"+number+"/"+c+1);
Deletion of the nucleus part from the cell copy n° 1 (N-TASQ channel)
selectWindow("Result of ntasq_cytocoloc_"+number+"/"+c+1);
run("Set 3D Measurements", "volume nb_of_obj._voxels integrated_density mean_gray_value minimum_gray_value
maximum_gray_value dots_size=5 font_size=10 show_numbers white_numbers");
run("3D Objects Counter", "threshold="+ntts+" slice=1 min.=2 max.=20000000 exclude_objects_on_edges objects
statistics"); Calculation of the FI (IntDen), the volume and the voxel number of the cytoplasmic N-TASQ foci selected
with the foregone N-TASQ threshold (ntts value)

        selectWindow("Results");
        q=nResults();
        NtcytocolocVolume=0;
        NtcytocolocNbvoxel=0;
        NtcytocolocIntDen=0;
        if (q>0) { Beginning of the loop allowing to go to the next foci
                for(f=0; f<q; f++) { Extraction of the FI, volume and voxel number values (below) of a foci
                NtcytocolocVolume = getResult("Volume (micron^3)", f);
                NtcytocolocNbvoxel = getResult("Nb of obj. voxels", f);
                NtcytocolocIntDen = getResult("IntDen", f);

                print("ntasq-cytocoloc_"+number+"/"+c+1+"/"+"object_n"+f+1+":", "Volume:", NtcytocolocVolume,
"nb_of_obj._voxels:", NtcytocolocNbvoxel, "IntDen:", NtcytocolocIntDen); Saving of the FI, volume and voxel number
values in a file
                }
                } Change of foci
        else {
                print("ntasq-cytocoloc_"+number+"/"+c+1+"/"+"object_n"+f+1+": no N-TASQ foci – cytoplasmic co-
localization");
                }

close("ntasq_cytocoloc_"+number+"/"+c+1); Close of the duplicated cell copy n° 1
close("nuc_cytocoloc_"+number+"/"+c+1); Close of the duplicated cell copy n° 2 (nucleus)
close("Result of ntasq_cytocoloc_"+number+"/"+c+1); Close of the nucleus-lacked cell image used for quantification
```

```
close("Objects map of Result of ntasq_cytocoloc_"+number+"/"+c+1); Close of the image generated after quantification
} Change of cell
```

Figure 47. Lines of code of the N-TASQ macro program 2.0 for the quantification of cytoplasmic N-TASQ *foci* number, FI and volume. This part of the N-TASQ macro program 2.0 allows to quantify the number, FI and the volume (as well as the voxel number) of each cytoplasmic N-TASQ *foci* inside each cell. To do this, each cell is duplicated, blurred and isolated two times, one of the copy (in DRAQ5 channel) is thresholded to only keep the nucleus and this copy is subtracted from the second one (in N-TASQ channel) in order to only keep the cytoplasmic data of this second image. Then the N-TASQ threshold is applied on this last nucleus-lacked image to only isolate small bright structures inside, quantify the number, FI and volume of these cytoplasmic N-TASQ *foci* and save it in a worksheet precising the name of the experiment, the cells number, the cytoplasmic N-TASQ *foci* number and for each the quantified values. Explanations about the function of some methods are in blue.

Next, the nucleus mask (DRAQ5 channel) is also merged (and not subtracted) with the whole cell (N-TASQ channel) to keep (and not delete) the nuclear part and thus define the nuclear N-TASQ fluorescent data ("Image calculator (AND)" method, **Figure 48**, **Figure S44**). Each cell is thus processed for characterizing both cytoplasmic (**Figure 47**) and nuclear N-TASQ *foci* (**Figure S44**). Of note, all these steps were performed in the different z-dimensions of cells, to take the size and shape of the *nuclei* in the different cells slices into account (**Figure S45**). Collectively, the N-TASQ macro program 2.0 comprises now 519 lines of code script which creates three summary images in the N-TASQ channel (z-stacked original image; **Figure S46**, left), DRAQ5 channel (z-stacked mask image; right) and both channels (z-stacked original image; middle). Some other options were introduced (not shown here) to be implemented as a function the analysis required: for instance, this macro program proposes the quantification of the background FI and the subcellular compartmentalization of N-TASQ *foci* as options, in order for the user to select the study of global *foci* or the distribution of cytoplasmic/nuclear *foci*.

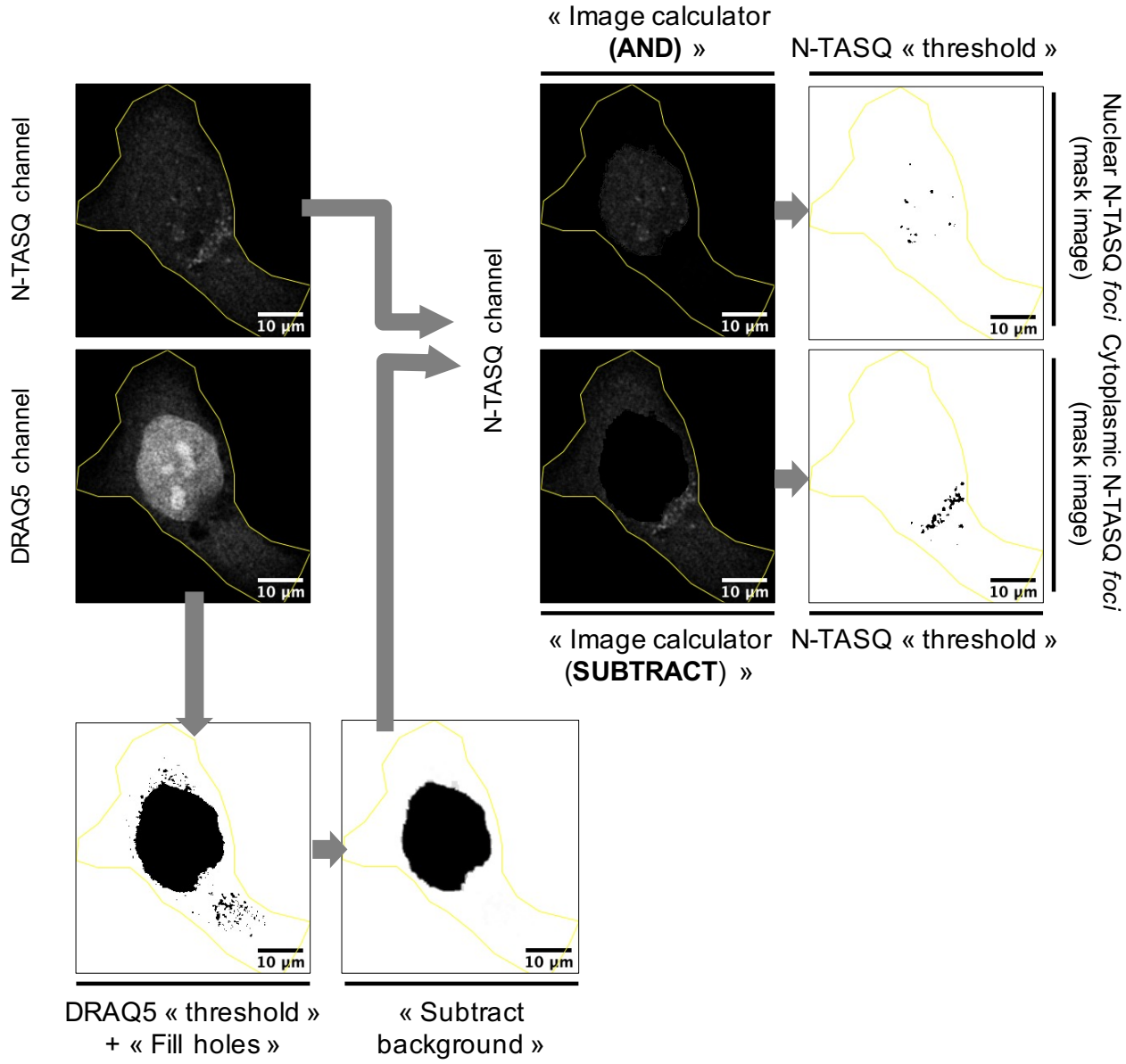

Figure 48. Processing of the optical images with the N-TASQ macro program 2.0 (Part 2/2). After the previous digital treatments of the N-TASQ (yellow) and DRAQ5 (blue) channels of the same optical image, the nucleus mask is obtained from the DRAQ5 channel ("Threshold" and "Fill holes" methods; bottom) and then processed with the N-TASQ channel in order to only keep the nuclear (*i.e.*, N-TASQ *foci* which co-localize with the nucleus mask; "Image calculator (AND)" method) or the cytoplasmic (*i.e.*, N-TASQ *foci* which not co-localize with the nucleus mask; "Image calculator (SUBTRACT)" method) N-TASQ *foci*. The N-TASQ *foci* are then studied separately ("Threshold" and "3D Object Counter" methods). 63x oil objective, then digital magnification (scale bar = 10 µm).

The 5 images analyzed, cumulating 45 MCF7 cells, with the N-TASQ macro program 2.0 revealed that these cells display a mean number of 12.2 cytoplasmic and 15.0 nuclear N-TASQ *foci*/cell, which represents a 45/55% ratio (**Table S27**). The cytoplasmic N-TASQ *foci* seem to be bigger (mean volume = 0.48 *versus* 0.37 μm^3) and brighter (normalized mean FI = 23.2 *versus* 17.4) than the nuclear ones, even if there are more big N-TASQ *foci* in the *nucleus* as compared to the cytoplasm. This could be explained by the proximity of G4 structures in the *nucleus* that generates clusters of G4s. It could be interesting to induce cytoplasmic

membrane-less organelles under stress condition to assess whether this macro program is fully responsive to these changes.

Parameters calculated	Co-localization macro program (2021)	N-TASQ macro program 1.0 (2022)	N-TASQ macro program 2.0 (2023)
Script lines of code	423	287	519
Cell number	**X** (Nuclei, automatic)	**X** (Cells, manual)	**X** (Cells, manual)
TASQ *foci* number	**X** (Nuclear)	**X** (Cellular)	**X** (Cellular)
TASQ cytoplasmic/nuclear discrimination			**X**
TASQ *foci* FI	**X**	**X**	**X**
TASQ *foci* volume		**X**	**X**
γH2AX *foci* number	**X**		
γH2AX *foci* FI	**X**		
TASQ/γH2AX *foci* coloc.	**X**		
Background FI		**X**	**X**
Summary processed optical images		**X** (one)	**X** (three)
Options-guided macro			**X** (1. Loading of previous ROI, 2. Background FI, 3. Global or subcellular *foci*)

Table 5. Comparative table of the macro programs. The table summarizes the parameters the different macro programs allow to measure as well as others added options.

In summary, we developed 2 macro programs for 2 different but complementary purposes: the N-TASQ macro program 1.0 was created and implemented to characterize the cellular TASQ *foci* through a quantification of their number, FI and volume; the N-TASQ macro program 2.0 was then created and implemented to discriminate between cytoplasmic from nuclear N-TASQ *foci*. These 2 macros thus offer different options that could be used in function of the information being sought.

C. Discussion and perspectives about the project outcomes

More than simple molecular tools for the study of the G4 structures *in vitro*, the biotinylated TASQs BioCyTASQ and BioTriazoTASQ turned out to be interesting G4 probes with applications in cells, what we reported via a publication into the journal JACS Au.[223] However, some drawbacks are associated with their use in cells, including the fact that 1/ we cannot rule out that their biotin appendage diverts their target engagement, owing to its ability to create H-bonds with possible cellular partners, and 2/ using a fluorescently labelled streptavidin is responsible for a quite saturated background FI owing to the natural biotin abundance. These 2 drawbacks are circumvented with the new generation of clickable TASQs[222] MultiTASQ and ^{az}MultiTASQ in which the biotin appendage is changed for an alkyne or an azide handle, that is, a bioorthogonal appendage devoid of any interaction with biomolecules while presenting a higher level of versatility as they can be functionalized *in situ* by click chemistry with a biotin or a fluorophore partner.

Fluorescently addressable biotinylated TASQs were used here for pre-targeting G4 imaging, implemented to assess whether PhpC, the most promising prototype of G4-destabilizer presented in Chapter I, is abile to decrease the number of folded G4s in MCF7 cells. We found that pre-incubating cells with PhpC does indeed a notable decrease (3.2-fold) of the number of TASQ *foci*, that is, of G4 *foci bone fide*, which is thus a qualitative demonstration of the ability of PhpC to modulate G4 landscapes in cells. These results, completed with those of the next Chapter III, were reported via a publication in the journal Chemical Communications.[255] We must now verify that this G4-destabilizing effect is dependent on its concentration, and also that it could be confirmed in a quantitative manner, which is precisely the topic of the next chapter.

From a technical point of view, these qualitative investigations provided me with the opportunity to create, develop and optimize macro programs aimed at numerically exploiting series of optical imaging. These experiments were further exploited one step further here providing a mechanistic link between G4s and DNA damage sites. It could be thus of interest now to confirm these results with additional experiments including DNase/RNase enzymatic treatment to confirm the nature of the TASQ *foci*, or co-localization experiments with other antibodies such as those raised against G3BP or TDP-43[256–258] to refine the nature of G4 condensates, or against Rab5 or Clathrin[259] to refine their cellular localization.

Some technical optimizations are also required to improve the reliability of these macros, such as for instance to obtain the mean gray value as FI data in addition of the IntDen (given that this last parameter depend on the *foci* area), or to find a way for the macro program no to stop if no *foci* are found in ROI. It could be also useful to automatize the definition of the N-TASQ threshold value in order to avoid any user bias when choosing this essential parameter.

Altogether, our results demonstrate that an optimized use of TASQs can make them promising yet indirect imaging probes for cellular G4s, which is an application that is fully complementary to their use as molecular baits to isolate and identify cellular G4s that will be detailed in the next chapter.

Chapter III - Optimization of a TASQ-mediated G-quadruplex-RNA-specific precipitation (G4RP) method for the study of the G-quadruplex transcriptomic landscape

A. Introduction to the chapter III

The development of the G-quadruplex-RNA-specific precipitation (G4RP) method via a collaboration between the team of Dr Judy M. Y. Wong (Faculty of Pharmaceutical Sciences, University of British Columbia, Vancouver, Canada) and our team led to 3 articles between 2018 and 2022.[91,120,121] This technique for G4-RNA study relies on a the purification of rG4s using a G4-specific multivalent molecular tool: Template-Assembled Synthetic G-Quartet (or TASQ), prior to their identification by sequencing (or by RT-qPCR for the G4RP-RT-qPCR). While the BioTASQ was used for G4-RNA in the original study (2018)[120] and then G4-DNA (G4DP method, 2023),[131] the BioCyTASQ was only used for G4-DNA.[131]

One of the goal of my PhD was then to import completely and optimize this technical know-how in our laboratory as well as work on the application of multivalent TASQs (*e.g.*, the biotinylated BioCyTASQ and the new clickable ^{az}MultiTASQ) for G4-RNA study. Also, as this technique could fit perfectly within the scope of my project regarding the previous *in cella* evaluations of the G4-destabilizer PhpC (see Chapter II), I decided to focus on such development (the RT-qPCR version of the G4RP).

B. Project organization and implementation

I. Optimization of the RNA extraction and G-quadruplex-RNA-specific precipitation (G4RP) protocols

1. The beginning of the project

The first tests of G4RP were performed using an ultrasonic cell homogenizer device (Branson 450 Digital Sonifier) working with 0.5-2x10^6 cells seeded until the RT-qPCR quantification. Through 5 different tests, I failed in obtaining decent results. Because this work was done in a blind manner, I decided to set up a gel electrophoresis monitoring, firstly trying denaturing 0.1% (w/v) SDS-PAGE with 1X MOPS buffer (**Figure S47-A**) without much success and then, a denaturing 6.7% (w/v) formaldehyde 1% (w/v) agarose gel in that same buffer (**Figure S47-B**) that was better. The only problem was the hazardous nature of working with gel and running buffer (around 200 mL) containing liquid formaldehyde. In a concern of safety, I then chose to keep agarose gel but switch from formaldehyde to bleach denaturing agent.

I then decided to focus on the *i.* preparation of new buffers, *ii.* optimization of the monitoring by gel electrophoresis (by changing the buffer for TAE and then TBE, doing the gel at 4 °C and increasing the % agarose from 1 to 1.5) (**Figure S47-C-E**), *iii.* addition of the monitoring by UV absorbance measurement, *iv.* compartmentalization and dissection of steps, and *v.* work on the reproducibility of the method step by step.

Regarding the reproducibility of the technique, I decided to *i.* count the cells number after the 48 h of growth, which obliged me to switch from cells scraping to cells trypsinization (further discussed hereafter), and *ii.* change the method of RNA purification. For the protection of samples from heat, I started to *i.* work integrally in ice-filled boxes, and *ii.* remove the sonication step for a thermostable alternative solution: the lysis with needle-equipped syringe. This lysis has also the advantages to be cheaper and easier to use than the sonication lysis.

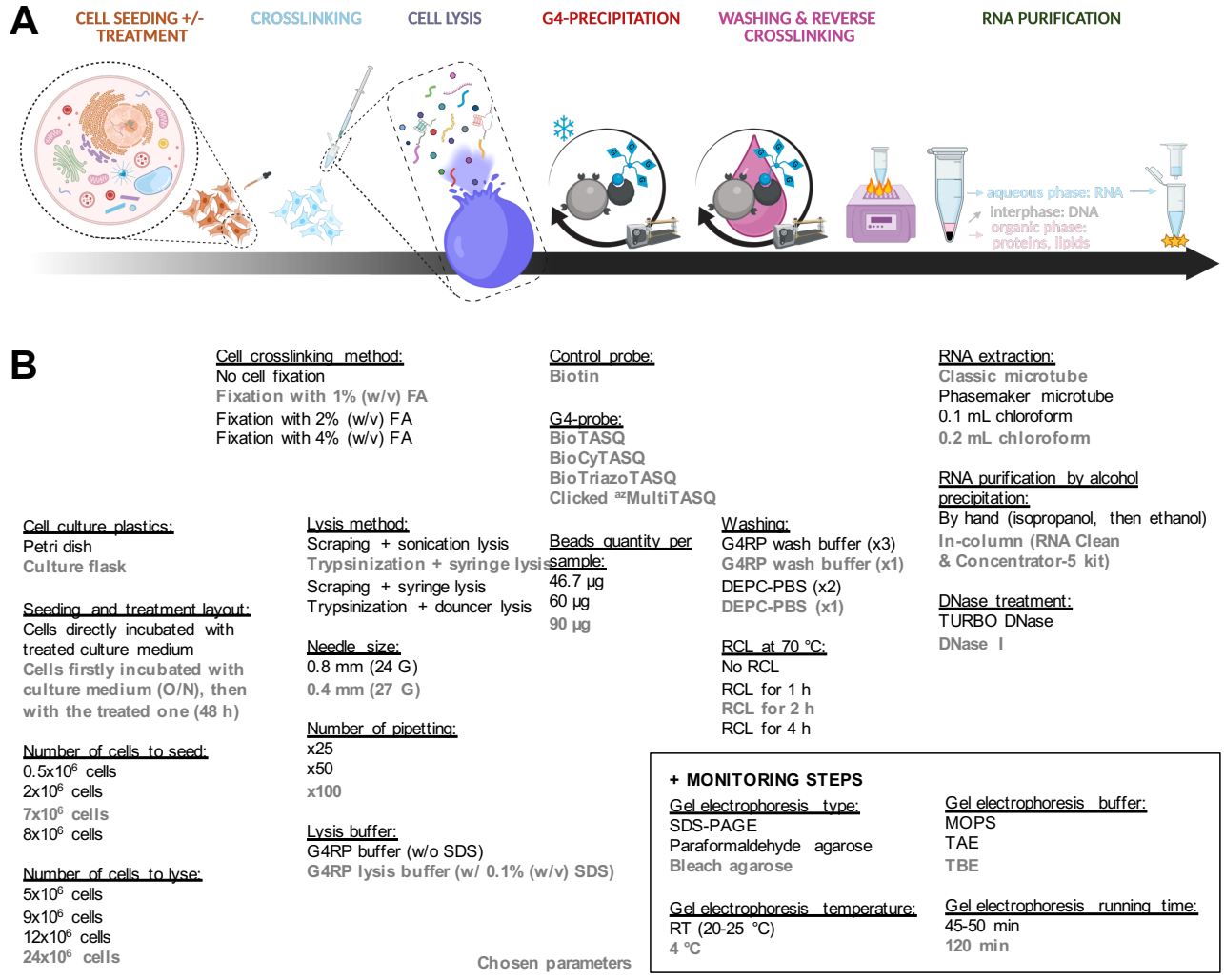

Figure 49. Summary of condition tested for the G4RP.v2 method. (**A**) Several conditions were tested for the following steps: cell seeding +/- treatment, crosslinking, cell lysis, G4-precipitation, washing & reverse crosslinking, RNA purification and monitoring steps. (**B**) Among the 61 individual parameters explored, some have been selected for the final G4RP.v2 method (bold grey). The panel A was created with BioRender.com

Before obtaining the final protocol of G4RP.v2 presented in this chapter, several assays were performed to optimize each step and choose the optimal parameters (**Figure 49**). These different optimizations were monitored by the two techniques previously mentioned: UV absorbance measurement and gel electrophoresis. The UV absorbance measurement was used to calculate an estimated concentration of nucleic acids and also assessed the quality of the samples using quality ratios (see the G4RP.v2 method, STEP A, sub-step 87-88). Different solutions were used as blank for the baseline of the UV-Vis

spectrophotometer: G4RP lysis buffer and UltraPure Distilled Water for raw lysate and purified RNA samples, respectively. Denaturing gel electrophoresis were run to *i.* visualize the recovery of nucleic acids through the different modifications of the protocol, *ii.* have a double check of the capture efficiency of nucleic acid sequences (here G4-RNA) by the G4 probes in comparison with the biotin control, *iii.* visualize the loss of the DNA fraction after RNA purification, and *iv.* estimate the size (with a RNA ladder) and the quality (distinct or smear bands) of the captured G4-RNA. Regarding the DNA fraction, the length of the human genomic DNA is around 3 100 000 000 bases (3.1 Gigabases)[260,261] while RNAs have length from < 50 bases to > 40 000 bases and mRNA an average length of 3 400 bases.[262,263] Thus, in the gels using raw lysates samples and with the RiboRuler High Range RNA Ladder I used, I was able to distinguish DNA as a high > 6 000 bases band and RNA as a medium 500-1 000 bases and a low < 200 bases bands. Several results obtained through these optimizations will be discussed further in this chapter (see **7. Alternative lysis methods**).

2. Optimization of the cell lysis step

For the next assays, the protocol was done until the cell lysis step (STEP 3) to compare different conditions allowing the better recovery of nucleic acids from cells. Due to the intrinsic variation of cell-based experiments, estimated values of RNA have to be compare between conditions done during the same optimization experiment (n° A-H, **Figure 50**, **Table S28**, **Figure 51**).

The initial condition for the cell lysis were *i.* the use of a 0.8 mm needle-equipped syringe, *ii.* 20 pipetting with the syringe and *iii.* a reverse crosslinking (RCL) at 70 °C for 1 h before the quantification. The number of cells to lyse was adjusted (STEP 2, sub-step 10) from $5x10^6$ (**Figure 50-A**, black line) to $9x10^6$ (red line) which allow for the recovery of 80.8 and 135.6 ng/µL of RNA (**Table S28-A**), respectively, and for a better visualization of the RNA bands in agarose gel (**Figure 51-A**). With $9x10^6$ cells, the contribution of SDS in G4RP lysis buffer was validated (STEP 3, sub-step 23) (**Figure 51-B**, red arrow): from 135.6 (without SDS, **Figure 50-B**, black line, **Table S28-B**) to 187.6 ng/µL (with 0.1% (w/v) SDS, red line) RNA. Also, 50 pipetting (instead of 20-25) with a 0.4 mm needle-equipped syringe (instead of 0.8 mm) was optimal to recover the highest quantity of RNA (**Figure 51-C**, red arrow), up to 88.4 ng/µL (**Figure 50-C**, red line, **Table S28-C**) of RNA (*versus* < 30.5 ng/µL for the other conditions). For these samples, an absorbance peak can be observed at 210-215 nm. Even though it could be attributed to the absorbance of DMSO (**Figure S48-A**, green line), these optimizing experiments did not include DMSO in the culture medium (contrarily to the final experiments, see **Figures S49-S51**, **Table S29** and the critical step n° v of STEP 1, sub-step 8). That 210-215 nm peak could rather originate in the supplemented DMEM used for these studies (**Figure S48-A**, orange line), which can still be present in samples despite the washing steps with DEPC-PBS (STEP 2, sub-step 12) and their resuspension in G4RP lysis buffer (STEP 3, sub-step 22). Another possible contribution is that of the 1% (w/v) formaldehyde (FA)/1X Fixing buffer (**Figure S48-B**, burgundy line) and the 1 M Glycine solution (**Figure S48-B**, pink line). However, a contribution of the G4RP buffer (**Figure S48-A**, black line), which was used as blank, can be excluded.

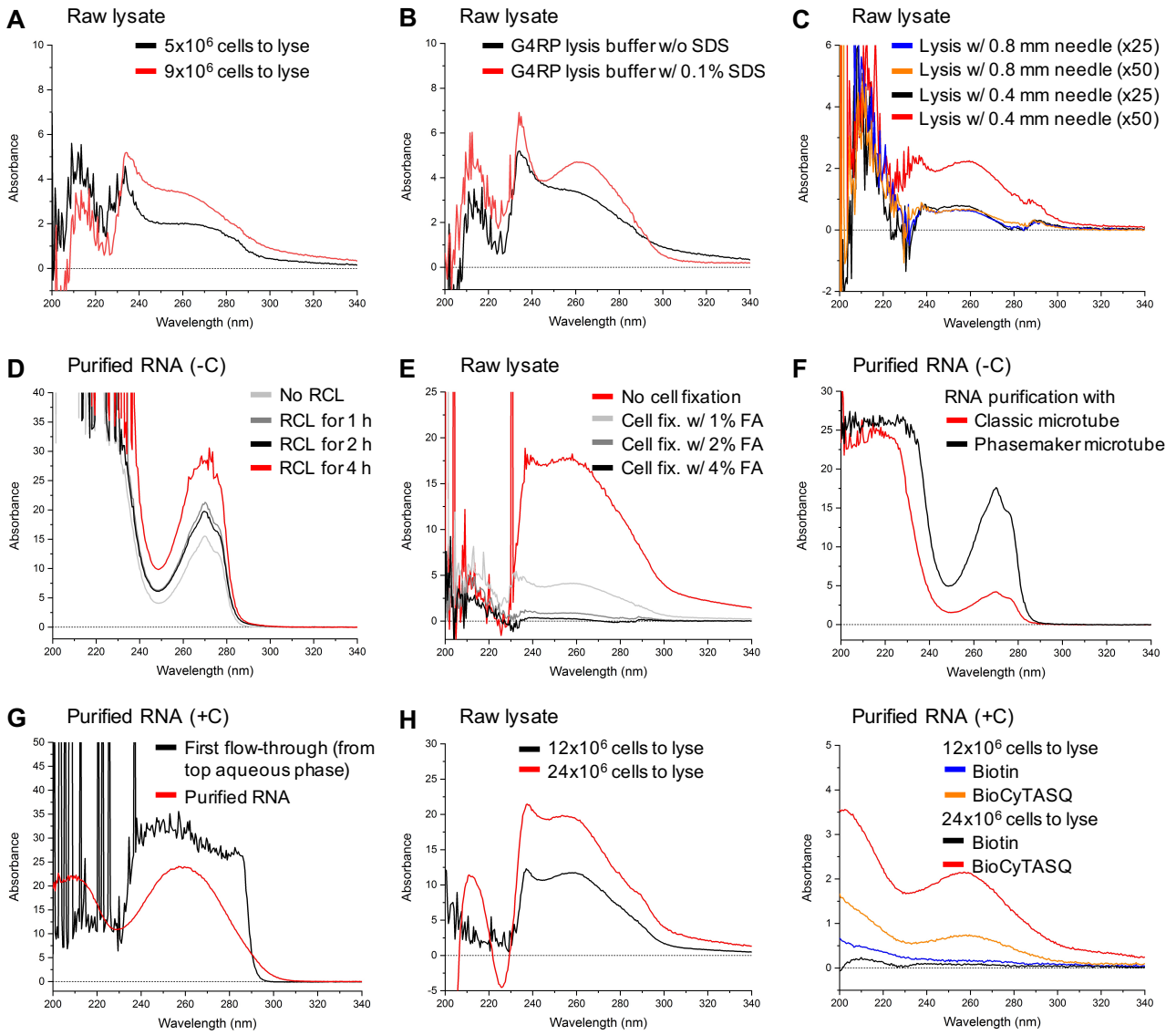

Figure 50. Monitoring of the G4RP.v2 method optimization by UV absorbance measurement. During the G4RP.v2 optimization, several Raw Lysate (after the lysis) or Purified RNA (after the RNA purification) samples were collected to evaluate the efficiency of parameters from G4RP.v2 steps by UV absorbance measurement (200-400 nm): (**A**) number of cells to lyse, (**B**) type of lysis buffer to use, (**C**) the size of the needle and the number of pipetting for the lyse, (**D**) the reverse crosslinking (RCL) time, (**E**) the % (w/v) of formaldehyde (FA) for cell fixation, (**F**) the type of microtube to use during the RNA purification, (**G**) the in-column RNA purification method and (**H**) the number of cells to lyse and its influence on the precipitation of G4s by Biotin or BioCyTASQ. Experiments A and B were performed at the same time. RNA samples purified by alcohol purification (precipitation with isopropanol and then ethanol) or in-column purification (precipitation with the RNA Clean & Concentrator-5 kit) are annotated “Purified RNA (-C)” or “Purified RNA (+C)”, respectively (C for “Column”). Different solutions were used as blank for the baseline of the UV-Vis spectrophotometer: G4RP lysis buffer and UltraPure Distilled Water for Raw Lysate and Purified RNA samples, respectively. For Raw lysate and Purified RNA samples, a dilution factor of 50 and 10, has been corrected here in Abs values, respectively. Absorbance, ratios and estimated RNA concentration values can be found in **Table S28.**

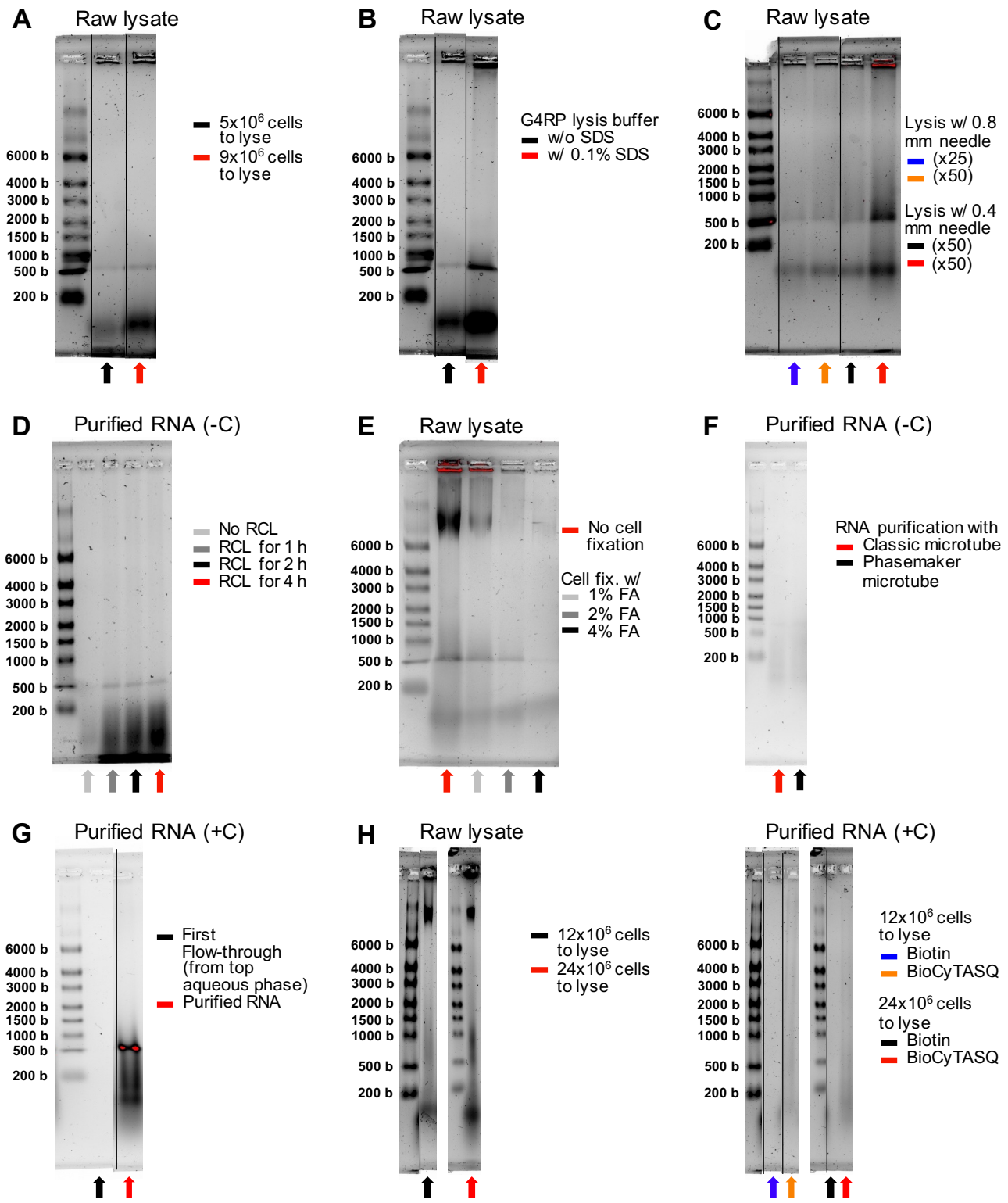

Figure 51. Monitoring of the G4RP.v2 method optimization by gel electrophoresis. During the G4RP.v2 optimization, several Raw Lysate (after the lysis) or Purified RNA (after the RNA purification) samples were collected to evaluate the efficiency of parameters from G4RP.v2 steps by gel electrophoresis (run at 100 V for 105 min at 4 °C): (**A**) number of cells to lyse, (**B**) type of lysis buffer to use, (**C**) the size of the needle and the number of pipetting for the lyse, (**D**) the reverse crosslinking (RCL) time, (**E**) the % (w/v) of formaldehyde (FA) for cell fixation, (**F**) the type of microtube to use during the RNA purification, (**G**) the the in-column RNA purification method and (**H**) the number of cells to lyse and its influence on the precipitation of G4s by Biotin or BioCyTASQ. Experiments A and B were performed at the same time. RNA samples purified by alcohol purification (precipitation with isopropanol and then ethanol) or in-column purification (precipitation with the RNA Clean & Concentrator-5 kit) are annotated “Purified RNA (-C)” or “Purified RNA (+C)”, respectively (C for “Column”). Gels were revelated with SYBR™ Gold Nucleic Acid Gel Stain. RiboRuler High Range RNA Ladder was used as ladder.

3. Optimization of the crosslinking and reverse crosslinking steps

The best reverse-crosslinking (RCL) time (STEP 5, sub-step 37) was determined using purified RNA samples, *i.e.*, precipitated with isopropanol (see below). This time appears to be 4 h (**Figure 50-D**, red line), which allows for recovering 821.6 ng/µL of RNA (360.8 ng/µL for no RCL, 524.4 for 1 h RCL, 496.4 for 2 h RCL, **Table S28-D**). However, the increase of the heating time at 70 °C may favor RNA degradation and then, shorter RNA sequences that could explain the increase of the < 200 bases band intensity observed by gel electrophoresis (**Figure 51-D**). Given the G4RP timing, a 2-h RCL step was kept (**Figure 50-D**, black line), which allows for the visualization of the high > 6 000 bases band in the raw lysates (**Figure S52**, black arrows), which totally disappear in purified RNA samples (**Figure 51-E-H**). At this point, we came to realize that the fixation step (STEP 2, sub-step 14) should be optimized as it influences the recovery of RNA from raw lysates, with 696.4, 164.8, 34.8 and 10.0 ng/µL for the no fixation, 1, 2 and 4% (w/v) FA fixation condition (**Figure 50-E**, **Table S28-E**), respectively (the RCL step being maintained at 70 °C for 2 h). This step fixation being essential for G4 structures maintenance, it was selected to be performed with 1% (w/v) FA.

4. Optimization of the RNA purification

The selected RNA purification method relied on the use of TRizol/chloroform RNA extraction (STEP 6, sub-step 38) followed by the RNA precipitation with isopropanol (first) and ethanol (second). The TRizol/chloroform extraction was performed in either classical (*i.e.*, 1.5 mL microtubes) or Phasemaker tubes before a centrifugation at 12 000 rpm for 15 min. The top aqueous phase (RNAs) recovered with Phasemaker tubes appeared to be pinkish (the color of TRizol) and the purified RNA obtained with, after the alcohol purifications, has a very high absorbance peak of 17.61 at 270 nm (**Figure 50-F**, black line, **Table S28-F**). This can be attributed to the residual presence of chloroform (regarding its atypical signature peak, **Figure S48-A**, burgundy line) and/or phenol (the major component of the TRIzol product, absorbing at 230-290 nm, **Figure S48-A**, red line). This peak hides the 260-nm one and thus, prevents determination. Moreover, both purified samples have a quality ratio indicating this chloroform/TRIzol contamination (R2= $A_{260\ nm}/A_{270\ nm}$ = 0.60-0.64 < 1.2, **Table S28-F**). The classical tubes were thus selected (less expensive) and the purification method changed as follows: *i.* an increase of the volume of chloroform from 0.1 mL to 0.2 mL for 1 mL TRIzol to improve the TRIzol trapping in the organic phase by chloroform and thus limit its recovery in the aqueous phase, and *ii.* a change in the RNA precipitation method, from alcohol precipitation to column-based purification using the RNA Clean & Concentrator-5 kit (STEP 6, sub-step 46). Of note, the DNase I provided in this kit was used instead of the DNase TURBO digestion I used formerly. The quality of this purified RNA named "Purified RNA (+C)" (**Figure 50-G**, red line) was totally satisfying regarding its quantity (*i.e.*, 957.2 ng/µL, **Table S28-G**) and quality (R1= $A_{260\ nm}/A_{230\ nm}$ between 1.8 and 2.2; R2= $A_{260\ nm}/A_{270\ nm}$ ≈ 1.2; R3= $A_{260\ nm}/A_{280\ nm}$ ≈ 1.8). This sample possesses also the right gel pattern with the medium 500-1 000 bases and the low < 200 bases bands (**Figure 51-G**), which confirms the complete removal of DNA traces.

5. Optimization of the G4-precipitation step

The complete G4RP protocol could thus be performed including the main G4-precipitation (STEP 4) and the optimized washing/cell lysis (STEP 3) and RCL steps (STEP 5, sub-step 37). It was of interest to better understand the G4-precipitation step: to this end, the different samples originating in the different sub-steps of this process (**Figure 52-A)** were analyzed: *i.* the supernatant after the lysis (called raw lysate; STEP 3, sub-step 25), *ii.* the supernatant after the G4-precipitation (called unbound; STEP 5, sub-step 32), *iii.* the supernatant after washing the beads with the G4RP buffer (called G4RP washing supernatant; STEP 5, sub-step 33), *iv.* the supernatant after washing the beads with DEPC-PBS (called DEPC-PBS washing supernatant; STEP 5, sub-step 34), *v*. the sample after its resuspension in DEPC-PBS supplemented with RNase OUT (called G4-precipitated and washed raw lysate; STEP 5, sub-step 35), and *vi.* the sample after RNA purification (called the purified RNA; STEP 6, sub-step 68). All of these samples were heated 2 h at 70 °C (for RCL; STEP 5, sub-step 37) before being loaded on a gel. These controls were done for two experiments performed with either $8x10^6$ (**Figure 52-B)** or $12x10^6$ cells (**Figure 52-C)**.

On these gels two main bands were observed at > 6 000 bases DNA band (**Figure S52**) present in the raw lysate sample (**Figure 52-C)**, hatched grey arrow) and < 200 bases RNA band present in several samples. When the precipitation was performed with the biotin control (**Figure 52-B-C**, dotted arrows), an important RNA band was observed in the unbound sample (dotted purple arrow) but not in the G4-precipitated and washed raw lysate (dotted yellow arrow), which means that biotin and beads (*i.e.*, MagneSphere®) do not precipitate any nucleic acids. As expected, no RNA band was found in the purified RNA (**Figure 52-C**, dotted red arrow). The G4-precipitation with the BioCyTASQ (**Figure 52-B-C**, solid arrows) led to a conflicting situation: on one hand, no band was observed in the unbound sample (**Figure 52-B**, solid purple arrow) but the RNA band was observable in the G4-precipitated and washed raw lysate (**Figure 52-B**, solid yellow arrow) which mean the BioCyTASQ was able to precipitate the majority of nucleic acids, implying an unexpected G4 fold for the majority of nucleic acids; on the other hand, a medium band was observable in the unbound sample (solid purple arrow) and a weak one in the G4-precipitated and washed raw lysate (solid yellow arrow), indicating that less of nucleic acids were precipitated by the BioCyTASQ, which may imply a better specificity. The difference between the two conditions could be explained by the difference of beads quantity as 60 *versus* 46.7 µg were used for the first and second conditions, respectively. These points will be discussed further hereafter (see **a. The cell growth** step). Interestingly, a high DNA band was observed in the first condition (**Figure 52-B)**, indicating that G4-DNA might have been precipitated by the BioCyTASQ, which justifies the RNA purification step.

The number of the washing steps was also optimized: in the original protocol, G4-precipitated samples were washed 3x with G4RP buffer and 2x with DEPC-PBS. These washing steps were decreased (STEP 5, sub-step 33-34) to 1x with G4RP wash buffer (**Figure 52-B,C**, blue arrows) and 1x with DEPC-PBS (**Figure**

52-B, green arrows). Gel electrophoresis controls indicated that these modifications did not disrupt the specific interactions with purified RNA.

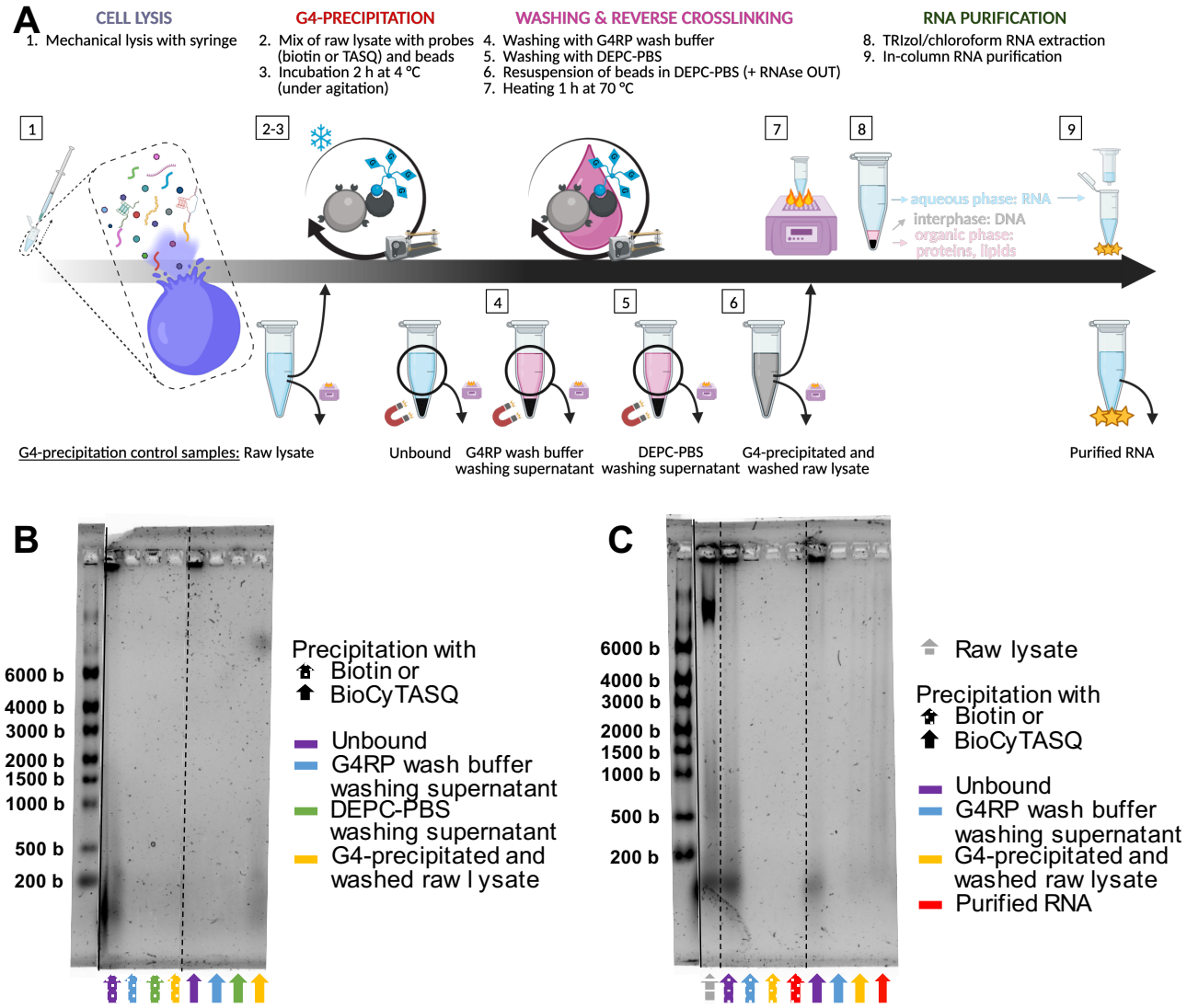

Figure 52. Monitoring of the G4-precipitation step of the G4RP.v2 method by gel electrophoresis. (**A**) During the G4-precipitation step, several control samples were collected to evaluate the potential efficiency of each sub-steps, *i.e.*, the cell lysis, G4-precipitation, both washing, reverse crosslinking and RNA purification. (**B-C**) The control samples collected were loaded and run on a denaturing agarose gel. These control samples are: the raw lysate (grey arrow), unbound (purple arrow), G4RP wash buffer washing supernatant (blue arrow), DEPC-PBS washing supernatant (green arrow), G4-precipitated and washed raw lysate (yellow arrow) and purified RNA (red arrow). Samples collected after the G4-precipitation, *i.e.*, all except the raw lysate (hatched arrow), were precipitated with either Biotin (dotted arrow) or BioCyTASQ (solid arrow). These two gels use samples from two distinct conditions: (**B**) $7x10^6$ MCF7 cells were seeded directly into the treated culture medium (*i.e.*, 0.4% (v/v) DMSO supplemented DMEM) 40 h, then $8x10^6$ cells were lysed and the G4-precipitation were performed with 60 µg of beads. (**C**) $8x10^6$ MCF7 cells were seeded into the culture medium for 18h, then replaced by the treated medium for 48 h, then $12x10^6$ cells were lysed and the G4-precipitation were performed with 46.7 µg of beads. Gels were revelated with SYBR™ Gold Nucleic Acid Gel Stain. RiboRuler High Range RNA Ladder was used as ladder. The panel A was created with BioRender.com

Given that only a fraction of the raw lysate was used (*i.e.*, 60 µL, representing *ca*. 15% of total volume, STEP 4, sub-step 26) to compare several G4-precipitation conditions, the number of pipetting (STEP 3, sub-step 23) was increased from 50 to 100, and that of the cells (STEP 2, sub-step 10) from $9x10^6$ (estimated RNA

recovered ≈ 100 ng/µL) to 12x10^6 (**Figure 50-H**, left, black line) and 24x10^6 (red line), which mechanically increased the amount of estimated RNA recovered in raw lysate (from 467.6 to 772.4 ng/µL (**Table S28-H**)),as also seen by gel analysis (**Figure 51-H**, left). Starting from 24x10^6 cells, the G4-precipitation of samples with the BioCyTASQ, followed by in-column RNA purification, allows the recovery of 30 µL of 85.2 ng/µL purified G4-RNA (**Figure 50-H**, right, red line, **Table S28-H**), *i.e*., 2.6 µg of purified G4-RNA. The control precipitation with biotin permitted to bind 26-fold less of purified RNA (*ca*. 0.1 µg of purified RNA, **Figure 50-H**, right, black line, **Table S28-H**). Using 12.5 µL (STEP 7, sub-step 70) of the 85.2 ng/µL purified G4-RNA for the RT-qPCR implies the use of 1.1 µg of G4-RNA, which is in line with the SuperScript™ III Reverse Transcriptase provider recommendations (*i.e.*, 10 pg-5 µg of total RNA). Collectively, these quantity/quality results (by UV absorbance measurement and gel electrophoresis) combined with qPCR amplification and dissociation curves (**Figures S49-S51-C,D**), support both the validity and efficiency of this optimized G4-RNA-precipitation method.

6. Comparison of the original G4RP *versus* G4RP.v2 protocols

61 individual parameters were assessed for assessing the validity of the G4RP protocol (**Figure 49**) and some important changes were made to optimize it, which results in the so called G4RP.v2 protocol (**Figure 53**). The main modifications are: *i.* the number of seeded cells (increased from 1x10^6 to 7x10^6 cells), *ii.* the cell culture plastics (changed from Petri dish to culture flask), *iii.* the addition of a cell counting step, *iv.* the lysis method (changed from scraping and sonication to trypsinization and pipetting), *v.* the volume of the raw lysate used to precipitate G4s (from 45 to 15%), *vi.* the G4-precipitation schedule (changed for a single incubation with the three components), *vii.* the washing step number (decreased from 5 to 2), *viii.* the RCL time (increased from 1 to 2 h), *ix.* the RNA purification method (changed for in-column purification) and finally, *x.* the schedule of the G4RP (with the introduction of an overnight protocol break during the RNA purification). These changes were made for increasing the practicability of the method (*e.g.*, G4-precipitation in one step), its reproducibility (*e.g.*, cell counting before the fixation) and efficiency (*e.g.*, RCL time) and even for personal preference (*e.g.*, lysis method). A series of checkpoints have been introduced in the protocol, notably through the two monitoring steps (*i.e.,* UV absorbance measurement and gel electrophoresis). Globally speaking, the G4RP.v2 is slightly longer than the original G4RP method, especially because of the new lysis method and the increase of the RCL time, the total protocol duration being estimated at one night plus 17 h for G4RP *versus* one night plus 19.5 h for G4RP.v2.

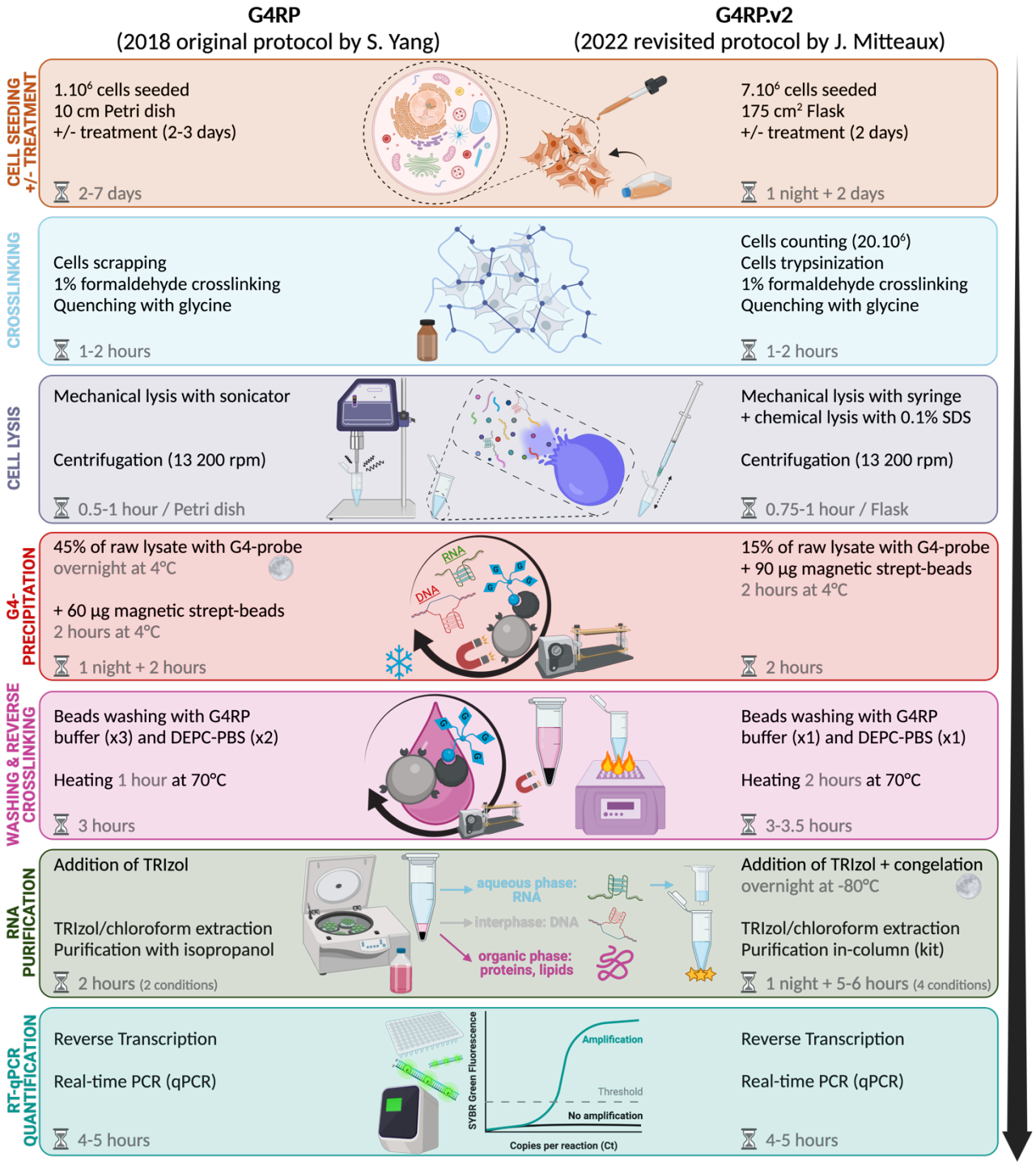

Figure 53. Schematic comparison of G4RP *versus* G4RP.v2 protocols. The G4RP.v2 protocol follows the same main experimental steps than the original G4RP protocol, *i.e.*, cell seeding & treatment (STEP 1), cell crosslinking (STEP 2), cell lysis (STEP 3), G4-precipitation (STEP 4), washing & reverse crosslinking (STEP 5), RNA purification (STEP 6) and RT-qPCR quantification (STEP 7). Several steps were changed and/or optimized, alternative steps were validated (for the cell lysis) and monitoring steps (*e.g.*, UV absorbance measurement and gel electrophoresis) were introduced in order to evaluate the optimizations and limits of the new method. Created with BioRender.com.

7. Alternative lysis methods

In addition to cell lysis by sonication (G4RP) and pipetting (G4RP.v2), two others techniques were explored for cell lysis: cell scraping and cell douncing (**Figure 54**).

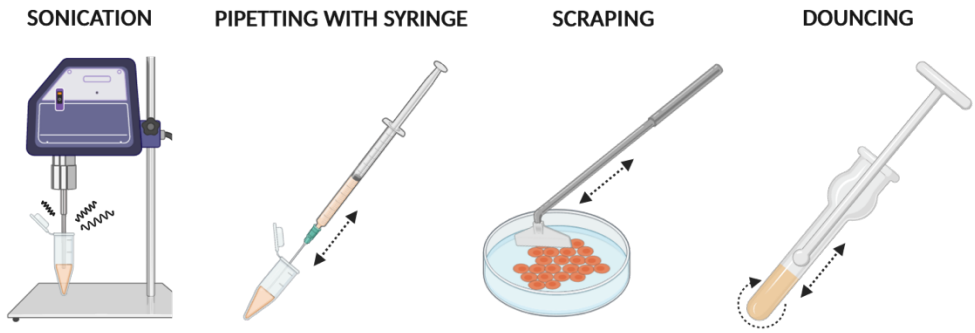

Figure 54. Schematic representation of the four mechanical lysis methods explored for the G4RP.v2. Cell sonication, pipetting with syringe, scraping and douncing are four mechanical lysis methods to lysis cells. Instead of the three others which are able to disrupt nuclear envelope, cell lysis with a douncer only allows for the recovery of cytosol components and intact organelles and nuclei. Created with BioRender.com

a. With a cell scraper (in addition to lysis with a syringe)

Alternative lysis methods were attempted, notably using cell scraper: to this end, $3.3x10^6$ cells were seeded in a culture flask or a Petri dish for a 48 h growth time, and $7.4x10^6$ cells were used for performing cell trypsinization and cell pipetting with 0.4 mm needle-equipped syringe or combining cell scraping and cell pipetting. Both UV absorbance measurement (**Figure 55-A**, **Table S30-a**) and gel electrophoresis (**Figure 55-B**) results show a better lysis efficiency for the combination of scraping and pipetting (**Figure 55**, red line), which led to an estimated RNA concentration of 634.8 ng/µL (*ca*. 1-log higher than with pipetting only (black line; 57.2 ng/µL)). The gel shows also the well disruption of the nuclear envelope with the high > 6 000 bases DNA band. This combination thus appears to be the best for cell lysis and allows for working with a lower cell density. However, the scraping step prevents the cell counting, which explains why the trypsinization/syringe lysis methods.

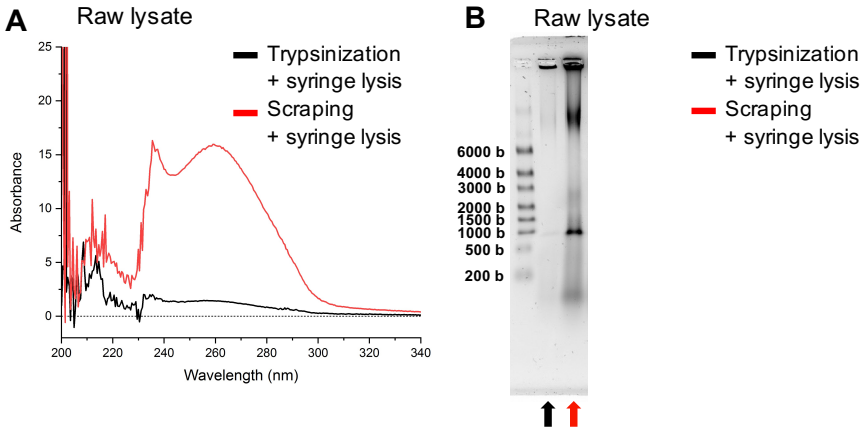

Figure 55. Monitoring lysis method with a cell scraper by UV absorbance measurement and gel electrophoresis. The experiment exploring the alternative cell lysis with a cell scraper was done with $7x10^6$ cells for each condition. Cells were either trypsinized and then lysed with a 0.4 nm needle-equipped syringe (50 pipetting) (black line) or scraped with a cell scraper and then lysed in the same way (red line). Monitoring was done by (**A**) UV absorbance measurements and (**B**) gel electrophoresis. Absorbance, ratios and estimated RNA concentration values can be found in **Table S30-a**. Gels were revelated with SYBR™ Gold Nucleic Acid Gel Stain. RiboRuler High Range RNA Ladder was used as ladder.

b. With a douncer (for cytoplasmic RNA only)

Another alternative lysis method was attempted, using a douncer (or "dounce homogenizer"), having in mind the possibility to perform G4RP.v2 with a different equipment that could be available in others laboratories. For these experiments, the G4RP.v2 protocol was performed till the lysis step (STEP 3, sub-step 22). $19x10^6$ cells were resuspended in the G4RP lysis buffer and lysed by 50 dounces. After several washing steps (with 400 µL of G4RP lysis buffer), samples were centrifuged at 13 200 rpm for 10 min at 4 °C, the supernatant recovered, the pellets resuspended separately in 10 µL of G4RP lysis buffer and sonicated 5 sec in ultrasonic bath sonicator, and all the samples were incubated for 2 h at 70 °C for RCL. UV absorbance measurement clearly shows that the douncer lysis worked well and that the majority of nucleic acid material is found in the raw lysates, with an estimated RNA concentration of 328.8 ng/µL (**Figure 56-A**, **Table S30-b-1**). This quantity corresponds to less than 50% of what is recovered after the syringe-based lysis (with $20x10^6$ cells, **Figure 59**, **Figure 62**, **Table S29**), which can be explained by the fact the douncer lysis does not affect nucleus integrity and allows for the recovery of cytosolic RNAs only. This was confirmed by the gel electrophoresis performed with the supernatants (**Figure 56-B**, solid arrows) where only the bottom band (corresponding to the < 200 bases RNA band) appears. Globally, this series of experiments indicate that the douncer method could be operative but also that care must be taken with the glass material (precisely, the cylindrical mortar part of the douncer): cellular material was lost at the bottom of the douncer and stayed there (Wash 1-2, solid arrows, **Figure 56-B**) without a stringent washing of it before each use, increasing then the risk of cross-contamination. Regarding the pellet samples (**Figure 56-B**, dotted arrows) some bands can be seen by gel (dotted green arrow) which seems to correspond to the DNA band which may be released from nuclei during the ultrasonic or heat treatment. In order to improve this method, $14x10^6$ cells were dounced either 50 or 100 times and two different washing methods were attempted. Douncing cells 50 or 100 times provided the same level of RNA recovery (219-297 ng/µL, **Figure 56-C** dark grey and light grey lines, **Table S30-b-2**) but too much douncing triggers material loss. To conclude, the lysis of cells by douncing appears to be a good and fast alternative to work with cytosolic RNA, and the quality of the samples obtained seemed to be suited to the rest of the G4RP.v2 protocol. However, the risk of cross-contamination is high with this technique and precautions must be applied to avoid it like an efficient cleaning of the douncer between each experiment (*e.g.*, 70% (v/v) Ethanol then RNase-free water washing, 2x; Wash, solid arrows, **Figure 56-D**).

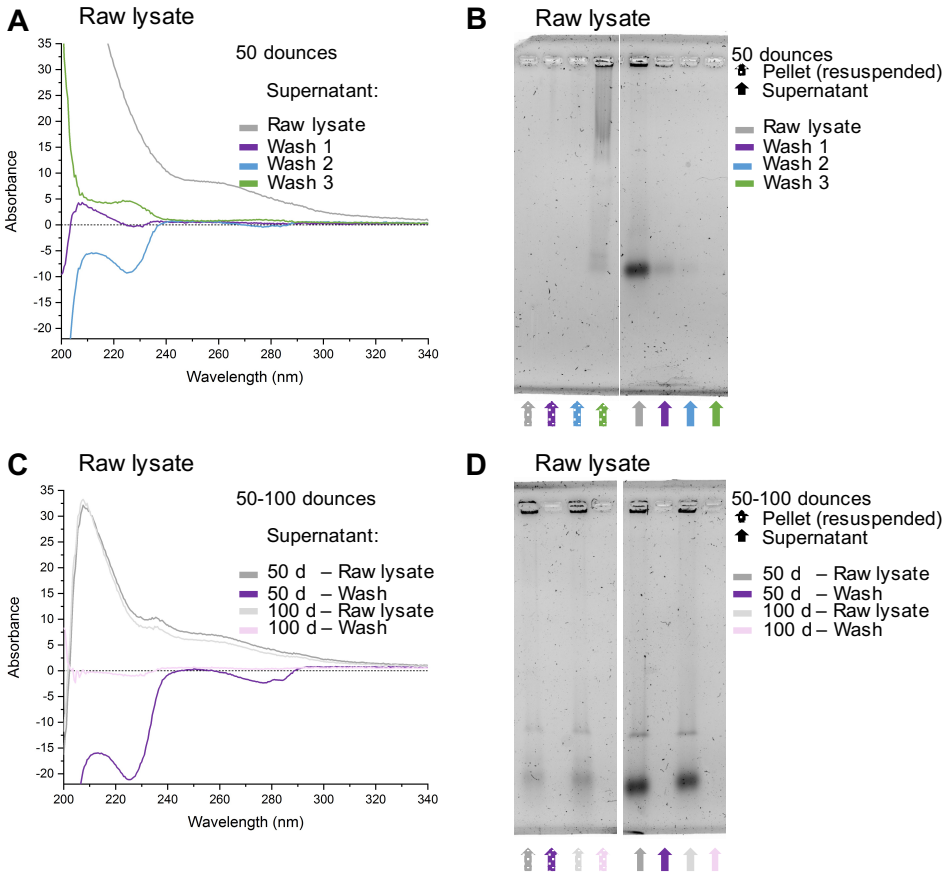

Figure 56. Monitoring lysis method with a douncer by UV absorbance measurement and gel electrophoresis. The two experiments exploring the alternative cell lysis with the douncer were done with (**A-B**) 19x10^6 cells dounced 50 times (raw lysate supernatant: grey symbols) and (**C-D**) 14x10^6 cells dounced 50 (raw lysate supernatant: dark grey symbols) or 100 times (raw lysate supernatant: light grey symbols), respectively. Raw lysate pellets were also kept for gel (dotted arrows). Several wash samples were collected in order to check the cleaning process between experiments and thus anticipate cross-contamination: Wash 1 (purple symbols), Wash 2 (blue symbols) and Wash 3 (green symbols) for the first experiment and "50 d – Wash" (dark purple symbols) and "100 d – Wash" (light purple symbols) for the second. Monitoring was done by UV absorbance measurements (**A, C**) and gel electrophoresis (**B, D**). Absorbance, ratios and estimated RNA concentration values can be found in **Table S30-b1-2**. Gels were revelated with SYBR™ Gold Nucleic Acid Gel Stain.

8. Last optimization steps

a. The cell growth step

The way cells are seeded and cultured can affect their viability and their permeability to various treatments. Also, the quantity of beads (*i.e.,* Streptavidin MagneSphere® Paramagnetic Particles) remained to be optimized. For the first experiment (**Figure 52-B)**, 7x10^6 MCF7 cells were seeded directly into the treated culture medium (*i.e.*, 0.4% (v/v) DMSO supplemented DMEM; this percentage take into account the preparation of the parent ligand solution at 20 mM in DMSO) and let in culture for 40 h. For the second experiment (**Figure 52-C)**, 8x10^6 MCF7 cells were firstly seeded into the culture medium (*i.e.*, supplemented DMEM), let in culture overnight (*i.e.*, 18 h) and then, the medium was then changed for the treated culture medium and cells were treated for 48 h (see the G4RP.v2 method, STEP 1, sub-steps 7-8). These different approaches have important morphological consequences, the cells being round (along with some floating cells) in the treated culture medium while well-spread cells for the 2-step incubation (**Figure 57**). The delay

between seeding and treatment (*i.e.*, overnight + 48 h) seems to be beneficial for cell state; these conditions were thus kept for the following experiments (STEP 1, sub-step 7).

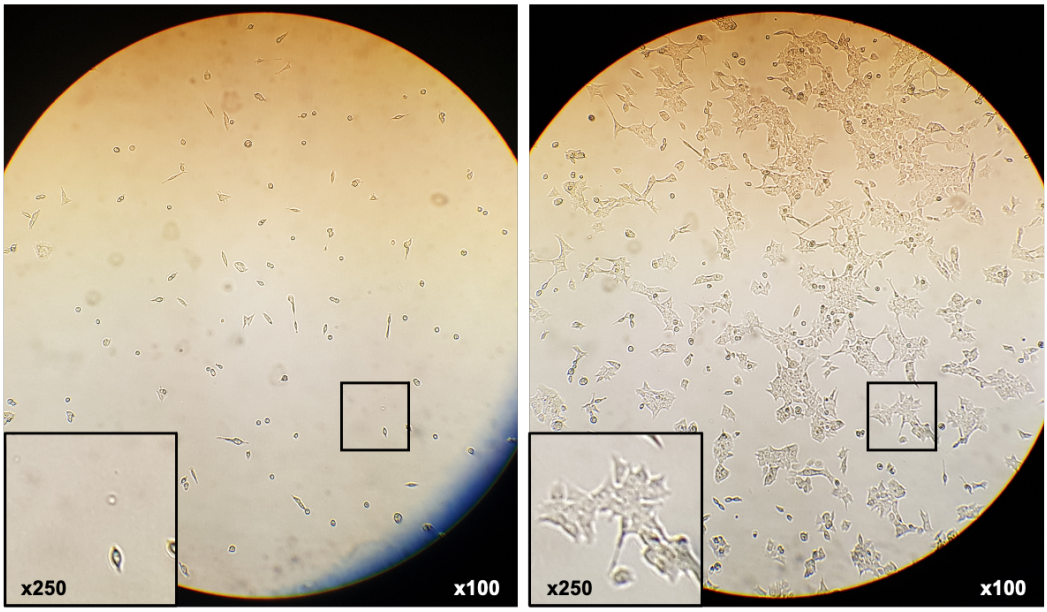

MCF7 cells 1 night after their seeding (day 2)

MCF7 cells after 1 night + 48 h incubation (day 4)

Figure 57. MCF7 cell density through the cell seeding & treatment step. MCF7 cells pictures took before (left) and after (right) 48 h incubation (STEP 1) without treatment through an optical binocular microscope (binocular loupe x10, objective loupe x10). (Insets) Chosen areas with 2.5x magnification.

b. The beads quantity

The initial conditions (**Figure 52-B)** on the use of 60 µg of beads per sample for the G4-precipitation step *versus* 46.7 µg for the second condition (**Figure 52-C)**. This *ca*. 22%-difference could explain the intensity increase of the < 200 bases RNA band for the unbound sample obtained after G4-precipitation with BioCyTASQ (**Figure 52-B,C**, solid purple arrow) and the intensity decrease of that same band for the G4-precipitated and washed raw lysate sample (solid yellow arrow). Therefore, the beads quantity was even increased to 90 µg (STEP 4, sub-step 28) in the final protocol to increase the amount of precipitated G4-RNAs usable for the next step, the RT-qPCR quantification.

c. The RT-qPCR experiments

The final step of the G4RP.v2 protocol is the quantification of the RNA by RT-qPCR. The procedure (**Figure Mat&Meth 8**) was created to automate the reverse transcription reaction (STEP 7, sub-step 75) to make it more reproducible. The first G4-RNA target was a G4 found in the 5'-UTR of the *NRAS* mRNA (simply referred to as *NRAS* G4 hereafter), which is one of the G4-RNA studied with the first version of the G4RP;[120] to this end, the same primers were used (**Tables Mat&Meth 12-13**, **Table S31**), to amplify a 215 nt-long amplicon from the mRNA (**Figure S53**).

Several experiments (**Figure 58-A**) were attempted to optimize the RT-qPCR step: for the input controls (**Figure 58-B**), the RNA samples were obtained directly from the purification of the raw Lysates without any G4-precipitation with G4-specific probes: we observed an overall improvement of the *NRAS* recovery (from Ct value = 34.01 (**Figure 58-A-B**, n° 1, blue line) to 25.41 (**Figure 58-A-B**, n° 5, red line), indicating a *NRAS* fold change of $2^{-(\Delta Ct)} = 2^{-(8.6)} = 388.02$) thanks to the different optimizations of the G4RP.v2 method. We also noticed that the *NRAS* recovery is not linked to the number of cells, which could mean that too many cells might have a small deleterious consequence on their viability. For the G4-precipitated samples (**Figure 58-C**), the precipitation was performed with a TASQ (see below), followed by the RNA purification and then a RT-qPCR quantification of the *NRAS* G4. The enrichment of *NRAS* by G4RP.v2 method is evident regarding Ct values going from 32.34 (**Figure 58-A,C**, n° 1, blue line) to 25.59 (**Figure 58-A,C**, n° 5, red line), representing a fold change of 107.63. This difference does not originate in the TASQ used as four different probes were used (BioTASQ, BioCyTASQ, Clicked ^{az}MultiTASQ and BioTriazoTASQ, see below), which provided similar G4-precipitation efficiency (**Figure 59**, **Table 6**, **Figure S49-E**). This enrichment is specifically due to the precipitation of G4s by TASQs given that the raw lysates treated with biotin as control led to a poor and uncertain Ct value > 30 (**Figure S54**). However, we found out that this enrichment is limited by the binding capacity of TASQs, the streptavidin-coated beads used for isolating the TASQs and/or the purification columns used for isolating the nucleic acids. Neither the increase in the number of cells (from $7x10^6$ to $24x10^6$), the number of pipetting (from 50 to 100) nor in the quantity of beads (from 46.7 to 90 µg) change the level of *NRAS* G4 recovery. These results indicate that a limiting factor could be the binding capacity of the columns used for the RNA purification; this issue could be tackled dividing the G4-precipitated samples in multiple aliquots that are subsequently processed individually and separately or trying to find a purification column with a higher binding capacity.

A

Summary of the experimental condition	Experiment n° 1	Experiment n° 2	Experiment n° 3	Experiment n° 4	Experiment n° 5
Number of cells used	< 4x10^6 cells	10x10^6 cells	7x10^6 cells	12x10^6 cells	24x10^6 cells
Lysis method	Sonication	Syringe (x50)	Syringe (x50)	Syringe (x100)	Syringe (x100)
Concentration of TASQ	95 µM	/	95 µM	95 µM	82 µM
Quantity of beads	96 µg	/	60 µg	46.7 µg	90 µg
Purification method	In-hand purif.	In-hand purif.	In-column purif.	In-column purif.	In-column purif.
Rev. Transcrip. method	Manual	Manual	Automated	Automated	Automated
Ct (dR; Threshold FI: 34)					
(5-25%) input control	34.01 (5%)	27.74 (25%)	25.65 (5%)	24.17 (5%)	25.41 (5%)
G4-precipitation with a TASQ	32.34 (BioTASQ)	/	25.72 (BioCyTASQ)	25.69 (BioCyTASQ)	25.59 (BioCyTASQ)

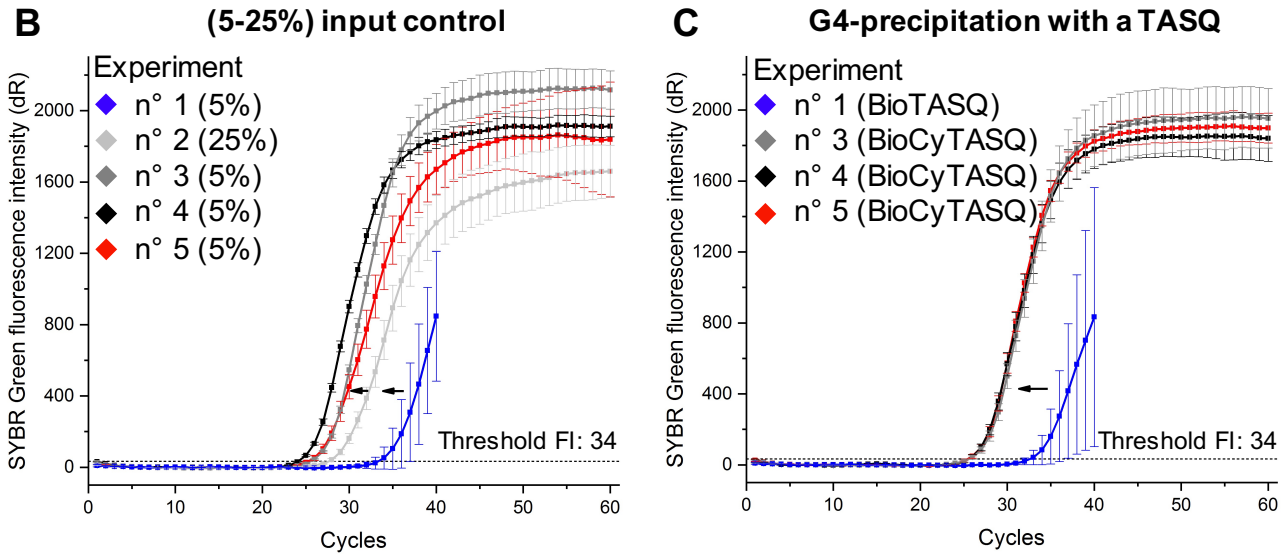

Figure 58. Monitoring the RT-qPCR step improvements of the G4RP.v2 method. (**A**) During the G4RP.v2 method optimization, 5 experiments of RT-qPCR with Purified RNA samples were performed representing the progression of the method from non-successful to final experiments with G4 ligands treatment. Among all peculiar parameters discussed throughout this chapter (Figure 49), several parameters are compared here: the number of cells used, lysis method, concentration of TASQ, quantity of beads, purification method and the reverse transcription method. All the Ct values (fluorescence intensity threshold: 34) obtained from the RT-qPCR quantification of (**B**) input control (5 or 25% from Raw Lysates) and (**C**) G4-precipitation with a TASQ (BioTASQ or BioCyTASQ) samples are presented in the table.

II. The G-quadruplex-RNA-specific precipitation (G4RP.v2) applied to two G4-RNAs with a panel of TASQs

1. Results of the G4RP.v2 method applied to two G-quadruplexes RNAs with a panoply of TASQs

After these rounds of optimization (**Figure 49**, **Figure 53**), which required 29 different experiments, the definitive G4RP.v2 protocol (see the method in Materials and Methods section) was used with different TASQs (**Figure Mat&Meth 9**) using the originally used BioTASQ[120] along with its derivative BioCyTASQ,[122,131,220,222,223] the clickable ^{az}MultiTASQ (clicked to a biotin few days before, see **Figure Mat&Meth 10**, **Tables Mat&Meth 14-15**)[222] and the latest TASQ prototype named BioTriazoTASQ.[264] These

investigations were performed using the *NRAS* G4 target (as above) along with a G4 found in the 5'-UTR of the *VEGFA* mRNA, simply referred to as *VEGFA* G4 hereafter (**Table Mat&Meth 12**, **Figure S55,** *VEGFA* amplicon length = 151 nt), which was also found in the initial protocol. Two controls were implemented during these experiments: *i.* the 5% input control (*i.e.*, the purified RNA sample obtained directly from 5% (volume) of the raw lysate sample without any precipitation with probe) to have a common parameter between all the biological replicates usable for normalization, and *ii.* the biotin control, in which biotin is used instead of TASQ to measure the unspecific binding of G4-RNAs on beads. The results were expressed as a G4RP-RT-qPCR signal (STEP 8, sub-step 83), in fold-change, which was calculated to compare the binding capacity of the different TASQs used against both *NRAS* and *VEGFA* G4s (**Figure 59**, **Table 6**).

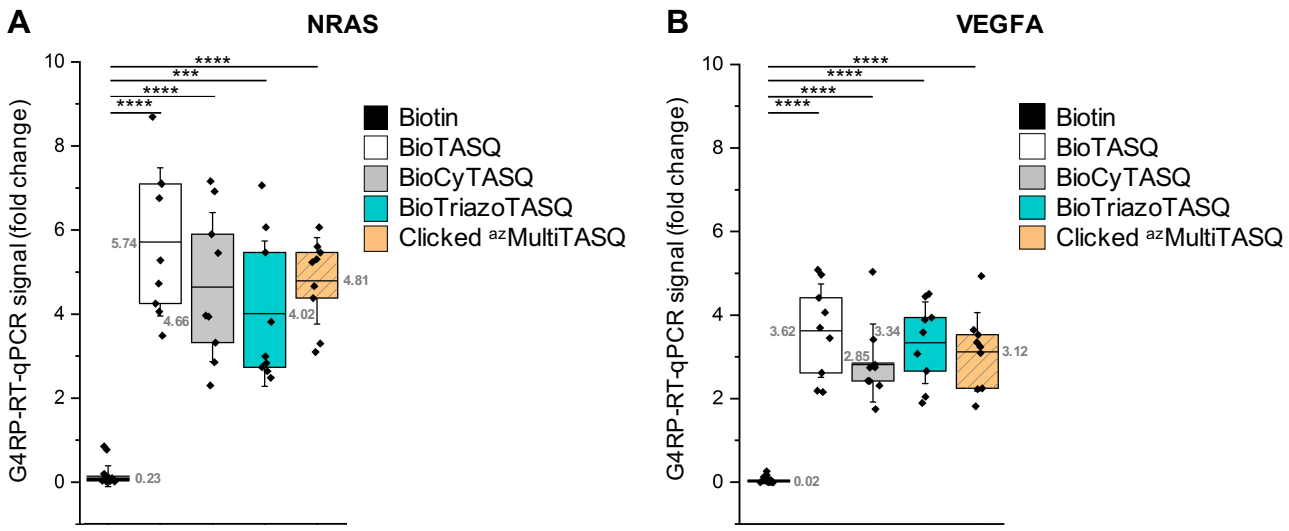

Figure 59. G4RP.v2 method with TASQs against G4-RNA *NRAS* and *VEGFA*. Quantification of the abundance (G4RP-RT-qPCR signal) of the two G4-RNAs (**A**) *NRAS* and (**B**) *VEGFA* from non-treated MCF7 cells (*i.e.*, cells only incubated with the treated culture medium: 0.4% (v/v) DMSO supplemented DMEM) by the G4RP.v2 method. A panel of TASQs was used at 82 µM for the G4-precipitation of nucleic acids from Raw Lysate samples: BioTASQ (white box), BioCyTASQ (grey box), BioTriazoTASQ (blue box) and Clicked ^{az}MultiTASQ (orange box). Biotin was used at 82 µM for the control precipitation (black box). Mean G4RP-RT-qPCR signals are shown in grey. Error bars represent SD from the mean for three independent experiments. For statistical hypothesis tests, Student's *t*-test and Welch's unequal variances *t*-test were used depending on variances equality. * $p < 0.05$, ** $p < 0.01$, *** $p < 0.001$, **** $p < 0.0001$.

Amplified RNA	***NRAS***				
(G4-) probe	Biotin	BioTASQ	BioCyTASQ	BioTriazoTASQ	Clicked ^{az}MultiTASQ
Mean G4RP-RT-qPCR signal	0.23 ± 0.33	5.74 ± 1.77	4.66 ± 1.78	4.02 ± 1.74	4.81 ± 1.03

Amplified RNA	***VEGFA***				
(G4-) probe	Biotin	BioTASQ	BioCyTASQ	BioTriazoTASQ	Clicked ^{az}MultiTASQ
Mean G4RP-RT-qPCR signal	0.02 ± 0.02	3.62 ± 1.12	2.85 ± 0.93	3.34 ± 0.97	3.12 ± 0.94

Table 6. G4RP.v2 results for G4-RNAs *NRAS* and *VEGFA*. Summary of the G4RP-RT-qPCR signal values (mean ± standard deviation) obtained by the G4RP.v2 quantification of the abundance of the two G4-RNAs *NRAS* (top) and *VEGFA* (bottom) from non-treated MCF7-cells.

For both G4-RNAs *NRAS* (**Figure 59-A**) and *VEGFA* (**Figure 59-B**), all TASQs efficiently precipitate G4s, leading to positive G4RP-RT-qPCR signal (expressed as Fold-Change, or simply "FC") (**Table 6**). In the initial publication,[120] a FC of *ca*. 2.9 was obtained for *NRAS* and 2.0 for *VEGFA* with the BioTASQ, which represent a FC_{NRAS}/FC_{VEGFA} ratio of 1.45. In comparison, the G4RP.v2 method provides a FC of 5.74 ± 1.77 for *NRAS* (**Figure 59-A**, white box) and 3.62 ± 1.12 for *VEGFA* (**Figure 59-B**, white box) with BioTASQ, corresponding to a FC_{NRAS}/FC_{VEGFA} ratio of 1.59, demonstrating the robustness of this revisited method. The global increase in these FC values between the original and the revisited protocols could originate in many different reasons, from a difference of the cell (different cell lines, passages numbers, culture method, etc.) or an increase of the G4-precipitated G4-RNA recovery with the G4RP.v2 method. The fact the FC_{NRAS}/FC_{VEGFA} ratio between the two G4-RNAs is similar (*ca*. 1.5) makes us confident as to the reliability of this protocol, and could be used as a characteristic G4RP signature for the MCF7 cells.

To go further into the details: concerning the *NRAS* G4s, the G4 probes BioCyTASQ, BioTriazoTASQ and the Clicked ^{az}MultiTASQ generated a significant FC of 4.66 ± 1.78 (**Figure 59-A**, grey box), 4.02 ± 1.74 (blue box) and 4.81 ± 1.03 (orange box), respectively, representing a similar binding capacity than the BioTASQ (5.74 ± 1.77). The Clicked ^{az}MultiTASQ also appears to give the most reproducible results. When comparing these FC values with the one of the biotin control (0.23 ± 0.33, **Figure 59-A**, black box, **Table 6**, top), a G4-specific-precipitation (G4sP) value (FC_{TASQ}/FC_{biotin} ratio) can be calculated for each TASQ: 24.96 for BioTASQ, 20.26 for BioCyTASQ, 17.48 for BioTriazoTASQ and 20.91 for the Clicked ^{az}MultiTASQ. Concerning the *VEGFA* G4s, the results are somewhat similar although with a lower amplitude: FC = 0.02 ± 0.02 for biotin (**Figure 59-B**, black box, **Table 6**, bottom), 3.62 ± 1.12 (G4sP= 181) for BioTASQ (white box), 2.85 ± 0.93 (G4sP= 142.5) for BioCyTASQ (grey box), 3.34 ± 0.97 (G4sP= 167) for BioTriazoTASQ (blue box) and 3.12 ± 0.94 (G4sP= 156) for the Clicked ^{az}MultiTASQ (orange box). Although the G4RP signals are globally lower for *VEGFA* G4s as compared to *NRAS* G4s, the TASQs showed a higher G4-specificity, their G4sP values being *ca*. 7-fold higher than those for *NRAS*.

III. Study of the ligand-induced effects on two G-quadruplexes RNAs

1. Preparation of the G-quadruplex-interacting molecules treatments

The revisited G4RP.v2 method has proved its efficiency and reliability through the purification by affinity using four different TASQs on two G4-RNAs, *NRAS* and *VEGFA* G4s. In order to expand the scope of the G4RP.v2 method, we decided to focus on the modulation of the RNA G4 landscapes by two G4-interacting compounds, BRACO-19[168,265] and PhpC, the former as a G4 stabilizer, already used in the original publication,[120] and the latter as a prototype of G4-destabilizer, identified in the Chapter I and assessed *in cella* in the Chapter II.

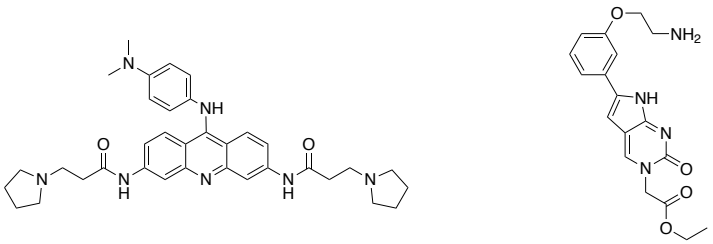

Figure 60. Structures of two G4 ligands, BRACO-19 and PhpC.

The toxicity of the two compounds were first assessed using the sulforhodamine B (SRB) assay on MCF7 cells (**Figure Mat&Meth 7** for the schematic representation; **Tables S32-S33**). A first series of experiences was performed with $6x10^4$ cells, in order to compare three methods of calculation of the cell viability: *i.* the Vichai & Kirtikara method,[266] using a negative control (*i.e.*, untreated cells) and a no growth control (*i.e.*, cells seeded, let in culture for 2 h then processed with the classical protocol),[266] *ii.* an intermediate method using the negative control and the background control (*i.e.*, no cells), and *iii.* a simple method, using only the negative control. It appears that the three methods provide similar results (**Figure S56**), with an IC_{50} of *ca*. 24.4 µM for BRACO-19 and 333.4 µM for PhpC (**Table S34**). Of note, given that some cell viability curves were found to go above 100% (**Figure S56**), which is the sign of a cell mortality in the untreated conditions, the number of seeded cells was decreased from $6x10^4$ cells to $4x10^4$. In these conditions (**Tables S32-S33**), BRACO-19 was found to be quite toxic (with an $IC_{50} = 18.7 \pm 2.8$ µM after 72 h-treatment, **Figure 61**, **Table 7**) and PhpC 20-fold less toxic than BRACO-19 (with an $IC_{50} = 387.9 \pm 41.4$ µM).

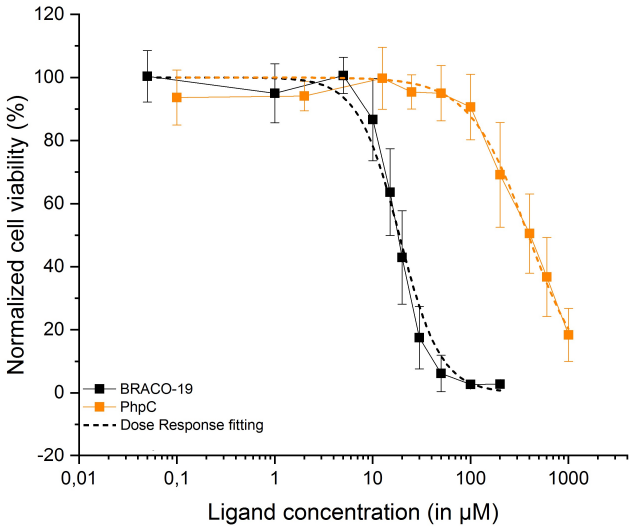

Figure 61. Cytotoxicity profile of BRACO-19 and PhpC. Sulforhodamine B (SRB) cytotoxicity assay was performed on MCF7 cells with the G4 ligands BRACO-19 (black square) and PhpC (orange square). Error bars represent SD from the mean for three independent experiments.

	Inhibitory concentration (IC) (in µM)		
G4 ligand	**IC_{20}**	**IC_{50}**	**IC_{80}**
BRACO-19	9.5 ± 2.0	18.7 ± 2.8	36.6 ± 4.3
PhpC	148.7 ± 26.7	387.9 ± 41.4	1012.0 ± 156.3

Table 7. IC values calculated by the SRB cytotoxicity assay for BRACO-19 and PhpC. Sulforhodamine B (SRB) cytotoxicity assay was performed on MCF7 cells with the G4 ligands BRACO-19 and PhpC and IC_x (x= 20, 50, 80) values, representing the ligand concentrations which allowed the inhibition of the cell viability of x%, were calculated.

2. Results of the G4RP.v2 method applied to cells treated with G-quadruplex-interacting compounds

The G4RP.v2 protocol was applied to cells treated with a concentration of BRACO-19/PhpC below their own IC_{20} values (IC_{20} BRACO-19 = 9.5 ± 2.0 µM, IC_{20} PhpC = 148.7 ± 26.7 µM): 8.4 µM (5 µg/mL) for BRACO-19, corresponding to the concentration used in the original publication,[120] and 90 µM for PhpC, which is calculated to be *ca*. 10-fold more concentrated than BRACO-19 because of the global weaker G4-affinity of PhpC for G4 binding (contrary to G4-stabilizer) evaluated by a series of *in vitro* experiments (see the fluorescence quenching and competitive FRET-melting assays in Chapter II). Untreated cells were used as control. As above, the G4RP.v2 method was monitored using two techniques, *i.e.*, UV absorbance measurement and gel electrophoresis (**Figures S49-S51-A,B**, **Table S29**). At the end of the RNA purification step, 30 µL of purified RNA at *ca.* 60 ng/µL were obtained (**Table S29**), corresponding to 1.8 µg of RNA; 0.75 µg of purified RNA were used for the RT-qPCR quantification, in line with the supplier's recommendations. Some examples of representative *NRAS* and *VEGFA* G4s amplification and dissociation curves and Ct values for these three conditions can be found as a supplementary material (**Figures S49-S51-C-E**).

Concerning the *NRAS* G4s (**Figure 62-A**): the biotin controls (black square) show an almost null FC (0.23 ± 0.33 µM) with no significant impact of the G4 ligand treatments (0.31 ± 0.23 (**Table 8**, top) and 0.23 ± 0.22 µM for BRACO-19- and PhpC-treated MCF7 cells, respectively, compared to non-treated (NT) cells). When using 3 TASQs for precipitating G4s, the treatment with BRACO-19 significantly increased the FC values: from 5.74 ± 1.77 to 15.66 ± 9.59 with BioTASQ (**Figure 62-A**, white square, **Table 8**, top), 4.66 ± 1.78 to 9.54 ± 5.23 with BioCyTASQ (grey square), and 4.81 ± 1.03 to 7.10 ± 1.74 with Clicked ^{az}MultiTASQ (orange square). The corresponding G4 ligand-specific modulatory effect values, calculated through the $FC_{BRACO\text{-}19}/FC_{NT}$ ratio, were 2.73 (BioTASQ), 2.05 (BioCyTASQ) and 1.48 (Clicked ^{az}MultiTASQ), found to be a bit lower than in the original report (*ca*. 4),[120] implying that the BRACO-19 effect was weaker in our conditions. These results show thus a moderate increase in the *NRAS* G4 landscape in MCF7 cells upon BRACO-19 treatment. The PhpC treatment shows, quite satisfyingly, the opposite effect, with a significant decrease in the FC values: from 5.74 ± 1.77 to 3.48 ± 0.66 with BioTASQ (**Figure 62-A**, white square, **Table 8**, top), 4.66 ± 1.78 to 2.42 ± 0.85 with BioCyTASQ (grey square), and 4.81 ± 1.03 to 2.28 ± 1.09 with Clicked ^{az}MultiTASQ (orange square). This corresponds to FC_{PhpC}/FC_{NT} ratios of 0.61, 0.52 and 0.47, respectively, which represent the very first demonstration of the G4-destabilizing effects of the PhpC on a biologically relevant G4-RNA in cells.

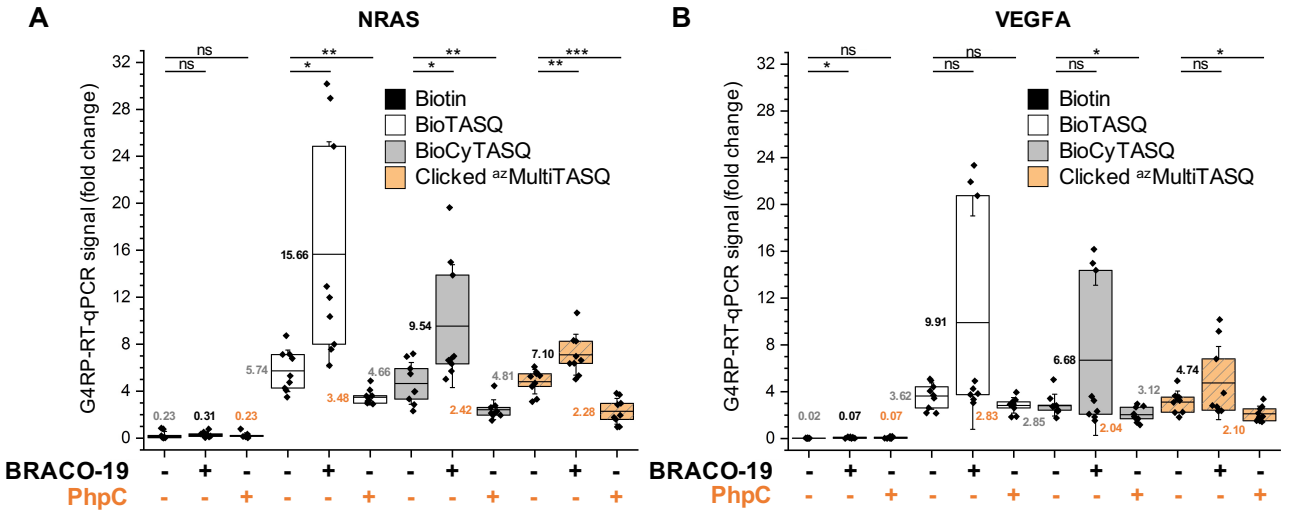

Figure 62. Application of the G4RP.v2 method for the assessment of the G4-RNA *NRAS* and *VEGFA* modulation by G4 ligands treatment. Quantification of the abundance (G4RP-RT-qPCR signal) modulation of the two G4-RNAs (**A**) *NRAS* and (**B**) *VEGFA* by 8.4 µM BRACO-19 (0.4% (v/v) DMSO) (+;-) or 90 µM PhpC (plus 0.4% (v/v) DMSO) (-;+) pre-treatment (48 h) of MCF7 cells via the G4RP.v2 method. For non-treated condition (-;-), cells were only incubated with the treated culture medium (0.4% (v/v) DMSO supplemented DMEM). A panoply of TASQs was used at 82 µM for the G4-precipitation of nucleic acids from Raw Lysate samples: BioTASQ (white box), BioCyTASQ (grey box) and Clicked ^{az}MultiTASQ (orange box). Biotin was used at 82 µM for the control precipitation (black box). Mean G4RP-RT-qPCR signals are shown in grey, black or orange for non-treated, BRACO-19 or PhpC-pre-treated MCF7 cells, respectively. Error bars represent SD from the mean for three independent experiments. For statistical hypothesis tests, Student's *t*-test and Welch's unequal variances *t*-test were used depending on variances equality. * $p < 0.05$, ** $p < 0.01$, *** $p < 0.001$, **** $p < 0.0001$.

Ampified RNA	***NRAS***					
(G4-) probe	Biotin			BioTASQ		
Treatment	NT	**BRACO-19**	PhpC	NT	**BRACO-19**	PhpC
Mean G4RP-RT-qPCR signal	0.23 ± 0.33	0.31 ± 0.23	0.23 ± 0.22	5.74 ± 1.77	15.66 ± 9.59	3.48 ± 0.66
(G4-) probe	BioCyTASQ			Clicked ^{az}MultiTASQ		
Treatment	NT	**BRACO-19**	PhpC	NT	**BRACO-19**	PhpC
Mean G4RP-RT-qPCR signal	4.66 ± 1.78	9.54 ± 5.23	2.42 ± 0.85	4.81 ± 1.03	7.10 ± 1.74	2.28 ± 1.09

Ampified RNA	***VEGFA***					
(G4-) probe	Biotin			BioTASQ		
Treatment	NT	**BRACO-19**	PhpC	NT	**BRACO-19**	PhpC
Mean G4RP-RT-qPCR signal	0.02 ± 0.02	0.07 ± 0.05	0.07 ± 0.07	3.62 ± 1.12	9.91 ± 9.12	2.83 ± 0.66
(G4-) probe	BioCyTASQ			Clicked ^{az}MultiTASQ		
Treatment	NT	**BRACO-19**	PhpC	NT	**BRACO-19**	PhpC
Mean G4RP-RT-qPCR signal	2.85 ± 0.93	6.68 ± 6.42	2.04 ± 0.63	3.12 ± 0.94	4.74 ± 3.13	2.10 ± 0.66

Table 8. Summary values of the G4-RNAs *NRAS* and *VEGFA* abundance modulated by G4 ligands. Summary of the G4RP-RT-qPCR signal values (mean ± standard deviation) obtained by the G4RP.v2 quantification of the abundance modulation of the two G4-RNAs *NRAS* (top) and *VEGFA* (bottom) by BRACO-19 or PhpC treatment. NT: no treatment.

The results obtained with *VEGFA* are less impressive (**Figure 62-B**, **Table 8**, bottom): the increase in the FC values for BRACO-19-treated cells are all non-significant (except for the biotin control (black square),

quite surprisingly): from 3.62 ± 1.12 to 9.91 ± 9.12 ($FC_{BRACO-19}/FC_{NT}$ ratio= 2.74) with BioTASQ (white square), 2.85 ± 0.93 to 6.68 ± 6.42 (2.34) with BioCyTASQ (grey square), and 3.12 ± 0.94 to 4.74 ± 3.13 (1.52) with Clicked ^{az}MultiTASQ (orange square). These results are therefore not in line with the initially ratio value of *ca.* 6 (with BioTASQ) reported in the original article.[120] Quite interestingly, the effect of PhpC on the *VEGFA* G4-precipitation was significant for both BioCyTASQ and Clicked ^{az}MultiTASQ, with FC from 2.85 ± 0.93 to 2.04 ± 0.63 (0.72) with BioCyTASQ (grey square), and 3.12 ± 0.94 to 2.10 ± 0.66 (0.67) with Clicked ^{az}MultiTASQ (orange square). The results obtained with BioTASQ (from 3.62 ± 1.12 to 2.83 ± 0.66 (FC_{PhpC}/FC_{NT} ratio= 0.78), white square) were non-significant due to the high variability of the experiments.

Collectively, these results indicate that the conditions in which cells were treated with BRACO-19 did not allow for monitoring clear effects on both *NRAS* and *VEGFA* G4s with all the TASQs, and that better results were obtained with *NRAS* G4s; conversely, the conditions in which cells were treated with PhpC led to a significant effect on the two G4s, which can be well-visualized with some TASQs. Also, these results indicate that the Clicked ^{az}MultiTASQ seems to be the most reliable probe to precipitate G4s from cells, from both an efficiency and reproducibility points of view.

C. Discussion and perspectives

The optimization of the G4RP protocol, which led to the G4RP.v2 protocol, was time- (*ca*. 5 full months of work) and material-demanding (*ca*. 30 different experiments were performed, with a lot of controls) but highly rewarding (specific techniques had to be learned, skills to be acquired).

From a technical point of view, monitoring RNA extraction by UV absorbance measurement and gel electrophoresis appeared to be suited and complementary techniques. While UV absorbance provides an approximative RNA quantity and useful information about its quality, gel electrophoresis allows for evaluating the efficiency of the cell lysis step by the direct observation of DNA and/or RNA electrophoretic bands. However, checking the quality of the purified RNA by gel was not very useful given the low quantity of RNA loaded (around 0.35 µg; the UV absorbance measurements were more sensitive and thus, informative here). Gel electrophoresis is more appropriated for the raw lysate samples but have to be run the day of the extraction for better results: I was used to run the gels the day after (for timing reasons), which explains why these gels appeared somewhat blurred, with partial nucleic acids degradation (**Figures S49-S51-B**). This was not the case for the gels loaded on the extraction day, notably during optimization experiments (**Figure 51**, Raw lysates samples), where bands were generally clearer and cleaner.

Combining cell scraping followed by cell lysis with a needle-equipped syringe provided the best RNA recovery efficiency among the several alternative attempts (**Figure 55**). However, this method was finally not retained given that I wanted to start every G4RP.v2 experiment with the same number of cells, which implied trypsinization and cell counting steps. I came to realize later that, at this stage, this parameter was not critical as the 5% input control allows for a systematic and reliable normalization during the RT-qPCR step. This parameter was however critical when cells were treated by ligands, to make the cell number/treatment

concentration ratio coherent and accurate. For the next developments of the G4RP.v2 technique, the use of this scraping-pipetting combination must be re-evaluated; also, the G4RP.v2 technique must now be applied at a transcriptome-wide scale, implying to fine-tune again the sonication step.

From a result point of view, the G4RP.v2 worked with three different TASQs, BioTASQ, BioCyTASQ and Clicked ^{az}MultiTASQ. The efficiency of the biotinylated TASQ was already established in the original protocol performed with the BioTASQ;[120] the results obtained herein with the Clicked ^{az}MultiTASQ (**Figure 59**, **Figure 62**, orange square) constitute a great advance in the development and use of multivalent TASQs and more generally versatile G4 tools in the G4 field.[222]

From a more general point of view, the G4RP.v2 technique allowed for assessing the global G4-RNAs *NRAS* and *VEGFA* landscapes in cells, and their modulation upon chemical treatment, what were reported via a publication in the journal Chemical Communications with some results from the Chapter II.[255] Globally speaking, the results were better for the *NRAS* G4s: as discussed above, the BRACO-19 treatment concentration has to be increased to obtain better results for the *VEGFA* G4s. More generally, dose-response G4RP.v2 experiments (*e.g.*, 3 different concentrations of ligands) could be interesting to better delineate the most effective concentration of both BRACO-19 and PhpC in cells. Also, the quantification of a non G4 housekeeping transcript is now required to validate completely this technique and use a classical transcript expression calculation (*e.g.*, $2^{-\Delta\Delta Ct}$).

Although some technical issues remain to be fixed, and some results improved (*e.g.*, *VEGFA*), the application of the G4RP.v2 method for the quantitative assessment of the PhpC effect on biological G4-RNAs is a success. Indeed, the modulation (decrease) of the natural abundance of two G4-RNAs, *NRAS* and *VEGFA*, by cell treatment with PhpC has been for the very first time demonstrated. Even if the exact mechanism by which PhpC exerts its effects remains to be deciphered (G4 destabilizing *per se*? facilitating the processivity of G4-helicase(s)/polymerase(s)? Both? Other?), the results reported herein are promising for the use of this molecule as a tool in the G4 field (*e.g.*, increasing the G4 landscape using PDS, decreasing it using PhpC) and even possibly as a drug for tackling G4-helicase deficiencies.[141] The application of the PhpC now needs the G4RP.v2 method to be performed at a transcriptome-wide scale (sequencing) to have a more precise idea of fields and diseases it might be useful to (G4-RNA-associated pathologies including neurodegenerative and infectious diseases, cancers).[135,144,153]

GENERAL CONCLUSIONS

The discovery of the G4 structures is intimately linked to the development and use of biophysical and biochemical methods such as UV absorption,[37] X-ray diffraction,[15] circular dichroism and PAGE.[16,54] They allowed for the identification of DNA as well as RNA G4-folding sequences, their structural characterization[267] and the characterization of G4-interacting molecules (*e.g.*, small molecules, proteins, aptamers).[268,269,213] G4s were initially seen as laboratory 'oddities' but the development of molecular biology techniques (*e.g.*, telomerase assay, gene reporter assay, RNAi),[77,86,102] combined with the use of G4 ligands (*e.g.*, BRACO-19, TMPyP4, PDS, Phen-DC_3) highlighted their possible biological functions, being linked to gene expression regulation, replication and transcription regulation, telomeres maintenance, DNA repair, proteins recruitment, etc.[135,270,271] These investigations also showed that an excessive formation of G4s, related to G4-helicase dysfunctions for instance, can be closely associated to neurodegenerative (*e.g.*, *C9orf72*-mediated ALS/FTD, Fragile X Syndrome)[153,152] and genetic diseases (*e.g.*, Bloom and Werner syndromes),[141,272] respectively. The quest for molecules able to interact with and modulate G4 structures in cells appear thus a useful strategy for the study of, and the development of potential treatments for, G4-associated diseases.

Our efforts described in chapter I are part of this objective, with the ultimate goal of identifying G4-destabilizing small molecules. We gathered promising candidates (based on already published molecules as well as reliable hypotheses) and assessed their G4-destabilizing properties *in vitro* using classical methods (*e.g.*, FRET-melting, CD titrations, PAGE analysis)[84,54,16] along with 2 newly developed assays, the G4-UNFOLD and qPCR Stop assays.[93] The former relies on the study of the kinetics of hybridization between an a G4-containing ON and its complementary sequence, the latter on that of the G4 structure-associated stalling of the *Taq* polymerase. We identified several promising small molecules, first and foremost the leading compound PhpC. Indeed, the wealth of data acquired with this molecule, highlighted by the newly developed scoring method, clearly identifies PhpC as the best G4-destabilizer from our series of candidates, with an established G4-destabilizing activity in 6 out of 7 *in vitro* assays performed. The next question was thus: is PhpC active in cells as well?

Optical imaging greatly contributed to gain insights into the biological relevance of G4s, using either antibodies (*e.g.*, BG4, D1),[114,198] nanobody (*e.g.*, SG4),[126] fluorescent G4 probes (*e.g.*, N-TASQ, PDP-Cy5, RHPS4)[208,212,214] or multivalent G4 molecular tools, both biotinylated[220,222,223] and clickable G4 ligands.[222,273,219,113] These multivalent tools can also be used for isolating G4s from cell extracts by affinity purification, with techniques such as G4RP-Seq and G4DP-Seq with biotinylated TASQs,[120,121,131] and G4-ChIP-Seq and G4 CUT&Tag with the BG4 antibody.[116,125]

We further develop the use of multivalent TASQs during this PhD project. In chapter II, we showed that the multivalent molecular tools BioCyTASQ and BioTriazoTASQ can be successfully implemented for the detection of G4s in cells and the study of their involvement in DNA double-stranded breaks (*via* a co-labelling

of γH2AX *foci*) by semi-quantitative analyses. We also demonstrated the global effect of the G4 destabilizer PhpC on the global G4 landscapes, which triggers a 3.2-fold decrease in the number of G4 *foci* number, quantified by an home-made macro program.

The experiments described in Chapter III results from the convergence of that described in Chapters I and II: indeed, they aim at providing a quantitative evaluation of the RNA G4 destabilizing properties of PhpC using multivalent TASQs (BioCyTASQ, BioTriazoTASQ, Clicked ^{az}MultiTASQ) in G4RP-RT-qPCR evaluation. To this end, the first G4RP-RT-qPCR protocol was optimized to lead to the G4RP.v2 method, which involves different cell lysis techniques and different go/no-go control steps. The G4RP.v2 method was used here to show that PhpC effectively destabilizes 2 G4-containing mRNAs, NRAS and VEGFA, with respective 1.6-/2.1-fold and 1.3-/1.5-fold decreases depending on the G4 tools used for the G4 precipitation.

In summary, this 3-year thesis project led to *i.* the development of 2 *in vitro* assays (the G4-UNFOLD and qPCR Stop assays) to assess small molecules effect on G4-DNA structures, *ii.* the identification of the first reliable prototype of G4 destabilizers, *iii.* the optimization of a scoring method for an easy classification of G4 destabilizer candidates, *iv.* the development of a new *in vitro* pull-down assay for assessing the properties of biotinylated TASQs (the qPCR pull-down assay), *v.* the validation of the use of 2 biotinylated TASQs (BioCyTASQ and BioTriazoTASQ) for G4 imaging in human cells, *vi.* the demonstration of the cellular properties of PhpC *via* an optimized semi-quantitative analysis (the N-TASQ macro program 2.0), *vii.* the optimization of an affinity purification method for the quantitative study of cellular G4-RNAs (G4RP.v2), and finally *viii*. the use of G4RP.v2 with several multivalent TASQs (BioCyTASQ, BioTriazoTASQ and clicked ^{az}MultiTASQ) for validating the G4-RNA-destabilizing effect of PhpC on the two G4-containing mRNAs *NRAS* and *VEGFA* in human cells.

Taken together, the results obtained through my PhD project support the DNA/RNA G4- destabilizing properties of the G-clamp analogue PhpC, demonstrated through both semi-quantitative and quantitative experiments, making it a promising tool for the G4 research, and possibly a promising candidate for treating G4-associated genetic dysfunctions. The protocols we developed also expand the scope of applications of TASQs, demonstrating that they are efficient tools for *in vitro* experiments, G4 imaging in human cells, and for the purification and quantification of G4-RNAs from cell lysates. Therefore, we do believe that these results have thus reached the goal heralded in the title of this manuscript as they have undoubtedly contributed to the development of methods and tools for the study of G-quadruplex DNA and RNA in human cells.

BIBLIOGRAPHY

(1) Miescher, F. Ueber Die Chemische Zusammensetzung Der Eiterzellen. *Medizinisch-chemische Untersuchungen* **1871**, *4*, 441–460.
(2) Dahm, R. Discovering DNA: Friedrich Miescher and the Early Years of Nucleic Acid Research. *Hum Genet* **2008**, *122* (6), 565–581. https://doi.org/10.1007/s00439-007-0433-0.
(3) Kossel, A. Ueber Die Herkunft Des Hypoxanthins in Den Organismen. *Z. Physiol. Chem.* **1881**, *5* (2–3), 152–157. https://doi.org/10.1515/bchm1.1881.5.2-3.152.
(4) Jones, M. E. Albrecht Kossel, a Biographical Sketch. *Yale Journal of Biology and Medicine* **1953**, *26*, 80–97.
(5) Levene, P. A. Recent Work in Biological Chemistry. *J. Am. Chem. Soc.* **1905**, *27* (11), 1445–1459. https://doi.org/10.1021/ja01989a010.
(6) Mandel, J. A.; Levene, P. A. On the Pyrimidin Bases of the Nucleic Acid Obtained from Fish Eggs. *Journal of Biological Chemistry* **1906**, *1* (4), 425–426. https://doi.org/10.1016/S0021-9258(17)46078-9.
(7) Mandel, J. A.; Jacobs, W. A.; Levene, P. A. On Nucleic Acids. *Experimental Biology and Medicine* **1908**, *5* (4), 92–94. https://doi.org/10.3181/00379727-5-54.
(8) Watson, T.; Crick, F. Molecular Structure of Nucleic Acids. *Nature* **1953**, *171*, 737–738.
(9) Franklin, R.; Gosling, R. G. Evidence for 2-Chain Helix in Crystalline Structur of Sodium Deoxyribonucleate. *Nature* **1953**, *171* (4356), 740–741.
(10) Wilkins, M. H. F. Molecular Structure of Deoxypentose Nucleic Acids. *Nature* **1953**, *171*, 738–740.
(11) Stefan, L.; Bertrand, B.; Richard, P.; Le Gendre, P.; Denat, F.; Picquet, M.; Monchaud, D. Assessing the Differential Affinity of Small Molecules for Noncanonical DNA Structures. *ChemBioChem* **2012**, *13* (13), 1905–1912. https://doi.org/10.1002/cbic.201200396.
(12) Felsenfeld, G.; Davies, D. R.; Rich, A. Formation of a Three-Stranded Polynucleotide Molecule. *Journal of the American Chemical Society* **1957**, *79* (8), 2023–2024.
(13) Htun, H.; Dahlberg, J. E. Topology and Formation of Triple-Stranded H-DNA. *Science* **1989**, *243* (4898), 1571–1576. https://doi.org/10.1126/science.2648571.
(14) Dalla Pozza, M.; Abdullrahman, A.; Cardin, C. J.; Gasser, G.; Hall, J. P. Three's a Crowd - Stabilisation, Structure, and Applications of DNA Triplexes. *Chem Sci* **2022**, *13* (35), 10193–10215. https://doi.org/10.1039/d2sc01793h.
(15) Gellert, M.; Lipsett, M. N.; Davies, D. R. Helix Formation by Guanylic Acid. *Proceedings of the National Academy of Sciences* **1962**, *48* (12), 2013–2018.
(16) Sen, D.; Gilbert, W. Formation of Parallel Four-Stranded Complexes by Guanine-Rich Motifs in DNA and Its Implications for Meiosis. *Nature* **1988**, *334*, 364–366.
(17) Spiegel, J.; Adhikari, S.; Balasubramanian, S. The Structure and Function of DNA G-Quadruplexes. *Trends in Chemistry* **2020**, *2* (2), 123–136. https://doi.org/10.1016/j.trechm.2019.07.002.
(18) Holliday, R. A Mechanism for Gene Conversion in Fungi. *Genet Res* **1964**, *5*, 282–304. https://doi.org/10.1017/S0016672308009476.
(19) Panayotatos, N.; Wells, R. D. Cruciform Structures in Supercoiled DNA. *Nature* **1981**, *289* (5797), 466–470. https://doi.org/10.1038/289466a0.
(20) Khristich, A. N.; Mirkin, S. M. On the Wrong DNA Track: Molecular Mechanisms of Repeat-Mediated Genome Instability. *J. Biol. Chem.* **2020**, *295* (13), 4134–4170. https://doi.org/10.1074/jbc.REV119.007678.
(21) Pohl, F. M. Ein modell der DNS-Struktur. *Naturwissenschaften* **1967**, *54* (23), 616. https://doi.org/10.1007/BF00591426.
(22) Ghosh, A.; Bansal, M. A Glossary of DNA Structures from A to Z. *Acta Crystallogr D Biol Crystallogr* **2003**, *59* (Pt 4), 620–626. https://doi.org/10.1107/s0907444903003251.
(23) Ravichandran, S.; Subramani, V. K.; Kim, K. K. Z-DNA in the Genome: From Structure to Disease. *Biophys Rev* **2019**, *11* (3), 383–387. https://doi.org/10.1007/s12551-019-00534-1.
(24) Thomas, M.; White, R. L.; Davis, R. W. Hybridization of RNA to Double-Stranded DNA: Formation of R-Loops. *Proc Natl Acad Sci U S A* **1976**, *73* (7), 2294–2298. https://doi.org/10.1073/pnas.73.7.2294.
(25) Chakraborty, P. New Insight into the Biology of R-Loops. *Mutation Research/Fundamental and Molecular Mechanisms of Mutagenesis* **2020**, *821*, 111711. https://doi.org/10.1016/j.mrfmmm.2020.111711.

(26) Schildkraut, C. L.; Richardson, C. C.; Kornberg, A. Ebzymic Synthesis of Deoxyribonucleic Acid XVII. Some Unusual Physical Properties of the Product Primed by Native DNA Templates. *J Mol Biol* **1964**, *9*, 24–45. https://doi.org/10.1016/s0022-2836(64)80089-9.
(27) Jensch, F.; Kemper, B. Endonuclease VII Resolves Y-Junctions in Branched DNA in Vitro. *EMBO J* **1986**, *5* (1), 181–189. https://doi.org/10.1002/j.1460-2075.1986.tb04194.x.
(28) McQuaid, K. T.; Pipier, A.; Cardin, C. J.; Monchaud, D. Interactions of Small Molecules with DNA Junctions. *Nucleic Acids Res* **2022**, *50* (22), 12636–12656. https://doi.org/10.1093/nar/gkac1043.
(29) Gehring, K.; Leroy, J.-L.; Guéron, M. A Tetrameric DNA Structure with Protonated Cytosine.Cytosine Base Pairs. *Nature* **1993**, *363* (6429), 561–565. https://doi.org/10.1038/363561a0.
(30) Mergny, J.-L.; Sen, D. DNA Quadruple Helices in Nanotechnology. *Chem. Rev.* **2019**, *119* (10), 6290–6325. https://doi.org/10.1021/acs.chemrev.8b00629.
(31) Griffith, J. D.; Comeau, L.; Rosenfield, S.; Stansel, R. M.; Bianchi, A.; Moss, H.; de Lange, T. Mammalian Telomeres End in a Large Duplex Loop. *Cell* **1999**, *97* (4), 503–514. https://doi.org/10.1016/S0092-8674(00)80760-6.
(32) Duquette, M. L.; Handa, P.; Vincent, J. A.; Taylor, A. F.; Maizels, N. Intracellular Transcription of G-Rich DNAs Induces Formation of G-Loops, Novel Structures Containing G4 DNA. *Genes Dev* **2004**, *18* (13), 1618–1629. https://doi.org/10.1101/gad.1200804.
(33) Bang, I. C. Chemische Und Physiologische Studien Über Die Guanylsäure. *Z. Physiol. Chem.* **1901**, *32*, 201–213.
(34) Donohue, J. Hydrogen-Bonded Helical Configurations of Polynucleotides. *Proceedings of the National Academy of Sciences* **1956**, *42*, 60–65.
(35) Arnott, S.; Chandrasekaran, R.; Marttila, C. M. Structures for Polyinosinic Acid and Polyguanylic Acid. *Biochemical Journal* **1974**, *141*, 537–543.
(36) Rich, A. The Molecular Structure of Polyionisinic Acid. *Biochimica et Biophysica Acta* **1958**, *29*, 502–509.
(37) Ralph, R. K.; Connors, W. J.; Khorana, H. G. Secondary Structure and Aggregation in Deoxyguanosine Oligonucleotides. *Journal of the American Chemical Society* **1962**, *84* (11), 2265–2266.
(38) Zimmerman, S. B.; Cohen, G. H.; Davies, D. R. X-Ray Fiber Diffraction and Model-Building Study of Polyguanylic Acid and Polyinosinic Acid. *J Mol Biol* **1975**, *92* (2), 181–192. https://doi.org/10.1016/0022-2836(75)90222-3.
(39) Kim, J.; Cheong, C.; Moore, P. B. Tetramerization of an RNA Oligonucleotide Containing a GGGG Sequence. *Nature* **1991**, *351* (6324), 331–332.
(40) Wei, D.; Parkinson, G. N.; Reszka, A. P.; Neidle, S. Crystal Structure of a C-Kit Promoter Quadruplex Reveals the Structural Role of Metal Ions and Water Molecules in Maintaining Loop Conformation. *Nucleic Acids Res* **2012**, *40* (10), 4691–4700. https://doi.org/10.1093/nar/gks023.
(41) Collie, G. W.; Sparapani, S.; Parkinson, G. N.; Neidle, S. Structural Basis of Telomeric RNA Quadruplex-Acridine Ligand Recognition. *J Am Chem Soc* **2011**, *133* (8), 2721–2728. https://doi.org/10.1021/ja109767y.
(42) Sasisekharan, V.; Zimmerman, S.; Davies, D. R. The Structure of Helical 5′-Guanosine Monophosphate. *Journal of Molecular Biology* **1975**, *92* (2), 171–179. https://doi.org/10.1016/0022-2836(75)90221-1.
(43) Pinnavaia, T. J.; Miles, H. T.; Becker, E. D. Self-Assembled 5'-Guanosine Monophosphate, Nuclear Magnetic Resonance Evidence for a Regular, Ordered Structure and Slow Chemical Exchange. *Journal of the American Chemical Society* **1975**, *97* (24), 7198–7200.
(44) Burge, S.; Parkinson, G. N.; Hazel, P.; Todd, A. K.; Neidle, S. Quadruplex DNA: Sequence, Topology and Structure. *Nucleic Acids Research* **2006**, *34* (19), 5402–5415. https://doi.org/10.1093/nar/gkl655.
(45) Ma, Y.; Iida, K.; Nagasawa, K. Topologies of G-Quadruplex: Biological Functions and Regulation by Ligands. *Biochemical and Biophysical Research Communications* **2020**, *531* (1), 3–17. https://doi.org/10.1016/j.bbrc.2019.12.103.
(46) Webba da Silva, M. Geometric Formalism for DNA Quadruplex Folding. *Chem. Eur. J.* **2007**, *13* (35), 9738–9745. https://doi.org/10.1002/chem.200701255.
(47) Karsisiotis, A. I.; Hessari, N. M.; Novellino, E.; Spada, G. P.; Randazzo, A.; Webba da Silva, M. Topological Characterization of Nucleic Acid G-Quadruplexes by UV Absorption and Circular Dichroism. *Angew. Chem. Int. Ed.* **2011**, *50* (45), 10645–10648. https://doi.org/10.1002/anie.201105193.
(48) Parkinson, G. N.; Lee, M. P. H.; Neidle, S. Crystal Structure of Parallel Quadruplexes from Human Telomeric DNA. *Nature* **2002**, *417* (6891), 876–880. https://doi.org/10.1038/nature755.

(49) Williamson, J. R.; Raghuraman, M. K.; Cech, T. R. Monovalent Cation-Induced Structure of Telomeric DNA: The G-Quartet Model. *Cell* **1989**, *59*, 871–880.
(50) Sen, D.; Gilbert, W. A Sodium-Potassium Switch in the Formation of Four-Stranded G4-DNA. *Nature* **1990**, *344*, 410–414.
(51) Haider, S.; Parkinson, G. N.; Neidle, S. Crystal Structure of the Potassium Form of an Oxytricha Nova G-Quadruplex. *Journal of Molecular Biology* **2002**, *320*, 189–200.
(52) Črnugelj, M.; Šket, P.; Plavec, J. Small Change in a G-Rich Sequence, a Dramatic Change in Topology: New Dimeric G-Quadruplex Folding Motif with Unique Loop Orientations. *J. Am. Chem. Soc.* **2003**, *125* (26), 7866–7871. https://doi.org/10.1021/ja0348694.
(53) Cheong, C.; Moore, P. B. Solution Structure of an Unusually Stable RNA Tetraplex Containing G- and U-Quartet Structures. *Biochemistry* **1992**, *31*, 8406–8414.
(54) Gray, D. M.; Bollum, F. J. A Circular Dichroism Study of Poly dG, Poly dC, and Poly dG:dC. *Biopolymers* **1974**, *13* (10), 2087–2102. https://doi.org/10.1002/bip.1974.360131011.
(55) Mergny, J.-L.; Li, J.; Lacroix, L.; Amrane, S.; Chaires, J. B. Thermal Difference Spectra: A Specific Signature for Nucleic Acid Structures. *Nucleic Acids Research* **2005**, *33* (16), e138–e138. https://doi.org/10.1093/nar/gni134.
(56) Wang, Y.; Patel, D. J. Solution Structure of the Human Telomeric Repeat d[AG3(T2AG3)3] G-Tetraplex. *Structure* **1993**, *1* (4), 263–282. https://doi.org/10.1016/0969-2126(93)90015-9.
(57) Joachimi, A.; Benz, A.; Hartig, J. S. A Comparison of DNA and RNA Quadruplex Structures and Stabilities. *Bioorganic & Medicinal Chemistry* **2009**, *17*, 6811–6815.
(58) Banco, M. T.; Ferré-D'Amaré, A. R. The Emerging Structural Complexity of G-Quadruplex RNAs. *RNA* **2021**, *27* (4), 390–402. https://doi.org/10.1261/rna.078238.120.
(59) Huppert, J. L.; Balasubramanian, S. Prevalence of Quadruplexes in the Human Genome. *Nucleic Acids Research* **2005**, *33* (9), 2908–2916. https://doi.org/10.1093/nar/gki609.
(60) Bedrat, A.; Lacroix, L.; Mergny, J.-L. Re-Evaluation of G-Quadruplex Propensity with G4Hunter. *Nucleic Acids Res* **2016**, *44* (4), 1746–1759. https://doi.org/10.1093/nar/gkw006.
(61) Puig Lombardi, E.; Londoño-Vallejo, A. A Guide to Computational Methods for G-Quadruplex Prediction. *Nucleic Acids Research* **2020**, *48* (1), 1–15. https://doi.org/10.1093/nar/gkz1097.
(62) Santos, T.; Salgado, G. F.; Cabrita, E. J.; Cruz, C. G-Quadruplexes and Their Ligands: Biophysical Methods to Unravel G-Quadruplex/Ligand Interactions. *Pharmaceuticals* **2021**, *14* (8), 769. https://doi.org/10.3390/ph14080769.
(63) Jin, R.; Breslauer, K. J.; Jones, R. A.; Gaffney, B. L. Tetraplex Formation of a Guanine-Containing Nonameric DNA Fragment. *Science* **1990**, *250* (4980), 543–548. https://doi.org/10.1126/science.2237404.
(64) Wang, Y.; de los Santos, C.; Gao, X.; Greene, K.; Live, D.; Patel, D. J. Multinuclear Nuclear Magnetic Resonance Studies of Na Cation-Stabilized Complex Formed by d(G-G-T-T-T-T-C-G-G) in Solution. *Journal of Molecular Biology* **1991**, *222* (3), 819–851.
(65) Aboul-ela, F.; Murchie, A. I. H.; Lilley, D. M. J. NMR Study of Parallel-Stranded Tetraplex Formation by the Hexadeoxynucleotide d(TG4T). *Nature* **1992**, *360*, 280–282.
(66) Kang, C.; Zhang, X.; Ratlifft, R.; Moyzis, R.; Rich, A. Crystal Structure of Four-Stranded Oxytricha Telomeric DNA. *Nature* **1992**, *356*, 126–131.
(67) Laughlan, G.; Murchie, H.; Norman, D. G.; Moore, M. H.; Moody, P. C. E.; Lilley, D. M. J.; Luisi, B. The High-Resolution Crystal Structure of a Parallel-Stranded Guanine Tetraplex. *Science* **1994**, *265* (5171), 520–524.
(68) Clark, G. R.; Pytel, P. D.; Squire, C. J.; Neidle, S. Structure of the First Parallel DNA Quadruplex-Drug Complex. *Journal of the American Chemical Society* **2003**, *125* (14), 4066–4067.
(69) Goodlett, D. R.; Camp, D. G.; Hardin, C. C.; Smith', R. D. Direct Observation of a DNA Quadruplex by Electrospray Ionization Mass Spectrometry. *Biological Mass Spectrometry* **1993**, *22* (3), 181–184.
(70) Haq, I.; Trent, J. O.; Chowdhry, B. Z.; Jenkins, T. C. Intercalative G-Tetraplex Stabilization of Telomeric DNA by a Cationic Porphyrin. *Journal of the American Chemical Society* **1999**, *121* (9), 1768–1779.
(71) Bolten, M.; Niermann, M.; Eimer, W. Structural Analysis of G-DNA in Solution: A Combination of Polarized and Depolarized Dynamic Light Scattering with Hydrodynamic Model Calculations. *Biochemistry* **1999**, *38* (38), 12416–12423.
(72) de Messieres, M.; Chang, J.-C.; Brawn-Cinani, B.; Porta, A. L. Single-Molecule Study of G-Quadruplex Disruption Using Dynamic Force Spectroscopy. *Physical Review Letters* **2012**, *109* (5), 058101.

(73) White, E. W.; Tanious, F.; Ismail, M. A.; Reszka, A. P.; Neidle, S.; Boykin, D. W.; Wilson, W. D. Structure-Specific Recognition of Quadruplex DNA by Organic Cations: Influence of Shape, Substituents and Charge. *Biophysical Chemistry* **2007**, *126* (1–3), 140–453.
(74) Redman, J. E. Surface Plasmon Resonance for Probing Quadruplex Folding and Interactions with Proteins and Small Molecules. *Methods* **2007**, *43* (4), 302–314.
(75) Smith, J. S.; Johnson, F. B. Isolation of G-Quadruplex DNA Using NMM-Sepharose Affinity Chromatography. *Methods in Molecular Biology* **2010**, *608*, 207–228.
(76) Müller, S.; Kumari, S.; Rodriguez, R.; Balasubramanian, S. Small-Molecule-Mediated G-Quadruplex Isolation from Human Cells. *Nat Chem* **2010**, *2* (12), 1095–1098. https://doi.org/10.1038/nchem.842.
(77) Zahler, A. M.; Williamson, J. R.; Cech, T. R.; Prescott, D. M. Inhibition of Telomerase by G-Quartet DNA Structures. *Nature* **1991**, *350* (6320), 718–720.
(78) Weitzmann, M. N.; Woodford, K. J.; Usdin, K. The Development and Use of a DNA Polymerase Arrest Assay for the Evaluation of Parameters Affecting Intrastrand Tetraplex Formation*. *The Journal of Biological Chemistry* **1996**, *271* (34), 20958–20964.
(79) Sun, D.; Thompson, B.; Cathers, B. E.; Salazar, M.; Kerwin, S. M.; Trent, J. O.; Jenkins, T. C.; Neidle, S.; Hurley, L. H. Inhibition of Human Telomerase by a G-Quadruplex-Interactive Compound. *Journal of Medicinal Chemistry* **1997**, *40* (14), 2113–2116.
(80) Perry, P. J.; Gowan, S. M.; Reszka, A. P.; Polucci, P.; Jenkins, T. C.; Kelland, L. R.; Neidle, S. 1,4- and 2,6-Disubstituted Amidoanthracene-9,10-Dione Derivatives as Inhibitors of Human Telomerase. *Journal of Medicinal Chemistry* **1998**, *41* (17), 3253–3260.
(81) Hagihara, M.; Yoneda, K.; Yabuuchi, H.; Okuno, Y.; Nakatani, K. A Reverse Transcriptase Stop Assay Revealed Diverse Quadruplex Formations in UTRs in mRNA. *Bioorg. Med. Chem. Lett.* **2010**, *20* (7), 2350–2353.
(82) Mendoza, O.; Gueddouda, N. M.; Boule, J.-B.; Bourdoncle, A.; Mergny, J.-L. A Fluorescence-Based Helicase Assay: Application to the Screening of G-Quadruplex Ligands. *Nucleic Acids Research* **2015**, *43* (11), e71–e71. https://doi.org/10.1093/nar/gkv193.
(83) Jamroskovic, J.; Obi, I.; Movahedi, A.; Chand, K.; Chorell, E.; Sabouri, N. Identification of Putative G-Quadruplex DNA Structures in S. Pombe Genome by Quantitative PCR Stop Assay. *DNA Repair* **2019**, *82*, 102678. https://doi.org/10.1016/j.dnarep.2019.102678.
(84) Mergny, J.-L.; Maurizot, J.-C. Fluorescence Resonance Energy Transfer as a Probe for G-Quartet Formation by a Telomeric Repeat. *ChemBioChem* **2001**, *2* (2), 124–132.
(85) Juskowiak, B.; Galezowska, E.; Zawadzka, A.; Gluszynska, A.; Takenaka, S. Fluorescence Anisotropy and FRET Studies of G-Quadruplex Formation in Presence of Different Cations. *Spectrochim Acta A Mol Biomol Spectrosc* **2006**, *64* (4), 835–843. https://doi.org/10.1016/j.saa.2005.08.012.
(86) Kumari, S.; Bugaut, A.; Huppert, J. L.; Balasubramanian, S. An RNA G-Quadruplex in the 5′ UTR of the NRAS Proto-Oncogene Modulates Translation. *Nat Chem Biol* **2007**, *3* (4), 218–221. https://doi.org/10.1038/nchembio864.
(87) Monchaud, D.; Allain, C.; Bertrand, H.; Smargiasso, N.; Rosu, F.; Gabelica, V.; Cian, A. D. Ligands Playing Musical Chairs with G-Quadruplex DNA: A Rapid and Simple Displacement Assay for Identifying Selective G-Quadruplex Binders. *Biochimie* **2008**, *90* (8), 1207–1230.
(88) Long, X.; Parks, J. W.; Bagshaw, C. R.; Stone, M. D. Mechanical Unfolding of Human Telomere G-Quadruplex DNA Probed by Integrated Fluorescence and Magnetic Tweezers Spectroscopy. *Nucleic Acids Research* **2013**, *41* (4), 2746–2755.
(89) Felsenstein, K. M.; Saunders, L. B.; Simmons, J. K.; Leon, E.; Calabrese, D. R.; Zhang, S.; Michalowski, A.; Gareiss, P.; Mock, B. A.; Schneekloth, J. S. Small Molecule Microarrays Enable the Identification of a Selective, Quadruplex-Binding Inhibitor of MYC Expression. *ACS Chem. Biol.* **2015**, *11* (1), 139–148.
(90) Le, D. D.; Di Antonio, M.; Chan, L. K. M.; Balasubramanian, S. G-Quadruplex Ligands Exhibit Differential G-Tetrad Selectivity. *Chem Commun (Camb)* **2015**, *51* (38), 8048–8050. https://doi.org/10.1039/c5cc02252e.
(91) Renard, I.; Grandmougin, M.; Roux, A.; Yang, S. Y.; Lejault, P.; Pirrotta, M.; Wong, J. M. Y.; Monchaud, D. Small-Molecule Affinity Capture of DNA/RNA Quadruplexes and Their Identification in Vitro and in Vivo through the G4RP Protocol. *Nucleic Acids Research* **2019**, *47* (11), 5502–5510. https://doi.org/10.1093/nar/gkz215.
(92) de Magis, A.; Kastl, M.; Brossart, P.; Heine, A.; Paeschke, K. BG-Flow, a New Flow Cytometry Tool for G-Quadruplex Quantification in Fixed Cells. *BMC Biology* **2021**, *19* (1), 45.

(93) Mitteaux, J.; Lejault, P.; Wojciechowski, F.; Joubert, A.; Boudon, J.; Desbois, N.; Gros, C. P.; Hudson, R. H. E.; Boulé, J.-B.; Granzhan, A.; Monchaud, D. Identifying G-Quadruplex-DNA-Disrupting Small Molecules. *J. Am. Chem. Soc.* **2021**, *143* (32), 12567–12577. https://doi.org/10.1021/jacs.1c04426.
(94) Luo, Y.; Granzhan, A.; Verga, D.; Mergny, J.-L. FRET-MC: A Fluorescence Melting Competition Assay for Studying G4 Structures in Vitro. *Biopolymers* **2021**, *112* (4), e23415. https://doi.org/10.1002/bip.23415.
(95) Esnault, C.; Magat, T.; El Aabidine, A. Z.; Garcia-Oliver, E.; Cucchiarini, A.; Bouchouika, S.; Lleres, D.; Goerke, L.; Luo, Y.; Verga, D.; Lacroix, L.; Feil, R.; Spicuglia, S.; Mergny, J.-L.; Andrau, J.-C. G4access Identifies G-Quadruplexes and Their Associations with Open Chromatin and Imprinting Control Regions. *Nature Genetics* **2023**, *55*, 1359–1369.
(96) Luo, Y.; Verga, D.; Mergny, J.-L. Iso-FRET: An Isothermal Competition Assay to Analyze Quadruplex Formation in Vitro. *Nucleic Acids Research* **2022**, *50* (16), e93. https://doi.org/10.1093/nar/gkac465.
(97) Grand, C. L.; Han, H.; Muñoz, R. M.; Weitman, S.; Von Hoff, D. D.; Hurley, L. H.; Bearss, D. J. The Cationic Porphyrin TMPyP4 Down-Regulates c-MYC and Human Telomerase Reverse Transcriptase Expression and Inhibits Tumor Growth in Vivo. *Mol Cancer Ther* **2002**, *1* (8), 565–573.
(98) Wilkinson, K. A.; Merino, E. J.; Weeks, K. M. Selective 2′-Hydroxyl Acylation Analyzed by Primer Extension (SHAPE): Quantitative RNA Structure Analysis at Single Nucleotide Resolution. *Nat Protoc* **2006**, *1* (3), 1610–1616. https://doi.org/10.1038/nprot.2006.249.
(99) Kwok, C. K.; Sahakyan, A. B.; Balasubramanian, S. Structural Analysis Using SHALiPE to Reveal RNA G-Quadruplex Formation in Human Precursor MicroRNA. *Angew. Chem. Int. Ed.* **2016**, *55* (31), 8958–8961. https://doi.org/10.1002/anie.201603562.
(100) Weldon, C.; Behm-Ansmant, I.; Hurley, L. H.; Burley, G. A.; Branlant, C.; Eperon, I. C.; Dominguez, C. Identification of G-Quadruplexes in Long Functional RNAs Using 7-Deazaguanine RNA. *Nat Chem Biol* **2017**, *13* (1), 18–20. https://doi.org/10.1038/nchembio.2228.
(101) Cogoi, S.; Quadrifoglio, F.; Xodo, L. E. G-Rich Oligonucleotide Inhibits the Binding of a Nuclear Protein to the Ki-Ras Promoter and Strongly Reduces Cell Growth in Human Carcinoma Pancreatic Cells. *Biochemistry* **2004**, *43* (9), 2512–2523. https://doi.org/10.1021/bi035754f.
(102) Wu, Y.; Shin-ya, K.; Brosh, R. M. FANCJ Helicase Defective in Fanconia Anemia and Breast Cancer Unwinds G-Quadruplex DNA To Defend Genomic Stability. *Mol Cell Biol* **2008**, *28* (12), 4116–4128. https://doi.org/10.1128/MCB.02210-07.
(103) Kumar, N.; Patowary, A.; Sivasubbu, S.; Petersen, M.; Maiti, S. Silencing C-MYC Expression by Targeting Quadruplex in P1 Promoter Using Locked Nucleic Acid Trap. *Biochem.* **2008**, *47* (50), 13179–13188.
(104) Williams, P.; Li, L.; Dong, X.; Wang, Y. Identification of SLIRP as a G Quadruplex-Binding Protein. *J Am Chem Soc* **2017**, *139* (36), 12426–12429. https://doi.org/10.1021/jacs.7b07563.
(105) Serikawa, T.; Eberle, J.; Kurreck, J. Effects of Genomic Disruption of a Guanine Quadruplex in the 5' UTR of the Bcl-2 mRNA in Melanoma Cells. *FEBS Lett* **2017**, *591* (21), 3649–3659. https://doi.org/10.1002/1873-3468.12855.
(106) Dang, D. T.; Nguyen, L. T. A.; Truong, T. T. T.; Nguyen, H. D.; Phan, A. T. Construction of a G-Quadruplex-Specific DNA Endonuclease. *Chem Commun (Camb)* **2021**, *57* (37), 4568–4571. https://doi.org/10.1039/d0cc05890d.
(107) Sarig, G.; Weisman-Shomer, P.; Erlitzki, R.; Fry, M. Purification and Characterization of qTBP42, a New Single-Stranded and Quadruplex Telomeric DNA-Binding Protein from Rat Hepatocytes. *J Biol Chem* **1997**, *272* (7), 4474–4482. https://doi.org/10.1074/jbc.272.7.4474.
(108) Isalan, M.; Patel, S. D.; Balasubramanian, S.; Choo, Y. Selection of Zinc Fingers That Bind Single-Stranded Telomeric DNA in the G-Quadruplex Conformation. *Biochemistry* **2001**, *40* (3), 830–836. https://doi.org/10.1021/bi001728v.
(109) Schaffitzel, C.; Berger, I.; Postberg, J.; Hanes, J.; Lipps, H. J.; Pluckthun, A. In Vitro Generated Antibodies Specific for Telomeric Guanine-Quadruplex DNA React with Stylonychia Lemnae Macronuclei. *Proc. Natl. Acad. Sci. U.S.A.* **2001**, *98* (15), 8572–8577. https://doi.org/10.1073/pnas.141229498.
(110) Law, M. J.; Lower, K. M.; Voon, H. P. J.; Hughes, J. R.; Garrick, D.; Viprakasit, V.; Mitson, M.; De Gobbi, M.; Marra, M.; Morris, A.; Abbott, A.; Wilder, S. P.; Taylor, S.; Santos, G. M.; Cross, J.; Ayyub, H.; Jones, S.; Ragoussis, J.; Rhodes, D.; Dunham, I.; Higgs, D. R.; Gibbons, R. J. ATR-X Syndrome Protein Targets Tandem Repeats and Influences Allele-Specific Expression in a Size-Dependent Manner. *Cell* **2010**, *143* (3), 367–378. https://doi.org/10.1016/j.cell.2010.09.023.

(111) Rodriguez, R.; Miller, K. M.; Forment, J. V.; Bradshaw, C. R.; Nikan, M.; Britton, S.; Oelschlaegel, T.; Xhemalce, B.; Balasubramanian, S.; Jackson, S. P. Small-Molecule–Induced DNA Damage Identifies Alternative DNA Structures in Human Genes. *Nat Chem Biol* **2012**, *8* (3), 301–310. https://doi.org/10.1038/nchembio.780.

(112) Lista, M. J.; Martins, R. P.; Billant, O.; Contesse, M.-A.; Findakly, S.; Pochard, P.; Daskalogianni, C.; Beauvineau, C.; Guetta, C.; Jamin, C.; Teulade-Fichou, M.-P.; Fåhraeus, R.; Voisset, C.; Blondel, M. Nucleolin Directly Mediates Epstein-Barr Virus Immune Evasion through Binding to G-Quadruplexes of EBNA1 mRNA. *Nat Commun* **2017**, *8*, 16043. https://doi.org/10.1038/ncomms16043.

(113) Masson, T.; Landras Guetta, C.; Laigre, E.; Cucchiarini, A.; Duchambon, P.; Teulade-Fichou, M.-P.; Verga, D. BrdU Immuno-Tagged G-Quadruplex Ligands: A New Ligand-Guided Immunofluorescence Approach for Tracking G-Quadruplexes in Cells. *Nucleic Acids Research* **2021**, *49* (22), 12644–12660. https://doi.org/10.1093/nar/gkab1166.

(114) Biffi, G.; Tannahill, D.; McCafferty, J.; Balasubramanian, S. Quantitative Visualization of DNA G-Quadruplex Structures in Human Cells. *Nature Chem* **2013**, *5* (3), 182–186. https://doi.org/10.1038/nchem.1548.

(115) Biffi, G.; Di Antonio, M.; Tannahill, D.; Balasubramanian, S. Visualization and Selective Chemical Targeting of RNA G-Quadruplex Structures in the Cytoplasm of Human Cells. *Nature Chemistry* **2014**, *6* (1), 75–80. https://doi.org/10.1038/nchem.1805.

(116) Hänsel-Hertsch, R.; Spiegel, J.; Marsico, G.; Tannahill, D.; Balasubramanian, S. Genome-Wide Mapping of Endogenous G-Quadruplex DNA Structures by Chromatin Immunoprecipitation and High-Throughput Sequencing. *Nat Protoc* **2018**, *13* (3), 551–564. https://doi.org/10.1038/nprot.2017.150.

(117) Matos-Rodrigues, G. Detection of Alternative DNA Structures and Its Implications for Human Disease. *Technology review* **2023**, *83*.

(118) Chambers, V. S.; Marsico, G.; Boutell, J. M.; Di Antonio, M.; Smith, G. P.; Balasubramanian, S. High-Throughput Sequencing of DNA G-Quadruplex Structures in the Human Genome. *Nat. Biotechnol.* **2015**, *33* (8), 877–881. https://doi.org/10.1038/nbt.3295.

(119) Kwok, C. K.; Balasubramanian, S. Targeted Detection of G-Quadruplexes in Cellular RNAs. *Angew. Chem. Int. Ed.* **2015**, *54* (23), 6751–6754. https://doi.org/10.1002/anie.201500891.

(120) Yang, S. Y.; Lejault, P.; Chevrier, S.; Boidot, R.; Robertson, A. G.; Wong, J. M. Y.; Monchaud, D. Transcriptome-Wide Identification of Transient RNA G-Quadruplexes in Human Cells. *Nat Commun* **2018**, *9* (1), 4730–4740. https://doi.org/10.1038/s41467-018-07224-8.

(121) Yang, S. Y.; Monchaud, D.; Wong, J. M. Y. Global Mapping of RNA G-Quadruplexes (G4-RNAs) Using G4RP-Seq. *Nat Protoc* **2022**, *17* (3), 870–889. https://doi.org/10.1038/s41596-021-00671-6.

(122) Feng, Y.; Tao, S.; Zhang, P.; Sperti, F. R.; Liu, G.; Cheng, X.; Zhang, T.; Yu, H.; Wang, X.; Chen, C.; Monchaud, D.; Zhang, W. Epigenomic Features of DNA G-Quadruplexes and Their Roles in Regulating Rice Gene Transcription. *Plant Physiology* **2022**, *188* (3), 1632–1648. https://doi.org/10.1093/plphys/kiab566.

(123) Amrane, S.; Jaubert, C.; Bedrat, A.; Rundstadler, T.; Recordon-Pinson, P.; Aknin, C.; Guédin, A.; De Rache, A.; Bartolucci, L.; Diene, I.; Lemoine, F.; Gascuel, O.; Pratviel, G.; Mergny, J.-L.; Andreola, M.-L. Deciphering RNA G-Quadruplex Function during the Early Steps of HIV-1 Infection. *Nucleic Acids Res* **2022**, *50* (21), 12328–12343. https://doi.org/10.1093/nar/gkac1030.

(124) Hui, W. W. I.; Simeone, A.; Zyner, K. G.; Tannahill, D.; Balasubramanian, S. Single-Cell Mapping of DNA G-Quadruplex Structures in Human Cancer Cells. *Sci Rep* **2021**, *11* (1), 23641.

(125) Lyu, J.; Shao, R.; Yung, P. Y. K.; Elsässer, S. J. Genome-Wide Mapping of G-Quadruplex Structures with CUT&Tag. *Nucleic Acids Res* **2022**, *50* (3), e13.

(126) Galli, S.; Melidis, L.; Flynn, S. M.; Varshney, D.; Simeone, A.; Spiegel, J.; Madden, S. K.; Tannahill, D.; Balasubramanian, S. DNA G-Quadruplex Recognition In Vitro and in Live Cells by a Structure-Specific Nanobody. *J Am Chem Soc* **2022**, *144* (50), 23096–23103.

(127) Kaya-Okur, H. S.; Wu, S. J.; Codomo, C. A.; Pledger, E. S.; Bryson, T. D.; Henikoff, J. G.; Ahmad, K.; Henikoff, S. CUT&Tag for Efficient Epigenomic Profiling of Small Samples and Single Cells. *Nature Communications* **2019**, *10* (1930).

(128) Guo, J. U.; Bartel, D. P. RNA G-Quadruplexes Are Globally Unfolded in Eukaryotic Cells and Depleted in Bacteria. *Science* **2016**, *353* (6306), 1382–1392. https://doi.org/10.1126/science.aaf5371.

(129) Su, H.; Xu, J.; Chen, Y.; Wang, Q.; Lu, Z.; Chen, Y.; Chen, K.; Han, S.; Fang, Z.; Wang, P.; Yuan, B.-F.; Zhou, X. Photoactive G-Quadruplex Ligand Identifies Multiple G-Quadruplex-Related Proteins with Extensive Sequence Tolerance in the Cellular Environment. *J Am Chem Soc* **2021**, *143* (4), 1917–1923. https://doi.org/10.1021/jacs.0c10792.

(130) Zhang, X.; Spiegel, J.; Martínez Cuesta, S.; Adhikari, S.; Balasubramanian, S. Chemical Profiling of DNA G-Quadruplex-Interacting Proteins in Live Cells. *Nat. Chem.* **2021**, *13* (7), 626–633. https://doi.org/10.1038/s41557-021-00736-9.

(131) Feng, Y.; He, Z.; Luo, Z.; Sperti, F. R.; Valverde, I. E.; Zhang, W.; Monchaud, D. Side-by-Side Comparison of G-Quadruplex (G4) Capture Efficiency of the Antibody BG4 versus the Small-Molecule Ligands TASQs. *iScience* **2023**, *26* (6), 106846. https://doi.org/10.1016/j.isci.2023.106846.

(132) Vannutelli, A.; Belhamiti, S.; Garant, J.-M.; Ouangraoua, A.; Perreault, J.-P. Where Are G-Quadruplexes Located in the Human Transcriptome? *NAR Genom Bioinform* **2020**, *2* (2), lqaa035. https://doi.org/10.1093/nargab/lqaa035.

(133) Todd, A. K.; Johnston, M.; Neidle, S. Highly Prevalent Putative Quadruplex Sequence Motifs in Human DNA. *Nucleic Acids Research* **2005**, *33* (9), 2901–2907. https://doi.org/10.1093/nar/gki553.

(134) Rhodes, D.; Lipps, H. J. G-Quadruplexes and Their Regulatory Roles in Biology. *Nucleic Acids Research* **2015**, *43* (18), 8627–8637. https://doi.org/10.1093/nar/gkv862.

(135) Varshney, D.; Spiegel, J.; Zyner, K.; Tannahill, D.; Balasubramanian, S. The Regulation and Functions of DNA and RNA G-Quadruplexes. *Nat Rev Mol Cell Biol* **2020**, *21* (8), 459–474. https://doi.org/10.1038/s41580-020-0236-x.

(136) Wieland, M.; Hartig, J. S. RNA Quadruplex-Based Modulation of Gene Expression. *Chemistry & Biology* **2007**, *14* (7), 757–763. https://doi.org/10.1016/j.chembiol.2007.06.005.

(137) Huang, H.; Zhang, J.; Harvey, S. E.; Hu, X.; Cheng, C. RNA G-Quadruplex Secondary Structure Promotes Alternative Splicing via the RNA-Binding Protein hnRNPF. *Genes Dev.* **2017**, *31* (22), 2296–2309. https://doi.org/10.1101/gad.305862.117.

(138) Le Sénéchal, R.; Keruzoré, M.; Quillévéré, A.; Loaëc, N.; Dinh, V.-T.; Reznichenko, O.; Guixens-Gallardo, P.; Corcos, L.; Teulade-Fichou, M.-P.; Granzhan, A.; Blondel, M. Alternative Splicing of BCL-x Is Controlled by RBM25 Binding to a G-Quadruplex in BCL-x Pre-mRNA. *Nucleic Acids Res* **2023**, *51* (20), 11239–11257. https://doi.org/10.1093/nar/gkad772.

(139) Tian, T.; Chen, Y.-Q.; Wang, S.-R.; Zhou, X. G-Quadruplex: A Regulator of Gene Expression and Its Chemical Targeting. *Chem* **2018**, *4*, 1314–1344.

(140) Brosh, R. M.; Matson, S. W. History of DNA Helicases. *Genes* **2020**, *11* (3), 255. https://doi.org/10.3390/genes11030255.

(141) Lejault, P.; Mitteaux, J.; Sperti, F. R.; Monchaud, D. How to Untie G-Quadruplex Knots and Why? *Cell Chemical Biology* **2021**, *28* (4), 436–455. https://doi.org/10.1016/j.chembiol.2021.01.015.

(142) Butler, T. J.; Estep, K. N.; Sommers, J. A.; Maul, R. W.; Moore, A. Z.; Bandinelli, S.; Cucca, F.; Tuke, M. A.; Wood, A. R.; Bharti, S. K.; Bogenhagen, D. F.; Yakubovskaya, E.; Garcia-Diaz, M.; Guilliam, T. A.; Byrd, A. K.; Raney, K. D.; Doherty, A. J.; Ferrucci, L.; Schlessinger, D.; Ding, J.; Brosh, R. M. Mitochondrial Genetic Variation Is Enriched in G-Quadruplex Regions That Stall DNA Synthesis in Vitro. *Human Molecular Genetics* **2020**, *29* (8), 1292–1309. https://doi.org/10.1093/hmg/ddaa043.

(143) Dalloul, Z.; Chenuet, P.; Dalloul, I.; Boyer, F.; Aldigier, J.-C.; Laffleur, B.; El Makhour, Y.; Ryffel, B.; Quesniaux, V. F. J.; Togbé, D.; Mergny, J.-L.; Cook-Moreau, J.; Cogné, M. G-Quadruplex DNA Targeting Alters Class-Switch Recombination in B Cells and Attenuates Allergic Inflammation. *Journal of Allergy and Clinical Immunology* **2018**, *142* (4), 1352–1355. https://doi.org/10.1016/j.jaci.2018.06.011.

(144) Ruggiero, E.; Richter, S. N. Viral G-Quadruplexes: New Frontiers in Virus Pathogenesis and Antiviral Therapy. In *Annual Reports in Medicinal Chemistry*; Elsevier, 2020; Vol. 54, pp 101–131. https://doi.org/10.1016/bs.armc.2020.04.001.

(145) Rauchhaus, J.; Robinson, J.; Monti, L.; Di Antonio, M. G-Quadruplexes Mark Sites of Methylation Instability Associated with Ageing and Cancer. *Genes* **2022**, *13* (9), 1665. https://doi.org/10.3390/genes13091665.

(146) Subramanian, M.; Rage, F.; Tabet, R.; Flatter, E.; Mandel, J.; Moine, H. G–Quadruplex RNA Structure as a Signal for Neurite mRNA Targeting. *EMBO Rep* **2011**, *12* (7), 697–704. https://doi.org/10.1038/embor.2011.76.

(147) Pandey, S.; Agarwala, P.; Jayaraj, G. G.; Gargallo, R.; Maiti, S. The RNA Stem–Loop to G-Quadruplex Equilibrium Controls Mature MicroRNA Production inside the Cell. *Biochemistry* **2015**, *54* (48), 7067–7078. https://doi.org/10.1021/acs.biochem.5b00574.

(148) Balasubramanian, S.; Hurley, L. H.; Neidle, S. Targeting G-Quadruplexes in Gene Promoters: A Novel Anticancer Strategy? *Nature Reviews Drug Discovery* **2011**, *10* (4), 261–275. https://doi.org/10.1038/nrd3428.

(149) Neidle, S. Quadruplex Nucleic Acids as Targets for Anticancer Therapeutics. *Nature Reviews*

Chemistry **2017**, *1* (5), 0041.
(150) DeJesus-Hernandez, M.; Mackenzie, I. R.; Boeve, B. F.; Boxer, A. L.; Baker, M.; Rutherford, N. J.; Nicholson, A. M.; Finch, N. A.; Flynn, H.; Adamson, J.; Kouri, N.; Wojtas, A.; Sengdy, P.; Hsiung, G.-Y. R.; Karydas, A.; Seeley, W. W.; Josephs, K. A.; Coppola, G.; Geschwind, D. H.; Wszolek, Z. K.; Feldman, H.; Knopman, D. S.; Petersen, R. C.; Miller, B. L.; Dickson, D. W.; Boylan, K. B.; Graff-Radford, N. R.; Rademakers, R. Expanded GGGGCC Hexanucleotide Repeat in Noncoding Region of C9ORF72 Causes Chromosome 9p-Linked FTD and ALS. *Neuron* **2011**, *72* (2), 245–256. https://doi.org/10.1016/j.neuron.2011.09.011.
(151) Renton, A. E.; Majounie, E.; Waite, A.; Simón-Sánchez, J.; Rollinson, S.; Gibbs, J. R.; Schymick, J. C.; Laaksovirta, H.; van Swieten, J. C.; Myllykangas, L.; Kalimo, H.; Paetau, A.; Abramzon, Y.; Remes, A. M.; Kaganovich, A.; Scholz, S. W.; Duckworth, J.; Ding, J.; Harmer, D. W.; Hernandez, D. G.; Johnson, J. O.; Mok, K.; Ryten, M.; Trabzuni, D.; Guerreiro, R. J.; Orrell, R. W.; Neal, J.; Murray, A.; Pearson, J.; Jansen, I. E.; Sondervan, D.; Seelaar, H.; Blake, D.; Young, K.; Halliwell, N.; Callister, J. B.; Toulson, G.; Richardson, A.; Gerhard, A.; Snowden, J.; Mann, D.; Neary, D.; Nalls, M. A.; Peuralinna, T.; Jansson, L.; Isoviita, V.-M.; Kaivorinne, A.-L.; Hölttä-Vuori, M.; Ikonen, E.; Sulkava, R.; Benatar, M.; Wuu, J.; Chiò, A.; Restagno, G.; Borghero, G.; Sabatelli, M.; Heckerman, D.; Rogaeva, E.; Zinman, L.; Rothstein, J. D.; Sendtner, M.; Drepper, C.; Eichler, E. E.; Alkan, C.; Abdullaev, Z.; Pack, S. D.; Dutra, A.; Pak, E.; Hardy, J.; Singleton, A.; Williams, N. M.; Heutink, P.; Pickering-Brown, S.; Morris, H. R.; Tienari, P. J.; Traynor, B. J. A Hexanucleotide Repeat Expansion in C9ORF72 Is the Cause of Chromosome 9p21-Linked ALS-FTD. *Neuron* **2011**, *72* (2), 257–268. https://doi.org/10.1016/j.neuron.2011.09.010.
(152) Wilson, D. M.; Cookson, M. R.; Van Den Bosch, L.; Zetterberg, H.; Holtzman, D. M.; Dewachter, I. Hallmarks of Neurodegenerative Diseases. *Cell* **2023**, *186* (4), 693–714. https://doi.org/10.1016/j.cell.2022.12.032.
(153) Balendra, R.; Isaacs, A. M. C9orf72-Mediated ALS and FTD: Multiple Pathways to Disease. *Nat Rev Neurol* **2018**, *14* (9), 544–558. https://doi.org/10.1038/s41582-018-0047-2.
(154) Wang, E.; Thombre, R.; Shah, Y.; Latanich, R.; Wang, J. G-Quadruplexes as Pathogenic Drivers in Neurodegenerative Disorders. *Nucleic Acids Research* **2021**, *49* (9), 4816–4830. https://doi.org/10.1093/nar/gkab164.
(155) Ellis, N. A.; Groden, J.; Ye, T.-Z.; Straughen, J.; Lennon, D. J.; Ciocci, S.; Proytcheva, M.; German, J. The Bloom's Syndrome Gene Product Is Homologous to RecQ Helicases. *Cell* **1995**, *83* (4), 655–666. https://doi.org/10.1016/0092-8674(95)90105-1.
(156) Sun, H.; Karow, J. K.; Hickson, I. D.; Maizels, N. The Bloom's Syndrome Helicase Unwinds G4 DNA. *Journal of Biological Chemistry* **1998**, *273* (42), 27587–27592. https://doi.org/10.1074/jbc.273.42.27587.
(157) Yu, C.-E.; Oshima, J.; Fu, Y.-H.; Wijsman, E. M.; Hisama, F.; Alisch, R.; Matthews, S.; Nakura, J.; Miki, T.; Ouais, S.; Martin, G. M.; Mulligan, J.; Schellenberg, G. D. Positional Cloning of the Werner's Syndrome Gene. *Science* **1996**, *272* (5259), 258–262. https://doi.org/10.1126/science.272.5259.258.
(158) Fry, M.; Loeb, L. A. Human Werner Syndrome DNA Helicase Unwinds Tetrahelical Structures of the Fragile X Syndrome Repeat Sequence d(CGG). *Journal of Biological Chemistry* **1999**, *274* (18), 12797–12802. https://doi.org/10.1074/jbc.274.18.12797.
(159) Levran, O.; Attwooll, C.; Henry, R. T.; Milton, K. L.; Neveling, K.; Rio, P.; Batish, S. D.; Kalb, R.; Velleuer, E.; Barral, S.; Ott, J.; Petrini, J.; Schindler, D.; Hanenberg, H.; Auerbach, A. D. The BRCA1-Interacting Helicase BRIP1 Is Deficient in Fanconi Anemia. *Nat Genet* **2005**, *37* (9), 931–933. https://doi.org/10.1038/ng1624.
(160) Levitus, M.; Waisfisz, Q.; Godthelp, B. C.; Vries, Y. de; Hussain, S.; Wiegant, W. W.; Elghalbzouri-Maghrani, E.; Steltenpool, J.; Rooimans, M. A.; Pals, G.; Arwert, F.; Mathew, C. G.; Zdzienicka, M. Z.; Hiom, K.; De Winter, J. P.; Joenje, H. The DNA Helicase BRIP1 Is Defective in Fanconi Anemia Complementation Group J. *Nat Genet* **2005**, *37* (9), 934–935. https://doi.org/10.1038/ng1625.
(161) Litman, R.; Peng, M.; Jin, Z.; Zhang, F.; Zhang, J.; Powell, S.; Andreassen, P. R.; Cantor, S. B. BACH1 Is Critical for Homologous Recombination and Appears to Be the Fanconi Anemia Gene Product FANCJ. *Cancer Cell* **2005**, *8* (3), 255–265. https://doi.org/10.1016/j.ccr.2005.08.004.
(162) London, T. B. C.; Barber, L. J.; Mosedale, G.; Kelly, G. P.; Balasubramanian, S.; Hickson, I. D.; Boulton, S. J.; Hiom, K. FANCJ Is a Structure-Specific DNA Helicase Associated with the Maintenance of Genomic G/C Tracts. *Journal of Biological Chemistry* **2008**, *283* (52), 36132–36139. https://doi.org/10.1074/jbc.M808152200.
(163) Kim, N. W.; Piatyszek, M. A.; Prowse, K. R.; Harley, C. B.; West, M. D.; Ho, P. L. C.; Coviello, G.

M.; Wright, W. E.; Weinrich, S. L.; Shay, J. W. Specific Association of Human Telomerase Activity with Immortal Cells and Cancer. *Science* **1994**, *266*, 2011–2015.

(164) Asai, A.; Oshima, Y.; Yamamoto, Y.; Uochi, T.; Kusaka, H.; Akinaga, S.; Yamashita, Y.; Pongracz, K.; Pruzan, R.; Wunder, E.; Piatyszek, M.; Li, S.; Chin, A. C.; Harley, C. B.; Gryaznov, S. A Novel Telomerase Template Antagonist (GRN163) as a Potential Anticancer Agent. *Cancer Res* **2003**, *63* (14), 3931–3939.

(165) Steensma, D. P.; Fenaux, P.; Van Eygen, K.; Raza, A.; Santini, V.; Germing, U.; Font, P.; Diez-Campelo, M.; Thepot, S.; Vellenga, E.; Patnaik, M. M.; Jang, J. H.; Varsos, H.; Bussolari, J.; Rose, E.; Sherman, L.; Sun, L.; Wan, Y.; Dougherty, S.; Huang, F.; Feller, F.; Rizo, A.; Platzbecker, U. Imetelstat Achieves Meaningful and Durable Transfusion Independence in High Transfusion-Burden Patients With Lower-Risk Myelodysplastic Syndromes in a Phase II Study. *J Clin Oncol* **2021**, *39* (1), 48–56. https://doi.org/10.1200/JCO.20.01895.

(166) Wheelhouse, R. T.; Sun, D.; Han, H.; Han, F. X.; Hurley, L. H. Cationic Porphyrins as Telomerase Inhibitors: The Interaction of Tetra-(N-Methyl-4-Pyridyl)Porphine with Quadruplex DNA. *Journal of the American Chemical Society* **1998**, *120* (13), 3261–3262.

(167) Shin-ya, K.; Wierzba, K.; Matsuo, K.; Ohtani, T.; Yamada, Y.; Furihata, K.; Hayakawa, Y.; Seto, H. Telomestatin, a Novel Telomerase Inhibitor from Streptomyces Anulatus. *Journal of the American Chemical Society* **2001**, *123*, 1262–1263.

(168) Read, M.; Harrison, R. J.; Romagnoli, B.; Tanious, F. A.; Gowan, S. H.; Reszka, A. P.; Wilson, W. D.; Kelland, L. R.; Neidle, S. Structure-Based Design of Selective and Potent G Quadruplex-Mediated Telomerase Inhibitors. *Proc. Natl. Acad. Sci. U.S.A.* **2001**, *98* (9), 4844–4849.

(169) Pennarun, G.; Granotier, C.; Gauthier, L. R.; Gomez, D.; Hoffschir, F.; Riou, J.-F.; Mergny, J.-L.; Mailliet, P.; Boussin, F. D. Apoptosis Related to Telomere Instability and Cell Cycle Alterations in Human Glioma Cells Treated by New Highly Selective G-Quadruplex Ligands. *Oncogene* **2005**, *24*, 2917–2928.

(170) Cian, A. D.; DeLemos, E.; Mergny, J.-L.; Teulade-Fichou, M.-P.; Monchaud, D. Highly Efficient G-Quadruplex Recognition by Bisquinolinium Compounds. *Journal of the American Chemical Society* **2007**, *129* (7), 1856–1857.

(171) De Cian, A.; Cristofari, G.; Reichenbach, P.; De Lemos, E.; Monchaud, D.; Teulade-Fichou, M.-P.; Shin-ya, K.; Lacroix, L.; Lingner, J.; Mergny, J.-L. Reevaluation of Telomerase Inhibition by Quadruplex Ligands and Their Mechanisms of Action. *Proceedings of the National Academy of Sciences* **2007**, *104* (44), 17347–17352. https://doi.org/10.1073/pnas.0707365104.

(172) Rodriguez, R.; Müller, S.; Yeoman, J. A.; Trentesaux, C.; Riou, J.-F.; Balasubramanian, S. A Novel Small Molecule That Alters Shelterin Integrity and Triggers a DNA-Damage Response at Telomeres. *J. Am. Chem. Soc.* **2008**, *130* (47), 15758–15759. https://doi.org/10.1021/ja805615w.

(173) Sanchez-Martin, V.; Soriano, M.; Garcia-Salcedo, J. A. Quadruplex Ligands in Cancer Therapy. *Cancers (Basel)* **2021**, *13* (13), 3156. https://doi.org/10.3390/cancers13133156.

(174) Xu, H.; Di Antonio, M.; McKinney, S.; Mathew, V.; Ho, B.; O'Neil, N. J.; Santos, N. D.; Silvester, J.; Wei, V.; Garcia, J.; Kabeer, F.; Lai, D.; Soriano, P.; Banáth, J.; Chiu, D. S.; Yap, D.; Le, D. D.; Ye, F. B.; Zhang, A.; Thu, K.; Soong, J.; Lin, S.; Tsai, A. H. C.; Osako, T.; Algara, T.; Saunders, D. N.; Wong, J.; Xian, J.; Bally, M. B.; Brenton, J. D.; Brown, G. W.; Shah, S. P.; Cescon, D.; Mak, T. W.; Caldas, C.; Stirling, P. C.; Hieter, P.; Balasubramanian, S.; Aparicio, S. CX-5461 Is a DNA G-Quadruplex Stabilizer with Selective Lethality in BRCA1/2 Deficient Tumours. *Nat Commun* **2017**, *8* (1), 14432. https://doi.org/10.1038/ncomms14432.

(175) Hilton, J.; Gelmon, K.; Bedard, P. L.; Tu, D.; Xu, H.; Tinker, A. V.; Goodwin, R.; Laurie, S. A.; Jonker, D.; Hansen, A. R.; Veitch, Z. W.; Renouf, D. J.; Hagerman, L.; Lui, H.; Chen, B.; Kellar, D.; Li, I.; Lee, S.-E.; Kono, T.; Cheng, B. Y. C.; Yap, D.; Lai, D.; Beatty, S.; Soong, J.; Pritchard, K. I.; Soria-Bretones, I.; Chen, E.; Feilotter, H.; Rushton, M.; Seymour, L.; Aparicio, S.; Cescon, D. W. Results of the Phase I CCTG IND.231 Trial of CX-5461 in Patients with Advanced Solid Tumors Enriched for DNA-Repair Deficiencies. *Nat Commun* **2022**, *13* (1), 3607. https://doi.org/10.1038/s41467-022-31199-2.

(176) Xu, H.; Hurley, L. H. A First-in-Class Clinical G-Quadruplex-Targeting Drug. The Bench-to-Bedside Translation of the Fluoroquinolone QQ58 to CX-5461 (Pidnarulex). *Bioorg Med Chem Lett* **2022**, *77*, 129016. https://doi.org/10.1016/j.bmcl.2022.129016.

(177) Koh, G. C. C.; Boushaki, S.; Zhao, S. J.; Pregnall, A. M.; Sadiyah, F.; Badja, C.; Memari, Y.; Georgakopoulos-Soares, I.; Nik-Zainal, S. The Chemotherapeutic Drug CX-5461 Is a Potent Mutagen in Cultured Human Cells. *Nat Genet* **2024**, *56* (1), 23–26. https://doi.org/10.1038/s41588-023-01602-9.

(178) Nikan, M. Template-Assembled Synthetic G-Quartets (TASQS), University of British Columbia,

2008. https://doi.library.ubc.ca/10.14288/1.0061694.
(179) Nikan, M.; Sherman, J. C. Template-Assembled Synthetic G-Quartets (TASQs). *Angew. Chem. Int. Ed.* **2008**, *47* (26), 4900–4902. https://doi.org/10.1002/anie.200704199.
(180) Stefan, L.; Guédin, A.; Amrane, S.; Smith, N.; Denat, F.; Mergny, J.-L.; Monchaud, D. DOTASQ as a Prototype of Nature-Inspired G-Quadruplex Ligand. *Chem. Commun.* **2011**, *47* (17), 4992. https://doi.org/10.1039/c0cc04960c.
(181) Xu, H.-J.; Stefan, L.; Haudecoeur, R.; Vuong, S.; Richard, P.; Denat, F.; Barbe, J.-M.; Gros, C. P.; Monchaud, D. Porphyrin-Templated Synthetic G-Quartet (PorphySQ): A Second Prototype of G-Quartet-Based G-Quadruplex Ligand. *Org. Biomol. Chem.* **2012**, *10* (27), 5212. https://doi.org/10.1039/c2ob25601k.
(182) Haudecoeur, R.; Stefan, L.; Denat, F.; Monchaud, D. A Model of Smart G-Quadruplex Ligand. *J. Am. Chem. Soc.* **2013**, *135* (2), 550–553. https://doi.org/10.1021/ja310056y.
(183) Haudecoeur, R.; Stefan, L.; Monchaud, D. Multitasking Water-Soluble Synthetic G-Quartets: From Preferential RNA-Quadruplex Interaction to Biocatalytic Activity. *Chem. Eur. J.* **2013**, *19* (38), 12739–12747. https://doi.org/10.1002/chem.201300791.
(184) Laguerre, A.; Desbois, N.; Stefan, L.; Richard, P.; Gros, C. P.; Monchaud, D. Porphyrin-Based Design of Bioinspired Multitarget Quadruplex Ligands. *ChemMedChem* **2014**, *9* (9), 2035–2039. https://doi.org/10.1002/cmdc.201300526.
(185) Fiel, R. J.; Munson, B. R. Binding of Mese-Tetra (4-N-Methylpyridyl) Prophine to DNA. *Nucleic Acids Research* **1980**, *8* (12), 2835–2842. https://doi.org/10.1093/nar/8.12.2835.
(186) Weisman-Shomer, P. The Cationic Porphyrin TMPyP4 Destabilizes the Tetraplex Form of the Fragile X Syndrome Expanded Sequence d(CGG)n. *Nucleic Acids Research* **2003**, *31* (14), 3963–3970. https://doi.org/10.1093/nar/gkg453.
(187) Ofer, N.; Weisman-Shomer, P.; Shklover, J.; Fry, M. The Quadruplex r(CGG)n Destabilizing Cationic Porphyrin TMPyP4 Cooperates with hnRNPs to Increase the Translation Efficiency of Fragile X Premutation mRNA. *Nucleic Acids Research* **2009**, *37* (8), 2712–2722.
(188) Morris, M. J.; Wingate, K. L.; Silwal, J.; Leeper, T. C.; Basu, S. The Porphyrin TmPyP4 Unfolds the Extremely Stable G-Quadruplex in MT3-MMP mRNA and Alleviates Its Repressive Effect to Enhance Translation in Eukaryotic Cells. *Nucleic Acids Research* **2012**, *40* (9), 4137–4145. https://doi.org/10.1093/nar/gkr1308.
(189) Zamiri, B.; Reddy, K.; Macgregor, R. B.; Pearson, C. E. TMPyP4 Porphyrin Distorts RNA G-Quadruplex Structures of the Disease-Associated r(GGGGCC)n Repeat of the C9orf72 Gene and Blocks Interaction of RNA-Binding Proteins. *Journal of Biological Chemistry* **2014**, *289* (8), 4653–4659. https://doi.org/10.1074/jbc.C113.502336.
(190) Joshi, S.; Singh, A.; Kukreti, S. Porphyrin Induced Structural Destabilization of a Parallel DNA G-quadruplex in Human MRP1 Gene Promoter. *J of Molecular Recognition* **2022**, *35* (3). https://doi.org/10.1002/jmr.2950.
(191) Waller, Z. A. E.; Sewitz, S. A.; Hsu, S.-T. D.; Balasubramanian, S. A Small Molecule That Disrupts G-Quadruplex DNA Structure and Enhances Gene Expression. *Journal of the American Chemical Society* **2009**, *131* (35), 12628–12633.
(192) Kaluzhny, D.; Ilyinsky, N.; Shchekotikhin, A.; Sinkevich, Y.; Tsvetkov, P. O.; Tsvetkov, V.; Veselovsky, A.; Livshits, M.; Borisova, O.; Shtil, A. Disordering of Human Telomeric G-Quadruplex with Novel Antiproliferative Anthrathiophenedione. *PLoS ONE* **2011**, *6* (11), e27151. https://doi.org/10.1371/journal.pone.0027151.
(193) O'Hagan, M. P.; Haldar, S.; Duchi, M.; Oliver, T. A. A.; Mulholland, A. J.; Morales, J. C.; Galan, M. C. A Photoresponsive Stiff-Stilbene Ligand Fuels the Reversible Unfolding of G-Quadruplex DNA. *Angew. Chem. Int. Ed.* **2019**, *58* (13), 4334–4338. https://doi.org/10.1002/anie.201900740.
(194) Neidle, S. Quadruplex Nucleic Acids as Novel Therapeutic Targets. *Journal of Medicinal Chemistry* **2016**, *59* (13), 5987–6011. https://doi.org/10.1021/acs.jmedchem.5b01835.
(195) Brown, B. A.; Li, Y.; Brown, J. C.; Hardin, C. C.; Roberts, J. F.; Pelsue, S. C.; Shultz, L. D. Isolation and Characterization of a Monoclonal Anti-Quadruplex DNA Antibody from Autoimmune "Viable Motheaten" Mice†,. *Biochemistry* **1998**, *37* (46), 16325–16337.
(196) Fernando, H.; Rodriguez, R.; Balasubramanian, S. Selective Recognition of a DNA G-Quadruplex by an Engineered Antibody. *Biochemistry* **2008**, *47* (36), 9365–9371.
(197) Henderson, A.; Wu, Y.; Huang, Y. C.; Chavez, E. A.; Platt, J.; Johnson, F. B.; Jr, R. M. B.; Sen, D.; Lansdorp, P. M. Detection of G-Quadruplex DNA in Mammalian Cells. *Nucleic Acids Research* **2013**, *42* (2), 860–869.

(198) Liu, H.-Y.; Zhao, Q.; Zhang, T.-P.; Wu, Y.; Xiong, Y.-X.; Wang, S.-K.; Ge, Y.-L.; He, J.-H.; Lv, P.; Ou, T.-M.; Tan, J.-H.; Li, D.; Gu, L.-Q.; Ren, J.; Zhao, Y.; Huang, Z.-S. Conformation Selective Antibody Enables Genome Profiling and Leads to Discovery of Parallel G-Quadruplex in Human Telomeres. *Cell Chemical Biology* **2016**, *23* (10), 1261–1270.

(199) Chen, Q.; Kuntz, I. D.; Shafer, R. H. Spectroscopic Recognition of Guanine Dimeric Hairpin Quadruplexes by a Carbocyanine Dye. *Proc Natl Acad Sci U S A* **1996**, *93* (7), 2635–2644.

(200) Li, Y.; Geyer, C. R.; Sen, D. Recognition of Anionic Porphyrins by DNA Aptamers. *Biochemistry* **1996**, *35* (21), 6911–6922.

(201) Allain, C.; Monchaud, D.; Teulade-Fichou, M.-P. FRET Templated by G-Quadruplex DNA: A Specific Ternary Interaction Using an Original Pair of Donor/Acceptor Partners. *J Am Chem Soc* **2006**, *128* (36), 11890–11893. https://doi.org/10.1021/ja062193h.

(202) Kong, D.-M.; Ma, Y.-E.; Wu, J.; Shen, H.-X. Discrimination of G-Quadruplexes from Duplex and Single-Stranded DNAs with Fluorescence and Energy-Transfer Fluorescence Spectra of Crystal Violet. *Chemistry* **2009**, *15* (4), 901–910.

(203) Drygin, D.; Siddiqui-Jain, A.; O'Brien, S.; Schwaebe, M.; Lin, A.; Bliesath, J.; Ho, C. B.; Proffitt, C.; Trent, K.; Whitten, J. P.; Lim, J. K. C.; Von Hoff, D.; Anderes, K.; Rice, W. G. Anticancer Activity of CX-3543: A Direct Inhibitor of rRNA Biogenesis. *Cancer Res* **2009**, *69* (19), 7653–7661. https://doi.org/10.1158/0008-5472.CAN-09-1304.

(204) Shivalingam, A.; Izquierdo, M. A.; Marois, A. L.; Vyšniauskas, A.; Suhling, K.; Kuimova, M. K.; Vilar, R. The Interactions between a Small Molecule and G-Quadruplexes Are Visualized by Fluorescence Lifetime Imaging Microscopy. *Nat Commun* **2015**, *6* (1), 8178. https://doi.org/10.1038/ncomms9178.

(205) Laguerre, A.; Wong, J. M. Y.; Monchaud, D. Direct Visualization of Both DNA and RNA Quadruplexes in Human Cells via an Uncommon Spectroscopic Method. *Sci Rep* **2016**, *6* (1), 32141. https://doi.org/10.1038/srep32141.

(206) Chen, X.-C.; Chen, S.-B.; Dai, J.; Yuan, J.-H.; Ou, T.-M.; Huang, Z.-S.; Tan, J.-H. Tracking the Dynamic Folding and Unfolding of RNA G-Quadruplexes in Live Cells. *Angew. Chem. Int. Ed.* **2018**, *57* (17), 4702–4706. https://doi.org/10.1002/anie.201801999.

(207) Tseng, T.-Y.; Chu, I.-T.; Lin, S.-J.; Li, J.; Chang, T.-C. Binding of Small Molecules to G-Quadruplex DNA in Cells Revealed by Fluorescence Lifetime Imaging Microscopy of o-BMVC Foci. *Molecules* **2018**, *24* (1), 35.

(208) Heald, R. A.; Modi, C.; Cookson, J. C.; Hutchinson, I.; Laughton, C. A.; Gowan, S. M.; Kelland, L. R.; Stevens, M. F. G. Antitumor Polycyclic Acridines. 8.1 Synthesis and Telomerase-Inhibitory Activity of Methylated Pentacyclic Acridinium Salts. *J Med Chem* **2001**, *45* (3), 590–597.

(209) Zhang, S.; Sun, H.; Chen, H.; Li, Q.; Guan, A.; Wang, L.; Shi, Y.; Xu, S.; Liu, M.; Tang, Y. Direct Visualization of Nucleolar G-Quadruplexes in Live Cells by Using a Fluorescent Light-up Probe. *Biochim. Biophys. Acta* **2018**, *1862* (5), 1101–1106.

(210) Zhang, S.; Sun, H.; Wang, L.; Liu, Y.; Chen, H.; Li, Q.; Guan, A.; Liu, M.; Tang, Y. Real-Time Monitoring of DNA G-Quadruplexes in Living Cells with a Small-Molecule FLuorescent Probe. *Nucleic Acids Research* **2018**, *46* (15), 7522–7532.

(211) Xu, S.; Li, Q.; Xiang, J.; Yang, Q.; Sun, H.; Guan, A.; Wang, L.; Liu, Y.; Yu, L.; Shi, Y.; Chen, H.; Tang, Y. Directly Lighting up RNA G-Quadruplexes from Test Tubes to Living Human Cells. *Nucleic Acids Res* **2015**, *43* (20), 9575–9586. https://doi.org/10.1093/nar/gkv1040.

(212) Laguerre, A.; Hukezalie, K.; Winckler, P.; Katranji, F.; Chanteloup, G.; Pirrotta, M.; Perrier-Cornet, J.-M.; Wong, J. M. Y.; Monchaud, D. Visualization of RNA-Quadruplexes in Live Cells. *J. Am. Chem. Soc.* **2015**, *137* (26), 8521–8525. https://doi.org/10.1021/jacs.5b03413.

(213) Monchaud, D. Quadruplex Detection in Human Cells. In *Annual Reports in Medicinal Chemistry*; Elsevier, 2020; Vol. 54, pp 133–160. https://doi.org/10.1016/bs.armc.2020.04.007.

(214) Wu, F.; Liu, C.; Chen, Y.; Yang, S.; Xu, J.; Huang, R.; Wang, X.; Li, M.; Liu, W.; Mao, W.; Zhou, X. Visualization of G-Quadruplexes in Gel and in Live Cells by a near-Infrared Fluorescent Probe. *Sens. Actuators B Chem.* **2016**, *236*, 268–275.

(215) Di Antonio, M.; Ponjavic, A.; Radzevičius, A.; Ranasinghe, R. T.; Catalano, M.; Zhang, X.; Shen, J.; Needham, L.-M.; Lee, S. F.; Klenerman, D.; Balasubramanian, S. Single-Molecule Visualization of DNA G-Quadruplex Formation in Live Cells. *Nat. Chem.* **2020**, *12* (9), 832–837. https://doi.org/10.1038/s41557-020-0506-4.

(216) Laguerre, A.; Stefan, L.; Larrouy, M.; Genest, D.; Novotna, J.; Pirrotta, M.; Monchaud, D. A Twice-As-Smart Synthetic G-Quartet: PyroTASQ Is Both a Smart Quadruplex Ligand and a Smart Fluorescent

Probe. *J. Am. Chem. Soc.* **2014**, *136* (35), 12406–12414. https://doi.org/10.1021/ja506331x.
(217) Yang, S. Y.; Amor, S.; Laguerre, A.; Wong, J. M. Y.; Monchaud, D. Real-Time and Quantitative Fluorescent Live-Cell Imaging with Quadruplex-Specific Red-Edge Probe (G4-REP). *Biochimica et Biophysica Acta (BBA) - General Subjects* **2017**, *1861* (5), 1312–1320. https://doi.org/10.1016/j.bbagen.2016.11.046.
(218) Tabor, N.; Ngwa, C.; Mitteaux, J.; Meyer, M. D.; Moruno-Manchon, J. F.; Zhu, L.; Liu, F.; Monchaud, D.; McCullough, L. D.; Tsvetkov, A. S. Differential Responses of Neurons, Astrocytes, and Microglia to G-Quadruplex Stabilization. *Aging* **2021**, *13* (12), 15917–15941. https://doi.org/10.18632/aging.203222.
(219) Lefebvre, J.; Guetta, C.; Poyer, F.; Mahuteau-Betzer, F.; Teulade, M.-P. Copper-Alkyne Complexation Is Responsible for the Nucleolar Localisation of Quadruplex Nucleic Acid Drugs Labelled by Click Chemistry. *Angew. Chem. Int. Ed.* **2017**, *56* (38), 11365–11369.
(220) Rota Sperti, F.; Charbonnier, T.; Lejault, P.; Zell, J.; Bernhard, C.; Valverde, I. E.; Monchaud, D. Biomimetic, Smart, and Multivalent Ligands for G-Quadruplex Isolation and Bioorthogonal Imaging. *ACS Chem. Biol.* **2021**, *16* (5), 905–914. https://doi.org/10.1021/acschembio.1c00111.
(221) Yasuda, M.; Ma, Y.; Okabe, S.; Wakabayashi, Y.; Su, D.; Chang, Y.-T.; Seimiya, H.; Tera, M.; Nagasawa, K. Target Identification of a Macrocyclic Hexaoxazole G-Quadruplex Ligand Using Post-Target-Binding Visualization. *Chemical Communications* **2020**, *56* (85), 12905–12908.
(222) Rota Sperti, F.; Mitteaux, J.; Zell, J.; Pipier, A.; Valverde, I. E.; Monchaud, D. The Multivalent G-Quadruplex (G4)-Ligands MultiTASQs Allow for Versatile Click Chemistry-Based Investigations. *RSC Chem. Biol.* **2023**, *4* (7), 456–465. https://doi.org/10.1039/D3CB00009E.
(223) Rota Sperti, F.; Dupouy, B.; Mitteaux, J.; Pipier, A.; Pirrotta, M.; Chéron, N.; Valverde, I. E.; Monchaud, D. Click-Chemistry-Based Biomimetic Ligands Efficiently Capture G-Quadruplexes in Vitro and Help Localize Them at DNA Damage Sites in Human Cells. *JACS Au* **2022**, *2* (7), 1588–1595. https://doi.org/10.1021/jacsau.2c00082.
(224) Robinson, J.; Stenspil, S. G.; Maleckaite, K.; Bartlett, M.; Di Antonio, M.; Vilar, R.; Kuimova, M. K. Cellular Visualization of G-Quadruplex RNA via Fluorescence- Lifetime Imaging Microscopy. *J Am Chem Soc* **2024**, *146* (1), 1009–1018. https://doi.org/10.1021/jacs.3c11908.
(225) Rota Sperti, F.; Mitteaux, J.; Zell, J.; Pipier, A.; Valverde, I. E.; Monchaud, D. The Multivalent G-Quadruplex (G4)-Ligands MultiTASQs Allow for Versatile Click Chemistry-Based Investigations. *bioRxiv 2022.10.28.512542* **2022**, 1–18. https://doi.org/10.1101/2022.10.28.512542.
(226) Monchaud, D.; Valverde, I. E.; Lejault, P.; Rota Sperti, F. Biomimetic G-Quartet Compounds (EP3889155 (A1)). EP3889155 (A1), October 6, 2021.
(227) Monchaud, D.; Valverde, I. E.; Lejault, P.; Rota Sperti, F. Biomimetic G-Quartet Compounds (WO2021198239 (A1)). WO2021198239 (A1), October 7, 2021.
(228) Kolb, H. C.; Finn, M. G.; Sharpless, K. B. Click Chemistry: Diverse Chemical Function from a Few Good Reactions. *Angew. Chem. Int. Ed.* **2001**, *40* (11), 2004–2021. https://doi.org/10.1002/1521-3773(20010601)40:11<2004::AID-ANIE2004>3.0.CO;2-5.
(229) Tornøe, C. W.; Meldal, M. Peptidotriazoles: Copper(l)-Catalyzed 1,3-Dipolar Cycloadditions on Solid-Phase. In *Peptides 2001*; Peptides 2001; American Peptide Society [u.a.]: San Diego, California, U.S.A, 2001; Vol. Peptides: the wave of the future; proceedings of the Second International and the Seventeenth American Peptide Symposium, June 9-14, 2001, San Diego, California, U.S.A, pp 263–264.
(230) Tornøe, C. W.; Christensen, C.; Meldal, M. Peptidotriazoles on Solid Phase: [1,2,3]-Triazoles by Regiospecific Copper(I)-Catalyzed 1,3-Dipolar Cycloadditions of Terminal Alkynes to Azides. *J. Org. Chem.* **2002**, *67* (9), 3057–3064. https://doi.org/10.1021/jo011148j.
(231) Agard, N. J.; Prescher, J. A.; Bertozzi, C. R. A Strain-Promoted [3 + 2] Azide−Alkyne Cycloaddition for Covalent Modification of Biomolecules in Living Systems. *J. Am. Chem. Soc.* **2004**, *126* (46), 15046–15047. https://doi.org/10.1021/ja044996f.
(232) Vuong, S.; Stefan, L.; Lejault, P.; Rousselin, Y.; Denat, F.; Monchaud, D. Identifying Three-Way DNA Junction-Specific Small-Molecules. *Biochimie* **2012**, *94* (2), 442–450. https://doi.org/10.1016/j.biochi.2011.08.012.
(233) Novotna, J.; Laguerre, A.; Granzhan, A.; Pirrotta, M.; Teulade-Fichou, M.-P.; Monchaud, D. Cationic Azacryptands as Selective Three-Way DNA Junction Binding Agents. *Org. Biomol. Chem.* **2015**, *13* (1), 215–222. https://doi.org/10.1039/C4OB01846J.
(234) Guyon, L.; Pirrotta, M.; Duskova, K.; Granzhan, A.; Teulade-Fichou, M.-P.; Monchaud, D. TWJ-Screen: An Isothermal Screening Assay to Assess Ligand/DNA Junction Interactions in Vitro. *Nucleic Acids Research* **2018**, *46* (3), e16–e16. https://doi.org/10.1093/nar/gkx1118.

(235) Duskova, K.; Lamarche, J.; Amor, S.; Caron, C.; Queyriaux, N.; Gaschard, M.; Penouilh, M.-J.; de Robillard, G.; Delmas, D.; Devillers, C. H.; Granzhan, A.; Teulade-Fichou, M.-P.; Chavarot-Kerlidou, M.; Therrien, B.; Britton, S.; Monchaud, D. Identification of Three-Way DNA Junction Ligands through Screening of Chemical Libraries and Validation by Complementary in Vitro Assays. *J. Med. Chem.* **2019**, *62* (9), 4456–4466. https://doi.org/10.1021/acs.jmedchem.8b01978.

(236) Morris, M. J.; Wingate, K. L.; Silwal, J.; Leeper, T. C.; Basu, S. The Porphyrin TmPyP4 Unfolds the Extremely Stable G-Quadruplex in MT3-MMP mRNA and Alleviates Its Repressive Effect to Enhance Translation in Eukaryotic Cells. *Nucleic Acids Research* **2012**, *40* (9), 4137–4145. https://doi.org/10.1093/nar/gkr1308.

(237) Laguerre, A.; Chang, Y.; Pirrotta, M.; Desbois, N.; Gros, C. P.; Lesniewska, E.; Monchaud, D. Surface-Promoted Aggregation of Amphiphilic Quadruplex Ligands Drives Their Selectivity for Alternative DNA Structures. *Org. Biomol. Chem.* **2015**, *13* (25), 7034–7039. https://doi.org/10.1039/C5OB00692A.

(238) Diabate, P. D.; Laguerre, A.; Pirrotta, M.; Desbois, N.; Boudon, J.; Gros, C. P.; Monchaud, D. DNA Structure-Specific Sensitization of a Metalloporphyrin Leads to an Efficient in Vitro Quadruplex Detection Molecular Tool. *New J. Chem.* **2016**, *40* (7), 5683–5689. https://doi.org/10.1039/C6NJ01012A.

(239) Jiang, X.; Gros, C. P.; Chang, Y.; Desbois, N.; Zeng, L.; Cui, Y.; Kadish, K. M. Tetracationic and Tetraanionic Manganese Porphyrins: Electrochemical and Spectroelectrochemical Characterization. *Inorg. Chem.* **2017**, *56* (14), 8045–8057. https://doi.org/10.1021/acs.inorgchem.7b00732.

(240) Wojciechowski, F.; Hudson, R. H. E. Peptide Nucleic Acid Containing a Meta-Substituted Phenylpyrrolocytosine Exhibits a Fluorescence Response and Increased Binding Affinity toward RNA. *Organic Letters* **2009**, *11* (21), 4878–4881. https://doi.org/doi/10.1021/ol9019474.

(241) Granzhan, A.; Largy, E.; Saettel, N.; Teulade-Fichou, M.-P. Macrocyclic DNA-Mismatch-Binding Ligands: Structural Determinants of Selectivity. *Chem. Eur. J.* **2010**, *16* (3), 878–889. https://doi.org/10.1002/chem.200901989.

(242) Waller, Z. A. E.; Sewitz, S. A.; Hsu, S.-T. D.; Balasubramanian, S. A Small Molecule That Disrupts G-Quadruplex DNA Structure and Enhances Gene Expression. *Journal of the American Chemical Society* **2009**, *131* (35), 12628–12633. https://doi.org/10.1021/ja901892u.

(243) NCBI Resource Coordinators. Database Resources of the National Center for Biotechnology Information. *Nucleic Acids Research* **2012**, *41* (D1), D8–D20. https://doi.org/10.1093/nar/gks1189.

(244) Duskova, K.; Lejault, P.; Benchimol, É.; Guillot, R.; Britton, S.; Granzhan, A.; Monchaud, D. DNA Junction Ligands Trigger DNA Damage and Are Synthetic Lethal with DNA Repair Inhibitors in Cancer Cells. *J. Am. Chem. Soc.* **2020**, *142* (1), 424–435. https://doi.org/10.1021/jacs.9b11150.

(245) Zell, J.; Duskova, K.; Chouh, L.; Bossaert, M.; Chéron, N.; Granzhan, A.; Britton, S.; Monchaud, D. Dual Targeting of Higher-Order DNA Structures by Azacryptands Induces DNA Junction-Mediated DNA Damage in Cancer Cells. *Nucleic Acids Research* **2021**, *49* (18), 10275–10288. https://doi.org/10.1093/nar/gkab796.

(246) Zimmer, J.; Tacconi, E. M. C.; Folio, C.; Badie, S.; Porru, M.; Klare, K.; Tumiati, M.; Markkanen, E.; Halder, S.; Ryan, A.; Jackson, S. P.; Ramadan, K.; Kuznetsov, S. G.; Biroccio, A.; Sale, J. E.; Tarsounas, M. Targeting BRCA1 and BRCA2 Deficiencies with G-Quadruplex-Interacting Compounds. *Mol Cell* **2016**, *61* (3), 449–460. https://doi.org/10.1016/j.molcel.2015.12.004.

(247) Moruno-Manchon, J. F.; Koellhoffer, E. C.; Gopakumar, J.; Hambarde, S.; Kim, N.; McCullough, L. D.; Tsvetkov, A. S. The G-Quadruplex DNA Stabilizing Drug Pyridostatin Promotes DNA Damage and Downregulates Transcription of Brca1 in Neurons. *Aging (Albany NY)* **2017**, *9* (9), 1957–1970. https://doi.org/10.18632/aging.101282.

(248) Pipier, A.; Devaux, A.; Lavergne, T.; Adrait, A.; Couté, Y.; Britton, S.; Calsou, P.; Riou, J. F.; Defrancq, E.; Gomez, D. Constrained G4 Structures Unveil Topology Specificity of Known and New G4 Binding Proteins. *Scientific Reports* **2021**.

(249) Bossaert, M.; Pipier, A.; Riou, J.-F.; Noirot, C.; Nguyên, L.-T.; Serre, R.-F.; Bouchez, O.; Defrancq, E.; Calsou, P.; Britton, S.; Gomez, D. Transcription-Associated Topoisomerase 2α (TOP2A) Activity Is a Major Effector of Cytotoxicity Induced by G-Quadruplex Ligands. *eLife* **2021**, *10*, e65184. https://doi.org/10.7554/eLife.65184.

(250) Porru, M.; Artuso, S.; Salvati, E.; Bianco, A.; Franceschin, M.; Diodoro, M. G.; Passeri, D.; Orlandi, A.; Savorani, F.; D'Incalci, M.; Biroccio, A.; Leonetti, C. Targeting G-Quadruplex DNA Structures by EMICORON Has a Strong Antitumor Efficacy against Advanced Models of Human Colon Cancer. *Mol Cancer Ther* **2015**, *14* (11), 2541–2551. https://doi.org/10.1158/1535-7163.MCT-15-0253.

(251) Marchetti, C.; Zyner, K. G.; Ohnmacht, S. A.; Robson, M.; Haider, S. M.; Morton, J. P.; Marsico, G.;

Vo, T.; Laughlin-Toth, S.; Ahmed, A. A.; Di Vita, G.; Pazitna, I.; Gunaratnam, M.; Besser, R. J.; Andrade, A. C. G.; Diocou, S.; Pike, J. A.; Tannahill, D.; Pedley, R. B.; Evans, T. R. J.; Wilson, W. D.; Balasubramanian, S.; Neidle, S. Targeting Multiple Effector Pathways in Pancreatic Ductal Adenocarcinoma with a G-Quadruplex-Binding Small Molecule. *J. Med. Chem.* **2018**, *61* (6), 2500–2517. https://doi.org/10.1021/acs.jmedchem.7b01781.

(252) Lee, W. T. C.; Yin, Y.; Morten, M. J.; Tonzi, P.; Gwo, P. P.; Odermatt, D. C.; Modesti, M.; Cantor, S. B.; Gari, K.; Huang, T. T.; Rothenberg, E. Single-Molecule Imaging Reveals Replication Fork Coupled Formation of G-Quadruplex Structures Hinders Local Replication Stress Signaling. *Nat Commun* **2021**, *12* (1), 2525. https://doi.org/10.1038/s41467-021-22830-9.

(253) Komůrková, D.; Svobodová Kovaříková, A.; Bártová, E. G-Quadruplex Structures Colocalize with Transcription Factories and Nuclear Speckles Surrounded by Acetylated and Dimethylated Histones H3. *Int J Mol Sci* **2021**, *22* (4), 1995. https://doi.org/10.3390/ijms22041995.

(254) François, M.; Leifert, W. R.; Hecker, J.; Faunt, J.; Fenech, M. F. Guanine-Quadruplexes Are Increased in Mild Cognitive Impairment and Correlate with Cognitive Function and Chromosomal DNA Damage. *DNA Repair (Amst)* **2016**, *46*, 29–36. https://doi.org/10.1016/j.dnarep.2016.08.001.

(255) Mitteaux, J.; Raevens, S.; Wang, Z.; Pirrotta, M.; Valverde, I. E.; Hudson, R. H. E.; Monchaud, D. PhpC Modulates G-Quadruplex-RNA Landscapes in Human Cells. *Chem Commun (Camb)* **2024**, *60* (4), 424–427. https://doi.org/10.1039/d3cc05155b.

(256) Tourrière, H.; Chebli, K.; Zekri, L.; Courselaud, B.; Blanchard, J. M.; Bertrand, E.; Tazi, J. The RasGAP-Associated Endoribonuclease G3BP Assembles Stress Granules. *Journal of Cell Biology* **2003**, *160* (6), 823–831. https://doi.org/10.1083/jcb.200212128.

(257) Neumann, M.; Sampathu, D. M.; Kwong, L. K.; Truax, A. C.; Micsenyi, M. C.; Chou, T. T.; Bruce, J.; Schuck, T.; Grossman, M.; Clark, C. M.; McCluskey, L. F.; Miller, B. L.; Masliah, E.; Mackenzie, I. R.; Feldman, H.; Feiden, W.; Kretzschmar, H. A.; Trojanowski, J. Q.; Lee, V. M.-Y. Ubiquitinated TDP-43 in Frontotemporal Lobar Degeneration and Amyotrophic Lateral Sclerosis. *Science* **2006**, *314* (5796), 130–133. https://doi.org/10.1126/science.1134108.

(258) Gomes, E.; Shorter, X. J. The Molecular Language of Membraneless Organelles. *Journal of Biological Chemistry* **2019**, *294* (18), 7115–7127.

(259) Podinovskaia, M.; Prescianotto, C.; Buser, D. P.; Spang, A. A Novel Live-C- Ell Imaging Assay Reveals Regulation of Endosome Maturation. *Cell Biology* **2021**, *10e70982*.

(260) International Human Genome Sequencing Consortium. Finishing the Euchromatic Sequence of the Human Genome. *Nature* **2004**, *431* (7011), 931–945. https://doi.org/10.1038/nature03001.

(261) Nurk, S.; Koren, S.; Rhie, A.; Rautiainen, M.; Bzikadze, A. V.; Mikheenko, A.; Vollger, M. R.; Altemose, N.; Uralsky, L.; Gershman, A.; Aganezov, S.; Hoyt, S. J.; Diekhans, M.; Logsdon, G. A.; Alonge, M.; Antonarakis, S. E.; Borchers, M.; Bouffard, G. G.; Brooks, S. Y.; Caldas, G. V.; Chen, N.-C.; Cheng, H.; Chin, C.-S.; Chow, W.; de Lima, L. G.; Dishuck, P. C.; Durbin, R.; Dvorkina, T.; Fiddes, I. T.; Formenti, G.; Fulton, R. S.; Fungtammasan, A.; Garrison, E.; Grady, P. G. S.; Graves-Lindsay, T. A.; Hall, I. M.; Hansen, N. F.; Hartley, G. A.; Haukness, M.; Howe, K.; Hunkapiller, M. W.; Jain, C.; Jain, M.; Jarvis, E. D.; Kerpedjiev, P.; Kirsche, M.; Kolmogorov, M.; Korlach, J.; Kremitzki, M.; Li, H.; Maduro, V. V.; Marschall, T.; McCartney, A. M.; McDaniel, J.; Miller, D. E.; Mullikin, J. C.; Myers, E. W.; Olson, N. D.; Paten, B.; Peluso, P.; Pevzner, P. A.; Porubsky, D.; Potapova, T.; Rogaev, E. I.; Rosenfeld, J. A.; Salzberg, S. L.; Schneider, V. A.; Sedlazeck, F. J.; Shafin, K.; Shew, C. J.; Shumate, A.; Sims, Y.; Smit, A. F. A.; Soto, D. C.; Sovic, I.; Storer, J. M.; Streets, A.; Sullivan, B. A.; Thibaud-Nissen, F.; Torrance, J.; Wagner, J.; Walenz, B. P.; Wenger, A.; Wood, J. M. D.; Xiao, C.; Yan, S. M.; Young, A. C.; Zarate, S.; Surti, U.; McCoy, R. C.; Dennis, M. Y.; Alexandrov, I. A.; Gerton, J. L.; Schatz, M. C.; Eichler, E. E.; Miga, K. H.; Phillippy, A. M. The Complete Sequence of a Human Genome. **2022**.

(262) Boivin, V.; Faucher-Giguère, L.; Scott, M.; Abou-Elela, S. The Cellular Landscape of Mid-size Noncoding RNA. *WIREs RNA* **2019**, *10* (4). https://doi.org/10.1002/wrna.1530.

(263) Piovesan, A.; Caracausi, M.; Antonaros, F.; Pelleri, M. C.; Vitale, L. GeneBase 1.1: A Tool to Summarize Data from NCBI Gene Datasets and Its Application to an Update of Human Gene Statistics. *Database* **2016**, *2016*, baw153. https://doi.org/10.1093/database/baw153.

(264) Rota Sperti, F. Even Smarter Molecular Tools for Studying Alternative Nucleic Acid Structures in Human Cells, Université de Bourgogne - Franche-Comté, Dijon, 2022. https://www.theses.fr/2022UBFCK064.

(265) Burger, A. M.; Dai, F.; Schultes, C. M.; Reszka, A. P.; Moore, M. J.; Double, J. A.; Neidle, S. The G-Quadruplex-Interactive Molecule BRACO-19 Inhibits Tumor Growth, Consistent with Telomere Targeting and Interference with Telomerase Function. *Cancer Res* **2005**, 9.

(266) Vichai, V.; Kirtikara, K. Sulforhodamine B Colorimetric Assay for Cytotoxicity Screening. *Nat Protoc* **2006**, *1* (3), 1112–1116. https://doi.org/10.1038/nprot.2006.179.
(267) Kwok, C. K.; Merrick, C. J. G-Quadruplexes: Prediction, Characterization, and Biological Application. *Trends in Biotechnology* **2017**, *35* (10), 997–1013. https://doi.org/10.1016/j.tibtech.2017.06.012.
(268) Umar, M. I.; Ji, D.; Chan, C.-Y.; Kwok, C. K. G-Quadruplex-Based Fluorescent Turn-On Ligands and Aptamers: From Development to Applications. *Molecules* **2019**, *24* (13), 2416. https://doi.org/10.3390/molecules24132416.
(269) Mendes, E.; Aljnadi, I. M.; Bahls, B.; Victor, B. L.; Paulo, A. Major Achievements in the Design of Quadruplex-Interactive Small Molecules. *Pharmaceuticals* **2022**, *15* (3), 300. https://doi.org/10.3390/ph15030300.
(270) Nakanishi, C.; Seimiya, H. G-Quadruplex in Cancer Biology and Drug Discovery. *Biochemical and Biophysical Research Communications* **2020**, *531* (1), 45–50. https://doi.org/10.1016/j.bbrc.2020.03.178.
(271) Vijay Kumar, M. J.; Morales, R.; Tsvetkov, A. S. G-Quadruplexes and Associated Proteins in Aging and Alzheimer's Disease. *Front. Aging* **2023**, *4*, 1164057. https://doi.org/10.3389/fragi.2023.1164057.
(272) Brosh, R. M.; Matson, S. W. History of DNA Helicases. *Genes* **2020**, *11* (3), 255. https://doi.org/10.3390/genes11030255.
(273) Di Antonio, M.; Biffi, G.; Mariani, A.; Raiber, E.-A.; Rodriguez, R.; Balasubramanian, S. Selective RNA Versus DNA G-Quadruplex Targeting by In Situ Click Chemistry. *Angew. Chem. Int. Ed.* **2012**, *51* (44), 11073–11078. https://doi.org/10.1002/anie.201206281.

APPENDICES

of

DOCTORAL THESIS OF THE UNIVERSITY OF BOURGOGNE FRANCHE-COMTÉ

prepared at the Institute of Molecular Chemistry of the University of Bourgogne (ICMUB)

Graduate School n°553

« Carnot Pasteur »

Thesis for the degree of Doctor of Philosophy (PhD)

in Chemical biology

by

Mr MITTEAUX Jérémie

Methods and tools for the study of G-quadruplex DNA and RNA in human cells

---

Thesis presented and defended in Dijon, on 13th December 2023

Jury composition:

Pr DENAT Franck	Professor and Director, ICMUB (Dijon)	President
Dr MILLEVOI Stefania	Senior INSERM researcher, CRCT (Toulouse)	Reviewer
Dr BRITTON Sébastien	CNRS researcher, IPBS (Toulouse)	Reviewer
Dr AMRANE Samir	INSERM researcher, ARNA/IECB (Bordeaux)	Examiner
Dr MONCHAUD David	Senior CRNS researcher, ICMUB (Dijon)	Supervisor
Dr GOBBO Jessica	Clinical research scientist, LNC Research Centre (Dijon)	Guest

LIST OF CONTENTS

ADDITIONAL FIGURES AND TABLES

I. Related to the Chapter I

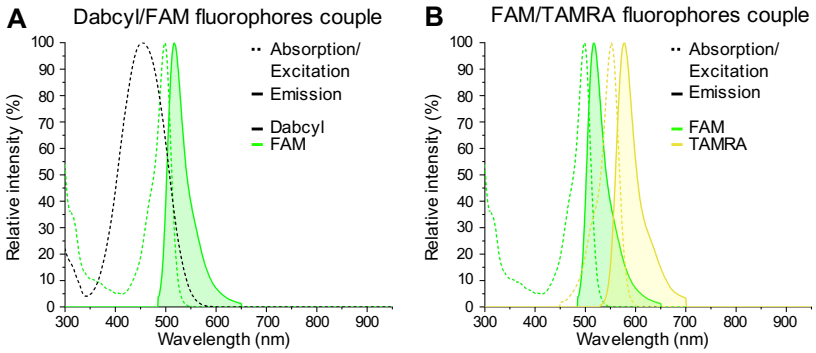

Figure S1. Spectra of the two fluorophores couples used in *in vitro* assays. (**A**) The dabcyl/FAM fluorophores couple was used in hPIF1 helicase and G4-UNFOLD assays where the dabcyl quenches the FAM emission. (**B**) The FAM/TAMRA fluorophores couple was used in FRET-melting assay where the TAMRA quenches the FAM emission. Dabcyl: dabcyl succinimidyl ester ($\lambda_{abs\ max}$= 452 nm; no emission). FAM: 6-carboxyfluorescein ($\lambda_{exc\ max}$= 498 nm; $\lambda_{em\ max}$= 517 nm). TAMRA: 5-carboxytetramethylrhodamine ($\lambda_{exc\ max}$= 552 nm; $\lambda_{em\ max}$= 576 nm). The fluorophores data set were taken on ThermoFisher's SpectraViewer tool.

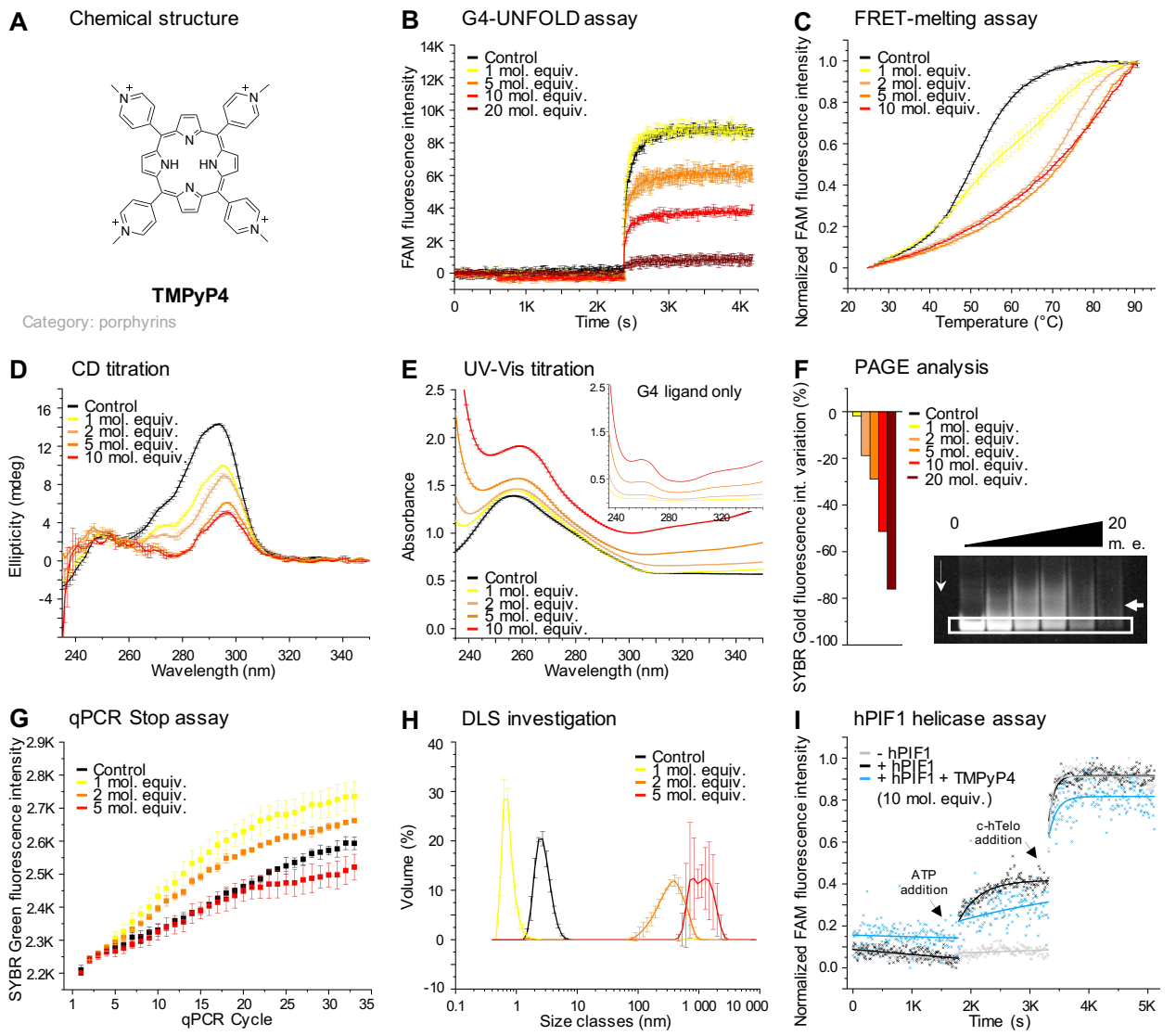

Figure S2. Summary card of TMPyP4 results. The (**A**) TMPyP4 small molecule effect on G4 was assessed by (**B**) G4-UNFOLD assay, (**C**) FRET-melting assay, (**D**) CD titration, (**E**) UV-Vis titration, (**F**) PAGE analysis, (**G**) qPCR Stop assay, (**H**) DLS investigation and (**I**) hPIF1 helicase assay with increasing concentrations (gradation from yellow to dark red). Controls are in black.

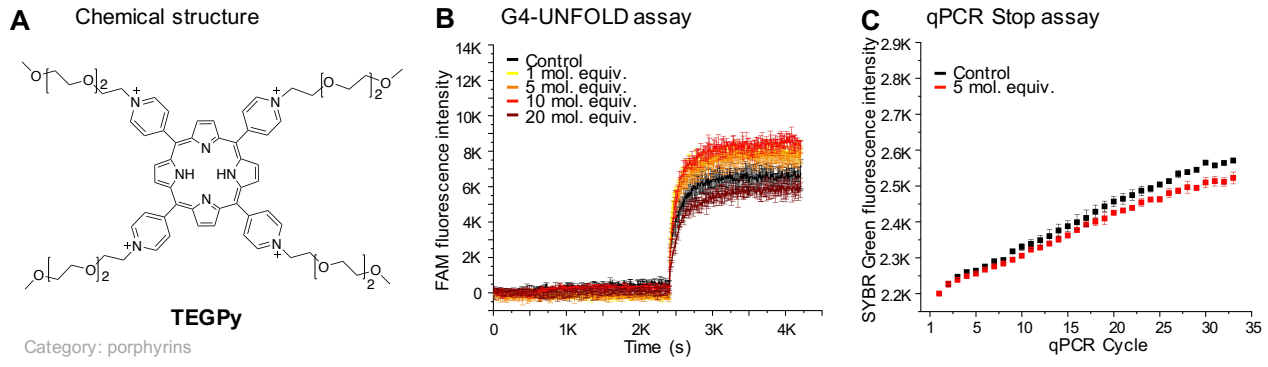

Figure S3. Summary card of TEGPy results. The (**A**) TEGPy small molecule effect on G4 was assessed by (**B**) G4-UNFOLD assay and (**C**) qPCR Stop assay with increasing concentrations (gradation from yellow to dark red). Controls are in black.

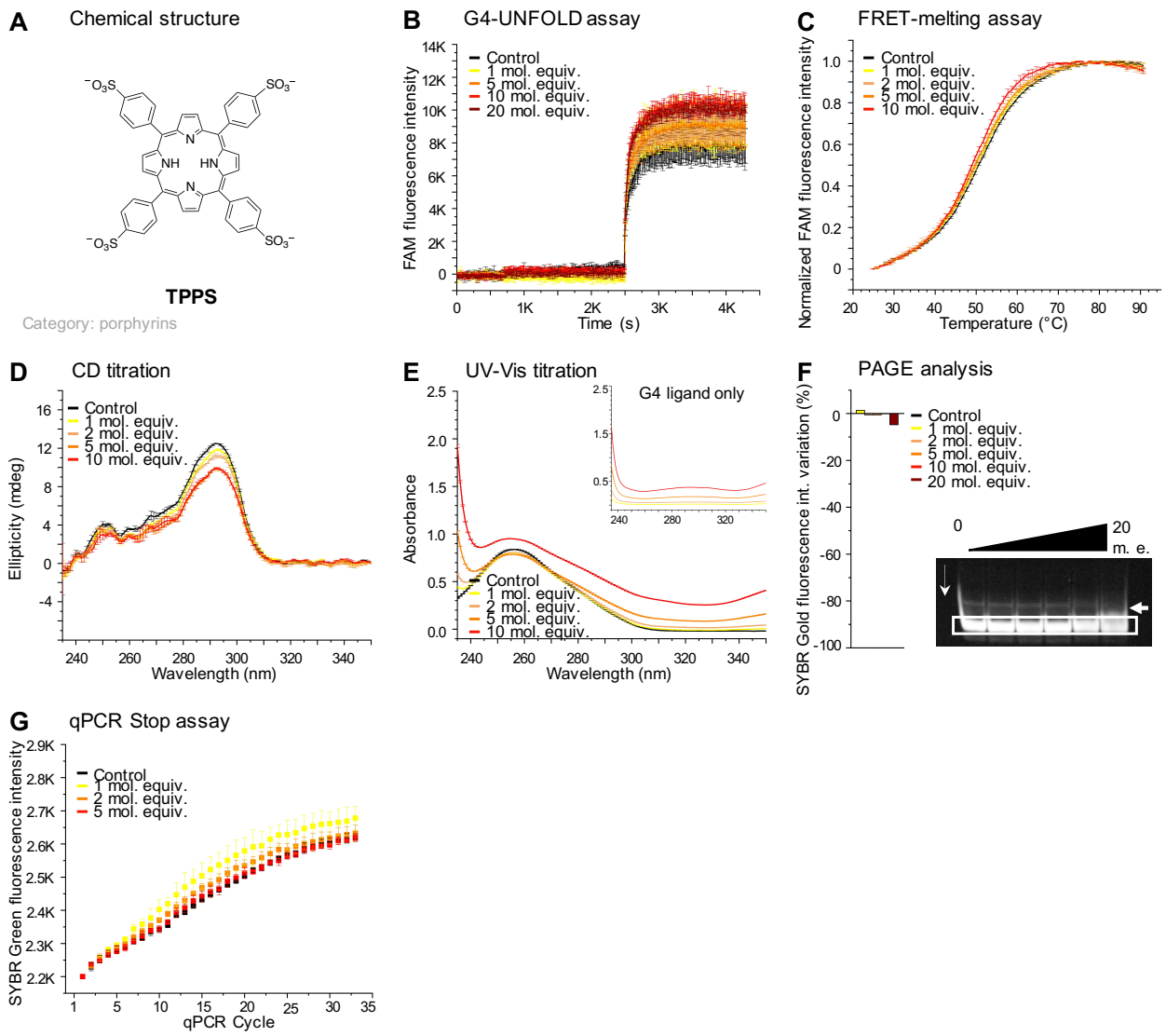

Figure S4. Summary card of TPPS results. The (**A**) TPPS small molecule effect on G4 was assessed by (**B**) G4-UNFOLD assay, (**C**) FRET-melting assay, (**D**) CD titration, (**E**) UV-Vis titration, (**F**) PAGE analysis and (**G**) qPCR Stop assay with increasing concentrations (gradation from yellow to dark red). Controls are in black.

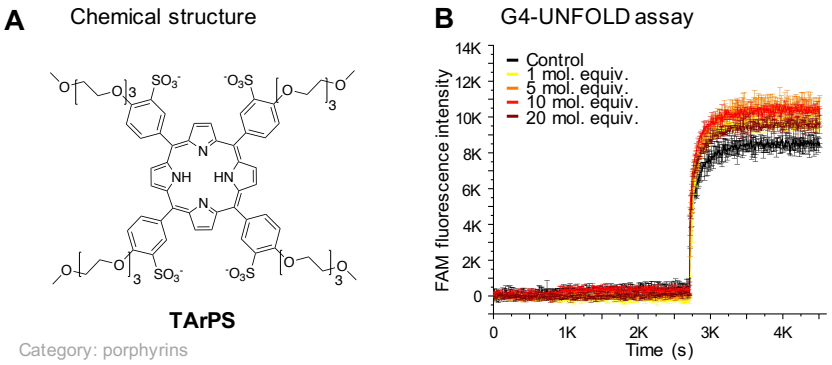

Figure S5. Summary card of TArPS results. The (**A**) TArPS small molecule effect on G4 was assessed by (**B**) G4-UNFOLD assay with increasing concentrations (gradation from yellow to dark red). Control is in black.

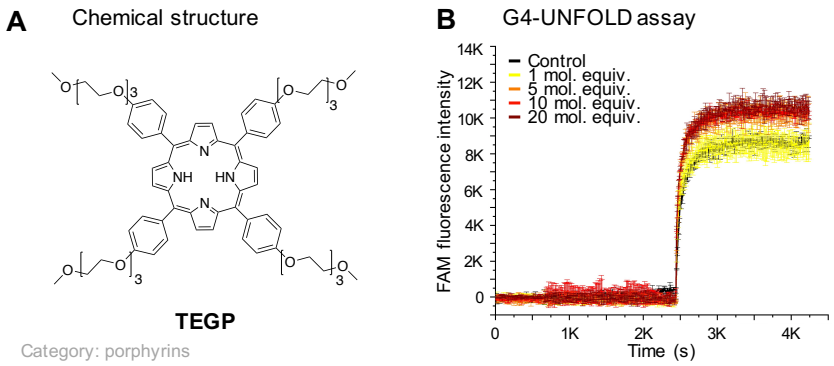

Figure S6. Summary card of TEGP results. The (**A**) TEGP small molecule effect on G4 was assessed by (**B**) G4-UNFOLD assay with increasing concentrations (gradation from yellow to dark red). Control is in black.

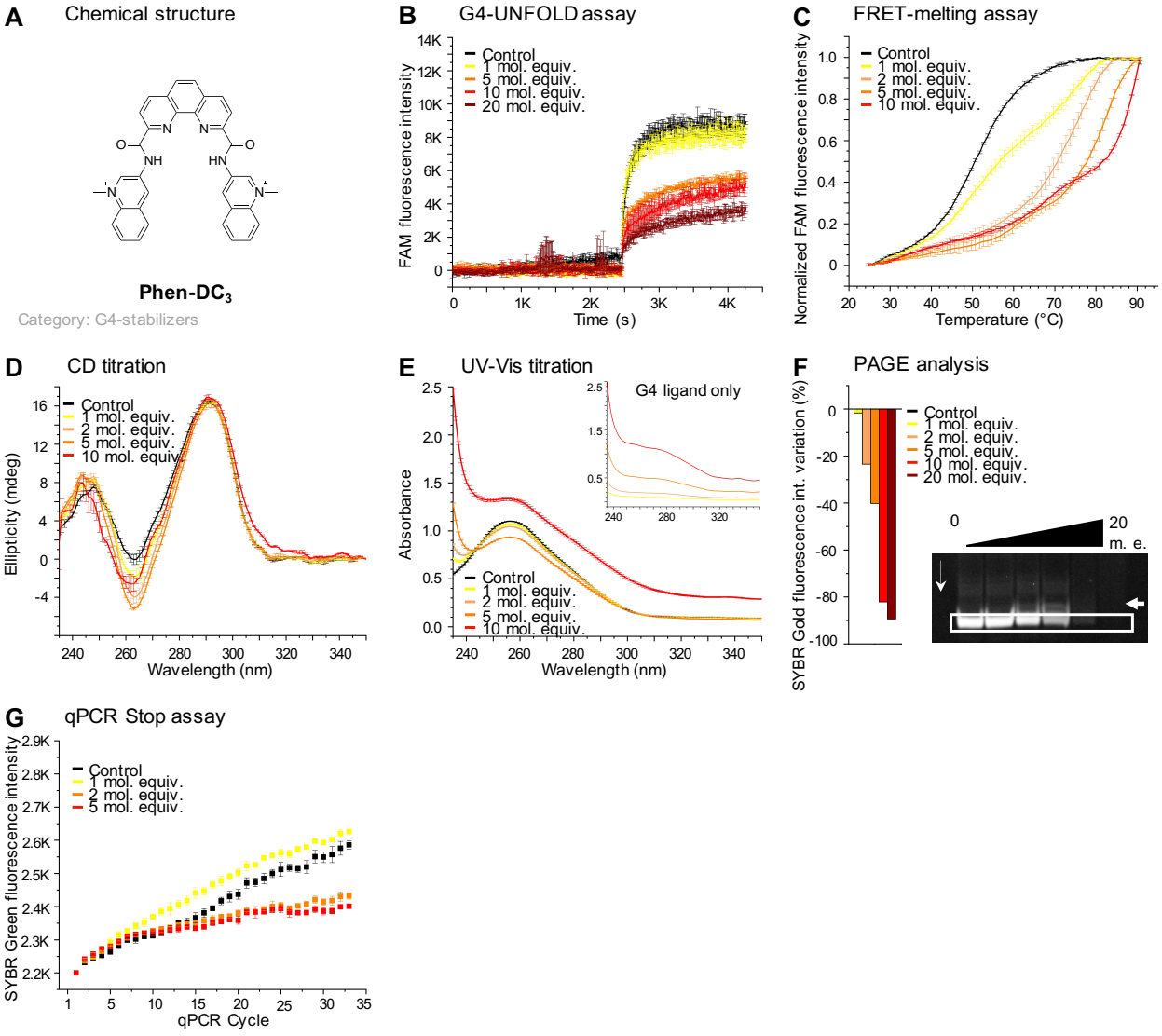

Figure S7. Summary card of Phen-DC$_3$ results. The (**A**) Phen-DC$_3$ small molecule effect on G4 was assessed by (**B**) G4-UNFOLD assay, (**C**) FRET-melting assay, (**D**) CD titration, (**E**) UV-Vis titration, (**F**) PAGE analysis and (**G**) qPCR Stop assay with increasing concentrations (gradation from yellow to dark red). Controls are in black.

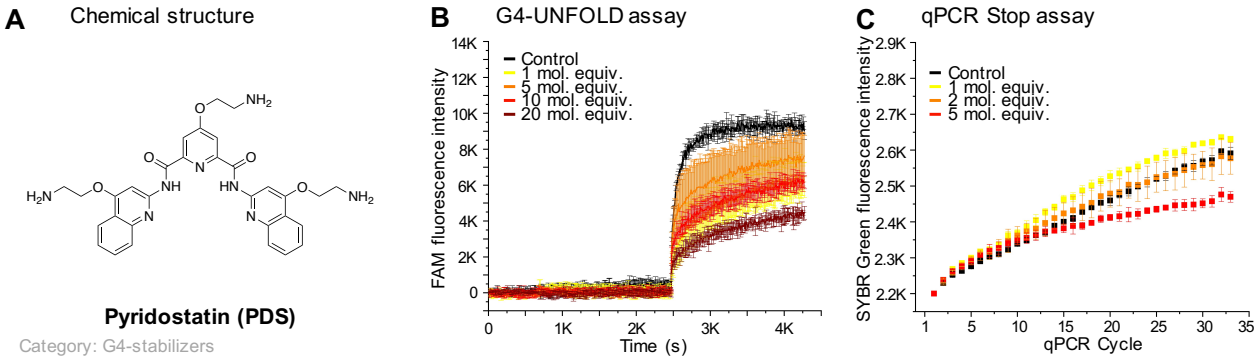

Figure S8. Summary card of PDS results. The (**A**) PDS small molecule effect on G4 was assessed by (**B**) G4-UNFOLD assay and (**C**) qPCR Stop assay with increasing concentrations (gradation from yellow to dark red). Controls are in black.

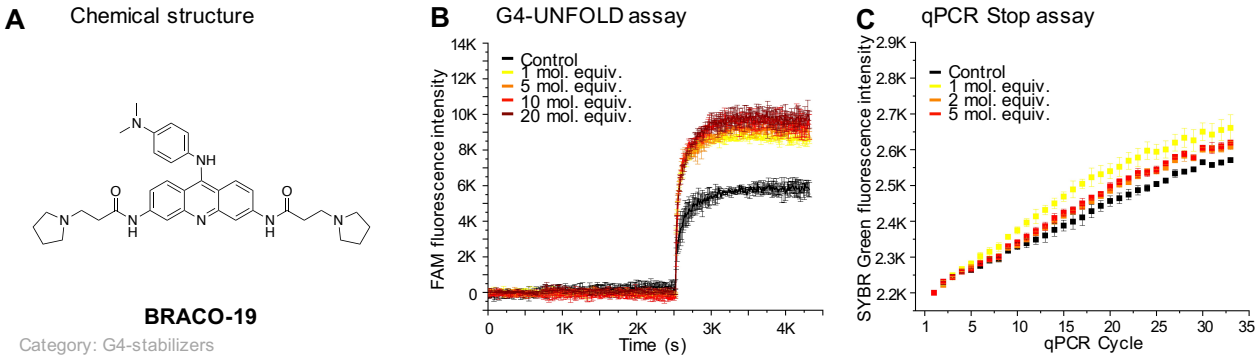

Figure S9. Summary card of BRACO-19 results. The (**A**) BRACO-19 small molecule effect on G4 was assessed by (**B**) G4-UNFOLD assay and (**C**) qPCR Stop assay with increasing concentrations (gradation from yellow to dark red). Controls are in black.

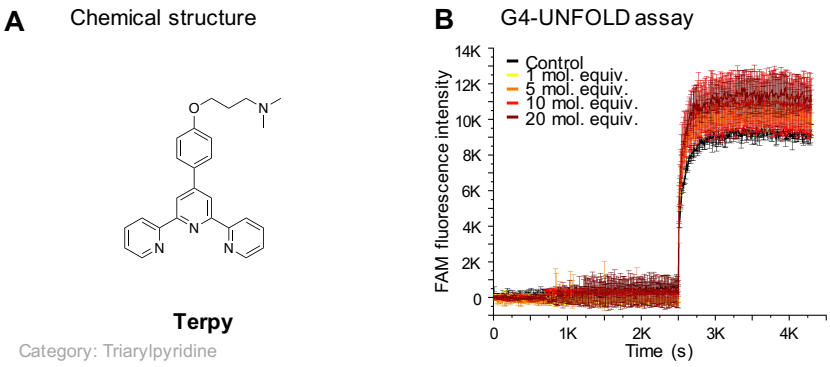

Figure S10. Summary card of Terpy results. The (**A**) Terpy small molecule effect on G4 was assessed by (**B**) G4-UNFOLD assay with increasing concentrations (gradation from yellow to dark red). Control is in black.

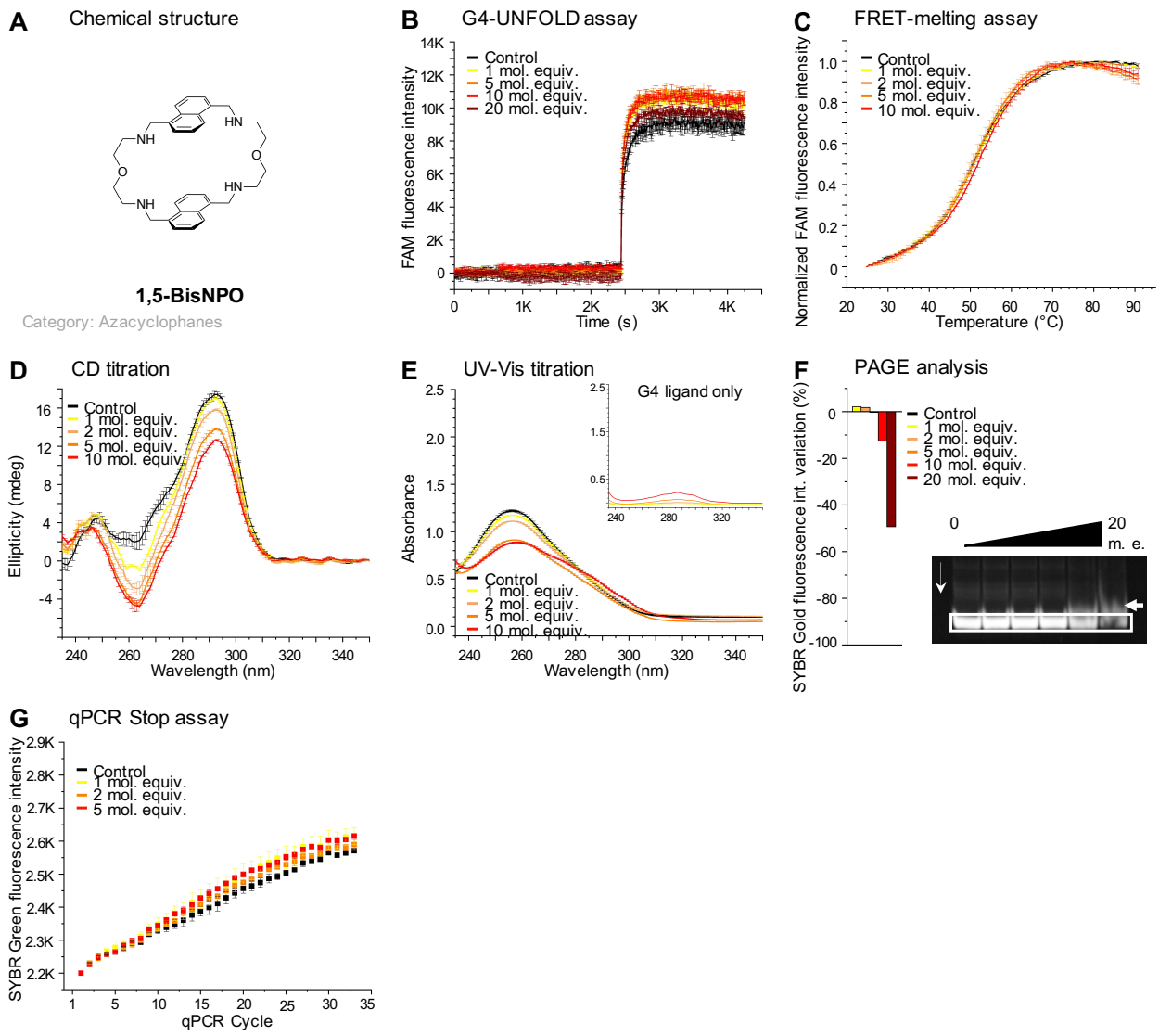

Figure S11. Summary card of 1,5-BisNPO results. The (**A**) 1,5-BisNPO small molecule effect on G4 was assessed by (**B**) G4-UNFOLD assay, (**C**) FRET-melting assay, (**D**) CD titration, (**E**) UV-Vis titration, (**F**) PAGE analysis and (**G**) qPCR Stop assay with increasing concentrations (gradation from yellow to dark red). Controls are in black.

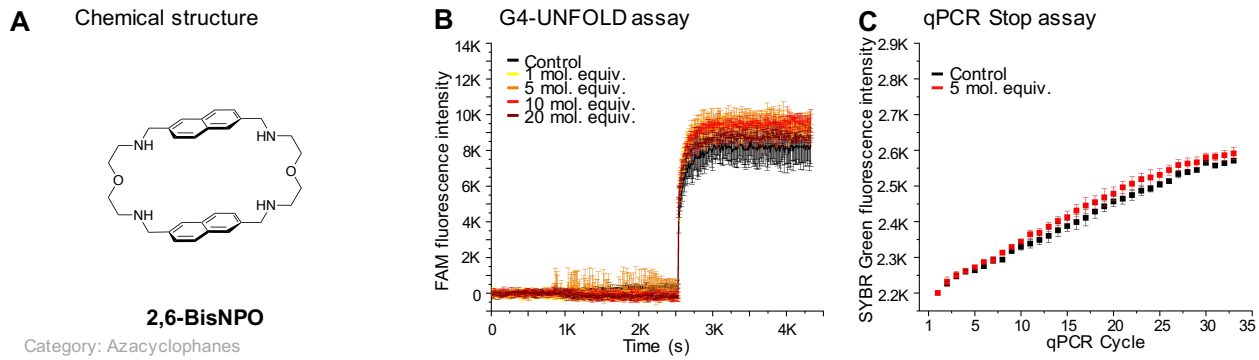

Figure S12. Summary card of 2,6-BisNPO results. The (**A**) 2,6-BisNPO small molecule effect on G4 was assessed by (**B**) G4-UNFOLD assay and (**C**) qPCR Stop assay with increasing concentrations (gradation from yellow to dark red). Controls are in black.

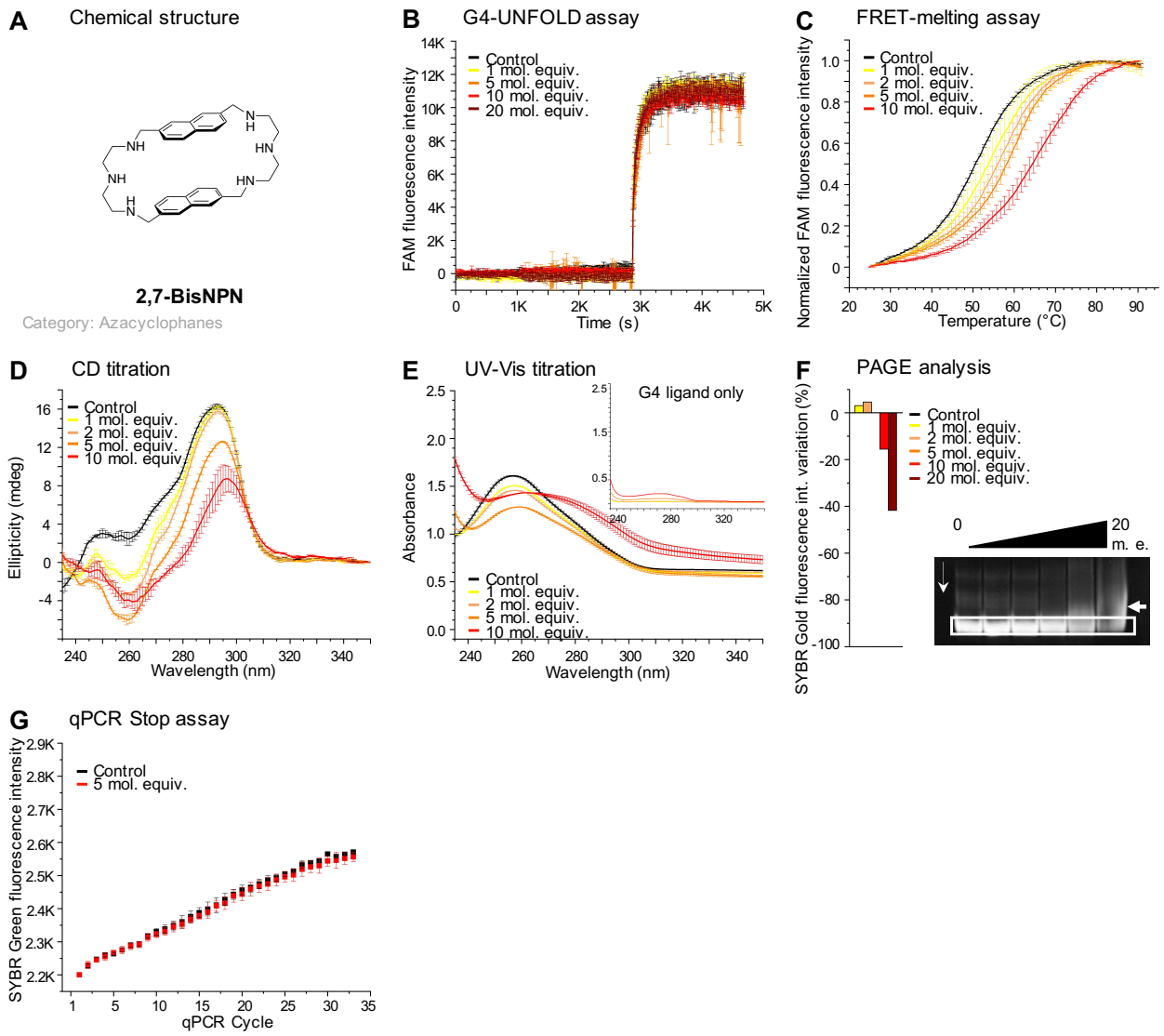

Figure S13. Summary card of 2,7-BisNPN results. The (**A**) 2,7-BisNPN small molecule effect on G4 was assessed by (**B**) G4-UNFOLD assay, (**C**) FRET-melting assay, (**D**) CD titration, (**E**) UV-Vis titration, (**F**) PAGE analysis and (**G**) qPCR Stop assay with increasing concentrations (gradation from yellow to dark red). Controls are in black.

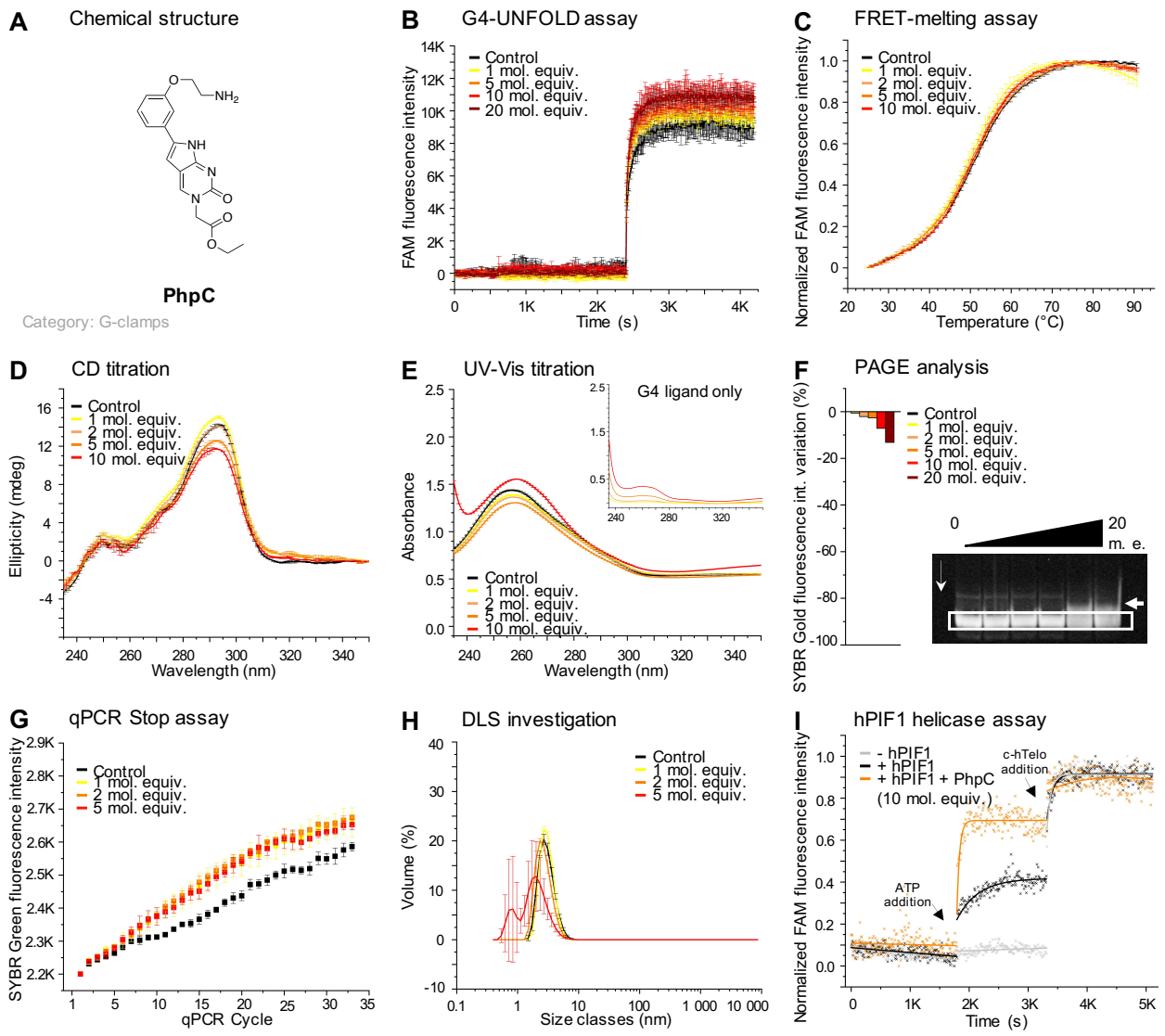

Figure S14. Summary card of PhpC results. The (**A**) PhpC small molecule effect on G4 was assessed by (**B**) G4-UNFOLD assay, (**C**) FRET-melting assay, (**D**) CD titration, (**E**) UV-Vis titration, (**F**) PAGE analysis, (**G**) qPCR Stop assay, (**H**) DLS investigation and (**I**) hPIF1 helicase assay with increasing concentrations (gradation from yellow to dark red). Controls are in black.

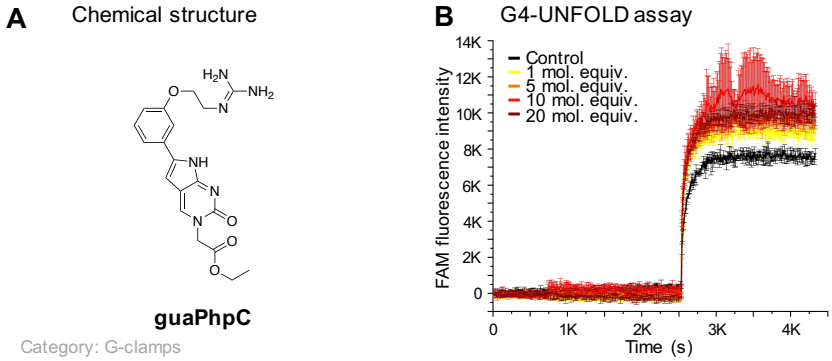

Figure S15. Summary card of guaPhpC results. The (**A**) guapPhpC small molecule effect on G4 was assessed by (**B**) G4-UNFOLD assay with increasing concentrations (gradation from yellow to dark red). Control is in black.

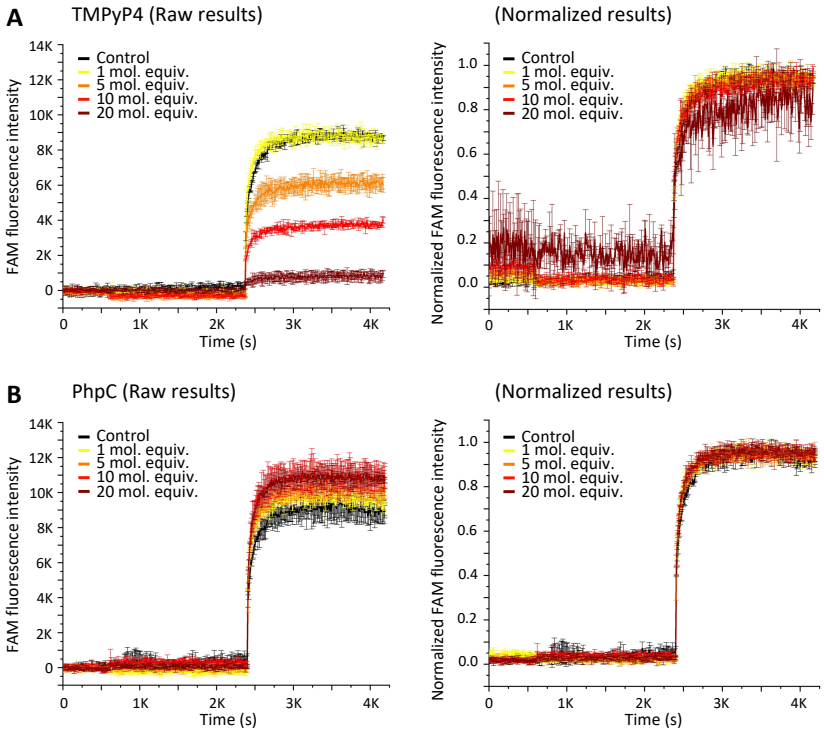

Figure S16. G4-UNFOLD raw and normalized curves obtained with 4 different concentrations of TMPyP4 or PhpC. The G4-UNFOLD assay was performed without (*i.e.*, Control, ON only with the Tris-HCl buffer 2: 20 mM Tris-HCl, 10 mM $MgCl_2$, 1 mM KCl, 99 mM NaCl, pH 7.2) or with the presence of (**A**) TMPyP4 or (**B**) PhpC (with the same Tris-HCl buffer 2 at 4 different concentrations of small molecules: 1, 5, 10 and 20 mol. equiv. (gradation from yellow to dark red). Controls are in black. For normalized data, a (0;1) normalization was applied to raw data. Error bars represent SD from the mean for three independent experiments.

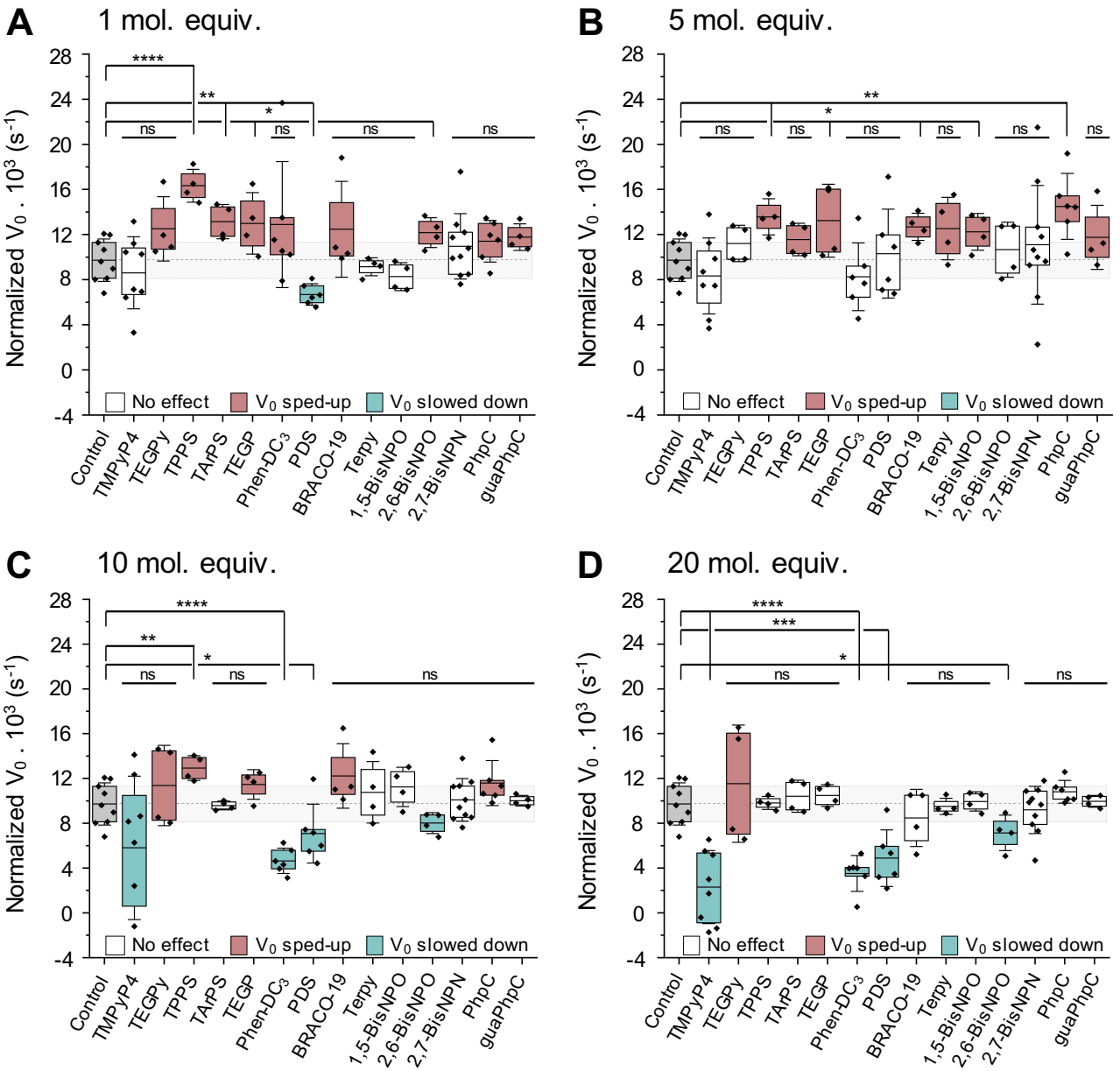

Figure S17. Normalized results obtained with 4 different concentrations of the 14 small molecules panoply assessed by G4-UNFOLD assay. The G4-UNFOLD assay was performed without (*i.e.*, V_0 Control, ON only with the Tris-HCl buffer 2: 20 mM Tris-HCl, 10 mM $MgCl_2$, 1 mM KCl, 99 mM NaCl, pH 7.2) or with the presence of a small molecule from the pre-selected small molecules panoply (with the same Tris-HCl buffer 2 at 4 different concentrations of small molecules: (**A**) 1, (**B**) 5, (**C**) 10 and (**D**) 20 mol. equiv. For normalized data, a (0;1) normalization was applied to raw data before the V_0 calculation. Mean V_0 values calculated correspond to the slope from the linear fit applied on the five first points after the c-hTelo addition. The capacity of small molecules to speed up (red boxes) or slow down (blue boxes) the c-hTelo hybridization speed in stabilizing or destabilizing the s-hTelo G4 was attributed in comparing Mean V_0 values (in s^{-1}): *i.* No effect if -SD V_0 Control < Mean V_0 small molecule < +SD V_0 Control, *ii.* G4-stabilizing effect if Mean V_0 small molecule < Mean V_0 Control or *iii.* G4-destabilizing effect if Mean V_0 small molecule > Mean V_0 Control. Error bars represent SD from the mean for at least four independent experiments. For statistical hypothesis tests, Student's *t*-test and Welch's unequal variances *t*-test were used depending on variances equality. * $p < 0.05$, ** $p < 0.01$, *** $p < 0.001$, **** $p < 0.0001$.

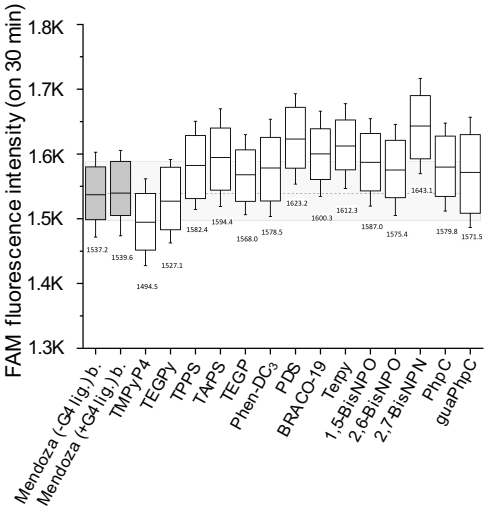

Figure S18. Results obtained with the 14 small molecules panoply measured alone with the plate-reader for G4-UNFOLD assay control. The FAM FI of the s-hTelo was monitored every 10 sec during 30 min after mixing this ON without (*i.e.*, V_0 Control, ON only with the Tris-HCl buffer 1/2: 20 mM Tris-HCl, 5 mM/10 mM $MgCl_2$, 1 mM KCl, 99 mM NaCl, pH 7.2) or with the presence of a small molecule from the pre-selected small molecules panoply (with the Tris-HCl buffer 2: 20 mM Tris-HCl, 10 mM $MgCl_2$, 1 mM KCl, 99 mM NaCl, pH 7.2) at 20 mol. equiv. Error bars represent SD from the mean of the 30 min data set.

	Small molecules alone	
	Mean of FAM FI	ΔFI
Tris-HCl buffer 1	1537.2 ± 65.5	/
Tris-HCl buffer 2	1539.6 ± 65.8	2.4
TMPyP4	1494.5 ± 67.1	-42.6
TEGPy	1527.1 ± 64.3	-10.1
TPPS	1582.4 ± 68.0	45.2
TArPS	1594.4 ± 75.3	57.2
TEGP	1568.0 ± 61.8	30.8
Phen-DC_3	1578.5 ± 75.1	41.3
PDS	1623.2 ± 69.8	86.0
BRACO-19	1600.3 ± 65.8	63.1
Terpy	1612.3 ± 65.5	75.1
1,5-BisNPO	1587.0 ± 67.5	49.9
2,6-BisNPO	1575.4 ± 70.4	38.2
2,7-BisNPN	1643.1 ± 73.5	106.0
PhpC	1579.8 ± 68.0	42.6
guaPhpC	1571.5 ± 85.1	34.4

Table S1. Summary FI and ΔFI values of the 14 small molecules panoply measured alone with the plate-reader for G4-UNFOLD assay control. Summary values of Mean FAM FI (or just FI) and ΔFI obtained in the control experiment of G4-UNDFOLD assay where the FAM FI of the s-hTelo was monitored every 10 sec during 30 min after mixing this ON without (*i.e.*, V_0 Control, ON only with the Tris-HCl buffer 1/2: 20 mM Tris-HCl, 5 mM/10 mM $MgCl_2$, 1 mM KCl, 99 mM NaCl, pH 7.2) or with the presence of a small molecule from the pre-selected small molecules panoply (with the Tris-HCl buffer

2: 20 mM Tris-HCl, 10 mM $MgCl_2$, 1 mM KCl, 99 mM NaCl, pH 7.2) at 20 mol. equiv. SD is from the mean of the 30 min data set. ΔFI= FI with small molecule – FI Control (Tris-HCl buffer 1).

A	**FRET-melting ($T_{1/2}$, °C)**				
	0 mol. equiv.	1 mol. equiv.	2 mol. equiv.	5 mol. equiv.	10 mol. equiv.
TMPyP4	50.6 ± 0.2	55.21 ± 1.8	68.8 ± 0.5	72.1 ± 0.2	70.5 ± 0.5
TPPS	50.6 ± 0.2	50.1 ± 0.1	49.6 ± 0.6	49.8 ± 0.1	49.0 ± 0.3
Phen-DC_3	50.6 ± 0.2	56.6 ± 1.1	70.6 ± 1.2	77.8 ± 0.5	81.5 ± 0.4
1,5-BisNPO	50.6 ± 0.2	50.8 ± 0.4	50.4 ± 0.8	50.8 ± 0.2	51.8 ± 0.3
2,7-BisNPO	50.6 ± 0.2	53.8 ± 2.1	56.0 ± 1.1	58.2 ± 0.9	64.4 ± 1.5
PhpC	50.6 ± 0.2	49.2 ± 0.8	50.2 ± 0.2	49.8 ± 0.8	50.2 ± 0.1

B	**FRET-melting ($\Delta T_{1/2}$, °C)**			
	1 mol. equiv.	2 mol. equiv.	5 mol. equiv.	10 mol. equiv.
TMPyP4	4.6	18.2	21.5	19.9
TPPS	-0.5	-1.0	-0.7	-1.6
Phen-DC_3	6.0	20.0	37.2	30.9
1,5-BisNPO	0.2	-0.2	0.2	1.2
2,7-BisNPO	3.2	5.4	7.5	13.8
PhpC	-1.4	-0.4	-0.8	-0.4

Table S2. Summary values of the 5 small molecules adjective panoply assessed by FRET-melting assay. Summary values of (**A**) $T_{1/2}$ (in °C) and (**B**) $\Delta T_{1/2}$ obtained in the FRET-melting assay performed without (*i.e.*, $T_{1/2}$ Control, 0 mol. equiv. row, ON only with CacoK10 buffer) or with the presence of a small molecule from the selected small molecules panoply (TMPyP4, TPPS, Phen-DC_3, 1,5-BisNPO, 2,7-BisNPN, PhpC) at 4 different concentrations of small molecules: 1, 2, 5 and 10 mol. equiv. Mean $T_{1/2}$ ± SD values calculated correspond to the melting temperature of the F21T G4 for three independent experiments. $\Delta T_{1/2}$= $T_{1/2}$ with small molecule – $T_{1/2}$ Control.

A	**CD at 293 nm (mdeg)**				
	0 mol. equiv.	1 mol. equiv.	2 mol. equiv.	5 mol. equiv.	10 mol. equiv.
TMPyP4	14.28 ± 0.07	9.51 ± 0.11	8.23 ± 0.30	5.23 ± 0.08	4.47 ± 0.11
TPPS	12.46 ± 0.02	11.85 ± 0.08	11.15 ± 0.18	9.81 ± 0.18	9.91 ± 0.01
Phen-DC_3	16.28 ± 0.14	16.32 ± 0.08	16.44 ± 0.09	16.08 ± 0.25	16.68 ± 0.01
1,5-BisNPO	17.42 ± 0.24	17.03 ± 0.16	15.81 ± 0.11	13.79 ± 0.02	12.66 ± 0.07
2,7-BisNPO	16.34 ± 0.20	16.23 ± 0.12	15.75 ± 0.22	12.39 ± 0.10	7.82 ± 1.81
PhpC	14.19 ± 0.14	15.06 ± 0.14	14.14 ± 0.07	12.58 ± 0.06	11.71 ± 0.00

B	**Variation of CD at 293 nm (%)**			
	1 mol. equiv.	2 mol. equiv.	5 mol. equiv.	10 mol. equiv.
TMPyP4	-33.3	-42.4	-63.3	-68.7
TPPS	-4.9	-10.5	-21.3	-20.5
Phen-DC_3	0.2	1.0	-1.2	2.5
1,5-BisNPO	-2.2	-9.2	-20.9	-27.3
2,7-BisNPO	-0.7	-3.6	-24.1	-52.1
PhpC	6.1	-0.3	-11.4	-17.5

Table S3. Summary values of the 5 small molecules adjective panoply assessed by Circular Dichroism titration. Summary values of (**A**) CD at 293 nm (or just CD; in mdeg; positive peak of the hTelo G4) and (**B**) CD variation obtained

in the CD titration performed without (*i.e.*, CD Control, 0 mol. equiv. row, ON only with CacoK10 buffer) or with the presence of a small molecule from the selected small molecules panoply (TMPyP4, TPPS, Phen-DC_3, 1,5-BisNPO, 2,7-BisNPN, PhpC) at 4 different concentrations of small molecules: 1, 2, 5 and 10 mol. equiv, in a titration manner. Mean CD ± SD values calculated correspond to the CD of the hTelo G4 during 10 min. CD variation= [(CD small molecule * 100)/CD Control] – 100.

A	**UV-Vis at 257 nm (complex)**					**UV-Vis at 257 nm (compound alone)**				
	0 mol. equiv.	1 mol. equiv.	2 mol. equiv.	5 mol. equiv.	10 mol. equiv.	0 mol. equiv.	1 mol. equiv.	2 mol. equiv.	5 mol. equiv.	10 mol. equiv.
TMPyP4	1.39 ± 0.01	1.44 ± 0.00	1.46 ± 0.00	1.57 ± 0.00	1.90 ± 0.01	0.01	0.09	0.17	0.45	0.91
TPPS	0.84 ± 0.00	0.80 ± 0.00	0.80 ± 0.00	0.78 ± 0.00	0.95 ± 0.00	0.004	0.02	0.05	0.14	0.29
Phen-DC_3	1.09 ± 0.01	1.07 ± 0.01	1.04 ± 0.00	0.93 ± 0.00	1.33 ± 0.02	0.08	0.11	0.20	0.52	1.20
1,5-BisNPO	1.21 ± 0.02	1.17 ± 0.00	1.11 ± 0.00	0.91 ± 0.00	0.89 ± 0.01	0.01	-0.03	-0.03	-0.01	0.07
2,7-BisNPO	1.61 ± 0.00	1.51 ± 0.00	1.46 ± 0.00	1.28 ± 0.00	1.42 ± 0.00	0.01	0.04	0.05	0.10	0.18
PhpC	1.44 ± 0.01	1.39 ± 0.01	1.36 ± 0.00	1.30 ± 0.00	1.55 ± 0.00	0.01	0.02	0.04	0.15	0.34

B	**Variation of UV-Vis at 257 nm (complex, %)**				**Variation of UV-Vis at 257 nm (comp. alone, %)**			
	1 mol. equiv.	2 mol. equiv.	5 mol. equiv.	10 mol. equiv.	1 mol. equiv.	2 mol. equiv.	5 mol. equiv.	10 mol. equiv.
TMPyP4	3.6	5.0	12.9	36.7	800	1600	4400	9000
TPPS	-4.8	-4.8	-7.1	13.1	400	1150	3400	7150
Phen-DC_3	-1.8	-4.6	-14.7	22.0	37.5	150	550	1400
1,5-BisNPO	-3.3	-8.3	-24.8	-26.4	-400	-400	-200	600
2,7-BisNPO	-6.2	-9.3	-20.5	-11.8	300	400	900	1700
PhpC	-3.5	-5.6	-9.7	7.6	100	300	1400	3300

Table S4. Summary values of the 5 small molecules adjective panoply assessed by UV-Vis titration. Summary values of (**A**) UV-Vis at 257 nm (or just UV; positive peak of the hTelo G4) and (**B**) UV variation (in %) obtained in the UV-Vis titration performed without (*i.e.*, UV Control, 0 mol. equiv. row, ± ON only with CacoK10 buffer) or with the presence of a small molecule from the selected small molecules panoply (TMPyP4, TPPS, Phen-DC_3, 1,5-BisNPO, 2,7-BisNPN, PhpC) at 4 different concentrations of small molecules: 1, 2, 5 and 10 mol. equiv, in a titration manner. UV-Vis titration of small molecules have also been monitored without the hTelo ON (compound alone). Mean UV ± SD values calculated correspond to the UV of the hTelo G4 during 10 min. UV variation= [(UV small molecule * 100)/UV Control] – 100. Comp.= compound.

A	**SYBR Gold fluorescence intensity (PAGE)**					
	0 mol. equiv.	1 mol. equiv.	2 mol. equiv.	5 mol. equiv.	10 mol. equiv.	20 mol. equiv.
TMPyP4	1165652	1143474	946045	828990	567120	279090
TPPS	922652	935313	917478	917744	921670	878931
Phen-DC_3	1174496	1155235	899367	702825	210164	124982
1,5-BisNPO	1288141	13168875	1311927	1284417	1127335	652839
2,7-BisNPO	1268097	1307083	1326832	1267322	1071228	739445
PhpC	1183049	1175663	1158332	1151716	1099066	1027728

B	**Variation of SYBR Gold fluorescence intensity (PAGE, %)**

	1 mol. equiv.	2 mol. equiv.	5 mol. equiv.	10 mol. equiv.	20 mol. equiv.
TMPyP4	-1.9	-18.8	-28.9	-51.3	-76.1
TPPS	1.4	-0.6	-0.5	-0.1	-4.7
Phen-DC_3	-1.6	-23.4	-40.2	-82.1	-89.4
1,5-BisNPO	2.2	1.8	-0.3	-12.5	-49.3
2,7-BisNPO	3.1	4.6	-0.1	-15.5	-41.7
PhpC	-0.6	-2.1	-2.7	-7.1	-13.1

Table S5. Summary values of the 5 small molecules adjective panoply assessed by PAGE analysis. Summary values of (**A**) SYBR Gold FI (or just FI) and (**B**) FI variation (in %) obtained in the PAGE analysis performed without (*i.e.*, FI Control, 0 mol. equiv. row, ON only with CacoK10 buffer) or with the presence of a small molecule from the selected small molecules panoply (TMPyP4, TPPS, Phen-DC_3, 1,5-BisNPO, 2,7-BisNPN, PhpC) at 5 different concentrations of small molecules: 1, 2, 5, 10 and 20 mol. equiv. FI values calculated correspond to the FI of the hTelo band in gel. FI variation= [(FI small molecule * 100)/FI Control] – 100.

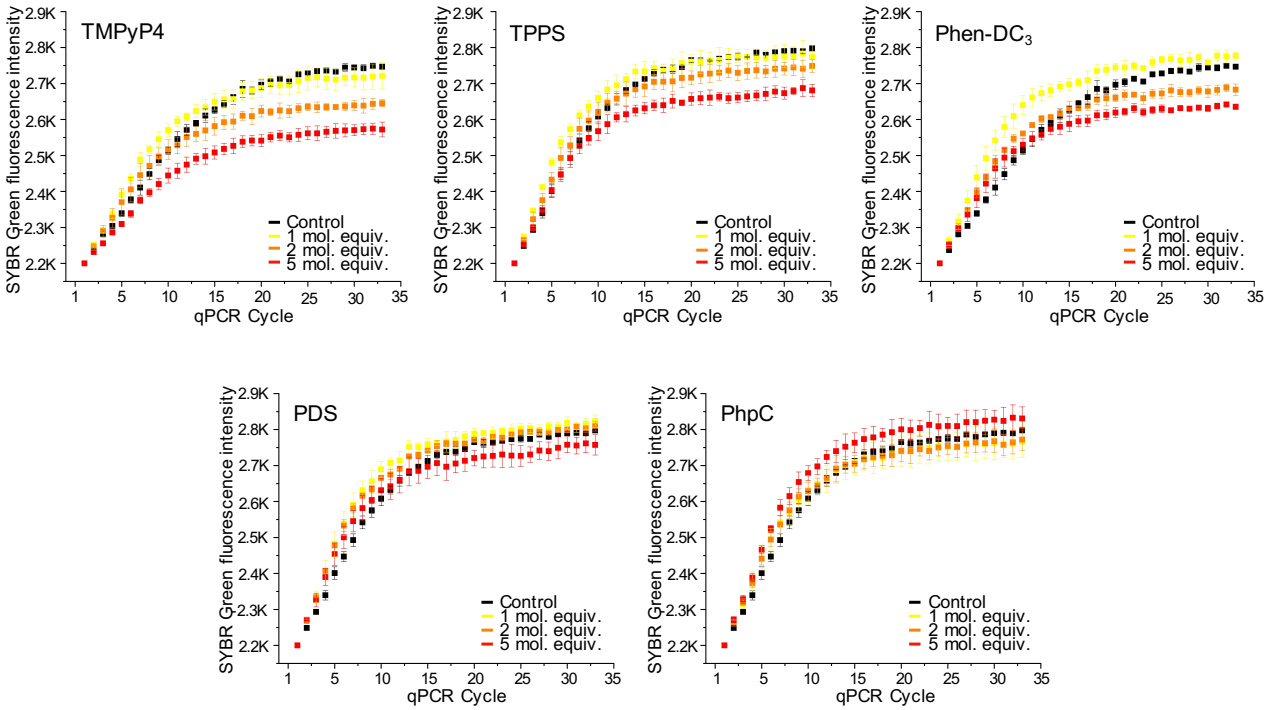

Figure S19. Experimental curves obtained with the 5 small molecules adjective panoply assessed by qPCR Stop assay with the *S. pombe* Non G4-strand ON. The qPCR Stop assay control was performed with the *S. pombe* Non G4-strand, without (*i.e.*, SYBR Green FI Control, ON only with the KCl) or with the presence of a small molecule from the reduced small molecules panoply (TMPyP4, TPPS, Phen-DC_3, PDS, PhpC) at 3 different concentrations of small molecules: 1, 2 and 5 mol. equiv. (gradation from yellow to dark red). Controls are in black. Error bars represent SD from the mean for six independent experiments.

A	***S. pombe* G4-strand**					
	1 mol. equiv.		**2 mol. equiv.**		**5 mol. equiv.**	
	Mean of SYBR Green FI	ΔFI	Mean of SYBR Green FI	ΔFI	Mean of SYBR Green FI	ΔFI
Control	2598.8 ± 23.5	/	/	/	/	/
TMPyP4	2709.2 ± 57.0	110.3	2650.8 ± 7.5	52.0	2538.7 ± 35.7	-60.2
TPPS	2693.0 ± 34.8	94.2	2642.7 ± 22.0	43.8	2610.2 ± 14.2	11.3
Phen-DC_3	2628.3 ± 14.1	29.5	2447.3 ± 21.0	-151.5	2403.0 ± 10.8	-195.8
PDS	2631.8 ± 26.5	33.0	2574.3 ± 27.8	-24.5	2482.5 ± 19.4	-116.3
PhpC	2692.7 ± 41.1	93.8	2698.3 ± 21.9	99.5	2670.7 ± 34.6	71.8

B	***S. pombe* Non G4-strand**					
	1 mol. equiv.		**2 mol. equiv.**		**5 mol. equiv.**	
	Mean of SYBR Green FI	ΔFI	Mean of SYBR Green FI	ΔFI	Mean of SYBR Green FI	ΔFI
Control	2752.5 ± 39.9	/	/	/	/	/
TMPyP4	2719.5 ± 40.9	-33.0	2662.8 ± 27.4	-89.7	2580.2 ± 23.0	-172.3
TPPS	2763.3 ± 38.1	10.8	2733.2 ± 21.6	-19.3	2694.7 ± 28.7	-57.8
Phen-DC_3	2774.0 ± 14.0	21.5	2689.2 ± 21.0	-63.3	2636.3 ± 16.7	-116.2
PDS	2779.7 ± 49.0	27.2	2778.0 ± 35.3	25.5	2734.0 ± 35.4	-18.5
PhpC	2761.3 ± 28.9	8.8	2765.7 ± 31.6	13.2	2787.2 ± 52.5	34.7

C	**Selectivity factor S (= $\Delta FI_{G4\text{-strand}} - \Delta FI_{Non\ G4\text{-strand}}$)**		
	1 mol. equiv.	2 mol. equiv.	5 mol. equiv.
TMPyP4	-3.3	-0.6	0.3
TPPS	8.7	-2.3	-0.2
Phen-DC_3	1.4	2.4	1.7
PDS	1.2	-1.0	6.3
PhpC	10.7	7.5	2.1

Table S6. Summary FI, ΔFI and Selectivity factor S values of the 5 small molecules adjective panoply assessed by qPCR Stop assay with the *S. pombe* G4 motif (G4-strand) and G4-complementary C-rich motif (Non G4-strand). Summary values of (**A-B**) SYBR Green FI (or just FI) and ΔFI and (C) Selectivity factor S obtained in the qPCR Stop assay performed with the *S. pombe* (**A**) G4-strand or (**B**) Non G4-strand, without (*i.e.*, SYBR Green FI Control, ON only with the KCl) or with the presence of a small molecule from the reduced small molecules panoply (TMPyP4, TPPS, Phen-DC_3, PDS, PhpC) at 3 different concentrations of small molecules: 1, 2 and 5 mol. equiv. Mean FI ± SD values calculated correspond to the FI value at the 33th (and last) qPCR cycle for six independent experiments. ΔFI= FI with small molecule – FI Control. Selectivity factor S= $\Delta FI_{\ G4\ Strand} - \Delta FI_{\ Non\ G4\text{-}strand}$.

	***S. pombe* G4-strand**	
	5 mol. equiv.	
	Mean of SYBR Green FI	ΔFI
Control	2571.0 ± 6.1	/
1,5-BisNPO	2615.3 ± 7.5	44.3
2,6-BisNPO	2591.3 ± 17.0	20.3
2,7-BisNPN	2556.3 ± 13.9	-14.7
BRACO-19	2619.7 ± 6.1	48.7
TEGPy	2522.3 ± 16.5	-48.7

Table S7. Summary FI and ΔFI of the additional 5 small molecules assessed by qPCR Stop assay with the *S. pombe* G4 motif (G4-strand). Summary values of SYBR Green FI (or just FI) and ΔFI obtained in the additional qPCR Stop assay performed with the *S. pombe* G4-strand, without (*i.e.*, SYBR Green FI Control, ON only with the KCl) or with the presence of additional small molecule (1,5-BisNPO, 2,6-BisNPO, 2,7-BisNPN, BRACO-19, TEGPy) at the 5 mol. equiv. concentration.

Mean FI ± SD values calculated correspond to the FI value at the 33th (and last) qPCR cycle for three independent experiments. ΔFI= FI with small molecule – FI Control.

A	**Scoring rules for**	
G4-UNFOLD assay		
Ranking design: if the strongest G4-stabilizer inhibits totally the c-hTelo hybridization and then the release of the FAM-labelled 15-nt ON too, there will be no FI increase after the addition of c-hTelo and thus the V_0 calculated will be of 0.0 s^{-1}. Mean V_0 ± SD of the Control= 51.5 ± 12.2 s^{-1} (**Table 3**). $\Delta V_{0\ min}$= -51.5 s^{-1} ($V_{0\ min}$= 0.0 s^{-1}), then $\Delta V_{0\ max}$= 51.5 s^{-1} ($V_{0\ max}$= 103.0 s^{-1}).		
Data used: Raw ΔV_0 (in s^{-1}) with the s-hTelo and with small molecule at 5 mol. equiv.		
G4-destabilizing (G4D) score	G4-stabilizing (G4S) score	Score
-12.2 < ΔV_0 < 12.2		**-0.1 decrement**
0.0 < ΔV_0 < 10.3	-10.3 < ΔV_0 < 0.0	**0.2**
10.3 < ΔV_0 < 20.6	-20.6 < ΔV_0 < -10.3	**0.4**
20.6 < ΔV_0 < 30.9	-30.9 < ΔV_0 < -20.6	**0.6**
30.9 < ΔV_0 < 41.2	-41.2 < ΔV_0 < -30.9	**0.8**
41.2 < ΔV_0 < 51.5 (and more)	-51.5 < ΔV_0 < -41.2	**1.0**

B	**Scoring rules for**	
qPCR Stop assay		
Ranking design: if the strongest G4-stabilizer inhibits totally the *Taq* polymerase replication of the G4-strand, there will be no SYBR Green FI increase above the initial FI value (*i.e.*, the FI at the first qPCR cycle) and thus the FI will be of 2200.0. Mean FI ± SD of the Control= 2598.8 ± 23.5 (**Table S6**). ΔFI_{min}= -398.8 (FI_{min}= 2200.0), then ΔFI_{max}= +398.8 (FI_{max}= 2997.6).		
Data used: ΔFI with the *S. pombe* G4-strand ON and with small molecule at 5 mol. equiv.		
G4-destabilizing (G4D) score	G4-stabilizing (G4S) score	Score
-23.5 < ΔFI < 23.5		**-0.1 decrement**
0.0 < ΔFI < 79.8	-79.8 < ΔFI < 0.0	**0.2**
79.8 < ΔFI < 159.5	-159.5 < ΔFI < -79.8	**0.4**
159.5 < ΔFI < 239.3	-239.3 < ΔFI < -159.5	**0.6**
239.3 < ΔFI < 319.0	-319.0 < ΔFI < -239.3	**0.8**
319.0 < ΔFI < 398.8 (and more)	-398.8 < ΔFI < -319.0	**1.0**

C	**Scoring rules for**	
FRET-melting assay		
Ranking design: if the strongest G4-destabilizer opens (or denatures) totally the G4 ON at room temperature (*i.e.*, at 25 °C), there will be a total dequenching of the FAM which will reach its maximal FI at 25 °C (the minimum temperature in the FRET-melting program). The T_{max} but also the $T_{1/2}$ will be thus 25.0 °C. Mean $T_{1/2}$ ± SD of the Control= 50.6 ± 0.2 °C (**Table S2**). $\Delta T_{1/2\ min}$= -25.6 °C ($T_{1/2\ min}$= 25.0 °C), then $\Delta T_{1/2\ max}$= 25.6 °C ($T_{1/2\ max}$= 76.2 °C).		
Data used: $\Delta T_{1/2}$ (in °C) with the F21T ON and with small molecule at 5 mol. equiv.		
G4-destabilizing (G4D) score	G4-stabilizing (G4S) score	Score
-0.2 < $\Delta T_{1/2}$ < 0.2		**-0.1 decrement**
-5.1 < $\Delta T_{1/2}$ < 0.0	0.0 < $\Delta T_{1/2}$ < 5.1	**0.2**
-10.2 < $\Delta T_{1/2}$ < -5.1	5.1 < $\Delta T_{1/2}$ < 10.2	**0.4**
-15.4 < $\Delta T_{1/2}$ < -10.2	10.2 < $\Delta T_{1/2}$ < 15.4	**0.6**
-20.5 < $\Delta T_{1/2}$ < -15.4	15.4 < $\Delta T_{1/2}$ < 20.5	**0.8**
-25.6 < $\Delta T_{1/2}$ < -20.5	20.5 < $\Delta T_{1/2}$ < 25.6 (and more)	**1.0**

D	**Scoring rules for**	
CD titration		
Ranking design: if the strongest G4-destabilizer opens (or denatures) totally the G4 ON, the CD peak at 293 nm will totally decrease until 0 mdeg. Mean CD ± SD of the Control varies depending on small molecule titration (**Table S3**). CD variation$_{min}$= -100% (CD$_{min}$= 0.0 mdeg), then CD variation$_{max}$= 100% (CD$_{max}$= Mean CD of the Control *2 mdeg).		
Data used: CD variation (in %) with the hTelo ON and with small molecule at 5 mol. equiv.		
G4-destabilizing (G4D) score	G4-stabilizing (G4S) score	Score
-SD < CD variation < SD		**-0.1 decrement**
-20.0 < CD variation < 0.0	0.0 < CD variation < 20.0	**0.2**
-40.0 < CD variation < -20.0	20.0 < CD variation < 40.0	**0.4**
-60.0 < CD variation < -40.0	40.0 < CD variation < 60.0	**0.6**
-80.0 < CD variation < -60.0	60.0 < CD variation < 80.0	**0.8**
-100.0 < CD variation < -80.0	80.0 < CD variation < 100.0 (and more)	**1.0**

E	**Scoring rules for**	
PAGE analysis		
Ranking design: this scoring is more subjective than the others because it relies on numeral values, PAGE band physical aspect and two *scenarii*. A small molecule acting on the G4 band will disturb the Control PAGE band which can only decrease in FI. Mean SYBR Gold FI of the Control varies depending on small molecule (**Table S5**). FI variation$_{min}$= -100% (FI$_{min}$= 0.0), while FI variation$_{max}$ is impossible. The effect has to be attributed depending on the observed *scenario* below. ***Scenario* 1:** if a small molecule stabilizes the G4, the apparent molecular size of the G4 band can remain, decrease (appearance of a lower band) or even disappear in the case of an aggregation (the compound/G4 complex is too big to enter in the gel). This is the case for the Phen-DC$_3$ and the TMPyP4. ***Scenario* 2:** if a small molecule destabilizes the G4, the apparent molecular size of the G4 band will increase (appearance of an upper, or shifted, band). This is the case for the 1,5-BisNPO, 2,7-BisNPN, PhpC and TPPS.		
Data used: FI variation (in %) with the hTelo ON and with small molecule at 5 mol. equiv.		
G4-destabilizing (G4D) score **(if *scenario* 2)**	G4-stabilizing (G4S) score **(if *scenario* 1)**	Score
-20.0 < FI variation < 0.0		**0.2**
-40.0 < FI variation < -20.0		**0.4**
-60.0 < FI variation < -40.0		**0.6**
-80.0 < FI variation < -60.0		**0.8**
-100.0 < FI variation < -80.0		**1.0**

Table S8. Summary of scoring rules used to calculate scores for the *in vitro*-assessed small molecules. The study of several small molecules with different *in vitro* assays, here (**A**) the G4-UNFOLD assay, (**B**) qPCR Stop assay, (**C**) FRET-melting assay, (**D**) CD titration and (**E**) PAGE analysis, implies the linking of the results obtained for a better macro-level analysis. For this, different scoring rules were elaborated to assign a score to every small molecule for each assay. These scores will thus be incorporated to obtain a small molecule total score.

A

	G4-destabilizing (G4D) and G4-stabilizing (G4S) scores									
	G4-UNFOLD assay		**qPCR Stop assay**		**FRET-melting assay**		**CD titration**		**PAGE analysis**	
Small m.	G4D	G4S	G4D	G4S	G4D	G4S	G4D	G4S	G4D	G4S
TMPyP4	0.0	0.4	0.0	0.2	0.0	1.0	0.8	0.0	0.0	0.4
TEGPy	0.3	0.0	0.0	0.2	/	/	/	/	/	/
TPPS	0.8	0.0	0.1	0.0	0.2	0.0	0.4	0.0	0.2	0.0
TArPS	0.6	0.0	/	/	/	/	/	/	/	/
TEGP	0.6	0.0	/	/	/	/	/	/	/	/
Phen-DC_3	0.0	0.4	0.0	0.6	0.0	1.0	0.2	0.0	0.0	0.6
PDS	0.0	0.1	0.0	0.4	/	/	/	/	/	/
BRACO-19	0.6	0.0	0.2	0.0	/	/	/	/	/	/
Terpy	0.8	0.0	/	/	/	/	/	/	/	/
1,5-BisNPO	0.6	0.0	0.2	0.0	0.0	0.2	0.4	0.0	0.2	0.0
2,6-BisNPO	0.1	0.0	0.1	0.0	/	/	/	/	/	/
2,7-BisNPN	0.4	0.0	0.0	0.1	0.0	0.4	0.4	0.0	0.2	0.0
PhpC	1.0	0.0	0.2	0.0	0.2	0.0	0.2	0.0	0.2	0.0
guaPhpC	0.6	0.0	/	/	/	/	/	/	/	/

B

	G4-destabilizing (G4D) and G4-stabilizing (G4S) total scores								
	G4-UNFOLD + qPCR Stop assays			**Two last assays + FRET-melting assay**			**Five assays**		
Small m.	G4D	G4S	Merging	G4D	G4S	Merging	G4D	G4S	Merging
TMPyP4	0.0	0.6	0.0	0.0	1.6	0.0	0.8	2.0	0.8
TEGPy	0.3	0.2	0.2	/	/	/	/	/	/
TPPS	0.9	0.0	0.0	1.1	0.0	0.0	1.7	0.0	0.0
TArPS	/	/	/	/	/	/	/	/	/
TEGP	/	/	/	/	/	/	/	/	/
Phen-DC_3	0.0	1.0	0.0	0.0	2.0	0.0	0.2	2.6	0.2
PDS	0.0	0.5	0.0	/	/	/	/	/	/
BRACO-19	0.8	0.0	0.0	/	/	/	/	/	/
Terpy	/	/	/	/	/	/	/	/	/
1,5-BisNPO	0.8	0.0	0.0	0.8	0.2	0.2	1.4	0.2	0.2
2,6-BisNPO	0.2	0.0	0.0	/	/	/	/	/	/
2,7-BisNPN	0.4	0.1	0.1	0.4	0.5	0.4	1.0	0.5	0.5
PhpC	1.2	0.0	0.0	1.4	0.0	0.0	1.8	0.0	0.0
guaPhpC	/	/	/	/	/	/	/	/	/

Table S9. Summary of scores and total scores calculated for the compilation of the *in vitro*-assessed small molecules. Summary G4-destabilizing (G4D), G4-stabilizing (G4S) and merging scores values of the 14 small molecules panoply calculated in following the scoring rules established (**A**) for each *in vitro* assays (G4-UNFOLD assay, qPCR Stop assay, FRET-melting assay, CD titration, PAGE analysis) and (**B**) for several assays combination: G4-UNFOLD plus qPCR Stop assays (total $score_{max}$= 2.0; left), G4-UNFOLD, qPCR Stop plus FRET-melting assays (total $score_{max}$= 3.0; middle) and the five assays (total $score_{max}$= 5.0; right). For a small molecule, the merging score corresponds to the shared value between G4D and G4S scores. This parameter shows the contradictory effect of a small molecule. G4D= G4-destabilizing. G4S= G4-stabilizing. Small m.= small molecules.

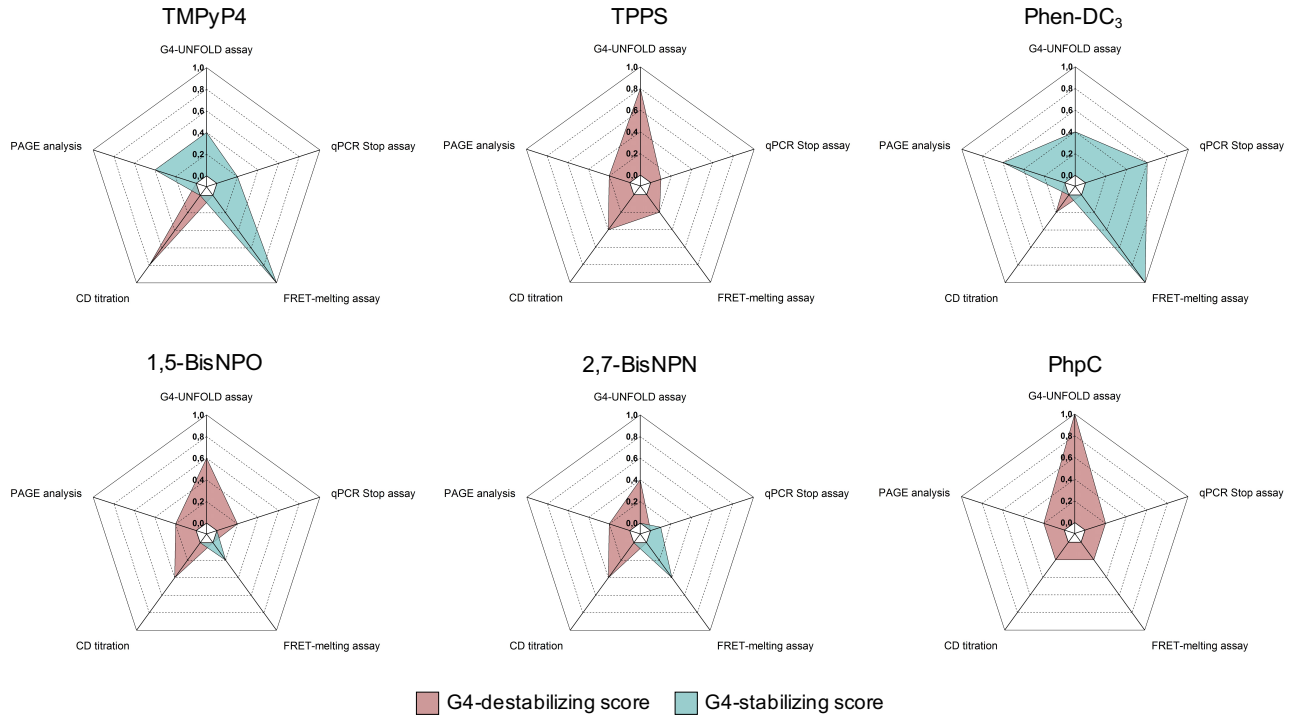

Figure S20. Additional radar chart representation of the effect-on-G4 scores calculated for the 6 small molecules panoply assessed by the five different *in vitro* assays. The 6 selected small molecules panoply was assessed at 5 mol. equiv. by the five *in vitro* assays. With the different scoring rules established (**Table S8**), G4-destabilizing (G4D, red box) and G4-stabilizing (G4S, blue box) scores were calculated and assigned to each small molecule in order to study and compare their effect on G4. Here each small molecule is represented separately with their scores by assays.

	Mean size classes of peaks (DLS, nm)			
	0 mol. equiv. (Control)	1 mol. equiv.	2 mol. equiv.	5 mol. equiv.
	% Intensity			
PhpC	3.6 / 396.1 / 5559.6 (n° 1)	3.6 / 164.2 / 5559.6	3.1 / 342.0 / 5559.6	3.1 / 164.2 / 5559.6
TMPyP4	3.1 / 220.2 / 5559.6 (n °2)	0.4 / 220.2	295.3	1281.3
	% Volume			
PhpC	2.7 (n° 1)	2.7	2.3	0.8 / 2.0
TMPyP4	2.7 (n °2)	0.7	396.1	825.0 / 1281.3

Table S10. Summary Volume and Intensity values assessed by Dynamic Light Scattering (DLS) investigation. Summary size values (nm) obtained in the DLS investigations performed without (0 mol. equiv., Control) or with the presence of the PhpC or TMPyP4 small molecules at 3 different concentrations of small molecules: 1, 2 and 5 mol. equiv. Results are shown according to the intensity (top) and volume (bottom) of particles. SD are not represented here.

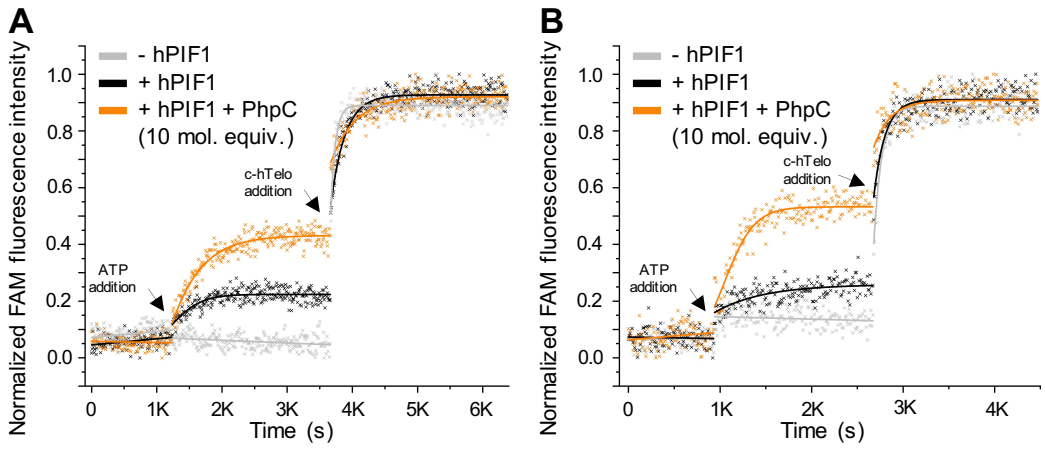

Figure S21. Additional results obtained with the small molecule PhpC assessed by hPIF1 helicase assay. The additional hPIF1 helicase assays were performed without hPIF1 (grey line) but also with hPIF1 without (black line) or with the presence of the PhpC (orange line) small molecule at 10 mol. equiv. concentration. hPIF1 was used at (**A**) 160 or (**B**) 170 nM.

	V_0 values at the ATP addition step					
	Exp. with PhpC or TMPyP4 [hPIF1]= 144 nM (**Figure 28-B**)		Additional exp. n° 1 [hPIF1]= 160 nM (**Figure S21-A**)		Additional exp. n° 2 [hPIF1]= 170 nM (**Figure S21-B**)	
	V_0 (s^{-1})	V_0 fold change	V_0 (s^{-1})	V_0 fold change	V_0 (s^{-1})	V_0 fold change
+ hPIF1 (no small molecule)	2.47	/	1.44	/	1.73	/
+ hPIF1 + PhpC 10 mol. equiv.)	5.97	2.42	3.21	2.23	2.66	1.54
+ hPIF1 + TMPyP4 10 mol. equiv.)	1.49	0.60	/	/	/	/

Table S11. Summary speed (v_0) values assessed by hPIF1 helicase assay. Summary V_0 values (s^{-1}) obtained in the hPIF1 helicase assay performed with the s-hTelo with hPIF1 without or with the presence of the PhpC and TMPyP4 small molecules at 10 mol. equiv. concentration. hPIF1 was used at 144, 160 and 170 nM. V_0 values calculated correspond to the slope from the linear fit applied on the five first points after the ATP addition.

A	**Fluorescence intensity (at 452 nm) titrations**							
	0 mol. equiv.		1 mol. equiv.		2 mol. equiv.		5 mol. equiv.	
	Mean FI	Var. (%)	Mean FI	Var. (%)	Mean FI	Var. (%)	Mean FI	Var. (%)
PhpC + GMP (in 1–100 mM K^+)	229.7 ± 1.5	/	225.7 ± 3.2	-1.7	222.0 ± 6.2	-3.4	213.7 ± 8.5	-7.0
PhpC + hTelo (in 1 mM K^+)	228.5 ± 0.7	/	196.5 ± 7.8	-14.0	178.5 ± 9.2	-21.9	145.5 ± 13.4	-36.3
PhpC + hTelo (in 10 mM K^+)	229.0 ± 0.0	/	208.5 ± 2.1	-9.0	190.5 ± 3.5	-16.8	159.0 ± 1.4	-30.6
PhpC + hTelo (in 100 mM K^+)	229.5 ± 0.7	/	214.0 ± 0.0	-6.8	196.5 ± 2.1	-14.4	171.5 ± 6.4	-25.3

B	**Relationship between FI quench and G4 stability**	
	FI quench (= Var. at 5 mol. equiv., %)	G4 stability by FRET-melting with hTelo alone ($\Delta T_{1/2}$, °C)
PhpC + hTelo (in 1 mM K^+)	-36.3	44.3 ± 0.7
PhpC + hTelo (in 10 mM K^+)	-30.6	50.3 ± 0.2
PhpC + hTelo (in 100 mM K^+)	-25.3	61.7 ± 0.1

Table S12. Summary values of the small molecule PhpC assessed by Fluorescence titrations. Summary (**A**) fluorescence intensity at 452 nm and (**B**) fluorescence quench at 5 mol. equiv. (plus $\Delta T_{1/2}$ of hTelo) values obtained in the fluorescence titrations (and FRET-melting assay) performed with PhpC and without or with the presence of the GMP or hTelo at 3 different concentrations of K^+: 1, 10 and 100 mM. For the FI quench, FI titration values at 5 mol. equiv. were used as well as $T_{1/2}$ values obtained with the hTelo alone in FRET-melting assay.

A	***H. sapiens* G4 ON**					
	G4 hTelo qSa		**G4 *c-MYC* qSa**		**G4 *c-KIT2* qSa**	
	Mean of SYBR Green FI	ΔFI	Mean of SYBR Green FI	ΔFI	Mean of SYBR Green FI	ΔFI
Control	2961.0 ± 31.5	/	2441.8 ± 14.5	/	2916.5 ± 45.2	/
PhpC (5 mol. equiv.)	3062.0 ± 62.5	101.0	2496.8 ± 8.7	55.0	3023.5 ± 32.5	107.0
PhpC (10 mol. equiv.)	3013.8 ± 96.7	52.8	2448.0 ± 18.1	6.3	3026.8 ± 63.6	110.3
PDS (5 mol. equiv.)	2897.8 ± 47.8	-63.3	2474.3 ± 18.5	32.5	2778.3 ± 47.6	-138.3
PDS (10 mol. equiv.)	2715.0 ± 54.2	-246.0	2511.8 ± 22.6	70.0	2576.8 ± 20.0	-339.8

B	***H. sapiens* Sc ON**					
	Sc hTelo qSa		**Sc *c-MYC* qSa**		**Sc *c-KIT2* qSa**	
	Mean of SYBR Green FI	ΔFI	Mean of SYBR Green FI	ΔFI	Mean of SYBR Green FI	ΔFI
Control	3117.3 ± 60.6	/	2978.8 ± 22.2	/	3096.8 ± 28.3	/
PhpC (5 mol. equiv.)	3129.3 ± 55.9	12.0	3099.8 ± 9.0	121.0	3145.5 ± 89.9	48.8
PhpC (10 mol. equiv.)	3059.8 ± 52.4	-57.5	3103.5 ± 40.3	124.8	3169.3 ± 40.0	72.5
PDS (5 mol. equiv.)	3127.3 ± 59.5	10.0	3057.3 ± 37.1	78.5	3150.5 ± 80.6	53.8
PDS (10 mol. equiv.)	3180.8 ± 35.4	63.5	3083.8 ± 45.0	105.0	3158.0 ± 48.5	61.3

Table S13. Summary values of the small molecules assessed by qPCR Stop assay with the three *H. sapiens* G4 motifs (G4 ON) and the scrambled version (Sc ON). Summary values of SYBR Green FI (or just FI) and ΔFI obtained in the qPCR Stop assays performed with the *H. sapiens* (**A**) G4 ON (hTelo qSa, *c-MYC* qSa, *c-KIT2* qSa) or (**B**) scrambled (Sc) ONS (Sc hTelo qSa, Sc *c-MYC* qSa, Sc *c-KIT2* qSa) without (*i.e.*, SYBR Green FI Control, ON only with the KCl) or with the presence of the PhpC and PDS small molecule at 2 different concentrations of small molecules: 5 and 10 mol. equiv. Mean FI ± SD values calculated correspond to the FI value at the 33th (and last) qPCR cycle for one experiment. ΔFI= FI with small molecule – FI Control.

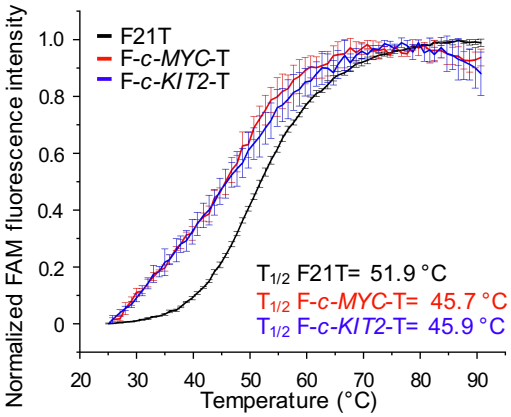

Figure S22. Experimental curves obtained with the three F21T, F-*c-MYC*-T and F-*c-KIT2*-T ONs assessed by FRET-melting assay. The FRET-melting assay was performed with the F21T (black line), F-*c-MYC*-T (red) and F-*c-KIT2*-T (blue) doubly labeled ONs with the FAM/TAMRA fluorophores couple. Mean $T_{1/2}$ (or T_m, in °C) values calculated correspond to the melting temperature of the ONs. Error bars represent SD from the mean for one experiment. The assay was kindly performed by Francesco Rota Sperti.

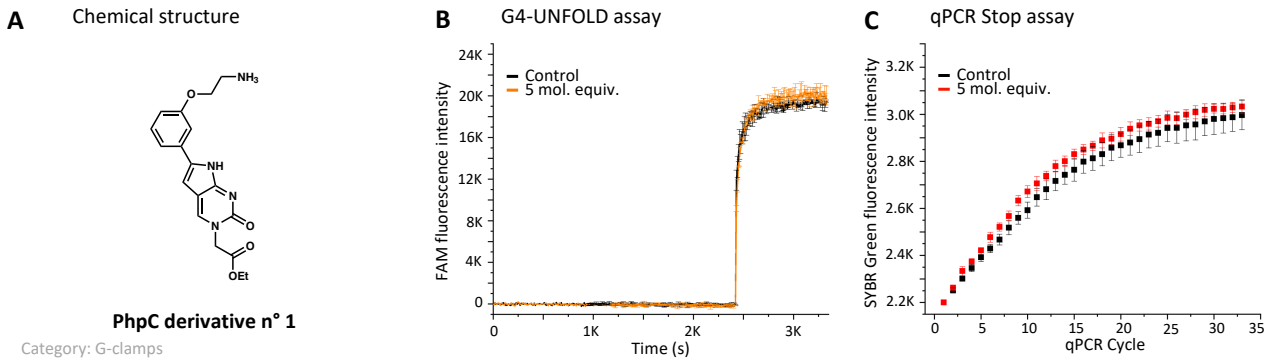

Figure S23. Summary card of PhpC derivative n° 1 results. The (**A**) PhpC derivative n° 1 small molecule effect on G4 was assessed by (**B**) G4-UNFOLD assay and (**C**) qPCR Stop assay at 5 mol. equiv. concentration (orange and red, respectively). Controls are in black.

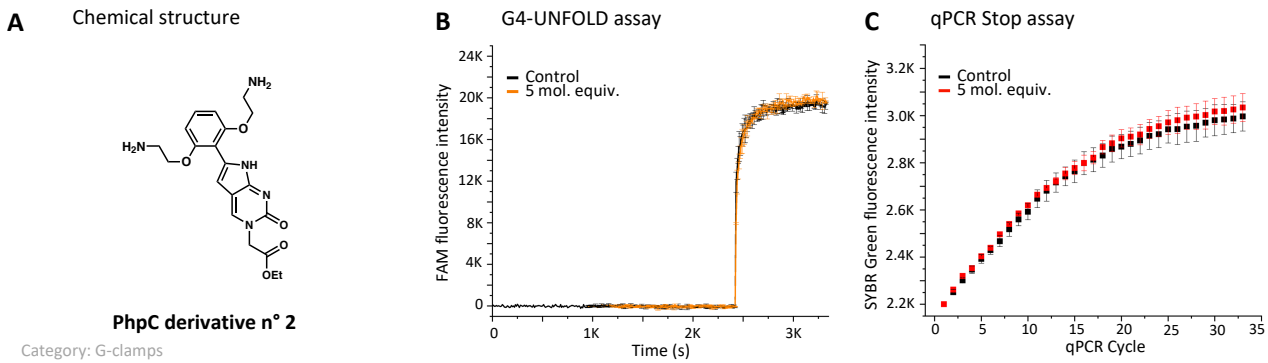

Figure S24. Summary card of PhpC derivative n° 2 results. The (**A**) PhpC derivative n° 2 small molecule effect on G4 was assessed by (**B**) G4-UNFOLD assay and (**C**) qPCR Stop assay at 5 mol. equiv. concentration (orange and red, respectively). Controls are in black.

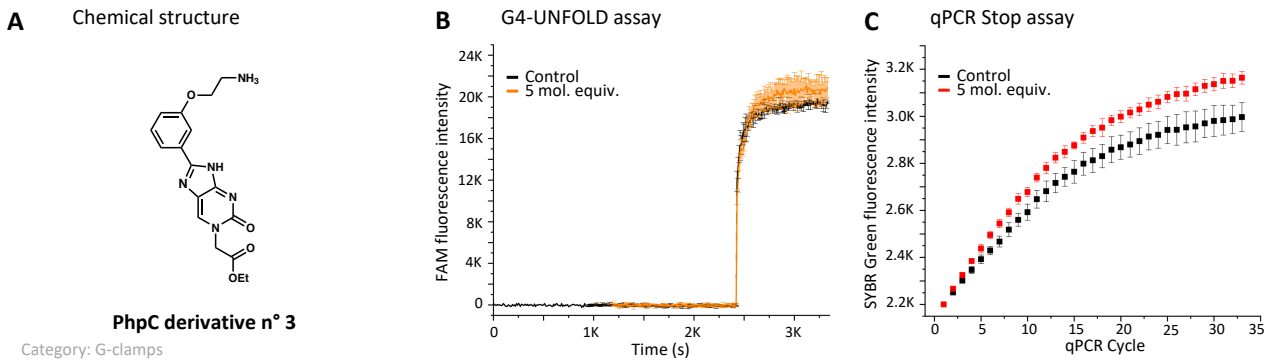

Figure S25. Summary card of PhpC derivative n° 3 results. The (**A**) PhpC derivative n° 3 small molecule effect on G4 was assessed by (**B**) G4-UNFOLD assay and (**C**) qPCR Stop assay at 5 mol. equiv. concentration (orange and red, respectively). Controls are in black.

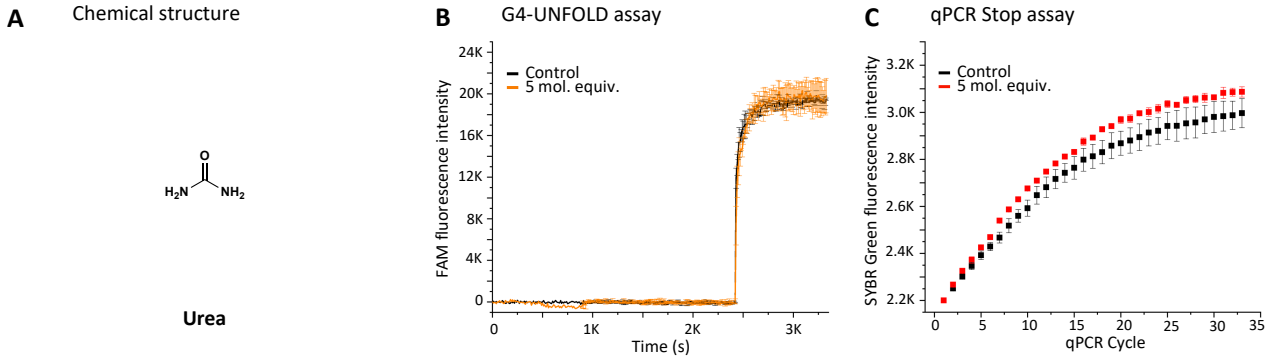

Figure S26. Summary card of urea results. The (**A**) urea denaturing agent effect on G4 was assessed by (**B**) G4-UNFOLD assay and (**C**) qPCR Stop assay at 5 mol. equiv. concentration (orange and red, respectively). Controls are in black.

	G4-UNFOLD (with hTelo)		**qPCR Stop assay** (with hTelo qSa)	
Small molecules	Mean of Raw V_0 (s^{-1})	ΔV_0 (s^{-1})	Mean of SYBR Green FI	ΔFI
Control	96.3 ± 6.0	/	2989.3 ± 33.3	/
PhpC	136.4 ± 25.3	40.1	3090.6 ± 35.2	101.3
PhpC derivative n° 1	127.5 ± 24.5	31.2	3058.7 ± 22.9	69.3
PhpC derivative n° 2	133.3 ± 19.4	37.0	3080.7 ± 54.2	91.4
PhpC derivative n° 3	119.9 ± 15.4	23.5	3155.1 ± 20.3	165.8
Urea	150.9 ± 28.4	54.5	3086.5 ± 39.6	97.1
PDS	64.2 ± 19.5	-32.1	2974.1 ± 26.7	-15.3

Table S14. Summary values of the PhpC derivatives assessed by G4-UNFOLD and qPCR Stop assay with the *H. sapiens* G4 hTelo. (Left) Summary values of V_0 and ΔV_0 (s^{-1}) obtained in the G4-UNFOLD assay performed with the s-hTelo ON and without (*i.e.*, V_0 Control, ON only with the Tris-HCl buffer 2: 20 mM Tris-HCl, 10 mM $MgCl_2$, 1 mM KCl, 99 mM NaCl, pH 7.2) or with the presence of small molecules (with the same Tris-HCl buffer 2) at 5 mol. equiv. concentration. Mean V_0 values calculated correspond to the slope from the linear fit applied on the five first points after the c-hTelo addition. SD is from the mean for at least four independent experiments. ΔV_0= V_0 with small molecule – V_0 Control. (Right) Summary SYBR Green FI (or just FI) and ΔFI obtained in the qPCR Stop assay performed with the *H. sapiens* hTelo qSa without (*i.e.*, SYBR Green FI Control, ON only with the KCl) or with the presence of small molecules at 5 mol. equiv. concentration. Mean FI values calculated correspond to the FI value at the 33th (and last) qPCR cycle. SD is from the

mean for three independent experiments. ΔFI= FI with small molecule – FI Control. (All) The small molecules used here are PhpC, PhpC derivative n° 1, n° 2, n° 3, urea and PDS.

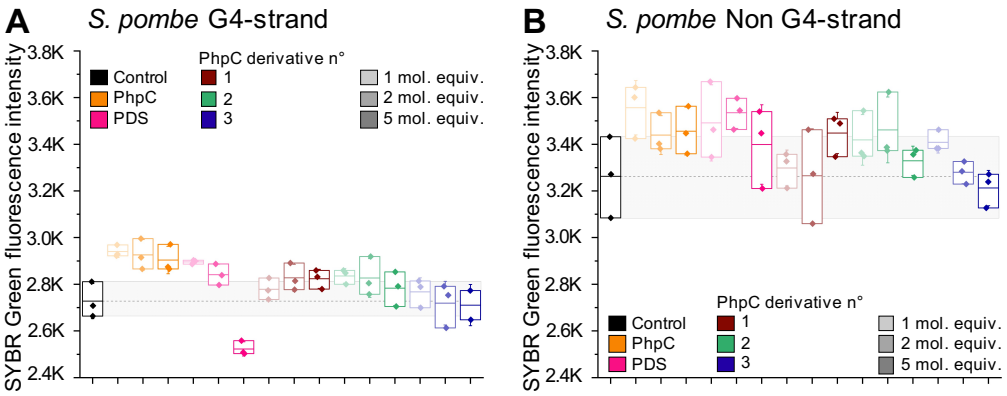

Figure S27. Results obtained with the PhpC derivatives assessed by qPCR Stop assay with *S. pombe* G4-strand ON from the original assay. The qPCR Stop assay was performed with the *S. pombe* (**A**) G4-strand or (**B**) Non G4-strand, without (*i.e.*, SYBR Green FI Control, ON only with the KCl) or with the presence of the PhpC (orange), PDS (pink), PhpC derivative n° 1 (burgundy), n° 2 (green) and n° 3 (blue) small molecules at 3 different concentrations: 1, 2 and 5 mol. equiv. (from light to dark hue). Mean FI values calculated correspond to the FI value at the 33th (and last) qPCR cycle. Error bars represent SD from the mean for one experiment.

A	***S. pombe* G4-strand**					
	1 mol. equiv.		**2 mol. equiv.**		**5 mol. equiv.**	
	Mean of SYBR Green FI	ΔFI	Mean of SYBR Green FI	ΔFI	Mean of SYBR Green FI	ΔFI
Control	2727.7 ± 75.4	/	/	/	/	/
PhpC	2940.0 ± 25.4	212.3	2925.7 ± 65.7	198.0	2903.7 ± 58.4	176
PDS	2896.0 ± 8.9	168.3	2841.0 ± 45.0	113.3	2523.0 ± 30.4	-204.7
PhpC der. n °1	2778.7 ± 46.2	51.0	2827.3 ± 58.2	99.7	2823.3 ± 40.7	95.7
PhpC der. n °2	2835.7 ± 31.4	108.0	2827.0 ± 83.2	99.3	2783.0 ± 74.3	55.3
PhpC der. n °3	2767.3 ± 60.5	39.7	2719.0 ± 93.7	-8.7	2710.5 ± 88.4	-17.2

B	***S. pombe* Non G4-strand**					
	1 mol. equiv.		**2 mol. equiv.**		**5 mol. equiv.**	
	Mean of SYBR Green FI	ΔFI	Mean of SYBR Green FI	ΔFI	Mean of SYBR Green FI	ΔFI
Control	3262.3 ± 174.2	/	/	/	/	/
PhpC	3556.3 ± 116.6	294.0	3439.3 ± 83.5	177.0	3456.3 ± 102.3	194.0
PDS	3491.7 ± 163.5	229.3	3535.0 ± 67.6	272.7	3399.0 ± 170.2	136.7
PhpC der. n °1	3298.7 ± 76.5	36.3	3265.0 ± 201.1	2.7	3448.3 ± 88.3	186.0
PhpC der. n °2	3418.7 ± 108.8	156.3	3461.3 ± 141.0	199.0	3329.3 ± 62.4	67.0
PhpC der. n °3	3408.7 ± 46.2	146.3	3279.7 ± 48.6	17.3	3212.3 ± 75.6	-50.0

Table S15. Summary values of the PhpC derivatives assessed by qPCR Stop assay with the *S. pombe* G4 motif (G4-strand) and the G4-complementary C-rich motif (Non G4-strand). Summary values of SYBR Green FI (or just FI) and ΔFI obtained in the qPCR Stop assays performed with the *S. pombe* (**A**) G4-strand or (**B**) Non G4-strand without (*i.e.*, SYBR Green FI Control, ON only with the KCl) or with the presence of the small molecules at 3 different concentrations: 1, 2 and 5 mol. equiv. Mean FI ± SD values calculated correspond to the FI value at the 33th (and last) qPCR cycle for one experiment. ΔFI= FI with small molecule – FI Control. The small molecules used here are PhpC, PDS, PhpC derivative n° 1, n° 2 and n° 3.

Scoring rules for				
G4-UNFOLD assay		**qPCR Stop assay**		
G4D score	G4S score	G4D score	G4S score	Score
$-6.0 < \Delta V_0 < 6.0$		$-33.3 < \Delta FI < 33.3$		**-0.1 decrement**
$0.0 < \Delta V_0 < 19.3$	$-19.3 < \Delta V_0 < 0.0$	$0.0 < \Delta FI < 157.9$	$-157.9 < \Delta FI < 0.0$	**0.2**
$19.3 < \Delta V_0 < 38.5$	$-38.5 < \Delta V_0 < -19.3$	$157.9 < \Delta FI < 315.7$	$-315.7 < \Delta FI < -157.9$	**0.4**
$38.5 < \Delta V_0 < 57.8$	$-57.8 < \Delta V_0 < -38.5$	$315.7 < \Delta FI < 473.6$	$-473.6 < \Delta FI < -315.7$	**0.6**
$57.8 < \Delta V_0 < 77.0$	$-77.0 < \Delta V_0 < -57.8$	$473.6 < \Delta FI < 631.4$	$-631.4 < \Delta FI < -473.6$	**0.8**
$77.0 < \Delta V_0 < 96.3$ (+)	$-96.3 < \Delta V_0 < -77.0$	$631.4 < \Delta FI < 789.3$ (+)	$-789.3 < \Delta FI < -631.4$	**1.0**

Table S16. Summary of the adapted scoring rules used to calculate scores for the PhpC derivatives assessed by G4-UNFOLD assay and qPCR Stop assay with the *H. sapiens* hTelo qSA. Summary of the adapted scoring rules used for results obtained in the G4-UNFOLD assay and qPCR Stop assay with the *H. sapiens* hTelo qSa performed without or with the presence of the PhpC, PhpC derivative n° 1, n° 2, n°3, urea and PDS small molecules at 5 mol. equiv. These scores will thus be incorporated to obtain a small molecule total score. G4D= G4-destabilizing. G4S= G4-stabilizing.

	G4-destabilizing (G4D) and G4-stabilizing (G4S) scores						
	G4-UNFOLD assay		**qPCR Stop assay**		**Two assays**		
Small molecules	G4D	G4S	G4D	G4S	G4D	G4S	Merging
PhpC	0.6	0.0	0.2	0.0	0.8	0.0	0.0
PhpC drv. n° 1	0.4	0.0	0.2	0.0	0.6	0.0	0.0
PhpC drv. n° 2	0.4	0.0	0.2	0.0	0.6	0.0	0.0
PhpC drv. n° 3	0.4	0.0	0.4	0.0	0.8	0.0	0.0
Urea	0.6	0.0	0.2	0.0	0.8	0.0	0.0
PDS	0.0	0.4	0.0	0.1	0.0	0.5	0.0

Table S17. Summary of scores and total scores calculated for the compilation of the PhpC derivatives assessed by G4-UNFOLD assay and qPCR Stop assay with the *H. sapiens* hTelo qSA. Summary G4-destabilizing (G4D), G4-stabilizing (G4S) and merging scores values of the PhpC, PhpC derivative n° 1, n° 2, n°3, urea and PDS small molecules calculated in following the adapted scoring rules established (**Table S16**) for each *in vitro* assays (G4-UNFOLD assay, qPCR Stop assay with the *H. sapiens* hTelo qSa) and for the combination of the two assays (total $score_{max}$= 2.0). For a small molecule, the merging score corresponds to the shared value between G4D and G4S scores. This parameter shows the contradictory effect of a small molecule. Drv.= derivative. G4D= G4-destabilizing. G4S= G4-stabilizing.

II. Related to the Chapter II

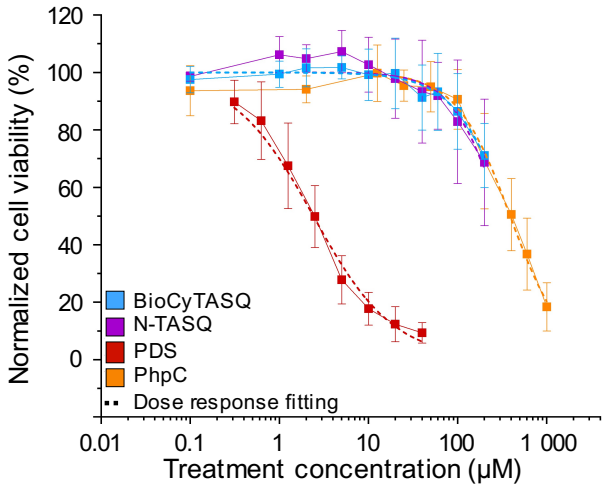

Figure S28. Cytotoxicity profile of BioCyTASQ, N-TASQ, PDS and PhpC. Sulforhodamine B (SRB) cytotoxicity assay was performed on MCF7 cells with the two G4 probes BioCyTASQ (blue square) and N-TASQ (purple) and the two G4 ligands PDS (red) and PhpC (orange). The dose response fitting curves are dashed. Error bars represent SD from the mean for three independent experiments. The PDS assessment was kindly performed by Angélique Pipier.

	Concentration (µM)									
BioCyTASQ	0.1	1	2	5	10	20	40	60	100	200
N-TASQ	0.1	1	2	5	10	20	40	60	100	200
PDS	0.3125	0.625	1.25	2.5	5	10	20	40	/	/
PhpC	0.1	2	12.5	25	50	100	200	400	600	1000

Table S18. Summary concentration range of G4 probes and ligands assessed by the SRB cytotoxicity assay. SRB cytotoxicity assay was performed on MCF7 cells with the G4 probes BioCyTASQ and N-TASQ and the G4 ligands PDS and PhpC. The concentration range used for this assay was established after a first SRB test using a wide concentration range. The PDS assessment was kindly performed by Angélique Pipier.

	Inhibitory concentrations (µM)		
	IC_{20}	IC_{50}	IC_{80}
BioCyTASQ	138.1 ± 15.3	386.3 ± 89.7	1080.2 ± 485.2
N-TASQ	127.4 ± 43.1	308.5 ± 192.2	746.9 ± 837.5
PDS	0.57 ± 0.11	2.40 ± 0.26	10.15 ± 1.11
PhpC	148.7 ± 26.7	387.9 ± 41.4	1012.0 ± 156.3

Table S19. Summary of the IC values obtained by the SRB cytotoxicity assay performed on G4 probes and ligands. SRB cytotoxicity assay was performed on MCF7 cells with the G4 probes BioCyTASQ and N-TASQ and the G4 ligands PDS and PhpC and the inhibitory concentrations x (IC_x) (x= 20, 50, 80) values, representing the ligand concentrations which allowed the inhibition of the cell viability of x%, were calculated. The PDS assessment was performed by Angélique Pipier.

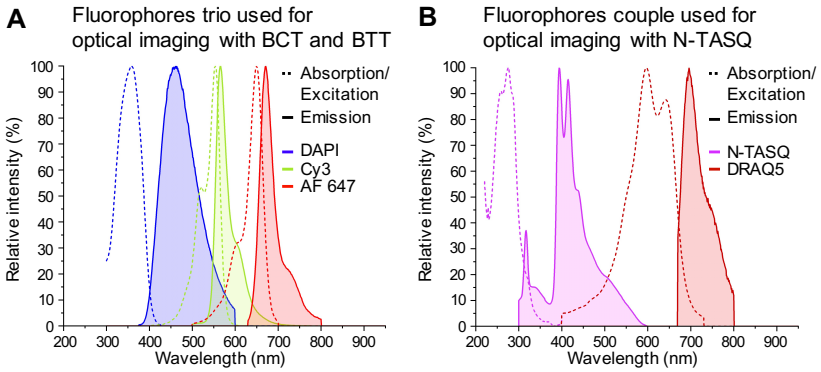

Figure S29. Spectra of the two different fluorophores combinations used for optical imaging. (**A**) The DAPI/Cy3/Alexa Fluor 647 fluorophores trio was used for optical imaging of G4s with the biotinylated TASQs (BioCyTASQ and BioTriazoTASQ). (**B**) The N-TASQ/DRAQ5 fluorophores couple was used for optical imaging of G4s with the smart N-TASQ. DAPI: 4',6-diamidino-2-phenylindole. Cy3: Cyanine 3. AF 647: Alexa Fluor 647. N-TASQ: Naphtho-TASQ. DRAQ5: 1,5-bis{[2-(di-methylamino)ethyl]amino}-4,8-dihydroxy-9,10-anthraquinone. The fluorophores data set were taken on ThermoFisher's SpectraViewer tool except for the G4 probe N-TASQ which was measured by Francesco Rota Sperti. AF = Alexa Fluor. BCT = BioCyTASQ. BTT = BioTriazoTASQ.

	Summary of maximum wavelengths of	
Fluorophore name	Absorption/Excitation ($\lambda_{exc\ max}$, nm)	Emission ($\lambda_{em\ max}$, nm)
N-TASQ	275	395
DAPI	358	460
Cy3	553	566
Alexa Fluor 647	647	672
DRAQ5	597	695

Table S20. Summary of maximum spectra wavelengths of the five fluorophores used for optical imaging. Summary of maximum absorption/excitation (($\lambda_{exc\ max}$) and emission (($\lambda_{em\ max}$) wavelengths for the five fluorophores used for optical imaging: N-TASQ, DAPI, Cy3, Alexa Fluor 647 and DRAQ5, ranked in the increasing order of their spectra wavelengths.

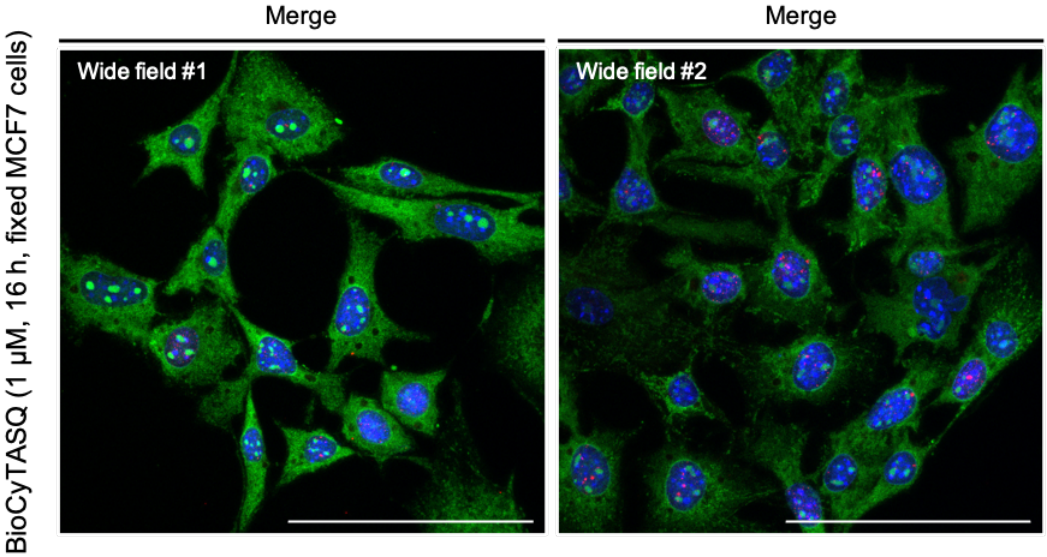

Figure S30. High-resolution wide optical images acquired with the G4 probe BioCyTASQ. The optical imaging was performed with MCF7 cells treated after cell fixation with BioCyTASQ (1 µM, 16 h), tagged with SA-Cy3 (green), which is followed by immunodetection of DNA damage nuclear γH2AX *foci* (with IgG-Alexa Fluor 647, red) and chromatin

staining by DAPI (blue). Two wide fields are shown here. 63x oil objective and then digital magnification (scale bar = 100 µm).

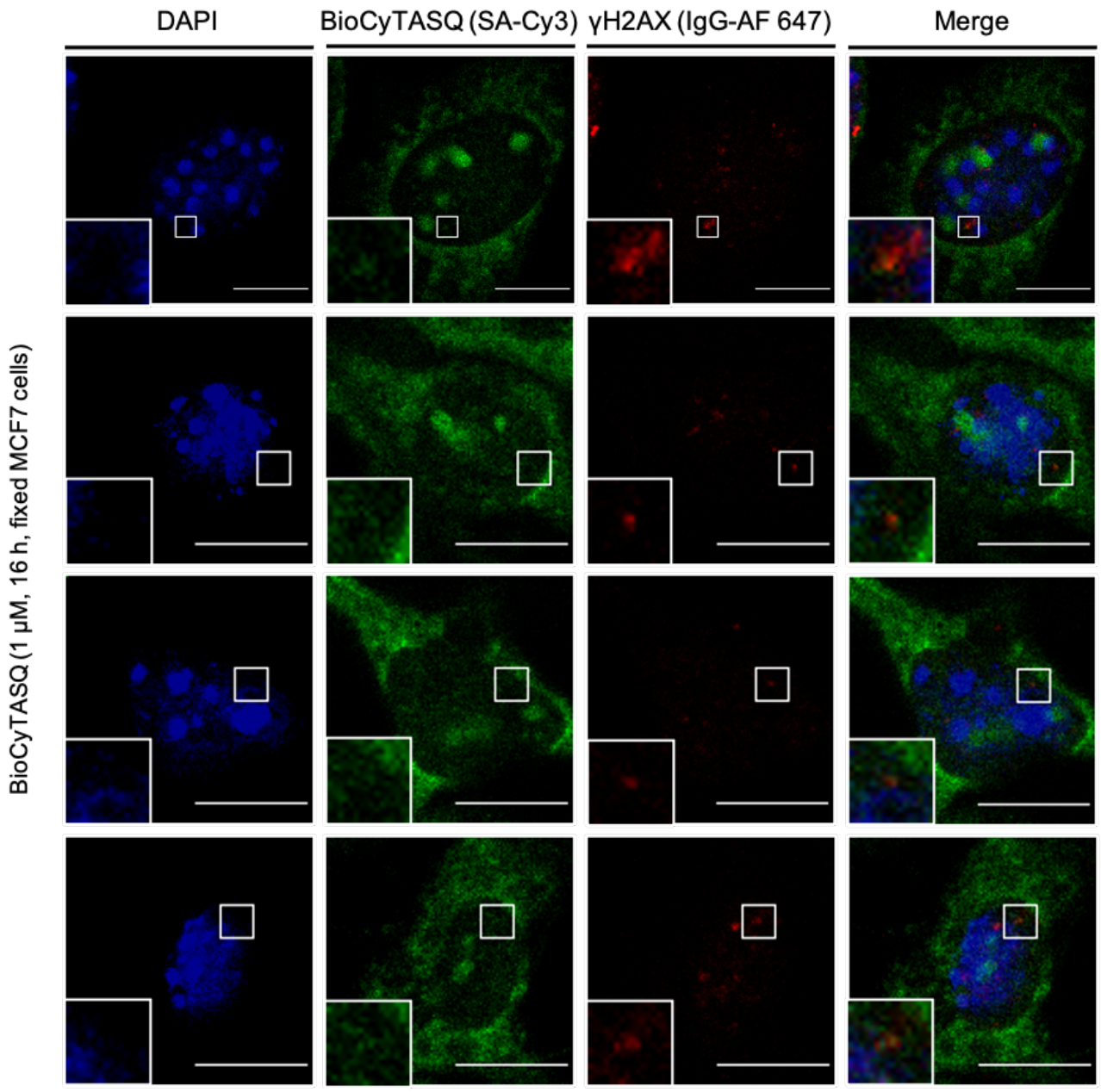

Figure S31. Additional high-resolution optical images acquired with the G4 probe BioCyTASQ (Part 1/2). The optical imaging was performed with MCF7 cells treated after cell fixation with BioCyTASQ (1 µM, 16 h), tagged with SA-Cy3 (green), which is followed by immunodetection of DNA damage nuclear γH2AX *foci* (with IgG-Alexa Fluor 647, red) and chromatin staining by DAPI (blue). Images are representative of the mean number of γH2AX *foci* per nucleus. Insets highlight nucleoplasmic sites where both nuclear TASQ and γH2AX *foci* co-localize. 63x oil objective, then digital magnification plus 3.9x magnification for insets (scale bar = 10 µm).

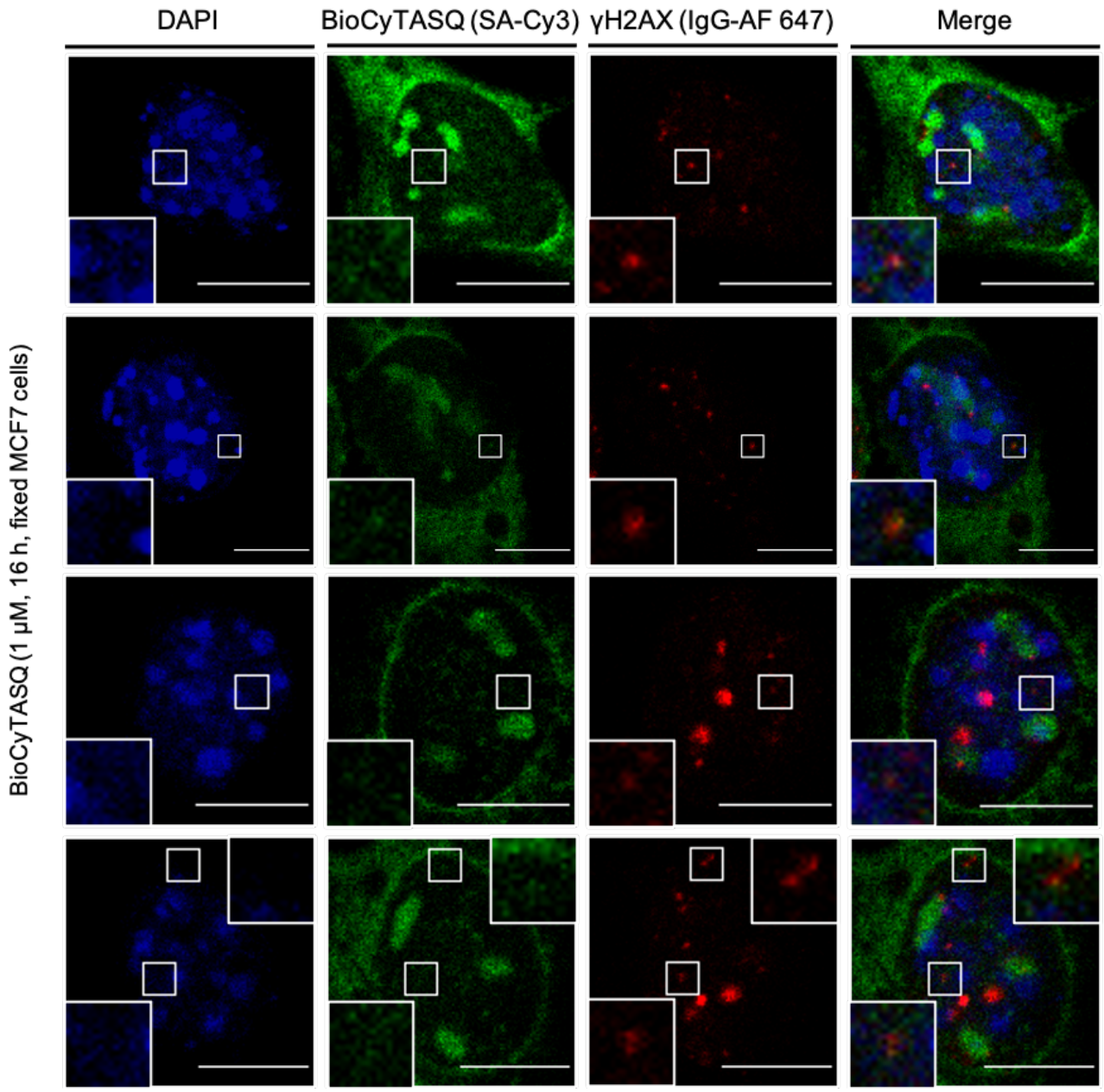

Figure S32. Additional high-resolution optical images acquired with the G4 probe BioCyTASQ (Part 2/2). The optical imaging was performed with MCF7 cells treated after cell fixation with BioCyTASQ (1 µM, 16 h), tagged with SA-Cy3 (green), which is followed by immunodetection of DNA damage nuclear γH2AX *foci* (with IgG-Alexa Fluor 647, red) and chromatin staining by DAPI (blue). Images are representative of the mean number of γH2AX *foci* per nucleus. Insets highlight nucleoplasmic sites where both nuclear TASQ and γH2AX *foci* co-localize. 63x oil objective, then digital magnification plus 3.9x magnification for insets (scale bar = 10 µm).

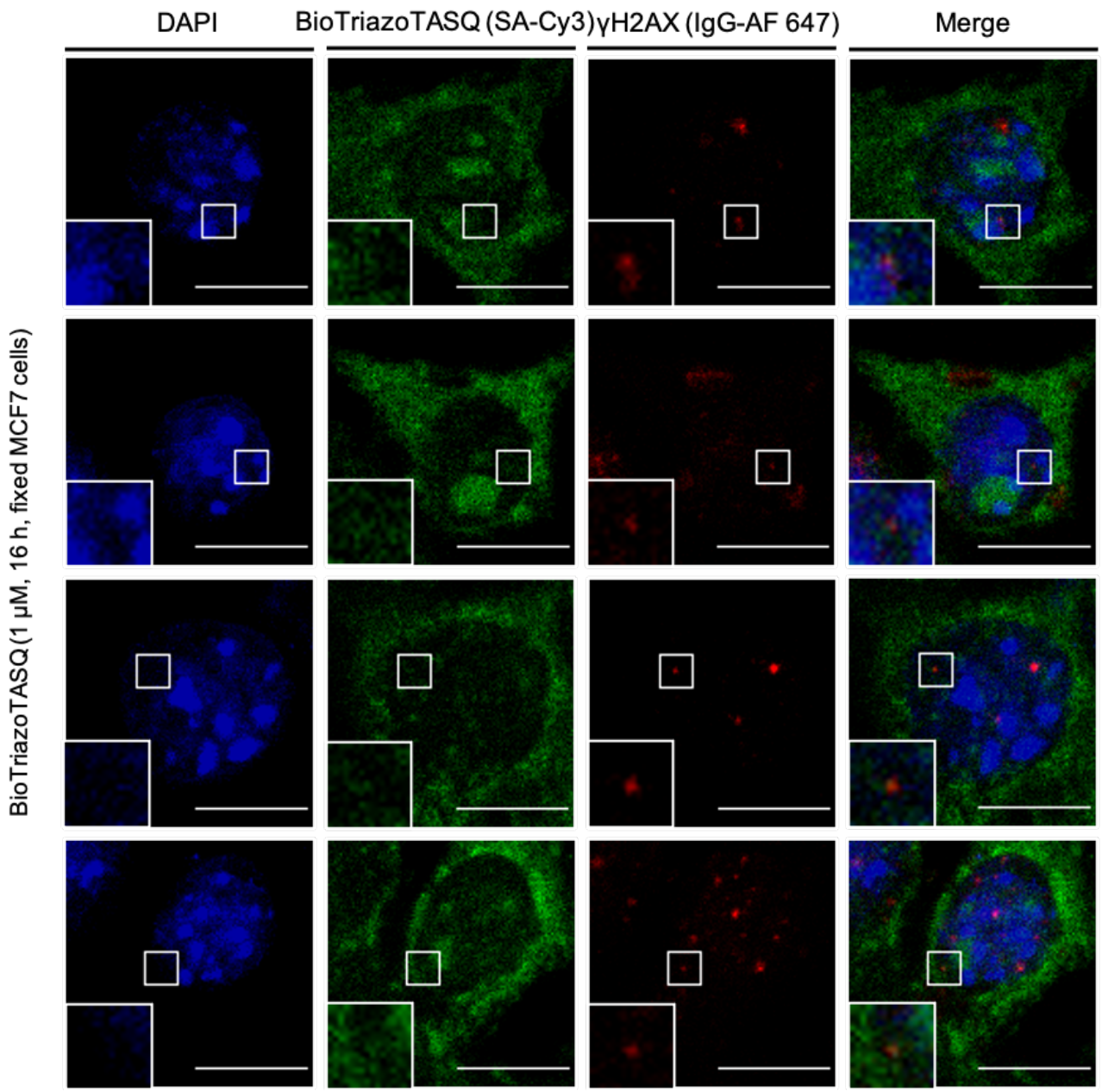

Figure S33. Additional high-resolution optical images acquired with the G4 probe BioTriazoTASQ (Part 1/2). The optical imaging was performed with MCF7 cells treated after cell fixation with BioTriazoTASQ (1 µM, 16 h), tagged with SA-Cy3 (green), which is followed by immunodetection of DNA damage nuclear γH2AX *foci* (with IgG-Alexa Fluor 647, red) and chromatin staining by DAPI (blue). Images are representative of the mean number of γH2AX *foci* per nucleus. Insets highlight nucleoplasmic sites where both nuclear TASQ and γH2AX *foci* co-localize. 63x oil objective, then digital magnification plus 3.9x magnification for insets (scale bar = 10 µm).

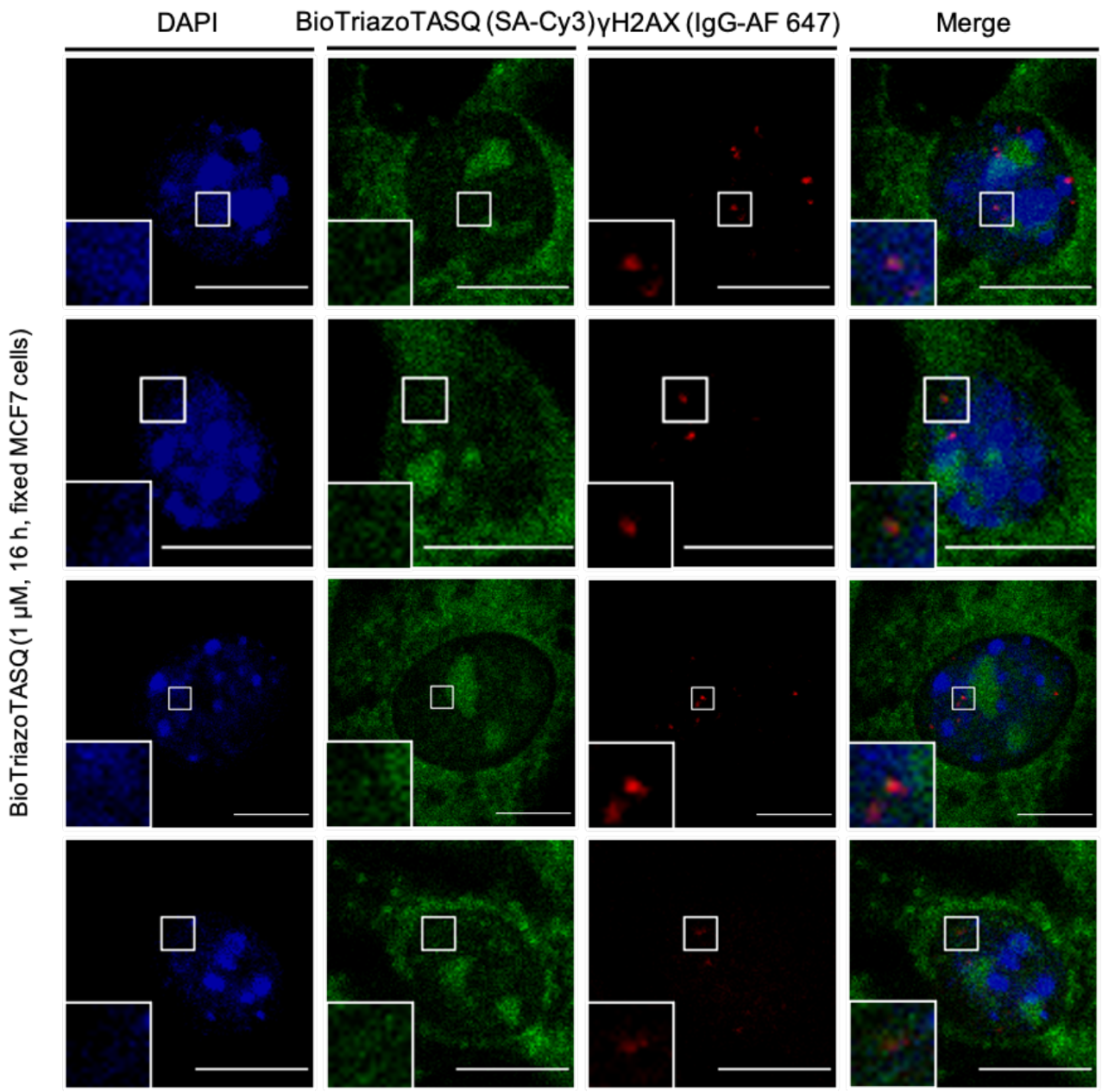

Figure S34. Additional high-resolution optical images acquired with the G4 probe BioTriazoTASQ (Part 2/2). The optical imaging was performed with MCF7 cells treated after cell fixation with BioTriazoTASQ (1 µM, 16 h), tagged with SA-Cy3 (green), which is followed by immunodetection of DNA damage nuclear γH2AX *foci* (with IgG-Alexa Fluor 647, red) and chromatin staining by DAPI (blue). Images are representative of the mean number of γH2AX *foci* per nucleus. Insets highlight nucleoplasmic sites where both nuclear TASQ and γH2AX *foci* co-localize. 63x oil objective, then digital magnification plus 3.9x magnification for insets (scale bar = 10 µm).

	Control	BioCyTASQ (1 µM, 24 h)	BioTriazoTASQ (1 µM, 24 h)
General parameters			
Number of images analysed	8	8	8
Nucleus data			
Total number of nuclei analysed	172.0	232.0	183.0
Nuclear TASQ *foci* data			
Total number of TASQ *foci* collected	5750.7	6889.3	8870.7
Mean number of TASQ *foci* per nucleus	20.6	27.8	32.9
Nuclear γH2AX *foci* data			
Mean number of γH2AX *foci* per nucleus	4.08	4.92	5.69
Nuclear TASQ and γH2AX *foci* comparative data			
Mean ratio of co-localized *foci*/all γH2AX *foci* per nucleus	/	2.7 %	2.9 %

Table S21. Intermediate summary values obtained from the high-resolution optical images sample acquired with the G4 probes BioCyTASQ and BioTriazoTASQ and used for the manual co-localization counting. Intermediate summary values obtained *via* the optical imaging performed with MCF7 cells non-treated (Control) or treated after cell fixation with BioCyTASQ or BioTriazoTASQ (1 µM, 16 h), tagged with SA-Cy3, which is followed by immunodetection of DNA damage nuclear γH2AX *foci* (with IgG-Alexa Fluor 647) and chromatin staining by DAPI. The values quantified are the number of nuclei, nuclear TASQ *foci* and nuclear γH2AX *foci* obtained by the optical images sample process with the co-localization macro program. The ratio of co-localized γH2AX/all γH2AX *foci* per nucleus was obtained by a manual counting on 23-32% of cells acquired.

	Control	BioCyTASQ (1 µM, 24 h)	BioTriazoTASQ (1 µM, 24 h)
General parameters			
Number of images analysed	24	24	24
Nucleus data			
Total number of nuclei analysed	719.0	719.0	793.0
Nuclear TASQ *foci* data			
Total number of TASQ *foci* collected	17 252.0	20 668.0	26 612.0
Mean number of TASQ *foci* per nucleus	23.99	28.75	33.56
Nuclear γH2AX *foci* data			
Total number of γH2AX *foci* collected	2 939.0	3 908.0	4 184.0
Nuclear TASQ and γH2AX *foci* comparative data			
Mean number of γH2AX *foci* per nucleus	4.09	5.44	5.28
Normalized mean ratio of co-localized *foci*/all γH2AX per nucleus (%) [a]	0.0	4.0 %	4.9 %

Table S22. Summary values obtained from the high-resolution optical images acquired with the G4 probes BioCyTASQ and BioTriazoTASQ and processed with co-localization macro program. Summary values obtained *via* the optical imaging performed with MCF7 cells non-treated (Control) or treated after cell fixation with BioCyTASQ or BioTriazoTASQ

(1 µM, 16 h), tagged with SA-Cy3, which is followed by immunodetection of DNA damage nuclear γH2AX *foci* (with IgG-Alexa Fluor 647) and chromatin staining by DAPI. The values quantified are the number of nuclei, nuclear TASQ *foci* and nuclear γH2AX *foci* obtained by the optical images process with the co-localization macro program. The ratio of co-localized γH2AX/all γH2AX per nucleus was also obtained automatically with the macro program.

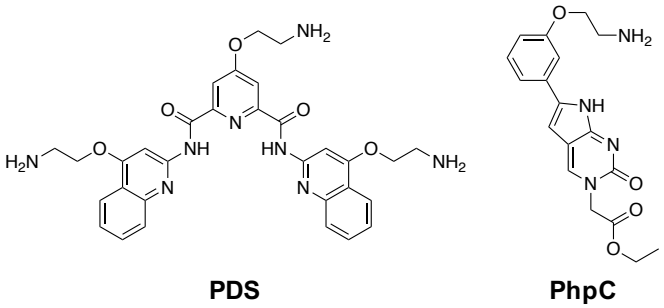

Figure S35. Chemical structures of the two G4 ligands incubated with cells. Are shown the G4-stabilizer PDS (left) used for optical imaging of G4s with the biotinylated BioTriazoTASQ and the *in vitro* G4-destabilizer PhpC (right) used for optical imaging of G4s with the N-TASQ.

	Control - PDS	**Control + PDS**	**BioTriazoTASQ (1 µM, 24 h) - PDS**	**BioTriazoTASQ (1 µM, 24 h) + PDS**
General parameters				
Number of images analysed	5	5	5	5
Nucleus data				
Total number of nuclei analysed	/	/	596.0	529.0
Total number of γH2AX$^+$ nuclei analysed	/	/	433.0	440.0
Nuclear TASQ *foci* data				
Mean number of TASQ *foci* per nucleus	0.0	0.0	38.98	35.72
Normalized mean number of TASQ *foci* per nucleus	0.0	0.0	1.0	0.93
Nuclear γH2AX *foci* data				
Mean number of γH2AX *foci* per nucleus	4.78	10.24	4.34	6.42
Normalized mean number of γH2AX *foci* per nucleus	1.0	2.21	1.0	1.49
Nuclear TASQ and γH2AX *foci* comparative data				
Mean number of co-localized *foci* per nucleus	0.0	0.0	0.83	1.58
Normalized mean number of co-localized *foci* per nucleus	/	/	1.0	1.89

Table S23. Summary values obtained from the high-resolution optical images acquired with the G4 probe BioTriazoTASQ and PDS-treated cells and processed with the co-localization macro program. Summary values obtained *via* the optical imaging performed with MCF7 cells live treated or not with PDS (+/- PDS; 5 µM, 6 h) and then treated after cell fixation with BioTriazoTASQ (+/- BTT; 1 µM, 16 h), tagged with SA-Cy3, which is followed by immunodetection of DNA damage nuclear γH2AX *foci* (with IgG-Alexa Fluor 647) and chromatin staining by DAPI. The values quantified are the number of nuclei, nuclear TASQ *foci*, nuclear γH2AX *foci* and ratio of co-localized γH2AX/all γH2AX per nucleus obtained by the optical images process with the co-localization macro program.

```
selectWindow("ntasq_"+number+".TIF"); Selection of the N-TASQ channel
        m=nsbg; The number of areas where the background FI has to be measured (previously chosen)
                FIbg=0;
                FIbgMean=0;
                if (m>0) {
                        for(s=0; s<m; s++) { Beginning of the loop allowing to position a new area
                        makeRectangle(500, 500, 56, 56); Size of the areas where to measure the background FI
                        waitForUser("Adjust your square n°"+s+1+"/"+m); Manual positioning of the areas on image

                                Stack.getDimensions(width, height, channels, slices, frames);
                                for (st=0; st<slices; st++) { Beginning of the loop allowing to go to the next z
                                setSlice(st+1);
                                run("Set Measurements...", "area integrated redirect=None decimal=1");

                                run("Measure"); Background FI quantification for this z of this image
                                FIbg = FIbg + getResult("IntDen", st); Addition of the background FI values
                                } Change of z-dimension
                        close("Results");
                        } Change of area
                        FIbgMean = FIbg/(m*st); Calculation of the mean background FI for this image
                        }
                print("int-background-mean-FI_"+number+"/"+nsbg+"/"+st+":", "IntDen:", FIbgMean); Data recovery
```

Figure S36. Lines of code of the N-TASQ macro program 1.0 for the quantification of background FI. This part of the N-TASQ macro program 1.0 allows to quantify the fluorescence (*i.e.*, the mean gray value) of the background without cells. To do this, the user has to position squared areas on the image where the background will be measured in each z-dimension. A mean background FI is then calculated in taking account of the number of areas and the number of z-dimension. Explanations about the function of some methods are in blue.

```
selectWindow("mask_stack_ntasq"+number+".TIF"); Selection of the image
roiManager("show all with labels"); Showing of the cells number and defined contours
run("Flatten");
run("Scale Bar...", "width=40 height=5 font=18 color=White background=None location=[Lower Right] bold overlay");
Addition of the scale bar
saveAs("png",save_directory+"ntasq_"+name+number+"_"+cond+"_defined_areas_overview"+".png"); Saving of the
summary image
close("ntasq_"+name+number+"_"+cond+"_defined_areas_overview"+".png");
close("mask_stack_ntasq"+number+".TIF");
close("ntasq_"+number+"_roi.TIF");
close("Results");
```

Figure S37. Lines of code of the N-TASQ macro program 1.0 for the creation of summary image. This part of the N-TASQ macro program 1.0 allows to save a summary image of cells field in which the cell contours, their number and the scale bar are shown. Explanations about the function of some methods are in blue.

```
for(c=0;c<roiManager("count");c++){ Beginning of the loop allowing to go to the next cell (ROI)
close("Results");
selectWindow("ntasq_"+number+"_foci.TIF");
roiManager("Select",c); Selection of the cell
run("Duplicate...", "title=int-ntasq_foci_"+number+"/"+c+1+" duplicate range=stack"); Duplication of the cell
run("Smooth", "stack"); Blurring of the cell
run("Clear Outside", "stack"); Deletion of the pixels values outside of the cell
run("Set 3D Measurements", "volume nb_of_obj._voxels integrated_density mean_gray_value minimum_gray_value
maximum_gray_value dots_size=5 font_size=10 show_numbers white_numbers");
run("3D Objects Counter", "threshold="+ntts+" slice=1 min.=2 max.=20000000 objects statistics"); Calculation of the FI
(IntDen), the volume and the voxel number of the N-TASQ foci selected with the foregone N-TASQ threshold (ntts
value)

        selectWindow("Results");
        m=nResults();
        NTfociVolume=0;
        NTfociNbvoxel=0;
        NTfociIntDen=0;
        if (m>0) {
                for(f=0; f<m; f++) { Addition of the FI, volume and voxel number values (below)
                NTfociVolume = getResult("Volume (micron^3)", f);
                NTfociNbvoxel = getResult("Nb of obj. voxels", f);
                NTfociIntDen = getResult("IntDen", f);

                print("int-ntasq-foci_"+number+"/"+c+1+"/"+"object_n"+f+1+":", "Volume:", NTfociVolume,
"nb_of_obj._voxels:", NTfociNbvoxel, "IntDen:", NTfociIntDen); Saving of the FI, volume and voxel number values in a
file
                }
                }
        else {
                print("int-ntasq-foci_"+number+"/"+c+1+"/"+"object_n"+f+1+":", m);
                }

close("int-ntasq_foci_"+number+"/"+c+1); Close of the duplicated cell used for N-TASQ foci quantification
close("Objects map of int-ntasq_foci_"+number+"/"+c+1); Close of the image generated after quantification
} Change of cell
```

Figure S38. Lines of code of the N-TASQ macro program 1.0 for the quantification of N-TASQ *foci* number, FI and volume. This part of the N-TASQ macro program 1.0 allows to quantify the number, FI and the volume (as well as the voxel number) of each N-TASQ *foci* inside each cell. To do this, each cell is duplicated, blurred, isolated and then, in applying a threshold on the image to only isolate small bright structures inside cells, the number, FI and volume of these N-TASQ *foci* are quantified and saved in a worksheet precising the name of the experiment, the cells number, the N-TASQ *foci* number and for each the quantified values. The only difference between the loop allowing the measure of cells data and this loop for N-TASQ *foci* data is the use of a threshold to only keep the *foci* inside of the cells. Explanations about the function of some methods are in blue.

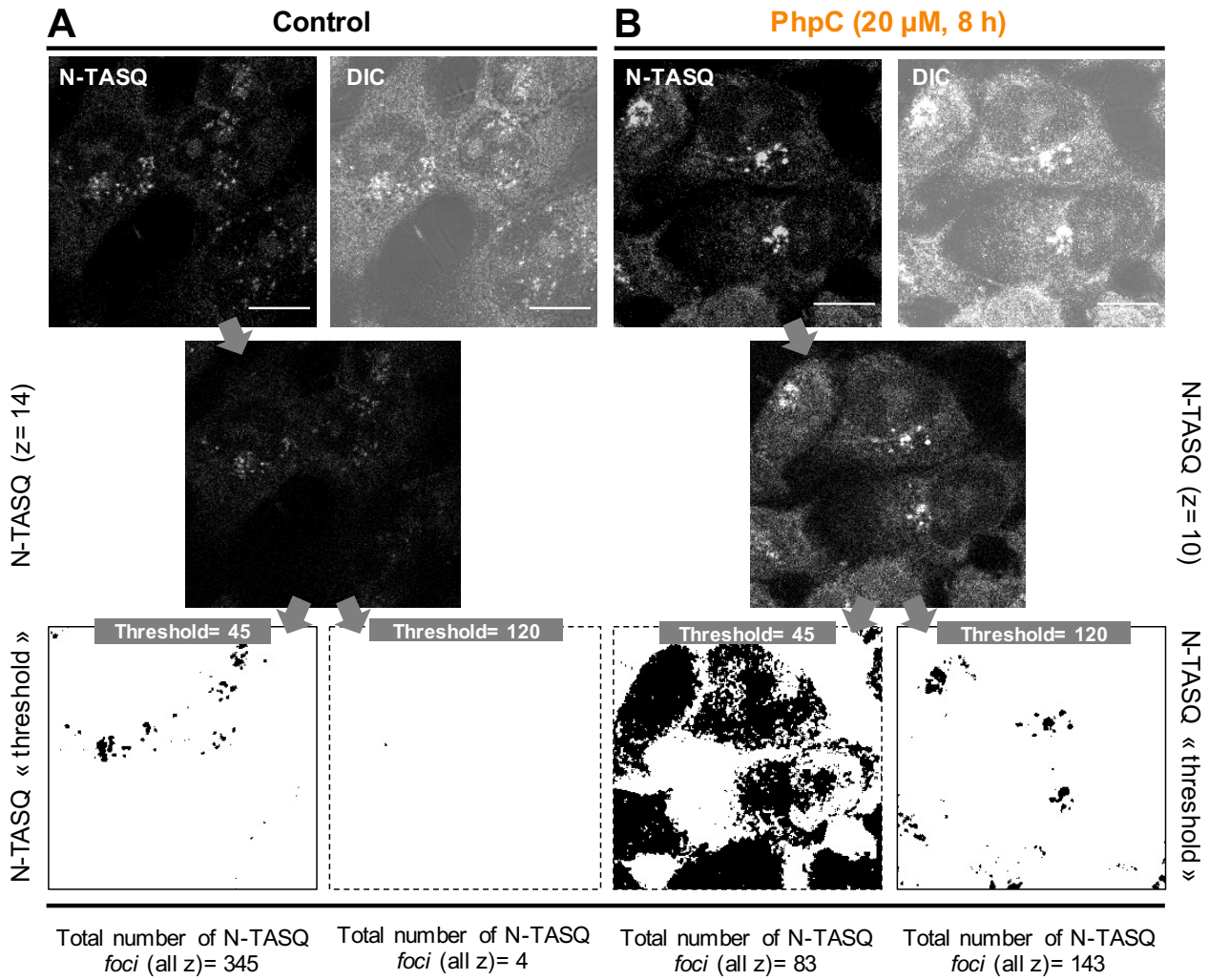

Figure S39. Methodology for the selection of the most adapted fluorescence threshold in each experimental condition for optical imaging. The optical imaging was performed with MCF7 cells (**A**) non-treated (Control) or (**B**) live treated with PhpC (20 µM, 8 h) and (**A-B**) N-TASQ (50 µM, 6 h; white) simultaneously. Images are representative of the mean number of N-TASQ *foci* per cell. 63x oil objective, then digital magnification (scale bar = 10 µm). The two selected fluorescence threshold values (*i.e.*, 45 and 120 for the non-treated (Control) and PhpC-treated MCF7 cells, respectively) were applied on the opposite condition in order to illustrate the use of these condition-depending threshold values.

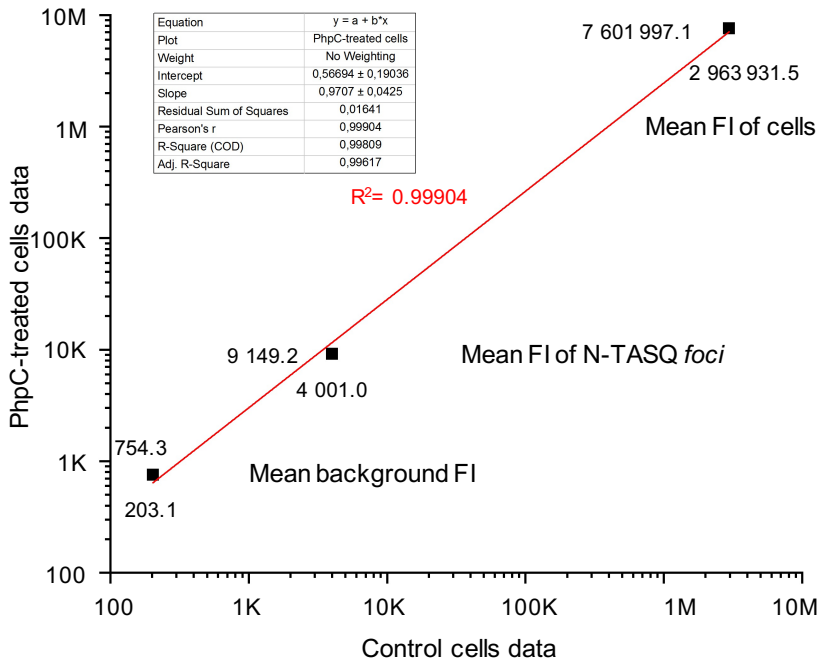

Figure S40. Correlation between different fluorescence parameters in each experimental condition obtained by optical imaging. The different raw fluorescence intensity (FI) values (*e.g.*, background FI, FI of cells, FI of N-TASQ *foci*) obtained by the optical images process with the N-TASQ macro program 1.0 show a correlation (R^2= 0.99904) between these FI values for non-treated (Control) and PhpC-treated MCF7 cells.

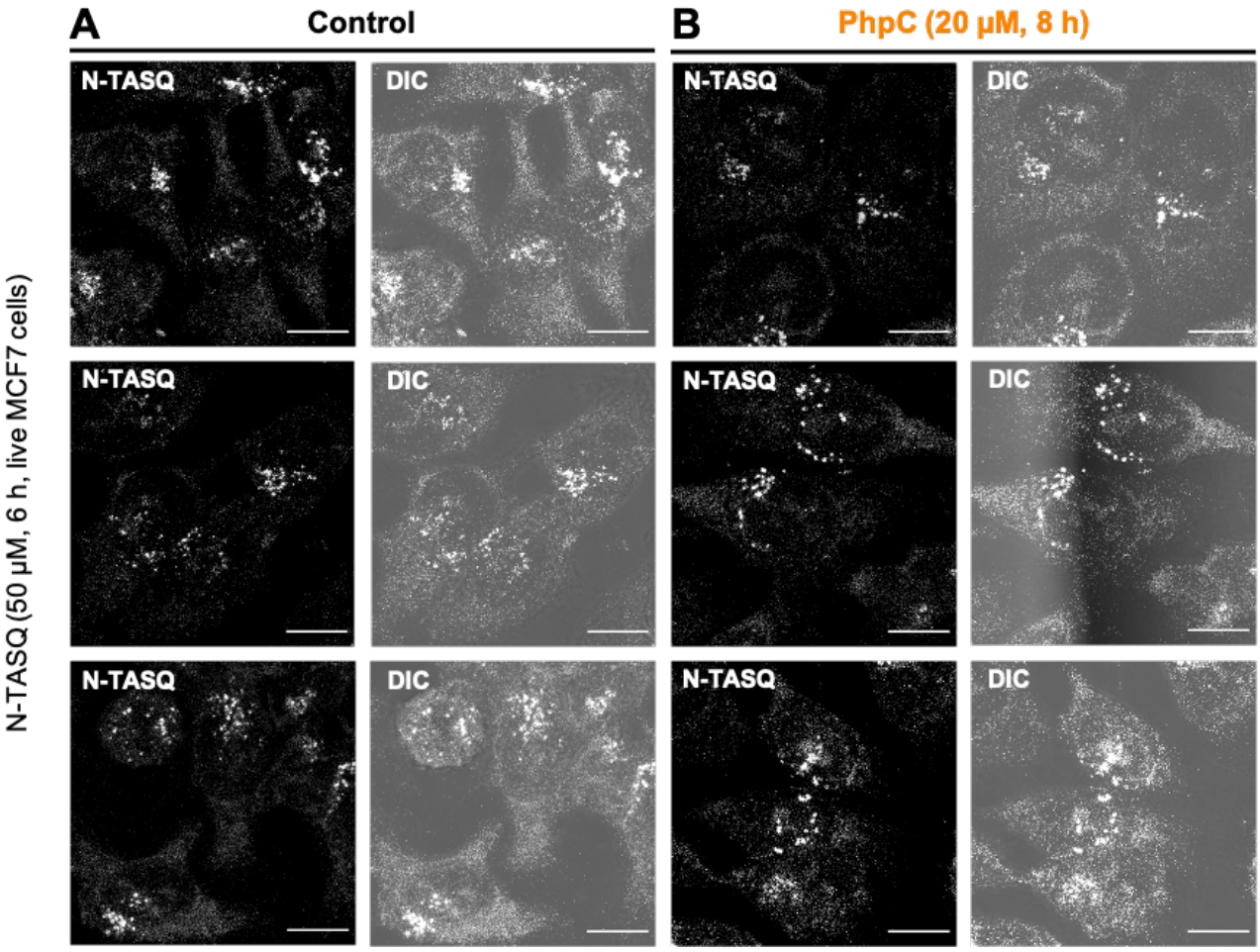

Figure S41. Additional high-resolution optical images acquired with the G4 probe N-TASQ and PhpC-treated cells. The optical imaging was performed with MCF7 cells (**A**) non-treated (Control) or (**B**) live treated with PhpC (20 µM, 8 h) and (A-B) N-TASQ (50 µM, 6 h; white) simultaneously. Images are representative of the mean number of N-TASQ *foci* per cell. 63x oil objective, then digital magnification (scale bar = 10 µm).

	Control	**PhpC (20 µM, 8 h)**
General parameters		
Number of images analysed	2	3
N-TASQ FI threshold	45	120
Mean background FI (IntDen)	203.14	754.27
Cell data		
Total number of cells analysed	84	118
Mean volume of cell (μm^3)	2 435.25	2 965.62
Mean FI of cell (IntDen)	2 963 931.49	7 601 997.14
Normalized mean FI of cell (IntDen) [a]	14 590.7	10 078.6
Global N-TASQ *foci* data		
Total number of N-TASQ *foci* collected	7 270	3 181
Mean number of N-TASQ *foci* per cell	86.6	27
Mean volume of N-TASQ *foci* (μm^3)	0.63	0.59
Mean FI of N-TASQ *foci* (IntDen)	4 001.00	9 149.18
Normalized mean FI of N-TASQ *foci* (IntDen) [a]	19.7	12.1
Portion of N-TASQ *foci* volume in total cell volume (%)	0.026	0.020
Portion of N-TASQ *foci* FI in total cell FI (%)	0.13	0.12
Portion of diffuse N-TASQ FI in total cell FI (%)	99.87	99.88
Number of big N-TASQ *foci* (volume > [2 * Mean volume]) per cell	3.2	1.8

Table S24. Summary values obtained from the high-resolution optical images acquired with the G4 probe N-TASQ and PhpC-treated cells and processed with the N-TASQ macro program 1.0. Summary values obtained *via* the optical imaging performed with MCF7 cells non-treated (Control) or live treated with PhpC (20 µM, 8 h) and N-TASQ (50 µM, 6 h) simultaneously. The values quantified are the number of cells and N-TASQ *foci* per cell and their respective FI and volume obtained by the optical images process with the N-TASQ macro program 1.0. Based on these data, others values were calculated as the portion of diffuse N-TASQ (%) and the number of big N-TASQ *foci* per cell [a] Normalization of FI has been made in dividing FI values from a condition by their respective Mean background FI. FI = Fluorescence intensity. IntDen = Integrated Density, *i.e.*, the product of area and mean gray value.

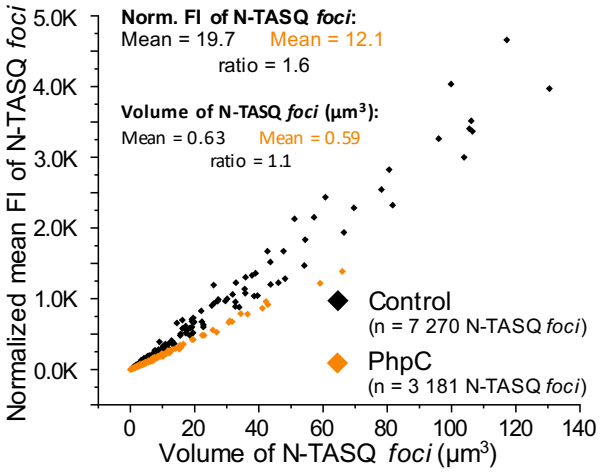

Figure S42. Additional quantitative results obtained from the high-resolution optical images acquired with the G4 probe N-TASQ and PhpC-treated cells. The optical imaging was performed with MCF7 cells non-treated (Control; black boxes) or live treated with PhpC (20 µM, 8 h; orange) and N-TASQ (50 µM, 6 h) simultaneously. Optical images were processed with the N-TASQ macro program 1.0 in order to count cells and N-TASQ *foci* per cell as well as their FI and volume (with the N-TASQ channel). A normalization was applied with the mean background FI of each image. The data set is from one technical experiment.

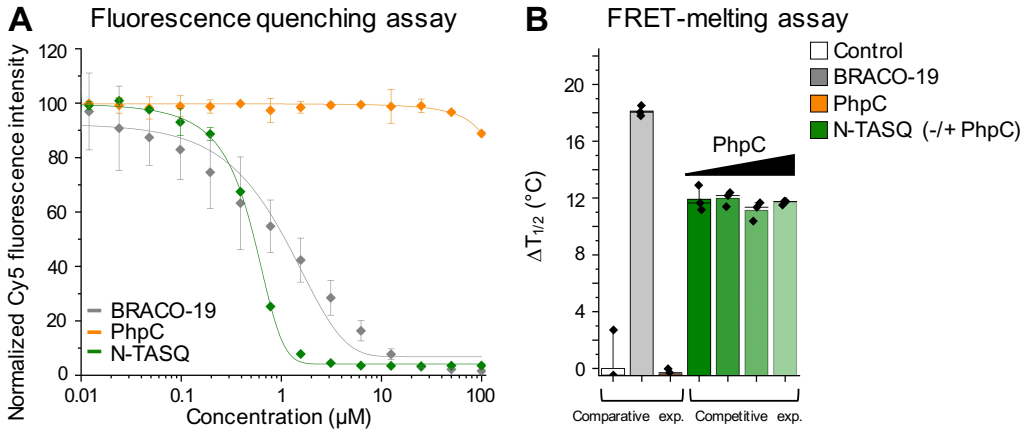

Figure S43. Fluorescence quenching and FRET-melting assays results. (**A**) The fluorescence quenching assay (FQA) was performed with the Cy5-labelled G4-RNA $^{5'}$Cy5-NRAS and G4-interacting molecules (BRACO-19 in grey, PhpC in orange, N-TASQ in green) at increasing concentrations. Error bars represent SD from the mean for three independent experiments. (**B**) The FRET-melting assay was performed with the G4-RNA F-NRAS-T and without (*i.e.*, $T_{1/2}$ Control, ON only with CacoK10 buffer) or with G4-interacting molecules (BRACO-19 in grey, PhpC in orange, N-TASQ in green) at 5 mol. equiv. For N-TASQ, competitive assay was conducted with increasing concentration of PhpC (up to 20 mol. equiv.; from light to dark hue). Mean $T_{1/2}$ (or T_m, in °C) values calculated correspond to the melting temperature of the F-NRAS-T G4. $\Delta T_{1/2}$= $T_{1/2}$ with G4-interacting molecule – $T_{1/2}$ Control. Error bars represent SD from the mean for three independent experiments. These assays were kindly performed by Sandy Raevens and Marc Pirrotta, respectively.

A	**Concentration range of G4-interacting molecules**														
Diluted solutions conc. (in µM)	0.00675	0.0135	0.027	0.05	0.11	0.217	0.43	0.87	1.74	3.47	6.94	13.89	27.78	55.55	111.11
Final conc. (in µM)	0.006	0.012	0.024	0.049	0.098	0.195	0.391	0.781	1.563	3.125	6.25	12.5	25	50	100
mol. equiv. (compared to $^{5'}$Cy5-ON)	0.3	0.6	1.2	2.45	4.9	9.75	19.55	39.05	78.15	156.25	312.5	625	1250	2500	5000

B	**Summary $^{app}K_D$ (µM)**		
	BRACO-19	PhpC	N-TASQ
$^{5'}$Cy5-NRAS	0.86 ± 0.26	>100	0.51 ± 0.01

Table S25. Summary data about the Fluorescence quenching assay (FQA). (**A**) Concentration range of the G4-interacting molecules (BRACO-19, PhpC, N-TASQ) used with the $^{5'}$Cy5-NRAS ON for the fluorescence quenching assay and (**B**) summary of the $^{app}K_D$ values obtained with the FQA performed with the G4-RNA $^{5'}$Cy5-NRAS and G4-interacting molecules (BRACO-19, PhpC, N-TASQ) at increasing concentrations.

	Mean $\Delta T_{1/2}$ (°C)			
G4-interacting molecules	No competitor	5 mol. equiv.	10 mol. equiv.	20 mol. equiv.
Control	0	/	/	/
BRACO-19	18.12 ± 0.37	/	/	/
PhpC	-3.38 ± 0.41	/	/	/
N-TASQ	11.91 ± 0.90	11.98 ± 0.52 (PhpC)	11.13 ± 0.67 (PhpC)	11.68 ± 0.15 (PhpC)

Table S26. Summary data about the FRET-melting assay. Summary of the $\Delta T_{1/2}$ (°C) values obtained with the FRET-melting assay performed with the G4-RNA F-NRAS-T and without (*i.e.*, Control, ON only with CacoK10 buffer) or with G4-interacting molecules (BRACO-19, PhpC, N-TASQ) at 5 mol. equiv. For N-TASQ, competitive assay was conducted with increasing concentration of PhpC (up to 20 mol. equiv.). Mean $T_{1/2}$ (or T_m, in °C) values calculated correspond to the melting temperature of the F-NRAS-T G4. $\Delta T_{1/2}$= $T_{1/2}$ with G4-interacting molecule – $T_{1/2}$ Control. SD is from the mean for three independent experiments.

```
for(c=0;c<roiManager("count");c++){ Beginning of the loop allowing to go to the next cell (ROI)
close("Results");

selectWindow("ntasq_"+number+"_nuccoloc.TIF");
roiManager("Select",c); Selection of a cell (N-TASQ channel)
run("Duplicate...", "title=ntasq_nuccoloc_"+number+"/"+c+1+" duplicate range=stack"); Duplication n° 1 of the cell
selectWindow("ntasq_nuccoloc_"+number+"/"+c+1);
run("Smooth", "stack"); Blurring of the cell copy n° 1
run("Clear Outside", "stack"); Deletion of the pixels values outside of the cell copy n° 1

selectWindow("nuc_"+number+"_nuccoloc.TIF");
roiManager("Select",c); Selection of the same cell (DRAQ5 channel)
run("Duplicate...", "title=nuc_nuccoloc_"+number+"/"+c+1+" duplicate range=stack"); Duplication n° 2 of the cell
selectWindow("nuc_nuccoloc_"+number+"/"+c+1);
run("Smooth", "stack"); Blurring of the cell copy n° 2
run("Clear Outside", "stack"); Deletion of the pixels values outside of the cell copy n° 2
setThreshold(nucts, 255); Isolation of the nucleus with DRAQ5 FI
run("Convert to Mask", "method=MaxEntropy background=Dark"); Creation of the nucleus mask
```

```
run("Fill Holes", "stack");
run("Subtract Background...", "rolling=3 light create stack");

imageCalculator("AND create stack", "ntasq_nuccoloc_"+number+"/"+c+1,"nuc_nuccoloc_"+number+"/"+c+1);
Merging of the nucleus part with the cell copy n° 1 (N-TASQ channel), thus deletion of the cytoplasm part
selectWindow("Result of ntasq_nuccoloc_"+number+"/"+c+1);
run("Set 3D Measurements", "volume nb_of_obj._voxels integrated_density mean_gray_value minimum_gray_value
maximum_gray_value dots_size=5 font_size=10 show_numbers white_numbers");
run("3D Objects Counter", "threshold="+ntts+" slice=1 min.=2 max.=20000000 objects statistics"); Calculation of the FI
(IntDen), the volume and the voxel number of the nuclear N-TASQ foci selected with the foregone N-TASQ threshold
(ntts value)

        selectWindow("Results");
        p=nResults();
        NTnuccolocVolume=0;
        NTnuccolocNbvoxel=0;
        NTnuccolocIntDen=0;
        if (p>0) { Beginning of the loop allowing to go to the next foci
                for(f=0; f<p; f++) { Extraction of the FI, volume and voxel number values (below) of a foci
        NTnuccolocVolume = getResult("Volume (micron^3)", f);
                NTnuccolocNbvoxel = getResult("Nb of obj. voxels", f);
                NTnuccolocIntDen = getResult("IntDen", f);

                print("ntasq-nuccoloc_"+number+"/"+c+1+"/"+"object_n"+f+1+":", "Volume:", NTnuccolocVolume,
"nb_of_obj._voxels:", NTnuccolocNbvoxel, "IntDen:", NTnuccolocIntDen); Saving of the FI, volume and voxel number
values in a file
                }
                } Change of foci
        else {
                print("ntasq-nuccoloc_"+number+"/"+c+1+"/"+"object_n"+f+1+": no N-TASQ foci - nucleus co-
localization");
                }

close("ntasq_nuccoloc_"+number+"/"+c+1); Close of the duplicated cell copy n° 1
close("nuc_nuccoloc_"+number+"/"+c+1); Close of the duplicated cell copy n° 2 (nucleus)
close("Result of ntasq_nuccoloc_"+number+"/"+c+1); Close of the cytoplasm-lacked cell image used for quantification
close("Objects map of Result of ntasq_nuccoloc_"+number+"/"+c+1); Close of the image generated after
quantification
} Change of cell
```

Figure S44. Lines of code of the N-TASQ macro program 2.0 for the quantification of nuclear N-TASQ *foci* number, FI and volume. This part of the N-TASQ macro program 2.0 allows to quantify the number, FI and the volume (as well as the voxel number) of each nuclear N-TASQ *foci* inside each cell. To do this, each cell is duplicated, blurred and isolated two times, one of the copy (in DRAQ5 channel) is thresholded to only keep the nucleus and this copy is merged with the second one (in N-TASQ channel) in order to only keep the nuclear data of this second image. Then the N-TASQ threshold is applied on this last cytoplasm-lacked image to only isolate small bright structures inside, quantify the number, FI and volume of these nuclear N-TASQ *foci* and save it in a worksheet precising the name of the experiment, the cells number, the nuclear N-TASQ *foci* number and for each the quantified values. Explanations about the function of some methods are in blue.

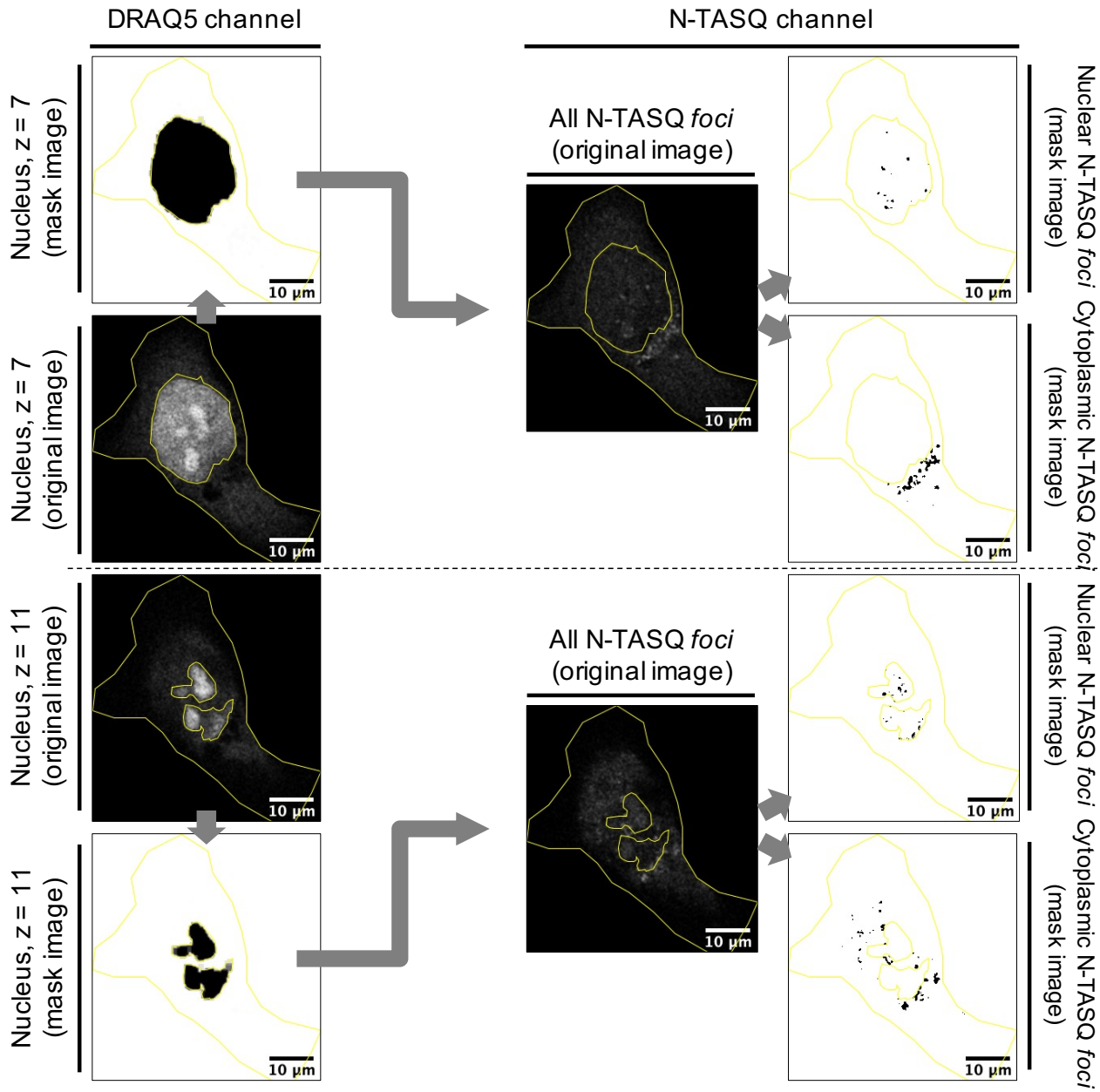

Figure S45. Additional processing of the optical images with the N-TASQ macro program 2.0. The optical imaging was performed with MCF7 cells live treated with N-TASQ (50 µM, 6 h), which is followed by a post-fixation chromatin staining by DRAQ5. Optical image was processed with the N-TASQ macro program 2.0 in order to study the N-TASQ *foci* subcellular compartmentalization. Here are shown two different z dimensions (z = 7 or 11) from the same optical image and the same cell showing the macro program 2.0 is able to separate the nuclear and cytoplasmic N-TASQ *foci* however the z-dimension of cells and then the size and shape of the nucleus. 63x oil objective, then digital magnification (scale bar = 10 µm).

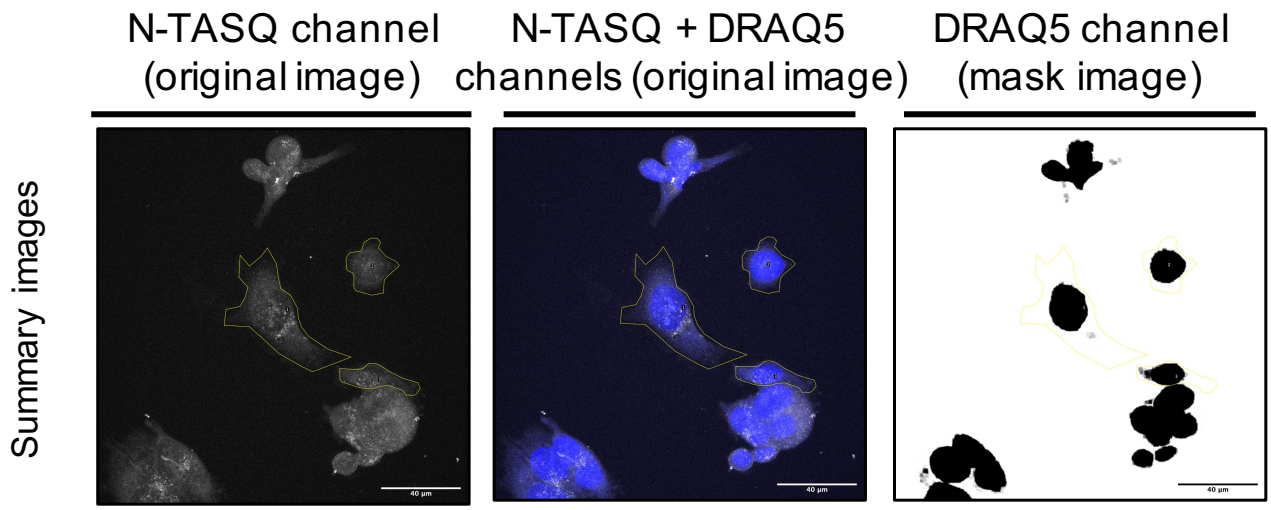

Figure S46. Summary processed optical images generated by the N-TASQ macro program 2.0. The optical imaging was performed with MCF7 cells live treated with N-TASQ (50 µM, 6 h), which is followed by a post-fixation chromatin staining by DRAQ5. Optical image was processed with the N-TASQ macro program 2.0 in order to study the N-TASQ *foci* subcellular compartmentalization. Here are shown the three different summary processed optical images generated by the program at the end of its process: the N-TASQ channel (z-stacked original image; left), the DRAQ5 channel (z-stacked mask image; right) and the both channels (z-stacked original image), in order to verify the program process and detect cells by their number. 63x oil objective, then digital magnification (scale bar = 10 µm).

	N-TASQ (50 µM, 6 h)
General parameters	
Number of images analysed	5
N-TASQ FI threshold	60
DRAQ5 FI threshold	50
Mean background FI (IntDen)	166.41
Cells data	
Total number of cells analysed	45.0
Mean volume of cell (µm^3)	2 253.2
Mean FI of cell (IntDen)	2 482 080.5
Normalized mean FI of cell (IntDen) [a]	14 915.7
Global N-TASQ *foci* data	
Total number of N-TASQ *foci* collected	1 223.0
Mean number of N-TASQ *foci* per cell	27.2
Mean volume of N-TASQ *foci* (µm^3)	0.42
Mean FI of N-TASQ *foci* (IntDen)	3 329.7
Normalized mean FI of N-TASQ *foci* (IntDen) [a]	20.0
Portion of N-TASQ *foci* volume in total cell volume (%)	0.50
Portion of N-TASQ *foci* FI in total cell FI (%)	3.65
Portion of diffuse N-TASQ FI in total cell FI (%)	96.35
Number of big N-TASQ *foci* (volume > [2 * Mean volume]) per cell	2.36
Cytoplasmic N-TASQ *foci* data	
Total number of cytoplasmic N-TASQ *foci* collected	548.0
Mean number of cytoplasmic N-TASQ *foci* per cell	12.2
Mean volume of cytoplasmic N-TASQ *foci* (µm^3)	0.48
Mean FI of cytoplasmic N-TASQ *foci* (IntDen)	3 860.6
Normalized mean FI of cytoplasmic N-TASQ *foci* (IntDen) [a]	23.2
Portion of cytoplasmic N-TASQ *foci* volume in total cell volume (%)	0.24
Portion of cytoplasmic N-TASQ *foci* FI in total cell FI (%)	1.89
Number of big cytoplasmic N-TASQ *foci* (volume > [2 * Mean volume]) per cell	1.09
Nuclear N-TASQ *foci* data	
Total number of nuclear N-TASQ *foci* collected	675.0
Mean number of nuclear N-TASQ *foci* per cell	15.0
Mean volume of nuclear N-TASQ *foci* (µm^3)	0.37
Mean FI of nuclear N-TASQ *foci* (IntDen)	2 898.6
Normalized mean FI of nuclear N-TASQ *foci* (IntDen) [a]	17.4
Portion of nuclear N-TASQ *foci* volume in total cell volume (%)	0.26
Portion of nuclear N-TASQ *foci* FI in total cell FI (%)	1.75
Number of big nuclear N-TASQ *foci* (volume > [2 * Mean volume]) per cell	1.27

Table S27. Summary values obtained from the high-resolution optical images acquired with the G4 probe N-TASQ and processed with the N-TASQ macro program 2.0. Summary values obtained *via* the optical imaging performed with MCF7 cells live treated with N-TASQ (50 µM, 6 h). The values quantified are the number of cells, cytoplasmic and nuclear N-TASQ *foci* per cell and their respective FI and volume obtained by the optical images process with the N-TASQ macro program 2.0. Based on these data, others values were calculated as the portion of diffuse N-TASQ (%) and the number of big N-TASQ *foci* per cell. [a] Normalization of FI has been made in dividing FI values from a condition by their respective Mean background FI. FI = Fluorescence intensity. IntDen = Integrated Density, *i.e.*, the product of area and mean gray value.

III. Related to the Chapter III

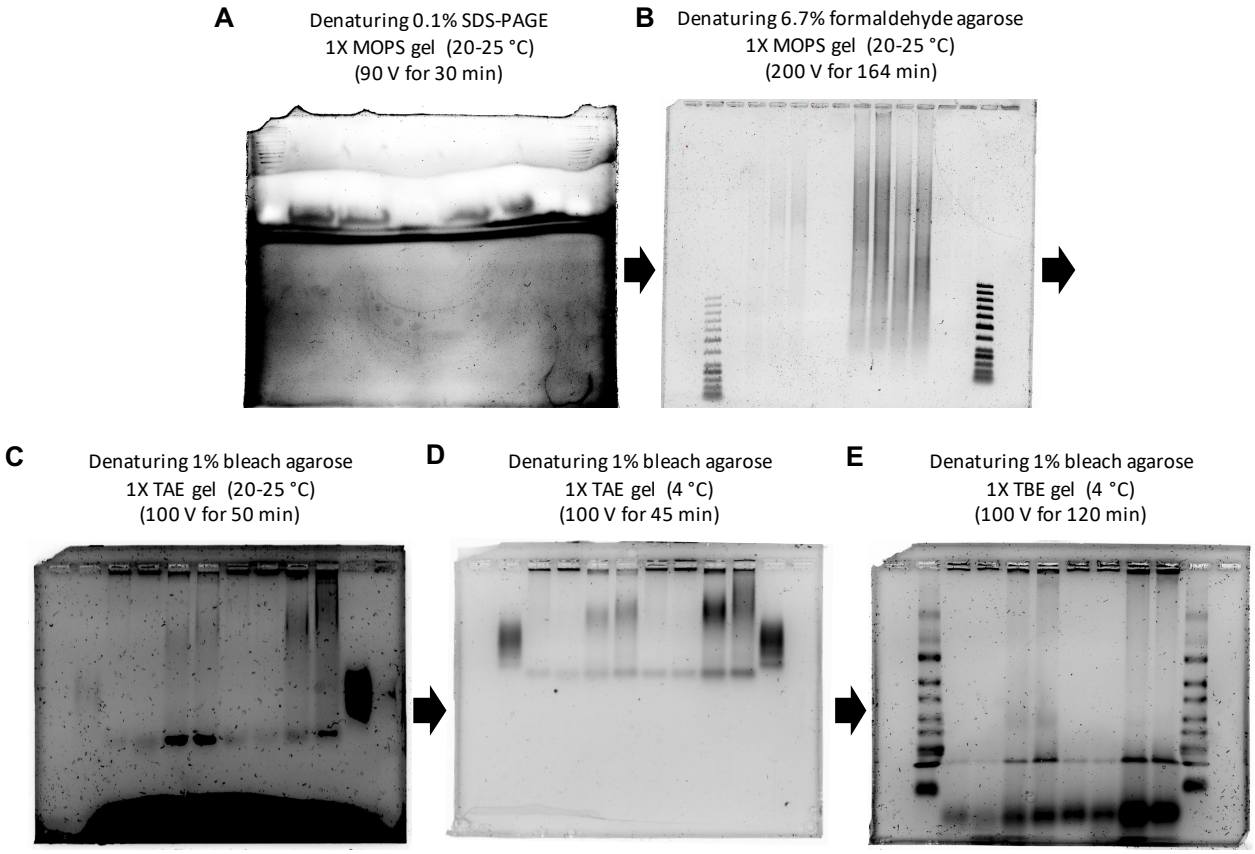

Figure S47. Representative gels of the optimization of the gel electrophoresis monitoring step. During the G4RP.v2 optimization, the RNA extraction from cells was studied firstly by running (**A**) denaturing 0.1% (w/v) SDS-PAGE 1X MOPS gel at RT, then (**B**) denaturing 6.7% (w/v) formaldehyde 1% (w/v) agarose and finally (**C-E**) denaturing 1% (v/v) bleach 1.5% (w/v) agarose gel. The same samples were used for these three last gels electrophoresis realized with 1X TAE (**C**) or 1X TBE (**D-E**) buffer. Gels were run progressively from RT (20-25 °C) (**A-C**) to 4 °C (**D-E**). Gels were revelated with SYBR™ Gold Nucleic Acid Gel Stain. 1 kb DNA Ladder or RiboRuler High Range RNA Ladder were used as ladder for A-B or C-D-E, respectively.

Optimi-zation exp. n°	Condition	Sample precipitation with	Sample purity	$A_{230\ nm}$	$A_{260\ nm}$	$A_{270\ nm}$	$A_{280\ nm}$	R1= $A_{260\ nm}/A_{230\ nm}$	R2= $A_{260\ nm}/A_{270\ nm}$	R3= $A_{260\ nm}/A_{280\ nm}$	RNA estimated C. (in ng/µL)
A	$5x10^6$ cells to lyse	No	Raw lysate	4.24	2.02	1.87	1.50	0.48	1.08	1.35	80.8
	$9x10^6$ cells to lyse	No	Raw lysate	2.42	3.39	2.93	2.19	1.40	1.16	1.55	135.6
B	G4RP lysis buffer w/o SDS	No	Raw lysate	2.42	3.39	2.93	2.19	1.40	1.16	1.55	135.6
	G4RP lysis buffer w/ 0.1% SDS	No	Raw lysate	5.01	4.69	4.35	3.20	0.94	1.08	1.47	187.6
C	Lysis w/ 0.8 mm needle (x25)	No	Raw lysate	0.62	0.61	0.35	0.09	0.98	1.74	6.78	24.4
	Lysis w/ 0.8 mm needle (x50)	No	Raw lysate	0.20	0.64	0.43	0.23	3.20	1.49	2.78	25.6
	Lysis w/ 0.4 mm needle (x25)	No	Raw lysate	0.77	0.76	0.36	0.11	0.99	2.11	6.91	30.4
	Lysis w/ 0.4 mm needle (x50)	No	Raw lysate	1.38	2.21	1.76	1.17	1.60	1.26	1.89	88.4
D	No RCL	No	Purified RNA (-C)	32.07	9.02	15.53	6.48	0.28	0.58	1.39	360.8
	RCL for 1 h	No	Purified RNA (-C)	sat.	13.11	21.29	9.42	/	0.62	1.39	524.4
	RCL for 2 h	No	Purified RNA (-C)	37.12	12.41	19.70	8.74	0.33	0.63	1.42	496.4
	RCL for 4 h	No	Purified RNA (-C)	sat.	20.54	28.42	14.33	/	0.72	1.43	821.6

Optimi-zation exp. n°	Condition	Sample precipitation with	Sample purity	$A_{230\ nm}$	$A_{260\ nm}$	$A_{270\ nm}$	$A_{280\ nm}$	R1= $A_{260\ nm}/A_{230\ nm}$	R2= $A_{260\ nm}/A_{270\ nm}$	R3= $A_{260\ nm}/A_{280\ nm}$	RNA estimated C. (in ng/µL)
E	No cell fixation	No	Raw lysate	1.26	17.41	15.21	11.69	13.82	1.14	1.49	696.4
	Cell fix. w/ 1% FA	No	Raw lysate	3.89	4.12	3.46	2.55	1.06	1.19	1.62	164.8
	Cell fix. w/ 2% FA	No	Raw lysate	0.004	0.87	0.58	0.40	217.5	1.50	2.18	34.8
	Cell fix. w/ 4% FA	No	Raw lysate	neg.	0.25	0.02	neg.	/	12.5	/	10.0
F	RNA purif. with classic microtube	No	Purified RNA (-C)	16.65	2.68	4.21	1.79	0.16	0.64	1.50	107.2
	RNA purif. with Phasemaker microtube	No	Purified RNA (-C)	25.80	10.61	17.61	7.53	0.41	0.60	1.41	424.4
G	First flow-through (from top aqueous phase)	No	Raw lysate	17.77	30.97	29.38	26.43	1.74	1.05	1.17	1 238.8
	Purified RNA	No	Purified RNA (+C)	10.94	23.93	20.54	12.95	2.19	1.17	1.85	957.2

Optimi-zation exp. n°	Condition	Sample precipitation with	Sample purity	$A_{230\ nm}$	$A_{260\ nm}$	$A_{270\ nm}$	$A_{280\ nm}$	R1= $A_{260\ nm}/A_{230\ nm}$	R2= $A_{260\ nm}/A_{270\ nm}$	R3= $A_{260\ nm}/A_{280\ nm}$	RNA estimated C. (in ng/µL)
H	12x10^6 cells to lyse	No	Raw lysate	3.07	11.69	9.62	7.01	3.81	1.22	1.67	467.6
	12x10^6 cells to lyse	Biotin	Purified RNA (+C)	0.23	0.16	0.14	0.12	0.70	1.14	1.33	6.40
	12x10^6 cells to lyse	BioCyTASQ	Purified RNA (+C)	0.57	0.72	0.61	0.42	1.26	1.18	1.71	28.8
	24x10^6 cells to lyse	No	Raw lysate	1.08	19.31	15.62	11.48	17.88	1.24	1.68	772.4
	24x10^6 cells to lyse	Biotin	Purified RNA (+C)	0.05	0.08	0.08	0.05	1.60	1.00	1.60	3.20
	24x10^6 cells to lyse	BioCyTASQ	Purified RNA (+C)	1.69	2.13	1.77	1.27	1.26	1.20	1.68	85.2

Table S28. Monitoring values of the G4RP.v2 method optimization obtained by UV absorbance measurement. The summary of peak Abs (λ_A= 230, 260, 270 and 280 nm), quality ratios and estimated RNA concentration values can be found for all the G4RP.v2 optimization experiments (/: no calculation possible; neg.: negative value; RCL: reverse crosslinking; sat.: saturated value; x25-50: number of pipetting). During these optimizations, several Raw Lysate (after the lysis) or Purified RNA (after the RNA purification) samples were collected in order to evaluate the efficiency of parameters from G4RP.v2 steps by UV absorbance measurement (200-400 nm). In that aim, the following parameters were assessed: (**A**) number of cells to lyse, (**B**) type of lysis buffer to use, (**C**) the size of the needle and the number of pipetting for the lyse, (**D**) the reverse crosslinking (RCL) time, (**E**) the % (w/v) of formaldehyde (FA) for cell fixation, (**F**) the type of microtube to use during the RNA purification, (**G**) the check of the in-column RNA purification method and (**H**) the number of cells to lyse and its influence on the precipitation of G4s by Biotin or BioCyTASQ. Experiments A and B were performed at the same time. RNA samples purified by hand alcohol purification (precipitation with isopropanol and then ethanol) or in-column purification (precipitation with the RNA Clean & Concentrator-5 kit) are annotated "Purified RNA (-C)" or "Purified RNA (+C)", respectively (C for "Column"). Different solutions were used as blank for the baseline of the UV-Vis spectrophotometer: G4RP lysis buffer and UltraPure Distilled Water for Raw Lysate and Purified RNA samples, respectively. For Raw lysate and Purified RNA samples, a dilution factor of 50 and 10, has been corrected here in Abs values, respectively.

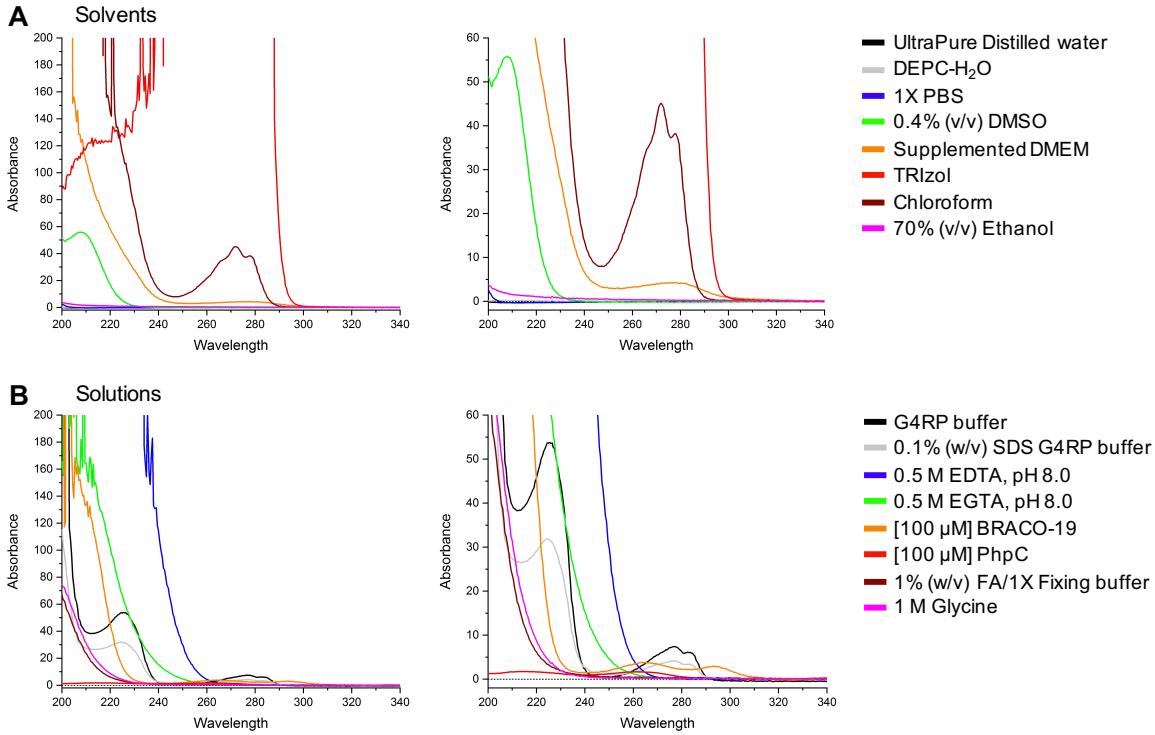

Figure S48. UV absorbance curves of several solvents and solutions used during the G4RP.v2 method. (**A**) The solvents are the UltraPure Distilled Water (black line), the DEPC-H_2O (grey line), the 1X PBS (blue line), 0.4% (v/v) DMSO (green line), the supplemented DMEM (orange line), TRIzol (red line), chloroform (burgundy line) and 70% (v/v) Ethanol (pink line). (**B**) The solutions are the G4RP buffer (black line), 0.1% (w/v) SDS G4RP buffer (grey line), the 0.5 M EDTA pH 8.0 buffer (blue line), the 0.5 M EGTA pH 8.0 buffer (green line), a [100 µM] BRACO-19 aqueous solution with 1% (v/v) DMSO (orange line), a [100 µM] PhpC aqueous solution (red line), the 1% (w/v) formaldehyde (FA)/1X Fixing buffer (burgundy line) and 1 M Glycine (pink line). The baseline was performed on air blank. A dilution factor of 10 was corrected here in Abs values of UltraPure Distilled Water, 1X PBS and [100 µM] PhpC. A dilution factor of 50 was corrected for the others. A zoom on small Abs curves is also shown (right).

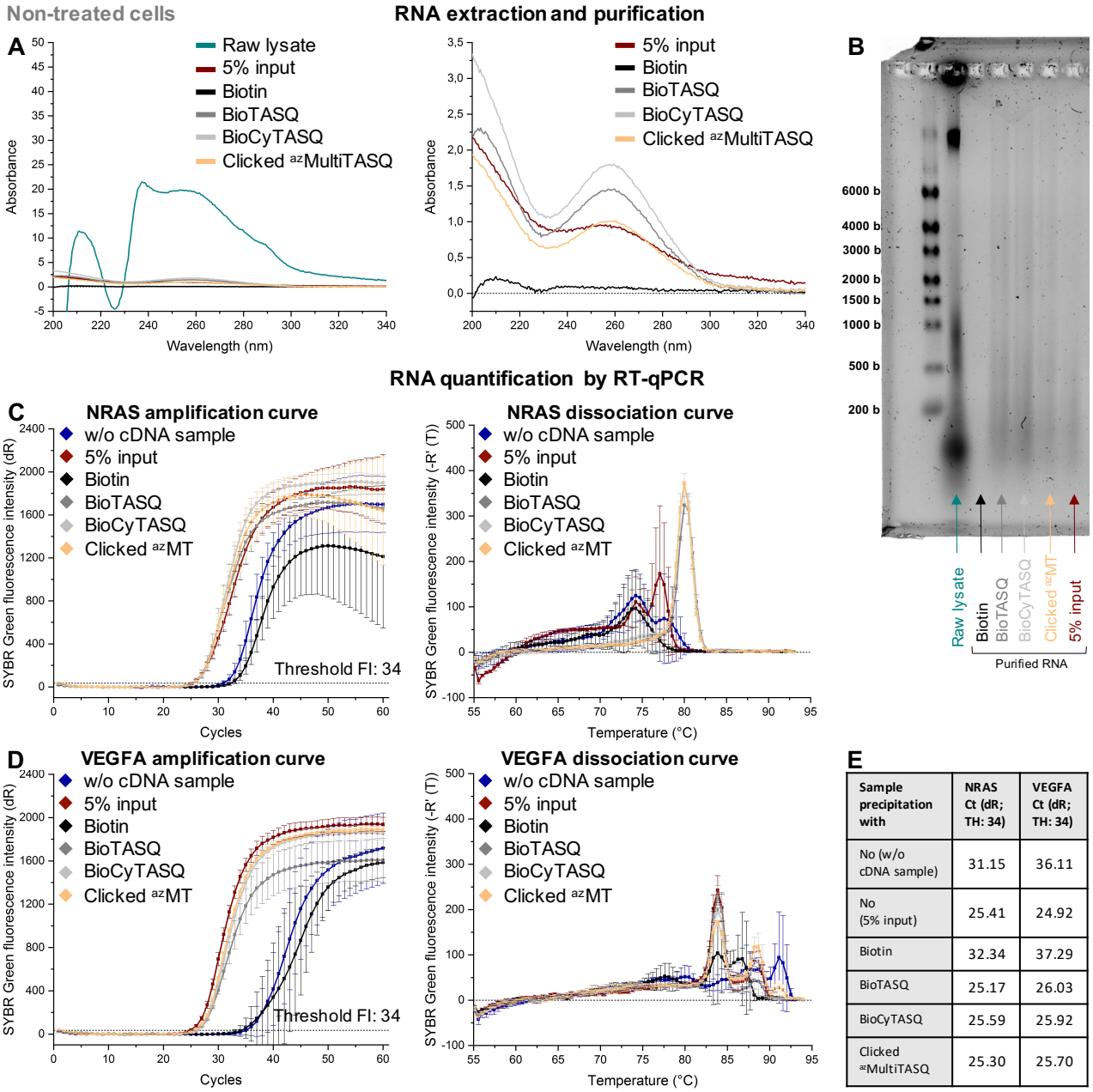

E

Sample precipitation with	NRAS Ct (dR; TH: 34)	VEGFA Ct (dR; TH: 34)
No (w/o cDNA sample)	31.15	36.11
No (5% input)	25.41	24.92
Biotin	32.34	37.29
BioTASQ	25.17	26.03
BioCyTASQ	25.59	25.92
Clicked azMultiTASQ	25.30	25.70

Figure S49. Monitoring data of the G4RP.v2 method performed with non-treated cells. (**A**) Representative UV absorbance (Abs, A) curves of the Raw lysate (*i.e.*, supernatant recovered after cell lysis, without any precipitation or RNA purification) (light blue line), the 5% input sample (*i.e.*, no precipitation control) (red line), the Biotin-precipitated sample (black line) and the three G4 probes BioTASQ- (dark grey line), BioCyTASQ- (light grey line) and Clicked ^{az}MultiTASQ-precipitated (orange line) samples (top left), with a zoom on small Abs curves (top right). For the Raw Lysate and the others samples (Purified RNA), a dilution factor of 50 and 10, has been corrected here in Abs values, respectively. (**B**) Quality check of Raw lysate or Purified RNA (Biotin, BioTASQ, BioCyTASQ, Clicked ^{az}MultiTASQ, 5% input) samples by a 1% (v/v) bleach 1.5% (w/v) agarose denaturing TBE gel electrophoresis. Gels were revealed with SYBR™ Gold Nucleic Acid Gel Stain. RiboRuler High Range RNA Ladder was used as ladder. (**C-D**) Representative amplification (left) and dissociation curves (right) obtained after the qPCR analysis of the G4-RNAs (**C**) NRAS and (**D**) VEGFA enrichment from water (w/o cDNA sample control) (dark blue line), 5% input (red line), Biotin- (black line), G4-ligand BioTASQ- (dark grey line), BioCyTASQ- (light grey line) or Clicked ^{az}MultiTASQ-precipitated (orange line) purified RNA. (**E**) Summary of Ct (dR) values obtained with amplification curves (threshold fluorescence intensity= 34) and fold change (G4RP-RT-qPCR signal) calculated with.

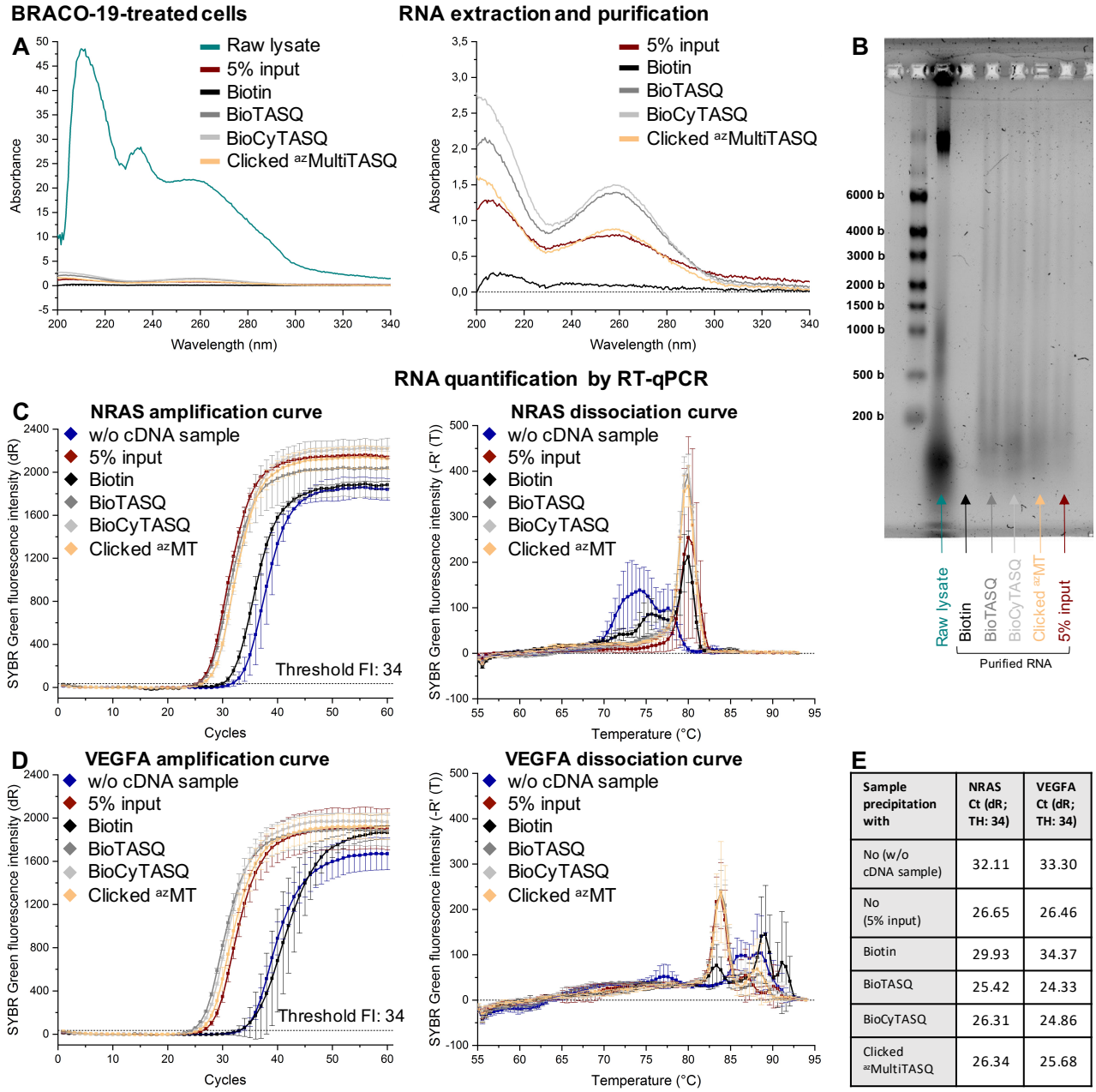

Sample precipitation with	NRAS Ct (dR; TH: 34)	VEGFA Ct (dR; TH: 34)
No (w/o cDNA sample)	32.11	33.30
No (5% input)	26.65	26.46
Biotin	29.93	34.37
BioTASQ	25.42	24.33
BioCyTASQ	26.31	24.86
Clicked azMultiTASQ	26.34	25.68

Figure S50. Monitoring data of the G4RP.v2 method performed with BRACO-19-treated cells. (**A**) Representative UV absorbance (Abs, A) curves of the Raw lysate (*i.e.*, supernatant recovered after cell lysis, without any precipitation or RNA purification) (light blue line), the 5% input sample (*i.e.*, no precipitation control) (red line), the Biotin-precipitated sample (black line) and the three G4 probes BioTASQ- (dark grey line), BioCyTASQ- (light grey line) and Clicked ^{az}MultiTASQ-precipitated (orange line) samples (top left), with a zoom on small Abs curves (top right). For the Raw Lysate and the others samples (Purified RNA), a dilution factor of 50 and 10, has been corrected here in Abs values, respectively. (**B**) Quality check of Raw lysate or Purified RNA (Biotin, BioTASQ, BioCyTASQ, Clicked ^{az}MultiTASQ, 5% input) samples by a 1% (v/v) bleach 1.5% (w/v) agarose denaturing TBE gel electrophoresis. Gels were revealed with SYBR™ Gold Nucleic Acid Gel Stain. RiboRuler High Range RNA Ladder was used as ladder. (**C-D**) Representative amplification (left) and dissociation curves (right) obtained after the qPCR analysis of the G4-RNAs (**C**) NRAS and (**D**) VEGFA enrichment from water (w/o cDNA sample control) (dark blue line), 5% input (red line), Biotin- (black line), G4-ligand BioTASQ- (dark grey line), BioCyTASQ- (light grey line) or Clicked ^{az}MultiTASQ-precipitated (orange line) purified RNA. (**E**) Summary of Ct (dR) values obtained with amplification curves (threshold fluorescence intensity= 34) and fold change (G4RP-RT-qPCR signal) calculated with.

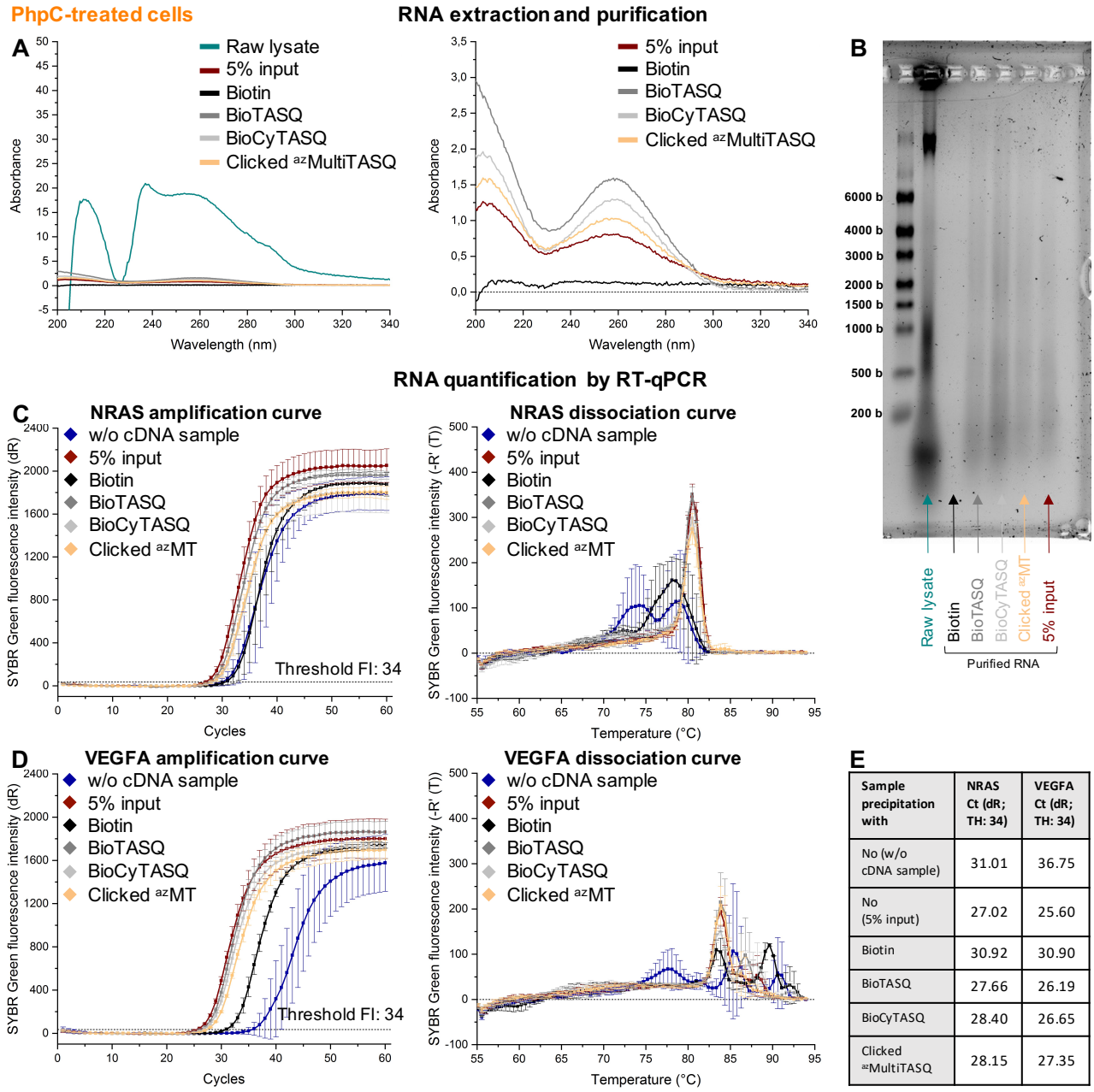

Sample precipitation with	NRAS Ct (dR; TH: 34)	VEGFA Ct (dR; TH: 34)
No (w/o cDNA sample)	31.01	36.75
No (5% input)	27.02	25.60
Biotin	30.92	30.90
BioTASQ	27.66	26.19
BioCyTASQ	28.40	26.65
Clicked azMultiTASQ	28.15	27.35

Figure S51. Monitoring data of the G4RP.v2 method performed with PhpC-treated cells. (**A**) Representative UV absorbance (Abs, A) curves of the Raw lysate (*i.e.*, supernatant recovered after cell lysis, without any precipitation or RNA purification) (light blue line), the 5% input sample (*i.e.*, no precipitation control) (red line), the Biotin-precipitated sample (black line) and the three G4 probes BioTASQ- (dark grey line), BioCyTASQ- (light grey line) and Clicked azMultiTASQ-precipitated (orange line) samples (top left), with a zoom on small Abs curves (top right). For the Raw Lysate and the others samples (Purified RNA), a dilution factor of 50 and 10, has been corrected here in Abs values, respectively. (**B**) Quality check of Raw Lysate or Purified RNA (Biotin, BioTASQ, BioCyTASQ, Clicked azMultiTASQ, 5% input) samples by a 1% (v/v) bleach 1.5% (w/v) agarose denaturing TBE gel electrophoresis. Gels were revealed with SYBR™ Gold Nucleic Acid Gel Stain. RiboRuler High Range RNA Ladder was used as ladder. (**C-D**) Representative amplification (left) and dissociation curves (right) obtained after the qPCR analysis of the G4-RNAs (**C**) NRAS and (**D**) VEGFA enrichment from water (w/o cDNA sample control) (dark blue line), 5% input (red line), Biotin- (black line), G4-ligand BioTASQ- (dark grey line), BioCyTASQ- (light grey line) or Clicked azMultiTASQ-precipitated (orange line) purified RNA. (**E**) Summary of Ct (dR) values obtained with amplification curves (threshold fluorescence intensity= 34) and fold change (G4RP-RT-qPCR signal) calculated with.

Condition	Sample precipitation with	Sample purity	$A_{230\ nm}$	$A_{260\ nm}$	$A_{270\ nm}$	$A_{280\ nm}$	R1= $A_{260\ nm}/A_{230\ nm}$	R2= $A_{260\ nm}/A_{270\ nm}$	R3= $A_{260\ nm}/A_{280\ nm}$	RNA estimated C. (in ng/µL)
Non-treated cells	No	Raw lysate	1.08	19.31	15.62	11.48	17.88	1.24	1.68	772.4
	No (5% input)	Purified RNA (+C)	0.93	0.93	0.79	0.58	1.00	1.18	1.60	37.2
	Biotin	Purified RNA (+C)	0.05	0.08	0.08	0.05	1.60	1.00	1.60	3.2
	BioTASQ	Purified RNA (+C)	0.81	1.45	1.16	0.74	1.79	1.25	1.96	58.0
	BioCyTASQ	Purified RNA (+C)	1.07	1.78	1.45	0.94	1.66	1.23	1.89	71.2
	Clicked ^{az}MultiTASQ	Purified RNA (+C)	0.65	1.00	0.82	0.54	1.54	1.22	1.85	40.0
BRACO-19-treated cells	No	Raw lysate	25.91	21.41	18.08	13.29	0.83	1.18	1.61	856.4
	No (5% input)	Purified RNA (+C)	0.61	0.81	0.67	0.49	1.33	1.21	1.65	32.4
	Biotin	Purified RNA (+C)	0.06	0.10	0.09	0.07	1.67	1.11	1.43	4.0
	BioTASQ	Purified RNA (+C)	0.82	1.39	1.14	0.76	1.70	1.22	1.83	55.6
	BioCyTASQ	Purified RNA (+C)	0.96	1.49	1.22	0.79	1.55	1.22	1.89	59.6
	Clicked ^{az}MultiTASQ	Purified RNA (+C)	0.57	0.88	0.72	0.48	1.54	1.22	1.83	35.2

Condition	Sample precipitation with	Sample purity	$A_{230\ nm}$	$A_{260\ nm}$	$A_{270\ nm}$	$A_{280\ nm}$	R1= $A_{260\ nm}/A_{230\ nm}$	R2= $A_{260\ nm}/A_{270\ nm}$	R3= $A_{260\ nm}/A_{280\ nm}$	RNA estimated C. (in ng/µL)
PhpC-treated cells	No	Raw lysate	4.80	18.40	14.77	10.76	3.83	1.25	1.71	736.0
	No (5% input)	Purified RNA (+C)	0.53	0.81	0.68	0.47	1.53	1.19	1.72	32.4
	Biotin	Purified RNA (+C)	0.07	0.14	0.12	0.11	2.00	1.17	1.27	5.6
	BioTASQ	Purified RNA (+C)	0.88	1.57	1.27	0.80	1.78	1.24	1.96	62.8
	BioCyTASQ	Purified RNA (+C)	0.58	1.30	1.04	0.67	2.24	1.25	1.94	52.0
	Clicked ^{az}MultiTASQ	Purified RNA (+C)	0.60	1.02	0.84	0.60	1.70	1.21	1.70	40.8

Table S29. Monitoring values of the application of the final G4RP.v2 method obtained by UV absorbance measurement. The summary of peak Abs (λ_A= 230, 260, 270 and 280 nm), quality ratios and estimated RNA concentration values can be found for all the G4RP.v2 final experiments (Non-treated, BRACO-19- and PhpC-treated cells conditions) and more precisely the following samples: Raw lysate (*i.e.*, supernatant recovered after cell lysis, without any precipitation or RNA purification), the 5% input sample (*i.e.*, no precipitation control), the Biotin-precipitated sample and the three G4 probes BioTASQ-, BioCyTASQ- and Clicked ^{az}MultiTASQ-precipitated samples. For the Raw Lysate and the others samples (Purified RNA), a dilution factor of 50 and 10, has been corrected here in Abs values, respectively.

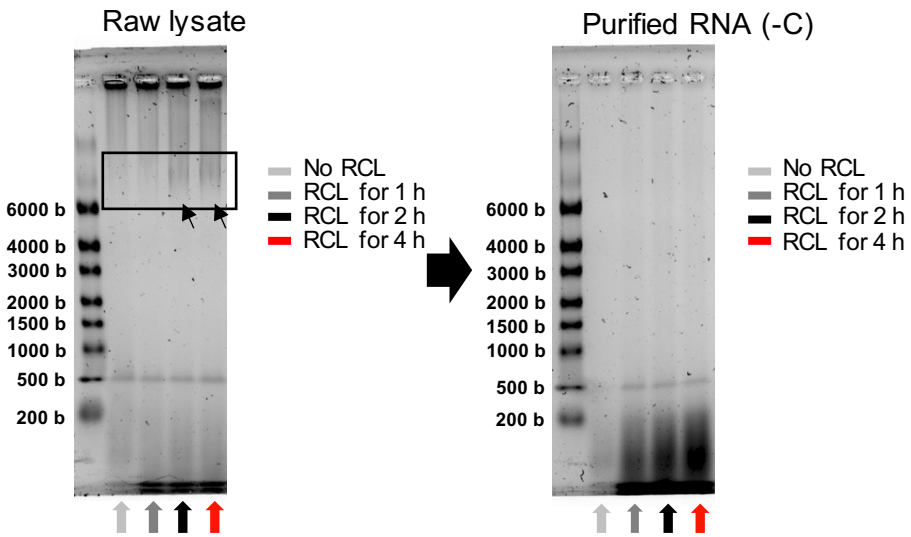

Figure S52. Representative gels of the parameters allowing the observation of the DNA band and the verification of the RNA purification step achievement. The > 6 000 bases DNA band (left) started to appear only after a reverse crosslinking of the biological material at 70 °C for 2 h and disappear from gel after the RNA purification (right). Gels were revelated with SYBR™ Gold Nucleic Acid Gel Stain. RiboRuler High Range RNA Ladder was used as ladder.

Alternative exp. n°	Condition	Sample precipitation with	Sample purity	$A_{230\,nm}$	$A_{260\,nm}$	$A_{270\,nm}$	$A_{280\,nm}$	R1= $A_{260\,nm}/A_{230\,nm}$	R2= $A_{260\,nm}/A_{270\,nm}$	R3= $A_{260\,nm}/A_{280\,nm}$	RNA estimated C. (in ng/µL)
a	Trypsinization + syringe lysis	No	Raw lysate	0.63	1.43	1.18	0.86	2.27	1.21	1.66	57.2
	Scraping + syringe lysis	No	Raw lysate	6.21	15.87	13.70	9.62	2.56	1.16	1.65	634.8
b-1	Douncer (50 dounces)	No	Raw lysate	17.65	8.22	6.85	5.29	0.47	1.2	1.55	328.8
	Douncer (50 dounces)	No	Wash 1	neg.	0.56	0.43	0.27	/	1.30	2.07	22.4
	Douncer (50 dounces)	No	Wash 2	neg.	0.70	0	neg.	/	/	/	28.0
	Douncer (50 dounces)	No	Wash 3	3.74	0.92	0.97	0.95	0.25	0.95	0.97	36.8
b-2	Douncer (50 dounces)	No	Raw lysate	13.67	7.43	6.23	4.71	0.54	1.19	1.58	297.2
	Douncer (50 dounces)	No	Wash	neg.	neg.	neg.	neg.	/	/	/	/
	Douncer (100 dounces)	No	Raw lysate	8.63	5.49	4.49	3.31	0.64	1.22	1.66	219.6
	Douncer (100 dounces)	No	Wash	0	0.49	0.42	0.45	/	1.17	1.09	19.6

Table S30. Monitoring values of the alternative lysis methods obtained by UV absorbance measurement. The summary of peak Abs (λ_A= 230, 260, 270 and 280 nm), quality ratios and estimated RNA concentration values can be found for all the experiment aiming to explore alternative lysis methods. Indeed, in addition to cell lysis by pipetting (50) with a needle-equipped syringe ("trypsinization + syringe lysis" condition, experiment a), alternative lysis methods were tried here: the cell lysis by cell scraping ("scraping + syringe lysis" condition, experiment a) or cell douncing (experiments b-1 and b-2). Exactly $3.3x10^6$, $19x10^6$ and $14x10^6$ cells were used for the a, b-1 and b-2 experiment, respectively. For the experiment a, the counting was done with the cells in culture flask (the "trypsinization + syringe lysis" condition) and I assumed I had the same for cells in the Petri dish (the "scraping + syringe lysis" condition). For all the samples a dilution factor of 50 has been corrected here in Abs values.

Primers		**Manual calculation**		**With ThermoFisher Tm Calculator**	
Name	Length (nt)	Melting temp.	PCR annealing temp.	Melting temp.	PCR annealing temp.
NRAS forward	23	66.0 °C	61.0 °C	60.0 °C	60.0 °C
NRAS reverse	23	68.0 °C	63.0 °C	59.9 °C	60.0 ° C
VEGFA forward	20	64.0 °C	59.0 °C	59.9 °C	59.9 °C
VEGFA reverse	20	64.0 °C	59.0 °C	61.2 °C	59.9 °C
	MEAN	65.5 °C	60.5 °C	60.3 °C	60.0 °C

Table S31. Summary of the melting and PCR annealing temperatures for the G4-RNAs NRAS and VEGFA primers couple. For manual calculation: Melting temperature (Tm)= [(4 °C per G/C) + (2 °C per A/T)]; PCR annealing temperature= Tm - 5 °C. For the use of the ThermoFisher Tm Calculator: the DNA polymerase option chose was the "DreamTaq DNA polymerase or other *Taq*-based DNA polymerase". Despite both manual and ThermoFisher automatic calculations, the PCR annealing (or hybridization) temperature should be around 60 °C.

Figure S53. Information about the target qPCR sequence for the G4-RNA NRAS quantification by RT-qPCR. The primers couple for the G4-RNA NRAS quantification by RT-qPCR was aligned with the *Homo sapiens* genome and transcriptome database with the Nucleotide BLAST tool of the NCBI website in order to find RNA sharing their sequences (the top 10 nucleotide sequence hits is shown) (top). Details of the first hit alignment with the primers couple is shown and give information about the location of these overlapping in the NRAS sequence (middle). The complete target qPCR sequence (or amplicon, after the qPCR) of NRAS is captioned with the primers couple location and Exon-Exon region (bottom).

A

Summary of the experimental condition	Experiment n° 1	Experiment n° 2	Experiment n° 3	Experiment n° 4	Experiment n° 5
Number of cells used	< $4x10^6$ cells	$10x10^6$ cells	$7x10^6$ cells	$12x10^6$ cells	$24x10^6$ cells
Lysis method	Sonication	Syringe (x50)	Syringe (x50)	Syringe (x100)	Syringe (x100)
Concentration of TASQ	95 µM	/	95 µM	95 µM	82 µM
Quantity of beads	96 µg	/	60 µg	46.7 µg	90 µg
Purification method	In-hand purif.	In-hand purif.	In-column purif.	In-column purif.	In-column purif.
Rev. Transcrip. method	Manual	Manual	Automated	Automated	Automated
Ct (dR; Threshold FI: 34)					
Precipitation with Biotin	32.02	/	29.72	30.50	32.34

B

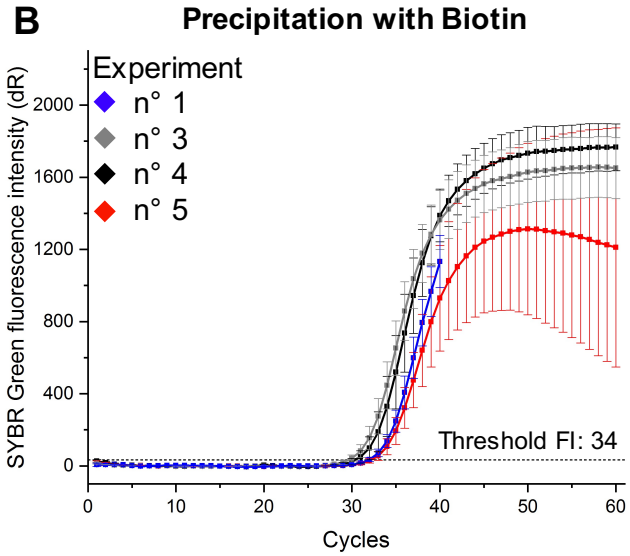

Figure S54. Additional monitoring of the RT-qPCR step improvement of the G4RP.v2 method. (**A**) During the G4RP.v2 method optimization, five experiments of RT-qPCR with Purified RNA samples were performed representing the progression of the method from non-successful to final experiments with G4 ligands treatment. Among all peculiar parameters discussed though this chapter, several parameters are compared here: the number of cells used, lysis method, concentration of TASQ, quantity of beads, purification method and the reverse transcription method. All the Ct values (fluorescence intensity threshold: 34) obtained from the RT-qPCR quantification of (**B**) precipitation with Biotin samples (control) are presented in the table.

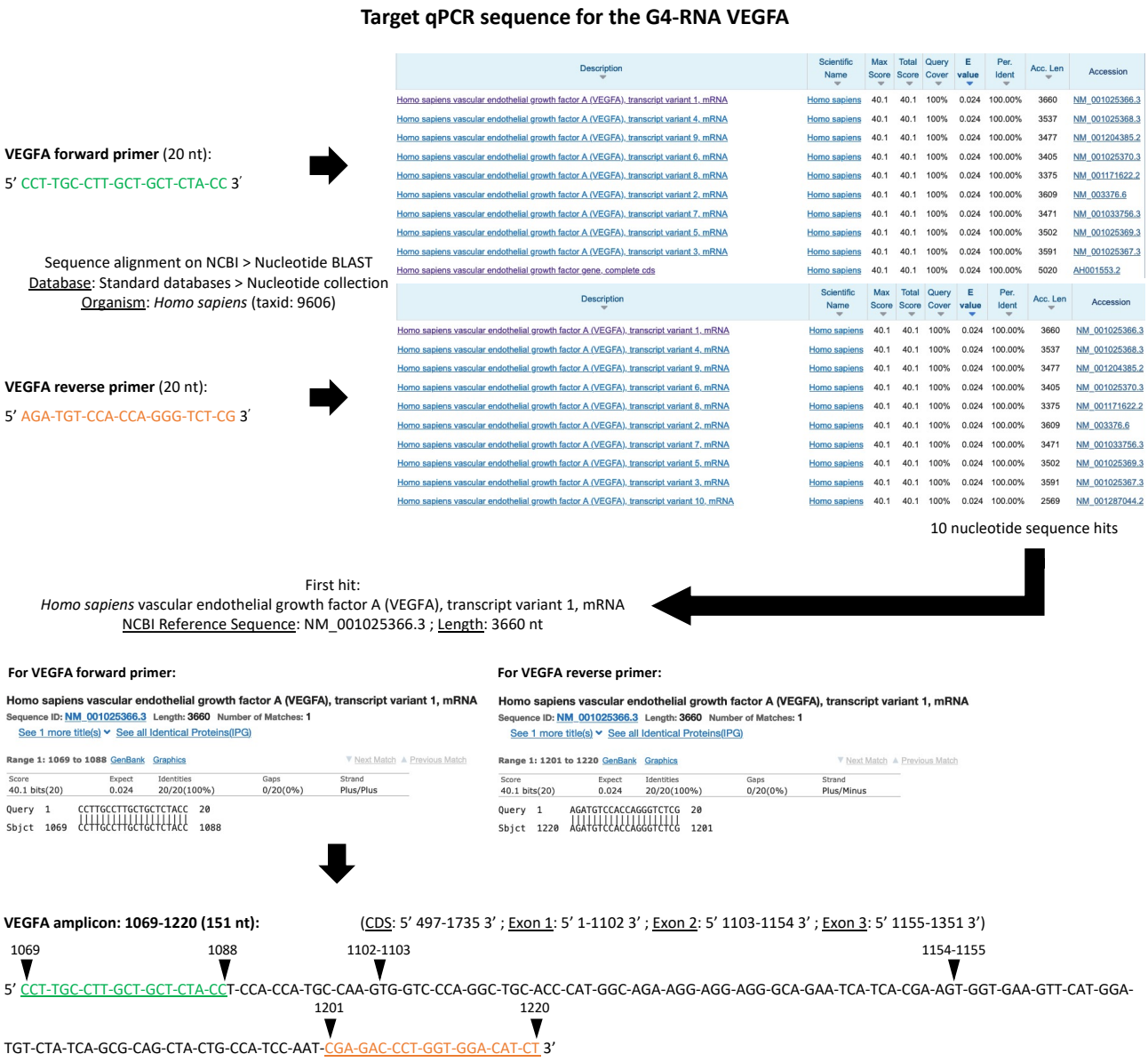

Figure S55. Information about the target qPCR sequence for the G4-RNA VEGFA quantification by RT-qPCR. The primers couple for the G4-RNA VEGFA quantification by RT-qPCR was aligned with the *Homo sapiens* genome and transcriptome database with the Nucleotide BLAST tool of the NCBI website in order to find RNA sharing their sequences (the top 10 nucleotide sequence hits is shown) (top). Details of the first hit alignment with the primers couple is shown and give information about the location of these overlapping in the VEGFA sequence (middle). The complete target qPCR sequence (or amplicon, after the qPCR) of VEGFA is captioned with the primers couple location and Exon-Exon region (bottom).

G4 ligand	5X Concentration (in µM)									
BRACO-19	0.25	5	25	50	75	100	150	250	500	1000
PhpC	0.5	10	62.5	125	250	500	1000	2000	3000	5000

Table S32. 5X Concentration range of G4 ligands used for the SRB assay. Sulforhodamine B (SRB) cytotoxicity assay was performed on MCF7 cells with the G4 ligands BRACO-19 and PhpC. The concentration range used for the SRB assay was established after a first SRB test using a wide concentration range. 5X G4 ligands concentrations were prepared in the helping microplate and 40 µL from that helping microplate were dispensed into the cell microplate (160 µL) for a 72 h incubation.

G4 ligand	Concentration (in µM)									
BRACO-19	0.05	1	5	10	15	20	30	50	100	200
PhpC	0.1	2	12.5	25	50	100	200	400	600	1000

Table S33. Concentration range of G4 ligands used for the SRB assay. Sulforhodamine B (SRB) cytotoxicity assay was performed on MCF7 cells with the G4 ligands BRACO-19 and PhpC. The concentration range used for the SRB assay was established after a first SRB test using a wide concentration range.

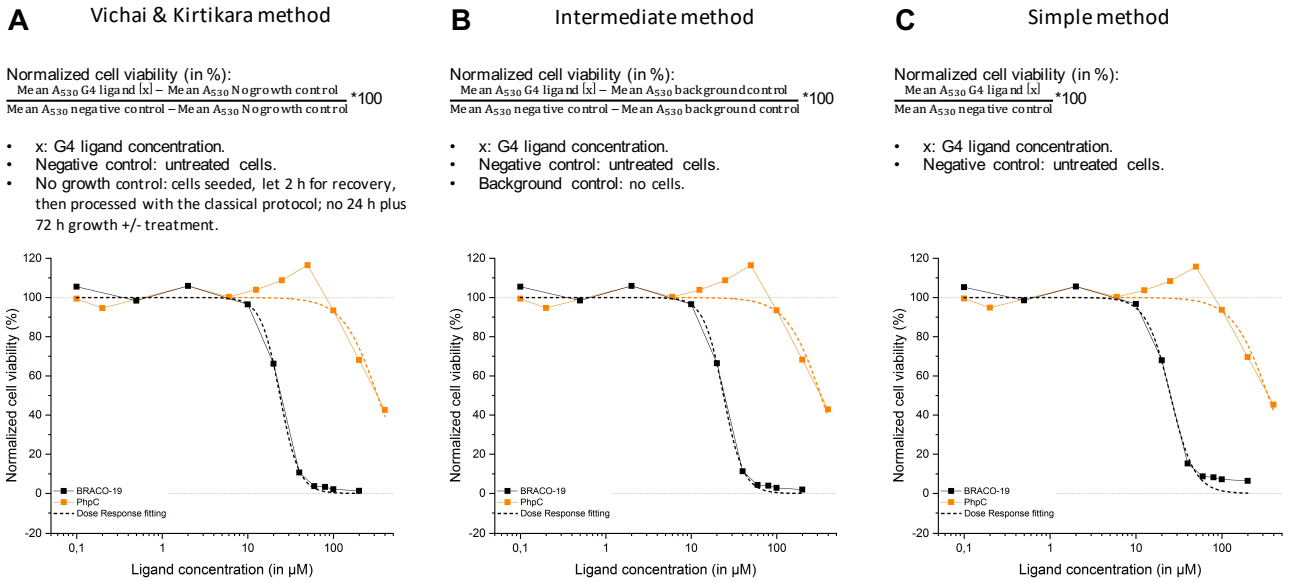

Figure S56. Comparison between three methods of SRB cytotoxicity assay and the calculation of the normalized cell viability. For the SRB cytotoxicity assay, a first assay was performed with $6x10^4$ cells in order to compare three method for cell viability calculation: (**A**) the Vichai & Kirtikara method, using the negative control (untreated cells) and the No growth control (cells seeded, let 2 h for recovery, then processed with the classical protocol; no 24h plus 72 h growth +/- treatment), (**B**) an intermediate method, using the negative control and the Background control (no cells) and (**C**) a simply method, using only the negative control. The three different formulas are shown on top of curves.

	Inhibitory concentration 50 (IC_{50}) (in µM)		
G4 ligand	**Vichai & Kirtikara method**	**Intermediate method**	**Simple method**
BRACO-19	23.7 ± 0.8	23.9 ± 0.8	25.2 ± 1.4
PhpC	327.0 ± 41.8	329.2 ± 42.2	344.2 ± 44.5

Table S34. Comparative summary of the inhibitory concentration 50 (IC_{50}) values calculated for the three methods of SRB cytotoxicity assay performed with the two G4 ligands BRACO-19 and PhpC. Three methods of sulforhodamine B (SRB) cytotoxicity assay were performed with $6x10^4$ cells MCF7 cells with the G4 ligands BRACO-19 and PhpC in order to compare them. The IC_{50} value, representing the ligand concentrations which allowed the inhibition of the cell viability of 50%, was calculated for the three methods.

G4RP.v2 experiment – Monitoring sheet

Experiment N°: ………….... Date: ……/……/…… Manipulator: ………………………………………..…………
Experimental condition: ……………………………..………………………………………………………………….

MAIN STEPS OF THE PROTOCOL DONE:
□ Cell treatment(s). □ Cell lysis. □ G4-precipitation. □ RNA purification.
□ Reverse transcription & qPCR quantification. □ UV absorbance measurement. □ Gel.

□ **STEP 1: CELL SEEDING & TREATMENT**
Cell type: ………………………… Cell Nb seeded: ………….. Treatment(s)? ……………….……………….
GROWTH **TREATMENT(S)**
START: Date: ……/……/…… Time: ………h……… START: Date: ……/……/…… Time: ………h………
END: Date: ……/……/…… Time: ………h……… END: Date: ……/……/…… Time: ………h………
Growth duration: ………h……… Treatment(s) duration: ………h………
Initial cell confluence/shape: ………………………..………………………………………………………….....
Final cell confluence/shape: …………………………………………………….…………….………………...

FRESH BUFFERS AND SOLUTION PREPARATION (+ other)
□ 1% (w/v) Formaldehyde/1X Fixing buffer. □ DEPC-PBS. □ 70% (v/v) ethanol.
□ G4RP lysis buffer. □ G4RP wash buffer. □ Centrifuge cooled down. □ Ice-filled box prepared.

□ **STEP 2-3: CELL CROSSLINKING – CELL LYSIS** ***(0-4 °C)***
Date: ……/……/…… Cell Nb used: …………… Fixation agent: ………… Lysis method: …………………

□ **STEP 4: G4-PRECIPITATION** ***(0-4 °C)***
Date: ……/……/…… G4-probe and control(s) used: ………………………………………………….………
Raw lysate supernatant vol.: …………… Probes concentration: ……………… Beads quantity: ……………
Start time: ………h……… End time: ………h……… Duration: ………h……… Temperature: ……………

□ **STEP 5: WASHING & REVERSE CROSSLINKING (RCL)** ***(0-4 °C)***
Date: ……/……/…… Nb of washing and buffers used to: ………………………………………………………
RCL: Start time: ………h……… End time: ………h……… Duration: ………h……… Temperature: ….…

□ **STEP 6: RNA PURIFICATION** ***(20-25 °C)***
Date: ……/……/…… Technique: ………………………………………………………………………………
TRIzol/chloroforme volume: …........... Top aqueous phase volume: ……..... DNAse I treatment? ……......

□ **STEP 7: REVERSE TRANSCRIPTION & qPCR QUANTIFICATION** ***(0-4 °C)***
Date: ……/……/…… Components of MM_A: □ Random hexamers. □ dNTP mix. □ Others? + □ RNA.
Components of MM_B: □ First strand buffer. □ DTT. □ RNase OUT. □ SSIII RT. □ Others?
Components of MM_C: □ Forward primer. □ Reverse primer. □ iTaq. □ Water. □ Others? + □ cDNA.
qPCR targets: ………………………………….................…… Nb of cycle: …….... Dissociation curve? ……...

□ **STEP A: UV ABSORBANCE MEASUREMENT** ***(0-4 °C)***
Date: ……/……/…… Buffer(s) used for baseline (raw/purified samples): ……………………/……………………
Raw: A_{230}= ………………… A_{260}= ………………… A_{270}= ………………… A_{280}= …………………
Purified: A_{230}= ………………… A_{260}= ………………… A_{270}= ………………… A_{280}= …………………
Contamination by organic compounds (R1= A_{260}/ A_{230}), TRIzol/chlorof. (R2= A_{260}/ A_{270}), proteins (R3= A_{260}/ A_{280}).
Estimated RNA conc. (ng/µL)= A_{260} * 40. Conc. obtained (raw/purified): ……………………/……………………

□ **STEP B: GEL ELECTROPHORESIS** ***(0-4 °C)***
Date: ……/……/…… □ Native/□ Denaturing gel. Buffer: ………………………… % agarose: ………………
Electrophoresis parameters: ……………………………………………………………………………………………
Electrophoresis: Start time: ………h……… End time: ………h……… Duration: ………h………
Revelation: Stain: …..………. Start time: ………h……… End time: ………h……… Duration: ……min…..

Did the samples have been frozen? (step, duration, T°C) ……..…………………………….………………….……

Problem(s) occurred? ………...…

FORMATION AND VALORIZATION

I. Courses followed (119 h)

- Introduction to histology, MOOC supervised by the University of Liège (Belgium) (25 h, **2020**)
- Research funding and valorization (6 h, **2020**)
- Industry organization and operation (7 h, **2020**)
- Intellectual property in scientific fields (7 h, **2021**)
- Introduction to consulting and contract research (12 h, **2020**)
- Introduction to research valorization and industrial transfer agreement (6 h, **2021**)
- Data analysis and statistics modelling (12 h, **2021**)
- Diagnostic strategies for cancers, MOOC supervised by the University of Paris (France) (22 h, **2021**)
- Scientific integrity in Research (12 h, **2022**)
- Critical ability and fallacious behaviors, MOOC supervised by the University of Cergy Paris (France) (10 h, **2022**)

II. Courses supervised (74 h)

Seminar

- General organic chemistry: nomenclature and stereochemistry (10 h, **2020**)

Practical work

- *Drosophila* genetics: hybridization analysis (10 h, **2020**)
- *Tenebrio* genomic DNA extraction and electrophoresis analysis (12 h, **2021**)
- Plasmid cloning and bacteria transformation (12 h, **2021**)
- Study of *nucleus* and mitosis in plants (30 h, **2021**)

III. Communications performed

Oral presentation

- *The Young Researchers Meeting 2021 of GDR RNA (GDR2083)* (online congress) (**2nd of June 2021**)
- XXII^{èmes} Journée de l'Ecole Doctorale (JED) Carnot-Pasteur (**30th of June 2023**)

Poster presentation

- *8th International Meeting on Quadruplex Nucleic Acids* (Marienbad, Czech Republic) (**27th of June – 1st of July 2022**) (Best Poster Presentation Award)
- *3rd PSL Chemical Biology Symposium* (Paris, France) (**12th – 13th of January 2023**)
- *3èmes Journées du GDR ChemBio* (Strasbourg, France) (**8th – 9th of June 2023**)

Figure S57. Best Poster Presentation award won at the 8th International Meeting on Quadruplex Nucleic Acids (G4thering) at Mariánske Lazné (Czech Republic) (2022/06/30). This award was shared with two others PhD students presented at this international congress.

IV. Publications

- Lejault Pauline, Mitteaux Jérémie, Rota Sperti Francesco and Monchaud David, *Cell Chem. Biol.* **2021**, *28* (4), 436-455
- Tabor Natalie, Ngwa Conelius, Mitteaux Jérémie, Meyer Matthew D., Moruno-Manchon Jose, Zhu Liang, Liu F., Monchaud David, McCullough Louise D. and Tsvetkov Andrey S., *Aging* **2021**, *13* (12), 15917-15941
- Mitteaux Jérémie, Lejault Pauline, Wojciechowski Filip, Joubert Alexandra, Boudon Julien, Desbois Nicolas, Gros Claude P., Hudson Robert H. E., Boulé Jean-Baptiste, Granzhan Anton and Monchaud David, *J. Am. Chem. Soc.* **2021**, *143* (32), 12567-12577
- Rota Sperti Francesco, Dupouy Baptiste, Mitteaux Jérémie, Pipier Angélique, Pirrotta Marc, Chéron Nicolas, Valverde Ibai E. and Monchaud David, *JACS Au* **2022**, *2* (7), 1588-1595
- Rota Sperti Francesco, Mitteaux Jérémie, Zell Joanna, Pipier Angélique, Valverde Ibai E. and Monchaud David, *RSC Chem. Biol.* **2023**, *4* (7), 456-465
- Turcotte Marc-Antoine, Bolduc François, Vannutelli Anaïs, Mitteaux Jérémie, Monchaud David and Perreault Jean-Pierre, *Biochimie* **2023**, *214* (Pt A), 24-32
- Mitteaux Jérémie, Raevens Sandy, Zi Wang, Pirrotta Marc, Valverde Ibai E., Hudson Robert H. E. and Monchaud David, *Chem. Commun. (Camb)* **2024**, *60* (4), 424-427

MATERIALS AND METHODS

I. Oligonucleotides (ONs)

Name	Nature	Length (in nucleotide)	Sequence	Experiment	Refer-ence
Dabcyl-labelled 49-nt ON	DNA	49	d[5′AAAAAAAAAAAGGGTTAGGGTTAGGGTTAGGGTATTCCGTTGAGCAGAG3′]-dabcyl	G4-UNFOLD and hPIF1 helicase assays	2
FAM-labelled 15-nt ON	DNA	15	FAM-d[5′CTCTGCTCAACGGAA3′]		
c-hTelo	DNA	49	d[5′CTCTGCTCAACGGAATACCCTAACCCTAACCCTAACCCTTTTTTTTTTT3′]		
Trap	DNA	15	d[5′TTCCGTTGAGCAGAG3′]	hPIF1 helicase	2
F21T	DNA	21	FAM-d[5′GGGTTAGGGTTAGGGTTAGGG3′]-TAMRA	FRET-melting assay	3
F-*c-KIT2*-T	DNA	21	FAM-d[5′CGGGCGGGCGCGAGGGAGGGG3′]-TAMRA		4
F-*c-MYC*-T	DNA	22	FAM-d[5′GAGGGTGGGGAGGGTGGGGAAG3′]-TAMRA		5
hTelo	DNA	22	d[5′AGGGTTAGGGTTAGGGTTAGGG3′]	CD/UV-Vis and fluorescence titrations, PAGE analyses, DLS investigations	6
(*S. pombe*) G4-strand	DNA	97	d[5′TAGCCATTCAGCCGTAACAGGCAGTGGAAGAGAGACAGACAGGGCAGGGCAGGGCAGGGCAGTACAGTAGAACCTAATGGTGTTTGATGGTATCTAA3′]	qPCR Stop assay with *S. pombe* G4	This thesis 7
(*S. pombe*) Non G4-strand	DNA	97	d[5′TTAGATACCATCAAACACCATTAGGTTCTACTGTACTGCCCTGCCCTGCCCTGCCCTGTCTGTCTCTCTTCCACTGCCTGTTACGGCTGAATGGCTA3′]		
G4-1 Reverse	DNA	25	d[5′TTAGATACCATCAAACACCATTAGG3′]		8
G4-1 Forward	DNA	20	d[5′TAGCCATTCAGCCGTAACAG3′]		
hTelo qSa	DNA	100	d[5′TAGCCATTCAGCCGTAACAGGCAGTGGAAGAGAGACAGACAGGGTTAGGGTTAGGGTTAGGGCAGTACAGTAGAACCTAATGGTGTTTGATGGTATCTAA3′]	qPCR Stop assay with *H. sapiens* G4s	This thesis
c-MYC qSa	DNA	101	d[5′TAGCCATTCAGCCGTAACAGGCAGTGGAAGAGAGACAGACAGAGGGTGGGGAGGGTGGGGAAGCAGTACAGTAGAACCTAATGGTGTTTGATGGTATCTAA3′]		
c-KIT2 qSa	DNA	100	d[5′TAGCCATTCAGCCGTAACAGGCAGTGGAAGAGAGACAGACACGGGCGGGCGCGAGGGAGGGGCAGTACAGTAGAACCTAATGGTGTTTGATGGTATCTAA3′]		
Sc hTelo qSa	DNA	100	d[5′TAGCCATTCAGCCGTAACAGGCAGTGGAAGAGAGACAGACAGAGTTAGTGTTAGAGTT		

			AGTGCAGTACAGTAGAACCTAATGGTGTTT GATGGTATCTAA$^{3'}$]		
Sc *c-MYC* qSa	DNA	101	d[$^{5'}$TAGCCATTCAGCCGTAACAGGCAGTGGA AGAGAGACAGACAGAGTGTGAGTAGAGTG AGTAAGCAGTACAGTAGAACCTAATGGTGT TTGATGGTATCTAA$^{3'}$]		
Sc *c-KIT2* qSa	DNA	100	d[$^{5'}$TAGCCATTCAGCCGTAACAGGCAGTGGA AGAGAGACAGACACGTGCGAGCGCGAGTG AGAGTCAGTACAGTAGAACCTAATGGTGTT TGATGGTATCTAA$^{3'}$]		
$^{5'}$Cy5-*NRAS*	RNA	18	Cy5-r[$^{5'}$GGGAGGGGCGGGUCUGGG$^{3'}$]	Fluorescence quenching assay	This thesis
F-*NRAS*-T	RNA	18	FAM-r[$^{5'}$GGGAGGGGCGGGUCUGGG$^{3'}$]-TAMRA	Competitive FRET-melting	This thesis
NRAS forward primer	DNA	23	d[$^{5'}$ATGACTGAGTACAAACTGGTGGT$^{3'}$]	G4RP.v2	[9]
NRAS reverse primer	DNA	23	d[$^{5'}$CATGTATTGGTCTCTCATGGCAC$^{3'}$]		
VEGFA forward primer	DNA	20	d[$^{5'}$CCTTGCCTTGCTGCTCTACC$^{3'}$]		
VEGFA reverse primer	DNA	20	d[$^{5'}$AGATGTCCACCAGGGTCTCG$^{3'}$]		

Table Mat&Meth 1. List of ONs used for the different Chapters experiments. All ONs used here were purchased from Eurogentec (Seraing, Belgium). The G4-1 reverse primer is usable with the G4-strand, hTelo qSa, *c-MYC* qSa, *c-KIT2* qSa, Sc hTelo qSa, Sc *c-MYC* qSa and Sc *c-KIT2* qSa, while the G4-1 forward primer is usable with the Non G4-strand. Cy5 (($\lambda_{exc\ max}$= 651 nm; $\lambda_{em\ max}$= 670 nm). Dabcyl: dabcyl succinimidyl ester ($\lambda_{abs\ max}$= 452 nm; no emission). FAM: 6-carboxyfluorescein ($\lambda_{exc\ max}$= 498 nm; $\lambda_{em\ max}$= 517 nm). TAMRA: 5-carboxytetramethylrhodamine ($\lambda_{exc\ max}$= 552 nm; $\lambda_{em\ max}$= 576 nm). qSa= qPCR Stop assay.

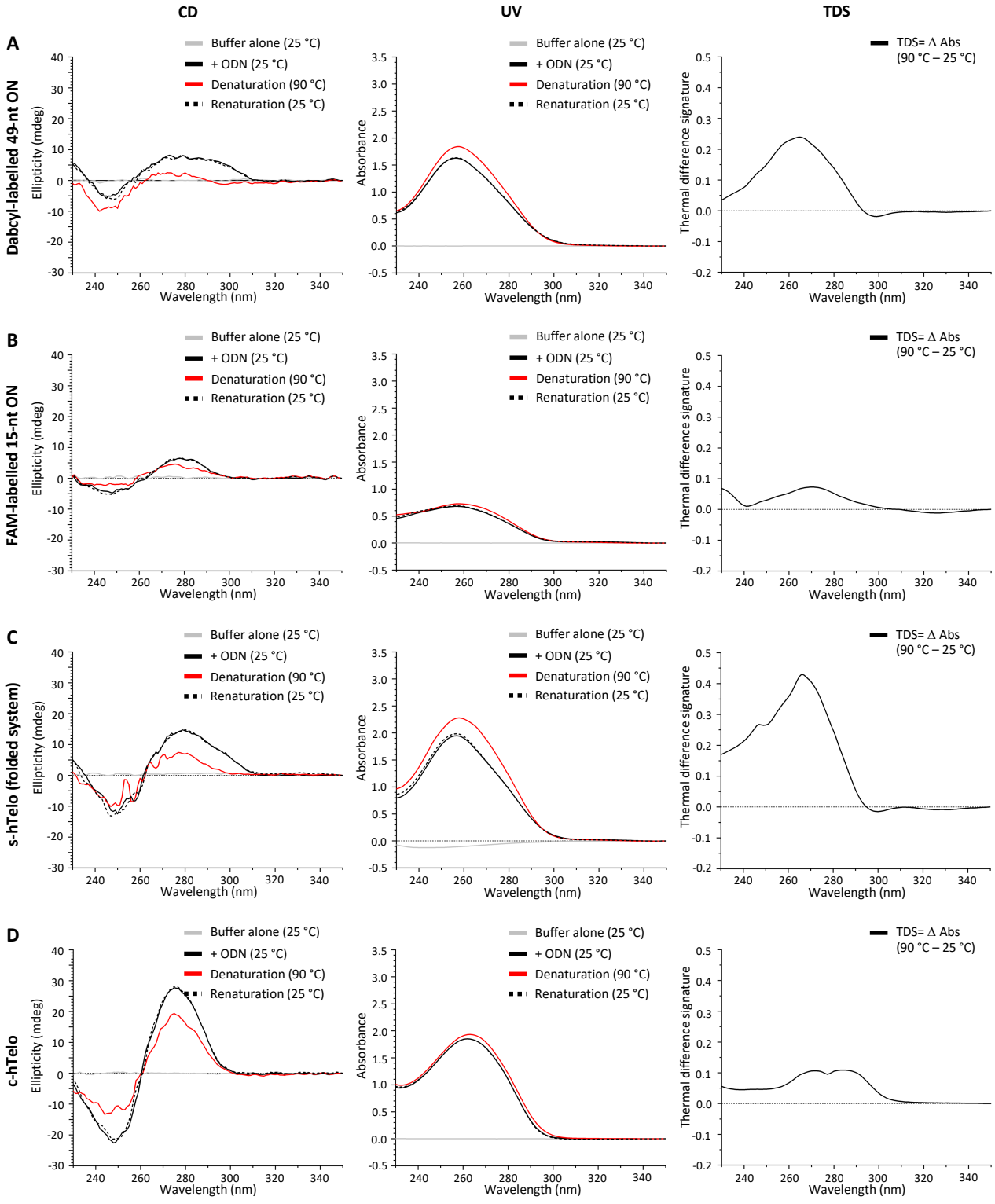

Figure Mat&Meth 1. *In vitro* structural characterization of ONs used for the different Chapters experiments (Part 1/4). The *in vitro* characterization of ONs was performed without (grey line) or with (3 µM) the (**A**) dabcyl-labelled 49-nt ON, (**B**) FAM-labelled 15-nt ON, (**C**) s-hTelo (folded system) or (**D**) c-hTelo at 25 °C (black solid line), then during denaturation (at 90 °C for 5 min, red line) and renaturation (return to 25 °C, black dashed line). 300 µL of mineral oil were added on top of the 100 µL of ON to avoid evaporation. Measures were performed in the preparation buffer of ONs: Tris-HCl buffer 1 (for ONs used in G4-UNFOLD and hPIF1 helicase assays). CD and UV spectra were recorded between 210-350 nm and the thermal difference signature (TDS) spectra were calculated as follow: TDS spectrum= UV spectrum at 90 °C (step 3) – UV spectrum at 25 °C (step 2). ODN= oligodesoxyribonucleotide.

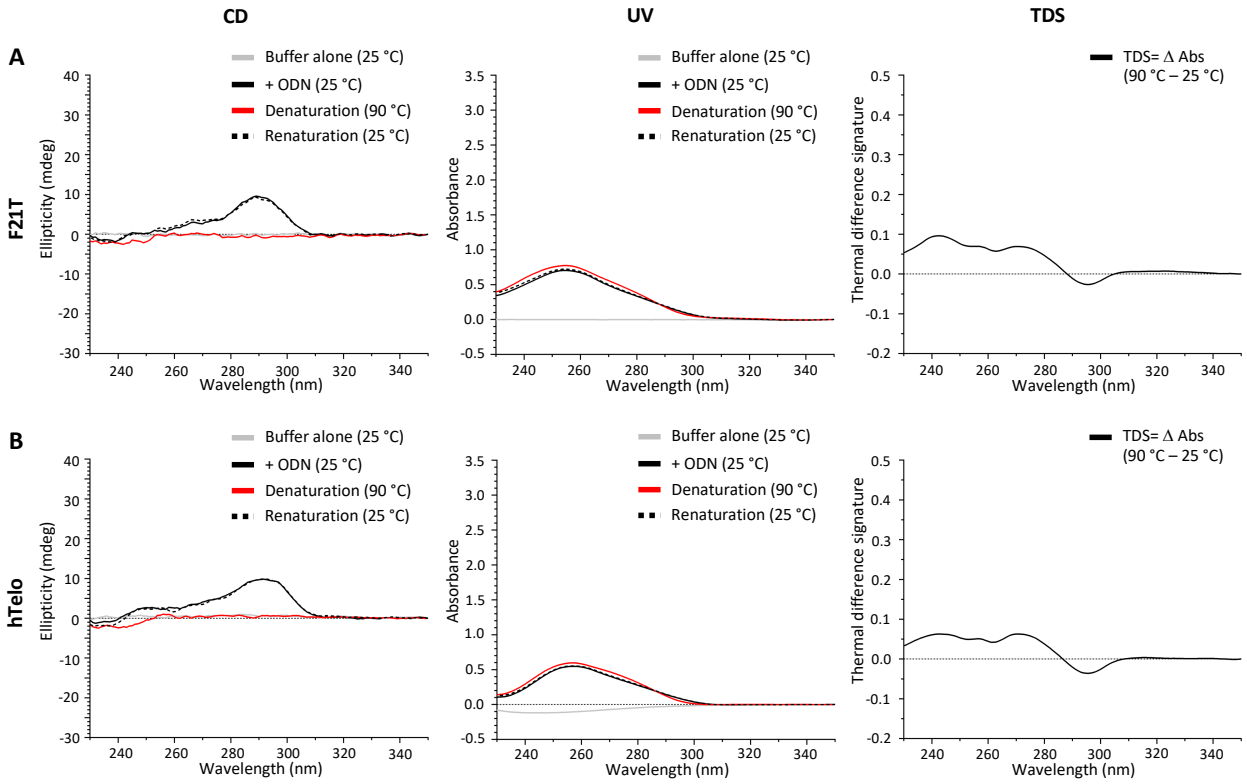

Figure Mat&Meth 2. *In vitro* structural characterization of ONs used for the different Chapters experiments (Part 2/4). The *in vitro* characterization of ONs was performed without (grey line) or with (3 µM) the (**A**) F21T or (**B**) hTelo at 25 °C (black solid line), then during denaturation (at 90 °C for 5 min, red line) and renaturation (return to 25 °C, black dashed line). 300 µL of mineral oil were added on top of the 100 µL of ON to avoid evaporation. Measures were performed in the preparation buffer of ONs: CacoK10 buffer (for ONs used in FRET-melting assay, CD/UV-Vis and fluorescence titrations, PAGE analyses and DLS investigations). CD and UV spectra were recorded between 210-350 nm and the thermal difference signature (TDS) spectra were calculated as follow: TDS spectrum= UV spectrum at 90 °C (step 3) – UV spectrum at 25 °C (step 2). ODN= oligodesoxyribonucleotide.

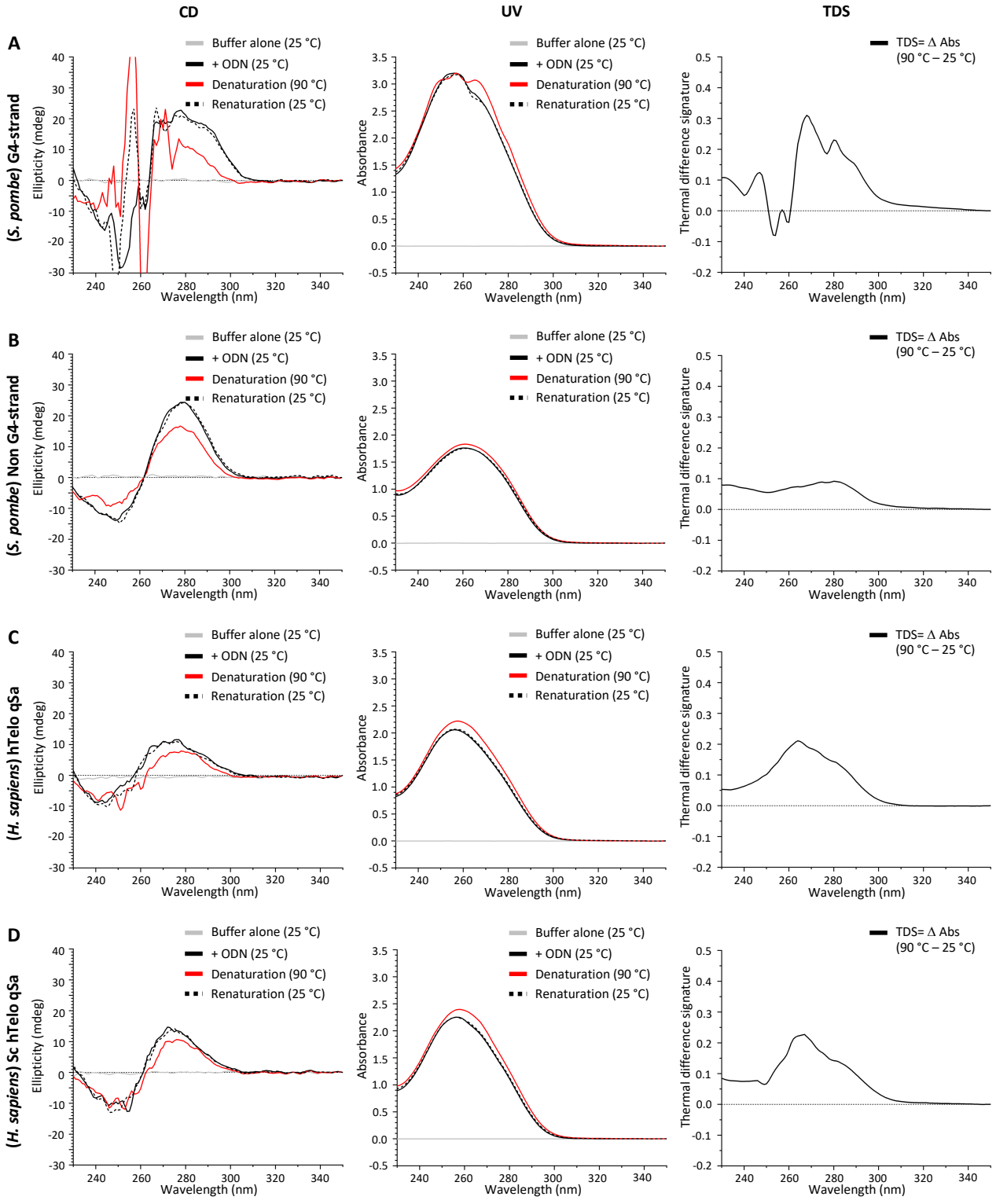

Figure Mat&Meth 3. *In vitro* structural characterization of ONs used for the different Chapters experiments (Part 3/4). The *in vitro* characterization of ONs was performed without (grey line) or with (3 µM) the (**A**) *S. pombe* G4-strand, (**B**) *S. pombe* Non G4-strand (**C**) *H. sapiens* hTelo qSa or (**D**) *H. sapiens* Sc hTelo qSa at 25 °C (black solid line), then during denaturation (at 90 °C for 5 min, red line) and renaturation (return to 25 °C, black dashed line). 300 µL of mineral oil were added on top of the 100 µL of ON to avoid evaporation. Measures were performed in the preparation buffer of ONs: 10 mM KCl (for ONs used in qPCR Stop assays). CD and UV spectra were recorded between 210-350 nm and the thermal difference signature (TDS) spectra were calculated as follow: TDS spectrum= UV spectrum at 90 °C (step 3) – UV spectrum at 25 °C (step 2). ODN= oligodesoxyribonucleotide.

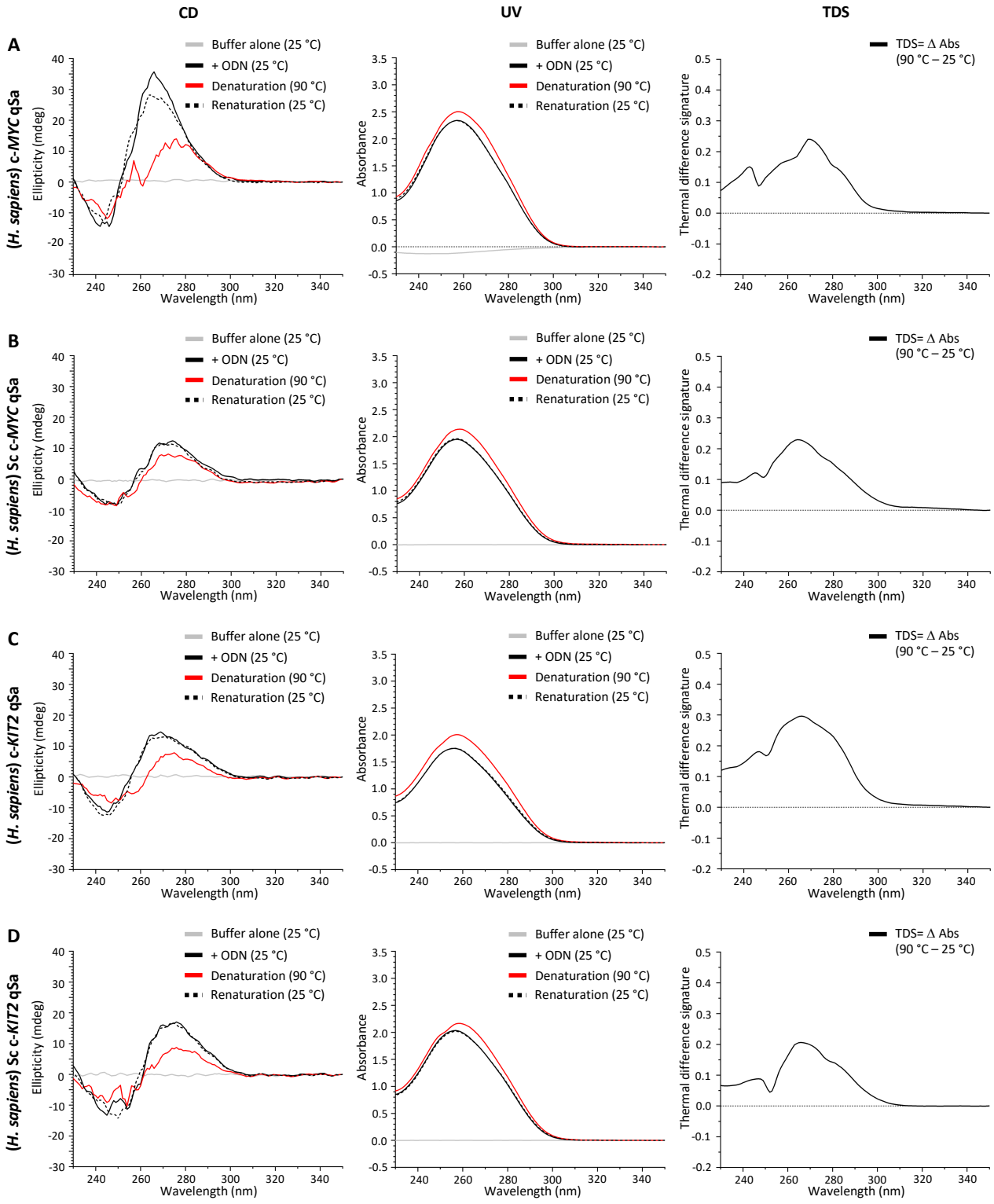

Figure Mat&Meth 4. *In vitro* structural characterization of ONs used for the different Chapters experiments (Part 4/4). The *in vitro* characterization of ONs was performed without (grey line) or with (3 µM) the (**A**) *H. sapiens* c-*MYC* qSa, (**B**) *H. sapiens* Sc c-*MYC* qSa (**C**) *H. sapiens* c-*KIT2* qSa or (**D**) *H. sapiens* Sc c-*KIT2* qSa at 25 °C (black solid line), then during denaturation (at 90 °C for 5 min, red line) and renaturation (return to 25 °C, black dashed line). 300 µL of mineral oil were added on top of the 100 µL of ON to avoid evaporation. Measures were performed in the preparation buffer of ONs: 10 mM KCl (for ONs used in qPCR Stop assays). CD and UV spectra were recorded between 210-350 nm and the thermal difference signature (TDS) spectra were calculated as follow: TDS spectrum= UV spectrum at 90 °C (step 3) – UV spectrum at 25 °C (step 2). ODN= oligodesoxyribonucleotide.

	Specific nucleic acids structures			
	CD signature peaks		TDS signature peaks	
	Positive band(s)	Negative band(s)	Positive band(s)	Negative band(s)
G-quadruplex (parallel/I)	260	240	243 (+/-), 273	295
G-quadruplex (hybrid/II)	260, 290	240		
G-quadruplex (anti-parallel/III)	240, 290	260		
i-Motif	288	260	239	295
Random coil	220, 273	250	/	/

Table Mat&Meth 2. Theoretical CD and TDS signatures of nucleic acids structures. The G-quadruplexes (parallel, hybrid, anti-parallel),[10,11] i-Motif[12,13] and random coils[12,13] structures possess atypical CD and TDS spectra with their positive(s) and/or negative(s) signature peaks.

	Oligonucleotides (ONs) studied *in vitro*				
	CD signature peaks		TDS signature peaks		Determined structure *in vitro* (CD/TDS):
	Positive band(s) (nm)	Negative band(s) (nm)	Positive band(s) (nm)	Negative band(s) (nm)	
ONs for the G4-UNFOLD assay					
Dabcyl-labelled 49-nt ON	276, 292	246	246, 265, 280	298	G4 hybrid and others **/** G4 and others
FAM-labelled 15-nt ON	280	247	271	325	Others **/** G4 and/or others
s-hTelo (folded system)	266, 279, 298	249	247, 266	299, 329	G4 hybrid and others **/** G4 and others
c-hTelo	276	248	271, 285	/	Random coil and others **/** G4 and/or others
ONs for the FRET-melting assay, CD/UV-Vis and fluorescence titrations, PAGE analysis, DLS investigations					
F21T	267, 290	237	242, 258, 272, 320	295	G4 hybrid **/** G4 hybrid and others
hTelo	250, 292	235	244, 257, 271, 315	295	G4 hybrid **/** G4 hybrid and others
ONs for the qPCR Stop assay					
(*S. pombe*) G4-strand	267, 278, 289	243, 251, 262	231, 247, 268, 281, 289	253, 260	G4 hybrid, random coil and others **/** G4 and others
(*S. pombe*) Non G4-strand	272, 279	249	282	/	Random coil and others **/** Others
(*H. sapiens*) hTelo qSa	273, 288	242	264, 272, 281	/	G4 hybrid and others **/** G4 and/or others
(*H. sapiens*) c-*MYC* qSa	254, 266	244	243, 257, 270, 282	/	G4 parallel and others **/** G4 and others
H. sapiens) c-*KIT2* qSa	269, 282	245	234, 246, 257, 266, 279	/	G4 and others **/** G4 and/or others
(*H. sapiens*) Sc hTelo qSa	274	248	246, 256, 266, 275, 282	/	Random coil **/** G4 and/or others
(*H. sapiens*) Sc c-*MYC* qSa	272	247	233, 245, 254, 264, 279	/	Random coil **/** G4 and/or others
H. sapiens) Sc c-*KIT2* qSa	274	249	247, 257, 266, 282	/	Random coil **/** G4 and/or others

Table Mat&Meth 3. Assignation of *in vitro* structure of ONs used for the different Chapters experiments. After obtaining the experimental CD and TDS spectra of ONs, their positive(s) and/or negative(s) signature peaks allowed their structural characterization.

II. Small molecules preparation for Chapter I

CRITICAL: Reagents and equipment can be obtained from various vendors and do not need to be from the ones specified here.

1. MATERIALS – Reagents

Chemical products and/or buffer components

- DMSO (Sigma-Aldrich, cat. n° D8418)

Molecular tools

- **1,5-BisNPO** (macrocyclic 1,5-bis-naphthalene) (produced in Anton Granzhan'lab, « Structure et Instabilité des Génomes », Paris, France).

- **2,6-BisNPO** (macrocyclic 2,6-bis-naphthalene) (produced in Anton Granzhan'lab, « Structure et Instabilité des Génomes », Paris, France).

- **2,7-BisNPN** (macrocyclic 2,7-bis-naphthalene) (produced in Anton Granzhan'lab, « Structure et Instabilité des Génomes », Paris, France).

- **BRACO-19** (N,N'-(9-(4-(dimethylamino)phenylamino)acridine-3,6-diyl)bis(3-(pyrrolidin-1-yl)propanamide)) (Sigma-Aldrich, cat. n° SML0560).

- **guaPhpC** (2-(6-(3-(2-(bis(tert-butyloxycarbonyl)methyleneamino)ethoxy)phenyl)pyrrolocytosin-1-yl)acetic acid) (produced by Filip Wojciechowski in Robert H. E. Hudson's lab, Department of Chemistry of The University of Western Ontario, Ontario, Canada).

- **PDS** (4-(2-Aminoethoxy)-N2,N6-bis(4-(2-aminoethoxy)quinolin-2-yl)pyridine-2,6-dicarboxamide hydrochloride) (Sigma-Aldrich, cat. n° SML2690).

- **Phen-DC$_3$** (3,3'-[1,10-Phenanthroline-2,9-diylbis(carbonylimino)]bis[1-methylquinolinium] 1,1,1-trifluoromethanesulfonate (1:2)) (Sigma-Aldrich, cat. n° SML2298).

- **PhpC** (ethyl 2-(6-(3-(2-(tert-butyloxycarbonylamino)ethoxy)phenyl)pyrrolocytosin-1-yl)acetate) (produced by Filip Wojciechowski in Robert H. E. Hudson's lab, Department of Chemistry of The University of Western Ontario, Ontario, Canada).

- **PhpC derivatives n° 1-3**: 1. (6-phenylpyrrolopyrimidin-3-yl)acetic acid, 2. ethyl 6-(2,6-(di(oxyethylaminum)phenyl)pyrrolocytosin-3-yl)acetate bis(trifluoroacetate) salt, 3. ethyl 6-(3-(oxyethylaminum)imidazolocytosin-3-yl)acetate trifluoroacetate salt (produced by Zi Wang in Robert H. E. Hudson's lab, Department of Chemistry of The University of Western Ontario, Ontario, Canada).

- **TArPS** (5,10,15,20-tetrakis[3-sulfonato-4-O-[2-[2-(2-methoxy)ethoxy]ethoxy]ethylphenyl]-21H,23H-porphyrin) (produced in lab by Nicolas Desbois & Claude P. Gros).

- **TEGP** (5,10,15,20-tetrakis-[4-(2-(2-(2-methoxy)-ethoxy)-ethoxy)-ethyl]-21H,23H-porphyrin) (produced in lab by Nicolas Desbois & Claude P. Gros).

- **TEGPy** (5,10,15,20-tetrakis-[N-(2-(2-(2-methoxy)-ethoxy)-ethoxy)-ethyl-4-pyridyl]-21H,23H-porphyrin) (produced in lab by Nicolas Desbois & Claude P. Gros).

- **Terpy** (produced in lab by Pauline Lejault).

- **TMPyP4** (5,10,15,20-tetrakis-[N-methyl-4-pyridyl]-21H,23H-porphyrin) (produced in lab by Nicolas Desbois & Claude P. Gros).

- **TPPS** (5,10,15,20-tetrakis[4-sulfonatophenyl]-21H,23H-porphyrin) (produced in lab by Nicolas Desbois & Claude P. Gros).

2. MATERIALS – Equipment

Devices and lab equipment

- Benchtop vortex (vendor of choice)
- Pipettes, single-channel (*e.g.* Finnpipette from Thermo Scientific, Nichipet EX-Plus II from Nichiryo)
- Tube rack (vendor of choice)
- Water purification system (PURELAB flex 3, ELGA LabWater, cat. n° PF3XXXXM1)

Consumables

- Filter tips, non-sterile (*e.g.* ClearLine, Fisherbrand SureOne, TipOne)
- Microtubes, with snap cap, DNase/RNase-free, non-sterile (1.5, 2, 5 mL) (*e.g.* ClearLine, Eppendorf)

Individual protection equipment

- Lab coat (vendor of choice)
- Nitrile gloves (*e.g.* Kimtech)

- Safety glasses (vendor of choice)

Waste management equipment

- Bin for biohazard and chemical hazard liquid waste
- Bin for biohazard and chemical hazard solid waste

(See the existing legislation in the country of use)

3. MATERIALS – Buffers and solutions preparation

For buffers and solutions preparation, I used UV-treated PURELAB ultrapure (type 1) water.

- **1 mM 1,5-BisNPO** (in ultrapure water)

  e.g. dissolve 0.66 mg of 1,5-BisNPO (M= 658.53 g/mol) in ultrapure water (*q.s.* 1 mL). Store at 4 °C.

- **1 mM 2,6-BisNPO** (in ultrapure water)

  e.g. dissolve 0.66 mg of 2,6-BisNPO (M= 658.53 g/mol) in ultrapure water (*q.s.* 1 mL). Store at 4 °C.

- **1 mM 2,7-BisNPN** (in ultrapure water)

  e.g. dissolve 0.73 mg of 2,7-BisNPN (M= 729.48 g/mol) in ultrapure water (*q.s.* 1 mL). Store at 4 °C.

- **1 mM BRACO-19** (in DMSO)

  e.g. dissolve 0.59 mg of BRACO-19 (M= 593.76 g/mol) in 1 mL of DMSO (*q.s.* ~ 1 mL). Store at 4 °C.

- **1 mM guaPhpC** (in ultrapure water)

  e.g. dissolve 0.40 mg of guaPhpC (M= 397.41 g/mol) in ultrapure water (*q.s.* 1 mL). Store at 4 °C.

- **1 mM PDS** (in DMSO)

  e.g. dissolve 0.60 mg of PDS (M= 596.64 g/mol) in DMSO (*q.s.* 1 mL). Store at 4 °C.

- **1 mM Phen-DC_3** (in ultrapure water)

  e.g. dissolve 0.85 mg of Phen-DC_3 (M= 848.75 g/mol) in ultrapure water (*q.s.* 1 mL). Store at 4 °C.

- **1 mM PhpC** (in ultrapure water)

  e.g. dissolve 0.36 mg of PhpC (M= 356.37 g/mol) in ultrapure water (*q.s.* 1 mL). Store at 4 °C.

- **1 mM PhpC derivative n° 1** (in ultrapure water)

e.g. dissolve 0.27 mg of PhpC derivative 1 (M= 269.26 g/mol) in ultrapure water (*q.s.* 1 mL). Store at 4 °C.

- **1 mM PhpC derivative n° 2** (in ultrapure water)
  e.g. dissolve 0.64 mg of PhpC derivative 2 (M= 643.50 g/mol) in ultrapure water (*q.s.* 1 mL). Store at 4 °C.

- **1 mM PhpC derivative n° 3** (in ultrapure water)
  e.g. dissolve 0.47 mg of PhpC derivative 3 (M= 471.39 g/mol) in ultrapure water (*q.s.* 1 mL). Store at 4 °C.

- **1 mM TArPS** (in ultrapure water)
  e.g. dissolve 1.58 mg of TArPS (M= 1583.72 g/mol) in DMSO (*q.s.* 1 mL). Store at 4 °C.

- **1 mM TEGP** (in DMSO)
  e.g. dissolve 1.26 mg of TEGP (M= 1263.49 g/mol) in DMSO (*q.s.* 1 mL). Store at 4 °C.

- **1 mM TEGPy** (in ultrapure water)
  e.g. dissolve 1.53 mg of TEGPy (M= 1527.1 g/mol) in ultrapure water (*q.s.* 1 mL). Store at 4 °C.

- **1 mM Terpy** (in DMSO)
  e.g. dissolve 0.41 mg of Terpy (M= 410.56 g/mol) in DMSO (*q.s.* 1 mL). Store at 4 °C.

- **1 mM TMPyP4** (in DMSO)
  e.g. dissolve 1.36 mg of TMPyP4 (M= 1363.6 g/mol) in DMSO (*q.s.* 1 mL). Store at 4 °C.

- 1 mM **TPPS** (in DMSO)
  e.g. dissolve 1.02 mg of TPPS (M= 1022.91 g/mol) in DMSO (*q.s.* 1 mL). Store at 4 °C.

- 1 M **Urea** (in ultrapure water)
  e.g. dissolve 3.00 mg of urea (M= 60.06 g/mol) in ultrapure water (*q.s.* 50 mL). Store at 4 °C.

III. G4-UNFOLD assay

CRITICAL: Reagents and equipment can be obtained from various vendors and do not need to be from the ones specified here.

1. MATERIALS – Reagents

Chemical products and/or buffer components

- HCl (Fisher Chemical, cat. n° H/1150)
- KCl (Sigma-Aldrich, cat. n° P3911)
- $MgCl_2$ (Sigma-Aldrich, cat. n° 208337)
- NaCl (VWR Chemicals, cat. n° 27810)
- Trizma® base (Sigma-Aldrich, cat. n° 933632)

2. MATERIALS – Equipment

Devices and lab equipment

- Benchtop centrifuge (vendor of choice)
- Benchtop heating block (ThermoMixer C, Eppendorf, cat. n° 5382 000.015)
- Benchtop vortex (vendor of choice)
- Pipettes, manual multichannel, 8 channels, 0.5-10 µL (Acura 855, Socorex, cat. n° 061132)
- pH meter (FiveEasy pH meter F20, Mettler Toledo, cat. n° 30266658)
  + pH electrode (LE438, Mettler Toledo, cat. n° 51340242)
- Pipettes, manual single-channel (*e.g.* Finnpipette from Thermo Scientific, Nichipet EX-Plus II from Nichiryo)
- Plate-reader (CLARIOstar Plus, BMG LABTECH)
- Tube rack (vendor of choice)
- UV-Vis spectrophotometer (Varian Cary 50 Probe, Agilent, no longer available for sale)
  + fibre-optic ultra-micro cell (Hellma TrayCell, Sigma-Aldrich, cat. n° Z802697)
- Water purification system (PURELAB flex 3, ELGA LabWater, cat. n° PF3XXXXM1)

Consumables

- Culture microplate, 96-wells, flat bottom, transparent plate, with lid (Corning-Falcon, cat. n° 353072)
- Filter tips, non-sterile (*e.g.* ClearLine, Fisherbrand SureOne, TipOne)
- Microtubes, with snap cap, DNase/RNase-free, non-sterile (0.5, 1.5, 2, 5 mL) (*e.g.* ClearLine, Eppendorf)

Individual protection equipment

- Lab coat (vendor of choice)
- Nitrile gloves (*e.g.* Kimtech)
- Safety glasses (vendor of choice)

Waste management equipment

- Bin for biohazard and chemical hazard liquid waste
- Bin for biohazard and chemical hazard solid waste

(See the existing legislation in the country of use)

Bioinformatics Softwares and Tools

- Cary WinUV software (Agilent), for the UV-Vis spectrophotometer
- Excel (Microsoft Corp.)
- OriginPro 9.1 (OriginLab Corp.)

3. MATERIALS – Buffers and solutions preparation

For buffers and solutions preparation, I used UV-treated PURELAB ultrapure (type 1) water.

- **1 M HCl** (in ultrapure water)
  e.g. add 8.35 mL of 37% (m/m) HCl* (M= 36.46 g/mol) in 91.65 mL of ultrapure water (*q.s.* 100 mL) (in that way). Store at 25 °C. *that 37% (m/m) HCl (d= 1.18) has a concentration of 11.97 M.

- **1 M KCl** (in ultrapure water)
  e.g. dissolve 7.46 g of KCl (M= 74.55 g/mol) in ultrapure water (*q.s.* 100 mL). Store at 4 °C.

- **Tris-HCl buffer 1** (20 mM Tris-HCl, 5 mM $MgCl_2$, 1 mM KCl, 99 mM NaCl, pH 7.2, in ultrapure water)
  e.g. mix 2 mL of 1 M Tris, 0.5 mL of 1 M $MgCl_2$, 0.1 mL of 1 M KCl, 9.9 mL of 1 M NaCl with 87.5 mL of ultrapure water. Adjust the pH to 7.2 with 1 M HCl (*q.s.* 100 mL). Store at 4 °C.

- **Tris-HCl buffer 2** (20 mM Tris-HCl, 10 mM $MgCl_2$, 1 mM KCl, 99 mM NaCl, pH 7.2, in ultrapure water)
  e.g. mix 2 mL of 1 M Tris, 1.0 mL of 1 M $MgCl_2$, 0.1 mL of 1 M KCl, 9.9 mL of 1 M NaCl with 87.0 mL of ultrapure water. Adjust the pH to 7.2 with 1 M HCl (*q.s.* 100 mL). Store at 4 °C.

- **1 M $MgCl_2$** (in ultrapure water)
  e.g. dissolve 0.95 g of KCl (M= 95.21 g/mol) in ultrapure water (*q.s.* 10 mL). Store at 4 °C.

- **1 M NaCl** (in ultrapure water)

  e.g. dissolve 2.92 g of NaCl (M= 58.44 g/mol) in ultrapure water (*q.s.* 50 mL). Store at 4 °C.

- **1 M Tris** (in ultrapure water)

  e.g. dissolve 2.42 g of Trizma base (M= 121.14 g/mol) in ultrapure water (*q.s.* 20 mL). Store at 4 °C.

4. METHODS – ONs and G4 ligands preparation

All oligonucleotides (ONs) used here were purchased from Eurogentec (Seraing, Belgium).

ON(s) necessitated for this technique is (are):

- dabcyl-labelled 49-nt ON
- FAM-labelled 15-nt ON
- c-hTelo

1) Dilute ONs in ultrapure water (18.2 MΩ.cm resistivity) at 500 µM for stock solutions
2) Determine the actual concentration of these stock solutions through a dilution to 5 µM theoretical concentration *via* a UV spectral analysis at 260 nm, with the molar extinction coefficient (ε) values provided by the manufacturer and the Beer-Lambert law formula: A= εlC.

s-hTelo (= dabcyl-labelled 49-nt ON + FAM-labelled 15-nt ON)

3) Prepare a semi-working solution of s-hTelo at 1 µM (1 µM and 0.85 µM for dabcyl-labelled 49-nt ON and FAM-labelled 15-nt ON, respectively):

   e.g. mix 2 µL of the 500 µM dabcyl-labelled 49-nt ON stock solution with 1.7 µL of 500 µM FAM-labelled 15-nt ON stock solution and 996.3 µL of Tris-HCl buffer **1** (*q.s.* 1 mL).
4) For the long and complementary folding of the high-order structures (*i.e.*, a G-quadruplex and a duplex), heat the 1 µM s-hTelo semi-working solution in following a decreasing temperature level: 90 °C for 5 min, 80 °C for 10 min, 60 °C for 1 h, 50 °C for 1 h, 40 °C for 1 h, 30 °C for 1 h, at RT for 1 h.
5) Aliquot the folded 1 µM s-hTelo semi-working solution in putting 100 µL in 10 0.5 mL-microtubes (or microtubes with a higher capacity).
6) Store at -20 °C.
7) When you need an aliquot for an experiment, chill one microtube slowly at RT and add 400 µL of the Tris-HCl buffer 1 to the 100 µL of folded 1 µM s-hTelo semi-working solution to obtain 500 µL of the folded 0.2 µM s-hTelo working solution.

c-hTelo (= complementary strand to the dabcyl-labelled 49-nt ON constituting the s-hTelo)

8) Prepare a working solution of c-hTelo at 2 µM:

e.g. mix 4 µL of the 500 µM c-hTelo stock solution with 996.0 µL of Tris-HCl buffer 1 (*q.s.* 1 mL).

9) Heat the 2 µM working solution at 90 °C for 5 min and then cool it on ice for at least 2 h.

CRITICAL STEP: I don't think this step is mandatory but I always prefer heating ONs in case the high concentrated stock solution favored aggregation induction which can affect ONs (de)hybridation.

10) Store at 4 °C.

CRITICAL STEP: The first time you prepare a new ON, be sure of the success of the folding process in checking the high-order structure presence by CD measurement.

G4 ligands

11) Dilute G4 ligands from 100 µM or 1 mM stock solution (if possible, in water) in Tris-HCl buffer 1 at 1-2-5-10 µM for working solutions and experiment with 1-2-5-10 mol. equiv. (*i.e.*, 40-80-200-400 nM), respectively.
12) Store at 4 °C.

5. METHODS – Step by step protocol

STEP 0: PROTOCOL PREPARATION (TIMING: 1 day)

1) Prepare the following buffers and solutions:
   Tris-HCl buffer 1 and Tris-HCl buffer 2 (see above). Store all buffers at 4 °C.
2) Prepare ONs and G4 ligands (see above).

STEP 1: MICROPLATE PREPARATION AND FLUORESCENCE MONITORING (TIMING: 1.5 h)

3) Make a master mix of the following components for n wells and gently mix:
   - 10.0 *n µL of [0.2 µM] s-hTelo
   - 38.0 *n µL of Tris-HCl buffer 2

CRITICAL STEPS: *i.* Being limited by the use of two 8-channels pipettes (one in each hand), only 16 microplate wells and thus conditions can be used in one experiment. *ii.* In order to have enough volume of master mix for all condition and thus all wells, it is better to prepare the mix for 2-3 additional wells depending on the total quantity of wells. *iii.* If possible, try to protect the s-hTelo from the light.

4) Dispense 48.0 µL of the master mix in each microplate well.

CRITICAL STEP: The number of microplate wells used per line must not be superior than the number of channels of your pipettes.

5) Put the microplate into the Plate-reader.
6) Monitor the FAM FI every 10 s during 10 min to verify whether the s-hTelo FI is stable and to have the baseline, then save it.
   (Parameters for the CLARIOstar Plus: Focal height= 4.5 mm; Fluorescein λ_{exc}= 482 ± 16 nm and λ_{em}= 530 ± 40 nm; Gain= 1300; Top optic acquisition; Setting time= 0.1 s; N° of flashes per well and cycle= 1; Cycle time= 10 s; Shake= none).
7) Add in each microplate well 2.0 µL of the buffer (Control) or small molecule (treatment) (**Table Mat&Meth 4**) and homogenize well the microplate in mixing slowly for 1-2 min on a laboratory rocker.
8) Monitor the FAM FI every 10 s during 10 min to verify whether the treatment modify the baseline, then save it.
9) Add, quickly and with the multi-channels pipettes, in each microplate well 2.2 µL of the [2 µM] c-hTelo in stirring rapidly the wells with the pipettes.
10) Monitor the FAM FI every 10 s during 30 min (the time to have the final plateau) to record the complete s-hTelo unwinding by the c-hTelo hybridization and its consequences on FI, then save it.

CRITICAL STEP: This last addition as well as the procedure launch on the plate-reader has to be very quick in order to record the increase of the FI.

Condition	**Volume (µL) (Final concentration)**				
Component	**Control**	**1 mol. equiv.**	**2 mol. equiv.**	**5 mol. equiv.**	**10 mol. equiv.**
[0.2 µM] s-hTelo	10.0 µL (40.0 nM)				
Tris-HCl buffer 2	38 µL (~ 0.7 mM KCl)				
Additional Tris-HCl buffer	2.0 µL	/	/	/	/
[1 µM] small molecule	/	2.0 µL (40.0 nM)	/	/	/
[2 µM] small molecule	/	/	2.0 µL (80.0 nM)	/	/
[5 µM] small molecule	/	/	/	2.0 µL (200.0 nM)	/
[10 µM] small molecule	/	/	/	/	2.0 µL (400.0 nM)
[2.0 µM] c-hTelo	2.2 µL (84.3 nM, thus 2.2 mol. equiv.)				
Volume total	**50.0 + 2.2 = 52.2 µL**				

Table Mat&Meth 4. Summary of experimental conditions applied for the G4-UNFOLD assay. The volume needed for each condition (Control, 1-2-5-10 mol. equiv. of small molecule) and the concentration are informed. A master mix can be prepared with the [0.2 µM] s-hTelo and the basal Tris-HCl buffer 2 (20 mM Tris-HCl, 10 mM $MgCl_2$, 1 mM KCl, 99 mM NaCl, pH 7.2), then 48.0 µL of this master mix have to be dispensed in each well microplate, the FI is monitored during

10 min, 2.0 µL of additional Tris-HCl buffer (Control) or small molecule (treatment) have to be added in appropriated wells, the FI is monitored again during 10 min, then 2.2 µL of the [2.0 µM] c-hTelo is added quickly and the FI is finally monitored during around 30 min. Bold bars separate the different steps.

STEP 2: DATA TREATMENT (TIMING: 20-40 min)

1) With the plate-reader system, export all the raw data of FAM fluorescence intensity (FI).
2) With your treatment software, (0;1) normalize (optional) or not the FI values of the last monitoring (*i.e.*, after the c-hTelo addition).
3) Take the five first points (*i.e.*, FI at 0, 10, 20, 30 and 40 s) after the c-hTelo addition. Due to fluorescence variability, if there is a sudden punctual decrease (often during 2-5 points) through the FI increase, do not take these decreasing points.
4) Display these five points in a FAM fluorescence intensity=f(time) function manner and apply a linear fitting on them.
5) The slope value of the fit right line obtained is the V_0 speed (s^{-1}).

   INFORMATION: For statistical hypothesis tests, Student's *t*-test and Welch's unequal variances *t*-test were used depending on variances equality. * $p < 0.05$, ** $p < 0.01$, *** $p < 0.001$, **** $p < 0.0001$.

6) Make your data representation with these values.

IV. FRET-melting assay

CRITICAL: Reagents and equipment can be obtained from various vendors and do not need to be from the ones specified here.

1. MATERIALS – Reagents

Chemical products and/or buffer components

- Cacodylic acid (Thermo Scientific, cat. n° A12075.09)
- KCl (Sigma-Aldrich, cat. n° P3911)
- LiCl (Strem Chemicals, cat. n° 93-0313)
- LiOH (Thermo Scientific, cat. n° A15519)

2. MATERIALS – Equipment

Devices and lab equipment

- Benchtop centrifuge (vendor of choice)
- Benchtop heating block (ThermoMixer C, Eppendorf, cat. n° 5382 000.015)
- Benchtop laboratory rocker (vendor of choice)
- Benchtop vortex (vendor of choice)
- Pipettes, manual single-channel (*e.g.* Finnpipette from Thermo Scientific, Nichipet EX-Plus II from Nichiryo)
- Real-time PCR system and thermocycler (Mx3005P, Agilent)
- Scissor (vendor of choice)
- Tube rack (vendor of choice)
- UV-Vis spectrophotometer (Varian Cary 50 Probe, Agilent, no longer available for sale)
  + fibre-optic ultra-micro cell (Hellma TrayCell, Sigma-Aldrich, cat. n° Z802697)
- Water purification system (PURELAB flex 3, ELGA LabWater, cat. n° PF3XXXXM1)

Consumables

- Filter tips, non-sterile (*e.g.* ClearLine, Fisherbrand SureOne, TipOne)
- Microtubes, with snap cap, DNase/RNase-free, non-sterile (1.5, 2, 5 mL) (*e.g.* ClearLine, Eppendorf)
- PCR plate, 96-wells (Agilent, cat. n° 401334)
  + optical strip caps (Agilent, cat. n° 401425)

Individual protection equipment

- Lab coat (vendor of choice)
- Nitrile gloves (*e.g.* Kimtech)

- Safety glasses (vendor of choice)

Waste management equipment

- Bin for biohazard and chemical hazard liquid waste
- Bin for biohazard and chemical hazard solid waste

(See the existing legislation in the country of use)

Bioinformatics Softwares and Tools

- Cary WinUV software (Agilent), for the UV-Vis spectrophotometer
- Excel (Microsoft Corp.)
- OriginPro 9.1 (OriginLab Corp.)

3. MATERIALS – Buffers and solutions preparation

For buffers and solutions preparation, I used UV-treated PURELAB ultrapure (type 1) water.

- **CacoK10 buffer** (10 mM lithium cacodylate buffer pH 7.2, 10 mM KCl, 90 mM LiCl, in ultrapure water)
  e.g. mix 10 mL of 100 mM lithium cacodylate buffer (pH 7.2), 10 mL of 100 mM KCl/900 mM LiCl with 80 mL of ultrapure water (*q.s.* 100 mL). Store at 25 °C.

- **100 mM KCl/900 mM LiCl** (in ultrapure water)
  e.g. dissolve 1.49 g of KCl (M= 74.55 g/mol) and 7.63 g of LiCl (M= 42.39 g/mol) in ultrapure water (*q.s.* 200 mL). Store at 4 °C.

- **1 M LiOH** (in ultrapure water)
  e.g. dissolve 2.01 g of cacodylic acid (M= 41.96 g/mol) in ultrapure water (*q.s.* 50 mL). Store at 4 °C.

- **100 mM lithium cacodylate buffer, pH 7.2** (100 mM cacodylic acid, 100 mM LiOH, pH 7.2, in ultrapure water)
  e.g. dissolve 5.52 g of cacodylic acid (M= 138 g/mol) in 40 mL of 1 M LiOH and ultrapure water. Adjust the pH to 7.2 (*q.s.* 400 mL). Store at 4 °C.

4. METHODS – ONs and G4 ligands preparation

All oligonucleotides (ONs) used here were purchased from Eurogentec (Seraing, Belgium).

ON(s) necessitated for this technique is (are):

- F21T

1) Dilute ONs in ultrapure water (18.2 MΩ.cm resistivity) at 500 µM for stock solutions.
2) Determine the actual concentration of these stock solutions through a dilution to 5 µM theoretical concentration *via* a UV spectral analysis at 260 nm, with the molar extinction coefficient (ε) values provided by the manufacturer and the Beer-Lambert law formula: A= εlC.
3) Prepare a working solution at 25 µM:
   e.g. mix 5 µL of the 500 µM stock solution with 10 µL of 100 mM lithium cacodylate buffer (pH 7.2), 10 µL of 100 mM KCl/900 mM LiCl and 75 µL of ultrapure water (*q.s.* 100 µL).
4) For the quick folding of the high-order structure, heat the 25 µM working solution at 90 °C for 5 min and then cool it on ice for at least 2 h.
5) Let the 25 µM working solution at 4 °C overnight.
6) Store at 4 °C.

CRITICAL STEP: The first time you prepare a new ON, be sure of the success of the folding process in checking the high-order structure presence by CD measurement.

G4 ligands

7) Dilute G4 ligands from 1 mM stock solution (if possible, in water) in CacoK10 buffer at 100 µM for working solution.
8) Store at 4 °C.

5. METHODS – Step by step protocol

STEP 0: PROTOCOL PREPARATION (TIMING: 3 h)

1) Prepare the following buffers and solutions:
   CacoK10 buffer, 100 mM KCl/900 mM LiCl, 1 M LiOH and 100 mM lithium cacodylate buffer (pH 7.2) (see above). Store all the buffers and solutions at 4 °C, except the CacoK10 buffer and the 1 M LiOH at room temperature (21-25 °C).
2) Prepare ONs and G4 ligands (see above).
3) Prepare the melting program (**Figure Mat&Meth 5**) for the real-time PCR system.

STEP 1: MIX AND MICROPLATE PREPARATION (TIMING: 20-30 min)

4) Make a master mix of the following components for n wells and gently mix:
   - 97.2 *n µL of CacoK10 buffer
   - 0.8 *n µL of [25 µM] ON

CRITICAL STEPS: *i.* In order to have enough volume of master mix for all condition and thus all wells, it is better to prepare the mix for 2-4 additional wells depending on the total quantity of wells. *ii.* If possible, try to protect the doubly fluorophores-labelled ON from the light.

5) Dispense 98.0 µL of the master mix in each microplate well.
6) Add in each microplate well 2.0 µL of buffer (Control) and/or small molecule (treatment) (**Table Mat&Meth 5**) and close the wells.

   CRITICAL STEP: In order to remove bubbles, altern these techniques: *i.* flick the bottom of the microplate wells to bring out bubbles from the liquid *ii.* centrifuge the microplate quickly (*e.g.*, reach 1 000 rpm and then stop it) to recover all drops.

7) Homogenize well the microplate in mixing normally for 2 min on a laboratory rocker.

Condition	**Volume (µL) (Final concentration)**				
Component	**Control**	**1 mol. equiv.**	**2 mol. equiv.**	**5 mol. equiv.**	**10 mol. equiv.**
[25 µM] ON	0.8 µL (200 nM)				
CacoK10 buffer	97.2 µL (~ 10 mM KCl)				
[100 µM] small molecule	/	0.2 µL (200 nM)	0.4 µL (400 nM)	1.0 µL (1000 nM)	2.0 µL (2000 nM)
Additional CacoK10 buffer	2.0 µL	1.8 µL	1.6 µL	1.0 µL	/
Volume total	**100.0 µL**				

Table Mat&Meth 5. Summary of experimental conditions applied for the FRET-melting assay. The volume needed for each condition (Control, 1-2-5-10 mol. equiv. of small molecule) and the concentration are informed. A master mix can be prepared with the ON studied and CacoK10 buffer, then 98 µL of this master mix have to be dispensed in each well microplate and the volume of additional CacoK10 (Control) and/or small molecule (treatment) have to be added in appropriated wells. Bold bars separate the different steps.

STEP 2: ACQUISITION (TIMING: 35 min)

8) Run the melting using the Molecular Beacon Melting Curve program and in selecting the appropriated positions and fluorophore filters (FAM). Use the 67 cycles procedure (**Figure Mat&Meth 5**).

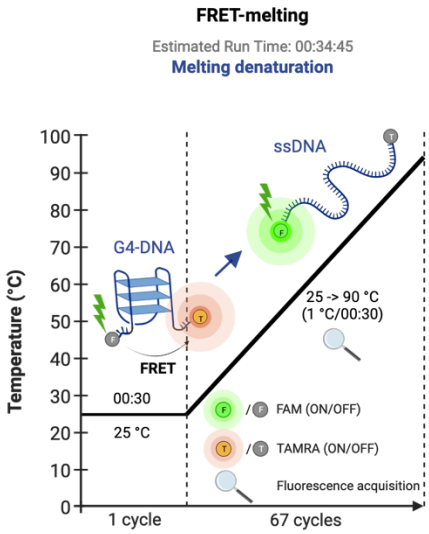

Figure Mat&Meth 5. Schematic representation of the melting procedure created for the FRET-melting assay method. The procedure is the common procedure we used in lab for the FRET-melting assay on the Real-time PCR system and thermocycler. During the melting, the G4 structure is denatured leading to a distance between the FAM and TAMRA fluorophores and thus liberating the FAM from the FRET interference caused by the TAMRA. The denaturation of the G4 structure is thus quantified indirectly via the FAM fluorescence intensity release and increase. Times showed represent hour:min:sec (or just min:sec). Created with BioRender.com

STEP 3: DATA TREATMENT (TIMING: 10-20 min)

9) With the Real-time PCR system, export the raw data of FAM fluorescence intensity (FI) by temperature.
10) With your treatment software, (0;1) normalize the FI values of the individual FI curves to make all the data comparable.
11) Display the normalized FI values in a Normalized FAM fluorescence intensity=f(temperature) function manner.
12) Recover the $T_{1/2}$ value (°C) either manually (more precise) or in applying a sigmoidal fitting (Boltzmann model) and taking the x0 value (more rapid).

    INFORMATION: For statistical hypothesis tests, Student's *t*-test and Welch's unequal variances *t*-test were used depending on variances equality. * $p < 0.05$, ** $p < 0.01$, *** $p < 0.001$, **** $p < 0.0001$.

13) Make your data representation with these values.

V. CD and UV-Vis titrations

CRITICAL: Reagents and equipment can be obtained from various vendors and do not need to be from the ones specified here.

1. MATERIALS – Reagents

Chemical products and/or buffer components

- Cacodylic acid (Thermo Scientific, cat. n° A12075.09)
- KCl (Sigma-Aldrich, cat. n° P3911)
- LiCl (Strem Chemicals, cat. n° 93-0313)
- LiOH (Thermo Scientific, cat. n° A15519)
- Mineral oil, pure (Thermo Scientific, cat. n° 415080010)

2. MATERIALS – Equipment

Devices and lab equipment

- Benchtop centrifuge (vendor of choice)
- Benchtop heating block (ThermoMixer C, Eppendorf, cat. n° 5382 000.015)
- Benchtop vortex (vendor of choice)
- Circular Dichroism (CD) spectropolarimeter (J-815, JASCO)
- Pipettes, manual single-channel (*e.g.* Finnpipette from Thermo Scientific, Nichipet EX-Plus II from Nichiryo)
- Quartz cuvette, rectangular, sub-micro, 100 µL, 10 mm path length, 2 mm interior width x 2.5 mm interior height (Starna Scientific, cat. n° 16R/100/Q/10/Z15)
  + vaned polyethylene plug stopper (Starna Scientific, cat. n° STP/C10.10)
- Quartz cuvettes rack (vendor of choice)
- Tube rack (vendor of choice)
- UV-Vis spectrophotometer (Varian Cary 50 Probe, Agilent, no longer available for sale)
  + fibre-optic ultra-micro cell (Hellma TrayCell, Sigma-Aldrich, cat. n° Z802697)
- Water purification system (PURELAB flex 3, ELGA LabWater, cat. n° PF3XXXXM1)

Consumables

- Filter tips, non-sterile (*e.g.* ClearLine, Fisherbrand SureOne, TipOne)
- Microtubes, with snap cap, DNase/RNase-free, non-sterile (1.5, 2, 5 mL) (*e.g.* ClearLine, Eppendorf)
- Nitrogen bottle, for the CD spectropolarimeter (Air Liquide, cat. n° I4001L50R2A001)

Individual protection equipment

- Lab coat (vendor of choice)
- Nitrile gloves (*e.g.* Kimtech)
- Safety glasses (vendor of choice)

Waste management equipment

- Bin for biohazard and chemical hazard liquid waste
- Bin for biohazard and chemical hazard solid waste

(See the existing legislation in the country of use)

Bioinformatics Softwares and Tools

- Cary WinUV software (Agilent), for the UV-Vis spectrophotometer
- Excel (Microsoft Corp.)
- OriginPro 9.1 (OriginLab Corp.)
- Spectra Manager 2, for the CD spectropolarimeter

3. MATERIALS – Buffers and solutions preparation

For buffers and solutions preparation, I used UV-treated PURELAB ultrapure (type 1) water.

- **CacoK10 buffer** (10 mM lithium cacodylate buffer pH 7.2, 10 mM KCl, 90 mM LiCl, in ultrapure water)
  e.g. mix 10 mL of 100 mM lithium cacodylate buffer (pH 7.2), 10 mL of 100 mM KCl/900 mM LiCl with 80 mL of ultrapure water (*q.s.* 100 mL). Store at 25 °C.

- **100 mM KCl/900 mM LiCl** (in ultrapure water)
  e.g. dissolve 1.49 g of KCl (M= 74.55 g/mol) and 7.63 g of LiCl (M= 42.39 g/mol) in ultrapure water (*q.s.* 200 mL). Store at 4 °C.

- **1 M LiOH** (in ultrapure water)
  e.g. dissolve 2.01 g of cacodylic acid (M= 41.96 g/mol) in ultrapure water (*q.s.* 50 mL). Store at 4 °C.

- **100 mM lithium cacodylate buffer, pH 7.2** (100 mM cacodylic acid, 100 mM LiOH, pH 7.2, in ultrapure water)
  e.g. dissolve 5.52 g of cacodylic acid (M= 138 g/mol) in 40 mL of 1 M LiOH and ultrapure water. Adjust the pH to 7.2 (*q.s.* 400 mL). Store at 4 °C.

4. METHODS – ONs and G4 ligands preparation

All oligonucleotides (ONs) used here were purchased from Eurogentec (Seraing, Belgium).

ON(s) necessitated for this technique is (are):

- hTelo

1) Dilute ONs in ultrapure water (18.2 MΩ.cm resistivity) at 500 µM for stock solutions
2) Determine the actual concentration of these stock solutions through a dilution to 5 µM theoretical concentration *via* a UV spectral analysis at 260 nm, with the molar extinction coefficient (ε) values provided by the manufacturer and the Beer-Lambert law formula: A= εlC.
3) Prepare a working solution at 50 µM:
   e.g. mix 10 µL of the 500 µM stock solution with 10 µL of 100 mM lithium cacodylate buffer (pH 7.2), 10 µL of 100 mM KCl/900 mM LiCl and 70 µL of ultrapure water (*q.s.* 100 µL).
4) For the quick folding of the high-order structure, heat the 50 µM working solution at 90 °C for 5 min and then cool it on ice for at least 2 h.
5) Let the 50 µM working solution at 4 °C overnight.
6) Store at 4 °C.

   CRITICAL STEP: The first time you prepare a new ON, be sure of the success of the folding process in checking the high-order structure presence by CD measurement.

G4 ligands

7) Dilute G4 ligands from 1 mM stock solution (if possible, in water) in CacoK10 buffer at 100 µM for working solutions.
8) Store at 4 °C.

5. METHODS – Step by step protocol

STEP 0: PROTOCOL PREPARATION (TIMING: 2 h)

1) Prepare the following buffers and solutions:
   CacoK10 buffer, 100 mM KCl/900 mM LiCl, 1 M LiOH and 100 mM lithium cacodylate buffer (pH 7.2) (see above). Store all the buffers and solutions at 4 °C, except the CacoK10 buffer and the 1 M LiOH at room temperature (21-25 °C).
2) Prepare ONs and G4 ligands (see above).

STEP 1: QUARTZ CUVETTE PREPARATION AND CD/UV-Vis MONITORING (TIMING: 1 h)

3) Make a master mix of the following components for n quartz cuvette and gently mix:
   - 88.0 *n µL of CacoK10 buffer
   - 6.0 *n µL of [50 µM] ON

CRITICAL STEP: In order to have enough volume of master mix for all condition and thus all quartz cuvettes, it is better to prepare the mix for 1-2 additional wells depending on the total quantity of wells.

4) Set the parameter of the Spectra Measurement program
   (Parameters for the JASCO J-815:
   GENERAL: Channel #1= CD; Channel #2= HT; Channel #3= Abs; Sensitivity= Standard; D.I.T.= 1 sec; Band width= 1.00 nm; Start= 350 nm; End= 210 nm; Data pitch= 1.0 nm; Start mode= Immediately; Scanning mode= Continuous; Scanning speed= 200 nm/min; Accumulation/Repeat= 3,
   CONTROL: Correction= Baseline,
   ACCESSORY: Temperature= 25.0 °C).
5) Put 100.0 µL of the CacoK10 buffer into the quartz cuvette.
6) Put the quartz cuvette into the CD spectropolarimeter and make the baseline of the software.
7) Empty the cuvette, dry it and dispense 94.0 µL of the master mix in each quartz cuvette.
8) Record the ellipticity (CD) as well as the absorbance to verify the secondary structure of the ON and to have this baseline control, then save it.
9) Add in quartz cuvette 3.0 µL of the [100 µM] small molecule (1 mol. equiv., **Table Mat&Meth 6**), mix well by up-and-down pipetting, record the data and then save it.
10) Add in quartz cuvette 3.0 µL of the [100 µM] small molecule (2 mol. equiv., **Table Mat&Meth 6**), mix well by up-and-down pipetting, record the data and then save it.
11) Add in quartz cuvette 11.0 µL of the [100 µM] small molecule (5 mol. equiv., **Table Mat&Meth 6**), mix well by up-and-down pipetting, record the data and then save it.
12) Add in quartz cuvette 1.7 µL of the [1 mM] small molecule (10 mol. equiv., **Table Mat&Meth 6**), mix well by up-and-down pipetting, record the data and then save it.
13) Clean the cuvette drastically: with dichloromethane, then acetone, then ethanol then water, then ethanol again and dry it (with pressurized air to be quick).

Condition	**Volume (µL) (Final concentration)**				
Component	**Control**	**1 mol. equiv.**	**2 mol. equiv.**	**~5 mol. equiv.**	**~10 mol. equiv.**
[50 µM] ON	6.0 µL (3.2 µM in V= 94.0 µL; 3.1 µM in V= 97.0 µL; 3.0 µM in V= 100.0 µL; 2.7 µM in V= 111.0 µL; 2.7 µM in V= 112.7 µL)				
CacoK10 buffer	88.0 µL (~ 10 mM KCl)				
[100 µM] small molecule	/	+ 3.0 µL (3.1 µM, in V= 97.0 µL)	/	/	/
[100 µM] small molecule	/	/	+ 3.0 µL (6.0 µM) in V= 100.0 µL)	/	/
[100 µM] small molecule	/	/	/	+ 11.0 µL (15.3 µM) in V= 111.0 µL)	/
[1 mM] small molecule	/	/	/	/	+ 1.7 µL (30.2 µM) in V= 112.7 µL)
Volume total	**94.0 + 3.0 + 3.0 + 11.0 + 1.7 = 112.7 µL**				

Table Mat&Meth 6. Summary of experimental conditions applied for the CD/UV-Vis titration. The volume needed for each titration condition (Control, 1-2-5-10 mol. equiv. of small molecule) and the concentrations at each step are informed. A master mix can be prepared with the [50 µM] ON studied and CacoK10 buffer, then 94 µL of this master mix have to be dispensed in a quart cuvette and the volume of small molecule (treatment) have to be added step by step in recording each step: addition of 3 µL of [100 µM] small molecule (1 mol. equiv.), then 3 µL again (2 mol. equiv.), then 11 µL (**~**5 mol. equiv.) and finally 1.7 µL of [1 mM] small molecule (**~**10 mol. equiv.). Bold bars separate the different steps.

STEP 2: DATA TREATMENT (TIMING: 20-30 min)

14) With the Spectra Manger system, export the raw data of CD and Absorbance.
15) With your treatment software, normalize the CD values (not the Absorbance) in setting the CD value at 350 nm of the individual CD curves to 0.0 mdeg to make all the data comparable. To do this, you can simply subtract to each worksheet column (corresponding to different quartz cuvette condition) the value allowing to have a CD value of 0.0 mdeg at 350 nm (1st line). Obviously, this value has to be subtracted for each wavelength (line) of its condition (column).
16) Make your data representation with these Normalized ellipticity or Raw absorbance values for CD and UV-Vis titration, respectively.

VI. Polyacrylamide Gel Electrophoresis (PAGE) analysis

CRITICAL: Reagents and equipment can be obtained from various vendors and do not need to be from the ones specified here.

1. MATERIALS – Reagents

Chemical products and/or buffer components

- Acrylamide : bis-Acrylamide 29:1, 40% solution (Fisher Bioreagents, cat. n° BP1408-1)
- Ammonium persulfate (Sigma-Aldrich, cat. n° A3678)
- Cacodylic acid (Thermo Scientific, cat. n° A12075.09)
- DNA gel loading dye, 6X (Thermo Scientific, cat. n° R0611)
- EDTA (Thermo Scientific, cat. n° 11843)
- KCl (Sigma-Aldrich, cat. n° P3911)
- LiCl (Strem Chemicals, cat. n° 93-0313)
- LiOH (Thermo Scientific, cat. n° A15519)
- Orthoboric acid (VWR Chemicals, cat. n° 20185)
- SYBR™ Gold Nucleic Acid Gel Stain (Invitrogen, cat. n° S11494)
- TEMED (N,N,N',N'-Tetramethylethylenediamine) (Sigma-Aldrich, cat. n° 411019)
- Trizma® base (Sigma-Aldrich, cat. n° 933632)

2. MATERIALS – Equipment

Devices and lab equipment

- Benchtop centrifuge (vendor of choice)
- Benchtop heating block (ThermoMixer C, Eppendorf, cat. n° 5382 000.015)
- Benchtop laboratory rocker (vendor of choice)
- Benchtop vortex (vendor of choice)
- Gel imager, with LMS-26 transilluminator (254/302/365 nm) (UVP MultiDoc-It Imaging System, Analytik Jena, cat. n° UVP97019704)
- Gel shovel (vendor of choice)
- Pipettes, manual single-channel (*e.g.* Finnpipette from Thermo Scientific, Nichipet EX-Plus II from Nichiryo)
- Tube rack (vendor of choice)
- UV-Vis spectrophotometer (Varian Cary 50 Probe, Agilent, no longer available for sale)
  + fibre-optic ultra-micro cell (Hellma TrayCell, Sigma-Aldrich, cat. n° Z802697)
- Vertical gel tank, complete (8-teeth combs, plain glass plate with 1 mm bonded spacers and notched glass plates (10 x 10 cm), gel gasting, sealing) (Fisher Scientific, cat. n° 11843293)

- Water purification system (PURELAB flex 3, ELGA LabWater, cat. n° PF3XXXXM1)

Consumables

- Filter tips, non-sterile (*e.g.* ClearLine, Fisherbrand SureOne, TipOne)
- Microtubes, with snap cap, DNase/RNase-free, non-sterile (1.5, 2, 5 mL) (*e.g.* ClearLine, Eppendorf)
- Tubes (15, 50 mL) (*e.g.* Falcon)

Individual protection equipment

- Lab coat (vendor of choice)
- Nitrile gloves (*e.g.* Kimtech)
- Safety glasses (vendor of choice)

Waste management equipment

- Bin for biohazard and chemical hazard liquid waste
- Bin for biohazard and chemical hazard solid waste

(See the existing legislation in the country of use)

Bioinformatics Softwares and Tools

- Cary WinUV software (Agilent), for the UV-Vis spectrophotometer
- Excel (Microsoft Corp.)
- OriginPro 9.1 (OriginLab Corp.)
- UVP software

3. MATERIALS – Buffers and solutions preparation

For buffers and solutions preparation, I used UV-treated PURELAB ultrapure (type 1) water.

- **10% (w/v) ammonium persulfate (APS)** (in ultrapure water)
  e.g. dissolve 500 mg of APS (M= 228.20 g/mol) in ultrapure water (*q.s.* 5 mL). Store at 4 °C.

- **CacoK10 buffer** (10 mM lithium cacodylate buffer pH 7.2, 10 mM KCl, 90 mM LiCl, in ultrapure water)
  e.g. mix 10 mL of 100 mM lithium cacodylate buffer (pH 7.2), 10 mL of 100 mM KCl/900 mM LiCl with 80 mL of ultrapure water (*q.s.* 100 mL). Store at 25 °C.

- **100 mM KCl/900 mM LiCl** (in ultrapure water)
  e.g. dissolve 1.49 g of KCl (M= 74.55 g/mol) and 7.63 g of LiCl (M= 42.39 g/mol) in ultrapure water (*q.s.* 200 mL). Store at 4 °C.

- **1 M LiOH** (in ultrapure water)
  e.g. dissolve 2.01 g of cacodylic acid (M= 41.96 g/mol) in ultrapure water (*q.s.* 50 mL). Store at 4 °C.

- **100 mM lithium cacodylate buffer, pH 7.2** (100 mM cacodylic acid, 100 mM LiOH, pH 7.2, in ultrapure water)
  e.g. dissolve 5.52 g of cacodylic acid (M= 138 g/mol) in 40 mL of 1 M LiOH and ultrapure water. Adjust the pH to 7.2 (*q.s.* 400 mL). Store at 4 °C.

- **1X TBE buffer** (in ultrapure water)
  e.g. dilute 100 mL of 10X TBE buffer with 900 mL of ultrapure water (*q.s.* 1 L). Store at 4 °C.

- **10X TBE buffer, pH 8.3** (in ultrapure water)
  e.g. dissolve 108 g of Trizma base (M= 121.14 g/mol), 55 g of orthoboric acid (M= 61.83 g/mol) and 9.3 g of EDTA (M= 292.25 g/mol) in ultrapure water (*q.s.* 1 L). Adjust the pH to 8.3 with 1 M HCl. Store at 25 °C.

4. METHODS – ONs and G4 ligands preparation

All oligonucleotides (ONs) used here were purchased from Eurogentec (Seraing, Belgium).

ON(s) necessitated for this technique is (are):

- hTelo

1) Dilute ONs in ultrapure water (18.2 MΩ.cm resistivity) at 500 µM for stock solutions
2) Determine the actual concentration of these stock solutions through a dilution to 5 µM theoretical concentration *via* a UV spectral analysis at 260 nm, with the molar extinction coefficient (ε) values provided by the manufacturer and the Beer-Lambert law formula: A= εlC.
3) Prepare a working solution at 50 µM:
   e.g. mix 10 µL of the 500 µM stock solution with 10 µL of 100 mM lithium cacodylate buffer (pH 7.2), 10 µL of 100 mM KCl/900 mM LiCl and 70 µL of ultrapure water (*q.s.* 100 µL).
4) For the quick folding of the high-order structure, heat the 50 µM working solution at 90 °C for 5 min and then cool it on ice for at least 2 h.
5) Let the 50 µM working solution at 4 °C overnight.
6) Store at 4 °C.

   CRITICAL STEP: The first time you prepare a new ON, be sure of the success of the folding process in checking the high-order structure presence by CD measurement.

G4 ligands

7) Dilute G4 ligands from 1 mM stock solution (if possible, in water) in CacoK10 buffer at 100 µM for working solutions.
8) Store at 4 °C.

5. METHODS – Step by step protocol

STEP 0: PROTOCOL PREPARATION (TIMING: 3 h)

1) Prepare the following buffers and solutions:
   10% (w/v) ammonium persulfate (APS), CacoK10 buffer, 100 mM KCl/900 mM LiCl, 1 M LiOH and 100 mM lithium cacodylate buffer (pH 7.2), 1X TBE buffer and 10X TBE buffer (pH 8.3) (see above). Store all the buffers and solutions at 4 °C, except the CacoK10 buffer, the 1 M LiOH and the 1X TBE buffer at room temperature (21-25 °C).
2) Prepare ONs and G4 ligands (see above).

STEP 1: MIX PREPARATION (TIMING: 1.5 h)

3) Mix gently all the components to prepare the sample to load (**Table Mat&Meth 7**).
4) Incubate the sample at 25 °C for 1 h under agitation.

Condition	**Volume (µL) (Final concentration)**					
Component	**Control**	**1 mol. equiv.**	**2 mol. equiv.**	**5 mol. equiv.**	**10 mol. equiv.**	**20 mol. equiv.**
[50 µM] ON	1.5 µL (6 µM)					
CacoK10 buffer	11.0 µL	10.25 µL	9.5 µL	7.25 µL	10.25 µL	9.5 µL
[100 µM] small molecule	/	0.75 µL (6 µM)	1.5 µL (12 µM)	3.75 µL (30 µM)	/	/
[1 mM] small molecule	/	/	/	/	0.75 µL (60 µM)	1.5 µL (120 µM)
Volume total	**12.5 µL**					

Table Mat&Meth 7. Summary of experimental conditions applied for the PAGE analysis. The volume needed for each condition (Control, 1-2-5-10-20 mol. equiv. of small molecule) and the concentration are informed. All the components have to be mix to have the sample without (Control) or with small molecule (treatment).

STEP 2: GEL PREPARATION AND ACQUISITION (TIMING: 1 h)

For a 8 wells 10x10 cm 20% (v/v) acrylamide:bis-acrylamide native TBE gel, prepare it as follows:

5) Mix 4.55 mL of the acrylamide:bis-acrylamide (29:1, 40%) solution with 4.45 mL of 1X TBE buffer and 90 µL of the 10% (w/v) APS.
6) Add quickly 9 µL of TEMED and mix again (*q.s.* ~ 9.1 mL).
7) Cast the mixture rapidly (do not forget combs!).
8) Let the gel polymerize for 15-20 min at RT.

PAUSE POINT: The gel can be easily stored for a week at 4 °C submerged in 1X TBE gel.

For the loading, electrophoresis and revelation steps, proceed as follows:

9) Mix 12.5 µL of the sample to load with 2.5 µL of the 6X DNA gel loading dye solution.
10) Load cautiously 10 µL in gel wells.
11) Run at 7 W for 15 min and then at 12 W for 35 min at 4 °C.
12) To prepare the relevation solution, mix 7.5 µL of SYBR™ Gold Nucleic Acid Gel Stain with 75 mL of 1X TBE buffer (1:10 000).
13) Incubate for 15 min at RT the gel submerged in the revelation solution on a benchtop laboratory rocker (protected from the light).
14) Image the gel with your standard gel imager and appropriate SYBR filters.

STEP 3: DATA TREATMENT (TIMING: 20-30 min)

15) With the UVP software system, load the pictures and quantify the intensity of the main band.
16) Make your data representation with these arbitrary intensity values.

VII. qPCR Stop assay

CRITICAL: Reagents and equipment can be obtained from various vendors and do not need to be from the ones specified here.

1. MATERIALS – Reagents

Chemical products and/or buffer components

- dNTP mix (Thermo Scientific, cat. n° R0191)
- iTaq™ Universal SYBR® Green Supermix (Bio-Rad, cat. n° 1725121)
- Cacodylic acid (Thermo Scientific, cat. n° A12075.09)
- KCl (Sigma-Aldrich, cat. n° P3911)
- LiCl (Strem Chemicals, cat. n° 93-0313)
- LiOH (Thermo Scientific, cat. n° A15519)

2. MATERIALS – Equipment

Devices and lab equipment

- Benchtop centrifuge (vendor of choice)
- Benchtop heating block (ThermoMixer C, Eppendorf, cat. n° 5382 000.015)
- Benchtop laboratory rocker (vendor of choice)
- Benchtop vortex (vendor of choice)
- Classical centrifuge (Universal 320 R, Hettich, cat. n° 1406)
- Dry ice box (vendor of choice)
- Ice maker (vendor of choice)
- Pipettes, manual single-channel (*e.g.* Finnpipette from Thermo Scientific, Nichipet EX-Plus II from Nichiryo)
- Real-time PCR system and thermocycler (Mx3005P, Agilent)
- Scissor (vendor of choice)
- Tube rack (vendor of choice)
- UV-Vis spectrophotometer (Varian Cary 50 Probe, Agilent, no longer available for sale)
  + fibre-optic ultra-micro cell (Hellma TrayCell, Sigma-Aldrich, cat. n° Z802697)
- Water purification system (PURELAB flex 3, ELGA LabWater, cat. n° PF3XXXXM1)

Consumables

- Filter tips, non-sterile (*e.g.* ClearLine, Fisherbrand SureOne, TipOne)
- Microtubes, with snap cap, DNase/RNase-free, non-sterile (1.5, 2, 5 mL) (*e.g.* ClearLine, Eppendorf)

- PCR plate, 96-wells (Agilent, cat. n° 401334)
  + optical strip caps (Agilent, cat. n° 401425)
- Tubes (15, 50 mL) (*e.g.* Falcon)

Individual protection equipment

- Lab coat (vendor of choice)
- Nitrile gloves (*e.g.* Kimtech)
- Safety glasses (vendor of choice)

Waste management equipment

- Bin for biohazard and chemical hazard liquid waste
- Bin for biohazard and chemical hazard solid waste

(See the existing legislation in the country of use)

Bioinformatics Softwares and Tools

- Cary WinUV software (Agilent), for the UV-Vis spectrophotometer
- Excel (Microsoft Corp.)
- MxPro QPCR software (Agilent), for the Real-time PCR system and thermocycler
- OriginPro 9.1 (OriginLab Corp.)

3. MATERIALS – Buffers and solutions preparation

For buffers and solutions preparation, I used UV-treated PURELAB ultrapure (type 1) water.

- **10 mM KCl** (in ultrapure water)
  e.g. dissolve 37.28 mg of KCl (M= 74.55 g/mol) in ultrapure water (*q.s.* 50 mL). Store at 4 °C.

- **380 mM KCl** (in ultrapure water)
  e.g. dissolve 1.42 g of KCl (M= 74.55 g/mol) in ultrapure water (*q.s.* 50 mL). Store at 4 °C.

- **100 mM KCl/900 mM LiCl** (in ultrapure water)
  e.g. dissolve 1.49 g of KCl (M= 74.55 g/mol) and 7.63 g of LiCl (M= 42.39 g/mol) in ultrapure water (*q.s.* 200 mL). Store at 4 °C.

- **1 M LiOH** (in ultrapure water)
  e.g. dissolve 2.01 g of cacodylic acid (M= 41.96 g/mol) in ultrapure water (*q.s.* 50 mL). Store at 4 °C.

- **100 mM lithium cacodylate buffer, pH 7.2** (100 mM cacodylic acid, 100 mM LiOH, pH 7.2, in ultrapure water)

  e.g. dissolve 5.52 g of cacodylic acid (M= 138 g/mol) in 40 mL of 1 M LiOH and ultrapure water. Adjust the pH to 7.2 (*q.s.* 400 mL). Store at 4 °C.

4. METHODS – ONs and G4 ligands preparation

All oligonucleotides (ONs) used here were purchased from Eurogentec (Seraing, Belgium).

ON(s) necessitated for this technique is (are):

S. pombe G4 sequences

- G4-strand (= antisense strand)
- No G4-strand (= the complementary strand of G4-strand; sense strand)
- G4-1 Forward primer (= the primer for the No G4-strand)
- G4-1 Reverse primer (= the primer for the G4-strand and all *H. sapiens* G4 sequences below)

Human G4 sequences

- hTelo qSa
- *c-MYC* qSa
- *c-KIT2* qSa
- Sc-hTelo qSa
- Sc *c-MYC* qSa
- Sc *c-KIT2* qSa

Template ONs (= G4-strand, No G4-strand, hTelo qSa, *c-MYC* qSa, *c-KIT2* qSa, Sc hTelo qSa, Sc *c-MYC* qSa, Sc *c-KIT2* qSa)

1) Dilute ONs in ultrapure water (18.2 MΩ.cm resistivity) at 500 µM for stock solutions.
2) Determine the actual concentration of these stock solutions through a dilution to 5 µM theoretical concentration *via* a UV spectral analysis at 260 nm, with the molar extinction coefficient (ε) values provided by the manufacturer and the Beer-Lambert law formula: A= εlC.
3) Prepare a semi-working solution at 50 µM:

   e.g. mix 10 µL of the 500 µM stock solution with 10 µL of 100 mM lithium cacodylate buffer (pH 7.2), 10 µL of 100 mM KCl/900 mM LiCl and 70 µL of ultrapure water (*q.s.* 100 µL).
4) For the quick folding of the high-order structure, heat the 50 µM working solution at 90 °C for 5 min and then cool it on ice for at least 2 h.

   CRITICAL STEP: Scrambled sequences (*i.e.*, Sc hTelo qSa, Sc *c-MYC* qSa, Sc *c-KIT2* qSa) having no G4-folding sequences, the folding process can be skipped.

5) Let the 50 µM semi-working solution at 4 °C overnight.
6) Prepare a working solution at 0.5 µM:
   e.g. mix 5 µL of the 50 µM semi-working solution with 495 µL of 10 mM KCl (*q.s.* 500 µL).
7) Store at 4 °C.

CRITICAL STEP: The first time you prepare a new ON, be sure of the success of the folding process in checking the high-order structure presence by CD measurement.

Primer ONs (= G4-1 Forward and Reverse)

8) Dilute ONs in ultrapure water (18.2 MΩ.cm resistivity) at 200 µM for stock solutions.
9) Determine the actual concentration of these stock solutions through a dilution to 5 µM theoretical concentration *via* a UV spectral analysis at 260 nm, with the molar extinction coefficient (ε) values provided by the manufacturer and the Beer-Lambert law formula: A= εlC.
10) Prepare a working solution at 6 µM:
    e.g. dilute 6 µL of the 200 µM stock solution with 194 µL of ultrapure water (*q.s.* 200 µL).
11) Store at 4 °C.

G4 ligands

12) Dilute G4 ligands from 1 mM or more stock solution (if possible, in water) with 10 mM KCl at 1.35-2.7-6.75-13.5 µM for working solutions and experiment with 1-2-5-10 mol. equiv. (*i.e.*, 67.5-135-337.5-675 nM), respectively.
13) Store at 4 °C.

5. METHODS – Step by step protocol

STEP 0: PROTOCOL PREPARATION (TIMING: 3 h)

1) Prepare the following buffers and solutions:
   10 mM KCl, 380 mM KCl, 100 mM KCl/900 mM LiCl, 1 M LiOH and 100 mM lithium cacodylate buffer (pH 7.2) (see above). Store all buffers and solutions at 4 °C, except 1 M LiOH at room temperature (21-25 °C).
2) Prepare ONs and G4 ligands (see above).
3) Prepare the qPCR program (**Figure Mat&Meth 6**) for the real-time PCR system.

STEP 1: qPCR MIX AND MICROPLATE PREPARATION (TIMING: 20-30 min)

4) Make a qPCR master mix of the following components for n wells and gently mix:
   - 2.65 *n µL of [380 mM] KCl
   - 1.35 *n µL of [0.5 µM] Template ON

- 0.5 *n µL of [6 µM] Primer ON
- 5 *n µL of [2X] *iTaq* Universal SYBR® Green Supermix

CRITICAL STEPS: *i.* In order to have enough volume of qPCR master mix for all condition and thus all wells, it is better to prepare the mix for 2-4 additional wells depending on the total quantity of wells. *ii.* Be careful to use the Primer ON appropriated for the Template ON (**Table Mat&Meth 1**). *iii.* If possible, try to protect the *iTaq* Universal SYBR® Green Supermix from the light.

5) Dispense 9.5 µL of the qPCR master mix in each microplate well.
6) Add in each microplate well 0.5 µL of buffer or small molecule treatment (**Table Mat&Meth 8**) and close the wells.

CRITICAL STEP: In order to remove bubbles, altern these techniques: *i.* flick the bottom of the microplate wells to bring out bubbles from the liquid *ii.* centrifuge the microplate quickly (*e.g.*, reach 1 000 rpm and then stop it) to recover all drops.

7) Homogenize well the microplate in mixing normally for 2 min on a laboratory rocker.

Condition	**Volume (µL) (Final concentration)**				
Component	**Control**	**1 mol. equiv.**	**2 mol. equiv.**	**5 mol. equiv.**	**10 mol. equiv.**
[0.5 µM] T. ON	1.35 µL (67.5 nM or 20.4 ng)				
[6 µM] P. ON	0.5 µL (300.0 nM or 22.9 ng)				
[380 mM] KCl	2.65 µL (~ 100.0 mM KCl)				
[2X] *iTaq*	5.0 µL (1X)				
Additional [380 mM] KCl	0.5 µL	/	/	/	/
[1.35 µM] small molecule	/	0.5 µL (67.5 nM)	/	/	/
[2.7 µM] small molecule	/	/	0.5 µL (135.0 nM)	/	/
[6.75 µM] small molecule	/	/	/	0.5 µL (337.5 nM)	/
[13.5 µM] small molecule	/	/	/	/	0.5 µL (675.0 nM)
Volume total	**10.0 µL**				

Table Mat&Meth 8. Summary of experimental conditions applied for the qPCR Stop assay. The volume needed for each condition (Control, 1-2-5-10 mol. equiv. of small molecule) and the concentration are informed. A master mix can be prepared with the Template and Primer ONs, the basal [380 mM] KCl and the [2X] *iTaq*, then 9.5 µL of this master mix have to be dispensed in each well microplate and 0.5 µL of additional KCl (Control) or small molecule (treatment) have to be added in appropriated wells. Bold bars separate the different steps. T.= Template. P.= Primer.

STEP 2: qPCR QUANTIFICATION (TIMING: 38 min)

8) Run the qPCR using the standard SYBR Green amplification program (with dissociation curve) and in selecting the appropriated positions and fluorophore filters (SYBR Green). Use the 33 cycles procedure (**Figure Mat&Meth 6**).

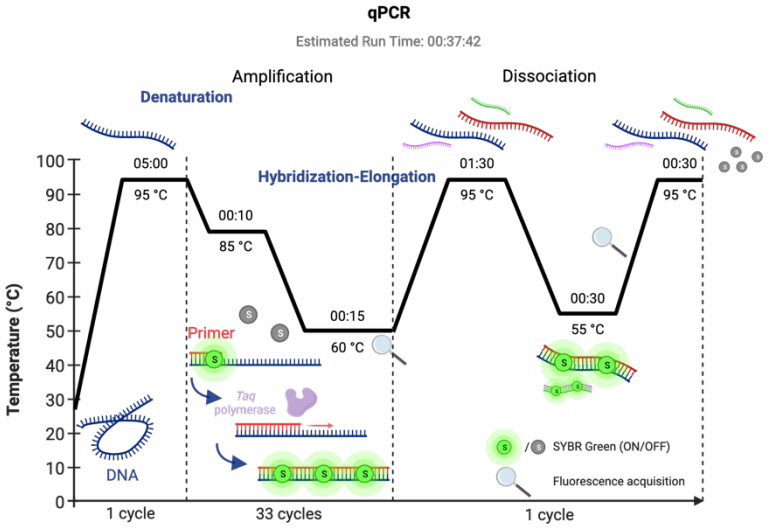

Figure Mat&Meth 6. Schematic representation of the qPCR procedure created for the qPCR Stop assay method. The procedure was created for the qPCR reaction on the Real-time PCR system and thermocycler. During the qPCR the DNAs (Template ONs) are amplified by polymerization into amplicons which are quantified via the SYBR Green (an intercalating agent) fluorescence intensity (amplification step). The dissociation step allows to evaluate the amplicons homogeneity. Times showed represent hour:min:sec (or just min:sec). Created with BioRender.com

STEP 3: DATA TREATMENT (TIMING: 10-20 min)

9) With the Real-time PCR system, export the raw data of SYBR Green fluorescence intensity (FI) by cycle.

10) With your treatment software, normalize the FI values in setting the starting emission of the individual FI curves to 2200.0 to make all the data comparable. To do this, you can simply subtract to each worksheet column (corresponding to different well microplate condition) the value allowing to have a FI of 2200.0 at the 1st qPCR cycle (1st line). Obviously, this value has to be subtracted to each qPCR cycle (line) of its condition (column).

11) Recover only the normalized FI values at the 33th (and last) qPCR cycle.

INFORMATION: For statistical hypothesis tests, Student's *t*-test and Welch's unequal variances *t*-test were used depending on variances equality. * $p < 0.05$, ** $p < 0.01$, *** $p < 0.001$, **** $p < 0.0001$.

12) Make your data representation with these values.

VIII. Dynamic Light Scattering

CRITICAL: Reagents and equipment can be obtained from various vendors and do not need to be from the ones specified here.

1. MATERIALS – Reagents

Chemical products and/or buffer components

- Cacodylic acid (Thermo Scientific, cat. n° A12075.09)
- KCl (Sigma-Aldrich, cat. n° P3911)
- LiCl (Strem Chemicals, cat. n° 93-0313)
- LiOH (Thermo Scientific, cat. n° A15519)

2. MATERIALS – Equipment

Devices and lab equipment

- Benchtop centrifuge (vendor of choice)
- Benchtop heating block (ThermoMixer C, Eppendorf, cat. n° 5382 000.015)
- Benchtop vortex (vendor of choice)
- Dynamic Light Scattering instrument (Zetasizer Nano ZSP, Malvern Panalytical)
- Pipettes, manual single-channel (*e.g.* Finnpipette from Thermo Scientific, Nichipet EX-Plus II from Nichiryo)
- Quartz cuvette, rectangular, semi-micro, 1 mL, 10 (interior and path length) x 4 mm (interior width) (Starna Scientific, cat. n° 29B-Q-10)
  + vaned polyethylene plug stopper (Starna Scientific, cat. n° STP/C10.10)
- Quartz cuvettes rack (vendor of choice)
- Tube rack (vendor of choice)
- UV-Vis spectrophotometer (Varian Cary 50 Probe, Agilent, no longer available for sale)
  + fibre-optic ultra-micro cell (Hellma TrayCell, Sigma-Aldrich, cat. n° Z802697)
- Water purification system (PURELAB flex 3, ELGA LabWater, cat. n° PF3XXXXM1)

Consumables

- Filter tips, non-sterile (*e.g.* ClearLine, Fisherbrand SureOne, TipOne)
- Microtubes, with snap cap, DNase/RNase-free, non-sterile (1.5, 2, 5 mL) (*e.g.* ClearLine, Eppendorf)
- PCR plate, 96-wells (Agilent, cat. n° 401334)
  + optical strip caps (Agilent, cat. n° 401425)
- Tubes (15, 50 mL) (*e.g.* Falcon)

Individual protection equipment

- Lab coat (vendor of choice)
- Nitrile gloves (*e.g.* Kimtech)
- Safety glasses (vendor of choice)

Waste management equipment

- Bin for biohazard and chemical hazard liquid waste
- Bin for biohazard and chemical hazard solid waste

(See the existing legislation in the country of use)

Bioinformatics Softwares and Tools

- Cary WinUV software (Agilent), for the UV-Vis spectrophotometer
- Excel (Microsoft Corp.)
- OriginPro 9.1 (OriginLab Corp.)
- Zetasizer software

3. MATERIALS – Buffers and solutions preparation

For buffers and solutions preparation, I used UV-treated PURELAB ultrapure (type 1) water.

- **CacoK10 buffer** (10 mM lithium cacodylate buffer pH 7.2, 10 mM KCl, 90 mM LiCl, in ultrapure water)
  e.g. mix 10 mL of 100 mM lithium cacodylate buffer (pH 7.2), 10 mL of 100 mM KCl/900 mM LiCl with 80 mL of ultrapure water (*q.s.* 100 mL). Store at 25 °C.

- **100 mM KCl/900 mM LiCl** (in ultrapure water)
  e.g. dissolve 1.49 g of KCl (M= 74.55 g/mol) and 7.63 g of LiCl (M= 42.39 g/mol) in ultrapure water (*q.s.* 200 mL). Store at 4 °C.

- **1 M LiOH** (in ultrapure water)
  e.g. dissolve 2.01 g of cacodylic acid (M= 41.96 g/mol) in ultrapure water (*q.s.* 50 mL). Store at 4 °C.

- **100 mM lithium cacodylate buffer, pH 7.2** (100 mM cacodylic acid, 100 mM LiOH, pH 7.2, in ultrapure water)
  e.g. dissolve 5.52 g of cacodylic acid (M= 138 g/mol) in 40 mL of 1 M LiOH and ultrapure water. Adjust the pH to 7.2 (*q.s.* 400 mL). Store at 4 °C.

4. METHODS – ONs and G4 ligands preparation

All oligonucleotides (ONs) used here were purchased from Eurogentec (Seraing, Belgium).

ON(s) necessitated for this technique is (are):

- hTelo

1) Dilute ONs in ultrapure water (18.2 MΩ.cm resistivity) at 500 µM for stock solutions
2) Determine the actual concentration of these stock solutions through a dilution to 5 µM theoretical concentration *via* a UV spectral analysis at 260 nm, with the molar extinction coefficient (ε) values provided by the manufacturer and the Beer-Lambert law formula: A= εlC.
3) Prepare a working solution at 50 µM:
   e.g. mix 30 µL of the 500 µM stock solution with 30 µL of 100 mM lithium cacodylate buffer (pH 7.2), 30 µL of 100 mM KCl/900 mM LiCl and 210 µL of ultrapure water (*q.s.* 300 µL).
4) For the quick folding of the high-order structure, heat the 50 µM working solution at 90 °C for 5 min and then cool it on ice for at least 2 h.
5) Let the 50 µM working solution at 4 °C overnight.
6) Store at 4 °C.

   CRITICAL STEP: The first time you prepare a new ON, be sure of the success of the folding process in checking the high-order structure presence by CD measurement.

G4 ligands

7) Dilute G4 ligands from 1 mM stock solution (if possible, in water) in CacoK10 buffer at 100 µM for working solutions.
8) Store at 4 °C.

5. METHODS – Step by step protocol

STEP 0: PROTOCOL PREPARATION (TIMING: 2 h)

1) Prepare the following buffers and solutions:
   CacoK10 buffer, 100 mM KCl/900 mM LiCl, 1 M LiOH and 100 mM lithium cacodylate buffer (pH 7.2) (see above). Store all the buffers and solutions at 4 °C, except the CacoK10 buffer and the 1 M LiOH at room temperature (21-25 °C).
2) Prepare ONs and G4 ligands (see above).

STEP 1: QUARTZ CUVETTE PREPARATION AND CD/UV-Vis MONITORING (TIMING: 1-2 h)

3) Set the parameter of the Zetasizer program
   (Parameters for the Zetasizer Nano ZSP in Manual Measurement mode:

MEASUREMENT: Type= size;

SAMPLE: Refractive indice= 1.5; Absorption= 0.01; Dispersant= Water; Temperature= 25 °C; Equilibration time= 30 sec; Measurement angle= 173 backscatter; Measurement duration= Automatic; Number of measurements= 3; Automatic attenuation selection= Yes; Analysis model= General purpose)

4) Put 300 µL of the [50 µM] ON into the quartz cuvette.
5) Put the quartz cuvette into the DLS instrument, record the data and then save it.
6) Add in quartz cuvette 1.5 µL of the [10 mM] small molecule (1 mol. equiv., **Table Mat&Meth 9**), mix well by up-and-down pipetting, record the data and then save it.
7) Add in quartz cuvette 1.5 µL of the [10 mM] small molecule (2 mol. equiv., **Table Mat&Meth 9**), mix well by up-and-down pipetting, record the data and then save it.
8) Add in quartz cuvette 4.5 µL of the [10 mM] small molecule (5 mol. equiv., **Table Mat&Meth 9**), mix well by up-and-down pipetting, record the data and then save it.
9) Clean the cuvette drastically: with dichloromethane, then acetone, then ethanol then water, then ethanol again and dry it (with pressurized air to be quick).

Condition	**Volume (µL) (Final concentration)**			
Component	**Control**	**1 mol. equiv.**	**2 mol. equiv.**	**5 mol. equiv.**
[50 µM] ON	300.0 µL (50.0 µM in V= 300.0 µL; 49.8 µM in V= 301.5 µL; 49.6 µM in V= 303.0 µL; 48.9 µM in V= 307.5 µL)			
[10 mM] small molecule	/	+ 1.5 µL (49.8 µM, in V= 301.5 µL)	/	/
[10 mM] small molecule	/	/	+ 1.5 µL (99.1 µM) in V= 303.0 µL)	/
[10 mM] small molecule	/	/	/	+ 4.5 µL (243.9 µM) in V= 307.5 µL)
Volume total	**300.0 + 1.5 + 1.5 + 4.5 = 307.5 µL**			

Table Mat&Meth 9. Summary of experimental conditions applied for the DLS investigation. The volume needed for each titration condition (Control, 1-2-5 mol. equiv. of small molecule) and the concentrations at each step are informed. The 300 µL of ON is putted on the quartz cuvette and the volume of small molecule (treatment) have to be added step by step in recording each step: addition of 1.5 µL of [10 mM] small molecule (1 mol. equiv.), then 1.5 µL again (2 mol. equiv.) and finally 4.5 µL (5 mol. equiv.). Bold bars separate the different steps.

STEP 2: DATA TREATMENT (TIMING: 10-20 min)

10) With the Zetasizer system and a home-made macro program, export the Intensity and Volume data.
11) With your treatment software, make your data representation of the Intensity or Volume=f(size classes).

IX. hPIF1 helicase assay

CRITICAL: Reagents and equipment can be obtained from various vendors and do not need to be from the ones specified here.

1. MATERIALS – Reagents

Chemical products and/or buffer components

- Adenosine 5'-triphosphate disodium salt hydrate (ATP) (Sigma-Aldrich, cat. n° A3377)
- Cacodylic acid (Thermo Scientific, cat. n° A12075.09)
- HCl (Fisher Chemical, cat. n° H/1150)
- hPIF1 enzyme (produced by Alexandra Joubert in Jean-Baptiste Boulé's lab, « Structure et Instabilité des Génomes » UMR CNRS-INSERM-MNHN, Paris , France)
- KCl (Sigma-Aldrich, cat. n° P3911)
- $MgCl_2$ (Sigma-Aldrich, cat. n° 208337)
- NaCl (VWR Chemicals, cat. n° 27810)
- Trizma® base (Sigma-Aldrich, cat. n° 933632)

2. MATERIALS – Equipment

Devices and lab equipment

- Benchtop centrifuge (vendor of choice)
- Benchtop heating block (ThermoMixer C, Eppendorf, cat. n° 5382 000.015)
- Benchtop vortex (vendor of choice)
- Pipettes, manual multichannel, 8 channels, 0.5-10 µL (Acura 855, Socorex, cat. n° 061132)
- pH meter (FiveEasy pH meter F20, Mettler Toledo, cat. n° 30266658)
  + pH electrode (LE438, Mettler Toledo, cat. n° 51340242)
- Pipettes, manual single-channel (*e.g.* Finnpipette from Thermo Scientific, Nichipet EX-Plus II from Nichiryo)
- Plate-reader (CLARIOstar Plus, BMG LABTECH)
- Tube rack (vendor of choice)
- UV-Vis spectrophotometer (Varian Cary 50 Probe, Agilent, no longer available for sale)
  + fibre-optic ultra-micro cell (Hellma TrayCell, Sigma-Aldrich, cat. n° Z802697)
- Water purification system (PURELAB flex 3, ELGA LabWater, cat. n° PF3XXXXM1)

Consumables

- Culture microplate, 96-wells, flat bottom, transparent plate, with lid (Corning-Falcon, cat. n° 353072)

- Filter tips, non-sterile (*e.g.* ClearLine, Fisherbrand SureOne, TipOne)
- Microtubes, with snap cap, DNase/RNase-free, non-sterile (0.5, 1.5, 2, 5 mL) (*e.g.* ClearLine, Eppendorf)

Individual protection equipment

- Lab coat (vendor of choice)
- Nitrile gloves (*e.g.* Kimtech)
- Safety glasses (vendor of choice)

Waste management equipment

- Bin for biohazard and chemical hazard liquid waste
- Bin for biohazard and chemical hazard solid waste

(See the existing legislation in the country of use)

Bioinformatics Softwares and Tools

- Cary WinUV software (Agilent), for the UV-Vis spectrophotometer
- Excel (Microsoft Corp.)
- OriginPro 9.1 (OriginLab Corp.)

3. MATERIALS – Buffers and solutions preparation

For buffers and solutions preparation, I used UV-treated PURELAB ultrapure (type 1) water.

- **50 mM ATP, pH 7.3** (in ultrapure water)
  e.g. mix 137.8 mg of ATP (M= 551.14 g/mol) in 5 mL of ultrapure water. Adjust the pH to 7.3 (*q.s.* 5 mL). Store at 4 °C. Around 1 mL of [1 M] LiOH is necessary.

- **1 M HCl** (in ultrapure water)
  e.g. add 8.35 mL of 37% (m/m) HCl* (M= 36.46 g/mol) in 91.65 mL of ultrapure water (*q.s.* 100 mL) (in that way). Store at 25 °C. *that 37% (m/m) HCl (d= 1.18) has a concentration of 11.97 M.

- **1 M KCl** (in ultrapure water)
  e.g. dissolve 7.46 g of KCl (M= 74.55 g/mol) in ultrapure water (*q.s.* 100 mL). Store at 4 °C.

- **Tris-HCl buffer 1** (20 mM Tris-HCl, 5 mM $MgCl_2$, 1 mM KCl, 99 mM NaCl, pH 7.2, in ultrapure water)
  e.g. mix 2 mL of 1 M Tris, 0.5 mL of 1 M $MgCl_2$, 0.1 mL of 1 M KCl, 9.9 mL of 1 M NaCl with 87.5 mL of ultrapure water. Adjust the pH to 7.2 with 1 M HCl (*q.s.* 100 mL). Store at 4 °C.

- **Tris-HCl buffer 2** (20 mM Tris-HCl, 10 mM $MgCl_2$, 1 mM KCl, 99 mM NaCl, pH 7.2, in ultrapure water)
  e.g. mix 2 mL of 1 M Tris, 1.0 mL of 1 M $MgCl_2$, 0.1 mL of 1 M KCl, 9.9 mL of 1 M NaCl with 87.0 mL of ultrapure water. Adjust the pH to 7.2 with 1 M HCl (*q.s.* 100 mL). Store at 4 °C.

- **1 M $MgCl_2$** (in ultrapure water)
  e.g. dissolve 0.95 g of KCl (M= 95.21 g/mol) in ultrapure water (*q.s.* 10 mL). Store at 4 °C.

- **1 M NaCl** (in ultrapure water)
  e.g. dissolve 2.92 g of NaCl (M= 58.44 g/mol) in ultrapure water (*q.s.* 50 mL). Store at 4 °C.

- **1 M Tris** (in ultrapure water)
  e.g. dissolve 2.42 g of Trizma base (M= 121.14 g/mol) in ultrapure water (*q.s.* 20 mL). Store at 4 °C.

4. METHODS – ONs and G4 ligands preparation

All oligonucleotides (ONs) used here were purchased from Eurogentec (Seraing, Belgium).

ON(s) necessitated for this technique is (are):

- dabcyl-labelled 49-nt ON
- FAM-labelled 15-nt ON
- c-hTelo
- Trap ON

1) Dilute ONs in ultrapure water (18.2 MΩ.cm resistivity) at 500 µM for stock solutions
2) Determine the actual concentration of these stock solutions through a dilution to 5 µM theoretical concentration *via* a UV spectral analysis at 260 nm, with the molar extinction coefficient (ε) values provided by the manufacturer and the Beer-Lambert law formula: A= εlC.

s-hTelo (= dabcyl-labelled 49-nt ON + FAM-labelled 15-nt ON)

3) Prepare a semi-working solution of s-hTelo at 1 µM (1 µM and 0.85 µM for dabcyl-labelled 49-nt ON and FAM-labelled 15-nt ON, respectively):
   e.g. mix 2 µL of the 500 µM dabcyl-labelled 49-nt ON stock solution with 1.7 µL of 500 µM FAM-labelled 15-nt ON stock solution and 996.3 µL of Tris-HCl buffer 1 (*q.s.* 1 mL).
4) For the long and complementary folding of the high-order structures (*i.e.*, a G-quadruplex and a duplex), heat the 1 µM s-hTelo semi-working solution in following a decreasing temperature level: 90 °C for 5 min, 80 °C for 10 min, 60 °C for 1 h, 50 °C for 1 h, 40 °C for 1 h, 30 °C for 1 h, at RT for 1 h.

5) Aliquot the folded 1 µM s-hTelo semi-working solution in putting 100 µL in 10 0.5 mL-microtubes (or microtubes with a higher capacity).
6) Store at -20 °C.
7) When you need an aliquot for an experiment, chill one microtube slowly at RT and add 400 µL of the Tris-HCl buffer 1 to the 100 µL of folded 1 µM s-hTelo semi-working solution to obtain 500 µL of the folded 0.2 µM s-hTelo working solution.

c-hTelo (= complementary strand to the dabcyl-labelled 49-nt ON constituting the s-hTelo)

8) Prepare a working solution of c-hTelo at 2 µM:
   e.g. mix 4 µL of the 500 µM c-hTelo stock solution with 996.0 µL of Tris-HCl buffer 1 (*q.s.* 1 mL).
9) Heat the 2 µM working solution at 90 °C for 5 min and then cool it on ice for at least 2 h.

   CRITICAL STEP: I don't think this step is mandatory but I always prefer heating ONs in case the high concentrated stock solution favored aggregation induction which can affect ONs (de)hybridation.

10) Store at 4 °C.

Trap (= complementary strand to the FAM-labelled 15-nt ON constituting the s-hTelo)

11) Prepare a working solution of Trap at 2 µM:
    e.g. mix 4 µL of the 500 µM Trap stock solution with 996.0 µL of Tris-HCl buffer 1 (*q.s.* 1 mL).
12) Heat the 2 µM working solution at 90 °C for 5 min and then cool it on ice for at least 2 h.

    CRITICAL STEP: i. I don't think this step is mandatory but I always prefer heating ONs in case the high concentrated stock solution favored aggregation induction which can affect ONs (de)hybridation.

13) Store at 4 °C.

    CRITICAL STEP: The first time you prepare a new ON, be sure of the success of the folding process in checking the high-order structure presence by CD measurement.

G4 ligands

14) Dilute G4 ligands from 100 µM or 1 mM stock solution (if possible, in water) in Tris-HCl buffer 1 at 1-2-5-10 µM for working solutions and experiment with 1-2-5-10 mol. equiv. (*i.e.*, 40-80-200-400 nM), respectively.
15) Store at 4 °C.

5. METHODS – Step by step protocol

STEP 0: PROTOCOL PREPARATION (TIMING: 1 day)

1) Prepare the following buffers and solutions:
   [50 mM] ATP, Tris-HCl buffer 1 and Tris-HCl buffer 2 (see above). Store all buffers at 4 °C.
2) Prepare ONs and G4 ligands (see above).

STEP 1: MICROPLATE PREPARATION AND FLUORESCENCE MONITORING (TIMING: 1.5 h)

3) Make a master mix of the following components for n wells and gently mix:
   - 10.0 *n µL of [0.2 µM] s-hTelo
   - 33.2 *n µL of Tris-HCl buffer 2
   - 5.0 *n µL of [2.0 µM] Trap

   CRITICAL STEPS: *i.* Being limited by the use of two 8-channels pipettes (one in each hand), only 16 microplate wells and thus conditions can be used in one experiment*. ii.* In order to have enough volume of master mix for all condition and thus all wells, it is better to prepare the mix for 2-3 additional wells depending on the total quantity of wells. *iii.* If possible, try to protect the s-hTelo from the light.

4) Dispense 48.2 µL of the master mix in each microplate well.

   CRITICAL STEP: The number of microplate wells used per line must not be superior than the number of channels of your pipettes.

5) Put the microplate into the Plate-reader.
6) Monitor the FAM FI every 10 s during 10 min to verify whether the s-hTelo FI is stable and to have the baseline, then save it.
   (Parameters for the CLARIOstar Plus: Focal height= 4.5 mm; Fluorescein λ_{exc}= 482 ± 16 nm and λ_{em}= 530 ± 40 nm; Gain= 1300; Top optic acquisition; Setting time= 0.1 s; N° of flashes per well and cycle= 1; Cycle time= 10 s; Shake= none).
7) Add in each microplate well 1.8 µL of the hPIF1 helicase ± buffer or small molecule treatment (**Table Mat&Meth 10**) and homogenize well the microplate in mixing slowly for 1-2 min on a laboratory rocker.
8) Monitor the FAM FI every 10 s during 10 min to verify whether the treatment modify the baseline, then save it.
9) Add, quickly and with the multi-channels pipettes, in each microplate well 5.0 µL of the [50 mM] ATP in stirring rapidly the wells with the pipettes.

10) Monitor the FAM FI every 10 s during 30 min (the time to have the semi-final plateau) to record the s-hTelo unwinding by the ATP-dependent hPIF1 and its consequences on FI, then save it.
11) Add, quickly and with the multi-channel pipettes, in each microplate well 5.0 µL of the [2 µM] c-hTelo in stirring rapidly the wells with the pipettes.
12) Monitor the FAM FI every 10 s during 30 min (the time to have the real final plateau) to record the complete s-hTelo unwinding by the c-hTelo hybridization and its consequences on FI, then save it.

CRITICAL STEP: The two last additions as well as the procedure launch on the plate-reader have to be very quick in order to record the increase of the FI.

Condition	**Volume (µL) (Final concentration)**		
Component	**-hPIF1**	**+hPIF1**	**+ hPIF1 + 10 mol. equiv.**
[0.2 µM] s-hTelo	10.0 µL (33.3 nM)		
Tris-HCl buffer 2	33.2 µL (~ 0.6 mM KCl)		
[2 µM] Trap	5 µL (166.7 nM)		
[10.8 µM] hPIF1	/	0.8 µL (143.0 nM)	
Additional Tris-HCl buffer	1.8 µL	1.0 µL	/
[20 µM] small molecule	/	/	1.0 µL (333.3 nM)
[50 mM] ATP	5.0 µL (4.2 mM)		
[2.0 µM] c-hTelo	5.0 µL (166.7 nM, thus 5.0 mol. equiv.)		
Volume total	**50.0 + 5.0 + 5.0 = 60.0 µL**		

Table Mat&Meth 10. Summary of experimental conditions applied for the hPIF1 helicase assay. The volume needed for each condition (Control, 10 mol. equiv. of small molecule) and the concentration are informed. A master mix can be prepared with the [0.2 µM] s-hTelo, the [2.0 µM] Trap and the basal Tris-HCl buffer 2 (20 mM Tris-HCl, 10 mM $MgCl_2$, 1 mM KCl, 99 mM NaCl, pH 7.2), then 48.2 µL of this master mix have to be dispensed in each well microplate, the FI is monitored during 10 min, 1.8 µL of the hPIF1 helicase ± buffer (Control) or small molecule (treatment) have to be added in appropriated wells, the FI is monitored again during 10 min, then 5.0 µL of the [50 mM] ATP is added quickly, the FI is monitored during around 30 min, then 5.0 µL of the [2.0 µM] c-hTelo is added quickly and the FI is finally monitored during around 30 min. Bold bars separate the different steps.

STEP 2: DATA TREATMENT (TIMING: 20-40 min)

13) With the plate-reader system, export all the raw data of FAM fluorescence intensity (FI).
14) With your treatment software, (0;1) normalize (optional) or not the FI values of the second to last monitoring (*i.e.*, after the ATP addition).
15) Take the five first points (*i.e.*, FI at 0, 10, 20, 30 and 40 s) after the c-hTelo addition. Due to fluorescence variability, if there is a sudden punctual decrease (often during 2-5 points) through the FI increase, do not take these decreasing points.

16) Display these five points in a FAM fluorescence intensity=f(time) function manner and apply a linear fitting on them.
17) The slope value of the fit right line obtained is the V_0 speed (s^{-1}).

    INFORMATION: For statistical hypothesis tests, Student's *t*-test and Welch's unequal variances *t*-test were used depending on variances equality. * $p < 0.05$, ** $p < 0.01$, *** $p < 0.001$, **** $p < 0.0001$.

18) Make your data representation with these values.

X. Sulforhodamine B (SRB) cytotoxicity assay

CRITICAL: Biological materials, reagents and equipment can be obtained from various vendors and do not need to be from the ones specified here.

1. MATERIALS – Biological materials

Cell line

- MCF7 (ECACC, cat. n° 86012803)

2. MATERIALS – Reagents

Cell culturing

- 1X PBS (Dutscher, cat. n° L0615)
- CO_2 bottle (Air Liquide, cat. n° I5100M14R0A001)
- Dulbecco's Modified Eagle Medium (DMEM) (Dutscher, cat. n° L0104)
- Fetal bovine serum (FBS) (Dutscher, cat. n° S1810)
- Penicillin-streptomycin (P-S) (Gibco, cat. n° 151-40-122)
- Trypsin (Dutscher, cat. n° L0910)

Chemical products and/or buffer components

- Acetic acid glacial (VWR Chemicals, cat. n° 20104.334)
- DMSO (Sigma-Aldrich, cat. n° D8418)
- Sulforhodamine B (SRB), sodium salt (Thermo Scientific, cat. n° A14769.14)
- Trichloroacetic acid (TCA) (Sigma-Aldrich, cat. n° T6399)
- Trizma® base (Sigma-Aldrich, cat. n° 933632)

Molecular tools

- BioCyTASQ (Sigma-Aldrich, cat. n° SCT246)
- BRACO-19 (Sigma-Aldrich, cat. n° SML0560)
- N-TASQ (produced in lab)
- PDS (Sigma-Aldrich, cat. n° SML2690)
- PhpC (produced by Robert H. E. Hudson's lab)

3. MATERIALS – Equipment

Devices and lab equipment

- Benchtop centrifuge (vendor of choice)
- Benchtop laboratory rocker (vendor of choice)

- Benchtop vortex (vendor of choice)
- Blow dryer (vendor of choice)
- Cell counting chamber / haemocytometer (Neubauer Improved, Brand, cat. n° 717820)
- Optical binocular microscope (vendor of choice)
- Pipet filler, motorized (*e.g.* Powerpette Pro, VWR, cat. n° 612-4552)
- Pipettes, manual multichannel, 8 channels, 0.5-10 µL (Acura 855, Socorex, cat. n° 061132)
- Pipettes, manual single-channel (*e.g.* Finnpipette from Thermo Scientific, Nichipet EX-Plus II from
- Plate-reader (CLARIOstar Plus, BMG LABTECH)
- Standard cell culture CO_2 incubator (BB 15, Thermo Scientific, cat. n° 51023121)
- Tube rack (vendor of choice)
- Water purification system (PURELAB flex 3, ELGA LabWater, cat. n° PF3XXXXM1)

Consumables

- Cell culture flasks (175 cm^2), with cap with filter membrane (Falcon, cat. n° 353112)
- Culture microplate, 96-wells, flat bottom, transparent plate, with lid (Corning-Falcon, cat. n° 353072)
- Filter tips, non-sterile and sterile (*e.g.* ClearLine, Fisherbrand SureOne, TipOne)
- Microtubes, with snap cap, DNase/RNase-free, non-sterile and sterile (1.5, 2, 5 mL) (*e.g.* ClearLine, Eppendorf)
- Serological pipets, sterile (*e.g.* Eppendorf, Falcon)
- Tubes (15, 50 mL) (*e.g.* Falcon)

Individual protection equipment

- Lab coat (vendor of choice)
- Nitrile gloves (*e.g.* Kimtech)
- Safety glasses (vendor of choice)
- Standard biosafety cabinet (vendor of choice)
- Standard fume hood (vendor of choice)

Waste management equipment

- Bin for biohazard and chemical hazard liquid waste
- Bin for biohazard and chemical hazard solid waste

(See the existing legislation in the country of use)

Bioinformatics Softwares and Tools

- Excel (Microsoft Corp.)
- OriginPro 9.1 (OriginLab Corp.)

4. MATERIALS – Buffers and solutions preparation

For buffers and solutions preparation, I used UV-treated PURELAB ultrapure (type 1) water.

- **1% (v/v) acetic acid**

  e.g. mix 500 µL of acetic acid glacial (M= 60.05) with 49.5 mL of ultrapure water (*q.s.* 50 mL). Store at 4 °C.

- **20 mM BRACO-19** (in DMSO)

  e.g. dissolve 11.9 mg of BRACO-19 (M= 593.76 g/mol) in 1 mL of DMSO (*q.s.* ~ 1 mL) under a safety cabinet. Store at 4 °C.

- **20 mM PhpC** (in ultrapure water)

  e.g. dissolve 3.56 mg of PhpC (M= 356.37 g/mol) in 500 µL of ultrapure water (*q.s.* ~ 500 µL) under a safety cabinet. Aliquote and store at -20 °C.

- **20 mM PDS** (in DMSO)

  e.g. dissolve 11.93 mg of PDS (M= 596.65 g/mol) in 1 mL of DMSO (*q.s.* ~ 1 mL) under a safety cabinet. Store at 4 °C.

- **0.057% (w/v) sulforhodamine B (SRB)** (in acetic acid)

  e.g. mix 285 mg of SRB (M= 580.65 g/mol) in 500 mL of 1% (v/v) acetic acid (*q.s.* ~ 500 mL). Store at 25 °C.

- **Supplemented DMEM** (culture medium) (10% (v/v) FBS, 1% (v/v) Pen-Strep, in DMEM)

  e.g. mix 56 mL of Fetal bovin serum and 6 mL of Penicillin-streptomycin (conc) with 500 mL of Dulbecco's Modified Eagle Medium (DMEM, High Glucose, w/ L-Glutamin, w/ Sodium Pyruvate) (*q.s.* 556 mL), under a safety cabinet. Store at 4 °C.

- **10% (w/v) trichloroacetic acid (TCA)** (in ultrapure water)

  e.g. dissolve 5 g of TCA (M= 163.39 g/mol) in 50 mL of ultrapure water (*q.s.* 50 mL). Store at 4 °C.

- **10 mM Trizma base, pH 10.5** (in ultrapure water)

e.g. dissolve 1.21 g of Trizma base (M= 121.14 g/mol) in 1 L of ultrapure water (*q.s.* 1 L). Store at 4 °C.

The solution below have to be fresh and then prepared the day of the G4 ligands addition (STEP 2, sub-step 6).

- **5% (v/v) DMSO supplemented DMEM**
  e.g. mix 750 µL of DMSO with 14.250 mL of Supplemented DMEM (*q.s.* 15 mL). Store at 4 °C.

5. METHODS – Step by step protocol

STEP 0: PROTOCOL PREPARATION (TIMING: 1 h)

1) Prepare the following buffers and solutions:
   1% (v/v) acetic acid, 20 mM G4 ligands (BRACO-19, PhpC), 0.057% (w/v) sulforhodamine B (SRB), supplemented DMEM, 10% (w/v) trichloroacetic acid (TCA), 10 mM Trizma base pH 10.5 (see above). Store all the buffers and solutions at 4 °C, except the 1% (v/v) acetic acid and the 0.057% (w/v) SRB at room temperature (RT; 21-25 °C).

   CRITICAL STEP: Try to prepare the G4 ligands in a sterile manner (*i.e.,* with RNase-free DMSO and water and/or 0.2 µm filtration).

STEP 1: CELL MICROPLATE PREPARATION (TIMING: 1 h)

2) On day 1 morning, $4x10^3$ MCF7 cells in exponential phase growth (in 160 µL; being $2.5x10^4$ cells/mL) are seeded per well of the 96-wells culture microplate in supplemented DMEM culture medium (10% (v/v) FBS, 1% (v/v) Pen-Strep). Allow cells to recover for 24 h under cell culture condition (37 °C, 5% CO_2).

   CRITICAL STEP: The last column (n° 12) can be kept for the background control: no cells.

STEP 2: HELPING MICROPLATE PREPARATION (TIMING: 1-2 h)

3) On day 2 morning, prepare freshly the following solution: 5% (v/v) DMSO supplemented DMEM.

   CRITICAL STEP: If possible with the concentration range, the use of a 2.5% (v/v) DMSO supplemented DMEM (and not 5%), thus 0.5% final (and not 1%), is encouraged for the cell care.

4) Prepare the helping microplate with the 5X G4 ligands concentration range in keeping two microplate lines for each G4 ligands (technical duplicate) (see **Tables S18 and S33** for the 1X final concentration range).

CRITICAL STEPS: i. Working with technical duplicate, for each biological singlicate, is enough. ii. Depending on the concentration range you want to assess, you can prepare G4 ligands concentrations individually with appropriated dilutions or in serial dilution (for each G4 ligands or for the whole microplate). iii. For each DMSO-dissolved G4 ligands, each 5X concentrations should be at the same DMSO percentage in the helping microplate, in diluting G4 ligands with the 5% (v/v) DMSO supplemented DMEM. Due to the maximal concentration I chose for BRACO-19 (5X= 1000 µM; 1X= 200 µM), from the 20 mM stock solution (100% DMSO), the DMSO percentage for each 5X concentrations was capped at 5% and thus 1% for the 1X G4 ligand in the cell microplate. For the concerned microplate lines, be sure to prepare the corresponding negative control (untreated cells) wells in taking account of the DMSO percentage (*i.e.*, with the 5% (v/v) DMSO supplemented DMEM) if applicable.

5) Homogenize well the helping microplate in mixing for 5 min on a laboratory rocker.

CRITICAL STEP: Centrifuging the helping microplate can help if there is some G4 ligands or supplemented DMEM (control; +/- DMSO) in wells corner. Then mix.

6) Dispense 40 µL of 5X G4 ligands or supplemented DMEM (control; +/- 5% (v/v) DMSO) from the helping microplate to the cell microplate (160 µL).

CRITICAL STEP: To avoid tips wasting, you can keep the same in starting by dispensing the supplemented DMEM (control; +/- 5% (v/v) DMSO) alone, then the helping microplate column containing the less concentrated 5X G4 ligands to the more concentrated.

7) Homogenize well the cell microplate in mixing slowly for 2 min on a laboratory rocker.
8) Incubate the cell microplate for 72 h under cell culture condition (37 °C, 5% CO_2).

STEP 3: CELL FIXATION (TIMING: 2-3 h)

9) On day 5, add 120 µL of cold 10% (w/v) TCA solution in each well of the cell microplate.

CRITICAL STEP: For an entire 96-wells microplate, prepare at least 12 mL of 10% (w/v) TCA solution.

10) Incubate the cell microplate for 1 h at 4 °C.
11) Empty the cell microplate.

CRITICAL STEP: To empty the cell microplate, you can just tap the microplate on a funnel placed on the bin for biohazard and chemical hazard liquid waste.

12) Wash the cell microplate carefully with water, empty and dry it in tapping on paper towel (x5).
13) Dry the cell microplate in allowing it at 25 °C overnight or with a blow dryer for 45 min.

CRITICAL STEPS: i. For the drying overnight, keep the microplate open but turned back on the lid to avoid condensation in the bottom of wells. ii. For the drying with blow dryer, do not let the blow dryer too close of the microplate to avoid a distortion of the plastic microplate.

PAUSE POINT: Once the cell microplate is fixed and dried, it can be stored indefinitely at RT.

STEP 4: CELL REVELATION (TIMING: 2 h)

14) Add 100 µL of the 0.057% (w/v) SRB solution per well of the cell microplate.

CRITICAL STEPS: i. Be careful to bubble. ii. For an entire 96-wells microplate, prepare at least 10 mL of 0.057% (w/v) SRB solution.

15) Incubate the cell microplate for 30 min at RT.
16) Discard the SRB.
17) Wash the cell microplate with ~150 µL of the 1% (v/v) acetic acid solution per well and discard it as fast as possible in tapping on the bin and paper towel (x3).

CRITICAL STEP: For an entire 96-wells microplate, prepare at least 50 mL of 1% (v/v) acetic acid solution.

18) Dry the cell microplate in allowing it at 25 °C overnight or with a blow dryer for 45 min.
19) Add 150 µL of cold 10 mM Trizma base pH 10.5 per well.
20) Incubate well the microplate for 5 min on a laboratory rocker.
21) Measure the absorbance at 530 nm of for each well with the plate-reader (CLARIOstar Plus).

INFORMATION: The λ_{max} of SRB in water is between 561 and 566 nm.

STEP 5: DATA TREATMENT (TIMING: 1-2 h)

22) Calculate the mean for the negative (untreated cells) and background (no cells) controls: Mean A_{530} negative control and Mean A_{530} background control.

23) CRITICAL STEP: Treat separately the negative control of water-dissolved G4 ligand lines (untreated cells, incubated with supplemented DMEM; the PhpC lines) and the DMSO-dissolved G4 ligand lines (untreated cells, incubated with 5% (v/v) DMSO supplemented DMEM; the BRACO-19 lines).

24) Calculate the mean for each G4 ligand concentration [x] and for each G4 ligand with technical duplicates $A_{530\,nm}$ data: Mean A_{530} G4 ligand [x].

25) Calculate the cell viability value for each G4 ligand concentration [x] and for each G4 ligand using the formula below:

Normalized cell viability (in %)=

$$\left[\left(\text{Mean } A_{530} \text{ G4 ligand [x]} - \text{Mean } A_{530} \text{ background control}\right) \Big/ \left(\text{Mean } A_{530} \text{ negative control} - \text{Mean } A_{530} \text{ background control}\right)\right] * 100$$

26) Calculate the Mean normalized cell viability values for each G4 ligand concentration [x] and for each G4 ligand with biological triplicate.

27) Make your data representation with these mean normalized cell viability values as a function of the G4 ligands concentration (in µM) (with a log10 abscissa axis).

28) Calculate inhibitory concentration values (*e.g.*, IC_{20}, IC_{50}, IC_{80}) in performing a sigmoidal fit (Dose Response) with OriginPro (OriginLab Corp.).

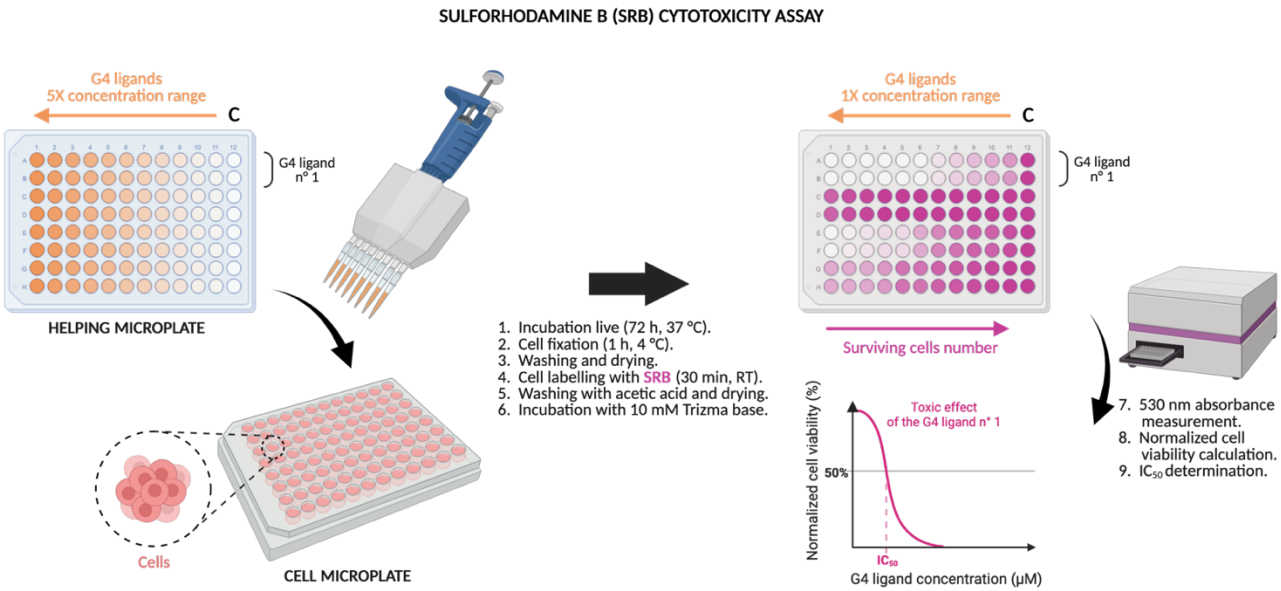

Figure Mat&Meth 7. Schematic representation of the Sulforhodamine B (SRB) cytotoxicity assay procedure. Cells potential toxicity effects of the two G4 ligands BRACO-19 and PhpC were assessed by the SRB assay using a Negative control (untreated cells) and a Background control (no cells). Created with BioRender.com

XI. Optical imaging

CRITICAL: Reagents and equipment can be obtained from various vendors and do not need to be from the ones specified here.

1. MATERIALS – Biological materials

Cell line

- MCF7 (ECACC, cat. n° 86012803)

2. MATERIALS – Reagents

Cell culturing

- 1X PBS (Dutscher, cat. n° L0615)
- CO_2 bottle (Air Liquide, cat. n° I5100M14R0A001)
- Dulbecco's Modified Eagle Medium (DMEM) (Dutscher, cat. n° L0104)
- Fetal bovine serum (FBS) (Dutscher, cat. n° S1810)
- Penicillin-streptomycin (P-S) (Gibco, cat. n° 151-40-122)
- Trypsin (Dutscher, cat. n° L0910)

Chemical products and/or buffer components

- Antibody anti-γH2AX (Sigma-Aldrich, cat. n° 05-636)
- Antibody anti-mouse – Alexa Fluor 647 (abcam, cat. n° ab150107)
- Bovin serum albumin (BSA) (VWR, cat. n° 1000-70)
- DAPI (Sigma-Aldrich, cat. n° D9542)
- DMSO (Sigma-Aldrich, cat. n° D8418)
- DRAQ5 (abcam, cat. n° ab108410)
- Fluoromount-G (Invitrogen, cat. n° 00-4958-02)
- Streptavidin-Cy3, SA-Cy3 (Thermo Scientific, cat. n° 434315)
- Triton X-100 (Sigma-Aldrich, cat. n° X100)

Molecular tools

- BioCyTASQ (Sigma-Aldrich, cat. n° SCT246)
- BioTriazoTASQ (produced in lab)
- N-TASQ (produced in lab)
- PDS (Sigma-Aldrich, cat. n° SML2690)
- PhpC (produced by Robert H. E. Hudson's lab)

3. MATERIALS – Equipment

Devices and lab equipment

- Benchtop centrifuge (vendor of choice)
- Benchtop heating block (ThermoMixer C, Eppendorf, cat. n° 5382 000.015)
- Benchtop laboratory rocker (vendor of choice)
- Benchtop vortex (vendor of choice)
- Blow dryer (vendor of choice)
- Cell counting chamber / haemocytometer (Neubauer Improved, Brand, cat. n° 717820)
- Confocal microscope (Leica TCS SP8, Leica Microsystems)
  + 63X objective lens
- Optical binocular microscope (vendor of choice)
- Pipet filler, motorized (*e.g.* Powerpette Pro, VWR, cat. n° 612-4552)
- Pipettes, manual multichannel, 8 channels, 0.5-10 µL (Acura 855, Socorex, cat. n° 061132)
- Pipettes, manual single-channel (*e.g.* Finnpipette from Thermo Scientific, Nichipet EX-Plus II from Nichiryo)
- Plate-reader (CLARIOstar Plus, BMG LABTECH)
- Standard cell culture CO_2 incubator (BB 15, Thermo Scientific, cat. n° 51023121)
- Tube rack (vendor of choice)
- Water purification system (PURELAB flex 3, ELGA LabWater, cat. n° PF3XXXXM1)

Consumables

- Cell culture flasks (175 cm^2), with cap with filter membrane (Falcon, cat. n° 353112)
- Cover glasses, round, 12 mm, #1 thickness (0.13 to 0.16 mm) (Marienfeld Superior, cat. n° 0111520)
- Culture microplate, 4-wells, flat bottom, transparent plate, with lid (NUNC, cat. n° 176740)
- Filter tips, sterile (*e.g.* ClearLine, Fisherbrand SureOne, TipOne)
- Microscope slides, 26x76x1 mm (Epredia, cat. n° AA00000112E01MNZ10)
- Microtubes, with snap cap, DNase/RNase-free, non-sterile (0.5, 1.5, 2, 5 mL) (*e.g.* ClearLine, Eppendorf)
- Serological pipets, sterile (*e.g.* Eppendorf, Falcon)
- Tubes (15, 50 mL) (*e.g.* Falcon)
- Tweezers (vendor of choice)

Individual protection equipment

- Lab coat (vendor of choice)
- Nitrile gloves (*e.g.* Kimtech)

- Safety glasses (vendor of choice)
- Standard biosafety cabinet (vendor of choice)

Waste management equipment

- Bin for biohazard and chemical hazard liquid waste
- Bin for biohazard and chemical hazard solid waste

(See the existing legislation in the country of use)

Bioinformatics Softwares and Tools

- Cary WinUV software (Agilent), for the UV-Vis spectrophotometer
- Excel (Microsoft Corp.)
- Fiji software[14]
- LAS X software (Leica Microsystems)
- OriginPro 9.1 (OriginLab Corp.)

4. MATERIALS – Buffers and solutions preparation

For buffers and solutions preparation, I used UV-treated PURELAB ultrapure (type 1) water.

- **Blocking buffer** (1% (w/v) BSA, 0.1% (v/v) Triton X-100, in 1X PBS)
  e.g. dissolve 500 mg of BSA in 50 µL of Triton X-100 and 49.95 mL of 1X PBS (*q.s.* 50 mL). Store at 4 °C.

- **1 mg/mL DAPI** (in 1X PBS)
  e.g. dissolve 1 mg of the DAPI with 1 mL of 1X PBS (*q.s.* 1 mL). Store at 4 °C and protect from light.

- **1 µg/mL DAPI** (in 1X PBS)
  e.g. dilute 10 µL of the 1 mg/mL DAPI solution in 9.99 mL of 1X PBS (*q.s.* 10 mL). Store at 4 °C and protect from light.

- **PBST solution** (0.1% (v/v) Triton X-100, in 1X PBS)
  e.g. dilute 0.5 mL of the Triton X-100 solution in 499.5 mL of 1X PBS (*q.s.* 500 mL). Store at RT.

- **50 µM PDS** (in DMSO)
  e.g. dilute 2.5 µL of the 20 mM PDS solution in 997.5 µL of DMSO (*q.s.* 1 mL). Store at 4 °C.

- **20 µM PhpC** (in ultrapure water)

e.g. dilute 1.0 µL of the 20 mM PhpC solution in 999.0 µL of ultrapure water (*q.s.* 1 mL). Store at 4 °C.

- **Supplemented DMEM** (culture medium) (10% (v/v) FBS, 1% (v/v) Pen-Strep, in DMEM) *e.g.* mix 56 mL of Fetal bovin serum and 6 mL of Penicillin-streptomycin (conc) with 500 mL of Dulbecco's Modified Eagle Medium (DMEM, High Glucose, w/ L-Glutamin, w/ Sodium Pyruvate) (*q.s.* 556 mL), under a safety cabinet. Store at 4 °C.

5. METHODS – Step by step protocol

STEP 0: PROTOCOL PREPARATION (TIMING: 1 h)

1) Prepare the following buffers and solutions:
   Blocking buffer, 1 µg/mL DAPI, PBST, 20-50 µM G4 ligands (PDS, PhpC), supplemented DMEM. Store all the buffers and solutions at 4 °C, except the PBST at room temperature (RT; 21-25 °C).

   CRITICAL STEP: Try to prepare the G4 ligands in a sterile manner (*i.e.,* with RNase-free DMSO and water and/or 0.2 µm filtration).

2) Clean the cover glasses: a 70% (v/v) Ethanol solution bath overnight, then dry them for one day

STEP 1: CELL MICROPLATE PREPARATION (TIMING: 1 h)

3) On day 1 morning, $6x10^4$ MCF7 cells in exponential phase growth (in 360 µL; being $1.7x10^5$ cells/mL) are seeded per cover glass-containing well of the 4-wells culture microplate in supplemented DMEM culture medium (10% (v/v) FBS, 1% (v/v) Pen-Strep). Allow cells to recover for 24 h under cell culture condition (37 °C, 5% CO_2).

STEP 2: HELPING MICROPLATE PREPARATION (TIMING: 2 days)

4) On day 2 morning, make the following treatment depending on the experiment (**Table Mat&Meth 11**):

Optical imaging with BioCyTASQ and BioTriazoTASQ (-/+ PDS)

- Pre-treatment with PDS (5 µM) or DMEM/DMSO solution (to have a similar final % DMSO) for 6 h at 37 °C
- Cell fixation with 100% Methanol for 10 min at -20 °C
- 1X PBS washing (3x)
- Cell blocking (and additional permeabilization) with blocking buffer for 10 min at RT
- Incubation with a mixed solution of TASQ (10 µM) and mouse anti-γH2AX IgG (1 µg/mL) for overnight (16 h) at 4 °C

- PBST washing (3x)
- Incubation with a mixed solution of SA-Cy3 (1 µg/mL) and donkey anti-mouse IgG–Alexa Fluor 647 (4 µg/mL) for 45 min at RT in dark chamber
- PBST washing (3x)
- Incubation with DAPI (1 µg/mL) for 5 min at RT in dark chamber
- PBST washing (3x)
- Water washing
- Slide mounting and sealing with Fluoromount-G, let dry some hour

Optical imaging with N-TASQ (-/+ PhpC)

- Pre-treatment with PhpC (20 µM) or DMEM solution for 2 h alone at 37 °C
- Addition of the N-TASQ (50 µM) and incubation for 6 h at 37 °C
- Cell fixation with 100% Methanol for 10 min at -20 °C
- 1X PBS washing (3x)
- (Optional: Incubation with DRAQ5 (5 µM) for 5 min at RT in dark chamber)
- (PBS washing (3x))
- Water washing
- Slide mounting and sealing with Fluoromount-G, let dry some hour

<table>
<tr><th colspan="6">Summary parameters used for optical imaging</th></tr>
<tr><td colspan="6">Optical imaging with the biotinylated BioCyTASQ and BioTriazoTASQ</td></tr>
<tr><td>Treatment conditions</td><td>Cell fixation conditions</td><td>G4 probe conditions</td><td>Primary antibody (or eq.)</td><td>Secondary antibody (or eq.)</td><td>Acquisition parameters</td></tr>
<tr><td rowspan="3">-/+ PDS, 5 µM, for 6 h at 37 °C, live cells</td><td rowspan="3">Cold methanol, for 10 min at -20 °C</td><td rowspan="3">BioCyTASQ or BioTriazoTASQ, 10 µM, for 16 h at 4 °C, post-fixed cells</td><td colspan="2">Streptavidin-Cy3, 1 µg/mL, for 45 min at 25 °C in dark chamber, post-fixed cells</td><td>λ_{exc}= 552 nm (2.0%); λ_{em}= 558-575 nm (gain = 50%)</td></tr>
<tr><td>Mouse anti-γH2AX IgG, 1 µg/mL, for 16 h at 4 °C, post-fixed cells</td><td>Donkey α-mouse IgG–Alexa Fluor 647, 4 µg/mL, for 45 min at 25 °C in dark chamber, post-fixed cells</td><td>λ_{exc}= 638 nm (0.1%); λ_{em}= 644-696 nm (gain = 50%)</td></tr>
<tr><td colspan="2">DAPI, 1 µg/mL, for 5 min at 25 °C in dark chamber, post-fixed cells</td><td>λ_{exc}= 405 nm (0.2%); λ_{em}= 448-475 nm (gain = 60%)</td></tr>
<tr><td colspan="6">Optical imaging with the N-TASQ</td></tr>
<tr><td>Treatment conditions</td><td>G4 probe conditions</td><td>Cell fixation conditions</td><td colspan="2">Other fluorophore conditions</td><td>Acquisition parameters</td></tr>
<tr><td rowspan="2">-/+ PhpC, 20 µM, for 8 h at 37 °C, live cells</td><td rowspan="2">N-TASQ, 50 µM, for 6 h at 37 °C, live cells</td><td rowspan="2">Cold methanol, for 10 min at -20 °C</td><td colspan="2" rowspan="2">-/+ DRAQ5, 5 µM, for 5 min at 25 °C, post-fixed cells</td><td>λ_{exc}= 405 nm (2%); λ_{em}= 450-530 nm (gain = 100%)</td></tr>
<tr><td>λ_{exc}= 638 nm (0.5%); λ_{em}= 680-720 nm (gain = 100%)</td></tr>
</table>

Table Mat&Meth 11. Summary parameters used for optical imaging. Summary parameters used for the optical imaging of G4s with the biotinylated TASQs: MCF7 cells non-treated or live treated with PDS (5 µM, 6 h) and then treated after cell fixation with BioCyTASQ or BioTriazoTASQ (1 µM, 16 h), tagged with SA-Cy3, which is followed by immunodetection of DNA damage nuclear γH2AX *foci* (with IgG-Alexa Fluor 647) and chromatin staining by DAPI; and for the optical imaging of G4s with the smart N-TASQ: MCF7 cells non-treated or live treated with PhpC (20 µM, 8 h) and N-TASQ (50 µM, 6 h) simultaneously. Eq.= equivalent fluorophore.

XII. G4RP.v2

CRITICAL: Biological materials, reagents and equipment can be obtained from various vendors and do not need to be from the ones specified here.

1. MATERIALS – Biological materials

Cell line

- MCF7 (ECACC, cat. n° 86012803)

2. MATERIALS – Reagents

Cell culturing

- 1X PBS (Dutscher, cat. n° L0615)
- CO_2 bottle (Air Liquide, cat. n° I5100M14R0A001)
- Dulbecco's Modified Eagle Medium (DMEM) (Dutscher, cat. n° L0104)
- Fetal bovine serum (FBS) (Dutscher, cat. n° S1810)
- Penicillin-streptomycin (P-S) (Gibco, cat. n° 151-40-122)
- Trypsin (Dutscher, cat. n° L0910)

Chemical products and/or buffer components

- 10X PBS (Dutscher, cat. n° X0515)
- 16% (w/v) Formaldehyde solution (Thermo Scientific, cat. n° 28908)
- Diethylpyrocarbonate (DEPC) (Sigma-Aldrich, cat. n° D5758)
- DMSO (Sigma-Aldrich, cat. n° D8418)
- DTT (Sigma-Aldrich, cat. n° D0632)
- EDTA (Thermo Scientific, cat. n° 11843)
- EGTA (Sigma-Aldrich, cat. n° E3889)
- Glycine (Sigma-Aldrich, cat. n° G8898)
- HCl (Fisher Chemical, cat. n° H/1150)
- HEPES (Thermo Scientific Chemicals, cat. n° 17257)
- KCl (Sigma-Aldrich, cat. n° P3911)
- KOH (Honeywell Fluka, cat. n° 30603)
- Liquid nitrogen (Air Liquide, cat. n° I4001XX3)
- NaCl (VWR Chemicals, cat. n° 27810)
- NaOH (Fisher Chemical, cat. n° S/4920/60)
- RNase OUT™, recombinant ribonuclease inhibitor (Invitrogen, cat. n° 10777019)
- SDS (Sigma-Aldrich, cat. n° L3771)

- Tergitol™ (Sigma-Aldrich, cat. n° NP40S)
- Trifluoroacetic acid (Fisher Chemical, cat. n° T/3258)
- Trizma® base (Sigma-Aldrich, cat. n° 933632)
- UltraPure Distilled Water (Invitrogen, cat. n° 10977035)

Molecular tools

- BioCyTASQ (Sigma-Aldrich, cat. n° SCT246)
- BioTASQ (produced in lab)
- BioTriazoTASQ (produced in lab)
- Biotin (Sigma-Aldrich, cat. n° B4501)
- BRACO19 (Sigma-Aldrich, cat. n° SML0560)
- Clickable ^{az}MultiTASQ (produced in lab)
- DBCO-PEG(4)-Biotin (Iris Biotech, cat. n° RL-2520)
- PhpC (produced by Robert H. E. Hudson's lab)
- Streptavidin MagneSphere® Paramagnetic Particles (Promega, cat. n° Z5481)

RNA purification kit, Reverse Transcription and qPCR products

- 5X First Strand buffer (see "SuperScript™ III Reverse Transcriptase kit")
- Chloroform (Carlo Erba, cat. n° 438603)
- dNTP mix (Thermo Scientific, cat. n° R0191)
- DTT [0.1 M] (see "SuperScript™ III Reverse Transcriptase kit")
- Ethanol absolute (VWR Chemicals, cat. n° 15338)
- iTaq™ Universal SYBR® Green Supermix (Bio-Rad, cat. n° 1725121)
- Random hexamers (Invitrogen, cat. n° N8080127)
- RNA Clean & Concentrator-5, supplied with DNase I (Zymo Research, cat. n° ZR1013)
- RNase OUT™, recombinant ribonuclease inhibitor (Invitrogen, cat. n° 10777019)
- SuperScript™ III Reverse Transcriptase kit (Invitrogen, cat. n° 18080044)
- TRIzol™ (Invitrogen, cat. n° 15596026)

Denaturating agarose gel reagents

- 2X RNA loading dye solution (see "RiboRuler High Range RNA Ladder, ready-to-use")
- Agarose (Lonza, cat. n° LON50004)
- Bleach (Orapi, cat. n° 619)
- EDTA (Thermo Scientific, cat. n° 11843)
- Orthoboric acid (VWR Chemicals, cat. n° 20185)

- RiboRuler High Range RNA Ladder, ready-to-use (Thermo Scientific, cat. n° SM1823)
- SYBR™ Gold Nucleic Acid Gel Stain (Invitrogen, cat. n° S11494)
- Trizma® base (Sigma-Aldrich, cat. n° 933632)

3. MATERIALS – Equipment

Devices and lab equipment

- Benchtop centrifuge (vendor of choice)
- Benchtop heating block (ThermoMixer C, Eppendorf, cat. n° 5382 000.015)
- Benchtop laboratory rocker (vendor of choice)
- Benchtop rotator (PTR-35, Grant-Bio, cat. n° 144208B)
- Benchtop vortex (vendor of choice)
- Cell counting chamber / haemocytometer (Neubauer Improved, Brand, cat. n° 717820)
- Compressed air system (vendor of choice)
- Dry ice box (vendor of choice)
- Freezer -80 °C (vendor of choice)
- Gel imager (ChemiDoc MP Imaging System, Bio-Rad, cat. n° 12003154)
  + Blot/UV/Stain-Free Sample Tray for ChemiDoc MP Imaging System (Bio-Rad, cat. n° 12003028)
- Gel shovel (vendor of choice)
- Ice maker (vendor of choice)
- Lyophilizer (Alpha 2-4 LD Plus, Christ, no longer available for sale)
- Magnetic rack (Magna GrIP Rack, Sigma-Aldrich, cat. n° 20-400)
- Mini Horizontal Electrophoresis System (Major Science, cat. n° MT108)
  + power supply (vendor of choice)
- Optical binocular microscope (vendor of choice)
- pH meter (FiveEasy pH meter F20, Mettler Toledo, cat. n° 30266658)
  + pH electrode (LE438, Mettler Toledo, cat. n° 51340242)
- Pipet filler, motorized (*e.g.* Powerpette Pro, VWR, cat. n° 612-4552)
- Pipettes, single-channel (*e.g.* Finnpipette from Thermo Scientific, Nichipet EX-Plus II from Nichiryo)
- Real-time PCR system and thermocycler (Mx3005P, Agilent)
- Refrigerated centrifuge (Universal 320 R, Hettich, cat. n° 1406)
  (or a classical centrifuge in a refrigerated room)
- Scissor (vendor of choice)
- Standard cell culture CO_2 incubator (BB 15, Thermo Scientific, cat. n° 51023121)
- Tube rack (vendor of choice)

- UV-Vis spectrophotometer (Varian Cary 50 Probe, Agilent, no longer available for sale)
  + fibre-optic ultra-micro cell (Hellma TrayCell, Sigma-Aldrich, cat. n° Z802697)
- Water purification system (PURELAB flex 3, ELGA LabWater, cat. n° PF3XXXXM1)

Consumables

- Cell culture flasks (175 cm^2), with cap with filter membrane (Falcon, cat. n° 353112)
- Filter 0.22 µm for bottle, sterile (Stericup quick release-GP sterile vacuum filtration system, Millipore, cat. n° S2GPU10RE)
- Filter 0.2 µm for syringe, sterile (Minisart NML, Sartorius, cat. n° 16534-K)
- Filter tips, non-sterile and sterile (*e.g.* ClearLine, Fisherbrand SureOne, TipOne)
- Microtubes, with snap cap, DNase/RNase-free, non-sterile and sterile (1.5, 2, 5 mL) (*e.g.* ClearLine, Eppendorf)
- PCR plate, 96-wells (Agilent, cat. n° 401334)
  + optical strip caps (Agilent, cat. n° 401425)
- PCR tubes (0.2 mL) (4TITUDE, cat. n° 4ti-0790)
- RNaseZap™ (Fisher Scientific, cat. n° AM9780)
- Serological pipets, sterile (*e.g.* Eppendorf, Falcon)
- Stericup Quick Release-GP Steril
- Syringe (Injekt®-F Solo 1 mL, Sterican, cat. n° 9166017V)
  + Hypodermic (dental) needle, G27, 0.40 x 40 mm, grey, sterile (Sterican, cat. n° 9186182)
- Syringe 50 mL (Omnifix Solo Luer-Lock 50 mL, B Braun, cat. n° 4617509F)
- Tubes (15, 50 mL) (*e.g.* Falcon)
- Wipes (*e.g.* Kimberly-Clarck)
- Wrapping film (Parafilm, Bemis, cat. n° PM996)

Individual protection equipment

- Cold insulating gloves, for liquid nitrogen manipulation (vendor of choice)
- Face shield, for liquid nitrogen manipulation (vendor of choice)
- Lab coat (vendor of choice)
- Nitrile gloves (*e.g.* Kimtech)
- Safety glasses (vendor of choice)
- Standard biosafety cabinet (vendor of choice)
- Standard fume hood (vendor of choice)

Waste management equipment

- Bin for biohazard and chemical hazard liquid waste
- Bin for biohazard and chemical hazard sharps objects
- Bin for biohazard and chemical hazard solid waste

(See the existing legislation in the country of use)

Bioinformatics Softwares and Tools

- Cary WinUV software (Agilent), for the UV-Vis spectrophotometer
- Excel (Microsoft Corp.)
- MxPro QPCR software (Agilent), for the Real-time PCR system and thermocycler
- OriginPro 9.1 (OriginLab Corp.)

4. MATERIALS – Buffers and solutions preparation

CAUTION: All buffers should be sterile and carefully prepared using DEPC-H_2O and/or RNase-free water. For buffers and solutions preparation, I used 1. DEPC-H_2O for final buffers and those used on living cells (DEPC-PBS, 5X Fixing buffer, G4RP buffers, glycine) and 2. RNase-free water for the other solutions (with UV-treated PURELAB ultrapure (type 1) water from ELGA LabWater device water or sterile UltraPure Distilled Water from Invitrogen).

For more information regarding molar weight of the G4 probes TASQs and Biotin molecules, see **Table Mat&Meth 14**.

- **1 mM BioCyTASQ** (in RNase-free water)

  1. Deprotect BioCyTASQ in removing BOC with TFA:

  Weight the empty tube that you will use.

  e.g. dissolve 2 mg of BioCyTASQ BOC-protected (M= 2333.76 g/mol) in 400 µL of TFA, incubate at 25 °C for 30 min. Add 1 mL of water, put a perforated cap on tube and cover the cap with wrapping film. Quick-freeze the tube with liquid nitrogen and lyophilize it overnight.

  2. Prepare **1 mM BioCyTASQ** (in RNase-free water):

  e.g. dissolve 1.43 mg of previous BioCyTASQ (BOC-deprotected, with TFA) (M= 2389.38 g/mol) in 600 µL of RNase-free water (*q.s.* 600 µL). Store at 4 °C.

- **1 mM BioTASQ** (in RNase-free water)

  1. Deprotect BioTASQ in removing BOC with TFA:

  Weight the empty tube that you will use.

e.g. dissolve 2 mg of BioTASQ BOC-protected (M= 2393.65 g/mol) in 400 µL of TFA, incubate at 25 °C for 30 min. Add 1 mL of water, put a perforated cap on tube and cover the cap with wrapping film. Quick-freeze the tube with liquid nitrogen and lyophilize it overnight.

2. Prepare **1 mM BioTASQ** (in RNase-free water):

e.g. dissolve 1.47 mg of previous BioTASQ (BOC-deprotected, with TFA) (M= 2449.26 g/mol) in 600 µL of RNase-free water (*q.s.* 600 µL). Store at 4 °C.

- **1 mM BioTriazoTASQ** (in RNase-free water)

  1. Deprotect BioTriazoTASQ in removing BOC with TFA:

  Weight the empty tube that you will use.

  e.g. dissolve 2 mg of BioTriazoTASQ BOC-protected (M= 2658.68 g/mol) in 400 µL of TFA, incubate at 25 °C for 30 min. Add 1 mL of water, put a perforated cap on tube and cover the cap with wrapping film. Quick-freeze the tube with liquid nitrogen and lyophilize it overnight.

  2. Prepare **1 mM BioTriazoTASQ** (in RNase-free water):

  e.g. dissolve 1.63 mg of previous BioTriazoTASQ (BOC-deprotected, with TFA) (M= 2714.29 g/mol) in 600 µL of RNase-free water (*q.s.* 600 µL). Store at 4 °C.

- **1 mM Biotin** (in RNase-free water)

  1. Prepare **10 mM Biotin** (in RNase-free water)

  e.g. dissolve 1.22 mg of Biotin (M= 244.31 g/mol) in 500 µL of RNase-free water (*q.s.* ~ 500 µL).

  2. Prepare the **1 mM Biotin** (in RNase-free water)

  e.g. mix 60 µL of 10 mM Biotin with 540 µL of RNase-free water (*q.s.* 600 µL). Store at 4 °C.

- **2 mM BRACO-19** (in DMSO)

  e.g. dissolve 1.19 mg of BRACO-19 (M= 593.76 g/mol) in 1 mL of DMSO (*q.s.* ~ 1 mL) under a safety cabinet. Store at 4 °C.

- **1 mM Clicked ^{az}MultiTASQ** (in RNase-free water)

  1. Deprotect Clickable ^{az}MultiTASQ in removing BOC with TFA:

  Weight the empty tube that you will use.

  e.g. dissolve 2 mg of Clickable ^{az}MultiTASQ BOC-protected (M= 2246.6 g/mol) in 400 µL of TFA, incubate at 25 °C for 30 min. Add 1 mL of water, put a perforated cap on tube and cover the cap with wrapping film. Quick-freeze the tube with liquid nitrogen and lyophilize it overnight.

  2. Prepare **2 mM Clickable ^{az}MultiTASQ** (in RNase-free water):

  e.g. dissolve 1.842 mg of previous Clickable ^{az}MultiTASQ (BOC-deprotected, with TFA) (M= 2302.24 g/mol) in 400 µL of RNase-free water (*q.s.* 400 µL).

3. Prepare **10 mM DBCO-PEG(4)-Biotin** (in RNase-free water):

e.g. dissolve 1.5 mg of DBCO-PEG(4)-Biotin (M= 749.92 g/mol) in 200 µL of RNase-free water (*q.s.* 200 µL).

4. Prepare the **1 mM Clicked ^{az}MultiTASQ** (= ^{az}MultiTASQ–DBCO-PEG(4)-Biotin):

e.g. mix 100 µL of 2 mM Clickable ^{az}MultiTASQ (BOC-deprotected, TFA in solution) (M= 1846.16 g/mol) with 22 µL of 10 mM DBCO-PEG(4)-Biotin and 78 µL of RNase-free water (*q.s.* 200 µL), to have a 1:1.1 ratio (Clickable ^{az}MultiTASQ:DBCO-PEG(4)-Biotin). Let the coupling reaction (click chemistry) occur at 37 °C for 1 h, under agitation. Check the percentage of conversion with a RP-HPLC-MS (normally, 1 h is enough for a 100% conversion seeable by the DBCO-PEG(4)-Biotin peak disappearance) (**Figures Mat&Meth 9-10**, **Tables Mat&Meth 14-15**).

5. The **1 mM Clicked ^{az}MultiTASQ** (M= 2596.08 g/mol) is now ready-to-use. Store at 4 °C.

- **DEPC-H_2O** (= 0.1% (v/v) DEPC-treated UltraPure Distilled Water)
  e.g. mix 500 µL of DEPC (M= 162.14 g/mol) with 499.5 mL of UltraPure Distilled Water.
  Filter sterilize (0.22 µm filter for bottle ; Stericup) under a safety cabinet. Store at 25 °C.

- **0.5 M EDTA, pH 8.0** (in RNase-free water)
  e.g. dissolve 4.38 g of EDTA (M= 292.25 g/mol) in RNase-free water (*q.s.* 30 mL). Adjust the pH to 8.0 with 1 M NaOH. Filter sterilize (0.2 µm filter for syringe) under a safety cabinet. Store at 4 °C.

- **0.5 M EGTA, pH 8.0** (in RNase-free water)
  e.g. dissolve 5.71 g of EGTA (M= 380.35 g/mol) in RNase-free water (*q.s.* 30 mL). Adjust the pH to 8.0 with 1 M NaOH. Filter sterilize (0.2 µm filter for syringe) under a safety cabinet. Store at 4 °C.

- **5X Fixing buffer** (250 mM HEPES KOH, 500 mM NaCl, 5 mM EDTA, 2.5 mM EGTA, in DEPC-H_2O)
  e.g. mix 25 mL of 1 M HEPES KOH buffer (pH 7.5), 50 mL of 1 M NaCl, 1 mL of 0.5 M EDTA (pH 8.0), 0.5 mL of 0.5 M EGTA (pH 8.0) with 23.5 mL DEPC-H_2O (*q.s.* 100 mL).
  Filter sterilize (0.2 µm filter for syringe) under a safety cabinet. Store at 4 °C.

- **G4RP buffer** (150 mM KCl, 25 mM Tris, 5 mM EDTA, 0.5 mM DTT, 0.5% (v/v) Tergitol, pH 7.4, in DEPC-H_2O)
  e.g. dissolve slowly 181.71 mg of Trizma base in 9 mL of 1 M KCl, 0.6 mL of 0.5 M EDTA pH 8.0, 3 mL of 10 mM DTT, 0.3 mL of Tergitol with DEPC-H_2O (*q.s.* 60 mL). Adjust the pH to 7.4 with 1 M HCl. Filter sterilize (0.2 µm filter for syringe) under a safety cabinet. Store at 4 °C.

- **1 M Glycine** (in DEPC-H_2O)

e.g. dissolve 3378.15 mg of glycine (M= 75.07 g/mol) in DEPC-H_2O (*q.s.* 45 mL).
Filter sterilize (0.2 µm filter for syringe) under a safety cabinet. Store at 4 °C.

- **1 M HCl** (in RNase-free water)
  e.g. add 8.35 mL of 37% (m/m) HCl* (M= 36.46 g/mol) in 91.65 mL of RNase-free water (*q.s.* 100 mL) (in that way). Store at 25 °C. *that 37% (m/m) HCl (d= 1.18) has a concentration of 11.97 M

- **1 M HEPES KOH buffer, pH 7.5** (in RNase-free water)
  e.g. dissolve 47.66 g of HEPES (M= 238.30 g/mol) in RNase-free water (*q.s.* 200 mL). Adjust the pH to 7.5 with 1 M KOH (around 20-30 mL). Filter sterilize (0.2 µm filter for syringe). Store at 4 °C.

- **1 M KCl** (in RNase-free water)
  e.g. dissolve 7.46 g of KCl (M= 74.55 g/mol) in RNase-free water (*q.s.* 100 mL). Store at 4 °C.

- **1 M KOH** (in RNase-free water)
  e.g. dissolve 11.22 g of KOH (M= 56.105 g/mol) in RNase-free water (*q.s.* 200 mL). Store at 4 °C.

- **1 M NaCl** (in RNase-free water)
  e.g. dissolve 5.84 g of NaCl (M= 58.44 g/mol) in RNase-free water (*q.s.* 100 mL). Store at 4 °C.

- **1 M NaOH** (in RNase-free water)
  e.g. dissolve 4 g of NaOH (M= 39.997 g/mol) in RNase-free water (*q.s.* 100 mL). Store at 25 °C.

- **20 mM PhpC** (in RNase-free water)
  e.g. dissolve 3.56 mg of PhpC (M= 356.37 g/mol) in 500 µL of RNase-free water (*q.s.* ~ 500 µL) under a safety cabinet. Aliquote and store at -20 °C.

- **20% (w/v) SDS** (in RNase-free water)
  e.g. dissolve slowly 10 g of SDS (M= 288.38 g/mol) in RNase-free water (*q.s.* 50 mL).
  Store at 25 °C. If it precipitates, warm at 37 °C and resuspend slowly.

- **Supplemented DMEM** (culture medium) (10% (v/v) FBS, 1% (v/v) Pen-Strep, in DMEM)
  e.g. mix 56 mL of Fetal bovin serum and 6 mL of Penicillin-streptomycin (conc) with 500 mL of Dulbecco's Modified Eagle Medium (DMEM, High Glucose, w/ L-Glutamin, w/ Sodium Pyruvate) (*q.s.* 556 mL), under a safety cabinet. Store at 4 °C.

- **1X TBE buffer** (in RNase-free water)
  e.g. dilute 100 mL of 10X TBE buffer with 900 mL of RNase-free water (*q.s.* 1 L). Store at 4 °C.

- **10X TBE buffer, pH 8.3** (in RNase-free water)
  e.g. dissolve 108 g of Trizma base (M= 121.14 g/mol), 55 g of orthoboric acid (M= 61.83 g/mol) and 9.3 g of EDTA (M= 292.25 g/mol) in RNase-free water (*q.s.* 1 L). Adjust the pH to 8.3 with 1 M HCl. Store at 25 °C.

The solutions below have to be fresh and then prepared the first day of the second phasis (experimental manipulation part). The final volumes described here are sufficient for an experiment with 3 conditions (= 3 flasks of cells with different treatments) in which 4 probes (*e.g.* biotin, BioTASQ, BioCyTASQ, Clicked ^{az}MultiTASQ) are tested for the G4-precipitation (*i.e.* 12 sub-conditions).

- **1% (w/v) Formaldehyde/1X Fixing buffer** (1% (w/v) formaldehyde, 50 mM HEPES KOH, 100 mM NaCl, 1 mM EDTA, 0.5 mM EGTA, in DEPC-H_2O)
  e.g. mix 1.9 mL of 16% (w/v) formaldehyde solution, 6 mL of 5X Fixing buffer with 22.1 mL of DEPC-H_2O (*q.s.* 30 mL). Store on ice, protected from light.

- **DEPC-PBS** (0.09% (v/v) DEPC, 1X PBS, in DEPC-H_2O)
  e.g. mix 4.5 mL of 10X PBS with 40.5 mL of DEPC-H_2O (*q.s.* 45 mL). Store on ice.

- **70% (v/v) Ethanol** (in RNase-free water)
  e.g. mix 7 mL of Ethanol absolute with 3 mL of RNase-free water. Store at 25 °C.

- **G4RP lysis buffer** (0.1% (w/v) SDS, 0.1 U/µL RNase OUT, in G4RP buffer)
  e.g. mix slowly 3.75 µL of 40 U/µL RNase OUT, 7.5 µL of 20% (w/v) SDS with 1488.75 µL of G4RP buffer (*q.s.* 1.5 mL). Mix by leading the tube with hands. Store at 4 °C (not on ice, to avoid SDS precipitation).

- **G4RP wash buffer** (0.1 U/µL RNase OUT, in G4RP buffer)
  e.g. mix 9 µL of 40 U/µL RNase OUT with 2391 µL of G4RP buffer (*q.s.* 2.4 mL). Store at 4 °C.

5. METHODS – Step by step protocol

The protocol schedule is separated on two phasis: *i.* a first phasis (STEP 1), the cell culture part, which is composed of cells seeding and growth (1 night), cells incubation with treatment (2 days) and protocol

preparation and a *ii.* second phasis (STEPS 2-8, A-B) which is the experimental manipulation part (around 24 h of manipulation spread over 2 days).

Here are the different steps of that G4RP.v2 protocol (TOTAL TIMING: 3-4 days + 2 nights + 21.25-25.5 h):

- STEP 0: PROTOCOL PREPARATION (TIMING: 1-2 day(s))
- STEP 1: CELL SEEDING & TREATMENT (TIMING: 1 night + 2 days)
- STEP 2: CELL CROSSLINKING (TIMING: 1-2 h)
- STEP 3: CELL LYSIS (TIMING: 2.25-3 h)
- STEP 4: G4-PRECIPITATION (TIMING: 2 h)
- STEP 5: WASHING & REVERSE CROSSLINKING (TIMING: 3-3.5 h)
- STEP 6: RNA PURIFICATION (TIMING: 1 night + 5-6 h)
- STEP 7: REVERSE TRANSCRIPTION & qPCR QUANTIFICATION (TIMING: 4-5 h)
- STEP 8: DATA TREATMENT (TIMING: 1-2 h)
- STEP A: UV ABSORBANCE MEASUREMENT (TIMING: 0.5-1 h)
- STEP B: GEL ELECTROPHORESIS (TIMING: 2.5-3 h)

These steps will be spread on five days following two phasis as previously said:

- A first phasis (cell culture part)
    - Day 1: STEPS 0-1 (cell seeding)
    - Day 2: STEPS 0-1 (cell treatment)
- A second phasis (experimental manipulation part)
    - Day 4: STEPS 2-6 (+ STEP A)
    - Day 5: STEPS 6-8 (+ STEPS A-B)

For that second phasis, I personally always had a work time of 15 h (7 am – 10 pm) and 9 h (9 am – 6 pm) for the day 4 and 5, respectively.

STEP 0: PROTOCOL PREPARATION (TIMING: 1-2 day(s))

1) Prepare the following buffers and solutions:

   1 mM Biotin, 2 mM BRACO-19, DEPC-H_2O, 5X Fixing Buffer, G4RP buffer, 1 M Glycine, 20 mM PhpC, 20% (w/v) SDS, supplemented DMEM, 1 mM TASQ (*e.g.,* BioTASQ, BioCyTASQ or Clicked ^{az}MultiTASQ) solution, 10X TBE buffer pH 8.3 and 1X TBE buffer (see above). Store all buffers and solutions at 4 °C, except DEPC-H_2O and 10X TBE buffer pH 8.3 at RT.

2) Prepare buffers from the RNA purification kit (*i.e.*, RNA Clean & Concentrator-5, supplied with DNase I):

   i. add 96 mL of 100% ethanol to the 24 mL RNA Wash Buffer concentrate, store at RT, ii. reconstitute the lyophilized DNase I (250 U) with 275 µL of DNase/RNase-free water, mix by gentle inversion and store aliquots at -20 °C.

3) Prepare qPCR primers couple in diluting them at [10 µM] in RNase-free UltraPure Distilled water.

4) Prepare the RT and qPCR programs for the real-time PCR system.
5) Prepare the denaturing agarose gel (1% (v/v) bleach, 1.5% (w/v) agarose, TBE) and store it at 4 °C.
6) Clean benchtops and materials (*e.g.,* pipettes) to use for the experiment with RNase decontaminant as the RNaseZap™ product.

CRITICAL STEP: Try to prepare all buffers and solutions in a RNase-free and sterile manner (*i.e.,* with RNase-free water and/or 0.2 µm filtration).

STEP 1: CELL SEEDING & TREATMENT (TIMING: 1 night + 2 days)

7) On day 1 afternoon, $7x10^6$ MCF7 cells in exponential phase growth (in 8 mL) are seeded per cell culture flasks (175 cm^2) in supplemented DMEM culture medium (10% (v/v) FBS, 1% (v/v) Pen-Strep). Allow cells to recover overnight under cell culture condition (37 °C, 5% CO_2). One cell flask can be prepared for non-treated cells (control) and two others for G4 ligand treated-cells (*e.g.,* with BRACO-19 or PhpC).
8) On day 2 morning, change the medium in adding and homogenizing the G4 ligand treatment with. Incubate cells for 48 h under cell culture condition (37 °C, 5% CO_2).

CRITICAL STEPS: i. Use culture medium suitable for your cell line. ii. Depending on cell lines you are using and RNA you want to target, the number of necessitated initial cells may vary. iii. If G4 ligand treatment is used, a dose-finding experiment should be performed before to make sure a suitable dose (*i.e.*, a low-toxic dose, < IC20) is chosen. iv. 8 mL of culture medium is sufficient for cell growth and allow to save G4 ligand treatment. v. If one of the G4 ligand treatments is dissolved in DMSO, make sure to keep the same % (v/v) of DMSO for all condition.

STEP 2: CELL CROSSLINKING (TIMING: 1-2 h)

That whole step was performed in an ice-filled box (unless otherwise indicated).

9) On day 4 morning, prepare freshly the following buffers and solutions:
   1% (w/v) Formaldehyde/1X Fixing buffer, DEPC-PBS, 70% (v/v) ethanol, G4RP lysis buffer and G4RP wash buffer. Store at 4 °C, but the ethanol RT, for day 5.
10) Unhook cells with trypsin, add an equal volume of supplemented DMEM, put it in 15 mL tubes and count cells with cell counting chamber to make sure having around $20x10^6$ cells. (at RT)

CRITICAL STEPS: i. A preliminary growth test should be made to check the final number of cells after that incubation step depending on cell lines you are using. ii. Cells can be crosslinked without any

counting step because the 5% input control will allow the normalization of data from that same condition whatever the starting material. iii. Several numbers of cells to lyse have been tried.

11) Centrifuge at 1 500 rpm (210 G) for 5 min at 4 °C.
12) Aspirate the supernatant and resuspend the cell pellet in 10 mL of DEPC-PBS.
13) Centrifuge at 1 500 rpm (210 G) for 5 min at 4 °C.
14) Aspirate the PBS, add 10 mL of 1% (w/v) Formaldehyde/1X Fixing buffer to the tube, vortex well and incubate on a benchtop laboratory rocker for 5 min at RT.

    CRITICAL STEPS: i. The incubation can be done simply in reversing hands. ii. Several fixation conditions have been tried**.**

15) Quench crosslink by adding glycine to a final concentration of 125 mM (*i.e.,* 1.43 mL of 1 M Glycine in the last 10 mL), vortex well and incubate on a benchtop laboratory rocker for 5 min at RT.

    TIMING: The duration of the formaldehyde crosslinking step is important.

    CRITICAL STEP: After the crosslinking step, keep the sample at 4 °C as much as possible (even during centrifugation).

16) Centrifuge at 1 500 rpm (210 G) for 5 min at 4 °C.
17) Remove the fixing solution and resuspend the cell pellet in 0.8 mL of DEPC-PBS.
18) Transfer into 1.5 mL microtubes.
19) Centrifuge at 1 500 rpm (210 G) for 3 min at 4 °C.

    CRITICAL STEP: The 3 min centrifugation allow to put the cell pellet along the tube corner, which facilitate the aspiration of the supernatant.

20) Aspirate the supernatant and wash again with 1 mL of DEPC-PBS.
21) Centrifuge at 1 500 rpm (210 G) for 3 min at 4 °C.

STEP 3: CELL LYSIS (TIMING: 2.25-3 h)

That whole step was performed in an ice-filled box (unless otherwise indicated).

If you are interested to study cytoplasmic RNA only, the cell lysis method using douncer may be sufficient. Other cell lysis methods can be applied.

22) Aspirate the supernatant and resuspend the pellet in 400 µL of G4RP lysis buffer (0.1% (w/v) SDS, 0.1 U/µL RNase OUT).
23) Make 100 quite fast pipetting (up-and-down) with a 0.4 mm needle-equipped syringe.

CRITICAL STEPS: i. For lysis, it is not necessary to aspirate all bubbles each time, just aspirate the buffer containing cells. ii. Depending on the number of cells the aspiration can be very slow, then use force for the release in order to press cells. iii. Be careful to not let buffer and/or bubble pass through the gasket to the piston of the syringe. If happens, disassemble the part of the syringe and aspirate the buffer with a pipette to not loose cells/lysate volume. iv. Quick spin the tube sometimes (*e.g.,* every 20 up-and-down) to gather non-lysed cells and then improve the pressing. v. Several conditions (*i.e.*, absence/presence of SDS, needle size, number of pipetting) have been tried.

24) Centrifuge at 13 200 rpm (16 550 G) for 10 min at 4 °C.
25) Recover the supernatant of that raw lysate to a new 1.5 mL tube.

CRITICAL STEP: To be sure you have well lysed cells and *nuclei* (if you are interested to study nuclear RNA), you can already make a gel electrophoresis (STEP B) and search for the DNA high > 6 000 bases DNA band.

PAUSE POINT: It is theoretically possible to freeze down the raw lysate supernatant for later processing. However, I always continued directly to the next step for optimal results.

STEP 4: G4-PRECIPITATION (TIMING: 2 h)

That whole step was performed in an ice-filled box (unless otherwise indicated).

26) Each raw lysate supernatant of around 380 µL can be homogenized and aliquoted into 0.2 mL PCR tubes as following:
    - 60 µL for the biotin control
    - 60 µL for the G4 probe TASQ experiment
    - 3 µL for the 5% input control (= 5% of the 60 µL starting material for G4-precipitation) That tube can be stored temporarily at 4 °C then process later with the other samples.
    - Around 8 µL for monitoring STEPS A-B (UV absorbance measurement and gel electrophoresis, respectively)

CRITICAL STEPS: i. The volume of raw lysate supernatant of 60 µL has been chose because this method has always been performed in assessing 3 differents TASQs at the same time (BioTASQ,

BioCyTASQ and Clicked ^{az}MultiTASQ). That volume can be increased depending on conditions you want to try (*e.g.*, antibodies, several G4-probes) and the abundance and/or the type of RNA you want to study (*e.g.,* lncRNA, miRNA). ii. To control the lysis step on that day 4, tubes for monitoring steps can be directly submitted to reverse crosslinking (STEP 5, sub-step 37) and UV absorbance measurement (STEP A) steps for nucleic acids quantification.

27) For each new experiment, wash Streptavidin MagneSphere® Paramagnetic Particles thrice with DEPC-PBS, then resuspend beads in 100 µL of DEPC-PBS to make a 6 µg/µL working stock.

CRITICAL STEPS: i. For each new experiment, a new working stock should be prepared with a new tube of beads. ii. For beads washing/resuspension, use a magnetic rack to pull beads to the tube corner, aspirate the buffer gently in keeping a magnet under the tube, then use wide-mouth tips to gently add buffer and homogenize beads inside. iii. For an experiment using that same precipitation condition (*i.e.*, the amount of beads, see below) for at least 7 sub-conditions to precipitate (with biotin or TASQ), 2 tubes of beads are necessary. iv. The amount of beads can be also optimized.

28) Add 15 µL of the 6 µg/µL beads solution (= 90 µg) to previous PCR tubes (for biotin control and G4-probe TASQ experiment) with wide-mouth tips.
29) Add 6.5 µL of 1 mM stock probe (biotin or TASQ) to a final concentration of 80 µM.
A final volume of 81.5 µL is fine.

CRITICAL STEP: i. The biotin and TASQ concentration can be increased if the G4-precipitation has trapped too few RNA targets. ii. The final volume can be adapted to be around 200 µL.

30) Incubate samples (with beads and probes together) for 2 h at 4 °C on a benchtop rotator.

CRITICAL STEP: Proposition for rotator parameters: orbital rotation of 35 rpm for 20 sec, then quick reciprocal vibration at 5° for 10 sec (with a 90° change after 5 sec).

STEP 5: WASHING & REVERSE CROSSLINKING (TIMING: 3-3.5 h)

That whole step was performed in an ice-filled box (unless otherwise indicated).

31) Use the magnetic rack to pull beads to the tube corner by leaving it on the magnet for 2 min.
32) Discard the supernatant (= unbound materials).
33) Wash beads gently one time with G4RP wash buffer (200 µL) and wide-mouth tips. Let incubate on a benchtop rotator for 5 min at RT. Discard the washing supernatant using a magnetic rack.

34) Wash beads gently one time with DEPC-PBS (200 µL) and wide-mouth tips. Let incubate on a benchtop rotator for 5 min at RT. Discard the washing supernatant using a magnetic rack.

CRITICAL STEPS: i. More washing steps can be added if necessary. ii. In order to control the efficiency of G4-precipitation condition and the softness of washing, several control samples can be kept for additional monitoring steps.

35) Resuspend beads in 100 µL of DEPC-PBS (supplemented with 1 µL of RNase OUT).
Take out the 5% input control tube that was stored in the sub-step 24 and add into that same DEPC-PBS/Rnase OUT mixture.
36) Transfer these samples to new 1.5 mL microtubes in resuspending well beads.
37) Incubate for 2 h at 70 °C on a benchtop heating block to reverse crosslink samples.

CRITICAL STEPS: i. The reverse crosslinking (RCL) duration is determinant for the RNA accessibility and the purity of the sample. Several RCL durations have been tried. ii. Working with RNase-free buffers and materials are essential to avoid RNase contamination and then RNA degradation during the heating step.

STEP 6: RNA PURIFICATION (TIMING: 1 night + 5-6 h)

38) (Under a standard fume hood) Add 1 mL of TRIzol as fast as possible to each tube and mix gently.
39) Quick-freeze samples with liquid nitrogen and store them overnight at -80 °C.

40) On day 5 morning, thaw samples for 5-6 min at 27 °C on a benchtop heating block and mix gently.
41) When it is completely thawed, let samples incubate with the TRIzol for 5 min at RT to dissociate any ribonucleoprotein complexes and other structures.
42) (Under a standard fume hood) Add 0.2 mL of chloroform in each tube. Make sure the cap is sealed and vigorously shake tubes for 15 sec at RT. Leave it for 3 min.

CRITICAL STEPS: i. Because TRizol/chloroform mixture leaks easily from microtubes, take care to keep cleaned gloves and put paper towels between your hand and tubes (places on a rack to shake all of them together) to avoid splashing the hazardous mixture on the working area. ii. Several conditions have been tried.

43) Centrifuge at 12 000 rpm (13 680 G) for 15 min at 4 °C. The mixture will separate into the top aqueous phase (RNAs), the middle interphase (DNA) and the bottom pink-colored organic phase (proteins). Manipulate tubes cautiously and maintain it in ice.

CRITICAL STEP: If the centrifuge is not placed under the fume hood, open doors and windows can avoid a too long risky exposition with volatile products.

44) Transfer the top aqueous phase (around 600 µL) into RNase-free tubes.
45) Add 1 volume of ethanol (95-100%) to 1 volume of aqueous phase (1:1), mix well (avoid vortexing)

Proceed with the RNA Clean-up protocol of the RNA Clean & Concentrator-5 kit provider, at RT:

46) Transfer the sample to the Zymo-Spin IC Column placed on a Collection Tube (or any RNase-free cap-free 2 mL microtube).

CRITICAL STEPS: i. Maximum volume of this column is 700 µL, so repeat the next step several time if necessary, in refilling the same column. ii. The maximum binding capacity of this column is supposed to be 10 µg RNA and the most I achieved to recover was 2.6 µg RNA. That recovery was enough for this study but it can be improved for less abundant target RNA study. To get more of RNA, the same top aqueous phase can be separated into two columns (and then the two purified RNA tubes be gathered) or another type of column can be tried. Several conditions (*i.e.*, method of purification) have been.

47) Centrifuge at 12 000 rpm (13 680 G) for 30 sec at RT and discard the flow-through (= the liquid in the bottom Collection Tube).
48) Add 400 µL of RNA Wash Buffer to the column.
49) Centrifuge at 12 000 rpm (13 680 G) for 30 sec at RT and discard the flow-through.

DNase I treatment (optional; the three next sub-steps 50-52)

50) Prepare the DNase I Reaction Mix (5 µL of reconstituted 1 U/µL DNase I in 35 µL of DNA Digestion Buffer) in an RNase-free microtube and mix by gentle inversion.
51) Add 40 µL of the DNase I Reaction Mix directly into the column matrix.
52) Incubate for 15 min at RT.
53) Add 400 µL of RNA Prep Buffer to the column.
54) Centrifuge at 12 000 rpm (13 680 G) for 30 sec at RT and discard the flow-through.
55) Add 700 µL of RNA Wash Buffer to the column.
56) Centrifuge at 12 000 rpm (13 680 G) for 30 sec at RT and discard the flow-through.
57) Add 400 µL of RNA Wash Buffer to the column.
58) Centrifuge at 12 000 rpm (13 680 G) for 30 sec at RT and discard the flow-through.
59) Ensure complete removal of the RNA Wash Buffer.
60) Carefully, transfer the column into a new RNase-free 1.5 mL microtube.
61) Add 15 µL of DNase/RNase-free water directly to the column matrix. Let 2 min.

62) Centrifuge at 12 000 rpm (13 680 G) for 30 sec at RT and discard the flow-through.
63) Keep the flow-through in the microtube (= 15 µL).
64) Add again 15 µL of DNase/RNase-free water directly to the same column matrix. Let 2 min.
65) Centrifuge at 12 000 rpm (13 680 G) for 30 sec at RT and discard the flow-through.
66) Keep the flow-through in the microtube (= 30 µL).
67) Incubate samples for 15 min at 55 °C on a benchtop heating block for RNA resolubilization.
68) Keep purified RNA samples on ice.

CRITICAL STEP: To control the concentration and purity of purified RNA, you can already check this information by UV absorbance measurement (STEP A).

PAUSE POINT: RNA sample can be stored long term (up to a year) at -80 °C in RNase-free metals-chelating buffers (*e.g.*, with EDTA), to inhibit RNase activity, and then thawed on ice for next processing. In our condition, with RNase-free water, the storage might be shorter. Avoid repeated freeze/thaw cycles. However, I always continued directly to the next step to avoid thawing.

STEP 7: REVERSE TRANSCRIPTION & qPCR QUANTIFICATION (TIMING: 4-5 h)

That whole step was performed in an ice-filled box (unless otherwise indicated).

CRITICAL STEPS: i. To preserve RNA integrity, it is preferential to mix stock products and master mixes by gently flicking the tube or pipetting up-and-down. Vortex is usually not recommended but one slow and very short (< 0.5 sec) vortexing should be fine to help homogenizing. ii. The following 20 µL reaction volume can be used for 10 pg-5 µg of total RNA or 10 pg-500 ng of mRNA (according to SuperScript™ III Reverse Transcriptase provider).

69) Make a master mix A (MM_A, **Table Mat&Meth 13**) of the following components and gently mix:
    - 1 µL of [50 µM] random hexamers
    - 1 µL of [10 mM] dNTP mix
70) Add the MM_A to 12.5 µL of purified RNA (sub-step 68) and gently mix = 14.5 µL of hybridization reaction.
71) Incubate for 5 min at 65 °C.
72) Place on ice for 5 min.
73) Make a master mix B (MM_B , **Table Mat&Meth 13**) of the following components and gently mix:
    - 4 µL of [5X] First Strand Buffer
    - 1 µL of [0.1 M] DTT
    - 0.25 µL of [100 mM] RNase OUT

- 0.25 µL of [200 U/µL] SuperScript III Reverse Transcriptase

74) Add the MM_B to the hybridization reaction tube and gently mix = 20 µL of Reverse Transcription reaction. Pulse spin by brief centrifugation if necessary.
75) Incubate for 5 min at RT. These sub-steps (75-77) can be performed on a thermocycler.
76) Incubate for 45 min at 55 °C.
77) Inactivate RT reaction by incubating for 15 min at 70 °C and cool down to RT.

CRITICAL STEP: i. cDNA sample (= RT sample) can be stored long term (up to a year) at -80 °C. The storage might be shorter at -20 °C (one month is fine). Avoid repeated freeze/thaw cycles. ii. To control the concentration and purity of cDNA, you can already check this information by UV absorbance measurement (STEP A).

Proceed to real-time PCR (qPCR) with the appropriate primer set.

78) For each appropriate primers couple, make a master mix C (MM_C, **Table Mat&Meth 13**) of the following components and gently mix:
    - 0.5 µL of [10 µM] forward primer
    - 0.5 µL of [10 µM] reverse primer
    - 5 µL of [2X] iTaq Universal SYBR® Green Supermix
    - 3 µL of RNase-free UltraPure Distilled water
79) Add 9 µL of appropriate MM_C in plate wells.
80) Add 1 µL of appropriate cDNA sample (or RNase-free UltraPure Distilled Water for "w/o cDNA sample" control) to the appropriate plate wells = 10 µL of qPCR reaction. If necessary, bring down qPCR reaction drops in the plate by brief centrifugation at 1 000 rpm (95 G) and stir slowly the plate for 1-2 min.
81) Run the qPCR using the standard SYBR Green amplification protocol (with dissociation curve) and in selecting the appropriated positions and fluorophore filters. Depending on starting materials, it should take around 20-40 cycles to reach exponential phase.

CRITICAL STEP: Primers couple should be adapted to the annealing (hybridization) temperature of 60 °C allowing a separation of the hybridization and elongation steps.

Name	Nature	Length (in nucleotide)	Sequence	Sub-step	Reference
NRAS forward primer	DNA	23	d[5′ATGACTGAGTACAAACTGGTGGT3′]	78	[9]
NRAS reverse primer	DNA	23	d[5′CATGTATTGGTCTCTCATGGCAC3′]	78	[9]
VEGFA forward primer	DNA	20	d[5′CCTTGCCTTGCTGCTCTACC3′]	78	[9]
VEGFA reverse primer	DNA	20	d[5′AGATGTCCACCAGGGTCTCG3′]	78	[9]

Table Mat&Meth 12. List of the primers couple used for the qPCR quantification of the G4-RNAs NRAS and VEGFA.

		Final concentration in					
Component	**Volume (µL)**	**MM_A**	**Hybridization reaction**	**MM_B**	**RT reaction**	**MM_C**	**qPCR reaction**
[50 µM] random hexamers	1	25 µM	3.45 µM	/	2.5 µM	/	250 nM
[10 mM] dNTP mix	1	5 mM	689.7 µM	/	500 µM	/	50 µM
Purified RNA	12.5	/	varies	/	varies	/	/
[5X] First Strand Buffer	4	/	/	3.6X	1X	/	0.1X
[0.1 M] DTT	1	/	/	18.18 mM	5 mM	/	500 µM
[100 mM] RNase OUT	0.25	/	/	4.55 mM	1.25 mM	/	125 µM
[200 U/µL] SuperScript III RT	0.25	/	/	9.1 U/µL	2.5 U/µL	/	0.25 U/µL
cDNA sample	1	/	/	/	/	/	varies
[10 µM] Forward primer	0.5	/	/	/	/	555.6 nM	500 nM
[10 µM] Reverse primer	0.5	/	/	/	/	555.6 nM	500 nM
[2X] iTaq Universal SYBR® Green Supermix	5	/	/	/	/	1.1X	1X
RNase-free UltraPure Distilled water	3	/	/	/	/	-	-
Volume total (in µL)	**/**	**2**	**14.5**	**5.5**	**20**	**9**	**10**

Table Mat&Meth 13. Summary of components used for the Reverse Transcription & qPCR quantification step. The volume needed for each sub-condition (MM_A, hybridization reaction, MM_B, RT reaction) and each primers couple (MM_C, qPCR reaction) and the concentration are informed.

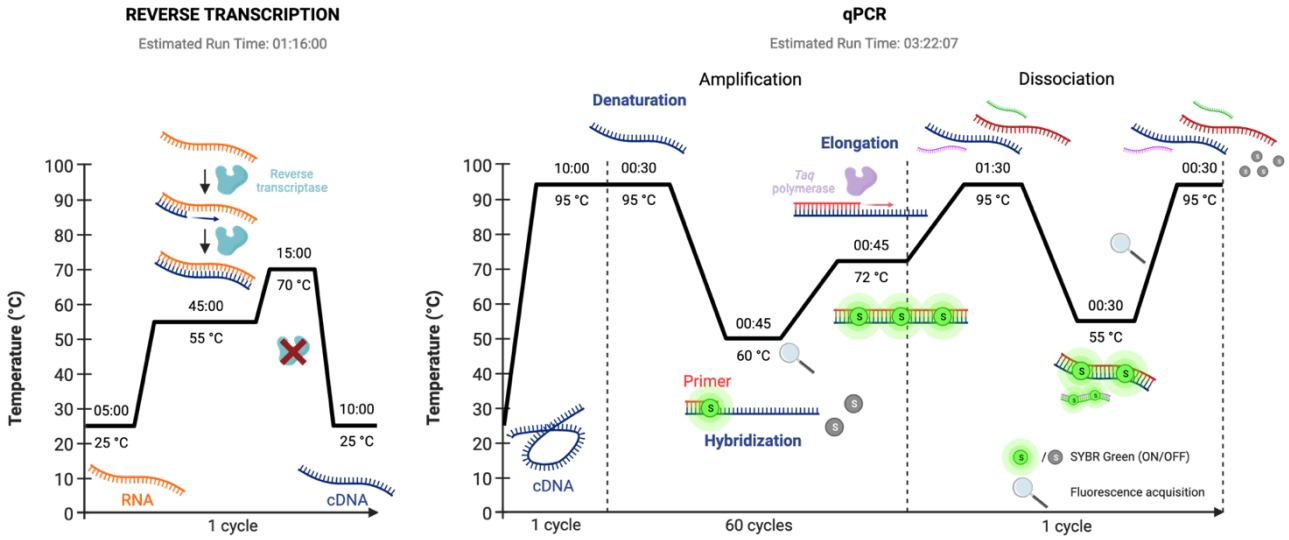

Figure Mat&Meth 8. Schematic representation of the Reverse Transcription and qPCR procedures created for the G4RP.v2 method. Two procedures were created to automate the Reverse Transcription (RT) and qPCR reactions (STEP 7) on the Real-time PCR system and thermocycler. During the RT reaction Purified RNAs are reverse transcribed into cDNAs while during qPCR the cDNAs are amplified by polymerization into amplicons which are quantified via the SYBR Green (an intercalating agent) fluorescence intensity (amplification step). The dissociation step allows to evaluate the amplicons homogeneity. Times showed represent hour:min:sec (or just min:sec). Created with BioRender.com.

STEP 8: DATA TREATMENT (TIMING: 1-2 h)

82) With the Real-time PCR system or the treatment software, determine a threshold for SYBR Green fluorescence intensity (FI) on a y=f(x)-type graph, *i.e.*, baseline-corrected raw SYBR Green FI on cycles: (dR)=f(cycles), and recover the Ct (dR) for each.

CRITICAL STEP: To determine a threshold for SYBR Green FI, put the ordinate (baseline-corrected raw SYBR Green FI (dR)) in log(y), focus only in the almost-vertical and parallel part of exponential curves and select the lowest FI validating these two last prerequisites (= the inflection point) to trace a threshold FI horizontal line. Put the ordinate back in linear y. To obtain the Ct (dR) value of an experimental condition, take the cycle number corresponding to the intersection point between that previous threshold FI line and the appropriate experimental amplification curve.

83) Normalize these Ct (dR) values using the formula below (or another):

G4RP-RT-qPCR signal (fold change)= $5*(2^{(\text{Mean Ct input}) - \text{Ct G4RP or biotin}})$

Mean Ct input corresponds to the mean of Ct obtained with the 5% input control, for each biological replicate. Ct G4RP (or biotin) corresponds to the individual technical Ct obtained with samples G4-precipitated with TASQ (or precipitated with biotin), for each biological replicate.

INFORMATION: For statistical hypothesis tests, Student's *t*-test and Welch's unequal variances *t*-test were used depending on variances equality. * $p < 0.05$, ** $p < 0.01$, *** $p < 0.001$, **** $p < 0.0001$.

84) Make your data representation with these fold change values.

6. METHODS – Monitoring steps

STEP A: UV ABSORBANCE MEASUREMENT (TIMING: 0.5-1 h)

That whole step was performed in an ice-filled box (unless otherwise indicated).

Because of the low range of your samples volume, prefer the use of UV-Vis spectrophotometer able to work with drop-size sub-samples (*e.g.*, 4 µL).

85) Make the baseline.

CRITICAL STEP: Use the appropriate buffer for baseline, *i.e.*, the G4RP lysis buffer for raw lysate and DNase/RNase-free water for purified RNA. An inappropriate baseline could lead to anormal UV absorbance curves (*e.g.*, strong negative part of the curve). If the G4RP lysis buffer is too cold, the SDS could be not completely dissolved and may need to be heated at 30-40 °C.

86) Measure the UV absorbance.

CRITICAL STEPS: i. Take back the drop in tube or for the gel electrophoresis (STEP B). ii. Clean well the material between each measurement to avoid cross-contamination between samples (*e.g.*, wash with water, then with 70% ethanol and dry it). iii. If the sample is too concentrated and you use a classical UV-Vis spectrophotometer with a fibre-optic ultra-micro cell, prefer the use of a different cap (the 50X instead of 10X) on your sample than diluting the sample which will make the baseline not appropriated anymore (*i.e.*, pH, salt and/or SDS concentration discord). iv. Several solutions and solvents absorbance have been measured in order to attribute absorbance peaks of samples.

87) For each sample, recover the peak absorbance value at following wavelengths (A_λ):
    - 230 nm for organic compounds absorbance
    - 260 nm for nucleic acids (DNA and RNA) absorbance
    - 270 nm for phenol(TRIzol)/chloroform absorbance
    - 280 nm for proteins absorbance
88) Calculate the following quality and quantity information for monitoring your G4RP protocol:
    - R1= $A_{260\,nm}/A_{230\,nm}$ for organic compounds contamination
      (Pure nucleic acids if R1= 1.8-2.2, contamination if R1< 1.8)
    - R2= $A_{260\,nm}/A_{270\,nm}$ for phenol (TRIzol)/chloroform contamination
      (Clean nucleic acids if R2= 1.2, contamination if R2< 1.2)

- R3= $A_{260\ nm}/A_{280\ nm}$ for proteins contamination
  (Pure RNA if R3≈ 2, pure DNA if R3≈ 1.8, protein contamination if R3< 1.8)
- RNA estimated concentration (in ng/µL)= $A_{260\ nm}$ * 40

STEP B: GEL ELECTROPHORESIS (TIMING: 2.5-3 h)

That whole step was performed in an ice-filled box (unless otherwise indicated).

For a 25 wells 105x83 mm 1% (v/v) bleach 1.5% (w/v) agarose denaturing TBE gel, prepare it as follows:

89) Mix 1.2 g of agarose with around 79.2 mL of 1x TBE buffer.
90) Boil the mixture for 10 min at 90 °C under a slow magnetic agitation (or use a microwave oven).
91) Add 0.8 mL of bleach and mix again in boiling and agitating for 5 min (*q.s.* ~ 80 mL).
92) Cool down quickly the mixture and cast it rapidly (do not forget combs!).

CRITICAL STEP: A high temperature and a slow agitation avoid normally the creation of too much bubbles. If not, try to not recover bubbles of Erlenmeyer flask walls and use a tip to chase them from the center of the gel.

93) Let the gel polymerize for 20 min at RT.

PAUSE POINT: The gel can be easily stored for a week at 4 °C submerged in 1X TBE gel.

For the loading, electrophoresis and revelation steps, proceed as follows:

94) Mix 4 µL of the sample to load (*e.g.*, raw lysate, purified RNA, others) with 0.5 µL of the 2X RNA loading dye solution (sufficient to benefit from the heavy glycerol and colored dye properties).

PAUSE POINT: Samples mixed with the 2X RNA loading dye solution can be stored at least two days at -20 °C.

95) Incubate for 10 min at 70 °C.
96) Chill on ice 5-10 min.
97) Load cautiously 4 µL in gel wells. For RiboRuler High Range RNA Ladder, load only 2 µL.
98) Run at 100 V for 1.75 h (105 min) at 4 °C.

CRITICAL STEPS: i. For a 1% agarose gel, the bromophenol blue and xylene cyanol dyes migration correspond to a 200-500 and 3 000-4 000 bases nucleic acid, respectively. ii. The electric tension

being the limiting parameter, you can set up the power supply at 100 V (electric tension), 300 mA (electric current) and 30 W (power). During the running, the power will be at ~12 W.

99) To prepare the relevation solution, mix 7.5 µL of SYBR™ Gold Nucleic Acid Gel Stain with 75 mL of 1X TBE buffer (1:10 000).
100) Incubate for 20 min at RT the gel submerged in the revelation solution on a benchtop laboratory rocker (protected from the light).
101) Image the gel with your standard gel imager and appropriate SYBR filters.

7. METHODS – Alternative lysis methods

a. With a cell scraper (in addition of lysis with syringe)

The cell lysis by scraping is another way to break cell membrane as well as nuclear envelope mechanically in using a plastic scraper on an adherent cell mat. For convenience, it is favorable to use Petri dish instead of culture flask for the cell culture given that it will allow to use cell scraper more easily. My aim here, as for the other alternative with a douncer, was to offer a protocol with a large possibility to perform G4RP.v2 depending on materials others laboratories have but also to relieve the lysis step. I combined here scraping and pipetting with needle-equipped syringe but scraping could be only executed.

Additional material: Cell scraper, sterile (blade length: 1.8 cm, Fisherbrand, cat. n° 08-100-241).

a1) Proceed like the classic G4RP.v2 protocol above until the cell treatment (STEP 2, sub-step 9).
a2) Aspirate the cell culture medium from Petri dish.
a3) Wash cells with 10 mL of DEPC-PBS.
a4) Aspirate the DEPC-PBS.
a5) Add 10 mL of 1% (w/v) Formaldehyde/1X Fixing buffer into the Petri dish and incubate on a benchtop laboratory rocker for 5 min at RT.
a6) Quench crosslink by adding glycine to a final concentration of 125 mM (*i.e.,* 1.43 mL of 1 M Glycine in the last 10 mL) and incubate on a benchtop laboratory rocker for 5 min at RT.
a7) Remove the fixing solution and add 0.8 mL of chilled DEPC-PBS into the Petri dish.
a8) Remove the DEPC-PBS and add 400 µL of G4RP lysis buffer into the Petri dish.
a9) Scrape cells vigorously and transfer the DEPC-PBS/raw lysate mixture into a 1.5 mL microtube.

CRITICAL STEPS: i. The scraping has to be controlled with short fast movements to avoid the projection of liquid and thus cells/raw lysate out of the dish. ii. To know if you are efficient or if you have to adjust your movement, you can check sometimes cell at the bottom of your Petri dish with an optical microscope.

a10) Make 50 quite fast pipetting (up-and-down) with a 0.4 mm needle-equipped syringe.
a11) Centrifuge at 13 200 rpm (16 550 G) for 10 min at 4 °C.
a12) Recover the supernatant of that raw lysate to a new 1.5 mL tube.
a13) Incubate for 2 h at 70 °C on a benchtop heating block to reverse crosslink samples.
a14) Check the results with UV absorbance measurement (STEP A) and gel electrophoresis (STEP B).

b. With a douncer (for cytoplasmic RNA only)

Invented by Alexander Dounce in 1955,[15] the dounce homogenizer (or "douncer") is a tool combined by three elements: a cylindrical glass tube (as a mortar), a glass "loose" pestle (with a clearance from the mortar of 63.5-127 µm) and a glass "tight" pestle (with a clearance of 12.7-63.5 µm). Douncing cells (*i.e.,* stroking with the douncer) is a simple technique allowing the membrane cell breakage and thus the recovery of cytosol components (*e.g.*, proteins, RNAs) and intact organelles and nucleus. The dounce movement I used here comprises of i. sticking the pestle into the bottom of the cylindrical mortar, ii. doing a 180° rotation, iii. doing a reverse 180° rotation and iv. pulling the pestle up (in keeping it at the bottom). For the experiments, I only used the tight pestle.

Additional material: Douncer (Dounce Tussue Grinder (15 mL), WHEATON, cat. n° 357544).

b1) Proceed like the classic G4RP.v2 protocol above until the lysis step (STEP 3, sub-step 22).

Before the lysis, the douncer materials have to be cleaned (the nine next sub-steps b2-b10):
b2) Wash the cylindrical mortar with 70% (v/v) Ethanol in douncing the pestle inside.
b3) Wash the cylindrical mortar with RNase-free water in douncing the pestle inside.
b4) Wash the cylindrical mortar with 70% (v/v) Ethanol in douncing the pestle inside.
b5) Wash the cylindrical mortar with RNase-free water in douncing the pestle inside.
b6) Dry the glass instruments with wipes.
b7) Wash the cylindrical mortar with 400 µL of DEPC-PBS in douncing the pestle inside (x2).
b8) Wash the cylindrical mortar with 400 µL of G4RP lysis buffer in douncing the pestle inside.
b9) Dry the glass instruments with wipes.
b10) Put the instruments on ice to keep it cold.

During the lysis:
b11) Put the pellet suspension (in G4RP lysis buffer) at the bottom of the cylindrical mortar.
b12) Make 50 dounces with the tight pestle, in staying in an ice-filled box.

CRITICAL STEP: Because of SDS in the G4RP lysis buffer, the douncing will create bubbles. When the lysis is finished, recover bubbles too.

b13) Between every different condition/experiment, clean the douncer materials in following the last cleaning process (the nine next sub-steps b2-b10).

After the lysis:

b14) Recover the raw lysate in a 1.5 mL tube.

b15) Centrifuge at 13 200 rpm (16 550 G) for 10 min at 4 °C.

b16) Recover the supernatant of that raw lysate to a new 1.5 mL tube.

b17) Incubate for 2 h at 70 °C on a benchtop heating block to reverse crosslink samples.

b18) Check the results with UV absorbance measurement (STEP A) and gel electrophoresis (STEP B).

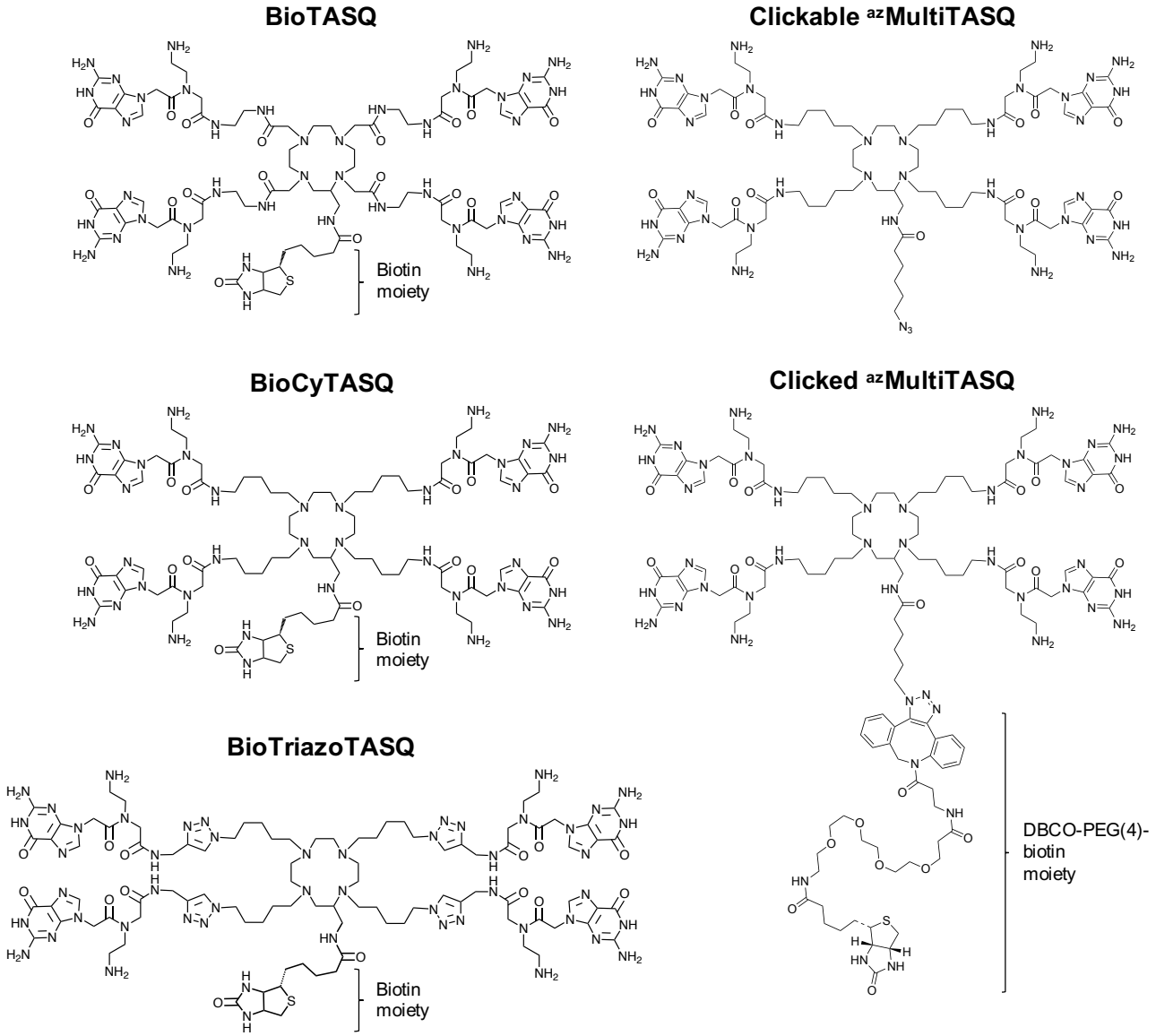

Figure Mat&Meth 9. Structures of G4-probes named TASQs. TASQs, for Template-Assembled Synthetic G-Quartets, are the G4-probes used through the G4RP.v2 method. The Clickable ^{az}MultiTASQ has to be "clicked" with a biotin moiety (here, the DBCO-PEG(4)-biotin) to be usable (see protocol above) while the BioTASQ, BioCyTASQ and BioTriazoTASQ already possess a biotin appendage.

Molar weight (in g/mol)	**Biotin**	**BioTASQ**	**BioCyTASQ**	**BioTriazoTASQ**	**Clickable ^{az}MultiTASQ**	**DBCO-PEG(4)-Biotin**	**Clicked ^{az}MultiTASQ** (^{az}MultiTASQ–DBCO-PEG(4)-Biotin)
BOC-protected	/	2393.65	2333.76	2658.68	2246.6	/	/
BOC-deprotected, with TFA	/	2449.26	2389.38	2714.29	2302.24	/	/
BOC-deprotected, TFA in solution	244.31	1993.18	1933.30	2258.21	1846.16	749.92	2596.08

Table Mat&Meth 14. **Summary of molar weight of G4 probes TASQs and Biotin molecules.** The G4 probes TASQs being produced in lab and stocked under a protected form (with BOC), their molar weight vary through the deprotection and solubilization process. For preparing precise TASQ solutions and monitoring them, here are their molar weight whether they are BOC-protected (stock form), BOC-deprotected with TFA presence or BOC-deprotected with TFA in solution (free TASQ form, in solution).

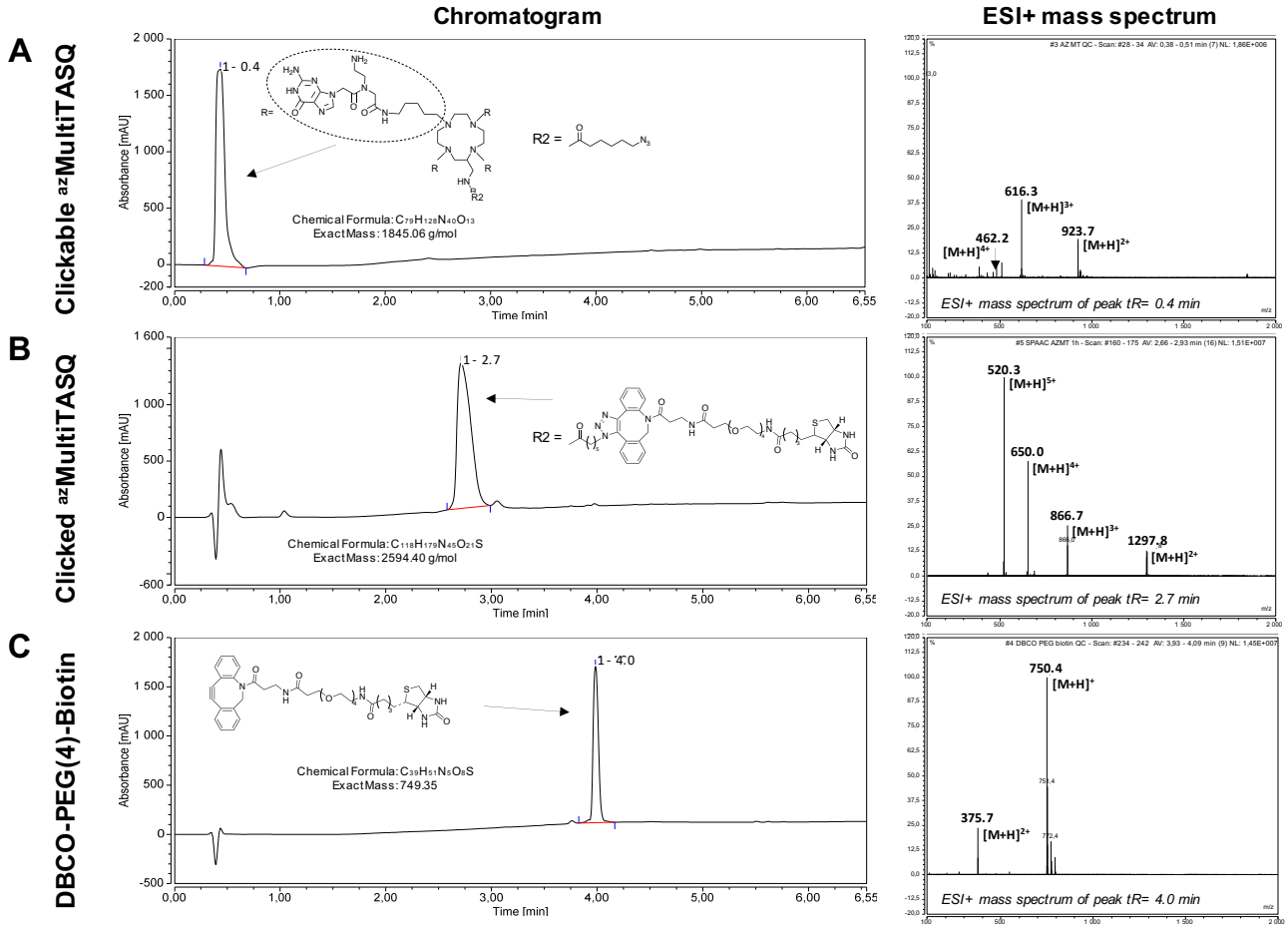

Figure Mat&Meth 10. RP-HPLC-MS elution profiles for the preparation of the Clicked azMultiTASQ. RP-HPLC-MS elution profiles of (A) the Clickable azMultiTASQ, (B) the Clicked azMultiTASQ (the G4-probe) and (C) the DBCO-PEG(4)-Biotin with the chromatogram of the elution (left) and the ESI+ mass spectrum of the major peak (right). The Clicked azMultiTASQ has been obtained after a coupling reaction (details are in the protocol above). (A) Clickable azMultiTASQ: tR= 0.4 min, m/z= 616.3 g/mol for $[M+H]^{3+}$; (B) Clicked azMultiTASQ: tR= 2.7 min, m/z= 520.3 g/mol for $[M+H]^{5+}$; (C) DBCO-PEG(4)-Biotin: tR= 4.0 min, m/z= 750.4 g/mol for $[M+H]^{+}$.

		m/z ratio				
Name	**Exact Mass (Da)**	**z= +1**	**z= +2**	**z= +3**	**z= +4**	**z= +5**
Clickable azMultiTASQ (BOC-deprotected, TFA in solution)	1845.06	Predicted values for $[M+H]^z$ ion:				
		1846.06	923.03	615.35	461.52	369.21
		Measured values:				
		/	923.7	616.3	462.2	/
Clicked azMultiTASQ (= azMultiTASQ–DBCO-PEG(4)-Biotin)	2594.40	Predicted values for $[M+H]^z$ ion:				
		2595.40	1297.7	865.13	648.85	519.08
		Measured values:				
		/	1297.8	866.7	650.0	520.3
DBCO-PEG(4)-Biotin	749.35	Predicted values for $[M+H]^z$ ion:				
		750.35	375.18	250.12	187.59	150.07
		Measured values:				
		750.4	375.7	/	/	/

Table Mat&Meth 15. Summary of mass information for the preparation of the Clicked azMultiTASQ. Summary of the exact mass (m) and the m/z ratio predicted and measured values for the Clickable azMultiTASQ, the Clicked azMultiTASQ (the G4-probe) and the DBCO-PEG(4)-Biotin. $[M+H]^z$ corresponds to a ion where "M+H" is the molecule (*i.e.,* a TASQ)

plus one hydrogen atom and “z” its ionic charge number. The m/z ratio corresponds to the exact mass of this $[M+H]^z$ ion divided by its charge number. “/” means no peak has been strongly detected.

BIBLIOGRAPHY

(1) Laguerre, A.; Hukezalie, K.; Winckler, P.; Katranji, F.; Chanteloup, G.; Pirrotta, M.; Perrier-Cornet, J.-M.; Wong, J. M. Y.; Monchaud, D. Visualization of RNA-Quadruplexes in Live Cells. *J. Am. Chem. Soc.* **2015**, *137* (26), 8521–8525. https://doi.org/10.1021/jacs.5b03413.

(2) Mendoza, O.; Gueddouda, N. M.; Boule, J.-B.; Bourdoncle, A.; Mergny, J.-L. A Fluorescence-Based Helicase Assay: Application to the Screening of G-Quadruplex Ligands. *Nucleic Acids Research* **2015**, *43* (11), e71–e71. https://doi.org/10.1093/nar/gkv193.

(3) Mergny, J.-L.; Maurizot, J.-C. Fluorescence Resonance Energy Transfer as a Probe for G-Quartet Formation by a Telomeric Repeat. *ChemBioChem* **2001**, *2* (2), 124–132.

(4) Stefan, L.; Bertrand, B.; Richard, P.; Le Gendre, P.; Denat, F.; Picquet, M.; Monchaud, D. Assessing the Differential Affinity of Small Molecules for Noncanonical DNA Structures. *ChemBioChem* **2012**, *13* (13), 1905–1912. https://doi.org/10.1002/cbic.201200396.

(5) Xu, H.-J.; Stefan, L.; Haudecoeur, R.; Vuong, S.; Richard, P.; Denat, F.; Barbe, J.-M.; Gros, C. P.; Monchaud, D. Porphyrin-Templated Synthetic G-Quartet (PorphySQ): A Second Prototype of G-Quartet-Based G-Quadruplex Ligand. *Org. Biomol. Chem.* **2012**, *10* (27), 5212. https://doi.org/10.1039/c2ob25601k.

(6) Mergny, J.-L.; Phan, A.-T.; Lacroix, L. Following G-Quartet Formation by UV-Spectroscopy. *FEBS Letters* **1998**, *435* (1), 74–78. https://doi.org/10.1016/S0014-5793(98)01043-6.

(7) Mitteaux, J.; Lejault, P.; Wojciechowski, F.; Joubert, A.; Boudon, J.; Desbois, N.; Gros, C. P.; Hudson, R. H. E.; Boulé, J.-B.; Granzhan, A.; Monchaud, D. Identifying G-Quadruplex-DNA-Disrupting Small Molecules. *J. Am. Chem. Soc.* **2021**, *143* (32), 12567–12577. https://doi.org/10.1021/jacs.1c04426.

(8) Jamroskovic, J.; Obi, I.; Movahedi, A.; Chand, K.; Chorell, E.; Sabouri, N. Identification of Putative G-Quadruplex DNA Structures in S. Pombe Genome by Quantitative PCR Stop Assay. *DNA Repair* **2019**, *82*, 102678. https://doi.org/10.1016/j.dnarep.2019.102678.

(9) Yang, S. Y.; Lejault, P.; Chevrier, S.; Boidot, R.; Robertson, A. G.; Wong, J. M. Y.; Monchaud, D. Transcriptome-Wide Identification of Transient RNA G-Quadruplexes in Human Cells. *Nat Commun* **2018**, *9* (1), 4730–4740. https://doi.org/10.1038/s41467-018-07224-8.

(10) Mergny, J.-L.; Li, J.; Lacroix, L.; Amrane, S.; Chaires, J. B. Thermal Difference Spectra: A Specific Signature for Nucleic Acid Structures. *Nucleic Acids Research* **2005**, *33* (16), e138–e138. https://doi.org/10.1093/nar/gni134.

(11) Karsisiotis, A. I.; Hessari, N. M.; Novellino, E.; Spada, G. P.; Randazzo, A.; Webba da Silva, M. Topological Characterization of Nucleic Acid G-Quadruplexes by UV Absorption and Circular Dichroism. *Angew. Chem. Int. Ed.* **2011**, *50* (45), 10645–10648. https://doi.org/10.1002/anie.201105193.

(12) Kypr, J.; Kejnovská, I.; Renciuk, D.; Vorlícková, M. Circular Dichroism and Conformational Polymorphism of DNA. *Nucleic Acids Res* **2009**, *37* (6), 1713–1725. https://doi.org/10.1093/nar/gkp026.

(13) Smiatek, J.; Chen, C.; Liu, D.; Heuer, A. Stable Conformations of a Single Stranded Deprotonated DNA I-Motif. *J Phys Chem B* **2011**, *115* (46), 13788–13795. https://doi.org/10.1021/jp208640a.

(14) Schindelin, J.; Arganda-Carreras, I.; Frise, E.; Kaynig, V.; Longair, M.; Pietzsch, T.; Preibisch, S.; Rueden, C.; Saalfeld, S.; Schmid, B.; Tinevez, J.-Y.; White, D. J.; Hartenstein, V.; Eliceiri, K.; Tomancak, P.; Cardona, A. Fiji: An Open-Source Platform for Biological-Image Analysis. *Nat Methods* **2012**, *9* (7), 676–682. https://doi.org/10.1038/nmeth.2019.

(15) Dounce, A. L.; Witter, R. F.; Monty, K. J.; Pate, S.; Cottone, M. A. A Method for Isolating Intact Mitochondria and Nuclei from the Same Homogenate, and the Influence of Mitochondrial Destruction on the Properties of Cell Nuclei. *The Journal of Cell Biology* **1955**, *1* (2), 139–153. https://doi.org/10.1083/jcb.1.2.139.